DISSERTATION

ZUR ERLANGUNG DES GRADES
„DOKTOR DER NATURWISSENSCHAFTEN“
(DR. RER. NAT.)

IM PROMOTIONSFACH CHEMIE

Bifunctional Carbanionic Synthesis of Bio-Based Thermoplastic Elastomers in Methyl *tert*-Butyl Ether

vorgelegt von
Moritz Meier-Merziger
geboren am 25.03.1995 in Darmstadt

Mainz 2024

JOHANNES GUTENBERG UNIVERSITÄT MAINZ

Fachbereich 09 – Chemie, Pharmazie, Geographie und Geowissenschaften der Johannes Gutenberg-Universität Mainz

Die als Dissertation vorgelegte Arbeit wurde im Zeitraum von April 2021 bis Juli 2024 am Department Chemie der Johannes Gutenberg-Universität Mainz im Arbeitskreis von [redacted] angefertigt.

Dekanin:

1. **Berichterstatter:**
2. **Berichterstatter:**

Tag der mündlichen Prüfung: 26.09.2024

Hiermit versichere ich gemäß § 10 Abs. 3d der Promotionsordnung vom 24.07.2007:

Ich habe die jetzt als Dissertation vorgelegte Arbeit selbst angefertigt und alle benutzten Hilfsmittel (Literatur, Apparaturen, Material) in der Arbeit angegeben. Ich hatte die hier als Dissertation vorgelegte Arbeit nicht als Prüfungsarbeit für eine andere staatliche oder andere wissenschaftliche Prüfung eingereicht. Ich hatte weder die hier vorgelegte Arbeit noch Teile davon bei einer anderen Fakultät bzw. einem anderen Fachbereich als Dissertation eingereicht.

Moritz Meier-Merziger

Für meine Familie

„Still round the corner there may wait,
A new Road or a secret gate.“

J. R. R. Tolkien

Danksagung

Author Contributions

Table of Content

Table of Content

Motivation and Objectives

Motivation and Objectives

In the last century, polymers have paved the way for many aspects of modern life by providing crucial properties, hardly accessible with traditional materials, such as metals or wood. Polymer-based innovations that go beyond the widely known commodity products such as thermoplastic packaging materials (i.e. polyethylene, polypropylene, polyethylene terephthalate, and polystyrene), polyvinyl chloride, polyurethanes, and synthetic rubber have shaped modern society in applications ranging from pharmaceutical formulations to electronic devices.[1]–[3]

A major concern with many polymer materials is their end-of-life fate. This represents a societal and political challenge, which plays a key role to reduce the environmental impact by lowering the amount of discarded polymers through the development and improvement of reuse and recycling pathways. Further, this aims to help reducing greenhouse gas emissions liberated by the production of the polymers.[4] Some polymer classes are intrinsically not recyclable by general thermoplastic processing techniques, i.e. extrusion and molding. This applies, for instance, to covalently cross-linked networks of elastomers or thermosets.[5],[6] As their unique properties are indispensable for several applications, vast efforts aim at comparable, yet (re)processible alternatives.

Figure 1. Overview of applications of thermoplastic elastomers.

ABA-triblock copolymers composed of high glass temperature (T_g) outer A-blocks and a low T_g B-midblock are known to show similar properties to chemically cross-linked networks. The immiscibility of the different blocks results in phase-separation within the bulk material.[7] At ambient temperatures, the high-T_g domains are vitrified, serving as reversible physical cross-

links. The low-T_g domains contribute rubbery characteristics, i.e., flexibility and elongation by chain entanglements. This type of material is referred to as "thermoplastic elastomer" (TPE), **Figure 1**. As described by G. Holden, TPEs are characterized as follows: *"They allow rubberlike articles to be produced using the rapid processing techniques developed by the thermoplastic industry".*[8]

While this advantage of reprocessability alone contributes to the greater sustainability of TPEs compared to elastomers, there are numerous additional aspects that can be addressed to increase the overall sustainability of these materials.[9] These handles include the synthesis process itself, as well as the selection of the crude feedstock.

An established pathway to obtain ABA-type triblock structures is the anionic polymerization. Introduced by Szwarc in the 1950s, the "living" behavior of this chain-growth polymerization is widely known for its high control, yielding precise polymers of adjustable molar mass and low dispersity.[10] The absence of termination and transfer reactions allows access to block copolymers *via* sequential addition of monomers. However, due to the high sensitivity of carbanions, this method requires high purity of all components as well as a considerable effort to run these multi-step procedures. One tool to minimize the required addition steps is the use of a bifunctional anionic initiator. Consequently, the chain-growth occurs in a telechelic manner at both ends of the growing chain and decreases the required number of monomer addition steps. As the use of bifunctional initiators in carbanionic polymerization is limited by their low solubility in commonly used hydrocarbons, more scarcely applied, polar solvents will be considered within this study. Many non-protic solvents, for instance tetrahydrofuran (THF), are out of scope for translation towards industry as the formation of peroxides prohibits large-scale applications. Surprisingly, the readily available solvent methyl *tert*-butyl ether (MTBE) has attracted minor attention so far, despite its significant advantages of moderate polarity and the absence of peroxide formation.[11] The increased polarity compared to hydrocarbons indicates that MTBE could be a highly promising alternative solvent for bifunctional carbanionic polymerization.[12],[13]

Given the limited knowledge regarding MTBE as a solvent in carbanionic polymerization, ***Objective*** ① of this thesis is to evaluate the suitability of MTBE as a solvent for this process. As THF is known for its poor stability towards alkyl lithium compounds, particularly at temperatures above -78 °C, better stability of MTBE would translate to a significant advantage.[14],[15] Questions that arise are: how does the reaction rate compare with traditional solvents, what is the degree of association of the living chain ends, and how does MTBE influence the kinetics of anionic copolymerization?

In addition to a more efficient synthesis route accessible *via* bifunctional initiation, the choice of monomer is another important aspect to enhance sustainability. Hence, bio-based monomers can be used to replace traditional fossil fuel-based monomers such as isoprene and styrene. As previously outlined by our group, various terpenes offer an excellent alternative owing to their great structural diversity, offering a broad range of properties.[16] For instance, *β*-farnesene is a relevant monomer not only because it is derived from a renewable feedstock, i.e., sugar cane, but also due to its unique features compared to its smaller homologue, isoprene. The T_g of polyfarnesene is low (< -70 °C) and practically independent of the microstructure in the polymer backbone, which is usually known to drastically influence the material properties of 1,3-dienes.[13] Therefore, many restrictions regarding reaction conditions, e.g. low solvent polarity, do not apply for *β*-farnesene, allowing for a much more versatile adjustment of reaction parameters.

As a low T_g is desired for the soft domains in TPEs, ***Objective*** ② is to use the abovementioned solvent MTBE as a medium for the bifunctional initiation of the bio-based monomer *β*-farnesene. To obtain fully bio-based TPEs, the outer high-T_g blocks also have to be constructed from a renewable source. Polylactide (PLA), known as one of the most abundant bio-based polymers, can be grafted on macromolecules bearing hydroxyl functionalities.[17] To introduce hydroxyl groups at a polydiene chain end, controlled termination using epoxides is a feasible and long-known pathway.[18] Since this is an established procedure, numerous glycidyl ethers were reported, which can even bear additional protected functionalities.[19],[20] Therefore, this part of the thesis investigates whether this process can be transferred to a bifunctional system that enables the simultaneous introduction of functionalities in α- and ω-position of a chain. The primary objective is to synthesize fully bio-based TPEs from *β*-farnesene and LL-dilactide (LLA).

To maximize the efficiency of the synthesis of fully bio-based TPEs, ***Objective*** ③ is to develop a one-pot synthesis approach, exclusively applying statistical anionic polymerization and relying on disparate reactivity ratios. Following the bifunctional polymerization of *β*-farnesene, a bio-based and anionically polymerizable second monomer should be used for the "hard" block. Again, a suitable candidate can be found in the group of terpenes. As introduced earlier by our group, polymers derived from nopadiene, a bicyclic 1,3-diene, have a considerably high T_g of ~ 160 °C that makes nopadiene a suitable substitute for polystyrene. Nopadiene can be derived from bio-renewable turpentine oil, which is sourced from pine trees.[21] As copolymerizations often result in gradient incorporation of the two comonomers, a preferred incorporation of *β*-farnesene may represent the most efficient route towards ABA-type tapered triblock copolymers. *In situ* ^{1}H NMR kinetics can be used to investigate the kinetics of the copolymerization, and the effect of reaction conditions will be examined. The

goal of this work is to identify suitable conditions that allow for the synthesis of two-sided tapered structures without requiring any further monomer addition steps.

Functional initiators and bifunctional initiators face similar challenges for their implementation in the field of carbanionic polymerization. Therefore, ***Objective*** ④ is to explore a new route to introduce functionality in α-position of polydienes. This project was designed in collaboration with the synthetic rubber company Arlanxeo. The introduction of hydrophilic groups at the chain end of a polydiene is a promising tool to enhance the poor filler-rubber interaction in rubber composites, an omnipresent challenge of the rubber industry.[22] As the major difficulty is attributed to solubility issues of the polar initiators in hydrocarbon solvents, detailed knowledge of the abovementioned objectives of bifunctional synthesis can be transferred to functional initiators.[19],[23] To further confirm successful chain end functionalization, the end-groups can be addressed *via* grafting LLA from the respective macroinitiators. This gives access to complex polymer structures, that extend the library of polymer architectures presented in this thesis, see **Figure 2**.

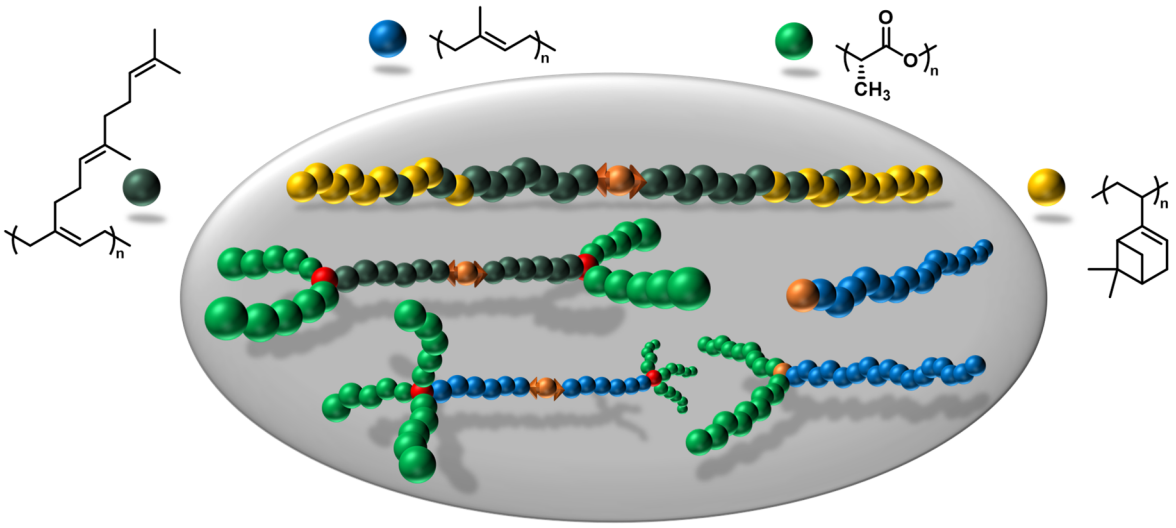

Figure 2. Overview of targeted polymer architectures of this thesis based on the monomers: *β*-farnesene, isoprene, LLA, and nopadiene.

As a prerequisite for this thesis, the ensuing chapter aims at a comprehensive overview of the state-of-the-art of the anionic polymerization of diene monomers, also highlighting their relevance in the field of thermoplastic elastomers. Recent advances, including new bio-based monomers, mechanistic insights, kinetics of statistical copolymerization, and the customization of material properties, will be covered in this compact *Perspective*.

References

[1] Mishra, M. *Concise encyclopedia of biomedical polymers and polymeric biomaterials (Volume I - II)*; CRC Press, **2017**.

[2] Sadasivuni, K. K.; Hegazy, S. M.; Abdullah Aly, A. A. M.; Waseem, S.; Karthik, K. Polymers in electronics. In *Polymer Science and Innovative Applications*; Mariam Al Ali AlMaadeed, Marcelo A. Carignano, Eds.; Elsevier, **2020**; pp 365‑392.

[3] Koltzenburg, S.; Maskos, M.; Nuyken, O.; Matyjaszewski, K.; Mülhaupt, R. *Polymer Chemistry*, 2nd edition 2023; Springer Berlin Heidelberg, **2023**.

[4] Jehanno, C.; Alty, J. W.; Roosen, M.; Meester, S. de; Dove, A. P.; Chen, E. Y.-X.; Leibfarth, F. A.; Sardon, H. Critical advances and future opportunities in upcycling commodity polymers. *Nature*, **2022**, *603* (7903), 803‑814.

[5] Post, W.; Susa, A.; Blaauw, R.; Molenveld, K.; Knoop, R. J. I. A Review on the Potential and Limitations of Recyclable Thermosets for Structural Applications. *Polymer Reviews*, **2020**, *60* (2), 359‑388.

[6] Fazli, A.; Rodrigue, D. Waste Rubber Recycling: A Review on the Evolution and Properties of Thermoplastic Elastomers. *Materials (Basel, Switzerland)*, **2020**, *13* (3).

[7] Holden, G.; Bishop, E. T.; Legge, N. R. Thermoplastic elastomers. *J. polym. sci., C Polym. symp.*, **1969**, *26* (1), 37‑57.

[8] Holden, G. *Understanding thermoplastic elastomers*; Hanser understanding books; Hanser, **2000**.

[9] Anastas, P.; Eghbali, N. Green chemistry: principles and practice. *Chemical Society reviews*, **2010**, *39* (1), 301‑312.

[10] Szwarc, M. 'Living' Polymers. *Nature*, **1956**, *178* (4543), 1168‑1169.

[11] Hamid, S. H.; Ali, M. A. Effect of MTBE Blending on the Properties of Gasoline. *Fuel Sci. Technol. Int.*, **1995**, *13* (5), 509‑544.

[12] Yu, Y.; Dubois, P.; Teyssié, P.; Jérôme, R. Difunctional Initiator Based on 1,3-Diisopropenylbenzene. 6. Synthesis of Methyl Methacrylate–Butadiene–Methyl Methacrylate Triblock Copolymers. *Macromolecules*, **1997**, *30* (15), 4254‑4261.

[13] Yoo, T.; Henning, S. K. Synthesis and Characterization of Farnesene-Based Polymers. *Rubber Chem. Technol.*, **2017**, *90* (2), 308‑324.

[14] Stanetty, P.; Mihovilovic, M. D. Half-Lives of Organolithium Reagents in Common Ethereal Solvents. *J. Org. Chem.*, **1997**, *62* (5), 1514‑1515.

[15] Clayden, J.; Yasin, S. A. Pathways for decomposition of THF by organolithiums: the role of HMPA. *New J. Chem.*, **2002**, *26* (2), 191‑192.

[16] Wahlen, C.; Frey, H. Anionic Polymerization of Terpene Monomers: New Options for Bio-Based Thermoplastic Elastomers. *Macromolecules*, **2021**, *54* (16), 7323‑7336.

[17] Frick, E. M.; Hillmyer, M. A. Synthesis and characterization of polylactide-block-polyisoprene-block-polylactide triblock copolymers: new thermoplastic elastomers containing biodegradable segments. *Macromol. Rapid Commun.*, **2000**, *21* (18), 1317‑1322.

[18] Richards, D. H.; Szwarc, M. Block polymers of ethylene oxide and its analogues with styrene. *Trans. Faraday Soc.*, **1959**, *55*, 1644.

[19] Tonhauser, C.; Frey, H. A road less traveled to functional polymers: epoxide termination in living carbanionic polymer synthesis. *Macromolecular rapid communications*, **2010**, *31* (22), 1938‑1947.

[20] Tonhauser, C.; Wilms, D.; Wurm, F.; Nicoletti, E. B.; Maskos, M.; Löwe, H.; Frey, H. Multihydroxyl-Functional Polystyrenes in Continuous Flow. *Macromolecules*, **2010**, *43* (13), 5582‑5588.

[21] Hahn, C.; Göttker-Schnetmann, I.; Tzourtzouklis, I.; Wagner, M.; Müller, A. H. E.; Floudas, G.; Mecking, S.; Frey, H. Nopadiene: A Pinene-Derived Cyclic Diene as a Styrene Substitute for Fully Biobased Thermoplastic Elastomers. *J. Am. Chem. Soc.*, **2023**, *145* (49), 26688-26698.

[22] Liu, X.; Zhao, S.; Zhang, X.; Li, X.; Bai, Y. Preparation, structure, and properties of solution-polymerized styrene-butadiene rubber with functionalized end-groups and its silica-filled composites. *Polymer*, **2014**, *55* (8), 1964‑1976.

[23] Schulz, D. N.; Halasa, A. F.; Oberster, A. E. Anionic polymerization initiators containing protected functional groups and functionally terminated diene polymers. *J. Polym. Sci. Polym. Chem. Ed.*, **1974**, *12* (1), 153‑166.

Abstract

Abstract

This thesis presents the synthesis of fully bio-based thermoplastic elastomers (TPEs) *via* anionic polymerization. TPEs are intrinsically more sustainable compared to classical irreversibly vulcanized elastomers. Consequently, bio-based TPEs and novel solvent options are investigated within this work. The first objective is to establish a more efficient synthesis route based on bifunctional initiation, wherein the solvent methyl *tert*-butyl ether (MTBE) is investigated for its ability to ensure a reliable and controlled anionic polymerization. Additionally, the utilization of renewable monomers as building blocks for TPEs addresses the urgent societal and political demand for increased sustainability. From this perspective, natural building blocks based on terpenes offer great structural diversity and are therefore used within this work to install different material properties. Thus, this dissertation aims to contribute to a more sustainable future of polymer materials.

Aiming at a general overview of the relevance of diene monomers in the anionic polymerization, **Chapter ①** gives a comprehensive compilation of findings of recent research in the form of a P*erspective* article. It features how the shift from established fossil fuel-based elastomers, produced from only three primarily used monomers, i.e., styrene, butadiene, and isoprene, towards bio-based feedstocks changes the perspective of research. These recently developed bio-based monomers in terms of polymer properties, mechanistic insights, and behavior in statistical copolymerization are covered.

As some relevant theoretical concepts for this thesis are not included in this first *Perspective* article, **Chapter ②** provides further insights. The general concept of TPEs is introduced, covering the origin of the reprocessability and the general concepts of phase behavior in the bulk of block copolymers. Different synthesis pathways towards ABA-type triblock copolymers are discussed. Since peculiar polymer architectures can be achieved by using bifunctional initiators, these are introduced in greater detail. Challenges and former reports of bifunctional initiators are evaluated. Furthermore, as statistical copolymerization is a key method in producing block-like tapered structures in an even more efficient manner, a general introduction is given regarding the concept of reactivity ratios as well as their determination.

The main objective of this work is to develop an efficient synthesis pathway for bio-based TPEs. As the greatest efficiency for the synthesis of ABA-type triblock structures is based on bifunctional initiators, suitable media have to be identified. The poor solubility of bifunctional initiators in hydrocarbons necessitates the use of more polar solvents. Traditionally, tetrahydrofuran (THF) is used on lab-scale. However, translation to industry is prohibited, as

the formation of peroxides and proton abstraction at ambient temperatures are major drawbacks of THF. Therefore, **Chapter ③** covers the investigation of MTBE as an alternative solvent that comprises solubility of bifunctional initiators, no peroxide formation, and ideally a higher stability towards alkyl lithium compounds. The latter is demonstrated by the 50 times longer half-life of *n*-butyl lithium in MTBE, compared to THF. As little is known about its general performance as reaction medium in the anionic polymerization, key kinetic parameters, i.e., propagation rates of the polymerization of 1,3-dienes are investigated as well. The trend of higher reaction rates compared to the traditionally used hydrocarbon solvent cyclohexane is determined for isoprene and *β*-farnesene – one "traditional" monomer and a renewable structure. Further, the "living" polydienyl lithium chains are predominantly present as non-aggregated unimers in MTBE. In addition to the homopolymerization, the established copolymerization system of styrene and isoprene is examined. The effect of an increasing MTBE fraction is investigated *via in situ* near-infrared (NIR) kinetics. The gradient structure, found in pure cyclohexane, successively changes to random monomer incorporation and ultimately yields an inverted, yet still close to random comonomer incorporation in pure MTBE. This is reflected by the reactivity ratios $r_S^{MTBE} = 1.82$ and $r_I^{MTBE} = 0.55$. The great potential identified for MTBE in carbanionic polymerization is used in the ensuing chapters of this work.

In **Chapter ④**, MTBE is utilized as a reaction medium for the bifunctional initiator 1,3-diisopropylene benzene. The excellent solubility of the bifunctional initiator in MTBE allows easy access to ABA-type triblock copolymers. To alleviate the current environmental challenges and to overcome the shrinking fossil fuel feedstock, a fully bio-based TPE is targeted. Therefore, *β*-farnesene is used for the middle block, as it can be derived from sugar cane and has a microstructure-independent low glass temperature (T_g). By controlled termination of the telechelic "living" polyfarnesene chains, hydroxyl groups are introduced *via* adding ethoxy ethyl glycidyl ether (EEGE) to the reaction. This affords low dispersity ($Đ$ = 1.07 to 1.10) and telechelic polyfarnesene macroinitiators, bearing two hydroxyl groups at each chain end. Subsequent organocatalyzed ring-opening polymerization (ROP) of LL-dilactide (LLA) yields *H*-shaped, fully bio-based triblock copolymers. The material features two distinct T_gs at – 66 °C and 51 °C, as well as gyroid or cylindrical morphologies, determined by transmission electron microscopy (TEM) and small-angle *X*-ray scattering (SAXS). A soft elastic material at room temperature is obtained.

Given the advantages of the moderately polar solvent MTBE, ensuring reliable solubility of a bifunctional initiator, and the low T_g of polyfarnesene, **Chapter ⑤** describes an even more efficient pathway towards ABA-type structures. To allow for a one-step synthesis and to avoid an elaborate multistep pathway, carbanionic polymerization is exclusively used in this chapter.

Nopadiene (Nopa) is chosen as a suitable comonomer, as PNopa exhibits a high T_g of ~ 160 °C and can be derived from the renewable feedstock pine tree. Excellent control of carbanionic copolymerization is confirmed by *in situ* ^{1}H NMR kinetics. By changing the reaction conditions, the reactivity ratios are tailored to yield a steep gradient comonomer incorporation, r_{Far}^{MTBE} = 10.8 and r_{Nopa}^{MTBE} = 0.093. Consequently, symmetric, two-sided tapered ABA-type triblock copolymers are accessible in a one-step approach, capitalizing on a difunctional initiator in MTBE. By changing the comonomer ratio, the material properties are tuned in a broad range: highly elastic materials with elongation exceeding 1300% as well as tough materials with Young modulus' exceeding 500 MPa are obtained. Characterization *via* SAXS, temperature-modulated differential scanning calorimetry (TM DSC), rheology, and dielectric spectroscopy are employed to relate the material properties to the phase state of the triblock copolymer. This revealed local phase segregation accompanied by respective T_gs of the domains, albeit in the absence of long-range order. Thus, it could be successfully demonstrated that it is possible to produce fully bio-based TPEs that are similar in their properties to fossil fuel-based materials *via* a one-pot and one-step synthesis.

Bifunctional initiators and functional initiators face similar challenges in their application in the field of carbanionic polymerization. Therefore, **Chapter ⑥** involves the translation of previous findings in terms of solubility issues of bifunctional initiators - Chapter 4 - to functional initiator structures. The project is the result of a collaboration with the synthetic rubber company Arlanxeo. The incorporation of functional groups at the chain end of polymer chains in elastomers is beneficial to improve filler-rubber interaction and helps to improve the performance in, for instance, tires as it lowers the rolling resistance and hence reduces fuel consumption. Further, functional groups at the chain end can be used in a subsequent reaction to access block structures. To this end, a heterotelechelic initiator for the formation of α-functionalized polyisoprene is developed. The initiator is accessed *via* titration using an iodine alkyl precursor and *tert*-butyl lithium. First, the functional alkyl lithium initiator, bearing two ketal-protected hydroxyl functionalities, is used for the carbanionic polymerization of isoprene. Low dispersity ($Đ$ < 1.1) polymers with a high 1,4-polyisoprene content (60%) are obtained after optimization of the required amount of polar modifiers. Matrix-assisted laser desorption/ionization time-of-flight mass spectroscopy (MALDI-ToF MS) measurements verify an effective end-group functionalization. Second, LLA is grafted from theses $(OH)_2$-PI macroinitiators to access A_2B-type block copolymers. Size-exclusion chromatography (SEC), NMR, and diffusion-ordered spectroscopy (DOSY) measurements are used to demonstrate successful chain-extension *via* lactide grafting. DSC experiments reveal two distinct T_gs, indicating phase-separation within the block copolymers. Hence, a heterotelechelic initiator for both carbanionic polymerization and ROP is introduced.

In the first appendix **Chapter A①**, an approach for TPEs based on a pure hydrocarbon medium is presented. The bifunctional initiator 1,3-bis(1-phenyl ethenyl) benzene (PEB) is used for its good solubility in cyclohexane. As such, a high 1,4-content can be achieved in the polymerization of 1,3-dienes, which in turn allows for the use of the readily available monomer isoprene. Subsequently, three hydroxyl groups are introduced simultaneously both in α- and *ω*-position by means of end-functionalization of the living anionic dilithiated PI-chains, with 1,2-isopropylidene glyceryl glycidyl ether (IGG) and subsequent acidic deprotection. These multi-hydroxyl PI-macroinitiators are used to initiate LLA in an organocatalyzed ROP. Thereby, *super-H*-shaped A_3BA_3-triblock structures are obtained. Thermal characterization reveals two distinct T_gs, suggesting phase-separation within the bulk material. PI-domains feature a low T_g in the range of - 55 °C to - 59 °C and the PLLA-domains show a T_g of 41 °C to 49 °C. Furthermore, the exact phase-separation and morphology is analyzed *via* TEM and SAXS, confirming cylindrical and lamellar morphologies. The combination of carbanionic synthesis and ROP of lactones is presented as a feasible pathway for complex polymer architectures.

Chapter A② presents a fundamental investigation on binary blends of polyfarnesene and polyisoprene as a model system towards super soft polymer melts. The expertise in the living diene polymerization gained before is used to synthesize a molar mass series of polyfarnesene samples in the range of 3.5 kg·mol^{-1} to 720 kg·mol^{-1}. To prepare polyfarnesene/polyisoprene blends, commercially available polyisoprene samples of the same molar mass are purchased. The addition of linear polyisoprene to the bottlebrush-architecture of polyfarnesene leads to dilation of the reputational “tube” that further reduces the - already low - plateau modulus of polyfarnesene. The work is based on a close collaboration with Prof. G. Floudas, with the syntheses of the polymer samples being contributed in the context of this thesis.

The research article presented in Chapter 4 is additionally published in a German journal. Appendix **Chapter A③** is the German translation of Chapter 4.

Kurzfassung

Die vorliegende Doktorarbeit beschreibt die Synthese vollständig biobasierter Thermoplastischer Elastomere (TPEs) mittels anionischer Polymerisation. TPEs sind intrinsisch nachhaltiger als klassische, vulkanisierte Elastomere. Folglich werden biobasierte TPEs und neue Lösemitteloptionen im Rahmen dieser Arbeit erforscht. Erstes Ziel ist es, eine effizientere Syntheseroute, basierend auf bifunktioneller Initiierung, zu etablieren, wobei das Lösemittel Methyl-*tert*-butylether (MTBE) auf seine Eignung hin untersucht wird, eine zuverlässige und kontrollierte Polymerisation zu gewährleisten. Daneben kann die Verwendung erneuerbarer Monomere als Bausteine für TPEs die gesellschaftlichen und politischen Forderungen nach mehr Nachhaltigkeit nachkommen. Aus diesem Gesichtspunkt bieten natürliche Strukturen der Terpene eine große strukturelle Vielfalt und werden daher in dieser Arbeit verwendet, um verschiedene Materialeigenschaften zu realisieren. Daher zielt die vorliegende Dissertation darauf ab, zu einer nachhaltigeren Zukunft von Polymermaterialien beizutragen.

Um einen allgemeinen Überblick über die Relevanz von Dien-Monomeren in der Carbanionischen Polymerisation zu erhalten, wird in **Kapitel ①** eine kompakte Zusammenstellung der Erkenntnisse in Form eines *Perspective*-Artikels gegeben. Dieser zeigt auf, wie der Wechsel von den etablierten Erdöl-basierten Elastomeren, welche auf nur drei verwendeten Monomeren, Styrol, Butadien und Isopren, basiert, zu biobasierten Rohstoffen den Blickwinkel der Wissenschaft verändert hat. Diese kürzlich entwickelten biobasierten Monomere werden in Bezug auf Polymereigenschaften, mechanistischen Erkenntnissen und deren Verhalten in statistischen Copolymerisationen behandelt.

Da nicht alle für diese Dissertation relevanten Konzepte in dem ersten *Perspective*-Artikel behandelt wurden, gibt **Kapitel ②** weitere Einblicke. Das generelle Konzept von TPEs, was den Ursprung der Wiederverarbeitbarkeit, sowie das generelle Konzept der Phasenseparation im Material von Blockcopolymeren umfasst, werden vorgestellt und die verschiedenen Synthesewege für ABA-Dreiblock Strukturen werden diskutiert. Da durch die Verwendung bifunktioneller Initiatoren ungewöhnliche Polymerarchitekturen erhalten werden können, werden diese genauer eingeführt und die zuvor berichteten Herausforderungen bifunktioneller Initiatoren werden evaluiert. Da statistische Copolymerisation eine Schlüsselmethode zur Herstellung blockartig verjüngter Strukturen in einer noch effizienteren Weise darstellt, wird eine generelle Einführung in das Konzept der Copolymerisationsparameter sowie deren Bestimmung gegeben.

Das Hauptziel dieser Arbeit ist die Entwicklung eines effizienten Synthesewegs für biobasierte TPEs. Da die höchste Effizienz für die Synthese von ABA-Dreiblock Copolymeren auf bifunktionellen Initiatoren basiert, soll ein geeignetes Medium für die Reaktion ausgemacht werden. Die schlechte Löslichkeit von bifunktionellen Initiatoren in Kohlenwasserstoffen erfordert die Verwendung polarer Lösemittel. Klassischerweise wird Tetrahydrofuran (THF) auf Labormaßstab eingesetzt. Jedoch ist die Verwendung auf industriellem Maßstab aufgrund der Nachteile von THF, wie Peroxidbildung und Protonenabstraktion bei Raumtemperatur, nicht realisierbar. Daher umfasst **Kapitel ③** die Untersuchung von MTBE als alternatives Lösemittel, welches die Löslichkeit bifunktioneller Initiatoren, keine Peroxidbildung sowie idealerweise eine höhere Stabilität gegen Alkyllithium Verbindungen umfasst. Letzteres konnte durch eine 50fach längere Halbwertszeit von *n*-Butyllithium im Vergleich zu Tetrahydrofuran nachgewiesen werden. Da nur wenig über das generelle Verhalten von MTBE als Reaktionsmedium in der anionischen Polymerisation bekannt ist, werden kinetische Parameter, wie Propagationskonstanten der Polymerisationen von 1,3-Dienen untersucht. Der Trend einer schnelleren Reaktionsrate im Vergleich zu dem traditionell verwendeten Lösemittel Cyclohexan, wird für Isopren und *β*-Farnesen – einem „traditionellen“ Monomer und einer erneuerbaren Struktur – bestimmt. Zudem kann gezeigt werden, dass die „lebenden“ Polydienyllithium Kettenenden in MTBE hauptsächlich als nicht aggregierte Unimere vorliegen. Neben den Homopolymeristionen wird das etablierte Copolymerisationssystem, bestehend aus Styrol und Isopren, untersucht. Der Effekt von steigendem MTBE-Anteil wird mittels *in situ* Nahinfrarot (NIR) Kinetik untersucht. Die Gradientenstruktur, welche in reinem Cyclohexan auftritt, verändert sich sukzessive hin zu zufälligem Monomereinbau und letztendlich zu einem invertiertem, jedoch trotzdem noch fast zufälligen Comonomereinbau in reinem MTBE. Dies spiegelt sich in den Copolymerisationsparametern $r_S^{MTBE} = 1.82$ und $r_I^{MTBE} = 0.55$ wider. Das für MTBE aufgezeigte große Potential in der Carbanionischen Polymerisation wird in den nachfolgenden Kapiteln dieser Arbeit angewandt.

In **Kapitel ④** wird MTBE als Reaktionsmedium für den bifunktionellen Initiator 1,3-Diisopropenylbenzol verwendet. Die ausgezeichnete Löslichkeit des bifunktionellen Initiators in MTBE erlaubt den einfachen Zugang zu ABA-Typ Dreiblockcopolymeren. Um die aktuellen ökologischen Herausforderungen zu bewältigen und das Schrumpfen der fossilen Rohstoffquellen zu überwinden, wird ein vollständig biobasiertes TPE entwickelt. Dazu wird *β*-Farnesen als Mittelblock verwendet, da es aus Zuckerrohr gewonnen werden kann und eine Mikrostruktur unabhängige niedrige Glasübergangstemperatur (T_g) besitzt. Durch kontrollierte Terminierung der “lebenden” telechelen Polyfarnesen-Ketten werden durch die Zugabe von Ethoxyethylglycidylether (EEGE) Hydroxylgruppen eingeführt. Somit ergeben sich eng verteilte ($Đ = 1.07$ bis 1.10) telechele Polyfarnesen Makroinitiatoren mit jeweils zwei

Hydroxylgruppen an jedem Kettenende. Anschließende organokatalysierte Ringöffnungspolymerisation (ROP) von L-Lactid führt zu *H*-förmigen völlig biobasierten Dreiblockcopolymeren. Das Material umfasst zwei getrennte T_gs, bei -66 °C und 51 °C sowie eine gyroide oder zylindrische Morphologie, welche über Transmission-Elektronenmikroskopie (TEM) und Kleinwinkel-Röntgenstreuung (SAXS) bestimmt werden. Ein bei Raumtemperatur weichelastisches Material wird erhalten.

Angesichts der Vorteile des moderat polaren Lösungsmittels MTBE, welches eine zuverlässige Löslichkeit eines bifunktionellen Initiators gewährleistet, und der niedrigen T_g von Polyfarnesen, beschreibt **Kapitel ⑤** einen noch effizienteren Weg zu ABA-Strukturen. Um eine Einstufensynthese zu ermöglichen und aufwendige Multistufen Synthesewege zu vermeiden, wird ausschließlich die Carbanionische Polymerisation in diesem Kapitel verwendet. Nopadiene wird als geeignetes Comonomer ausgewählt, da es einen hohen T_g von ~ 160 °C aufweist und aus der erneuerbaren Rohstoffquelle Pinie gewonnen werden kann. Die hohe Kontrolle in der Carbanionischen Copolymerisation wird durch *in situ* ^{1}H NMR Kinetik Experimente bestätigt. Durch das Variieren der Reaktionsbedingungen werden die Copolymerisationsparameter so verändert, dass ein steiler Comonomer Gradienteneinbau, $r_{Far}^{MTBE} = 10.8$ und $r_{Nopa}^{MTBE} = 0.093$, erhalten wird. Somit sind symmetrische beidseitig verjüngte ABA-Dreiblockcopolymere unter Verwendung eines bifunktionellen Initiators in MTBE zugänglich. Durch das Variieren des Comonomerverhältnisses werden die Materialeigenschaften in einem weiten Bereich angepasst: hoch elastische Materialien mit Bruchdehnung von über 1300%, sowie zähe Materialien mit E-Modulen, welche 500 MPa überschreiten. Charakterisierungen mittels SAXS, Temperatur modulierter dynamischer Differenzkalorimetrie (TM-DSC), Rheologie und Dielektrische Spektroskopie werden eingesetzt, um die Materialeigenschaften mit dem Phasenzustand der Dreiblockcopolymere in Verbindung zu setzten. Dies ergibt lokale Phasenseparation in Verbindung mit den jeweiligen T_gs der Domänen trotz des Ausbleibens einer Fernordnung. Somit zeigt sich, dass es möglich ist, völlig biobasierte TPEs mit vergleichbaren Eigenschaften zu erdölbasierten Materialen in einer Einstufensynthese herzustellen.

Bifunktionelle Initiatoren und funktionelle Initiatoren zeichnen sich durch ähnliche Herausforderungen für Ihre Verwendung in der Carbanionischen Polymerisation aus. Daher umfasst **Kapitel ⑥** den Transfer vorheriger Erkenntnisse in Bezug auf Löslichkeitsprobleme von Bifunktionellen Initiatoren - Kapitel 4 – auf funktionelle Initiatoren. Die Projektergebnisse gehen aus einer Kollaboration mit der Synthetik-Kautschuk Firma Arlanxeo hervor. Das Einbringen von funktionellen Gruppen an das Kettenende von Elastomeren ist von Vorteil, um die Füller-Polymer Wechselwirkung zu verbessern und somit die Performance in beispielsweise Reifen zu verbessern, da es den Rollwiederstand erniedrigt und somit den

Kraftstoffverbrauch verringert. Zudem können funktionelle Gruppen am Kettenende für eine anschließende Reaktion verwendet werden, um Blockstrukturen zu erhalten. Zu diesem Zweck wird ein heterotelecheler Initiator zur Herstellung von α-funktionalisiertem Polyisopren entwickelt. Der Initiator wird über Titration einer Iod-Alkyl Vorstufe mit *tert*-Butyllithium hergestellt. Zuerst wird der funktionelle Initiator, welcher zwei Ketal-geschützte Hydroxylgruppen trägt, zur carbanionischen Polymerisation von Isopren verwendet. Eng verteilte ($Đ < 1.1$) Polymere mit hohem 1,4-Polyisopren Anteil (60%) werden nach Optimierung der benötigten Menge polarer Additive erhalten. Mittels Matrix unterstützte Laser-Desorption/Ionisation Flugzeit Massenspektroskopie (MALDI-ToF MS) wird die effektive Endfunktionalisierung bestätigt. Daraufhin wird L-Lactid, ausgehend von den erhaltenen $(OH)_2$-PI-Makroinitiatoren, polymerisiert, um A_2B-Blockcopolymere zu erhalten. Größenausschluss-Chromatographie (SEC), NMR Spektroskopie und diffusionsspektroskopische NMR (DOYS) Experimente werden verwendet, um die erfolgreiche Kettenerweiterung der Lactid-Polymerisation zu zeigen. DSC-Experimente zeigen zwei getrennte T_gs, was auf eine Phasenseparation des Copolymers hinweist. Somit kann ein heterotelecheler Initiator für die carbanionische Polymerisation sowie ROP vorgestellt werden.

Im ersten Anhang **Kapitel A①**, wird ein Verfahren zur Herstellung von TPEs in puren Kohlenwasserstoffen als Lösemittel vorgestellt. Hierzu wird der bifunktionelle Initiator, 1,3-Bis(1-phenylethenyl)benzol aufgrund seiner guten Löslichkeit in Cyclohexan verwendet. Dadurch kann ein hoher 1,4-Anteil bei der Polymerisation von 1,3-Dienen erreicht werden, was wiederum die Verwendung des weit verbreiteten Monomeres Isopren erlaubt. Anschließend, werden jeweils drei Hydroxylgruppen simultan in α- und ω-Position durch Endfunktionalisierung der „lebenden" di-lithiierten PI-Ketten mittels 1,2-Isopropylidenglycerylglycidylether (IGG) und anschließender sauren Entschützung eingeführt. Diese multihydroxyl PI-Makroinitiatoren werden zur Initiierung von L-Lactid in einer organokatalysierten ROP verwendet. Somit sind *super-H*-förmige A_3BA_3-Dreiblockstrukturen zugänglich. Thermische Charakterisierung zeigt zwei getrennte T_gs, was auf eine Phasenseparation im Material schließen lässt. Die PI-Domänen weisen einen niedrigen T_g im Bereich von – 55 °C bis – 59 °C und die PLLA-Domänen eine T_g von 41 °C bis 49 °C auf. Zudem wird die genaue Phasenseparation und Morphologie mittels TEM und SAXS untersucht, wodurch zylindrische und lamellare Morphologien bestätigt werden. Die Kombination von Carbanionischischer Polymerisation mit ROP von Lactonen wird als geeigneter Syntheseweg für komplexe Polymerstrukturen präsentiert.

Kapitel A② umfasst eine grundlegende Untersuchung von binären Mischungen aus Polyfarnesen und Polyisopren als Modellsystem für superweiche Polymerschmelzen. Die

zuvor gewonnenen Erkenntnisse zur kontrollierten Polymerisation werden genutzt, um eine Molekulargewichtsreihe von Polyfarnesen Proben im Bereich von 3.5 $kg \cdot mol^{-1}$ bis 720 $kg \cdot mol^{-1}$ zu synthetisieren. Um Polyfarnesen/Polyisopren Mischungen herzustellen, werden kommerziell erhältliche Polyisoprenproben mit gleichem Molekulargewicht gekauft. Die Zugabe von linearem Polyisopren zu Polyfarnesen mit Bürsten-Architektur führt zu einer Erweiterung des Durchmessers der „Ketten"-Reptation, wodurch das ohnehin schon niedrige Plateaumodul von Polyfarnesen weiter verringert werden kann. Die Arbeit basiert auf einer engen Kollaboration mit Prof. G. Floudas und die Synthese der Polymerproben wird im Rahmen dieser Arbeit beigesteuert.

Der in Kapitel 4 vorgestellt wissenschaftliche Artikel ist zusätzlich in einem Deutschen Journal veröffentlicht. Das Anhang **Kapitel A③** ist die deutsche Übersetzung von Kapitel 4.

Graphical Abstract

Graphical Abstract

Chapter 1: Green Perspective Drives the Renaissance of Anionic Diene Polymerization

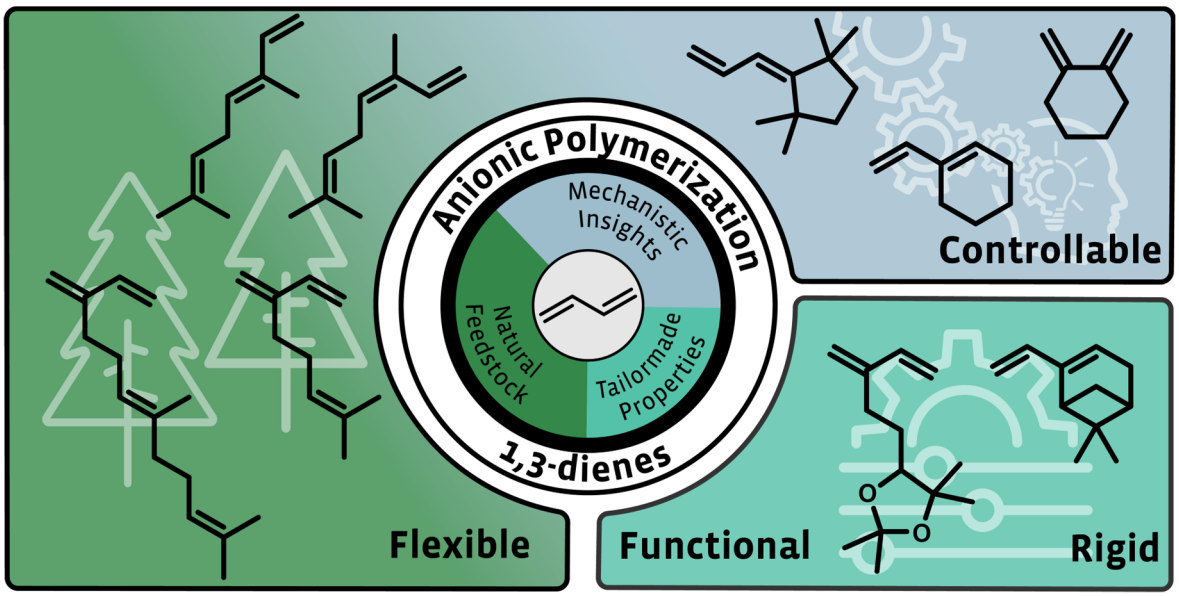

Chapter 3: Spotlight on Methyl *tert*-Butyl Ether: Unveiling Its Role in Living Anionic Polymerization

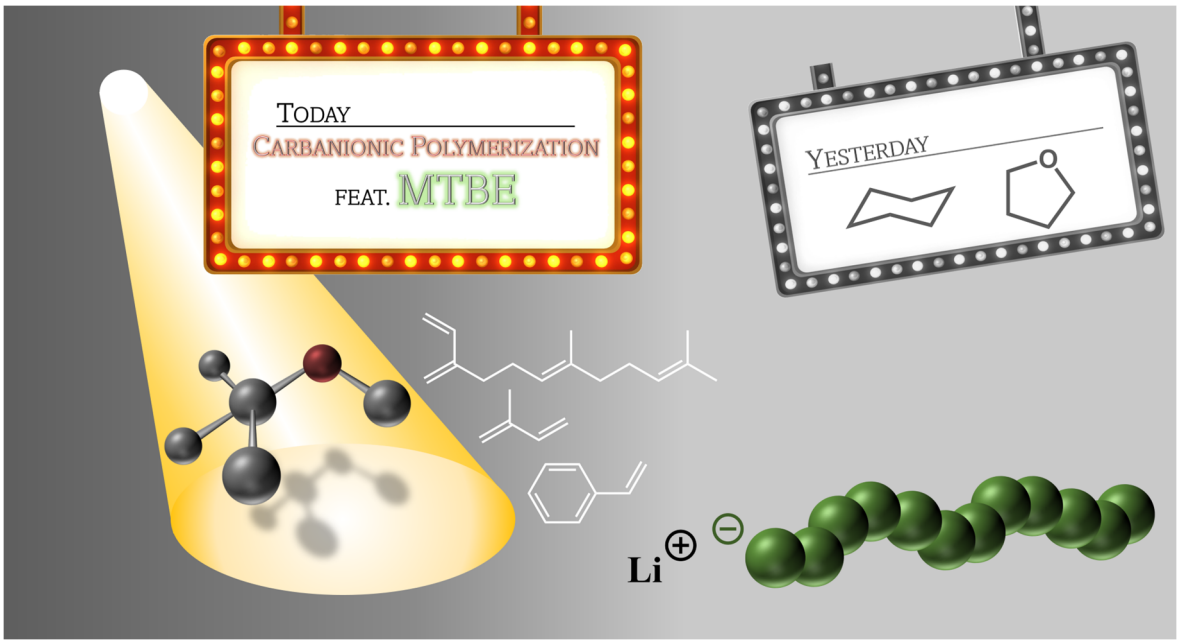

Chapter 4: Bifunctional Carbanionic Synthesis of Fully Bio-Based Triblock Structures Derived from *β*-Farnesene and LL-Dilactide: Thermoplastic Elastomers

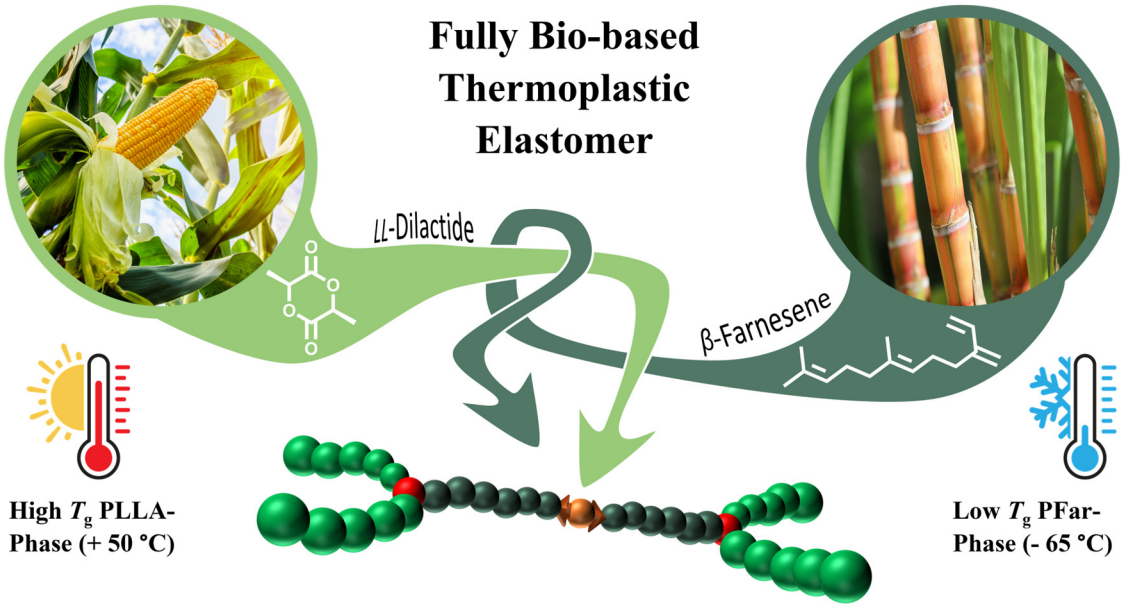

Chapter 5: One-Step Synthesis of Fully Bio-based Two-Sided Tapered ABA-Type Thermoplastic Elastomers

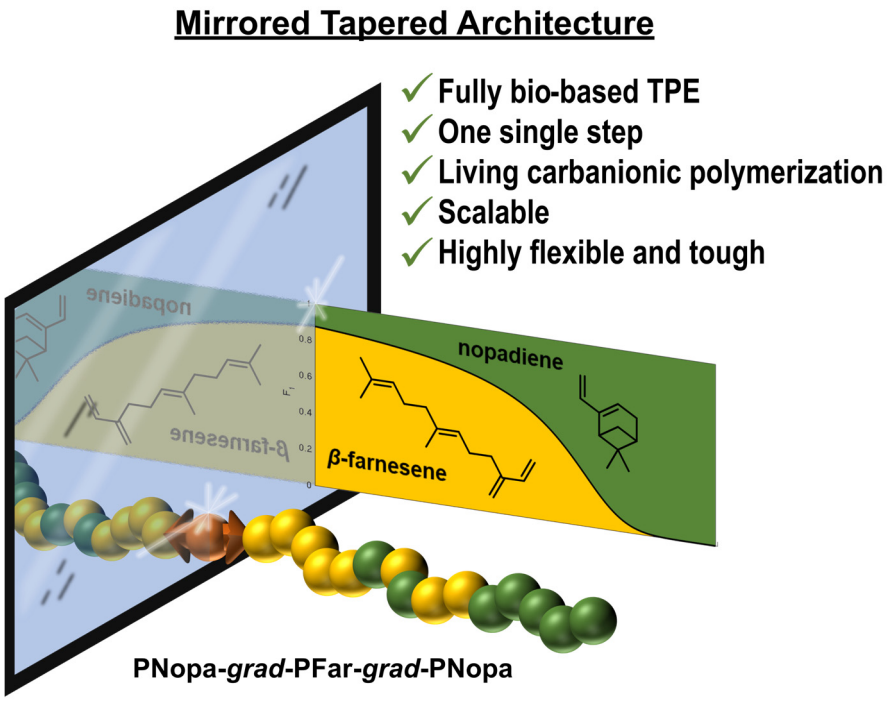

Chapter 6: Heterotelechelic Initiation to access A_2B-type Block Copolymers via LL-Dilactide Grafting from α-Functionalized Polyisoprene

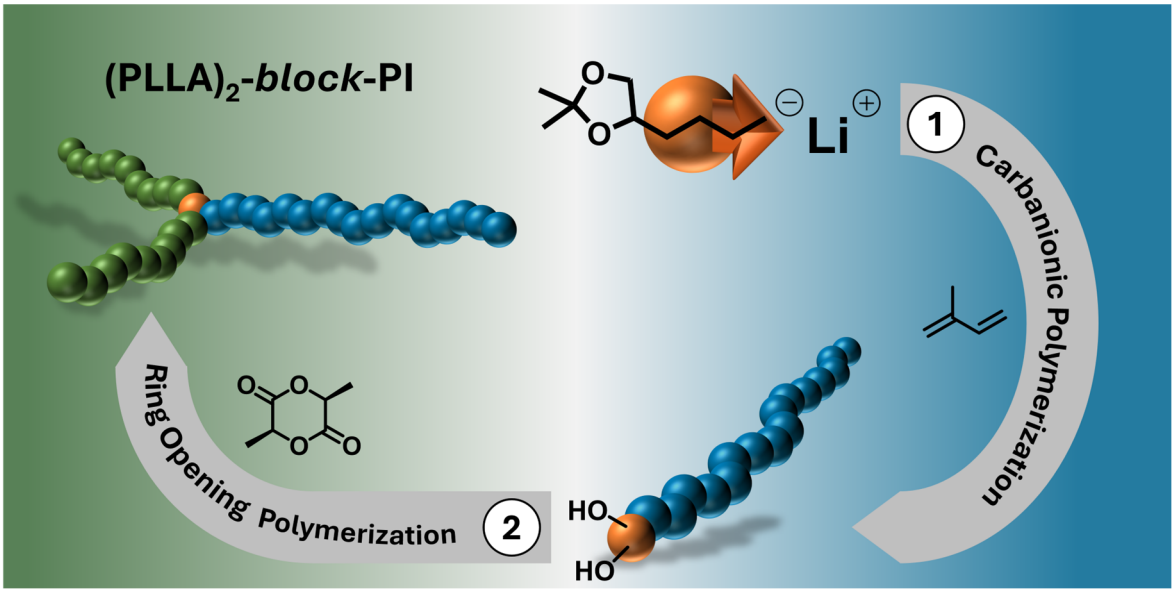

Chapter A1: Synthesis of Phase-Separated *super-H*-shaped Triblock Architectures: Poly(L-Lactide) grafted from Telechelic Polyisoprene

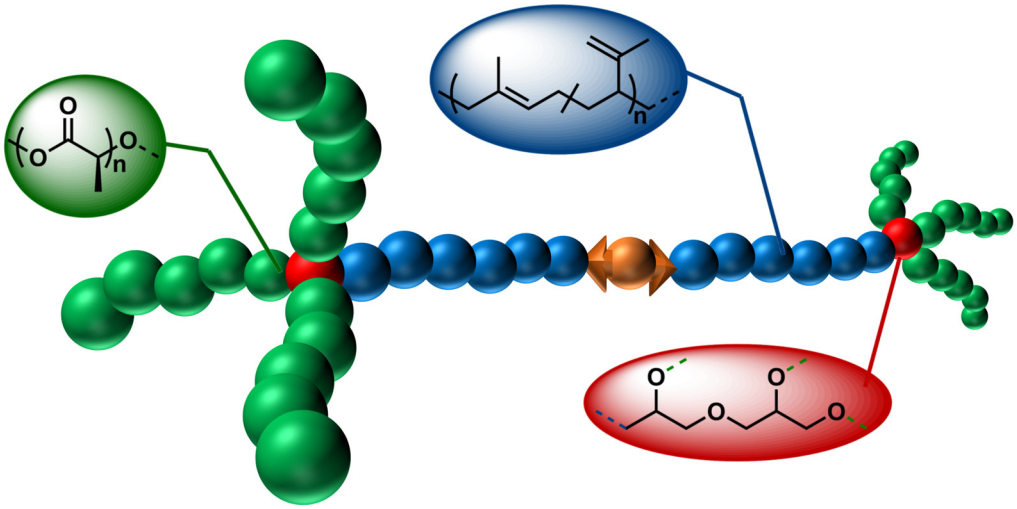

Chapter A2: Supersoft Polymer Melts in Binary Blends of bottlebrush *cis*-1,4-polyfarnesene and *cis*-1,4-polyisoprene

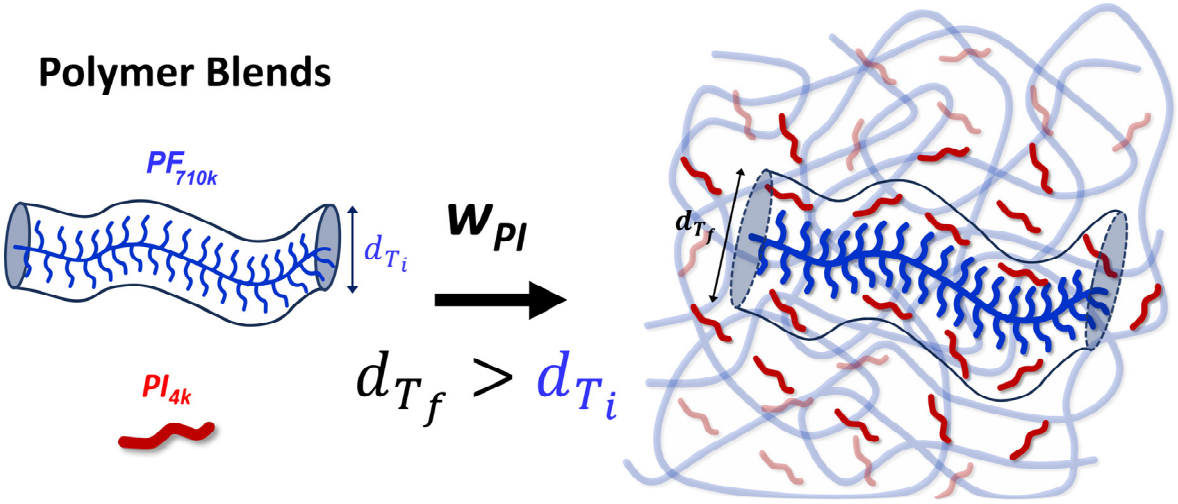

Chapter 1

Green Perspective Drives the Renaissance of Anionic Diene Polymerization

Moritz Rauschenbach,[a] *Moritz Meier-Merziger,*[a] *and Holger Frey* [a]*

* Corresponding author
All authors have contributed equally

[a] Department of Chemistry, Johannes Gutenberg University Mainz, Duesbergweg 10-14, 55128 Mainz, Germany

Published in: *Polymer Chemistry*, **2024**, 15 (42), 4297-4311.
https://doi.org/10.1039/D4PY00805G

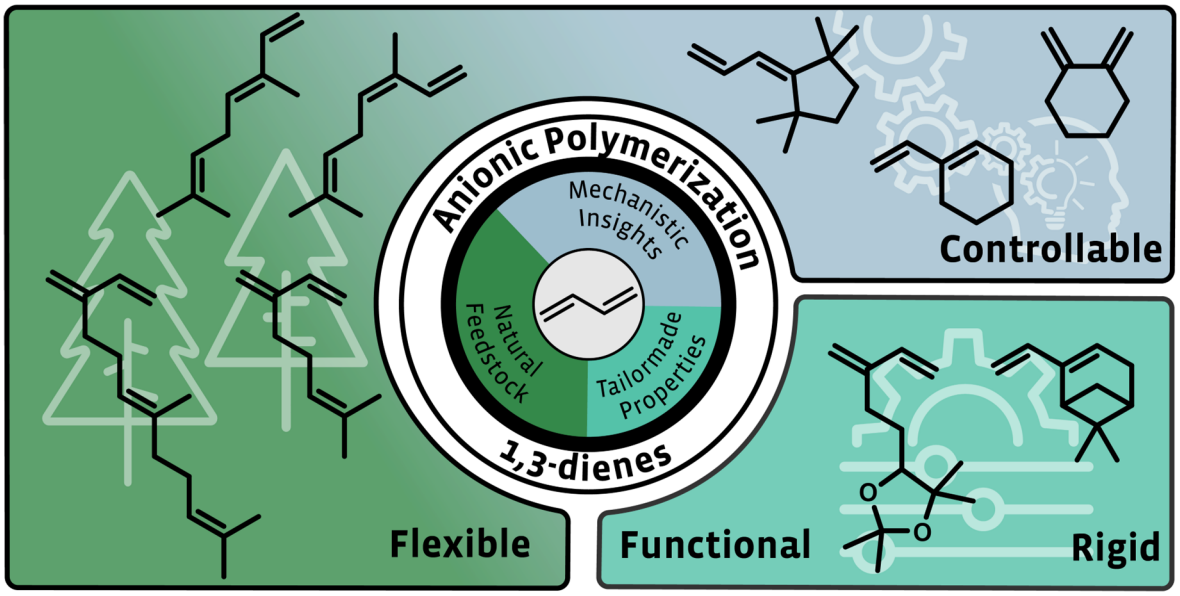

The following publication is adapted with permission from Rauschenbach, M.; Meier-Merziger, M.; and Frey, H.; Green Perspective Drives the Renaissance of Anionic Diene Polymerization, *Polymer Chemistry*, **2024,** 15 (42), 4297-4311.

1. Introduction

Polydienes played a pivotal role in the initiation of macromolecular science when Staudinger introduced the term "macromolecule" in 1920, specifically referring to polyisoprene (PI).[1],[2] Although the first anionic diene polymerization was observed already a decade earlier by Matthews,[3] who stored isoprene in the presence of sodium, it was *IG Farben* that later commercialized the alkali metal-initiated polybutadiene as "Buna". This development was prompted by a substantial increase in demand for natural rubber.[4],[5] From a molecular perspective, natural rubber derived from *hevea brasiliensis,* consists of 1,4-*cis* (>98%) polyisoprene.[6] Nowadays, synthetic rubber is produced on megaton scale and is often combined or blended with natural rubber.[7] Both synthetic and natural possess a double bond per repeating unit, rendering them suitable for crosslinking. The resulting elastomers are used for applications as diverse as tires and medical gloves. The anionic polymerization of dienes continues to garner significant attention in today's industrial and scientific research.[8] This leads to continuous new insights also for the established dienes such as butadiene (B) and isoprene (I). Synthetic rubber offers advantages over natural rubber due to its versatile and adjustable properties, since the exact chemical nature of the polymer can be influenced during the polymerization process.[9] The commercial importance also arises from the option to produce homo- and copolymers with controlled molar masses and the capability to precisely regulate microstructure to meet a variety of material specifications.[10] Moreover, 1,3-dienes are used in copolymers such as acrylonitrile-butadiene-styrene (ABS) and styrene-butadiene-styrene (SBS), which are frequently utilized materials. SBS and the analogue SIS using I instead of B have been investigated in-depth and became commercialized under various trade names (i.e. *Styroflex*®).[11] S/I-copolymers have remained a key research topic of our group, elucidating how different polymerization conditions affect the statistical copolymerization and the resulting monomer gradients and mechanical properties[5],[12]–[17] Consecutive monomer addition steps can be used to generate precisely defined multiblock copolymers (MBCP) that are not accessible by other techniques.[5],[13]–[15] The knowledge of the incorporation mode of two monomers within a polymer chain, based on their reactivity ratios, can be used to reduce required monomer addition steps to increase efficiency. Therefore, *in situ* kinetics measurements relying on ^{1}H NMR kinetics or near infrared (NIR) kinetics have become the methods of choice to determine the reactivity ratios of a large variety of copolymerizations.[16]–[23] Furthermore, in recent years new diene monomers have been introduced that extend the range of materials beyond polybutadiene and polyisoprene.

Polydienes are commonly synthesized by anionic or catalytic polymerization techniques. Catalytic strategies are carried out on large commercial scale. Recently the long-time challenge

of incorporation of polar monomers was achieved by the groups of Cui and Mecking who were the first to report on the catalytic polymerization of functional dienes.[24],[25] Nonetheless, a detailed overview of the catalytic polymerization of 1,3-dienes will not be covered in greater extent in this review. Readers are referred to recently published reviews.[26],[27] Properties found and discussed for polydiene materials naturally apply regardless of the polymerization technique used. The main advantage found in catalytic polymerization is the high control of stereoselectivity.[26] The development of a Gd-based catalyst enabled similarly high 99.9% *cis*-1,4-polyisoprene stereocontrol as known from natural rubber.[28]

Due to the high basicity of the carbanion, the highest extent of control in anionic polymerization is achieved by the challenging break-seal method.[29] This requires not only a synthetic skillset, but also glassblowing skills. The more accessible high vacuum technique, that has long been established, enables still exceptional control over the polymerization. This allows to synthesize new polydienes and to investigate the impact of polymerization conditions. Besides the established production of polydienes *via* batch synthesis, also continuous flow reactors for the carbanionic polymerization can be employed for dienes.[30]–[33]

Moreover, Haddleton and coworkers reported on the anionic diene polymerization without monomer/solvent purification steps, making it even more widely applicable for low molar mass polymers.[34],[35] With respect to precision, anionic polymerization surpasses the catalytic approach, thanks to its distinctive living character, which enables to synthesize of a wide range of polymer architectures and tapered compositions in copolymers.[8]

In recent years, there has been a notable trend in academic research as well as in industry towards bio-derived monomers. Efforts to tailor material properties for enhanced performance accompany this shift, with the aim of matching or surpassing the properties of established fossil fuel-based materials. In this review we will cover 1,3-dienes beyond their classical representatives butadiene and isoprene. A selection of the discussed mono- and disubstituted 1,3-dienes is shown in **Figure 1**. While some can be found in nature, additional synthetic modification steps are required for others. The number of synthetically obtained 1,3-dienes for the anionic polymerization is steadily increasing.

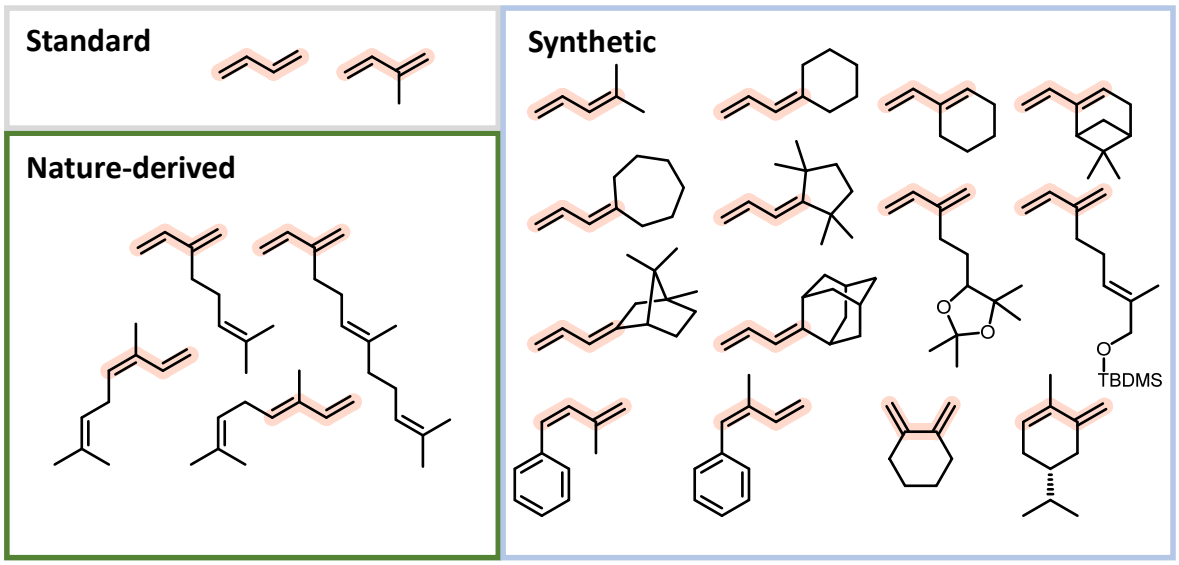

Figure 1. Overview of a selection of 1,3-dienes discussed in this perspective. Reactive diene moieties are marked for each monomer.

2. Is the Anionic Polymerization of Dienes Genuinely a Coordinative Process?

Butadiene and isoprene are the most investigated diene monomers to date. They both can lead to different isomeric units along the chain, namely regio- and stereostructure (**Scheme 1**b). As detailed by Carlotti et al.,[9] varying the microstructure is a powerful method to adjust the materials' properties, for instance for tire applications, where high degrees of elasticity over a broad temperature range are desired, which are usually correlated with a high 1,4-content. This involves minimizing the glass temperature as much as possible to achieve the widest possible application temperature range. The overall regio- and stereochemistry of the anionic polymerization of 1,3-dienes has been widely discussed in the last decade with respect to their dependency on the counter ion,[10],[36],[37] solvent,[10],[38] and the presence of a polar modifier.[17],[20] The formation of aggregates during the polymerization in non-polar solvents and their suppression by the use of polar solvents or modifiers was found to be one of the key aspects of the propagation mechanism. The number of the aggregating chains evolves from the kinetic order, expressed by the following **Equation 1**:

$$\log(k_{\text{app}}) \sim \frac{1}{n}\log\,[\text{Ini}]_0 \qquad \textbf{(1)}$$

k_{app} gives the apparent rate constant of the propagation, $[\text{Ini}]_0$ the initial concentration of the initiator and n the number of aggregating chains. Hereby, the aggregates are in an equilibration with the unimers which are considered to be the active species capable of sustaining the propagation mechanism, see **Scheme 1**. M. Szwarc already reported that the relative rates of propagation for isoprene and butadiene are ordered as isoprene > butadiene, while both

exhibit a number of aggregating chains of n = 4.[10],[39] However, it was found that polyisoprenyl lithium aggregation also depends on the concentration of active chain ends. An overall equilibration between tetramers and dimers was observed, with n approaching ~2 with decreasing concentration.[10],[38] β-Myrcene and β-farnesene, although kinetically investigated under the assumption of tetramer formation, have not been explored with respect to their aggregation behavior.[20],[21] The observation that their propagation rate surpasses that of isoprene suggests the presence of an equilibrium solely between dimers and unimers. It should be noted that this assumption has not yet been empirically confirmed.

Scheme 1. a) Aggregation equilibrium of polyisoprenyl lithium in non-polar solvents in analogy to Müller and Matyjaszewski; b) possible microstructures of PI and their respective glass temperatures.[38],[40]

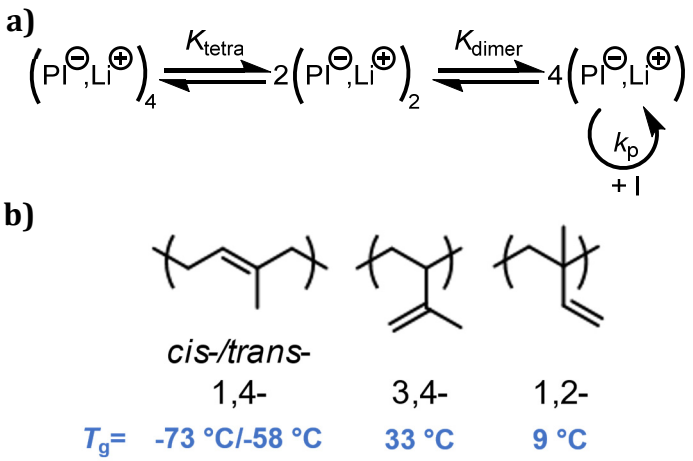

The coordination of the counterion to the incoming monomer and its spatial orientation mainly dictate the regioselectivity, see **Scheme 2**. In non-polar media, it has been reported to undergo a six-membered transition state, where the diene is added in a *cis*-form, explaining overall high amount of 1,4-addition. The final *cis/trans* ratios have been extensively elucidated by Gebert et al. who suggested an isomerization of the *cis*-oriented chain end to a *trans*-form before the next monomer addition.[38],[41],[42] Worsfold and Bywater further proposed that the isomerization occurs in competition with the monomer addition.[10],[43] Based on these fundamental investigations, the final ratio of *cis* and *trans* 1,4-units can be explained.

Scheme 2. Proposed mechanism of the polymerization of isoprene with lithium as counter ion in apolar or polar media, respectively; image is reproduced from Barent et al.[41]

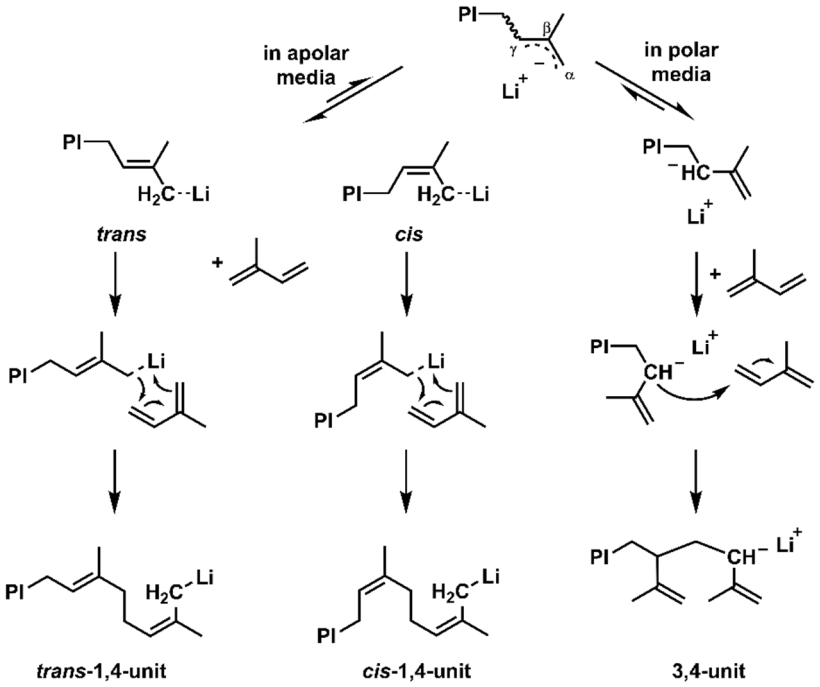

By changing the counterion from Li^+ to Na^+ or K^+, for instance, the interionic distance increases, which reduces the 1,4-content of polydienes.[10],[44] Based on the industrially most popular diene representative 1,3-butadiene, Carlotti and coworkers have investigated the impact of bimetallic initiator systems with lithium and potassium or calcium, respectively. They studied the influence of the additional coordinative center on the microstructure. While the addition of potassium led to an expected increase of 1,2-units, the designed calcium-lithium initiators enabled high control towards *trans*-1,4-units.[45],[46] Reviewing the accessible microstructures of polybutadiene, Carlotti *et al*. also reported on the combined effect of both variation of the counterions as well as changing to polar solvents.[9] The polymerization in polar solvents, e.g. THF, or the addition of polar modifiers are both associated with a suppression of the coordination between the chain end, the counterion and the diene. As a consequence, increased vinyl content enhances the backbone rigidity of the polydiene, which is reflected by a rise of the glass temperature (**Scheme 1**b).[38],[41] However, the influence of solvents on the anionic polymerization will be discussed below in greater detail.

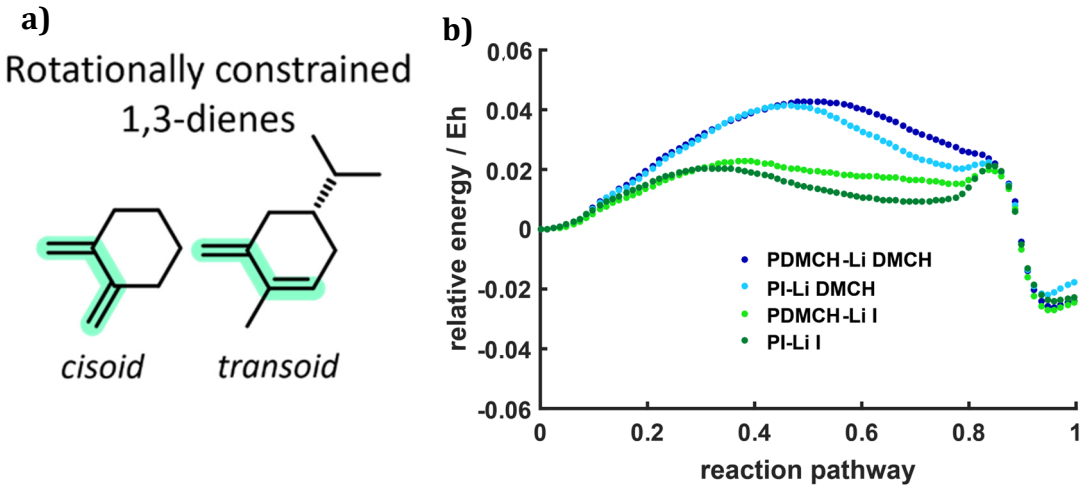

Figure 2. a) Rotationally constrained dienes with a *cisoid* (DMCH) and a *transoid* (IMMCH) geometry; b) Reaction pathways for the four possible propagation steps of the copolymerization of isoprene and DMCH (Addition of DMCH, blue; Addition of isoprene, green), image is reproduced from Barent et al.[41]

A rather new aspect in this field is the examination of the orientation of the double bonds to each other in the 1,3-diene scaffold. In this regard, DFT calculations can give mechanistical insight which goes beyond the mere consumption in a copolymerization. In a recent publication we investigated rotationally constrained dienes.[41] Two model compounds were synthesized to obtain a *cisoid* and a *transoid* monomer as shown in **Figure 2**a. DFT calculations identified deviations of the torsion angle in both monomers and allow an assumption regarding the reactivity given by the electron densities. A crucial finding from the simulation is that if a fixed *transoid* geometry is present, only one of the double bonds can coordinate with the lithium counterion. This crucial step should prevent the polymerization. In contrast, the *cisoid* model compound coordinates with both double bonds, albeit a distortion of the ring is required. Consequently, only homopolymers with the *cisoid* 1,2-dimethylene-cyclohexane (DMCH) were obtained and copolymerization with isoprene was achieved. DFT calculations show that the energy required for the polymerization of DMCH is significantly increased compared to isoprene due to a required distortion of the ring, see **Figure 2**b. Empirically, this was observed *via in situ* ^{1}H NMR kinetics. In the copolymerization with isoprene, isoprene is consumed predominantly, resulting in a gradient structure along the chain. The homopolymerization of DMCH itself required unusual conditions to keep the growing chain in solution: high temperatures of 140 °C were applied in the solvent tetralin. Noteworthy, the analysis of P(DMCH) confirmed the exclusive formation of 1,4-units and a T_g of 53 °C. In contrast, no polymers were obtained with the *transoid* monomer IMMCH. In 2015, Ishizone and coworkers described the anionic polymerization of the *transoid*-fixed benzofulvene in both

polar and apolar media.[47]–[49] This can be attributed to the conjugation with the aromatic ring that leads to a planar cross-conjugated π-system resulting in a higher reactivity. The removal of the aromatic ring, e.g., in methylene cyclopentane resulted in the expected reduction of the reactivity. For this monomer 70 °C and a reaction time of 4 days were required to achieve full conversion.[50] Consequently, it can be concluded that *transoid* dienes are not suitable for the living anionic polymerization in non-polar solvents at mild conditions.

3. Controlling the Microstructure of Polydienes

The resulting microstructure is directly dependent on the propagation mechanism, as introduced previously. Primarily for rubber applications, 1,4-repeating units are favored because of the known low T_g of the polymers and lower entanglement molar mass.[5],[44] One the other hand, for specific post-polymerization modification reactions[51],[52] or to suppress crystallization as for hydrogenated polybutadiene,[53] an increased vinyl content is targeted. Polydienes, such as polyisoprene, were investigated to understand their microstructural changes with regard to solvent polarity. It is noted that polymerization in polar solvents like THF results in significantly higher content of 3,4- and 1,2-units. The system's polarity can be tailored *via* exact amounts of polar modifiers into non-polar solvents. Morton and Fetters reported that for isoprene the addition of aliquots of THF initially increases the propagation rate.[54] However, further addition leads to a subsequent decrease, as Bywater previously demonstrated for styrene.[55] Recently, we have been able to give a detailed view on the impact of THF on the statistical copolymerization of styrene and isoprene, relying on online NIR monitoring of the anionic copolymerization. By increasing the THF concentration the vinyl content of the isoprene-units increases.[17] In analogy, polymerization of the analogous *β*-myrcene was investigated to compare the influence of DTHFP and TMEDA as polar modifiers with the established THF. As shown in **Table 4**, both DTHFP and TMEDA show a stronger influence on the microstructure.[20],[56] The addition of 2 equivalents with respect to the lithium ion concentration gives a dominance in 3,4-units (>57%). Undesirably, this leads to an increase of the original low glass temperature. Polydiene based elastomer chains usually exhibit a T_g below -60 °C. When gradually increasing the ratio of vinylic units, the T_g of polyisoprene can reach 0 °C.[57] Although the T_g of polydienes show this dependency on the proportion of the different microstructures, polyfarnesene, discussed later in this perspective, shows a different behavior. Due to its long side-chain in every repeating unit the T_g remains nearly unaffected by increasing the vinyl content as illustrated in **Figure 3**.

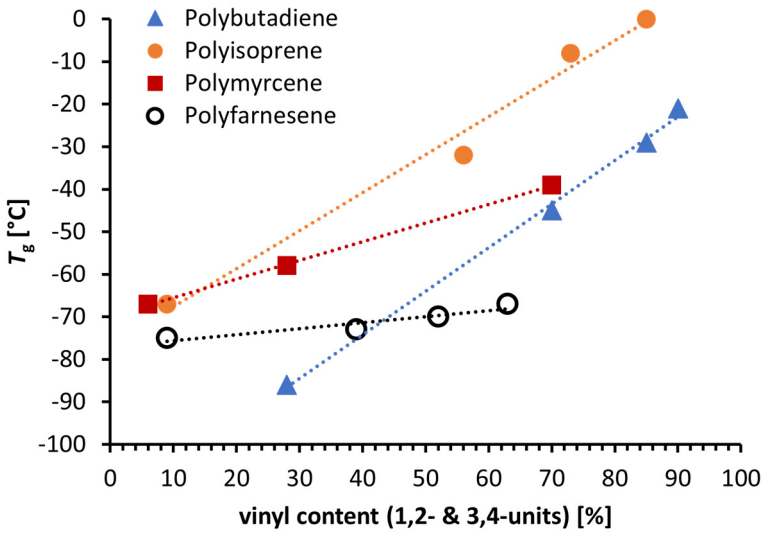

Figure 3. Dependency of glass temperature of polydienes on the vinyl content. The values are combined from several original works.[57] – [60]

In addition to altering the system's polarity, it is well-known that increasing bulkiness of the substituent results in an almost exclusive formation of *cis*-1,4-units. This was demonstrated for the anionic polymerization of 2-substituted 1,3-butadiene derivatives with a methyl, ethyl, *n*-propyl or isopropyl group.[61] – [63] Pendant phenyl groups, as seen in 1-phenyl butadiene (PhB), 1-phenyl isoprene and 4-phenyl isoprene, have demonstrated a predominant occurrence of 1,4-addition (>80%), even in the polar solvent THF.[64] – [66] Furthermore, Ishizone and coworkers achieved control over the incorporation by designing rather unusual allylidene monomers.[67],[68] The reported butadiene-derivatives were 1,1-disubtituted with increasing bulkiness of the pendant group. Various substituents, ranging from two methyl groups to a bornane ring and even the adamantly group, were attached to the dienyl-unit. Hence, the sterically hindered 1,4-addition could be further prohibited with increasing bulkiness, which is underlined by the absence of 1,2-units. The structures shown in **Figure 4a** were sufficiently effective to increase the 3,4-units to more than 20% in apolar media. The bulky substituents of the structures in **Figure 4b** almost exclusively result in 3,4-incorporation. As a result, these polymers turned out to be very stiff materials with high glass temperatures of nearly 200°C in case of the pendant bornane-ring. In theory, this might allow for application in thermoplastic elastomers (TPEs) as a hard segment, but may also lead to extremely high processing temperatures.

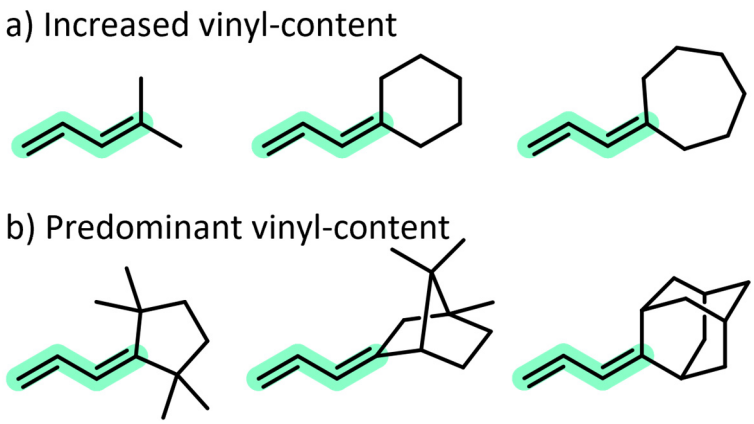

Figure 4. 1,1-Disubstituted 1,3-dienes studied with respect to their behavior in the anionic polymerization, reported by Ishizone et al.[67],[68]

The monomer vinyl cyclohexane (VCH) serves a model compound with one double bond sterically hindered within a cyclic structure. The key question was whether VCH behaves as a 1,3-diene or as a styrenic vinyl monomer in the anionic polymerization in non-polar media. In analogy to other diene structures, the homopolymerization in cyclohexane (CHx) lead to a predominant formation of 64% 1,4-units.[69] The extent of 1,4-incorporation is comparable to the allylidene cyclohexane with a reported 66% 1,4-units when polymerized in benzene.[68] However, the added rigidity from the ring in the backbone increased the T_g to 78 °C. The microstructure of PVCH was adjusted to enhance the vinyl content, reaching up to 78% of 3,4-PVCH upon addition of the polar modifier THF. The resulting material properties, with a T_g of up to 89 °C, are much closer to those of PS (T_g = 100 °C).[70] Likewise, the hydrogenation leads to a high amount of poly(vinylcyclohexane) segments, as obtained by hydrogenation of PS.

4. Bio-Derived Diene Alternatives

The dwindling fossil resources evolved to be a major motivation in finding new substitutes for established systems such as polydiene-based (co)polymers. Wahlen et al. presented a wide scope of terpene monomers that are amenable to the anionic polymerization.[71] Predominantly, *β*-myrcene (Myr) and *β*-farnesene (Far) have gained significant attention owing to their structural similarity to the 2-substituted isoprene framework and their bio-based origin from turpentine oil and sugar cane, respectively. Both monomers show similar dependencies of the polymer structures on the polymerization conditions and result in comparable polymer properties. A highly 1,4-dominated microstructure is obtained when polymerizing in apolar solvents, which results in a similarly low T_g as polyisoprene, with T_g < -60 °C (**Figure 3**).[57],[59] This renders PFar and PMyr suitable for the application as soft phase in thermoplastics elastomers. Combinations with polystyrene or polylactide as the

vitrified plastic domains have also been reported to date. When polystyrene is used for the rigid phase, classical linear ABA-triblock copolymers were synthesized. Sequential addition yields block-architectures whereas tapered structures are obtained by statistical copolymerization.[20],[22],[59] This will be discussed in greater detail in one of the following sections. By the combination with polylactide as the rigid phase even more complex architectures were realized, e.g., graft polymers and *H*-shaped triblock structures, see **Figure 5**.[72] – [74]

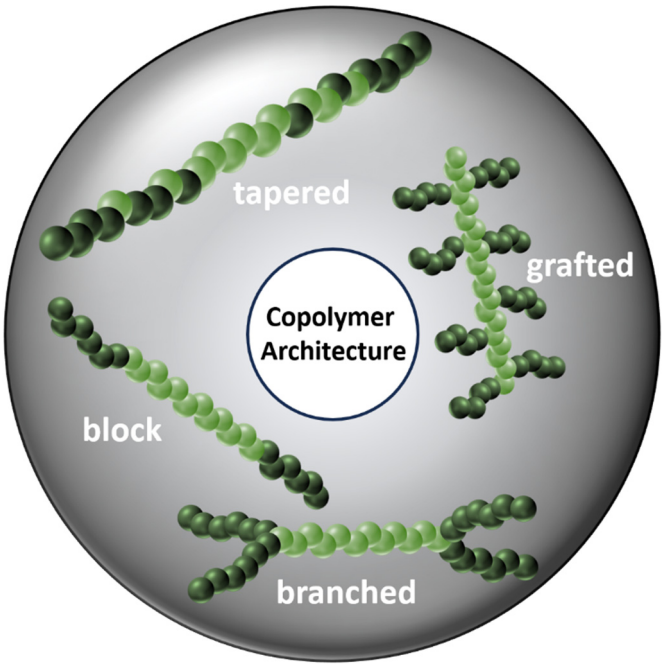

Figure 5. Different copolymer architectures for TPEs based on block, tapered and branched triblock structures as well as graft-copolymers.[21],[72] – [75]

Nevertheless, due to the increasing length of the side chains in PMyr and PFar, that do not contribute to the polymers backbone, the entanglement molar mass increases from 7 kg·mol^{-1} for PI, 18 kg·mol^{-1} for PMyr to 50 kg·mol^{-1} for PFar.[76] – [78] This effect has considerable consequences for elastic mechanical properties that are strongly dependent on the entanglements of the polymer chains. Therefore, higher molar masses compared to PI are required for PFar to obtain similar mechanic properties.

The first report on the anionic polymerization of *β*-myrcene in our group focused on the behavior in statistical copolymerizations with isoprene, styrene and 4-methyl styrene (4MS).[22] *In situ* ^{1}H NMR kinetics were performed revealing *β*-myrcene as a suitable substitute for isoprene with similar behavior in the copolymerization with styrene. Both systems show a steep gradient, as discussed later in this perspective. This was further investigated using the *in situ* NIR method.[20] A series of S/Myr-copolymers were synthesized to investigate the impact of an increasing THF content on the gradient structure of the copolymers. It was shown that

the gradient structure can be tuned by a variety of modifiers, even to a complete inversion, similar to the behavior observed earlier for isoprene.[17] Furthermore, we showed that Far forms a gradient structure in the statistical copolymerization with styrene and that the polymerization in cyclohexane get significant faster moving up the homologous series of terpenes: $k_{p,I} < k_{p,Myr} < k_{p,Far}$.[16],[20],[21]

Although renewable feedstocks are one of the most important research fields, their impact on nature and, above all, the possible competition with food sources should always be considered as well. *β*-Farnesene, relatively price competitive due to its use as sustainable jet fuel besides its application in materials, is mainly derived from sugar cane.[79] PFar products are already widely available in industry, e.g., PFar-diol is used for the preparation of polyurethanes.[57],[80] Therefore, additional feedstocks are being sought. It was already shown that heterotrophic as well as lithoautotrophic bacteria are capable of producing Far from cultivation on a variety of substrates.[81]

Furthermore, the additional double bonds in the side-chain allow post-modification with respect to thiol-ene click and epoxidation, respectively.[82],[83] Thereby, these monomers offer the possibility of introducing functionalities along the chains, which would require suitable protecting groups if introduced prior polymerization. This will be addressed in a later section. In addition to these aforementioned examples, there are also less known representatives in the field of terpenes. For instance, our group reported on the anionic polymerization of *β*-ocimene (Oc).[84] As Oc resembles a 1,2-disubstitued diene it naturally occurs as a mixture of the *cis* and *trans*-isomer. The anionic polymerization in cyclohexane resulted in an unusually high dispersity up to 2. *In situ* ^{1}H NMR kinetics revealed a preferred consumption of the *trans*-isomer over the *cis*-form ($r_{trans} = 3.16$ and $r_{cis} = 0.316$) turning the apparent ocimene homopolymerization into a copolymerization of the two stereoisomers. Surprisingly, the addition of styrene inverted the trend to an accelerated consumption of the *cis*-isomer. Taking advantage of these findings, both isomers were isolated by polymerization of the respective other isomer. Consequently, the NMR kinetics with styrene could be performed separately. The values given in **Table 2** reveal the presumed consumption of styrene over the *trans*-isomer ($r_{trans} = 0.628$ and $r_S = 1.59$), while the *cis*-isomer yields an almost random incorporation of both monomers ($r_{cis} = 1.01$ and $r_S = 0.98$). This phenomenon is quite uncommon in the field of carbanionic polymerization, as mostly gradient incorporations are obtained. An overview of a broad range of diene copolymerizations and their respective reactivity ratios are given in **Table 2**. For reference, the established S/I-copolymerization in cyclohexane shows a steep gradient, characterized by $r_I = 10$ and $r_S = 0.015$.[17]

1,3-Diene structures offer potential beyond low T_g and high elasticity, as their structures can be highly diverse. Ishizone et al. presented a variety of 1,1-disubstituted dienes that possess cyclic structural elements and were already discussed in more detail earlier in this perspective.[67],[68] Their uncommon high T_gs are attributed to the rigidity of the ring structure and the resulting high content of 3,4-units. Cyclic elements can also be incorporated by 1,2-subsitution as mentioned for the monomer VCH.[69] With the monomer nopadiene (Nopa), 1*R*,5*S*-2-ethenyl-6,6-dimethylbicyclo[3.1.1]hept-2-ene, our group recently presented a sterically even more demanding monomer, due to its bicyclic structure. Thereby, a strikingly high T_g of 160 °C for PNopa can be achieved. Nopadiene was therefore presented as a potential bio-based substitute of styrene in TPE materials. Nopa can be derived from myrtenal or nopol, again originating from *β*-pinene. An exclusive diene structured and fully bio-based TPE can be obtained using the monomers Myr and Nopa.[85] Furthermore, we also developed a one-step synthesis for TPEs. By precisely controlling the reaction conditions, we achieved reactivity ratios that favor the incorporation of low T_g polyfarnesene, followed by high T_g polynopadiene. Since a bifunctional initiator was employed for this reaction, a telechelic polymerization was realized and thus, in one step, two-sided tapered ABA-triblock structures are accessible.[75]

The diversity of natural sourced compounds, e.g. terpenes, offer great potential to customize material properties. However, many parameters must be considered. As many bio-based monomers have expanded the portfolio of polymers accessible *via* carbanionic polymerization, a compilation of a variety of the resulting diene polymers in terms of their glass temperature is listed in **Table 1**. The data show the enormous diversity of diene structures and their potential in the field of materials science, as they can be tailored to a wide range of thermal properties. Among those listed, 4,8-dimethylnon-1,3,7-triene (DMNT) has not yet been presented in an original work yet.

Table 1. Summary of a variety of polydienes accessible *via* carbanionic polymerization, listed with increasing glass temperatures.

Polymer	**1,4** [%]	T_g [°C]	Ref.	**Polymer**	**1,4** [%]	T_g [°C]	Ref.
Polybutadiene	72	-86	[57]	PolyDMNT	74	-30	-
Polyfarnesene	91	-75	[57]	Poly*rac*ocimene	15	-26	[84]
Polyfarnesene	61	-73	[57]	Polybutadiene	10	-21	[57]
Polyfarnesene	48	-70	[57]	Polyisoprene	15	0	[57]
Polymyrcene	94	-67	[58]	PolyMyrDOL	67	11	[86]
Polyisoprene	91	-67	[57]	Poly4PhI	94	48	[66]
Polyfarnesene	37	-66	[72]	PolyDMCH	100	53	[41]
Polymyrcene	72	-58	[60]	Poly1PhI	35	65	[66]
PolyMyrOSi	69	-53	[58]	PolyVCH	22	89	[69]
Polybutadiene	30	-45	[57]	Polynopadiene	51	158	[85]
Polymyrcene	30	-39	[59]	Poly(Aad)*	0.0	178	[67]
Polyisoprene	44	-32	[57]	Poly(ATMC5)**	0.0	194	[68]

* 2-allylidene-adamantane (Aad) ** 2-allylidene-1,1,3,3-tetramethylcyclopentane (ATMC5)

5. New Solvents for the Anionic Polymerization of 1,3-Dienes

Usually the requirements for solvents used in the carbanionic polymerization are (i) aprotic nature and (ii) high base-stability. Often non-polar solvents like cyclohexane or benzene are used, as is mostly the case for butadiene and isoprene systems. The reason for this is the previously introduced solvent effect on the microstructure and the associated change in material properties. For this reason, cyclohexane, hexane mixtures, benzene, and toluene are established solvents. Toluene is less favored due to reported transfer reactions.[87] For specific demands, e.g., solubility of bifunctional initiators, functional initiators and monomers, tetrahydrofuran (THF) is primarily used to increase the polarity and suppress aggregation. However, proton abstraction at ambient temperatures restrict its use to low temperatures, usually -78 °C.[88],[89] However, the polymerization of dienes is thermodynamically hindered at these low temperatures. Gallei et al. took advantage of this to access block copolymers by using a one-pot synthesis of styrene/myrcene mixtures. Only styrene polymerizes at low temperatures, whereas myrcene requires temperatures above -30 °C in THF to polymerize.[90]

Further, the awareness of sustainability and a shift towards more bio-based systems has led to a reconsideration of solvents, as they make up a large proportion of a synthesis. Consequently, bio-based, more sustainable solvents are currently under investigation, see **Figure 6**.

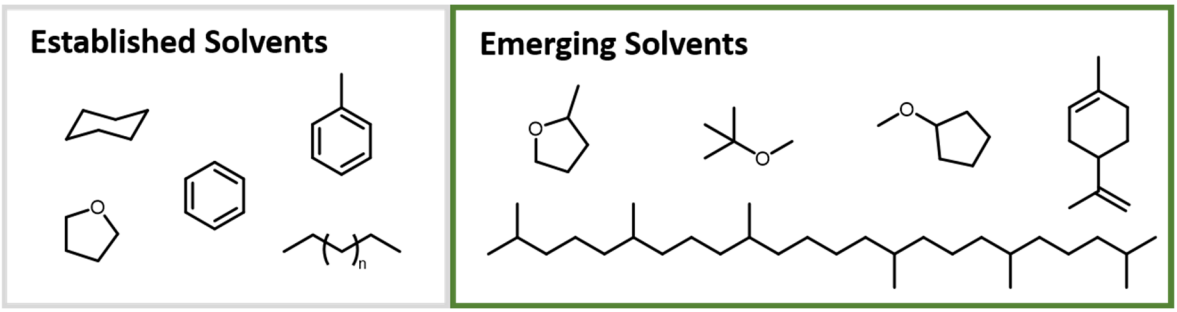

Figure 6. Established and emerging solvents for the anionic polymerization.

Looking beyond butadiene and isoprene, other new and often bio-based monomers facilitates the use of more polar solvents. As introduced beforehand, PFar maintains a low T_g in a polar medium, whereas the syntheses of other polydienes still require an apolar solvent to achieve similar material properties. The Schlaad group investigated the polymerization of isoprene and *β*-myrcene in a variety of "green" solvents, i.e. limonene, 2-methyl tetrahydrofuran (2-MeTHF) and cyclopentyl methyl ether (CPME).[91],[92] On the one hand, 2-MeTHF appeared to have almost the same impact on the microstructure as THF, affording a majority of 3,4-incoorporation (54%). On the other hand, CPME yielded a major fraction of 1,4-units of 64%. The apolar solvent limonene strikingly resulted in 90% 1,4-incorporation. In all solvents, dispersities below 1.15 were obtained. Recently, CPME has also been employed for the copolymerization of styrene with isoprene or 1,3-pentadiene, as well as for the copolymerization of isoprene and 1,3-pentadiene. Kinetic studies were conducted to assess its suitability for use in anionic polymerization.[93] Additionally, 2-MeTHF and CPME were both evaluated as additives in the anionic polymerization of 1,3-cyclohexadiene. Notably, CPME in a toluene system demonstrated promising results, with quantitative yields and successful achievement of targeted molar masses, while maintaining low dispersities of Đ < 1.12.[94] In addition, Haddleton et al. investigated the use of squalane, bearing a C_{30} framework, in its unpurified form as polymerization medium. Despite the high dispersity (*Đ*=1.84), attributed to the absence of purification steps, the low polarity yielded 94% of 1,4-incorporation.[35] In one of our recent works, we showed that the moderately polar solvent methyl *tert*-butyl ether (MTBE) is ideally suited to solvate the bifunctional initiator 1,3-diisopropenyl benzene (DIB). A synergy can be found, as MTBE enables a reliable bifunctional initiation as it prevents aggregation, while the associated increase in vinyl content does not affect the properties of PFar.[72],[75] MTBE, besides being cheap due to industrial scale production for

petrol-additives, can potentially be obtained from renewable feedstocks, i.e. bio-methanol and bio-isobutylene.[95] It is therefore somewhat surprising that it has not received more attention in carbanionic polymerization to date. This can certainly be attributed to the prevalence of the classical systems established over decades.

6. Behavior of 1,3-Dienes in the Statistical Copolymerization

The statistical copolymerization of styrene and butadiene towards so-called "*tapered*" block copolymers was patented as early as 1958 by *Phillips Petroleum Company*.[96],[97] Further development by *Shell Co*. resulted in gradient copolymers for commercial application.[98] The statistical copolymerization is an efficient tool to form block-like, tapered structures that still retain microphase segregation. Therefore, the investigation of the gradient incorporation within a copolymerization is of significant interest. In recent works we compared tapered multiblock copolymers composed of isoprene and styrene with their respective analogues obtained *via* sequential monomer addition. SAXS patterns revealed weaker segregation, clearly attributed to a reduced effective Flory-Huggins parameter, χ_{eff}.[14] Consequently, the order-disorder transition (ODT) temperature, T_{ODT}, decreases, which is desirable for industrial applications targeting high-speed processing through melt extrusion.[11] The synthesis of tapered block copolymers relies on significantly different reactivity ratios.[99],[100] In 2013, we reported on *in situ* ^{1}H NMR spectroscopy to track the individual comonomer consumption throughout the carbanionic copolymerization. The decreasing integrals of the respective monomer signals can be used to calculate the reactivity ratios of each system. By this means, one can directly monitor the copolymerization of isoprene and styrene in apolar media, demonstrating the formation of a steep gradient. The associated reactivity ratios have been determined to be $r_I = 11$ and $r_S = 0.053$. This can be attributed to the faster cross-propagation rate of S to I, compared to *vice versa* ($k_{SI} >> k_{IS}$).[16],[101] Therefore, by initiation of a monomer mixture, two blocks, PI-*grad*-PS, linked by a short gradient structure are obtained. This can be repeated multiple times to generate multiblock copolymers with exceptional material properties, while minimizing the number of reaction steps required.[5],[13]–[15],[102] Driven by the interest for bio-based monomers we also investigated the terpenes *β*-myrcene and *β*-farnesene in the copolymerization with styrene. Both show an even steeper gradient when combined with styrene. **Table 2** summarizes 1,3-dienes that have been investigated regarding statistical copolymerization with styrene. First, butadiene and monosubstituted 1,3-dienes form very pronounced gradients. Secondly, the homopolymerization becomes less preferred when additional substituents are introduced to the monomer scaffold. For instance, VCH with its one double bond captured in the ring is consumed slower than styrene, indicating that the

cross-over reaction is highly dependent on the sterics of the respective 1,3-diene. Furthermore, the aforementioned ocimene and its two isomers reveal the impact of the configuration of the double bonds. While the *trans*-isomer is consumed first when both isomers are polymerized together, the reactivity order inverts when both are copolymerized with styrene. This observation was supported by ^{1}H NMR chemical titration, which revealed a suprising interaction between styrene and solely the *cis*-isomer.

Table 2. Summary of reported reactivity ratios for the copolymerizations of 1,3-dienes with styrene in cyclohexane, together with resulting monomer gradients.

Diene	Solvent	T [°C]	r_{diene}	r_S	Molar gradient	Ref.
β-myrcene	CHx	20	40	0.024		[20]
β-farnesene	CHx	23	27	0.037		[21]
butadiene	CHx	25	15.5	0.04	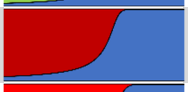	[10]
isoprene	CHx	20	10.1	0.013	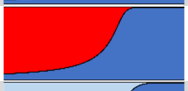	[16]
4PhI	CHx	25	9.2	0.109	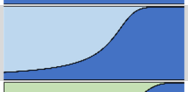	[66]
MyrDOL	CHx	25	5.2	0.19	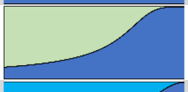	[86]
1PhI	CHx	25	3.38	0.3	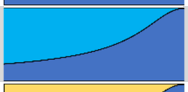	[66]
nopadiene	CHx	25	3.26	0.31		[85]
cis-ocimene	CHx	23	1.015	0.985	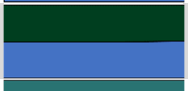	[84]
trans-ocimene	CHx	23	0.62	1.59	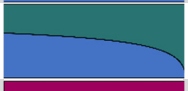	[84]
VCH	CHx	25	0.39	2.56	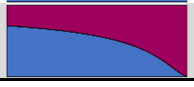	[69]

The copolymerization of two 1,3-dienes, mostly with isoprene as a comonomer, has also been investigated, see **Table 3**. Generally, less noticeable gradients in comparison to diene/S-systems are observed. The *β*-myrcene derivative MyrDOL has been found to form the steepest gradients when copolymerized with either isoprene or *β*-myrcene, respectively. However, this monomer can hardly be compared with other systems due to its increased polarity resulting from the functional side-chain, which is expected to reduce the formation of aggregates, similar to a modifier. Noteworthy, the copolymerization of isoprene with the DMCH and VCH, which are both rotationally constrained, results in a favored consumption of isoprene.

Table 3. Reported reactivity ratios for the copolymerization between two 1,3-dienes in apolar media, together with resulting monomer gradients.

Diene 1	Diene 2	Solvent	*T* [°C]	r_1	r_2	Molar gradient	Ref.
MyrDOL	isoprene	CHx	25	9.22	0.11	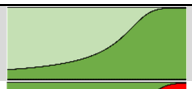	[86]
β-myrcene		CHx	23	4.4	0.23	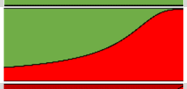	[22]
butadiene		*n*-hexane	20	2.82	0.42	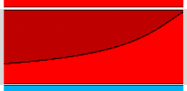	[103]
1PhI		CHx	25	0.865	1.155		[66]
VCH		CHx	25	<<1	>>1		[69]
DMCH		CHx	25	0.087	11.51		[41]
MyrDOL	*β*-myrcene	CHx	25	6.22	0.16		[86]
nopadiene		CHx	25	0.13	7.49		[85]
nopadiene	*β*-farnesene	CHx	25	0.155	6.50	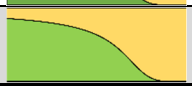	[75]

More recently, we implemented NIR-spectroscopy to track the monomer consumption.[16] The reactions can be tracked directly in the stirred polymerization solution in the reactor, which means that the product formed can be directly characterized with respect to its monomer gradient in the chains. Using *in situ* NIR spectroscopy, we studied the influence of polar modifiers, i.e. THF and DTHFP, in the copolymerizations of I/S and Myr/S. Gradually increasing the ratio of [THF]/[Li] can be used as a tool to control the molar composition of the copolymer chains, as indicated by the profiles shown in **Table 4**. Both isoprene and *β*-myrcene are incorporated in a reduced manner, when the polarity of the system increases, resulting in a preferred consumption of styrene.[17],[20] In case of the copolymerization of *β*-myrcene and styrene DTHFP and TMEDA were shown to have a much stronger impact compared to THF. Already 0.5 eq of [DTHFP]/[Li] influences the copolymerization even more than 20 eq of THF. Only 2 eq of either DTHFP or TMEDA already lead to an enhanced incorporation of styrene, as indicated by reactivity ratios of $r_S \geq 17.5$ and $r_{Myr} \leq 0.15$, respectively.[20],[56]

Table 4. Reported reactivity ratios on the copolymerization of dienes with styrene in the presence of polar modifier, together with resulting molar gradients of the chains.

Diene	Polar Modifier	eq	T [°C]	r_{Diene}	r_S	Molar gradient	Ref.
Isoprene	THF	0.5	20	2.856	0.093	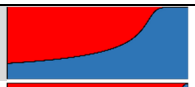	[17]
Isoprene	THF	2	20	1.06	0.262		
Isoprene	THF	20	20	0.374	0.925		
Isoprene	THF	240	20	0.148	4.196		
β-Myrcene	THF	0.5	20	12.3	0.082	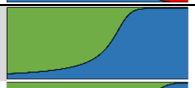	[20]
β-Myrcene	THF	2	20	4.38	0.23	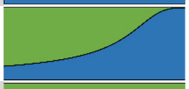	
β-Myrcene	THF	20	20	0.87	1.15		
β-Myrcene	THF	240	20	0.17	5.77	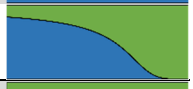	
β-Myrcene	DTHFP	0.5	20	0.41	2.42		
β-Myrcene	DTHFP	2	20	0.056	18.0	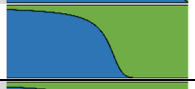	
β-Myrcene	TMEDA	2	-	0.15	17.52	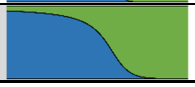	[56]

7. Functional Polydienes *via* Functional Monomers or Post-Polymerization Modification

So far, all presented polydienes discussed solely consist of carbon and hydrogen. In many rubber applications inorganic fillers are used to reduce cost and also to enhance mechanical performance (i.e. modulus, tensile strength etc.). A common filler material used is silica, which is poorly dispersed in a fully non-polar diene material. Silica is known to enhance the performance of tires, one of the main applications of rubber, e.g., by increasing the wet grip for higher safety standards and reduces the rolling resistance to lower fuel consumption.[104] In this context, the incompatibility of hydrophilic fillers and hydrophobic polydienes has led to an increased interest in modifying polydienes. Early works showed that functionalities have to be separated from the propagating diene unit to prevent the so-called "*backside-collapse*" as an undesired side reaction (**Scheme 3**).[44],[105],[106]

Scheme 3: Proposed mechanism of the backside-collapse, as described by original works of Takenaka et al.[105],[106]

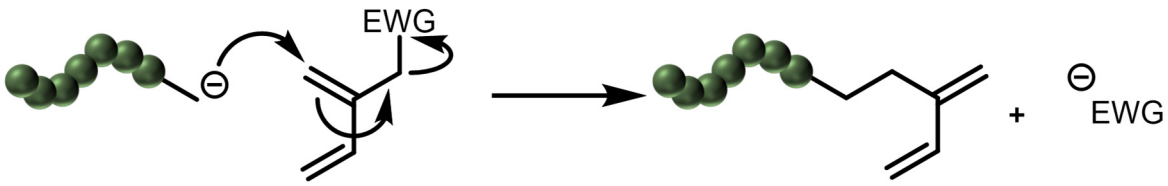

Our group reported on two approaches of functional diene-monomers. Both are based on *β*-myrcene as a precursor that was converted to a hydroxyl-functionalized structure. As free hydroxyl groups are incompatible in the anionic polymerization, suitable protecting groups must be employed. A single hydroxyl group was protected using a siloxyl functionality (MyrOSi), and a dioxolane-based structure (MyrDOL) was used to incorporate two protected hydroxyl groups. Both functional monomers had a modifier effect on the polymerization, as the masked polar functionalities can interact with the counterion and thereby influence the polymerization mechanism. In this case, the diene acts both as a monomer as well as a modifier. The functionalized *β*-myrcene derivatives, MyrOSi and MyrDOL, showed 31% 3,4-units when polymerized in cyclohexane.[58],[86]

Copolymers offer vast possibilities to tune, combine or design materials properties. A variety of copolymers exclusively synthesized *via* anionic polymerization were discussed before. Beyond this, there is a broad field of copolymers that are composed of monomers that require different polymerization techniques. This can be accomplished by preparing a macroinitiator from monomer A. Subsequently, Poly(A) serves as macroinitiator for monomer B to form Poly(A)-*b*-Poly(B) block copolymers in a second reaction using a different polymerization technique. For this purpose, functional groups, e.g. hydroxyl groups, have to be incorporated at the polydiene framework. Controlled end-functionalization of carbanionic living chains is a suitable pathway. Lithium, commonly present as a counterion has the advantage of forming highly stable ion pairs with oxygen. Hence, by using an epoxide in the termination step of a carbanionic synthesis, lithium alkoxides are formed that are not capable of polymerizing any further. As a result, exactly one epoxide monomer is introduced at each chain end reaching a degree of functionalization of up to 99%.[107],[108] Based on the large variety of epoxides available, this method offers vast potential for elaborate architectures. We recently applied this method to a bifunctional system to simultaneously introduce hydroxyl groups at both chain ends. Whereas ethylene oxide is known to introduce one hydroxyl group, ethoxy ethyl glycidyl ether (EEGE) and isopropylidene glyceryl glycidyl ether (IGG) can be used to introduces two and three hydroxyl groups, respectively. Ultimately, this yields telechelic OH_2-polydiene-OH_2 and OH_3-polydiene-OH_3 macroinitiators. *Via* subsequent organocatalyzed chain extension

relying on the ring-opening polymerization of LL-dilactide (LLA), elaborate architectures, e.g., *H-,* and *super-H*-shaped triblock copolymers are accessible.[72],[109]

Another example for the subsequent formation of a second polymer is grafting from a macroinitiator bearing suitable functional groups at the chains. The high abundance of unsaturated groups found in polydienes was used to introduce functionalities in a post-polymerization pathway. This was demonstrated by the group of Li et al. by epoxidation of PMyr.[74],[110] Another efficient pathway is based on the use of polymers derived from functional monomers, e.g. polyMyrOSi, that can be exploit as macroinitiator after the cleavage of the protecting group. Again, by LLA grafting so-called bottlebrush structures are accessible.[58]

The coupling of polymers offers a third option for producing block copolymers, especially elaborate architectures. Coupling in the carbanionic polymerization can be achieved directly by introducing multifunctional coupling reagents, e.g. chlorosilanes, at the living polymer chains.[111] In this manner, complex branched structures can be realized in addition to linear ones, enhancing the material properties in terms of lower viscosity in melt and solution found for commercial products like Styrolux.[11] Our group introduced a *tetra*-functional silyl compound to produce well-defined multiblock star polymers.[112],[113] In the past, this has been pushed to the limit, with reports of up to 128-arm star polymers.[114] The versatile chemistry of polydienes has recently been exploited by Hirschberg et al. who used epoxidized PI to couple with living polystyrenyl chains to obtain *pom-pom* architectures.[115]

8. Current Challenges

Anionic polymerization is still the benchmark when it comes to high precision polymer synthesis. Since polymer chains can be obtained with high uniformity, details of structure-property correlations can be determined with great accuracy. The current shift towards more sustainable feedstocks comes with an increased diversity of diene structures and transforms the deemed “old-fashioned” and fossil fuel-based status of carbanionic polymerization. This motivates fundamental works of carbanionic polymerization to further investigate the mechanism and to develop high performance materials. As most products based on dienes are used as high-volume materials, the economy of scale is a key factor in this area.

An aspect not to be neglected is the responsibility of the industrialized countries to regulate the usage of the available farmland between the production of renewable raw materials and agriculture. For that reason, many different feedstocks are under investigation to obtain dienes *via* truly sustainable pathways. One approach can be found by utilizing bacteria that are capable of turning waste streams into precious resources.[81] Another approach addresses

turpentine oil as a feedstock, which does not compete with food production. This shows that the future holds many challenges when fossil fuel-based isoprene and butadiene are to be replaced as standard diene-building blocks. New routes are therefore mandatory to adapt the variety of new monomers to specific material properties. Other aspects such as more sustainable solvents or more efficient processes are also driving current research.

9. Conclusion

In this perspective, we have reflected on the significance of polydienes in the past and on current developments. With the high precision of the anionic polymerization a variety of 1,3-dienes have been successfully polymerized in a living manner. Besides resembling the properties of fossil fuel-based polybutadiene or polyisoprene with bio-based candidates, the synthesis of rigid polydienes like polynopadiene was recently achieved, showing promising performance as a substitute for polystyrene. This allows the synthesis of fully diene-based TPEs. The elasticity of polydienes can be either tuned by the addition of different polar modifier as well as by the changing the substitution pattern of the monomer. This change has great impact on the reactivity ratios when copolymerized with styrene. While monosubstituted 1,3-dienes showed a block-like polymer composition, disubstituted 1,3-dienes reacted almost randomly with styrene in apolar media. This increase in steric demand is directly related to the resulting microstructure of the polydiene. Further, if the degrees of freedom are reduced to a minimum *via* constrained 1,3-dienes of a *cisoid* or *transoid* structure, respectively, the requirement of a *cisoid*-state was revealed. A large variety of copolymerizations and their respective reactivity ratios within the field of dienes in the carbanionic polymerization was presented, alongside with insights into new emerging fields including new monomers, solvents and modifiers. We emphasize that the findings of the past years, summarized herewith, are beneficial to create new innovations in the future and is of general relevance for the field of carbanionic polymerization and polydienes in general.

References

[1] Frey, H.; Johann, T. Celebrating 100 years of "polymer science": Hermann Staudinger's 1920 manifesto. *Polym. Chem.*, **2020**, *11* (1), 8‑14.

[2] Staudinger, H.; Fritschi, J. Über Isopren und Kautschuk. 5. Mitteilung. Über die Hydrierung des Kautschuks und über seine Konstitution. *Helvetica Chimica Acta*, **1922**, *5* (5), 785‑806.

[3] Mollwo Perkin, F. Natural and Synthetic Rubber. *J R Soc Arts*, **1912**, *61* (3134), 85‑102.

[4] Holt, A. Neuere Arbeiten auf dem Kautschukgebiet. *Angewandte Chemie*, **1914**, *27*, 153‑158.

[5] Steube, M.; Johann, T.; Barent, R. D.; Müller, A. H.; Frey, H. Rational design of tapered multiblock copolymers for thermoplastic elastomers. *Progress in Polymer Science*, **2022**, *124*, 101488.

[6] Thomas, S.; Chan, C. H.; Pothen, L. A.; K. R., R.; Maria, H. J. *Natural Rubber Materials 1*; Royal Society of Chemistry, **2014**.

[7] Official Website of Malaysian Rubber Council. *Rubber Industry: Industry Overview*. www.myrubbercouncil.com/industry/world_production.php (accessed 2024-07-08).

[8] Ntetsikas, K.; Ladelta, V.; Bhaumik, S.; Hadjichristidis, N. Quo Vadis Carbanionic Polymerization? *ACS polymers Au*, **2023**, *3* (2), 158‑181.

[9] Forens, A.; Roos, K.; Dire, C.; Gadenne, B.; Carlotti, S. Accessible microstructures of polybutadiene by anionic polymerization. *Polymer*, **2018**, *153*, 103‑122.

[10] Hsieh, H. L.; Quirk, R. P. *Anionic Polymerization*:*Principles and Practical Applications*; Plastics Engineering Ser, v.34; Chapman and Hall/CRC, **1996**.

[11] Knoll, K.; Nießner, N. Styrolux + and styroflex + - from transparent high impact polystyrene to new thermoplastic elastomers: Syntheses, applications and blends with other styrene based polymers. *Macromol. Symp.*, **1998**, *132* (1), 231‑243.

[12] Galanos, E.; Wahlen, C.; Butt, H.-J.; Frey, H.; Floudas, G. Phase Diagram of Tapered Copolymers Based on Isoprene and Styrene. *Macromol. Chem. Phys.*, **2022**, *223* (10).

[13] Grune, E.; Appold, M.; Müller, A. H. E.; Gallei, M.; Frey, H. Anionic Copolymerization Enables the Scalable Synthesis of Alternating (AB)n Multiblock Copolymers with High Molecular Weight in n/2 Steps. *ACS Macro Lett.*, **2018**, *7* (7), 807‑810.

[14] Barent, R. D.; Perevyazko, I.; Mikusheva, N.; Floudas, G.; Frey, H. Linear (IS) n I Multiblock Copolymers: Tailoring the Softness of Thermoplastic Elastomers by Flexible Polyisoprene End Blocks. *Macromolecules*, **2023**, *56* (15), 5792‑5802.

[15] Steube, M.; Johann, T.; Galanos, E.; Appold, M.; Rüttiger, C.; Mezger, M.; Gallei, M.; Müller, A. H. E.; Floudas, G.; Frey, H. Isoprene/Styrene Tapered Multiblock Copolymers with up to Ten Blocks: Synthesis, Phase Behavior, Order, and Mechanical Properties. *Macromolecules*, **2018**, *51* (24), 10246‑10258.

[16] Steube, M.; Johann, T.; Plank, M.; Tjaberings, S.; Gröschel, A. H.; Gallei, M.; Frey, H.; Müller, A. H. E. Kinetics of Anionic Living Copolymerization of Isoprene and Styrene Using in Situ NIR Spectroscopy: Temperature Effects on Monomer Sequence and Morphology. *Macromolecules*, **2019**, *52* (23), 9299‑9310.

[17] Steube, M.; Johann, T.; Hübner, H.; Koch, M.; Dinh, T.; Gallei, M.; Floudas, G.; Frey, H.; Müller, A. H. E. Tetrahydrofuran: More than a “Randomizer” in the Living Anionic Copolymerization of Styrene and Isoprene: Kinetics, Microstructures, Morphologies, and Mechanical Properties. *Macromolecules*, **2020**, *53* (13), 5512‑5527.

[18] Natalello, A.; Werre, M.; Alkan, A.; Frey, H. Monomer Sequence Distribution Monitoring in Living Carbanionic Copolymerization by Real-Time 1 H NMR Spectroscopy. *Macromolecules*, **2013**, *46* (21), 8467‑8471.

[19] Tiedemann, P. von; Blankenburg, J.; Maciol, K.; Johann, T.; Müller, A. H. E.; Frey, H. Copolymerization of Isoprene with p -Alkylstyrene Monomers: Disparate Reactivity Ratios and the Shape of the Gradient. *Macromolecules*, **2019**, *52* (3), 796‑806.

[20] Fuchs, D. A. H.; Hübner, H.; Kraus, T.; Niebuur, B.-J.; Gallei, M.; Frey, H.; Müller, A. H. E. The effect of THF and the chelating modifier DTHFP on the copolymerisation of *β*-myrcene and styrene: kinetics, microstructures, morphologies, and mechanical properties. *Polym. Chem.*, **2021**, *12* (32), 4632‑4642.

[21] Wahlen, C.; Blankenburg, J.; Tiedemann, P. von; Ewald, J.; Sajkiewicz, P.; Müller, A. H. E.; Floudas, G.; Frey, H. Tapered Multiblock Copolymers Based on Farnesene and Styrene: Impact of Biobased Polydiene Architectures on Material Properties. *Macromolecules*, **2020**, *53* (23), 10397‑10408.

[22] Grune, E.; Bareuther, J.; Blankenburg, J.; Appold, M.; Shaw, L.; Müller, A. H. E.; Floudas, G.; Hutchings, L. R.; Gallei, M.; Frey, H. Towards bio-based tapered block copolymers: the behaviour of myrcene in the statistical anionic copolymerisation. *Polym. Chem.*, **2019**, *10* (10), 1213‑1220.

[23] Wadgaonkar, S. P.; Schüttner, S.; Berger-Nicoletti, E.; Müller, A. H. E.; Frey, H. Anionic Copolymerization of 4-Trimethylsilylstyrene: From Kinetics to Gradient and Block Copolymers. *Macromolecules*, **2022**, *55* (11), 4721‑4732.

[24] Yao, C.; Liu, N.; Long, S.; Wu, C.; Cui, D. Highly cis-1,4-selective coordination polymerization of polar 2-(4-methoxyphenyl)-1,3-butadiene and copolymerization with isoprene using a β-diketiminato yttrium bis(alkyl) complex. *Polym. Chem.*, **2016**, *7* (6), 1264‑1270.

[25] Leicht, H.; Göttker-Schnetmann, I.; Mecking, S. Stereoselective Copolymerization of Butadiene and Functionalized 1,3-Dienes. *ACS Macro Lett.*, **2016**, *5* (6), 777‑780.

[26] Ricci, G.; Pampaloni, G.; Sommazzi, A.; Masi, F. Dienes Polymerization: Where We Are and What Lies Ahead. *Macromolecules*, **2021**, *54* (13), 5879‑5914.

[27] Friebe, L.; Nuyken, O.; Obrecht, W. Neodymium-Based Ziegler/Natta Catalysts and their Application in Diene Polymerization. In *Neodymium Based Ziegler Catalysts ‑ Fundamental Chemistry*; Nuyken, O., Ed.; Advances in polymer science; Springer Berlin Heidelberg, **2006**; pp 1‑154.

[28] Kaita, S.; Doi, Y.; Kaneko, K.; Horiuchi, A. C.; Wakatsuki, Y. An Efficient Gadolinium Metallocene-Based Catalyst for the Synthesis of Isoprene Rubber with Perfect 1,4-Cis Microstructure and Marked Reactivity Difference between Lanthanide Metallocenes toward Dienes As Probed by Butadiene−Isoprene Copolymerization Catalysis. *Macromolecules*, **2004**, *37* (16), 5860‑5862.

[29] Hadjichristidis, N.; Iatrou, H.; Pispas, S.; Pitsikalis, M. Anionic polymerization: High vacuum techniques. *J. Polym. Sci. A Polym. Chem.*, **2000**, *38* (18), 3211‑3234.

[30] Wurm, F.; Wilms, D.; Klos, J.; Löwe, H.; Frey, H. Carbanions on Tap ‑ Living Anionic Polymerization in a Microstructured Reactor. *Macromol. Chem. Phys.*, **2008**, *209* (11), 1106‑1114.

[31] Tonhauser, C.; Wilms, D.; Wurm, F.; Nicoletti, E. B.; Maskos, M.; Löwe, H.; Frey, H. Multihydroxyl-Functional Polystyrenes in Continuous Flow. *Macromolecules*, **2010**, *43* (13), 5582‑5588.

[32] Iida, K.; Chastek, T. Q.; Beers, K. L.; Cavicchi, K. A.; Chun, J.; Fasolka, M. J. Living anionic polymerization using a microfluidic reactor. *Lab on a chip*, **2009**, *9* (2), 339‑345.

[33] Pérez, K.; Leveneur, S.; Burel, F.; Legros, J.; Vuluga, D. Anionic synthesis and end-functionalization of polymyrcene in a flow microreactor system. *React. Chem. Eng.*, **2023**, *8* (2), 432‑441.

[34] Zhang, J.; Pointer, W.; Patias, G.; Al-Shok, L.; Hand, R. A.; Smith, T.; Haddleton, D. M. End functionalization of polyisoprene and polymyrcene obtained by anionic polymerization via one-pot ring-opening mono-addition of epoxides. *European Polymer Journal*, **2023**, *183*, 111755.

[35] Zhang, J.; Aydogan, C.; Patias, G.; Smith, T.; Al-Shok, L.; Liu, H.; Eissa, A. M.; Haddleton, D. M. Polymerization of Myrcene in Both Conventional and Renewable Solvents: Postpolymerization Modification via Regioselective Photoinduced Thiol-Ene Chemistry for Use as Carbon Renewable Dispersants. *ACS Sustainable Chem. Eng.*, **2022**, *10* (29), 9654–9664.

[36] Tobolsky, A. V.; Rogers, C. E. Anionic polymerization of isoprene: Effect of ionic character of the growing ion pair on polymer structure. *J. Polym. Sci.*, **1959**, *38* (133), 205–207.

[37] Tobolsky, A. V.; Rogers, C. E. Isoprene polymerization by organometallic compounds. II. *J. Polym. Sci.*, **1959**, *40* (136), 73–89.

[38] Müller, A. H. E.; Matyjaszewski, K., Eds. *Controlled and living polymerizations*:*Methods and materials*; Wiley-VCH-Verl., **2009**.

[39] Szwarc, M. 'Living' Polymers. *Nature*, **1956**, *178* (4543), 1168–1169.

[40] Mark, J. E., Ed. *Physical properties of polymers handbook*, 2nd ed.; Springer, **2007**.

[41] Barent, R. D.; Wagner, M.; Frey, H. Geometric requirements for living anionic polymerization: polymerization of rotationally constrained 1,3-dienes. *Polym. Chem.*, **2022**, *13* (38), 5478–5485.

[42] Gebert, W.; Hinz, J.; Sinn, H. Umlagerungen bei der durch Lithiumbutyl initiierten Polyreaktion der Diene Isopren und Butadien. *Die Makromolekulare Chemie*, **1971**, *144* (1), 97–115.

[43] Worsfold, D. J.; Bywater, S. Lithium Alkyl Initiated Polymerization of Isoprene. Effect of Cis/Trans Isomerization of Organolithium Compounds on Polymer Microstructure. *Macromolecules*, **1978**, *11* (3), 582–586.

[44] Hadjichristidis, N.; Hirao, A., Eds. *Anionic Polymerization*; Springer Japan, **2015**.

[45] Carlotti, S.; Ménoret, S.; Barabanova, A.; Desbois, P.; Deffieux, A. Retarded Anionic Polymerization: Copolymerization of Butadiene and Styrene in the Presence of Alkyllithium and n , s -Dibutylmagnesium or Triisobutylaluminium Derivatives. *Macromol. Chem. Phys.*, **2004**, *205* (5), 656–663.

[46] Forens, A.; Roos, K.; Dire, C.; Gadenne, B.; Carlotti, S. Anionic Polymerization of Butadiene Using Lithium/Potassium Multi-metallic Systems: Influence on Polymerization Control and Polybutadiene Microstructure. *Chin J Polym Sci*, **2020**, *38* (4), 357‑362.

[47] Kosaka, Y.; Goseki, R.; Kawauchi, S.; Ishizone, T. Living Anionic Polymerization of Benzofulvene in Hydrocarbon Solvent. *Macromol. Symp.*, **2015**, *350* (1), 55‑66.

[48] Kosaka, Y.; Kawauchi, S.; Goseki, R.; Ishizone, T. High Anionic Polymerizability of Benzofulvene: New Exo-Methylene Hydrocarbon Monomer. *Macromolecules*, **2015**, *48* (13), 4421‑4430.

[49] Kosaka, Y.; Kitazawa, K.; Inomata, S.; Ishizone, T. Living Anionic Polymerization of Benzofulvene: Highly Reactive Fixed Transoid 1,3-Diene. *ACS Macro Lett.*, **2013**, *2* (2), 164‑167.

[50] Kobayashi, S.; Lu, C.; Hoye, T. R.; Hillmyer, M. A. Controlled polymerization of a cyclic diene prepared from the ring-closing metathesis of a naturally occurring monoterpene. *J. Am. Chem. Soc.*, **2009**, *131* (23), 7960‑7961.

[51] Rüttiger, C.; Appold, M.; Didzoleit, H.; Eils, A.; Dietz, C.; Stark, R. W.; Stühn, B.; Gallei, M. Structure Formation of Metallopolymer-Grafted Block Copolymers. *Macromolecules*, **2016**, *49* (9), 3415‑3426.

[52] Gabor, A. H.; Lehner, E. A.; Mao, G.; Schneggenburger, L. A.; Ober, C. K. Synthesis and Lithographic Characterization of Block Copolymer Resists Consisting of Both Poly(styrene) Blocks and Hydrosiloxane-Modified Poly(diene) Blocks. *Chem. Mater.*, **1994**, *6* (7), 927‑934.

[53] Rodgers, B., Ed. *Rubber compounding*:*Chemistry and applications*, Second edition; Taylor & Francis, **2016**.

[54] Morton, M.; Fetters, L. J. Homogeneous anionic polymerization. V. Association phenomena in organolithium polymerization. *J. Polym. Sci. A Gen. Pap.*, **1964**, *2* (7), 3311‑3326.

[55] Bywater, S.; Worsfold, D. J. Anionic Polymerization of Styrene Effect of Tetrahydrofuran. *Can. J. Chem.*, **1962**, *40* (8), 1564‑1570.

[56] Shaw, L.; Hutchings, L. R. Tales of the unexpected. The non-random statistical copolymerisation of myrcene and styrene in the presence of a polar modifier. *Polym. Chem.*, **2020**, *11* (44), 7020‑7025.

[57] Yoo, T.; Henning, S. K. Synthesis and Characterization of Farnesene-Based Polymers. *Rubber Chem. Technol.*, **2017**, *90* (2), 308‑324.

[58] Wahlen, C.; Rauschenbach, M.; Blankenburg, J.; Kersten, E.; Ender, C. P.; Frey, H. Myrcenol-Based Monomer for Carbanionic Polymerization: Functional Copolymers with Myrcene and Bio-Based Graft Copolymers. *Macromolecules*, **2020**, *53* (20), 9008‑9017.

[59] Bolton, J. M.; Hillmyer, M. A.; Hoye, T. R. Sustainable Thermoplastic Elastomers from Terpene-Derived Monomers. *ACS Macro Lett.*, **2014**, *3* (8), 717‑720.

[60] Zhang, J.; Lu, J.; Su, K.; Wang, D.; Han, B. Bio-based *β*-myrcene-modified solution-polymerized styrene‑butadiene rubber for improving carbon black dispersion and wet skid resistance. *J. Appl. Polym. Sci.*, **2019**, *136* (45), 1‑10.

[61] Ohno, R.; Tanaka, Y.; Kawakami, M. Synthesis and Characterization of 2-Alkylbutadiene Polymers. II. Stereospecific Polymerization of 2-Ethyl-, 2-n-Propyl-, 2-Isopropyl-, and 2-n-Butylbutadienes. *Polym J*, **1973**, *4* (1), 56‑60.

[62] Suzuki, T.; Tsuji, Y.; Takegami, Y.; Harwood, H. J. Microstructure of Poly(2-phenylbutadiene) Prepared by Anionic Initiators. *Macromolecules*, **1979**, *12* (2), 234‑239.

[63] Ding, Y. X.; Weber, W. P. Regio- and stereospecific 1,4-polymerization of 2-(triethylsilyl)-1,3-butadiene. *Macromolecules*, **1988**, *21* (2), 530‑532.

[64] Suzuki, T.; Tsuji, Y.; Takegami, Y. Microstructure of Poly(1-phenylbutadiene) Prepared by Anionic Initiators. *Macromolecules*, **1978**, *11* (4), 639‑644.

[65] Suzuki, T.; Tsuji, Y.; Watanabe, Y.; Takegami, Y. Characterization of Living Anion Chain End of Oligomeric 1-Phenyl-1,3-butadienyllithium. *Polym J*, **1979**, *11* (8), 651‑660.

[66] Rauschenbach, M.; Stein, L.; Linden, G.; Barent, R.; Heinze, K.; Frey, H. Anionic Polymerization of Phenyl-Substituted Isoprene Derivatives: Polymerization Behaviour and Cyclization-Enabled Fluorescence. *Polym. Chem.*, **2024**, Accepted Manuscript.

[67] Goseki, R.; Miyai, S.; Uchida, S.; Ishizone, T. Polymerizability of exomethylene monomers based on adamantyl frameworks. *Polym. Chem.*, **2021**, *12* (25), 3602‑3611.

[68] Uchida, S.; Togii, K.; Miyai, S.; Goseki, R.; Ishizone, T. Allylidene Monomers: Anionically Polymerizable 1,1-Disubstituted 1,3-Diene Derivatives. *Macromolecules*, **2020**, *53* (22), 10107‑10116.

[69] Hahn, C.; Rauschenbach, M.; Frey, H. Merging Styrene and Diene Structures to a Cyclic Diene: Anionic Polymerization of 1-Vinylcyclohexene (VCH). *Angew. Chem. Int. Ed.*, **2023**, *62* (28), e202302907.

[70] Haynes, W. M.; Lide, D. R.; Bruno, T. J. *CRC Handbook of Chemistry and Physics:A Ready-Reference Book of Chemical and Physical Data*, 95th ed; CRC Press, **2015**.

[71] Wahlen, C.; Frey, H. Anionic Polymerization of Terpene Monomers: New Options for Bio-Based Thermoplastic Elastomers. *Macromolecules*, **2021**, *54* (16), 7323–7336.

[72] Meier-Merziger, M.; Imschweiler, J.; Hartmann, F.; Niebuur, B.-J.; Kraus, T.; Gallei, M.; Frey, H. Bifunctional Carbanionic Synthesis of Fully Bio-Based Triblock Structures Derived from *β*-Farnesene and ll-Dilactide: Thermoplastic Elastomers. *Angew. Chem. Int. Ed.*, **2023**, *62* (42), e202310519.

[73] Zhou, C.; Wei, Z.; Lei, X.; Li, Y. Fully biobased thermoplastic elastomers: synthesis and characterization of poly(l -lactide)-b-polymyrcene-b-poly(l -lactide) triblock copolymers. *RSC Adv.*, **2016**, *6* (68), 63508–63514.

[74] Zhou, C.; Wei, Z.; Jin, C.; Wang, Y.; Yu, Y.; Leng, X.; Li, Y. Fully biobased thermoplastic elastomers: Synthesis of highly branched linear comb poly(*β*-myrcene)-graft-poly(l-lactide) copolymers with tunable mechanical properties. *Polymer*, **2018**, *138*, 57–64.

[75] Meier-Merziger, M.; Fotaras, N.; Tzourtzouklis, I.; Allouch, C.; Wagner, M.; Müller, A. H. E.; Frey, H. One-Step Synthesis of Fully Bio-based Two-Sided Tapered ABA-Type Thermoplastic Elastomers. *ACS Sustainable Chem. Eng.*, **2024**, *12* (24), 9922–9933.

[76] Iacob, C.; Yoo, T.; Runt, J. Molecular Dynamics of Polyfarnesene. *Macromolecules*, **2018**, *51* (13), 4917–4922.

[77] Fetters, L. J.; Lohse, D. J.; Richter, D.; Witten, T. A.; Zirkel, A. Connection between Polymer Molecular Weight, Density, Chain Dimensions, and Melt Viscoelastic Properties. *Macromolecules*, **1994**, *27* (17), 4639–4647.

[78] Fetters, L. J. Determination of the Inermolecular Entanglement Coupling Spacing in Polyisoprene by Viscosity Measurments. *J. Res. Natl. Bur. Stds.*, **1965** (69A), 33–37.

[79] Oßwald, P.; Whitside, R.; Schäffer, J.; Köhler, M. An experimental flow reactor study of the combustion kinetics of terpenoid jet fuel compounds: Farnesane, p-menthane and p-cymene. *Fuel*, **2017**, *187*, 43–50.

[80] Zhang, J.; Chen, J.; Yao, M.; Jiang, Z.; Ma, Y. Hydrolysis-resistant polyurethane elastomers synthesized from hydrophobic bio-based polyfarnesene diol. *J. Appl. Polym. Sci.*, **2019**, *136* (25), 1–10.

[81] Milker, S.; Holtmann, D. First time *β*-farnesene production by the versatile bacterium Cupriavidus necator. *Microbial cell factories*, **2021**, *20* (1), 89.

[82] Matic, A.; Schlaad, H. Thiol-ene photofunctionalization of 1,4-polymyrcene. *Polym. Int.*, **2018**, *67* (5), 500‑505.

[83] Matic, A.; Hess, A.; Schanzenbach, D.; Schlaad, H. Epoxidized 1,4-polymyrcene. *Polym. Chem.*, **2020**, *11* (7), 1364‑1368.

[84] Wadgaonkar, S. P.; Wagner, M.; Baptista, L. A.; Cortes-Huerto, R.; Frey, H.; Müller, A. H. E. Anionic Polymerization of the Terpene-Based Diene *β*-Ocimene: Complex Mechanism Due to Stereoisomer Reactivities. *Macromolecules*, **2023**, *56* (2), 664‑677.

[85] Hahn, C.; Göttker-Schnetmann, I.; Tzourtzouklis, I.; Wagner, M.; Müller, A. H. E.; Floudas, G.; Mecking, S.; Frey, H. Nopadiene: A Pinene-Derived Cyclic Diene as a Styrene Substitute for Fully Biobased Thermoplastic Elastomers. *J. Am. Chem. Soc.*, **2023**, *145* (49), 26688-26698.

[86] Hahn, C.; Wagner, M.; Müller, A. H. E.; Frey, H. MyrDOL, a Protected Dihydroxyfunctional Diene Monomer Derived from *β*-Myrcene: Functional Polydienes from Renewable Resources via Anionic Polymerization. *Macromolecules*, **2022**, *55* (10), 4046‑4055.

[87] Gatzke, A. L.; Vanzo, E. Chain transfer to toluene in n-butyl-lithium initiated polymerization of styrene. *Chem. Commun. (London)*, **1967** (22), 1180.

[88] Bates, R. B.; Kroposki, L. M.; Potter, D. E. Cycloreversions of anions from tetrahydrofurans. Convenient synthesis of lithium enolates of aldehydes. *J. Org. Chem.*, **1972**, *37* (4), 560‑562.

[89] Ogle, C. A.; Strickler, F. H.; Gordon, B. Reaction of polystyryllithium with tetrahydrofuran. *Macromolecules*, **1993**, *26* (21), 5803‑5805.

[90] Bareuther, J.; Plank, M.; Kuttich, B.; Kraus, T.; Frey, H.; Gallei, M. Temperature Variation Enables the Design of Biobased Block Copolymers via One-Step Anionic Copolymerization. *Macromolecular rapid communications*, **2020**, e2000513.

[91] Glatzel, J.; Noack, S.; Schanzenbach, D.; Schlaad, H. Anionic polymerization of dienes in ‘green’ solvents. *Polym. Int.*, **2021**, *70* (2), 181‑184.

[92] Dev, A.; Rösler, A.; Schlaad, H. Limonene as a renewable unsaturated hydrocarbon solvent for living anionic polymerization of *β*-myrcene. *Polym. Chem.*, **2021**, *12* (21), 3084‑3087.

[93] Fu, Y.; Yang, S.; Xiong, Q.; Gu, Z.; Dai, Q.; Tan, H.; Le Zhou; Geng, M.; Xie, F.; Yi, W.; Li, L.; Liu, K. Synthesis, kinetic study and characterization of C5 -dienes/styrene copolymers via living anionic polymerization in cyclopentyl methyl ether solvent. *Polym. Int.*, **2023**, *73* (4), 326‑336.

[94] Natori, I.; Natori, S.; Taehee, J.; Ogino, K. The last challenge for living anionic polymerization of 1,3-cyclohexadiene with the s-butyllithium/cyclopentyl methyl ether system. *Polymer*, **2022**, *250*, 124821.

[95] Wilson, J.; Gering, S.; Pinard, J.; Lucas, R.; Briggs, B. R. Bio-production of gaseous alkenes: ethylene, isoprene, isobutene. *Biotechnology for biofuels*, **2018**, *11* (234), 1‑11.

[96] Legge, N. R. Thermoplastic Elastomers. *Rubber Chemistry and Technology*, **1987**, *60* (3), 83‑117.

[97] Porter, L. M. Block polymers and process for preparation thereof. GB 888624 (A).

[98] Holden, G.; Milkovich, R. Block polymers of monovinyl aromatic hydrocarbons and conjugated dienes. US 3265765 (A).

[99] Worsfold, D. J. Anionic copolymerization of styrene and isoprene in cyclohexane. *J. Polym. Sci. A-1 Polym. Chem.*, **1967**, *5* (11), 2783‑2789.

[100] Kraus, G.; Rollmann, K. W. Some effects of monomer sequence on the viscoelastic behavior of random copolymers of butadiene and styrene. *Angew. Makromol. Chemie*, **1971**, *16* (1), 271‑296.

[101] Grune, E.; Johann, T.; Appold, M.; Wahlen, C.; Blankenburg, J.; Leibig, D.; Müller, A. H. E.; Gallei, M.; Frey, H. One-Step Block Copolymer Synthesis versus Sequential Monomer Addition: A Fundamental Study Reveals That One Methyl Group Makes a Difference. *Macromolecules*, **2018**, *51* (9), 3527‑3537.

[102] Wang, W.; Lu, W.; Goodwin, A.; Wang, H.; Yin, P.; Kang, N.-G.; Hong, K.; Mays, J. W. Recent advances in thermoplastic elastomers from living polymerizations: Macromolecular architectures and supramolecular chemistry. *Progress in Polymer Science*, **2019**, *95*, 1‑31.

[103] Hill, D.; O'Donnell, J. H.; O'Sullivan, P. W.; McGrath, J. E.; Wang, I. C.; Ward, T. C. Anionic copolymerization of butadiene and isoprene: Applicability of the terminal model to high conversion. *Polym. Bull.*, **1983**, *9* (6-7).

[104] Hayichelaeh, C.; Reuvekamp, L. A. E. M.; Dierkes, W. K.; Blume, A.; Noordermeer, J. W. M.; Sahakaro, K. Promoting Interfacial Compatibility of Silica-Reinforced Natural Rubber Tire Compounds Byaliphatic Amine. *Rubber Chemistry and Technology*, **2018**, *91* (2), 433‑452.

[105] Takenaka, K.; Nakashima, D.; Miya, M.; Takeshita, H.; Shiomi, T. Anionic polymerization of 2-(N,N-bistrimethylsilylaminomethyl)-1,3-butadiene and 2-(4-(N,N-bistrimethylsilylamino)butyl)-1,3-butadiene. *e-J. Soft Mater.*, **2013**, *9* (0), 14‑19.

[106] Takenaka, K.; Akagawa, Y.; Takeshita, H.; Miya, M.; Shiomi, T. Polymerization of 1,3-Dienes Containing Functional Groups 6: Unexpected Collapse of Monomer Structure in the Anionic Polymerization of 2-Ethoxymethyl-1,3-butadiene. *Polym J*, **2009**, *41* (2), 106‑107.

[107] Tonhauser, C.; Frey, H. A road less traveled to functional polymers: epoxide termination in living carbanionic polymer synthesis. *Macromolecular rapid communications*, **2010**, *31* (22), 1938‑1947.

[108] Dreier, P.; Ahn, J.; Chang, T.; Frey, H. End Group Functionality of 95-99%: Epoxide Functionalization of Polystyryl-Lithium Evaluated via Solvent Gradient Interaction Chromatography. *Macromol. Rapid Commun.*, **2022**, e2200560.

[109] Meier-Merziger, M.; Fickenscher, M.; Hartmann, F.; Kuttich, B.; Kraus, T.; Gallei, M.; Frey, H. Synthesis of phase-separated super-H-shaped triblock architectures: poly(l-lactide) grafted from telechelic polyisoprene. *Polym. Chem.*, **2023**, *14* (23), 2820‑2828.

[110] Zhou, C.; Wei, Z.; Wang, Y.; Yu, Y.; Leng, X.; Li, Y. Fully biobased thermoplastic elastomers: Synthesis of highly branched star comb poly(*β*-myrcene)-graft-poly(l-lactide) copolymers with tunable mechanical properties. *European Polymer Journal*, **2018**, *99*, 477‑484.

[111] Hadjichristidis, N.; Pitsikalis, M.; Pispas, S.; Iatrou, H. Polymers with complex architecture by living anionic polymerization. *Chem. Rev.*, **2001**, *101* (12), 3747‑3792.

[112] Tiedemann, P. von; Maciol, K.; Preis, J.; Sajkiewicz, P.; Frey, H. Rapid one-pot synthesis of tapered star copolymers via ultra-fast coupling of polystyryllithium chain ends. *Polym. Chem.*, **2019**, *10* (14), 1762‑1768.

[113] Tiedemann, P. von; Yan, J.; Barent, R. D.; Spontak, R. J.; Floudas, G.; Frey, H.; Register, R. A. Tapered Multiblock Star Copolymers: Synthesis, Selective Hydrogenation, and Properties. *Macromolecules*, **2020**, *53* (11), 4422‑4434.

[114] Roovers, J.; Zhou, L. L.; Toporowski, P. M.; van der Zwan, M.; Iatrou, H.; Hadjichristidis, N. Regular star polymers with 64 and 128 arms. Models for polymeric micelles. *Macromolecules*, **1993**, *26* (16), 4324‑4331.

[115] Hirschberg, V.; Schußmann, M. G.; Röpert, M.-C.; Dingenouts, N.; Buchheiser, S.; Nirschl, H.; Berson, J.; Wilhelm, M. Supertough Thermoplastic Elastomers of Polystyrene and Polyisoprene via the Pom-Pom Topology. *Macromolecules*, **2024**, *57* (7), 3387‑3396.

Chapter 2

Theoretical Background

This chapter gives an overview of the theoretical background of relevant topics not covered by the *Perspective* article presented in **Chapter 1**. Given the primary objective of the presented thesis is the synthesis of bio-based thermoplastic elastomers (TPE's), this term, along with the basics of block copolymers will be introduced in greater detail. Additionally, the specialized field of bifunctional initiators for the carbanionic polymerization will be discussed. This is followed by a general introduction to the kinetic investigation to define the foundation for its later implementation.

Block Copolymers

Customizing polymer properties to a specific application is one of the core elements in polymer chemistry. Some demands can be met by simply choosing from the broad range of available polymer materials, i.e., thermoplastics, thermosets, or elastomers, whereas others require more detailed consideration. The first approach, which may seem obvious, is to suppress unfavorable properties or to create desired new features by using additives for a material or by blending different materials.[1] This is a common practice, for example, to cost-effectively reduce the brittle properties of materials, e.g. polylactide (PLA) or polyvinylchloride (PVC) by adding plasticizers.[2] – [4] Thereby, limitations for applications that require mechanical toughness, i.e., elongation at break and impact strength, can be overcome. Even though this is a reasonable approach to meet certain properties, its drawbacks should not be neglected. First, the long-term stability of these materials is questionable, as low molar mass plasticizer molecules migrate out of the material over time, causing drastically decreasing performance.[5] Second, as some plasticizers are known to show toxicity, e.g. phthalates, the rising awareness in this regard is currently driving research to explore suitable alternatives.[6] Polymer blends, on the other hand, are often immiscible, and the weak interactions between the segregated phases cause poor mechanical properties.[7]

One approach to overcome immiscibility is to chemically link two types of polymers by covalent bonds to yield copolymers. While a random distribution of two monomers along a polymer chain results in a homogeneous material, an initial polymerization of monomer A, followed by polymerization of monomer B results in a block copolymer, i.e. poly(A)-*b*-poly(B). This is usually achieved *via* controlled chain-growth polymerization. Still, both polymer blocks of copolymers are usually immiscible, similar to polymer blends. But as they are linked *via* covalent bonds the phase separation of block copolymers is limited to the scale of the polymer

chain. The result is a domain structure of the copolymer often referred to as nano- or microphase separation, see **Figure 1**a. ABA-type tri- or $A(BA)_n$ multiblock copolymers have another advantage, as the different individual domains can be linked through others *via* bridging as illustrated in **Figure 1**b & c.

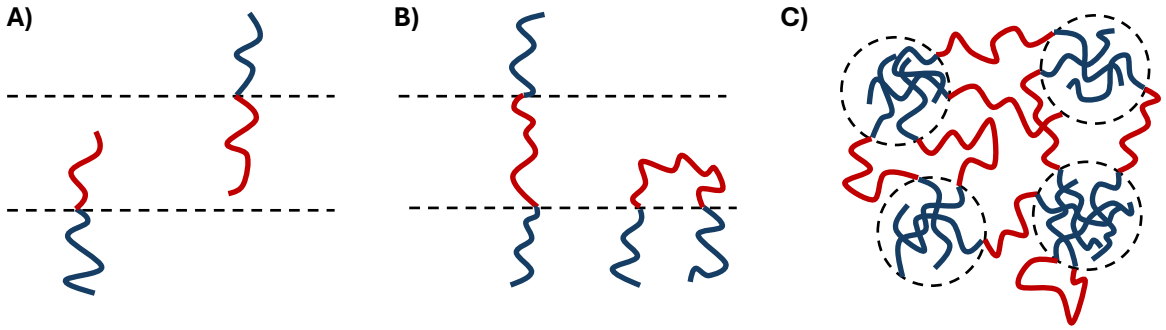

Figure 1. Illustration of the domain linkage in: A) an AB-diblock copolymer; B) bridging within an ABA-triblock copolymer; C) ABA-triblock in a spherical morphology.

The thermodynamics of mixing can be expressed by the Gibbs free molar energy, $\Delta G_{mix,m}$, which depends on the molar enthalpy of mixing, $\Delta H_{mix,m}$, the molar entropy of mixing, $\Delta S_{mix,m}$, and the temperature (T), see **Equation 1**.[8]

$$\Delta G_{mix,m} = \Delta H_{mix,m} - T\,\Delta S_{mix,m} \quad \textbf{(1)}$$

In analogy with an alchemist's Latin proverb, lat. *similia similibus solvuntur* – "similar substances will dissolve similar substances", the enthalpy ($\Delta H_{mix,m} > 0$) of two incompatible blocks contribute towards phase separation within a block copolymer, poly(A)-*b*-poly(B). A more detailed examination of the miscibility of block copolymers can be found in the Flory-Huggins-Theory. The Flory-Huggins interaction parameter, χ, can be used to express the interaction of two polymers. Thereby, the enthalpy term, $\Delta H_{mix,m}$, can be written as:[1]

$$\Delta H_{mix,m} = R \cdot T \cdot \chi \cdot \phi_A \cdot \phi_B \quad \textbf{(2)}$$

R represents the universal gas constant and ϕ_A and ϕ_B refer to the volume fractions of each block. **Equation 3** describes the dependency of χ, on the interaction energies of each possible monomer pair, ε_{AA}, ε_{BB} and ε_{AB}. The number of neighboring monomer units is expressed by the parameter z and k_B is the Boltzmann constant.[2]

$$\chi = \left(\frac{z}{k_B \cdot T}\right) \cdot \left[\varepsilon_{AB} - \frac{1}{2}(\varepsilon_{AA} + \varepsilon_{BB})\right] \quad \textbf{(3)}$$

In accordance with **Equation 4**, the entropic effect loses significance with increasing degree of polymerization (N_A and N_B). Notably, the term gains a stronger influence with higher

temperatures, see **Equation 1**, which is the reason why some copolymers transform into the disordered state (DIS) at elevated temperatures.[1]

$$\Delta S_{\mathrm{mix,m}} = -R\left(\frac{\phi_{\mathrm{A}}}{N_{\mathrm{A}}}\cdot \ln\phi_{\mathrm{A}} + \frac{\phi_{\mathrm{B}}}{N_{\mathrm{B}}}\ln\phi_{\mathrm{B}}\right) \quad \textbf{(4)}$$

Hence, the phase separation of a block copolymer is favored with a higher Flory-Huggins interaction parameter and higher degree of polymerization, usually expressed by the product, χN. Whereas the parameter χ is a constant for each copolymer combination, N can be tailored by the molar mass of the polymer. Mean-field predictions show that a value of $(\chi N)_{\mathrm{ODT}} \sim 10.5$ reflects the order-disorder transition (ODT) of a symmetric diblock copolymer.[3] The morphology of a block copolymer is mainly dependent on the volume fractions of the two blocks A and B as well as the extent of incompatibility of both blocks. If a strongly segregated linear block copolymer, poly(A)-*b*-poly(B), with a minority fraction of poly(A) is examined, a spherical (S) morphology of poly(A) in a continuous phase of the respective other block is obtained. Exceeding ~13 vol% of poly(A) leads to hexagonal ordered cylindrical (H) morphology and above ~30 vol% a lamellar (L) alignment is obtained. Eventually, poly(B) becomes the minority fraction, and the morphologies are obtained in a reversed manner.[11] **Figure 2** shows a theoretical phase diagram and the different possible morphologies of a linear AB-diblock copolymer. The disordered state (DIS) describes miscibility of the two polymer blocks and the absence of phase separation.

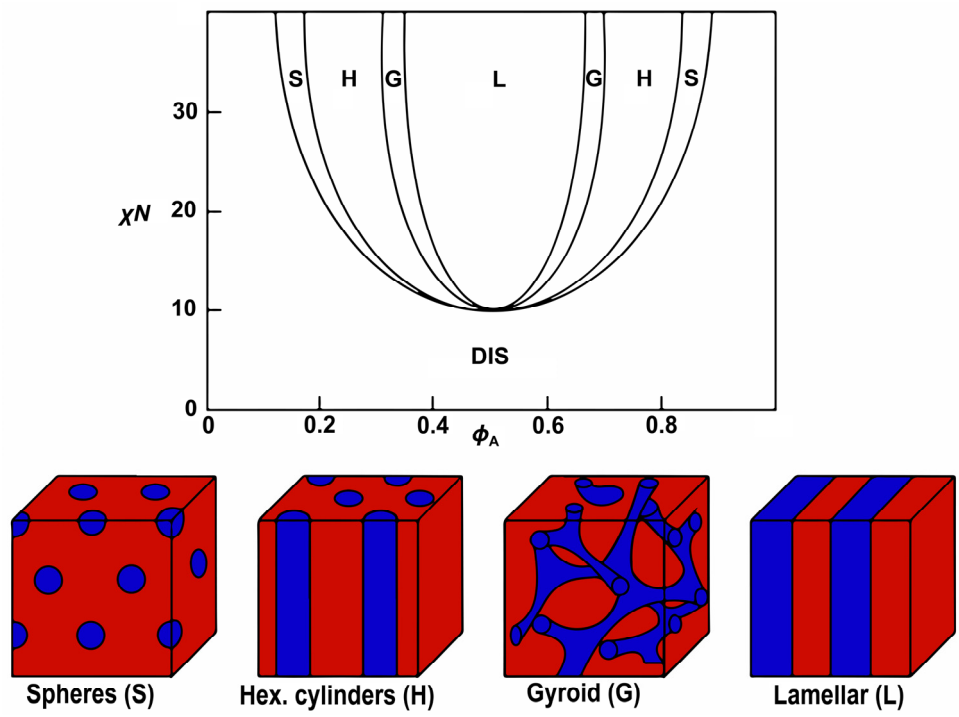

Figure 2. Phase diagram of a poly(A)-*b*-poly(B) block copolymer indicating the different possible morphology dependent on the volume fraction of the polymer block A, ϕ_{A}, and the product χN. Graphic modified from ©2022 Katsuhiro Endo, *Springer Nature*, licensed under CC BY 4.0.[12]

While branched structures result in shifts of this theoretical phase diagram due to curvature at the interface of the blocks, linear ABA-triblock copolymers are found to follow a similar phase diagram as simple AB-diblocks.[13],[14] At comparable chain length and composition, triblock copolymers are generally weaker ordered compared to diblocks due to a significantly reduced conformational entropy as two block-junctions need to be located at the domain boundary.[15] In addition, the triblock copolymers bear the abovementioned advantage of flexible bridging of the vitrified, high T_g polymer domains. Thereby, a new class of materials can be obtained, namely thermoplastic elastomers (TPEs).

Thermoplastic Elastomers

TPEs combine features of the two general polymer classes: thermoplastics and elastomers. On the one hand, thermoplastics can be easily processed as the individual polymer chains can rearrange themselves when exceeding a polymer-characteristic temperature. For amorphous thermoplastics this is the glass temperature (T_g), whereas crystalline or semi-crystalline polymers also have a melting point (T_m) that has to be considered. Elastomers on the other hand, are covalently crosslinked polymer chains, consisting of low T_g materials. The downside of elastomers is that reshaping or processing is impossible, as they have to be cured in the final shape of their application. Both features, thermal processing and elasticity due to cross-links, can be found in TPEs, albeit avoiding covalent chain links.

The origin of these properties is the abovementioned physical cross-linking and bridging of phase separated ABA-triblock copolymers. To yield TPE properties, poly(A) must have a high T_g, e.g. polystyrene (PS), and poly(B) should possess a low T_g, as is the case for polybutadiene (PB). Thereby, the poly(A) domains are vitrified at the application temperature, whereas the linked poly(B) domains lead to elasticity, enhanced further by their entanglements. Thus, the covalent cross-linking usually present in elastomers is replaced by physical cross-linking through the vitrified poly(A)-domains. These physical cross-links are reversible and heating the material above the T_g of the glassy high T_g domains allows for the use of standard thermal processing techniques of the thermoplastic industry, i.e., extrusion and injection molding. This also offers potential recyclability and reprocessing.[16],[17] Nevertheless, some disadvantages of the TPE concept should be mentioned. For example, the temperature range for utilization is restricted by the T_gs of the domains. For instance, classical styrene-butadiene-styrene (SBS)-TPEs can only be used up to a temperature of approximately 100 °C, which corresponds to the T_g of PS.[18] Other classical elastomers, e.g. silicones or butadiene rubber can withstand much more heat and are therefore still irreplaceable in applications which require a high heat resistance, e.g. use as tires, seals etc.[19] Further, the solubility of TPEs offers the advantage of solvent casting, but also leads to the disadvantage of poor solvent resistance.

The synthesis of TPEs requires a certain extent of control of structural parameters to obtain block copolymers. Therefore, chain growth polymerizations, e.g. carbanionic polymerization, are usually carried out using sequential monomer addition steps to generate $A(BA)_n$ block structures, see **Figure 3**. Developing more efficient pathways is a crucial field of research. For instance, some monomer combinations are known to yield block-like "tapered" copolymers *via* statistical copolymerization. Under specific reaction condition, one monomer is incorporated faster. This leads to the formation of a polymer chain region rich in monomer A, and eventually a pure monomer-B polymer chain end when monomer A is fully consumed. These copolymers are usually referred to as tapered (general gradient) copolymers, poly(A)-*grad*-poly(B). Clearly, the synthesis of tapered block copolymers is more economic and efficient than sequential block copolymers, as they require fewer reaction steps.[20] They may even be advantageous, as they show better processability due to a lowered order-disorder temperature.[21] Since the nature of the gradient plays a crucial role, a detailed introduction to copolymerization kinetics is given later in this section.

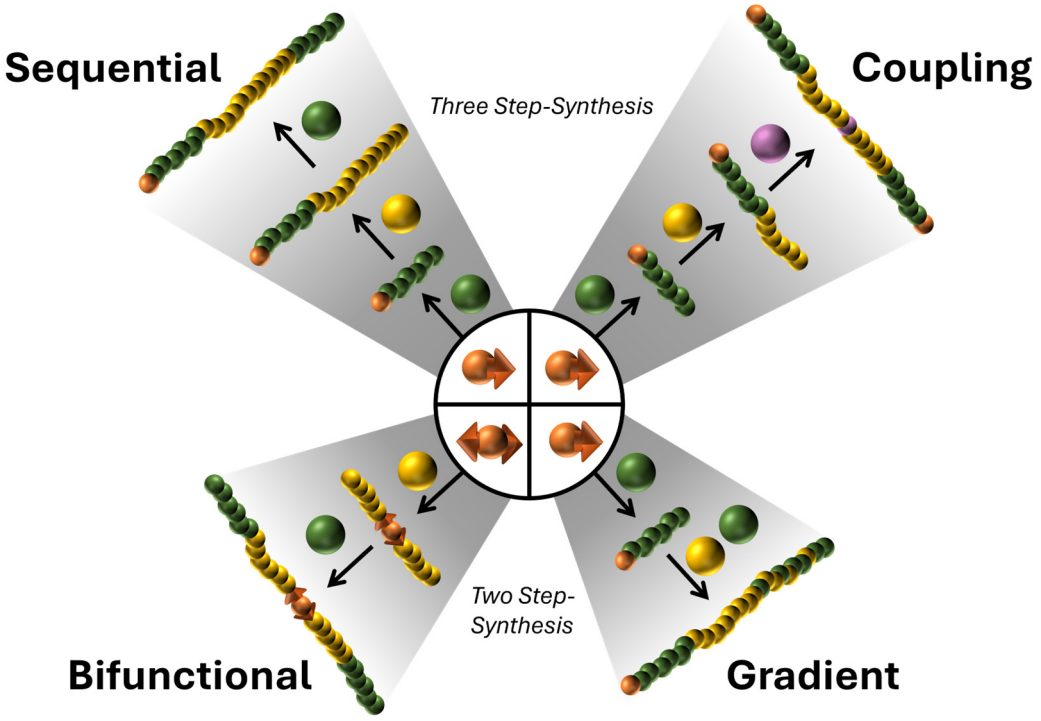

Figure 3. Different possible pathways to ABA-triblock copolymers in the field of carbanionic polymerization.

Another pathway comprises a coupling agent that can be introduced to a living polymerization of a diblock polymer to form the respective triblock. This is already an established route in industry to not only yield linear but branched and star structures by using di-, tri- or multi-functional coupling reagents.[22],[23] As another alternative shown in **Figure 3**, a bifunctional initiator can be used to reduce the required monomer addition steps further.

Bifunctional Initiators

The higher efficiency of the synthesis sequence when utilizing a bifunctional initiator for the synthesis of triblock structures has resulted in great interest in this specific pathway. In addition, it enables the synthesis of some monomer sequences that are not accessible by sequential monomer addition due to the vast differences of nucleophilicity of several monomer types. A polymethylmethacrylate (PMMA) anion is not sufficiently nucleophilic to initiate 1,3-dienes, whereas *vice versa* synthesis of such blocks is feasible. Therefore, bifunctional initiators can be used to access PMMA-*b*-PB-*b*-PMMA triblock copolymers.[24]

Some of the very first initiator systems in the field of living anionic polymerization are indeed bifunctional initiators, such as sodium/naphthalene.[25] As this particular initiator is limited to a polar solvent, e.g. tetrahydrofuran (THF), the relevance for the synthesis of butadiene or isoprene based TPEs is limited due to the strong effect of the polarity of the solvent on the resulting polymers' properties.[26] The increased polarity leads to a change in microstructure of 1,3-dienes and increases the T_g to a point that it is unsuitable for any application. A detailed explanation of the effect of the solvent polarity on the microstructure can be found in **Chapter 1**.

To assure a low T_g for polydienes, e.g. polybutadiene and polyisoprene, apolar solvents are therefore indispensable. However, this causes a conflict with most bifunctional initiators, as these tend to aggregate in non-polar solvents or even precipitate, i.e. become insoluble. This results in either broad distributions of the polymers or even disable any polymer formation.

Different approaches have been described in literature to circumvent the formation of aggregates in the case of bifunctional initiators. The *seeding technique,* for instance, relies on a sequential addition of monomers to first form oligomers with an increased solubility, adding the majority of monomer in a second addition step.[22],[27] The downside of this approach is a broadening of the molecular weight distribution.[28]

Another approach is to incorporate sterically demanding groups, e.g. phenyl groups, into the dilithiated initiator structure to prevent the formation of aggregates. In this context, multiple derivatives of the general structure of 1,3-di-(1-phenylethenyl)benzene (PEB) were introduced, see **Figure 4**b.[29] – [34] They are converted to the respective dilithiated structure by the addition of two equivalents of butyl lithium (BuLi), i.e. *sec*- and *tert*-BuLi as shown in **Figure 4**a. The formation of the benzylic anion is desired, as homopolymerization is impossible due to bulkiness of the phenyl substituents. Despite several successful reports on the utilization of these structures, doubt has been expressed, whether high control can be achieved and that most probably multifunctional or monofunctional side products are always

present.[28],[35],[36] Some reports on an enhanced performance upon the addition of polar modifiers, e.g. triethylamine, have been published, albeit with the downside of an increased vinyl content within the 1,3-diene polymerization. This effect of polar modifiers was described for the rather simple structure, 1,3-diisopropenyl benzene (DIB), which was successfully used to synthesize ABA-triblock copolymers from polybutadiene and polymethylmethacrylates.[24],[37] – [40]

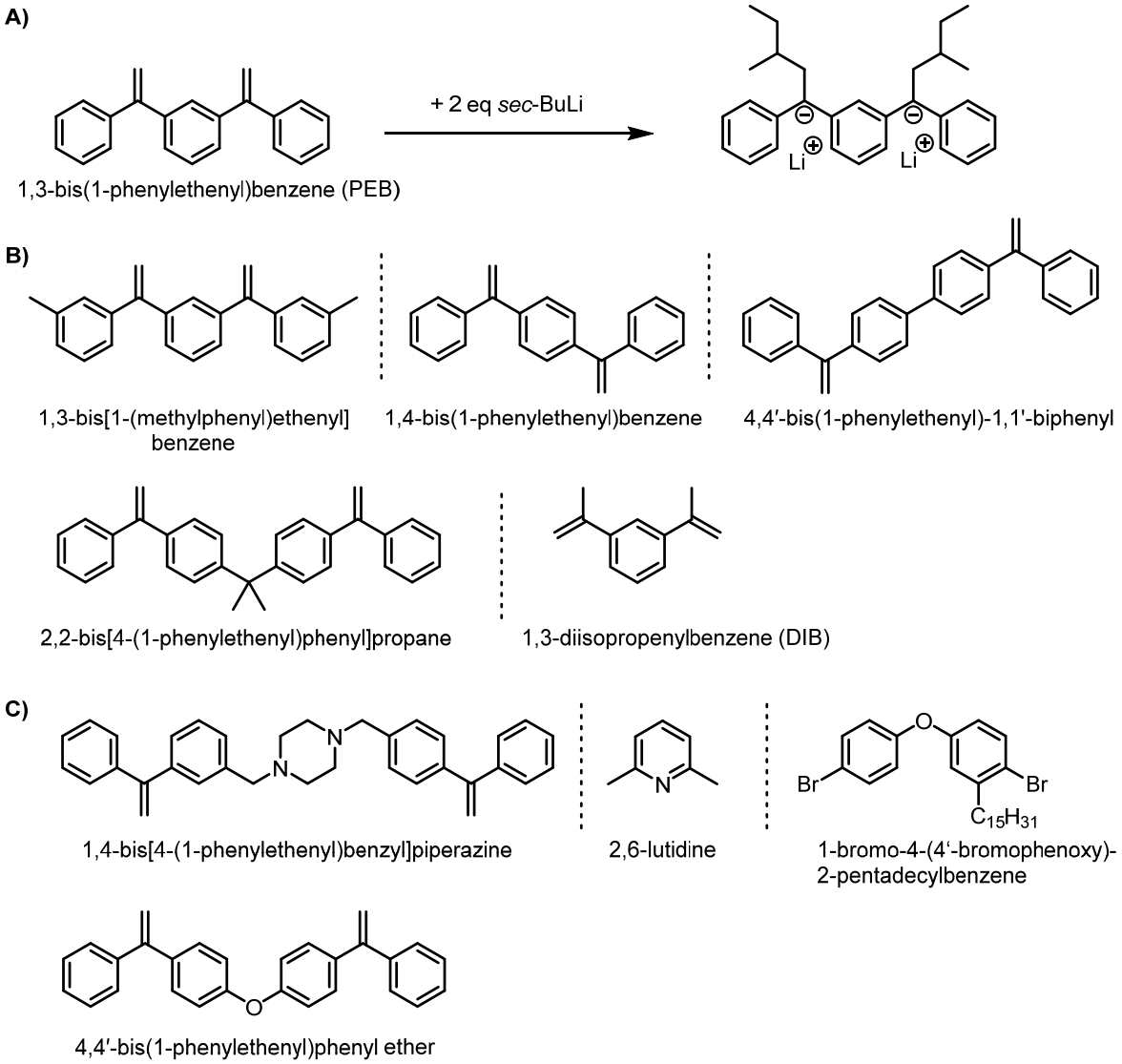

Figure 4. Overview of different bifunctional initiators for the carbanionic polymerization: A) general activation pathway of 1,3-bis(1-phenylethenyl)benzene[29]; B) pure hydrocarbon structures (1,3-bis[1-(methylphenyl)ethenyl]benzene[31], 1,4-bis(1-phenylethenyl)benzene[32], 4,4′-bis(1-phenylethenyl)-1,1′-biphenyl[33], 2,2-bis[4-(1-phenylethenyl)phenyl]propane[29], 1,3-diisopropenylbenzene[34]); C) structures containing hetero atoms (4,4′-bis[(1-phenylethenyl)phenyl] ether[41], 1,4-bis[4-(1-phenylethenyl)benzyl] piperazine[30], 2,6-lutidine[42], 1-brom-4-(4'-bromphenoxy)-2-pentadecylbenzol[43]).

If the synthesis and the required application allow the use of polar solvents the synthesis gets more controlled. For example, naphthalene lithium in THF can be used to synthesize α,ω-epoxidized polyisoprene *via* controlled end-functionalization with epichlorohydrin. Likewise, propylene oxide can be used to introduce hydroxyl groups simultaneously at both chain ends to yield a α,ω-diols.[26],[44] These structures are highly valuable precursors for subsequent polymerization, i.e., polyurethane synthesis, graft-polymers or epoxy-based networks.[45],[46]

Recently, bifunctional initiators were successfully designed for pure hydrocarbon solvents, which are somehow different in structure, as they also comprise hetero atoms in their framework. Consequently, the di-lithiated structures are kept in solution by the intrinsically increased polarity of the structures, see **Figure 4**c. Highly efficient bifunctional initiators are accessible, albeit with the drawback of a very demanding synthesis route of the structures, limiting their industrial use.[30],[43] In addition, the introduction of polar groups enhances the formation of vinyl content in a similar way to the addition of external modifiers, e.g., the amine in 2,6-lutidine yields a 1,4-content in PI of 50%, whereas pure hydrocarbon systems yield ~93%.[42]

The utilization of bifunctional initiators in industry is mentioned in several patents by Kraton and BASF, but their actual commercial use for the synthesis of ABA-triblocks has not been confirmed.[47],[48]

Kinetics of Homopolymerizations and Copolymerizations

The knowledge of the kinetics, i.e. reaction rates and elementary steps, of a polymerization is vital to gain a full picture of the polymerization mechanism and resulting polymer properties, e.g., molar mass and distribution. For example, a broad dispersity of ~1.3 in the field of living polymerization is often associated with slow initiation.[49] An accurate investigation of a polymerization kinetics can be used to prove such an assumption. Moreover, the synthesis of sequential block copolymers, i.e. multiblock copolymers, require precise knowledge of the polymerization kinetics to ensure complete monomer consumption before the next monomer addition step.[50] In general, an anionic polymerization can be described by the decrease in monomer concentration over time (t), the rate constant (k_p) and the numbers of active chains – equal to the initiator concentration ($[Ini]_0$), see **Equation 5**. The initial monomer concentration is expressed as ($[M]_0$).

$$\frac{d[M]_0}{dt} = k_p \cdot [M]_0 \cdot [Ini]_0 \quad \textbf{(5)}$$

The "livingness" of a controlled polymerization is indicated by the absence of any termination or transfer reaction. Thereby, the $[Ini]_0$ is assumed to be constant, indicating pseudo-first order kinetics. The experimentally accessible apparent rate constant, k_{app}, can be transferred to the general rate constant (k_p) using:

$$k_p = \frac{k_{app}}{[Ini]^{1/n}} \quad \textbf{(6)}$$

The exponent, $1/n$, associated with the degree of aggregation (n) will be discussed further below. The differential equation can then be expressed as follows:

$$\frac{d[M]_0}{dt} = k_{app} \cdot [M]_0 \quad \textbf{(7)}$$

A linear logarithmic plot following **Equation 8** can be used to determine the apparent rate constant from the slope of the fit.

$$\ln\left(\frac{[M]_t}{[M]_0}\right) = k_{app} \cdot t \quad \textbf{(8)}$$

The half-life time ($t_{1/2}$) in case of pseudo-first order kinetics can therefore be expressed by:

$$t_{1/2} = -\frac{\ln(2)}{k_{app}} \quad \textbf{(9)}$$

To obtain a comparable value for different polymerizations, the apparent rate constant can be related to the $[Ini]_0$ of the polymerization. Most carbanionic polymerizations have an equilibrium of formed aggregates of the active chain ends, which affects the kinetics of the polymerization.[51] As only the unimeric structures can proceed in the propagation, this equilibrium is expressed by the following **Scheme 1**, where n is the degree of aggregation and K_{agg} /K_{diss} are the equilibrium constants of aggregation and dissociation.

Scheme 1. Propagation mechanism of a living carbanionic polymerization of monomer A indicating the aggregation equilibrium.

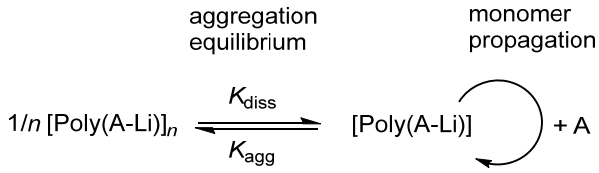

The general rate constant, k_p, contains the usually unknown K_{agg}, the degree of aggregation and the unknown monomer propagation rate constant of the non-aggregated chains, k_p'.

$$k_p = k_p' \cdot \left(K_{agg}\right)^{-1/n} \quad \textbf{(10)}$$

To determine the number of aggregated species, **Equation 6** can be transferred to a linear double logarithmic plot. Apparent rate constants at different $[Ini]_0$ have to be determined experimentally. The slope of the respective plot, **Equation 11**, gives the reverse degree of association. The well-studied monomer styrene forms dimers in hydrocarbon solvents, whereas the 1,3-dienes butadiene and isoprene, have been reported to form tetramers that transform to dimers at lower concentrations.[52],[53]

$$\ln(k_{app}) = \frac{1}{n} \cdot \ln([Ini]) + \ln(k_p) \quad \textbf{(11)}$$

The rate constants dependency on the temperature (T), the pre-exponential factor (A) and the activation energy (E_A) can be expressed by the Arrhenius **Equation 12**.

$$k_p = A \cdot e^{-\frac{E_A}{R \cdot T}} \quad \textbf{(12)}$$

The plot of the logarithmic apparent rate constant ($\ln(k_p)$) versus T^{-1} can be used to determine the E_A from its slope, see **Equation 13**. R refers to the molar gas constant.

$$\ln(k_p) = \ln(A) - \frac{E_A}{R} \cdot T^{-1} \quad \textbf{(13)}$$

Moving from homopolymerization to copolymerization increases the complexity of the kinetic investigation, as different possible pathways must be considered. In **Figure 5** all four possible pathways of an anionic copolymerization are illustrated. They comprise the homo-propagation of each monomer, M_1 and M_2, which are associated with the respective propagation rates, k_{11} and k_{22}. Cross-propagation, i.e. the change of a M_1-chain end to a M_2-chain end are described with the cross-propagation rates, k_{12} and k_{21}.

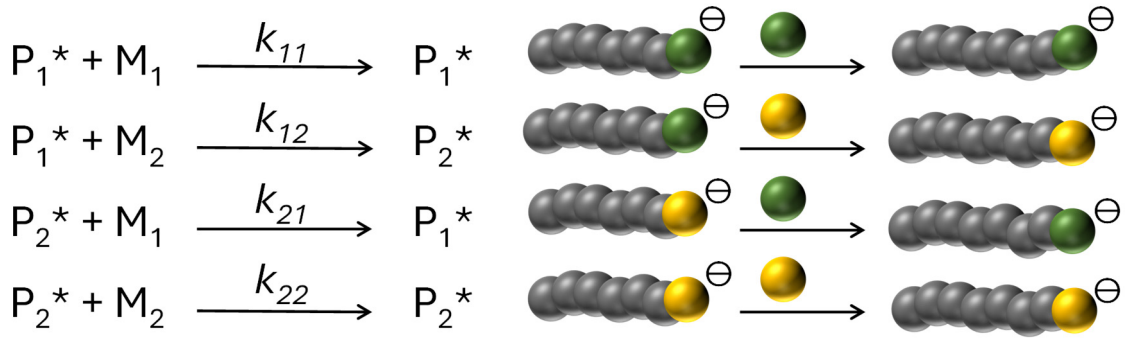

Figure 5. Possible reaction steps in a living anionic copolymerization indicating the propagation rate constants, k_{11} and k_{22} as well as the different crossover constants, k_{12} and k_{21}, visualizing the active chain ends monomer by color, adapted from Steube et al.[54]

The relation of these different pathways can be expressed by the reactivity ratios, r_1 and r_2. They are defined as the quotient of the homo-propagation rate constants and the cross-propagation rate constants:

$$r_1 = \frac{k_{11}}{k_{12}}; \quad r_2 = \frac{k_{22}}{k_{21}} \tag{14}$$

Different models were reported for the determination of these reactivity ratios. Varying assumptions can be made to reduce the complexity of the kinetic investigation. For instance, the Jaacks[55] equation, **Equation 15**, can be used to determine the reactivity ratios from the individual monomer consumption, assuming that the chain ends' nature has no influence on the propagation.

$$\log\frac{[\mathrm{M_1}]_t}{[\mathrm{M_1}]_0} = r_1 \cdot \log\frac{[\mathrm{M_2}]_t}{[\mathrm{M_2}]_0}; \qquad r_2 = 1/r_1 \tag{15}$$

Therefore, this model is referred to as a "non-terminal", or ideal model. The individual active chain ends [P_1*] and [P_2*] can be simplified to [P*], and the four possible rate constants are reduced to just two:

$$k_{11} = k_{21} = k_1\,;\; k_{12} = k_{22} = k_2 \tag{16}$$

The individual monomer consumption can be written as shown in **Equations 17** and **18**. Solving these differential equations gives **Equation 19** that can be expressed in a logarithmic form and is referred to as the abovementioned Jaacks-fit, **Equation 15**.

$$\frac{\mathrm{d}[\mathrm{M_1}]}{\mathrm{d}t} = k_1[\mathrm{P^*}][\mathrm{M_1}] \tag{17}$$

$$\frac{\mathrm{d}[\mathrm{M_2}]}{\mathrm{d}t} = k_2[\mathrm{P^*}][\mathrm{M_2}] \tag{18}$$

$$\frac{\mathrm{d}[\mathrm{M_1}]}{\mathrm{d}[\mathrm{M_2}]} = r_1\frac{[\mathrm{M_1}]}{[\mathrm{M_2}]} \tag{19}$$

A more complex terminal model was described by Meyer and Lowry in 1965 with the restriction: $r_1 \neq 1$; $r_2 \neq 1$, see **Equation 22**.[56] Based on the general concept for the reactivity ratios and monomer consumption, introduced by Mayo and Lewis in 1944, **Equation 20**,[57] its integrated form can be used to yield the reactivity ratios.

$$\frac{\mathrm{d}[\mathrm{M_1}]}{\mathrm{d}[\mathrm{M_2}]} = \frac{[\mathrm{M_1}](r_1[\mathrm{M_1}]+[\mathrm{M_2}])}{[\mathrm{M_2}]([\mathrm{M_1}]+r_2[\mathrm{M_2}])} \tag{20}$$

Using the definition of the monomer feed, f_1, **Equation 21**, the integrated form can be expressed as followed:

$$f_1 = \frac{[M_1]}{[M_1]+[M_2]}; \qquad f_{1,0} = \frac{[M_1]}{[M_1]+[M_2]} \tag{21}$$

$$\frac{[M]}{[M]_0} = \left(\frac{f_1}{f_{1,0}}\right)^{\frac{r_2}{1-r_2}} \cdot \left(\frac{f_2}{f_{2,0}}\right)^{\frac{r_1}{1-r_1}} \cdot \left(\frac{f_{1,0}-\left(\frac{1-r_2}{2-r_1-r_2}\right)}{f_1-\left(\frac{1-r_2}{2-r_1-r_2}\right)}\right)^{\frac{1-r_1r_2}{(1-r_1)(1-r_2)}} \tag{22}$$

The reactivity ratios can then be extracted from non-linear fitting. Researchers agree that a model with the least number of parameters should be used to reduce the probability of overfitting.[54],[58] – [60] Therefore, the ideal, non-terminal model, e.g. Jaacks-fit, should be considered first. If the data deviates from the linearity of this fit, the more complex terminal models, e.g. Meyer-Lowry, should be used.

In the past, the determination was difficult because monitoring of the monomer consumption *via* sampling was complex, and calculation tools were limited. Modern *in-situ* methods for direct tracking of monomer consumption and computational assisted calculation tools have simplified the determination of reactivity ratios of copolymerizations. Several analytic methods were introduced to track the monomer conversions in real time. For example, *in situ* near infrared (NIR)[61],[62] and mid-IR[63] spectroscopy and *in situ* NMR[64],[65] spectroscopy are known to give access to copolymerization kinetics. These differ in their implementation possibilities, their advantages and disadvantages.

In situ NMR, for instance, is a very fast and obvious method to gain precise data regarding individual monomer consumption, which requires only small quantities of the samples. One disadvantage is, that the polymerizations are restricted to the scale of an NMR-tube limiting various reaction parameters, e.g. concentration, molar mass and temperature. Further, to obtain reliable and quantitative results, the intervals between data points are restricted by the relaxation delay of the protons under investigation. Consequently, only few data points can be monitored for very fast reactions. Despite being an established procedure, *in situ* NMR kinetics of a "living" carbanionic polymerization requires precise consideration due the high reactivity of the highly nucleophilic carbanions.

In comparison to *in situ* NMR techniques, the NIR method has the advantage of not being limited to a specific reaction vessel. The sensor can be built in various set-ups, e.g. reaction flasks or reactors, and therefore allows for a much broader scope of adjustable reaction parameters. Additionally, the polymerization reactions can be performed under process monitoring in scale-up and pilot scale reactors, to evaluate the kinetics-properties relations. The downside is that the minimum scale set by the sensor size is considerable larger compared to a 5 mm NMR-tube, which makes handling and rection set-ups more complex and more time-consuming. Both techniques require a high level of technical considerations in case of the

carbanionic (co)polymerization to ensure an absolutely inert environment, which is key for this sensitive polymerization technique. However, in recent years both techniques have led to a detailed understanding of gradients and reactivity ratios in the living anionic copolymerization.

References

[1] Utracki, L. A.; Favis, B. D. Polymer Alloys and Blends. In *Composites and specialty applications*; Cheremisinoff, N. P., Ed.; Handbook of polymer science and technology, vol 4; Marcel Dekker, **1989**; pp 121‑185.

[2] Godwin, A. D. Plasticizers. In *Applied Plastics Engineering Handbook*; Elsevier, **2024**; pp 595‑618.

[3] Mascia, L.; Xanthos, M. An overview of additives and modifiers for polymer blends: Facts, deductions, and uncertainties. *Adv Polym Technol*, **1992**, *11* (4), 237‑248.

[4] Anderson, K.; Schreck, K.; Hillmyer, M. Toughening Polylactide. *Polymer Revs.*, **2008**, *48* (1), 85‑108.

[5] Jacobsen, S.; Fritz, H. G. Plasticizing polylactide? the effect of different plasticizers on the mechanical properties. *Polym. Eng. Sci.*, **1999**, *39* (7), 1303‑1310.

[6] Eales, J.; Bethel, A.; Galloway, T.; Hopkinson, P.; Morrissey, K.; Short, R. E.; Garside, R. Human health impacts of exposure to phthalate plasticizers: An overview of reviews. *Environment international*, **2022**, *158*, 106903.

[7] Paul, D. R.; Barlow, J. W. Polymer Blends. *Journal of Macromolecular Science, Part C*, **1980**, *18* (1), 109‑168.

[8] Elias, H.-G. *An introduction to polymer science*, 1. ed.; VCH, **1997**.

[9] Mai, Y.; Eisenberg, A. Self-assembly of block copolymers. *Chemical Society reviews*, **2012**, *41* (18), 5969‑5985.

[10] Glaser, J.; Medapuram, P.; Beardsley, T. M.; Matsen, M. W.; Morse, D. C. Universality of block copolymer melts. *Physical review letters*, **2014**, *113* (6), 68302.

[11] Matsen, M. W.; Schick, M. Self-assembly of block copolymers. *Current Opinion in Colloid & Interface Science*, **1996**, *1* (3), 329‑336.

[12] Endo, K.; Matsuda, Y.; Tanaka, S.; Muramatsu, M. A phase-field model by an Ising machine and its application to the phase-separation structure of a diblock polymer. *Scientific reports*, **2022**, *12* (1), 10794.

[13] Matsen, M. W. Effect of Architecture on the Phase Behavior of AB-Type Block Copolymer Melts. *Macromolecules*, **2012**, *45* (4), 2161‑2165.

[14] Hadjichristidis, N.; Iatrou, H.; Behal, S. K.; Chludzinski, J. J.; Disko, M. M.; Garner, R. T.; Liang, K. S.; Lohse, D. J.; Milner, S. T. Morphology and miscibility of miktoarm styrene-diene copolymers and terpolymers. *Macromolecules*, **1993**, *26* (21), 5812‑5815.

[15] Mai, S.-M.; Mingvanish, W.; Turner, S. C.; Chaibundit, C.; Fairclough, J. P. A.; Heatley, F.; Matsen, M. W.; Ryan, A. J.; Booth, C. Microphase-Separation Behavior of Triblock Copolymer Melts. Comparison with Diblock Copolymer Melts. *Macromolecules*, **2000**, *33* (14), 5124‑5130.

[16] Holden, G. *Understanding thermoplastic elastomers*; Hanser understanding books; Hanser, **2000**.

[17] Banerjee, S. S.; Bhowmick, A. K. High-temperature thermoplastic elastomers from rubber-plastic blends: A state-of-the-art review. Rubber Chemistry and Technology, 90(1), 1-36. *Rubber Chem. Technol.*, **2017**, *90* (1), 1‑36.

[18] Fox, T. G.; Flory, P. J. The glass temperature and related properties of polystyrene. Influence of molecular weight. *Journal of Polymer Science*, **1954**, *14* (75), 315‑319.

[19] Shit, S. C.; Shah, P. A Review on Silicone Rubber. *Natl. Acad. Sci. Lett.*, **2013**, *36* (4), 355‑365.

[20] Beginn, U. Gradient copolymers. *Colloid Polym Sci*, **2008**, *286* (13), 1465‑1474.

[21] Barent, R. D.; Perevyazko, I.; Mikusheva, N.; Floudas, G.; Frey, H. Linear (IS) n I Multiblock Copolymers: Tailoring the Softness of Thermoplastic Elastomers by Flexible Polyisoprene End Blocks. *Macromolecules*, **2023**, *56* (15), 5792‑5802.

[22] Knoll, K.; Nießner, N. Styrolux + and styroflex + - from transparent high impact polystyrene to new thermoplastic elastomers: Syntheses, applications and blends with other styrene based polymers. *Macromol. Symp.*, **1998**, *132* (1), 231‑243.

[23] Polymeropoulos, G.; Zapsas, G.; Ntetsikas, K.; Bilalis, P.; Gnanou, Y.; Hadjichristidis, N. 50th Anniversary Perspective : Polymers with Complex Architectures. *Macromolecules*, **2017**, *50* (4), 1253‑1290.

[24] Yu, J. M.; Dubois, P.; Teyssié, P.; Jérôme, R. Syndiotactic Poly(methyl methacrylate) (sPMMA)−Polybutadiene (PBD)−sPMMA Triblock Copolymers: Synthesis, Morphology, and Mechanical Properties. *Macromolecules*, **1996**, *29* (19), 6090‑6099.

[25] Szwarc, M. 'Living' Polymers. *Nature*, **1956**, *178* (4543), 1168‑1169.

[26] Yoo, T.; Henning, S. K. Synthesis and Characterization of Farnesene-Based Polymers. *Rubber Chem. Technol.*, **2017**, *90* (2), 308‑324.

[27] Yu, Y. S.; Dubois, P.; Teyssié, P.; Jérôme, R. Difunctional Anionic Initiator Based on 1,3-Diisopropenylbenzene. 5. Effect of Polar Additives and Initiator Seeding on the Synthesis

of Poly(styrene- b -butadiene- b -styrene) Copolymers. *Macromolecules*, **1997**, *30* (24), 7356-7362.

[28] Bandermann, F.; Speikamp, H.-D.; Weigel, L. Bifunctional anionic initiators: A critical study and overview. *Makromol. Chem.*, **1985**, *186* (10), 2017-2024.

[29] Tung, L. H.; Lo, G. Y.-S.; Beyer, D. E. Dilithium Anionic Initiators Based on Double 1,1-Diphenylethylene Compounds. *Macromolecules*, **1978**, *11* (3), 616-617.

[30] Schultz, A. R.; Bobade, S.; Scott, P. J.; Long, T. E. Hydrocarbon-Soluble Piperazine-Containing Dilithium Anionic Initiator for High Cis -1,4 Isoprene Polymerization. *Macromol. Chem. Phys.*, **2018**, *219* (1), 1700201.

[31] Tung, L. H.; Lo, G. Y.-S. Studies on Dilithium Initiators. 1. Hydrocarbon-Soluble Initiators 1,3-Phenylenebis(3-methyl-1-phenylpentylidene)dilithium and 1,3-Phenylenebis[3-methyl-1-(methylphenyl)pentylidene]dilithium. *Macromolecules*, **1994**, *27* (8), 2219-2224.

[32] A. Yamagishi; M. Szwarc; L. Tung; Grace Y-S. Lo. Spectroscopic and Kinetic Studies of Addition of Double 1,1-Diphenylethylenes to Lithium Polystyryl in Benzene. *Macromolecules*, **1978**, *11* (3), 607-615.

[33] Rosser, R. W.; Neville, R. G. Disubstituted p -phenylene monomers. α-methyl- and α-phenyl-vinyl derivatives of benzene, biphenyl, p -terphenyl, and p , p ′-diphenoxiybiphenyl. *J. Appl. Polym. Sci.*, **1969**, *13* (1), 215-225.

[34] Beinert, G.; Lutz, P.; Franta, E.; Rempp, P. A bifunctional anionic initiator soluble in non-polar solvents. *Makromol. Chem.*, **1978**, *179* (2), 551-555.

[35] Bastelberger, T.; Höcker, H. Divinylidene compounds and their role as key compounds for the synthesis of blockcopolymers. *Angew. Makromol. Chemie*, **1984**, *125* (1), 53-67.

[36] Quirk, R. P.; Ma, J.-J. Dilithium initiators based on 1,3-bis(1- phenylethenyl)benzene. Tetrahydrofuran and lithium sec-butoxide effects. *Polym. Int.*, **1991**, *24* (4), 197-206.

[37] Foss, R. P.; Jacobson, H. W.; Sharkey, W. H. A New Difunctional Anionic Initiator. *Macromolecules*, **1977**, *10* (2), 287-291.

[38] Yu, Y.; Dubois, P.; Teyssié, P.; Jérôme, R. Difunctional Initiator Based on 1,3-Diisopropenylbenzene. 6. Synthesis of Methyl Methacrylate−Butadiene−Methyl Methacrylate Triblock Copolymers. *Macromolecules*, **1997**, *30* (15), 4254-4261.

[39] Yu, Y. S.; Dubois, P.; Jérôme, R.; Teyssié, P. Difunctional Initiators Based on 1,3-Diisopropenylbenzene. 3. Synthesis of a Pure Dilithium Adduct and Its Use as Difunctional Anionic Polymerization Initiator. *Macromolecules*, **1996**, *29* (8), 2738‑2745.

[40] Yu, J. M.; Dubois, P.; Jérôme, R. Synthesis and Properties of Poly[isobornyl methacrylate (IBMA)- b -butadiene (BD)- b -IBMA] Copolymers: New Thermoplastic Elastomers of a Large Service Temperature Range. *Macromolecules*, **1996**, *29* (23), 7316‑7322.

[41] Neville, R. G.; Rosser, R. W. Thermally stable polymer precursors. Diisopropenyl and bis (1-phenylvinyl) p -phenylene oxide monomers. *Die Makromolekulare Chemie*, **1969**, *123* (1), 19‑28.

[42] Ying, W. B.; Ko, N. Y.; Yao, C. K.; Kwak, N. H.; Zhang, R.; Lee, K. J.; Lee, B. A Convenient Dual-Side Anionic Initiator Based on 2,6-Luditine/s-Butyl Lithium. *Macromol. Res.*, **2019**, *27* (6), 601‑605.

[43] Matmour, R.; More, A. S.; Wadgaonkar, P. P.; Gnanou, Y. High performance poly(styrene-b-diene-b-styrene) triblock copolymers from a hydrocarbon-soluble and additive-free dicarbanionic initiator. *Journal of the American Chemical Society*, **2006**, *128* (25), 8158‑8159.

[44] Gao, B.; Sun, L.; Chen, X.; Zhai, X.; Zheng, J.; Ye, X.; Lu, J.; Feng, A.; Zhang, L. Preparation of bis-epoxy end capped macromonomers through anionic or RAFT polymerization. *J. Appl. Polym. Sci.*, **2022**, *139* (43).

[45] Haese, M. den; Gemoets, H. P. L.; van Aken, K.; Pitet, L. M. Fully biobased triblock copolymers generated using an unconventional oscillatory plug flow reactor. *Polym. Chem.*, **2022**, *13* (30), 4406‑4415.

[46] Zhang, J.; Chen, J.; Yao, M.; Jiang, Z.; Ma, Y. Hydrolysis-resistant polyurethane elastomers synthesized from hydrophobic bio-based polyfarnesene diol. *J. Appl. Polym. Sci.*, **2019**, *136* (25).

[47] Bronstert, K.; Knoll, K.; Haedicke, E. Living polymers, process for their preparation and their use for preparing telechelic polymers. EP19910115439 19910912.

[48] Willis, C. L.; Goodwin, D. E.; Haddix, G. W.; Tutunjian, P. N.; Cocchiara, J. P.; Atwood, H. E.; Stevens, C. A. Anionic Polymerization Diinitiator and Process for Preparing Same. US20070876596 20071022.

[49] Gold, L. Statistics of Polymer Molecular Size Distribution for an Invariant Number of Propagating Chains. *The Journal of Chemical Physics*, **1958**, *28* (1), 91‑99.

[50] Steube, M.; Johann, T.; Galanos, E.; Appold, M.; Rüttiger, C.; Mezger, M.; Gallei, M.; Müller, A. H. E.; Floudas, G.; Frey, H. Isoprene/Styrene Tapered Multiblock Copolymers with up to Ten Blocks: Synthesis, Phase Behavior, Order, and Mechanical Properties. *Macromolecules*, **2018**, *51* (24), 10246‑10258.

[51] Korotkov, A. A.; Chesnokova, N. N.; Trukhmanova, L. B. Polymerization of isoprene with a butyl lithium catalyst. *Polymer Science U.S.S.R.*, **1960**, *1* (1), 10‑20.

[52] Worsfold, D. J. Anionic copolymerization of styrene and isoprene in cyclohexane. *J. Polym. Sci. A-1 Polym. Chem.*, **1967**, *5* (11), 2783‑2789.

[53] Worsfold, D. J.; Bywater, S. Degree of Association of Polystyryl-, Polyisoprenyl-, and Polybutadienyllithium in Hydrocarbon Solvents. *Macromolecules*, **1972**, *5* (4), 393‑397.

[54] Steube, M.; Johann, T.; Barent, R. D.; Müller, A. H.; Frey, H. Rational design of tapered multiblock copolymers for thermoplastic elastomers. *Progress in Polymer Science*, **2022**, *124*, 101488.

[55] Jaacks, V. A Novel Method of Determination of Reactivity Ratios in Binary and Ternary Copolymerizations. *Makromol. Chem.*, **1972**, *161* (1), 161‑172.

[56] Meyer, V. E.; Lowry, G. G. Integral and differential binary copolymerization equations. *J. Polym. Sci. A Gen. Pap.*, **1965**, *3* (8), 2843‑2851.

[57] Mayo, F. R.; Lewis, F. M. Copolymerization. I. A Basis for Comparing the Behavior of Monomers in Copolymerization; The Copolymerization of Styrene and Methyl Methacrylate. *J. Am. Chem. Soc.*, **1944**, *66* (9), 1594‑1601.

[58] Roald Hoffmann; Vladimir I Minkin; Barry K Carpenter. Ockham's Razor and chemistry. *Bulletin de la Societe Chimique de France*, **1996**, *2* (133), 117‑130.

[59] Hawkins, D. M. The problem of overfitting. *J. Chem. Inf. Comput. Sci.*, **2004**, *44* (1), 1‑12.

[60] Beckingham, B. S.; Sanoja, G. E.; Lynd, N. A. Simple and Accurate Determination of Reactivity Ratios Using a Nonterminal Model of Chain Copolymerization. *Macromolecules*, **2015**, *48* (19), 6922‑6930.

[61] Miller, C. E.; Eichinger, B. E.; Gurley, T. W.; Hermiller, J. G. Determination of microstructure and composition in butadiene and styrene-butadiene polymers by near-infrared spectroscopy. *Anal. Chem.*, **1990**, *62* (17), 1778‑1785.

[62] Steube, M.; Johann, T.; Hübner, H.; Koch, M.; Dinh, T.; Gallei, M.; Floudas, G.; Frey, H.; Müller, A. H. E. Tetrahydrofuran: More than a "Randomizer" in the Living Anionic

Copolymerization of Styrene and Isoprene: Kinetics, Microstructures, Morphologies, and Mechanical Properties. *Macromolecules*, **2020**, *53* (13), 5512‑5527.

[63] Quinebèche, S.; Navarro, C.; Gnanou, Y.; Fontanille, M. In situ mid-IR and UV‑visible spectroscopies applied to the determination of kinetic parameters in the anionic copolymerization of styrene and isoprene. *Polymer*, **2009**, *50* (6), 1351‑1357.

[64] Obermeier, B.; Wurm, F.; Frey, H. Amino Functional Poly(ethylene glycol) Copolymers via Protected Amino Glycidol. *Macromolecules*, **2010**, *43* (5), 2244‑2251.

[65] Natalello, A.; Werre, M.; Alkan, A.; Frey, H. Monomer Sequence Distribution Monitoring in Living Carbanionic Copolymerization by Real-Time 1 H NMR Spectroscopy. *Macromolecules*, **2013**, *46* (21), 8467‑8471.

Chapter 3

Spotlight on Methyl *tert*-Butyl Ether: Unveiling Its Role in Living Anionic Polymerization

Moritz Meier-Merziger,[a] *Dominik A. H. Fuchs*,[a] *Holger Frey*,[a]* *and Axel H. E. Müller* [a]*

* Corresponding authors

[a] Department of Chemistry, Johannes Gutenberg University Mainz, Duesbergweg 10-14, 55128 Mainz, Germany

Published in: *Macromolecules* , **2024**, 57 (16), 8154-8161.
https://doi.org/10.1021/acs.macromol.4c01262

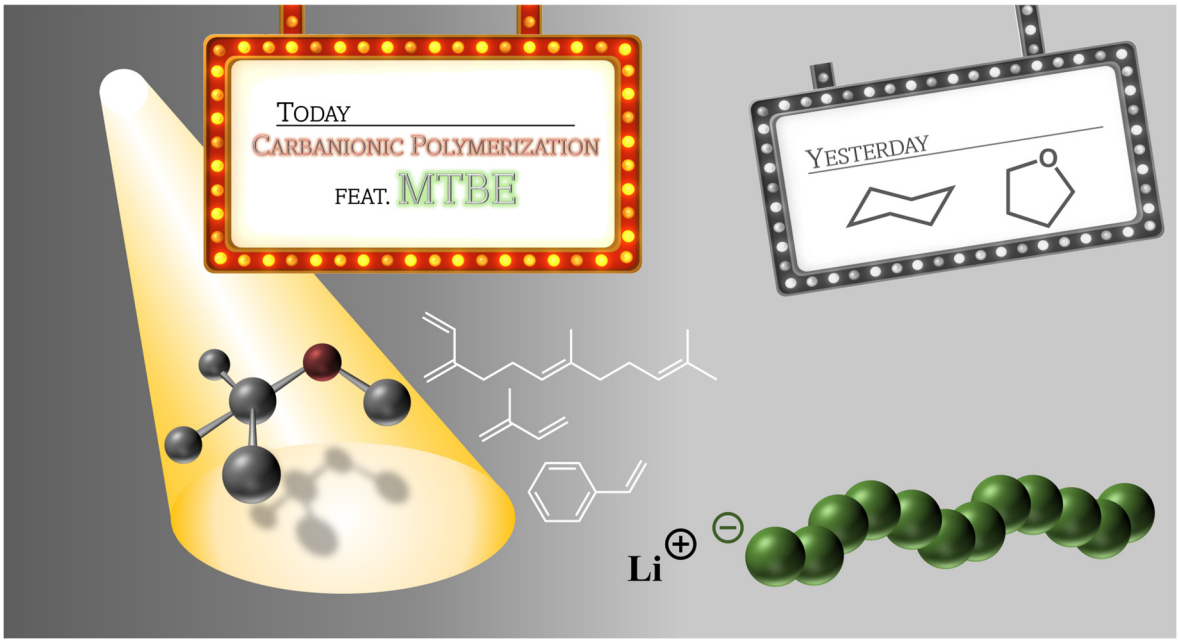

The following publication is adapted with permission from Meier-Merziger, M.; Fuchs, D. A. H.; Frey H.; Müller, A. H. E.; Spotlight on Methyl tert-Butyl Ether - Underrated or Overlooked? Unveiling Its Role for Living Anionic Polymerization, *Macromolecules*, **2024**, 57 (16), 8154-8161.

Abstract

The moderately polar solvent methyl *tert*-butyl ether (MTBE) was investigated as reaction medium for the carbanionic polymerization of the 1,3-dienes isoprene and *β*-farnesene. Key characteristics of MTBE, e.g., 50 times longer half-life of *n*-butyl lithium compared to tetrahydrofuran and polymerization rate constants were determined. *In situ* ^{1}H NMR kinetics showed a polymerization rate in MTBE in between the commonly utilized solvents cyclohexane and tetrahydrofuran for diene polymerization. Remarkably, the living polydienyl lithium chains in MTBE are predominantly present as non-aggregated unimers. The copolymerization of styrene and isoprene in cyclohexane with increasing MTBE fraction was investigated via *in situ* near-infrared kinetics. The gradient structure successively changes to random monomer incorporation and ultimately yields an inverted, yet still almost random incorporation in pure MTBE, reflected by the reactivity ratios r_S^{MTBE} = 1.82 and r_I^{MTBE} = 0.55. A spotlight is placed on the great potential of this highly available, albeit rarely used solvent for anionic polymerization.

Introduction

The choice of a solvent is often crucial in determining the success of a synthesis. This particularly applies to ionic polymerizations. In the case of carbanionic polymerization, the main requirement is a non-protic solvent and the strict absence of all protic impurities. Therefore, non-polar hydrocarbon solvents, e.g., alkanes, toluene or benzene, have been primarily used,[1],[2] some of which bear disadvantages. For example, transfer reactions were reported for toluene.[3] Carbanionic ion pairs form aggregates with lihium counterions, posing a well-known problem for the solubility of bifunctional initiators.[4]–[6] Thus, non-protic ether solvents, predominantly tetrahydrofuran (THF), have been used in this case. The better solvation of the counterion prevents formation of aggregates. However, the increased polarity affects the resulting microstructure, namely regio- and stereostructure, of a poly(1,3-diene) leading to a low extent of 1,4-incorporation and consequently an undesired high glass temperature (T_g) for, e.g. polybutadiene and polyisoprene. In addition, THF is notorious for its decomposition reactions with alkyl lithium compounds, limiting its use to low temperatures.[7] The half-life of *n*-butyl lithium in THF at 20 °C was reported to be just 107 min.[8] Finally, ether solvents are also known to form peroxides, restricting or even prohibiting their use in large-scale industrial processes.

Surprisingly, very little research has been published on the use of solvents of intermediate polarity for the anionic polymerization. One representative of this class is methyl *tert*-butyl ether (MTBE). One the one hand MTBE shows improved safety due to the absence of peroxide formation.[9] Secondly, one expects higher stability towards alkyl lithium compounds due to fewer protons in α-position as well as significant steric hindrance and moderate polarity, reflected by a dielectric constant, $\varepsilon^{MTBE} = 2.6$, in between the non-polar cyclohexane (CHx; $\varepsilon^{CHx} = 2.02$) and THF, $\varepsilon^{THF} = 7.6$.[10] – [12] Despite these advantages, MTBE has received surprisingly little attention, although it is readily available on large scale. In a few works MTBE was used as a polar modifier to modify the vinyl content of polybutadiene and to randomize the copolymerization of butadiene with styrene or divinylbenzene.[13]–[16] The addition of 40 equivalents of MTBE relative to *n*-BuLi in cyclohexane at 50 °C led to an increase of the vinyl content from ~7% to 28%.[13],[17] This effect is much weaker than the ~41% vinyl content reported for 45 equivalents of THF in hexane at 50 °C.[18] Another interesting feature of MTBE is its greater solvating strength for bifunctional initiators preventing aggregation.[19],[20] This is primarily relevant for diene monomers, for which the change in the resulting microstructure is not of great concern for their properties. This refers for instance to the microstructure-independent low T_g of polyfarnesene (PFar).[20],[21] Consequently, we recently introduced the bifunctional synthesis of fully bio-based thermoplastic elastomers in MTBE.[22],[23] The use of

MTBE as a neat solvent for carbanionic polymerization was reported in 1987 in a Czech patent, targeting the bifunctional synthesis of SBS rubber.[24]–[27] Surprisingly, this has been almost overlooked ever since.

Increasing awareness for sustainability has resulted in the examination of new bio-based solvents in recent years. For instance, Schlaad et al. introduced DL-limonene and 2-methyltetrahydrofuran (2-MeTHF) as more sustainable solvents for carbanionic polymerization.[28],[29] Other examples comprise the hydrogenated triterpene squalane, bearing a C_{30} framework, and cyclopentyl methyl ether.[30],[31] The drawback of these solvents is their limited accessibility, which makes large-scale application unlikely. MTBE, which is already available on large scale due to multiple industrial applications, e.g., as fuel component, is therefore much more attractive. Even though today's MTBE large-scale production relies on a fossil feedstock, the high demand has resulted in a variety of alternative bio-based production pathways. MTBE can be obtained from methanol, easily available in a sustainable manner, and isobutylene.[32] The latter can be synthesized from carbon dioxide and green hydrogen in the zirconium oxide catalyzed isosynthesis.[33]–[35] The process can also be operated with syngas from biomass or biomass can be used directly to afford isobutylene *via* fermentation.[36]–[39] Despite the many benefits, it is important to also be aware of the reported disadvantages of MTBE, such as health concerns linked to endocrine disruption and incompatibility with some established metalation reactions, e.g., Grignard reagent formation.[40],[41]

This work presents the first fundamental examination of MTBE as a solvent for carbanionic polymer synthesis. It covers an investigation on the stability towards alkyl lithium compounds in comparison to the established polar solvent THF. Further, the performance in the anionic polymerization is quantified and demonstrated by investigating the kinetics of the homopolymerization of isoprene and *β*-farnesene as well as the copolymerization of isoprene and styrene using increasing fractions of MTBE.

Results and Discussion

Stability of THF and MTBE Towards Butyl Lithium

To compare the stability of alkyl lithium compounds in THF and MTBE, the nucleophile *n*-butyl lithium (*n*-BuLi) was chosen. Its more widely used isomer, *sec*-BuLi, is not feasible for this investigation due to its rapid decomposition in THF even at lower temperatures (78 min at – 20 °C).[8] The reaction was investigated by *in situ* ^{1}H NMR kinetics at 20 °C by tracking the decrease of the methylene signal of *n*-BuLi at ~ -0.75 ppm, see **Figure S1** (Supporting

Information). **Figure 1a** shows that the concentration of *n*-BuLi decreases rapidly. The pseudo-first order plot of $\ln([BuLi]_0/[BuLi])$ vs time is linear with a half-life of 44 min. Detailed information on the NMR method is given in the **Supporting Information**.

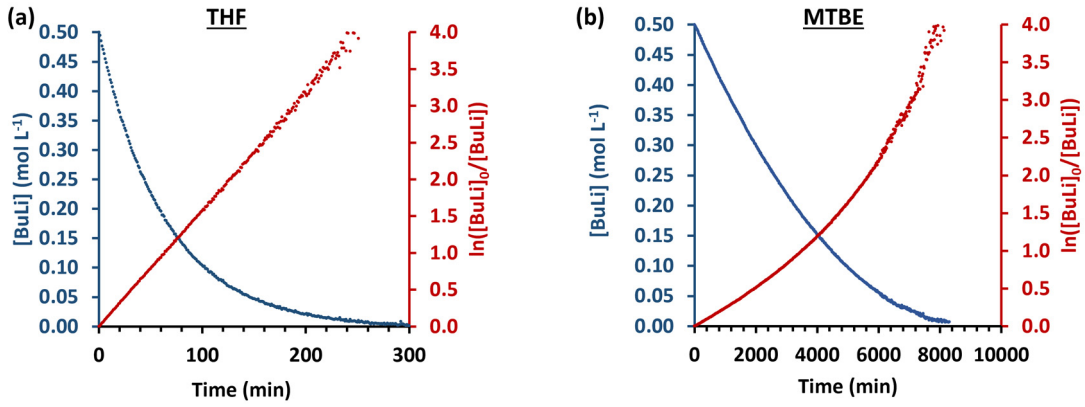

Figure 1. Decrease of *n*-BuLi concentration at 20 °C (blue), along with the pseudo-first order plot (red); (a) in THF, (b) in MTBE.

In contrast, the decomposition of MTBE is more than 50 times slower than THF, with a half-life of ~ 2600 min, see **Figure 1b** and **Figure S2**. Since neither the pseudo-first order, nor the pseudo-second order plot (1/[BuLi] vs time, **Figure S3**) follow a linear trend, the consumption of *n*-BuLi cannot easily be assigned to a specific kinetic order. We assume that a secondary process emerges during the decomposition of MTBE. As known in literature, the methoxy group of MTBE can be deprotonated under harsh conditions using *sec*-BuLi and potassium *tert*-butoxide.[42] This implies the following proposed reaction shown in **Scheme 1**.

Scheme 1. Proposed decomposition reaction of MTBE in the presence of *n*-BuLi.

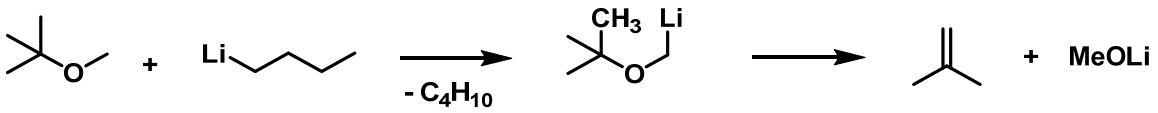

As a result, isobutylene and lithium methoxide are produced. Evidence for this can be found in the *in situ* ^{1}H NMR kinetics in **Figure S2**. While the characteristic *n*-BuLi signal at ca. -0.75 ppm decreases, new signals emerge at 4.7 ppm and 1.8 ppm. They can be attributed to the olefin and methyl signal of isobutylene, respectively. Their formation follows the expected integral ratio of two and six protons. Simultaneously, lithium methoxide is formed, in which we assume the origin of the deviating kinetics. Polar structures are known to affect the kinetics of carbanionic polymerization.[1],[43]

The far higher stability of MTBE compared to THF indicates that it is ideally suited as an alternative solvent for the carbanionic polymerization, as investigated in the following.

Kinetics of Polymerization of Isoprene in MTBE

The diene monomers isoprene and *β*-farnesene (Far) were investigated for their polymerization kinetics in MTBE. Isoprene is a commonly utilized monomer of which many data regarding polymerization rates, aggregation number, and polymer microstructure in classical solvents are known, rendering it highly suitable for comparison. *β*-Farnesene on the other hand, is much better suited for synthesis in polar media for its microstructure-independent low T_g.[20]

The polymerization of isoprene was performed at three different temperatures, 23 °C, 30 °C and 40 °C. Polymerizations were investigated using *in situ* ^{1}H NMR kinetic experiments following the decrease of the methine signal of isoprene at ~ 6.6 ppm, see **Figure S4**. **Figure 2a** shows the linear pseudo-first order plots indicating living polymerization of isoprene in MTBE.

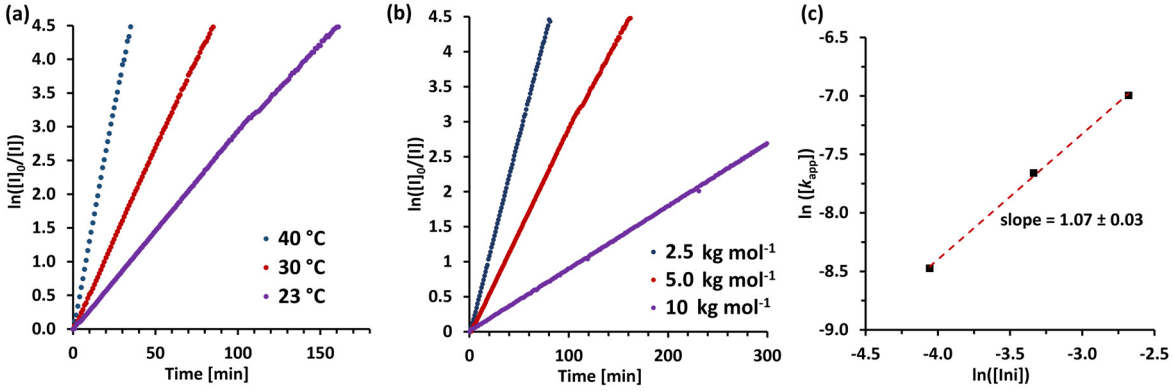

Figure 2. *In situ* ^{1}H NMR kinetics results of isoprene polymerization in MTBE using *sec*-BuLi as initiator; (a) pseudo-first-order plots at different temperatures at $[Ini]_0 \approx 35$ mmol L^{-1}; (b) pseudo-first-order plots using different $[Ini]_0$ at 23 °C; (c) double logarithmic plot of the apparent rate constants of isoprene at different initiator concentrations at 23 °C.

The apparent rate constant, k_{app}, is the slope of the pseudo first-order plot, and **Equation 1** renders the rate constant, k_p^{MTBE}, using the initiator concentration $[Ini]_0$ and the aggregation number *n*,

$$k_p = \frac{k_{app}}{[Ini]_0^{1/n}} \quad \textbf{(1)}$$

These values were compared to previously reported values of isoprene polymerized in cyclohexane, see **Table 1**.[44],[45] The propagation rate of isoprene in MTBE is about one magnitude higher than in cyclohexane. In contrast, the propagation rate in THF is four times higher than in MTBE, $k_p^{THF,29\,°C} = 105 \cdot 10^{-3}$ M^{-1} s^{-1}.[46]

An important factor that needs to be considered is the degree of aggregation of the active chain ends, *n*, in the respective solvents. Polyisoprenyl lithium chains are known to form tetramers in cyclohexane at concentrations relevant to polymerization.[47] The higher polarity of MTBE suggests a change in the aggregation state. **Equation 2** was used to determine the aggregation number.

$$\ln k_{app} = (1/n) \ln[\mathrm{Ini}]_0 \qquad \textbf{(2)}$$

The polymerization was performed at three different initiator concentrations, $[\mathrm{Ini}]_0$, targeting different molar masses of 2.5 kg mol^{-1}, 5 kg mol^{-1} and 10 kg mol^{-1}, see **Figure 2**b. The initiator concentrations were determined from the number-average molar masses of the polymers determined by ^{1}H NMR (see **Table 1**). Based on the linear fit (**Figure 2**c) an aggregation number of $n \approx 1$ was determined, suggesting the unimeric nature of polyisoprenyl lithium chains in MTBE. Additional information on the polymerization kinetics, e.g. time-conversion plots, SEC traces and NMR spectra, can be found in **Figures S5, S6, S10, S12 and S13**.

Table 1. Summary of polymerization rates of isoprene and *β*-farnesene in MTBE and published values obtained in cyclohexane (CHx), assuming *n*=1 in MTBE and *n*=4 in cyclohexane.

Temperature [°C]	**$[\mathrm{Ini}]_0$** [a] [mmol·L^{-1}]	**k_{app}^{MTBE}** [10^{-3}·s^{-1}]	**k_p^{MTBE}** [10^{-3}·M^{-1}·s^{-1}]	**k_p^{CHx}** [10^{-3}·M$^{-1/4}$·s^{-1}]
Isoprene				
23	35.5	0.47	13.3	0.61[44] [b]
30	36.9	0.89	24.1	1.47[45] [c]
40	37.1	2.11	56.9	3.81[45] [c]
Farnesene				
23	34.9	0.80	22.9	3.23[48] [b]
30	35.7	1.57	44.0	6.31[48] [b]
40	34.3	3.69	107.6	23.1[48] [b]

[a] Calculated using $M_n = M_{Mon} \cdot [M]_0 \cdot [Ini]_0^{-1}$; $[I]_0$= 1.94 mol L^{-1}, $[Far]_0$= 0.65 mol L^{-1}. [b] Determined by *in situ* ^{1}H NMR kinetics;[44],[48] [c] Determined by *in situ* NIR kinetics.[45]

Kinetics of Polymerization of *β*-Farnesene in MTBE

The conversion of *β*-farnesene (Far) can be tracked by *in situ* ^{1}H NMR kinetics following the decrease of the proton at ~ 6.4 ppm. The respective spectra are presented in **Figure S7**. Following the investigation for isoprene we investigated the dependence on temperature and initiator concentration. The linearity of the pseudo-first order plots, see **Figure 3a** and **b**,

proves the living behavior, and using **Equation 1** the apparent rate constants were converted to the respective rate constants of Far in MTBE, k_p^{MTBE}, summarized in **Table 1**. As evident from **Figure 3c**, polyfarnesenyl lithium chains in MTBE form primarily unimers (aggregation number of $n \approx 1$), similar to polyisoprenyl lithium. Additional data are presented in **Figures S8, S9, S11, S14 and S15**.

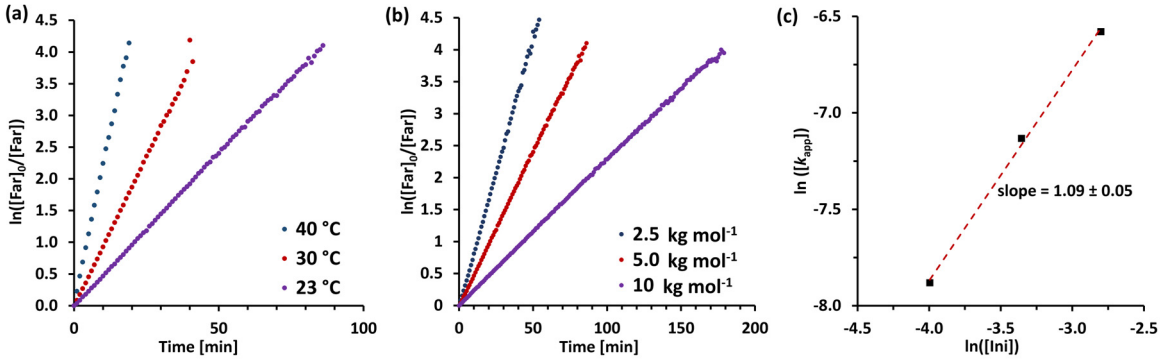

Figure 3. *In situ* ^{1}H NMR kinetics results of *β*-farnesene polymerization in MTBE using *sec*-BuLi as initiator; (a) pseudo-first-order plots at different temperatures at $[Ini]_0 \approx 35$ mmol L^{-1}; (b) pseudo-first-order plots using different $[Ini]_0$ at 23 °C; (c) double logarithmic plot of the apparent rate constants of isoprene at different initiator concentrations at 23 °C.

As observed earlier, *β*-farnesene reacts faster than myrcene and isoprene in cyclohexane. This was associated to the bulky chain ends of the longer homologous, decreasing their aggregation.[48],[49] Further it is evident that in MTBE *β*-farnesene polymerizes about 70% faster than isoprene, independent of the temperature. Taking the absence of aggregation into account, this is unexpected, considering the bulkiness of the monomer and the chain end. The full set of rate constants is analyzed by an Arrhenius plot (**Equation 3**; **Figure 4)**.

$$\ln k_p = \ln A + E_A/RT \qquad \textbf{(3)}$$

The activation energies, E_A, of both *β*-farnesene and isoprene are much lower in MTBE than in cyclohexane. This can be attributed to the fact that the activation energy in cyclohexane also contains the enthalpy of the aggregation/dissociation equilibrium. Further polymer characteristics, e.g. microstructure and molar mass determinations via SEC and NMR, are summarized in **Table S1**.

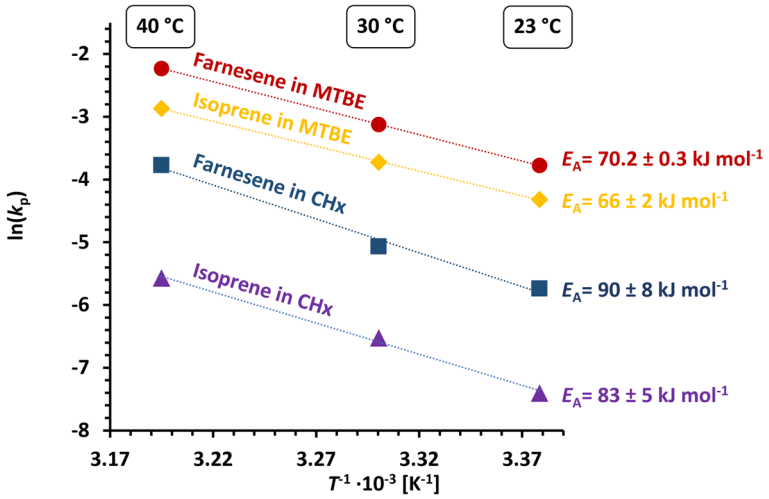

Figure 4. Arrhenius plots of isoprene and *β*-farnesene polymerization in MTBE and cyclohexane.

Noteworthy, the change in polarity of the solvent influences the resulting microstructure of the respective polydienes. For example, *β*-farnesene polymerized in hydrocarbons leads to ~ 93% of 1,4-units and ~ 7% 3,4-units, which decreases to approximately 62% 1,4-units and 38% 3,4-units when polymerized in MTBE.[22] In contrast, the effect on the polyisoprene microstructure is slightly stronger, as the amount of vinyl units increases to approx. 49% 3,4-units and 4% 1,2-units, whereas the amount of 1,4-units decreases to 47%. In comparison, the higher polarity of THF is known to further increase the vinyl content to 62% 3,4-units, 24% 1,2-units and only 14% of 1,4-units.[29]

Copolymerization of Isoprene and Styrene in MTBE/Cyclohexane Mixtures

Recently, our group utilized MTBE as a solvent for the bifunctional copolymerization of *β*-farnesene and nopadiene (Nopa), a biobased 1,2-substituded bicyclic 1,3-diene. Herein, the change from cyclohexane to MTBE showed only minor variation of the respective reactivity ratios of the copolymerization (r_{Far}^{CHx} = 6.5, r_{Nopa}^{CHx} = 0.156 and r_{Far}^{MTBE} = 7.23, r_{Nopa}^{MTBE} = 0.138).[23] In the following section, the copolymerization of styrene (S) and isoprene (I), as an established copolymerization pair in carbanionic polymerization, is investigated in MTBE/cyclohexane mixtures.

The copolymerization in pure cyclohexane leads to a steep comonomer gradient along the chain, reflected by the reactivity ratios r_I^{CHx} = 10 and r_S^{CHx} = 0.015, respectively.[50] The change in the polarity of the reaction medium is known to have a strong impact on the copolymerization and the associated reactivity ratios. Polar additives, like THF or 2,2-di(2-tetrahydrofurfuryl)propane (DTHFP), are known to entirely invert the comonomer gradient,

and consequently styrene is preferably incorporated during the copolymerization.[49],[50] The copolymerization of styrene and isoprene with increasing MTBE content was therefore investigated using *in situ* near-infrared (NIR) kinetics. The procedure followed the protocol explained in a previous publication.[45]

The ratio [MTBE]/[Li] in cyclohexane was steadily increased until MTBE was present as a pure solvent. The reactivity ratios are determined from the individual monomer consumptions using the non-terminal (Jaacks)[51],[52] and terminal model (Meyer and Lowry)[53]. Preferentially, the non-terminal model — assuming an ideal copolymerization ($r_1 \cdot r_2$=1) — is used, since it is less prone to overfitting compared to the more complex terminal model.[54] The non-linear Meyer-Lowry fit was only used for the ratios [MTBE]/[Li] = 0, 5 and 20, as the data deviated from linearity in the respective Jaacks fit.[53] Exemplary, the NIR kinetic results in neat MTBE is presented in **Figure 5**.

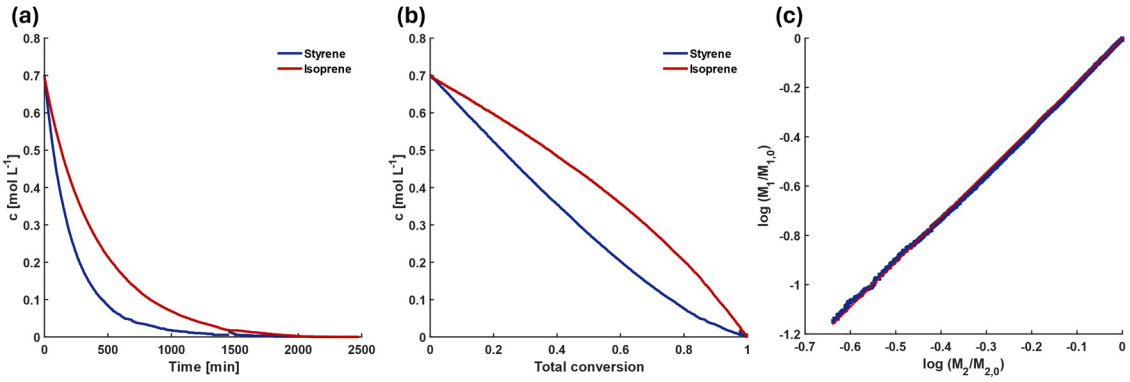

Figure 5. *In situ* NIR kinetics of the copolymerization of styrene and isoprene in neat MTBE at 20 °C, (a) time-conversion plot, (b) monomer consumption vs. total consumption, (c) Jaacks-fit of the copolymerization, r_I=0.55 and r_S=1.82.

All kinetic results are summarized in **Table 2** and additional data is given in the SI (**Figures S18-25**). The effect of the MTBE content on the reactivity ratios is shown in **Figure 6**.

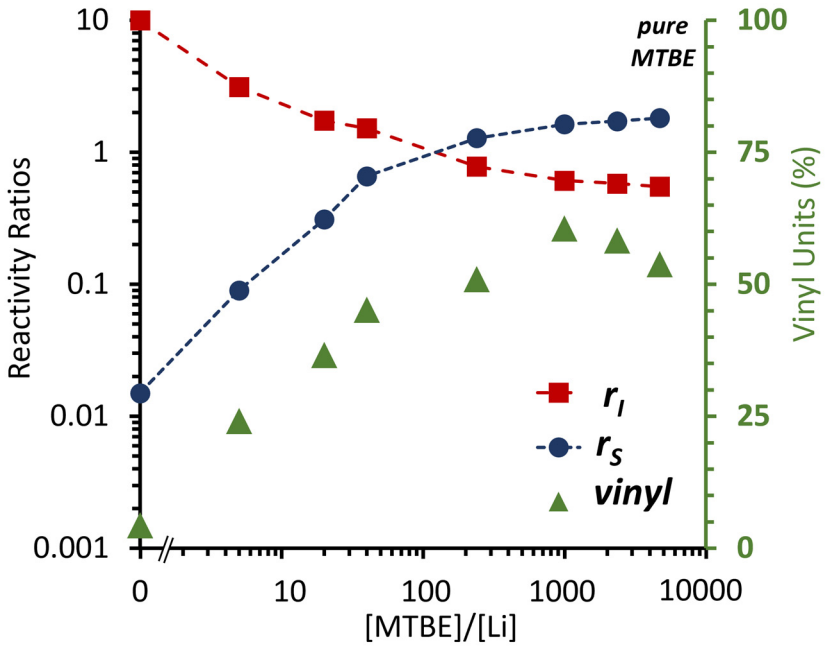

Figure 6. Effect of the addition of MTBE on the reactivity ratios of the copolymerization of S, red, and I, blue, and the amount if vinyl units, green; lines connecting the symbols are a guide to the eye only; measured with *in situ* NIR kinetics at 20 °C.

It is evident that the reactivity ratios converge and eventually invert, so that finally styrene is incorporated first. By interpolation we see that a random copolymer ($r_S = r_I \approx 1$) is expected at [MTBE]/[Li] ≈ 166 (3.5 vol%) and no significant change is observed by exceeding a [MTBE]/[Li] ratio of 1000 equivalents. Additionally, the reaction half-life, $t_{1/2}$ (inverse rate), is decreased by the addition of MTBE up to 1000 eq, whereas further addition of MTBE leads to an increase in reaction time again. Eventually, the half-life of isoprene even exceeds the $t_{1/2}$ in pure cyclohexane, see **Figure S29**. A similar minimum of $t_{1/2}$ was observed with THF as ligand at a THF/Li ratio ≈ 80 already.[50] Analogously, randomization with THF is already achieved at [THF]/[Li] ≈ 6.[50] Noteworthy, an additional *in situ* NMR kinetic experiment in neat MTBE showed nearly identical results to the one obtained *via* the *in situ* NIR measurement, proving the comparability of both techniques. The reactivity ratios in neat MTBE, determined by either NMR or NIR are in good agreement, r_S^{MTBE} = 1.82 (NIR); 1.87 (NMR) and r_I^{MTBE} = 0.55 (NIR); 0.53 (NMR), and reveal a weak compositional gradient not very far from an ideal, random incorporation of styrene and isoprene. This is also reflected by a the low so-called blockiness of the styrene content, see **Figure S30**. This is in line with results obtained in previous works where the addition of polar modifiers, e.g., THF or DTHFP, was used to manipulate the tapered structure of diene/styrene copolymers.[49],[50] Notably, the gradient is much weaker than in pure THF, where $r_S^{THF} \approx 9$ and $r_I^{THF} \approx 0.1$ was reported.[55] Thus, pure MTBE is a suitable solvent to synthesize near-random S/I copolymers.

Table 2. Polymer characteristics of all synthesized S/I copolymers.

[MTBE] /[Li] [a]	MTBE [vol%]	M_n^{SEC} [b] [kg·mol^{-1}]	$Đ$ [b]	r_I [c]	r_S [c]	1,4- [d] [%]	3,4- [d] [%]	1,2- [d] [%]	T_g [e] [°C]	Volume Gradient [f]
***In situ* NIR kinetics**										
0 Ref: [50]	0	88.2	1.06	10.03	0.015	96	3.8	0.6	-39/83	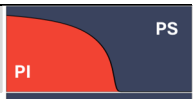
5	0.1	88.3	1.04	3.13	0.09	75.9	22.6	1.5	-14	
20	0.4	89.6	1.04	1.74	0.31	63.4	34.9	1.7	11	
40	0.9	86.4	1.04	1.52	0.66	54.8	42.3	2.9	24	
240	5.1	90.4	1.04	0.78	1.28	49.0	48.3	2.7	32	
1000	21.3	83.7	1.04	0.61	1.63	39.4	56.5	4.1	33	
2350	50.0	94.6	1.05	0.58	1.72	41.7	53.9	4.4	33	
pure MTBE	100	84.1	1.06	0.55	1.82	46.2	51.3	2.5	29	
***In situ* ^{1}H NMR kinetics**										
pure MTBE	100	4.1	1.11	0.53	1.87	45.7[g]	50.4[g]	3.9[g]	NA	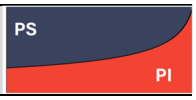

[a] Equivalents based on the [MTBE]/[Li]. [b] Determined by SEC (eluent: THF, PS-calibration). [c] Determined from the Jaacks-Fit or Mayer-Lowry-Fit. [d] Determined by ^{1}H NMR.[56] [e] Glass temperature determined *via* DSC using a heat rate of 10 K min^{-1}. [f] Volume gradients were determined assuming the following densities of the homopolymers: ρ_{PS}=0.97 g·cm^{-3}, ρ_{PI}=0.83 g·cm^{-3}, respectively.[57] [g] Values taken from PI homopolymerization in pure MTBE, see Table S1.

The increasing polarity of the medium affects the fraction of resulting vinyl units, i.e. 3,4- and 1,2-units, as can be seen in **Figure 6** and **S26** and **Table 2**. Exceeding 1000 eq of MTBE has no further significant impact on the reactivity ratios. This is also evident from thermal properties determined by DSC experiments, **Figures S27** and **S28**. The near random S/I-copolymers show only one mixed T_g in the range of -14 °C to 33 °C, depending on the content of vinyl units.

Conclusions

MTBE, produced on megaton scale, offers numerous advantages beyond the absence of peroxide formation, making it particularly preferable to other ethers for large-scale processes. The key objective of this work was to give a fundamental introduction and overview of the characteristics of MTBE as a moderately polar solvent for the carbanionic polymerization. As one key result, the study reveals that MTBE shows a more than 50 times higher stability towards alkyl lithium compounds than THF, the most often used polar solvent. *In situ* ^{1}H NMR kinetics of isoprene and *β*-farnesene polymerizations show a propagation rate in MTBE in between those in THF and cyclohexane. In pronounced contrast to cyclohexane and similar to THF the chain ends are present as non-aggregated unimers, leading to higher reaction rates for propagation. *In situ* NIR kinetics revealed that the effect of MTBE on the copolymerization of styrene and isoprene as a relevant copolymerization system in cyclohexane is weaker than that of THF, eventually yielding an inverted near-random incorporation of both comonomers in neat MTBE. Due to its higher stability, moderate polarity, excellent solubility of bifunctional initiators, and absence of peroxide formation, MTBE as a cheap and very abundant chemical has great potential for further applications in polymer chemistry. The use of this solvent for polar and heterocyclic monomers is subject of future investigations.

References

[1] Hsieh, H. L.; Quirk, R. P. *Anionic Polymerization*:*Principles and Practical Applications*; Plastics Engineering Ser, v.34; Chapman and Hall/CRC, **1996**.

[2] Hadjichristidis, N.; Iatrou, H.; Pispas, S.; Pitsikalis, M. Anionic polymerization: High vacuum techniques. *J. Polym. Sci. A Polym. Chem.*, **2000**, *38* (18), 3211‐3234.

[3] Gatzke, A. L. Chain transfer in anionic polymerization. Determination of chain-transfer constants by using carbon-14-labeled chain transfer agents. *J. Polym. Sci. A-1 Polym. Chem.*, **1969**, *7* (8), 2281‐2292.

[4] Sanderson, R. D.; Roediger, A. H. A.; Summers, G. J. Hydrocarbon-soluble difunctional organolithium anionic initiators. A gas‐liquid chromatographic study of the reaction of sec -butyllithium with m -divinylbenzene. *Polym. Int.*, **1994**, *35* (3), 263‐272.

[5] Margerison, D.; Newport, J. P. Degree of association of n-butyl lithium in hydrocarbon media. *Trans. Faraday Soc.*, **1963**, *59*, 2058.

[6] Hadjichristidis, N.; Pitsikalis, M.; Pispas, S.; Iatrou, H. Polymers with complex architecture by living anionic polymerization. *Chem. Rev.*, **2001**, *101* (12), 3747‐3792.

[7] Clayden, J.; Yasin, S. A. Pathways for decomposition of THF by organolithiums: the role of HMPA. *New J. Chem.*, **2002**, *26* (2), 191‐192.

[8] Stanetty, P.; Mihovilovic, M. D. Half-Lives of Organolithium Reagents in Common Ethereal Solvents. *J. Org. Chem.*, **1997**, *62* (5), 1514‐1515.

[9] Hamid, S. H.; Ali, M. A. Effect of MTBE Blending on the Properties of Gasoline. *Fuel Sci. Technol. Int.*, **1995**, *13* (5), 509‐544.

[10] Zhang, H.; Zeng, Z.; Ma, F.; Wu, Q.; Wang, X.; Cheng, S.; Xie, J. Cyclopentylmethyl Ether, a Non-Fluorinated, Weakly Solvating and Wide Temperature Solvent for High-Performance Lithium Metal Battery. *Angew. Chem. Int. Ed.*, **2023**, *62* (21), e202300771.

[11] Critchfield, F. E.; Gibson, J. A.; Hall, J. L. Dielectric Constant and Refractive Index from 20 to 35° and Density at 25° for the System Tetrahydrofuran–Water. *J. Am. Chem. Soc.*, **1953**, *75* (23), 6044‐6045.

[12] Songsiri, N.; Rempel, G. L.; Prasassarakich, P. Liquid-Phase Synthesis of Isoprene from Methyl tert -Butyl Ether and Formalin Using Keggin-Type Heteropolyacids. *Ind. Eng. Chem. Res.*, **2016**, *55* (33), 8933‐8940.

[13] Iovu, M. C.; Buzdugan, E.; Teodorescu, M.; Britchi, A. G.; Hubca, G.; Iovu, H. Copolymerization of styrene with butadiene using methyl tert -butyl ether as active center modifier. *Angew. Makromol. Chemie*, **1999**, *271* (1), 18‑23.

[14] Iovu, M.-C.; Mapolie, S.; Britchi, A. G. Styrene-butadiene rubber synthesized by anionic polymerization. *Macromol. Symp.*, **2001**, *165* (1), 55‑62.

[15] Iovu, M.-C.; Buzdugan, E.; Ghioca, P.; Britchi, A. G. Random Anionic Polymerization of Styrene with Butadiene using Methyl Tert-Butyl Ether/n-Butyl Lithium as Initiator System. Reation Mechanism and Kinetic Model. *Rev. Roum. Chim.*, **2003**, *48* (2), 163‑171.

[16] Novoa-Carballal, R.; Nosov, S.; Pfaff, S.; Schmalz, H.; Müller, A. H. E. Hyperbranched and Hyperstar Polybutadienes via Anionic Self-Condensing Vinyl Copolymerization. *Macromolecules*, **2021**, *54* (12), 5774‑5783.

[17] Uraneck, C. A. Influence of temperature on microstructure of anionic-initiated polybutadiene. *J. Polym. Sci. A-1 Polym. Chem.*, **1971**, *9* (8), 2273‑2281.

[18] Antkowiak, T. A.; Oberster, A. E.; Halasa, A. F.; Tate, D. P. Temperature and concentration effects on polar-modified alkyllithium polymerizations and copolymerizations. *J. Polym. Sci. A-1 Polym. Chem.*, **1972**, *10* (5), 1319‑1334.

[19] Yu, Y.; Dubois, P.; Teyssié, P.; Jérôme, R. Difunctional Initiator Based on 1,3-Diisopropenylbenzene. 6. Synthesis of Methyl Methacrylate–Butadiene–Methyl Methacrylate Triblock Copolymers. *Macromolecules*, **1997**, *30* (15), 4254‑4261.

[20] Yoo, T.; Henning, S. K. Synthesis and Characterization of Farnesene-Based Polymers. *Rubber Chem. Technol.*, **2017**, *90* (2), 308‑324.

[21] Wahlen, C.; Frey, H. Anionic Polymerization of Terpene Monomers: New Options for Bio-Based Thermoplastic Elastomers. *Macromolecules*, **2021**, *54* (16), 7323‑7336.

[22] Meier-Merziger, M.; Imschweiler, J.; Hartmann, F.; Niebuur, B.-J.; Kraus, T.; Gallei, M.; Frey, H. Bifunctional Carbanionic Synthesis of Fully Bio-Based Triblock Structures Derived from *β*-Farnesene and ll-Dilactide: Thermoplastic Elastomers. *Angew. Chem. Int. Ed.*, **2023**, *62* (42), e202310519.

[23] Meier-Merziger, M.; Fotaras, N.; Tzourtzouklis, I.; Allouch, C.; Wagner, M.; Müller, A. H. E.; Frey, H. One-Step Synthesis of Fully Bio-based Two-Sided Tapered ABA-Type Thermoplastic Elastomers. *ACS Sustainable Chem. Eng.*, **2024,** *12* (26), 9922-9933.

[24] Čermák, J., Hašová, V.; Mačka, M.; Petrů, V.; Pleska, A.; Reiss, J.; Sufčák, M.; Večerka, F.; Vyoral, L. Způsob roztokové kopolymerace konjugovaných dienů s vinylaromatickými uhlovodíky. CZ 254630.

[25] Horák, Z.; Hlavatá, D.; Hromádková, J.; Kotek, J.; Hašová, V.; Mikešová, J.; Pleska, A. Effect of selected structural parameters of styrene-butadiene block copolymers on their compatibilization efficiency in polystyrene/polybutadiene blends. *J. Polym. Sci. B Polym. Phys.*, **2002**, *40* (23), 2612-2623.

[26] Hlavatá, D.; Hromádková, J.; Fortelný, I.; Hašová, V.; Pulda, J. Compatibilization efficiency of styrene-butadiene triblock copolymers in polystyrene-polypropylene blends with varying compositions. *J. Appl. Polym. Sci.*, **2004**, *92* (4), 2431-2441.

[27] Fortelný, I.; Minkova, L. I.; Kotek, J.; Lapčíková, M.; Michálková, D. Morphology and mechanical properties of polypropylene/polystyrene blends compatibilized with styrene-butadiene block copolymers. *Polym. Eng. Sci.*, **2012**, *52* (1), 191-204.

[28] Dev, A.; Rösler, A.; Schlaad, H. Limonene as a renewable unsaturated hydrocarbon solvent for living anionic polymerization of *β*-myrcene. *Polym. Chem.*, **2021**, *12* (21), 3084-3087.

[29] Glatzel, J.; Noack, S.; Schanzenbach, D.; Schlaad, H. Anionic polymerization of dienes in 'green' solvents. *Polym. Int.*, **2021**, *70* (2), 181-184.

[30] Zhang, J.; Aydogan, C.; Patias, G.; Smith, T.; Al-Shok, L.; Liu, H.; Eissa, A. M.; Haddleton, D. M. Polymerization of Myrcene in Both Conventional and Renewable Solvents: Postpolymerization Modification via Regioselective Photoinduced Thiol-Ene Chemistry for Use as Carbon Renewable Dispersants. *ACS Sustainable Chem. Eng.*, **2022**, *10* (29), 9654-9664.

[31] Fu, Y.; Yang, S.; Xiong, Q.; Gu, Z.; Dai, Q.; Tan, H.; Le Zhou; Geng, M.; Xie, F.; Yi, W.; Li, L.; Liu, K. Synthesis, kinetic study and characterization of C5 -dienes/styrene copolymers via living anionic polymerization in cyclopentyl methyl ether solvent. *Polym. Int.*, **2023**, *73* (4), 326-336.

[32] Nawaz, Z. Methyl-Tert-Butyl-Ether Synthesis Reactor Modelling and Optimization Using an Aspen Custom Modeler. *Hung. J. Ind. Chem.*, **2017**, *45* (2), 1-7.

[33] Bown, R. M.; Joyce, M.; Zhang, Q.; Reina, T. R.; Duyar, M. S. Identifying Commercial Opportunities for the Reverse Water Gas Shift Reaction. *Energy Tech*, **2021**, *9* (11).

[34] Zhu, M.; Ge, Q.; Zhu, X. Catalytic Reduction of CO2 to CO via Reverse Water Gas Shift Reaction: Recent Advances in the Design of Active and Selective Supported Metal Catalysts. *Trans. Tianjin Univ.*, **2020**, *26* (3), 172-187.

[35] Wu, X.; Tan, M.; Tian, S.; Song, F.; Ma, Q.; He, Y.; Yang, G.; Tsubaki, N.; Tan, Y. Designing ZrO2-based catalysts for the direct synthesis of isobutene from syngas: The studies on Zn promoter role. *Fuel*, **2019**, *243*, 34‑40.

[36] Fukada, H.; FUJII, T.; OGAWA, T. Microbial production of C3- and C4-hydrocarbons under aerobic conditions. *Agricultural and Biological Chemistry*, **1984**, *48* (6), 1679‑1682.

[37] Wilson, J.; Gering, S.; Pinard, J.; Lucas, R.; Briggs, B. R. Bio-production of gaseous alkenes: ethylene, isoprene, isobutene. *Biotechnology for biofuels*, **2018**, *11*, 234.

[38] van Leeuwen, B. N. M.; van der Wulp, A. M.; Duijnstee, I.; van Maris, A. J. A.; Straathof, A. J. J. Fermentative production of isobutene. *Applied microbiology and biotechnology*, **2012**, *93* (4), 1377‑1387.

[39] Rauch, R.; Hrbek, J.; Hofbauer, H. Biomass Gasification for Synthesis Gas Production and Applications of the Syngas. *WIRS Energy Environ*, **2014**, *3* (4), 343‑362.

[40] Moser, G. J.; Wolf, D. C.; Sar, M.; Gaido, K. W.; Janszen, D.; Goldsworthy, T. L. Methyl tertiary butyl ether-induced endocrine alterations in mice are not mediated through the estrogen receptor. *Toxicological Sciences*, **1998**, *41* (1), 77‑87.

[41] Jordan, A.; Hall, C. G. J.; Thorp, L. R.; Sneddon, H. F. Replacement of Less-Preferred Dipolar Aprotic and Ethereal Solvents in Synthetic Organic Chemistry with More Sustainable Alternatives. *Chem. Rev.*, **2022**, *122* (6), 6749‑6794.

[42] Corey, E. J.; Eckrich, T. M. t-Butoxymethyllithium: Direct preparation from t-butyl methyl ether and applications as a hydroxymethyl anion equivalent. *Tetrahedron Lett.*, **1983**, *24* (31), 3165‑3168.

[43] Bywater, S. Anionic Polymerization of Olefins. In *Non-Radical Polymerisation*; Comprehensive Chemical Kinetics; Elsevier, **1976**; pp 1‑65.

[44] Tiedemann, P. von; Blankenburg, J.; Maciol, K.; Johann, T.; Müller, A. H. E.; Frey, H. Copolymerization of Isoprene with p -Alkylstyrene Monomers: Disparate Reactivity Ratios and the Shape of the Gradient. *Macromolecules*, **2019**, *52* (3), 796‑806.

[45] Steube, M.; Johann, T.; Plank, M.; Tjaberings, S.; Gröschel, A. H.; Gallei, M.; Frey, H.; Müller, A. H. E. Kinetics of Anionic Living Copolymerization of Isoprene and Styrene Using in Situ NIR Spectroscopy: Temperature Effects on Monomer Sequence and Morphology. *Macromolecules*, **2019**, *52* (23), 9299‑9310.

[46] Morton, M.; Bostick, E. E.; Livigni, R. A.; Fetters, L. J. Homogeneous anionic polymerization. IV. Kinetics of butadiene and isoprene polymerization with butyllithium. *J. Polym. Sci. A Gen. Pap.*, **1963**, *1* (5), 1735‑1747.

[47] Worsfold, D. J.; Bywater, S. Degree of Association of Polystyryl-, Polyisoprenyl-, and Polybutadienyllithium in Hydrocarbon Solvents. *Macromolecules*, **1972**, *5* (4), 393‑397.

[48] Wahlen, C.; Blankenburg, J.; Tiedemann, P. von; Ewald, J.; Sajkiewicz, P.; Müller, A. H. E.; Floudas, G.; Frey, H. Tapered Multiblock Copolymers Based on Farnesene and Styrene: Impact of Biobased Polydiene Architectures on Material Properties. *Macromolecules*, **2020**, *53* (23), 10397‑10408.

[49] Fuchs, D. A. H.; Hübner, H.; Kraus, T.; Niebuur, B.-J.; Gallei, M.; Frey, H.; Müller, A. H. E. The effect of THF and the chelating modifier DTHFP on the copolymerisation of *β*-myrcene and styrene: kinetics, microstructures, morphologies, and mechanical properties. *Polym. Chem.*, **2021**, *12* (32), 4632‑4642.

[50] Steube, M.; Johann, T.; Hübner, H.; Koch, M.; Dinh, T.; Gallei, M.; Floudas, G.; Frey, H.; Müller, A. H. E. Tetrahydrofuran: More than a “Randomizer” in the Living Anionic Copolymerization of Styrene and Isoprene: Kinetics, Microstructures, Morphologies, and Mechanical Properties. *Macromolecules*, **2020**, *53* (13), 5512‑5527.

[51] Jaacks, V. Eine neuartige Methode zur Bestimmung von Copolymerisationsparametern. *Angew. Chem.*, **1967**, *79* (9), 419.

[52] Jaacks, V. A Novel Method of Determination of Reactivity Ratios in Binary and Ternary Copolymerizations. *Makromol. Chem.*, **1972**, *161* (1), 161‑172.

[53] Meyer, V. E.; Lowry, G. G. Integral and differential binary copolymerization equations. *J. Polym. Sci. A Gen. Pap.*, **1965**, *3* (8), 2843‑2851.

[54] Hawkins, D. M. The problem of overfitting. *J. Chem. Inf. Comput. Sci.*, **2004**, *44* (1), 1‑12.

[55] Spirin, Y. L.; Arest-Yakubovich, A. A.; Polyakov, D. K.; Gantmakher, A. R.; Medvedev, S. S. Polymerization catalyzed by lithium and lithium alkyl. *J. Polym. Sci.*, **1962**, *58* (166), 1181‑1189.

[56] Meier-Merziger, M.; Fickenscher, M.; Hartmann, F.; Kuttich, B.; Kraus, T.; Gallei, M.; Frey, H. Synthesis of phase-separated super-H-shaped triblock architectures: poly(l-lactide) grafted from telechelic polyisoprene. *Polym. Chem.*, **2023**, *14* (23), 2820‑2828.

[57] Fetters, L. J.; Lohse, D. J.; Richter, D.; Witten, T. A.; Zirkel, A. Connection between Polymer Molecular Weight, Density, Chain Dimensions, and Melt Viscoelastic Properties. *Macromolecules*, **1994**, *27* (17), 4639‑4647.

Supporting Information

1. Experimental Section

All experiments had to be performed under inert atmosphere in absence of any protic impurities. Therefore, the glassware was flame-dried at least three times before usage, and high-vacuum (10^{-3} mbar) techniques were used to transfer monomers and solvents. The argon used was treated by passing through cyclohexane/BuLi/diphenylethylene solutions to remove any remaining reactive substances.

1.1. Materials

All chemicals were used as received from the respective suppliers and all treatments are indicated at the point of the procedure. Substances were obtained from the following suppliers: *Amyris*: *β*-farnesene (95%); *Fisher Scientific:* THF (99.8%), cyclohexane (99.8%), isopropyl alcohol (99.8%); *Thermo Fisher:* MTBE (99.9%); *Thermo Scientific: n*-BuLi (2.5 mol L^{-1}), *sec*-BuLi (2.5 mol L^{-1}), isoprene (98%), calcium hydride (93%), basic aluminum oxide (40-300 µm 60A), *Sigma Aldrich:* styrene (99%), toluene (99.8%); *Lanxess:* trioctyl aluminum; *TCI:* diphenyl ethylene (98%); *Deutero*: cyclohexane-d_{12} (99.5%), chloroform-d_1 (99.5%).

1.2. Instruments

Nuclear Magnetic Resonance Spectroscopy (NMR). Measurements were performed on different NMR instruments. All 400 MHz spectra were recorded on either *Bruker Avance II HD* 400 MHz *(*5 mm *BBFO-head* with z-gradient, ATM and *SampleXPress 60* autosampler) or *Bruker Avance III HD* 400 MHz (5 mm N_2-cooled *BBO-cryo-head (BB/H+F)* with z-gradient, ATM and *SampleXPress 60* autosampler). Whereas 500 MHz spectra were measured on a *Bruker Avance III* 500 MHz instrument (5 mm *BBFO-Probe* with z-gradient and ATM, temperature control was done with a *VTU* (variable temperature unit) with an accuracy of ± 0.1 K). Data processing was done using the software *MestReNova* by *Mestrelab Research S.L.*, Spain.

Size Exclusion Chromatography (SEC). Samples were prepared at a concentration of 1 mg mL^{-1} in THF. They were measured using an Agilent *1260 Infinity II* setup using a *MZ-Gel SDPlus e5/e3/100* column set provided by *MZ-Analysentechnik,* Mainz, Germany. All measured samples were normalized to an internal toluene standard. Samples were referenced to either polyisoprene or polystyrene calibration standards obtained from *Polymer Standard Service*, Mainz, Germany.

Differential Scanning Calorimetry (DSC). Thermal analysis of the copolymers was performed using a *TA Instruments DSC 250* in combination with a *TA Instruments RCS 90* cooling system from *Waters Corporation*, United States. Experiments were performed using a heating rate of 10 K min^{-1}, and the instrument was calibrated using a two-point calibration of indium and *n*-octane.

1.3. *In Situ* ^{1}H NMR Determination of the Half-life of *n*-BuLi

The solvents MTBE and THF were dried over *n*-BuLi and diphenylethylene and freshly distilled when used. The solvent was inserted into an argon filled glovebox. For the measurement of THF, 0.8 mL of THF was added to an NMR tube and sealed with a septa cap. It was taken out of the glovebox and cooled in an isopropyl alcohol bath (cooled to < -20 °C). Then, 0.2 mL of 2.5 mol L^{-1} *n*-BuLi stock solution in hexane/cyclohexane was added. The NMR tube was kept at < -20 °C, until it was directly inserted into the NMR instrument, which was already set to 20 °C. *In situ* ^{1}H NMR kinetics were recorded without the addition of deuterated solvent. To obtain quantitative proton signals, the delay was set to 60 seconds and 1-scan spectra were recorded to yield a data point each minute.

For MTBE a similar procedure was applied. Again, 0.8 mL of solvent (MTBE) was added to an NMR tube with the addition of 0.05 mL of deuterated cyclohexane (C_5D_{12}). After removal from the glovebox the NMR tube was cooled to < -20 °C in an isopropyl alcohol cooling bath and 0.2 mL of 2.5 mol L^{-1} *n*-BuLi stock solution in hexane/cyclohexane was added. Keeping the NMR tube at < -20 °C it was moved to the NMR instrument. It was inserted to the NMR instrument, already set to 20 °C. As the measurement was carried out over a period of over 5 days, the measurement was performed with the addition of a deuterated solvent to minimize the drift of the spectra. It was recorded with a relaxation delay of 60 seconds and 16 scans per spectra to yield a higher signal-to-noise ratio. Thereby, every 16 min a data point is collected.

1.4 *In Situ* ^{1}H NMR Kinetics of Homopolymerization of Isoprene

MTBE was dried over *n*-BuLi and diphenylethylene and freshly distilled when used. Isoprene was first freed from its stabilizer by passing through alkaline aluminum oxide and dried for 24 hours over calcium hydride. Hydrogen and other gases were removed *via* three *freeze-pump-thaw* cycles. A second empty reaction flask was loaded with 10 vol% of 25 wt% trioctyl aluminum solution in cyclohexane, and cyclohexane was removed under vacuum. Then isoprene was transferred from calcium hydride onto trioctyl aluminum and stirred for

24 hours. Isoprene was transferred into an empty flask and along with dry MTBE inserted into an argon filled glove box. NMR tubes were loaded with 0.1 g (0.489 mmol) of isoprene and 0.7 mL MTBE each. The tubes were sealed with a septa cap and removed from the glove box. The *in situ* ^{1}H NMR kinetic was measured without the addition of deuterated solvents and initiated with 15.6 µL of 1.3 mol L^{-1} *sec*-BuLi solution in hexane/cyclohexane. The NMR experiment was performed with a relaxation delay of 60 seconds, and 1-scan spectra were recorded until no monomer signal remained. The kinetics data were measured at 23 °C, 30 °C and 40 °C. The polymerization was terminated by the addition of one drop degassed isopropyl alcohol and the product was precipitated in pure isopropyl alcohol.

1.5. *In Situ* ^{1}H NMR Kinetics of Homopolymerization of *β*-Farnesene

MTBE was dried over *n*-BuLi and diphenylethylene and freshly distilled when used. *β*-Farnesene was first freed from its stabilizer by passing through alkaline aluminum oxide and dried 24 hours over calcium hydride. Hydrogen and other gases were removed by vacuum. Then 10 vol% of 25 wt% trioctyl aluminum solution in cyclohexane was added and stirred for another 24 hours. Cyclohexane was removed under vacuum. Then *β*-farnesene was distilled, and along with MTBE inserted into an argon filled glove box. NMR tubes were loaded with 0.1 g (0.489 mmol) of *β*-farnesene and 0.7 mL MTBE each. The tubes were sealed with a septa cap and removed from the glove box. The *in situ* ^{1}H NMR kinetics were measured without the addition of deuterated solvents and initiated with 15.6 µL of 1.3 mol L^{-1} *sec*-BuLi solution in hexane/cyclohexane. NMR experiments were performed with a relaxation delay of 60 seconds, and 1-scan spectra were recorded until no monomer signal remained. The kinetics were measured at 23 °C, 30 °C and 40 °C. The polymerization was terminated by the addition of one drop degassed isopropyl alcohol and precipitated in pure isopropyl alcohol.

1.6. *In Situ* ^{1}H NMR Kinetics of the Copolymerization Styrene and Isoprene

MTBE was dried over *n*-BuLi and diphenylethylene and freshly distilled when used. Isoprene and styrene were first freed from their stabilizer by passing through alkaline aluminum oxide and dried 24 hours over calcium hydride. Hydrogen and other gases were removed *via* three *freeze-pump-thaw* cycles. A second empty reaction flask was loaded with 10 vol% of 25 wt% trioctyl aluminum solution in cyclohexane and cyclohexane was removed under vacuum. Then the monomers were transferred from calcium hydride onto trioctyl aluminum and stirred for another 24 hours. Isoprene and styrene were transferred into an empty flask and along with dry MTBE transferred into an argon filled glove box. An NMR tube was loaded with 0.55 mL

MTBE, 0.052 g (0.76 mmol) isoprene and 0.078 g (0.75 mmol) styrene. The tube was sealed with a septa cap and removed from the glove box. The *in situ* ^{1}H NMR kinetics were measured without the addition of deuterated solvents and initiated with 14.5 µL of 1.3 mol L^{-1} *sec*-BuLi solution in hexane/cyclohexane. The NMR experiment was performed with a relaxation delay of 60 seconds and 1-scan spectra were recorded until no monomer signals remained. The kinetics were measured at 23 °C. The polymerization was terminated by the addition of one drop degassed isopropyl alcohol and the product precipitated in pure isopropyl alcohol.

1.7. *In Situ* NIR Kinetics of the Copolymerization Styrene and Isoprene

The NIR set-up and data analysis have been described in previous publications.[1] Solvents and monomers were dried as in the other experiments, and they were cryo-transferred into an ampule rather than the glovebox. Cyclohexane was dried under reflux with sodium and benzophenone. After drying, indicated by a blue coloration, the solvent was transferred into the NIR-reaction flask (Morton flask glass reactor), which was equipped with the NIR probe head, the monomer glass ampule, a temperature probe and an additional glass joint. All reactions were carried out under the same conditions, only the amount of MTBE added varies. The synthesis of P($S_{0.5}$-*co*-$I_{0.5}$) with [MTBE]/[Li] = 5 is described as an example. Both dried monomers (48.35 ml, 0.483 mol) isoprene and (55.3 ml, 0.483 ml) styrene were cryo-transferred into an ampule and added to the reaction flask, containing 585 ml cyclohexane and 0.62 ml MTBE. The polymerization was initiated with 0.8 ml (1.04 mmol; 1 eq) of a 1.3 M *sec*-BuLi solution. The addition of the initiator resulted in a color change from colorless to pale yellow at the beginning of the reaction, indicating the preferred isoprene polymerization, to red at the end of the polymerization, indicating the preferred styrene incorporation at this point. After a reaction time of 600 minutes and no further decrease of the NIR signal at 6138 cm^{-1}, the reaction was completed and terminated by adding 2 ml of degassed isopropanol under argon counterflow. The resulting colorless polymer was precipitated in a 3:1 mixture of methanol:isopropanol, dried under reduced pressure and stored at -20 °C.

The reaction temperature was monitored with a temperature probe, and a cryostat was used to maintain a reaction temperature of 20 °C. In all copolymerizations the measured reaction temperature increase did not exceed 10 °C. Previous works demonstrated that the effect of temperature is negligible compared to the effect the modifiers have on the reactivity ratios.[1],[2]

2. Kinetics of *n*-BuLi decomposition in THF and MTBE

The kinetics of *n*-BuLi decomposition in THF was tracked *via in situ* ^{1}H NMR kinetics, using the methylene signal at ~ -0.75 ppm. A delay of 60 s between each data point was selected to ensure a full relaxation of the proton signal and 1-scan spectra were recorded. The decrease in the proton integral can be seen in **Figure S1**:

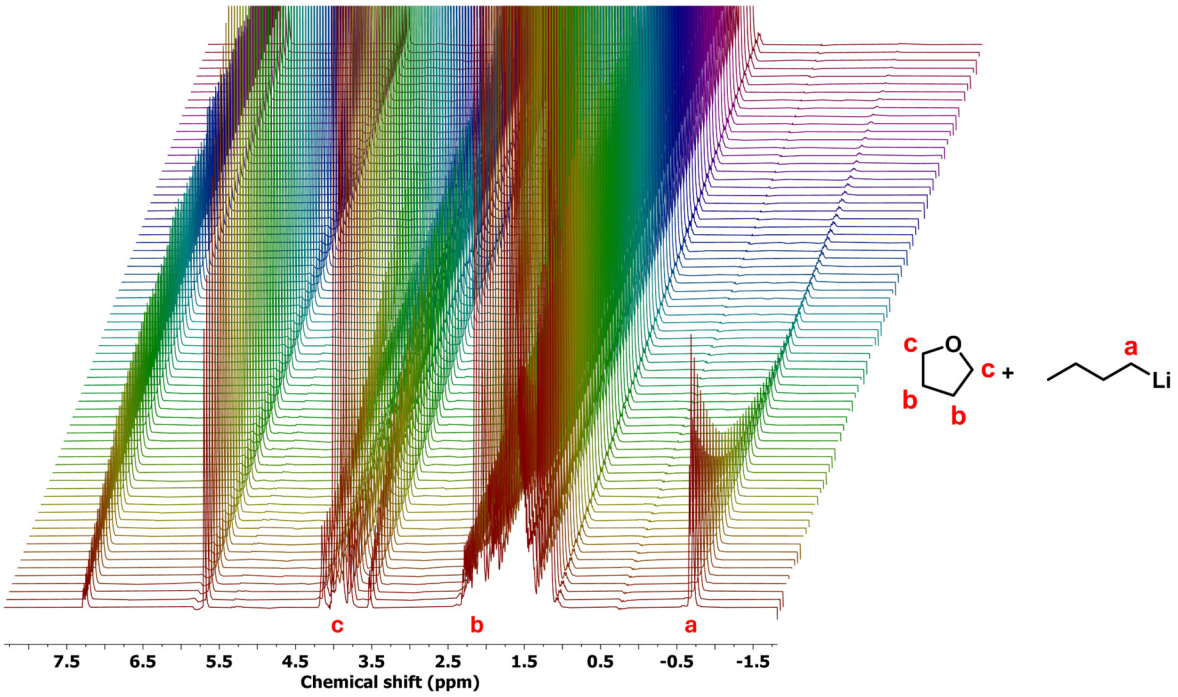

Figure S1. ^{1}H NMR kinetic of *n*-BuLi in THF, 1-scan spectra recorded with a delay of 60 s without deuterated solvent at 400 MHz, proton signals assigned to THF and *n*-BuLi, every 5th spectrum is shown.

A similar procedure was performed for *n*-BuLi in MTBE. However, as the process is much slower, 16-scan spectra with a delay of 60 s in between each pulse were recorded, yielding an even better signal-to-noise ratio, see **Figure S2**.

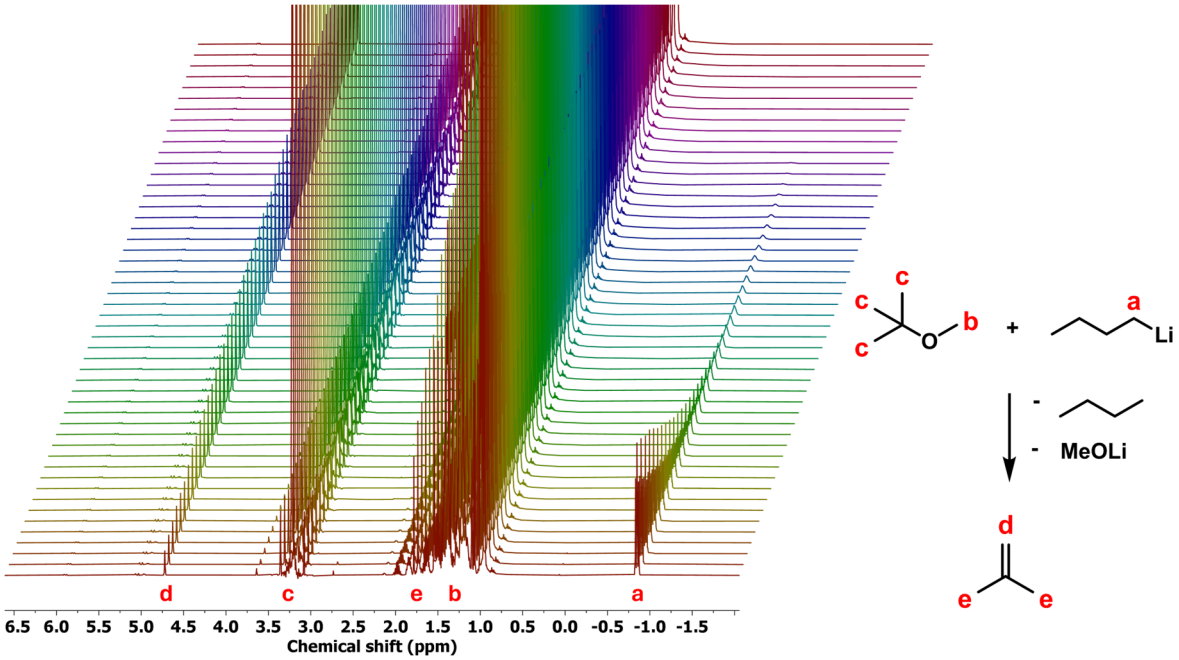

Figure S2. ^{1}H NMR kinetics of *n*-BuLi in MTBE, 16-scan spectra recorded with a delay of 60 s without deuterated solvent at 500 MHz, proton signals assigned to MTBE, *n*-BuLi and isobutylene, every 10th spectrum is shown.

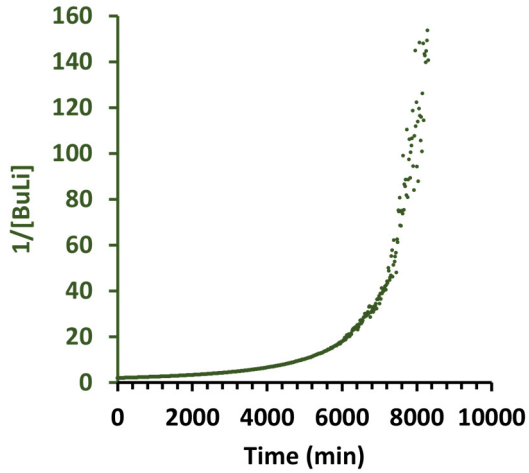

Figure S3. Plot of *n*-BuLi in MTBE shown as 1/[BuLi] vs time, corresponding to a second order plot.

3. Homopolymerization of Isoprene and *β*-Farnesene in MTBE

Homopolymerizations of isoprene were performed in MTBE at 23 °C, 30 °C and 40 °C. *In situ* ^{1}H NMR kinetics were measured, and the consumption of isoprene was tracked by following the decrease of the proton integral of the conjugated diene at ~ 6.6 ppm. The respective spectra are presented in **Figure S4** for the polymerization at 23 °C.

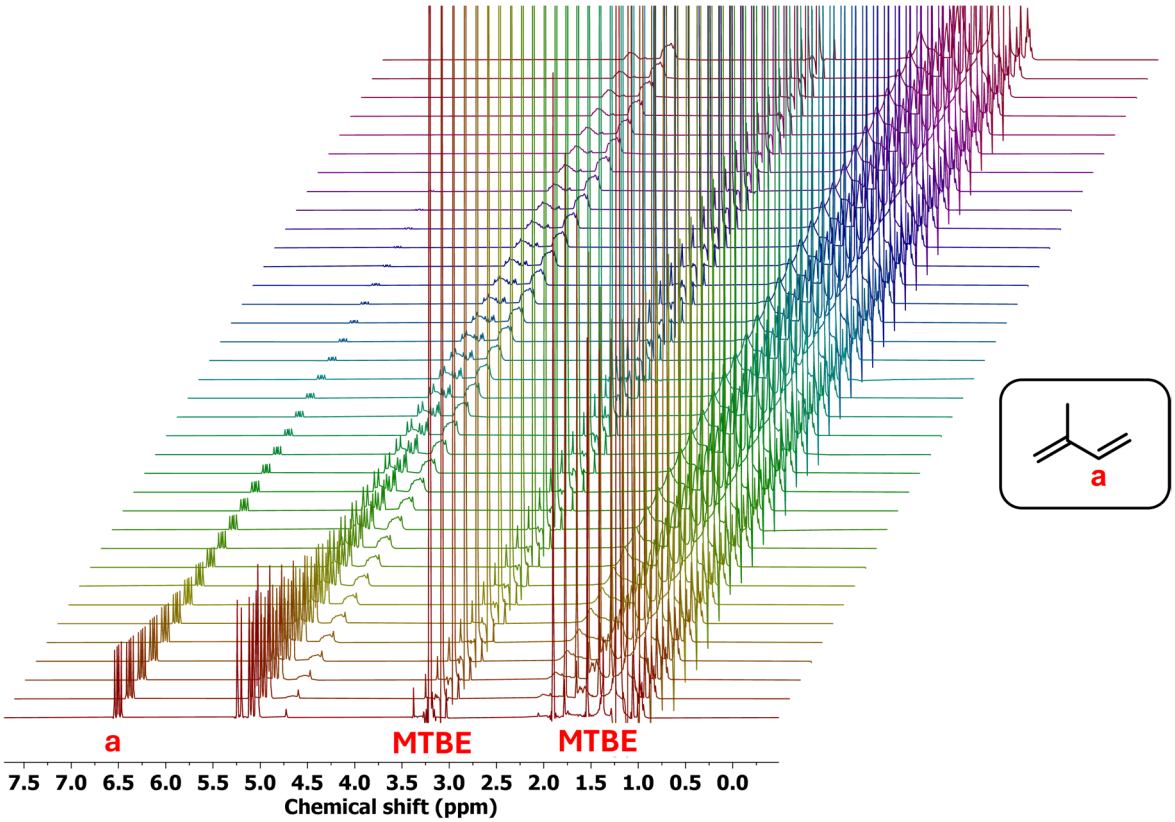

Figure S4. *In situ* ^{1}H NMR kinetics of isoprene in MTBE, 1-scan spectra recorded with a delay of 60 s without deuterated solvent at 400 MHz. The characteristic diene proton signal at 6.6 ppm was used to determine the consumption of isoprene, every 5th spectrum is shown.

Olefin signals in the range of 4.5 ppm to 5.3 ppm represent the methylene protons of the diene structure. The signals change from sharp signals originating from the monomer to broad signals assigned to the olefinic protons of the polymer backbone. The time-conversion plot for each polymerization is presented in **Figure S5**, indicating faster consumption of isoprene at higher temperatures.

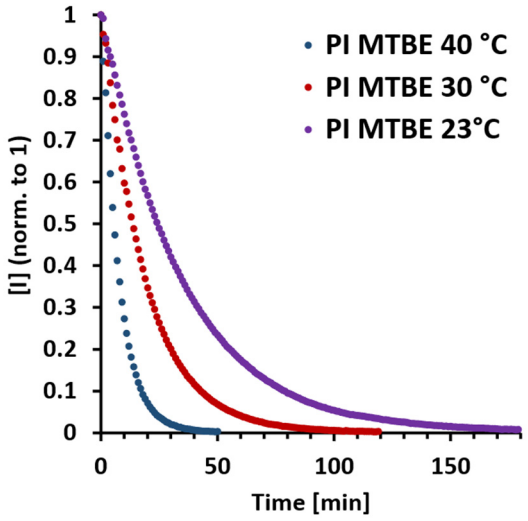

Figure S5. Time-conversion plots of the homopolymerization of isoprene in MTBE carried out at 23 °C, 30 °C, and 40 °C.

Additionally, the homopolymerization of isoprene in MTBE was investigated at three different initiator concentrations to determine the degree of aggregation. The time-conversion plots of the respective *in situ* ^{1}H NMR kinetics are shown in the following **Figure S6**:

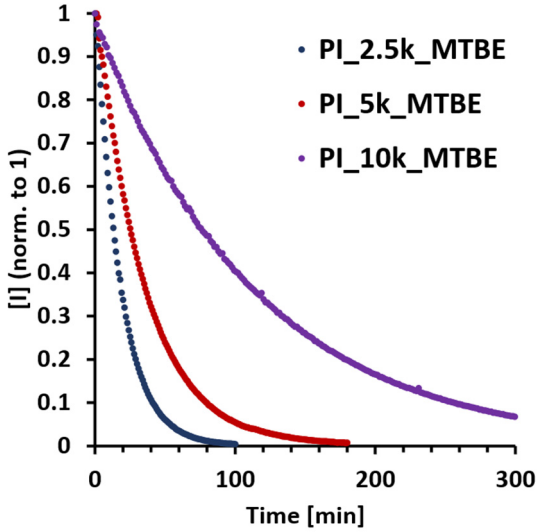

Figure S6. Time-conversion plots of the homopolymerizations of isoprene in MTBE targeting a molar mass of 2.5 kg·mol^{-1}, 5 kg·mol^{-1}, and 10 kg·mol^{-1}, respectively.

The homopolymerization was likewise performed for *β*-farnesene in MTBE. **Figure S7** exemplarily shows the *in situ* ^{1}H NMR kinetics of *β*-farnesene polymerized in MTBE at 23 °C. The time-conversion plots of the polymerizations performed at three different temperatures, 23 °C, 30 °C, and 40 °C, are presented in **Figure S8**. The results of the homopolymerizations targeting different molar masses can be followed in **Figure S9**.

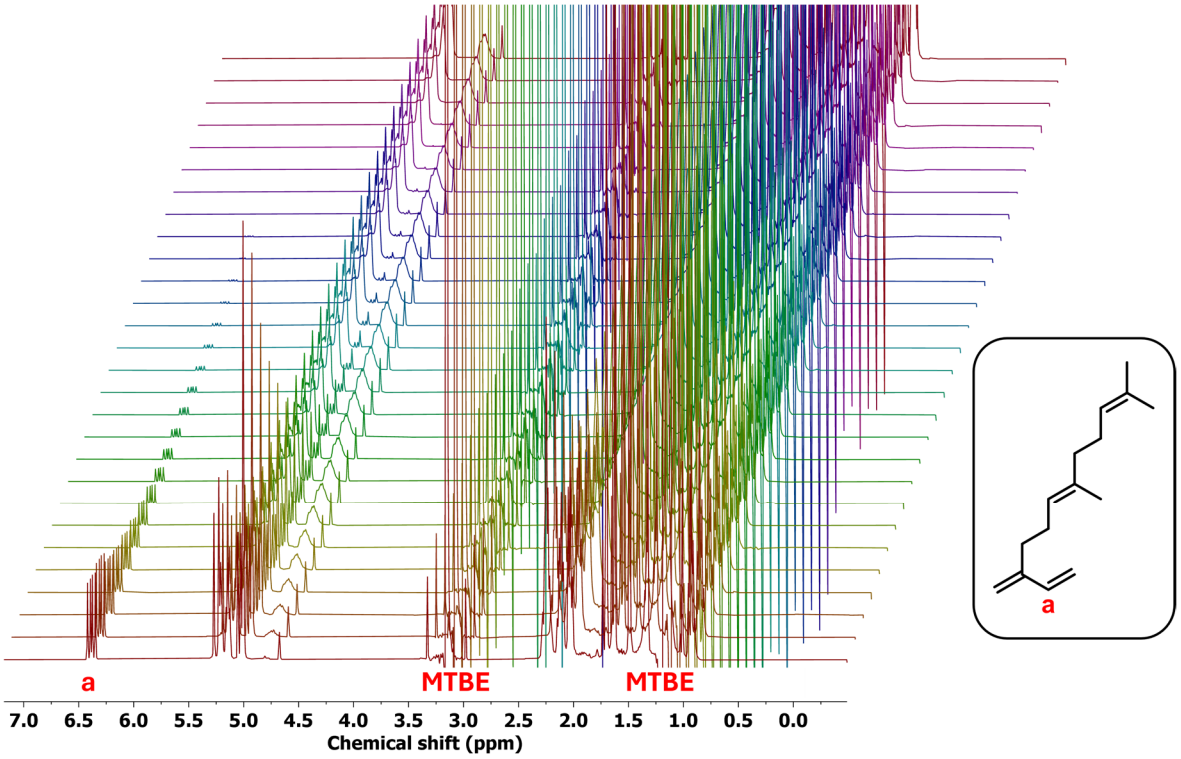

Figure S7. *In situ* ^{1}H NMR kinetics of *β*-farnesene in MTBE, 1-scan spectra recorded with a delay of 60 s without deuterated solvent at 400 MHz. The characteristic diene proton signal at ~ 6.4 ppm was used to determine the consumption of *β*-farnesene, every 5th spectrum is shown.

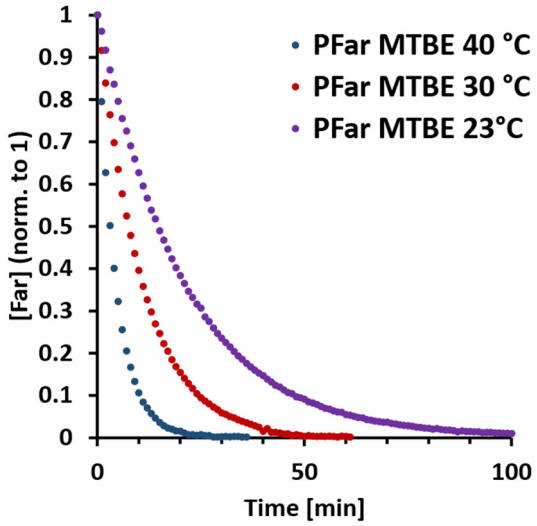

Figure S8. Time-conversion plots of the homopolymerization of *β*-farnesene in MTBE carried out at 23 °C, 30 °C, and 40 °C.

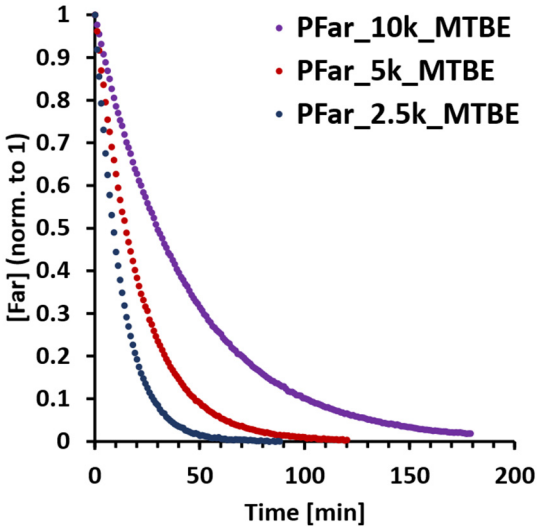

Figure S9. Time-conversion plots of the homopolymerizations of *β*-farnesene in MTBE at 23 °C targeting a molar mass of 2.5 kg·mol^{-1}, 5 kg·mol^{-1}, and 10 kg·mol^{-1}, respectively.

For all kinetics samples polymer characteristics, e.g., the initiator concentration $[Ini]_0$, molar mass by SEC (M_n^{SEC}) and by NMR (M_n^{NMR}) as well as their respective microstructure are summarized in the following **Table S1**:

Table S1. Summary of all collected data of polymer samples obtained in the *in situ* ^{1}H NMR kinetics of isoprene, $[I]_0$ = 1.94 mol·L^{-1}, and *β*-farnesene, $[Far]_0$ = 0.65 mol·L^{-1}, polymerized in MTBE.

$M_n^{theo.}$ [kg·mol^{-1}]	Temp. [°C]	$[Ini]_0$ [a] [mmol·L^{-1}]	M_n^{SEC} [b] [kg·mol^{-1}]	$Đ$ [b]	M_n^{NMR} [c] [kg·mol^{-1}]	1,4- [c] [%]	3,4- [c] [%]	1,2- [c] [%]
Isoprene								
5.0	23	35.5	5.6	1.11	3.7	45.7	50.4	3.9
5.0	30	36.9	5.8	1.11	3.6	47.3	49.0	3.7
5.0	40	37.1	5.5	1.11	3.6	48.5	48.3	3.1
2.5	23	68.6	2.7	1.06	1.9	46.2	49.1	4.7
10.0	23	17.3	15.7	1.05	7.7	47.3	49.1	3.6
Farnesene								
5.0	23	34.9	4.2	1.15	3.8	60.9	39.1	0.0
5.0	30	35.7	4.1	1.16	3.7	59.7	40.3	0.0
5.0	40	34.3	4.1	1.16	3.9	63.0	37.0	0.0
2.5	23	60.7	2.2	1.10	2.2	64.4	35.6	0.0
10.0	23	18.4	9.7	1.04	7.2	60.0	40.0	0.0

[a] Calculated using the absolute molar mass M_n^{NMR} and total volume of the reaction mixture. [b] Determined by SEC (eluent: THF, PI-calibration). [c] Determined by ^{1}H NMR.[3],[4]

4. NMR Spectra of Homopolymers

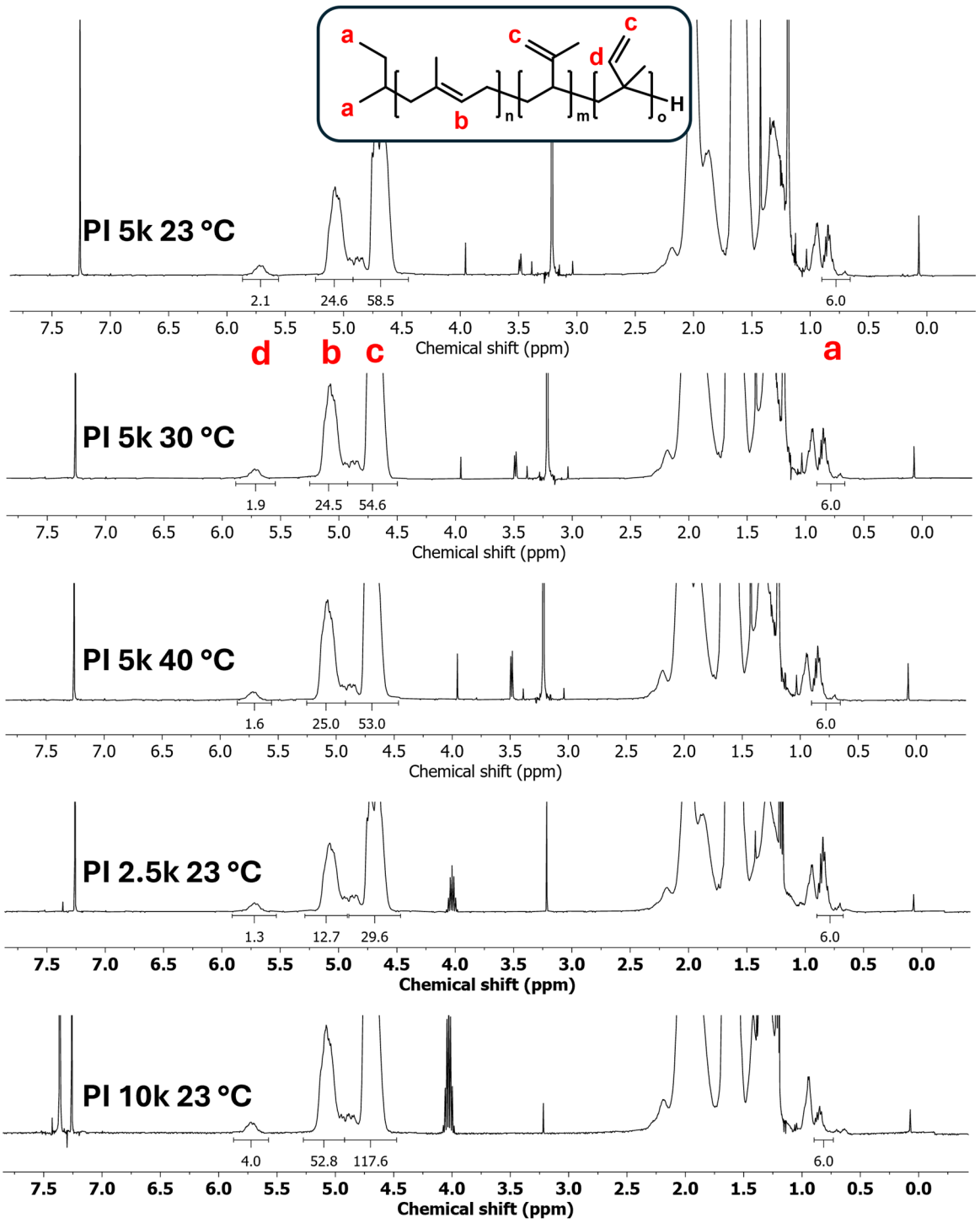

Figure S10. ^{1}H NMR spectra of all PI samples and their proton integrals assigned to the respective characteristic microstructure, measured in $CDCl_3$ at 400 MHz.

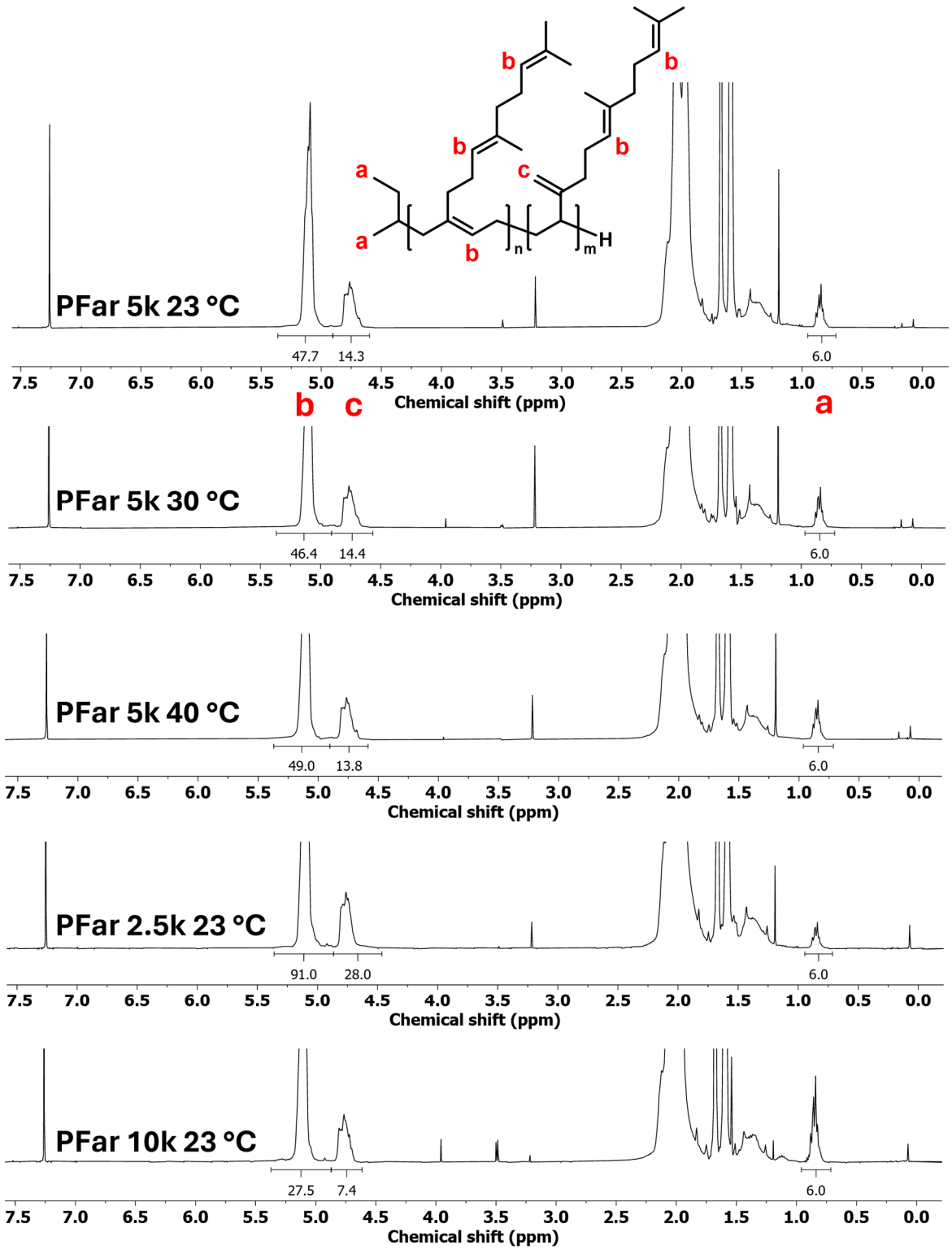

Figure S11. ^{1}H NMR spectra of all PFar samples and their proton integrals assigned to the respective characteristic microstructure, measured in $CDCl_3$ at 400 MHz.

5. SEC Results

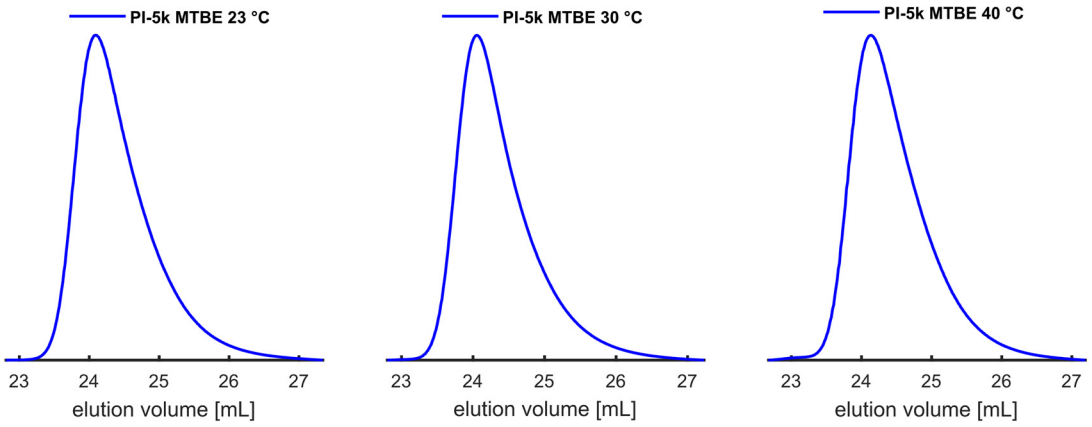

Figure S12. SEC traces of *in situ* ^{1}H NMR kinetics PI-samples of polymerizations performed at different temperatures, measured in THF using a PI-calibration. For M_n and dispersity, see Table S1.

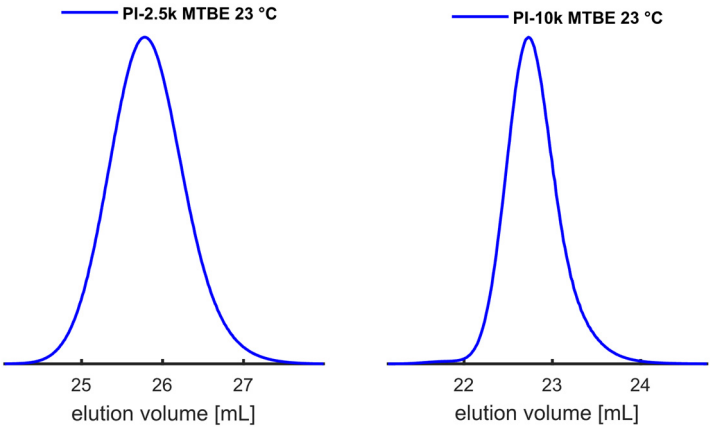

Figure S13. SEC traces of *in situ* ^{1}H NMR kinetics PI-samples targeting 2.5 kg·mol^{-1} and 10 kg·mol^{-1}, measured in THF using a PI-calibration. For M_n and dispersity, see Table S1.

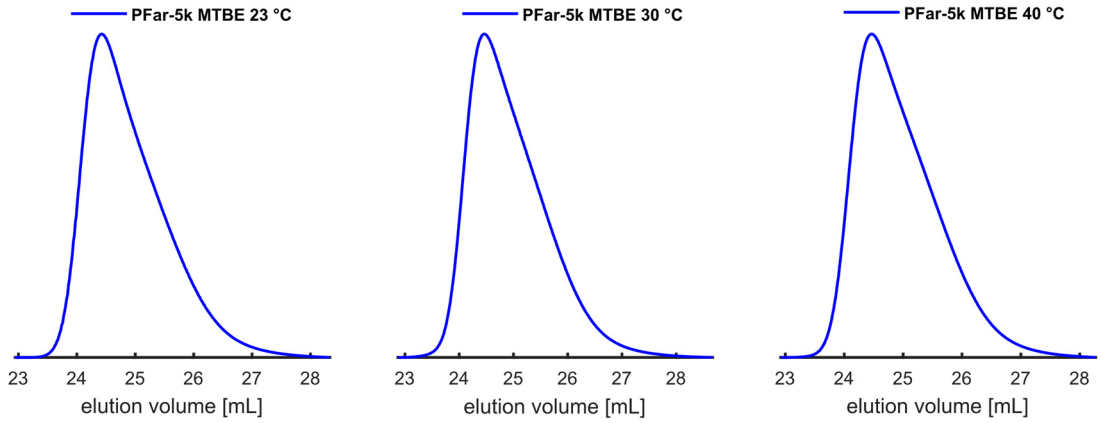

Figure S14. SEC traces of *in situ* ^{1}H NMR kinetics PFar-samples of polymerizations performed at different temperatures, measured in THF using a PI-calibration. For M_n and dispersity, see Table S1.

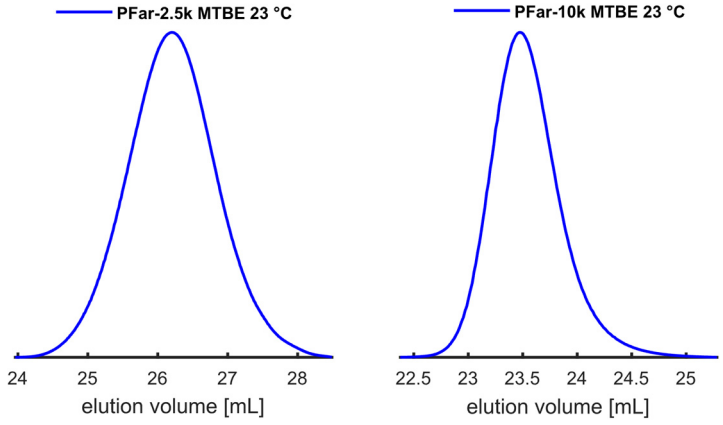

Figure S15. SEC traces of *in situ* ^{1}H NMR kinetics PFar-samples targeting 2.5 kg·mol^{-1} and 10 kg·mol^{-1}, measured in THF using a PI-calibration. For M_n and dispersity, see Table S1.

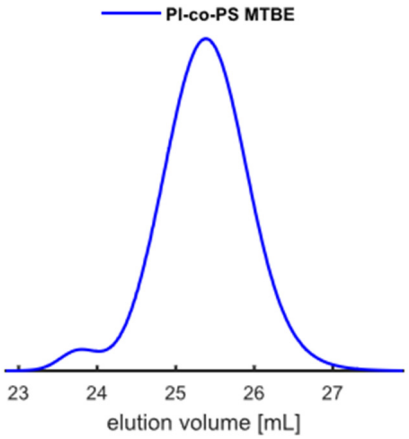

Figure S16. SEC trace of *in situ* ^{1}H NMR kinetics sample of the copolymerization of isoprene and styrene in MTBE at 23 °C, measured in THF with a PS-calibration.

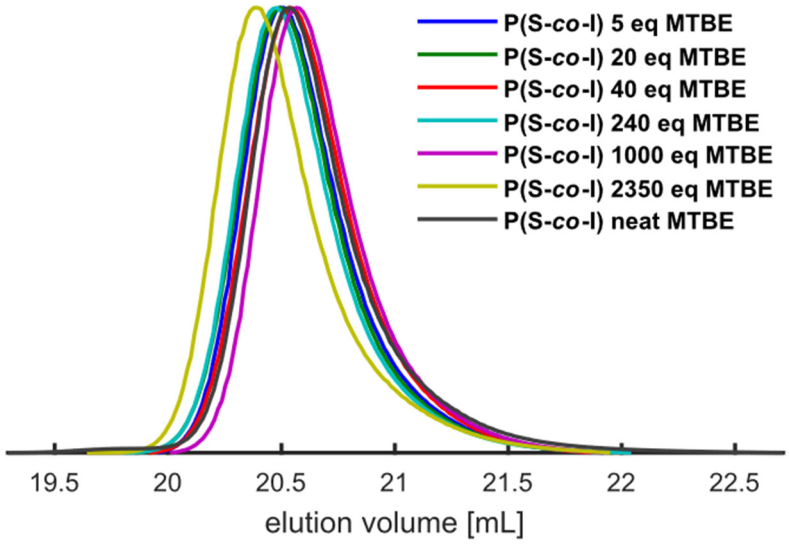

Figure S17. SEC trace of *in situ* NIR kinetic samples of the copolymerization of isoprene and styrene in cyclohexane with different equivalents of MTBE at 20 °C, measured in THF with a PS-calibration.

6. Copolymerization of Isoprene and Styrene

6.1 *In situ* ^{1}H NMR Kinetics

The copolymerization of isoprene and styrene was investigated both *via in situ* ^{1}H NMR kinetics and *in situ* NIR kinetics. First, neat MTBE was used as a solvent in the NMR experiment, see **Figure S18**. The individual monomer consumption is plotted versus time and total conversion and the Jaacks equation,[5] **Equation S1**, is used to determine the reactivity ratios, r_I and r_S. All three plots are illustrated in **Figure S19**, and the results is summarized in **Table 2**.

$$\ln\frac{[M_1]_0}{[M_1]_t} = r_1 \ln\frac{[M_2]_0}{[M_2]_t}; \qquad r_2 = 1/r_1 \tag{S1}$$

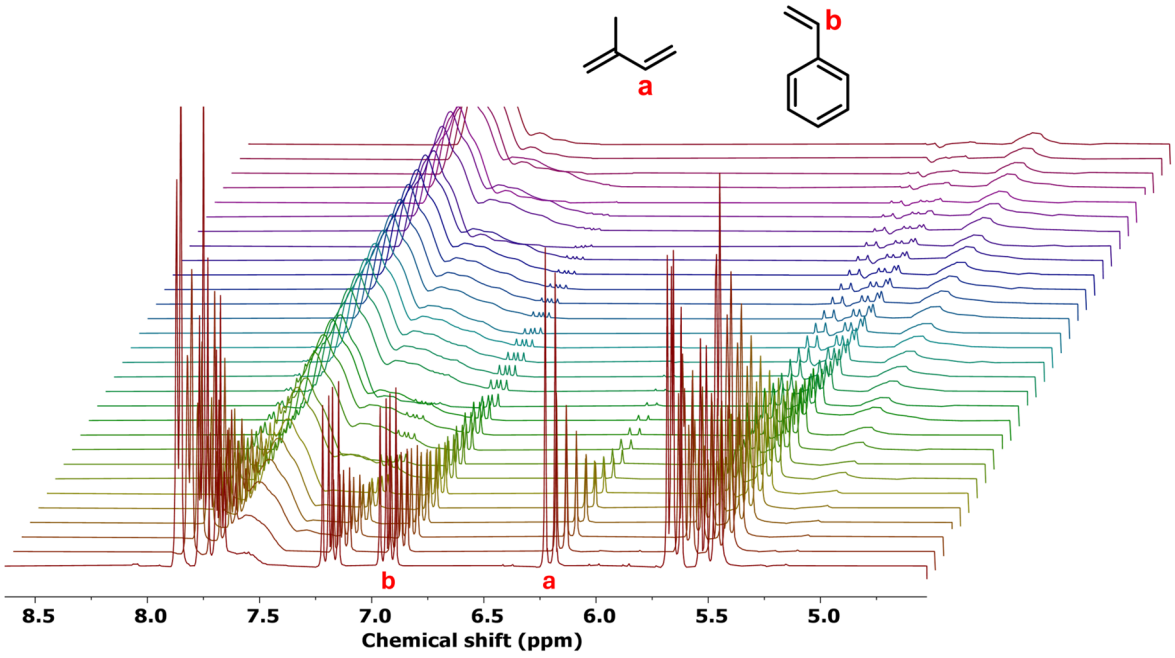

Figure S18. *In situ* ^{1}H NMR spectra of the copolymerization of styrene and isoprene in neat MTBE, measured in non-deuterated MTBE at 23 °C and 400 MHz.

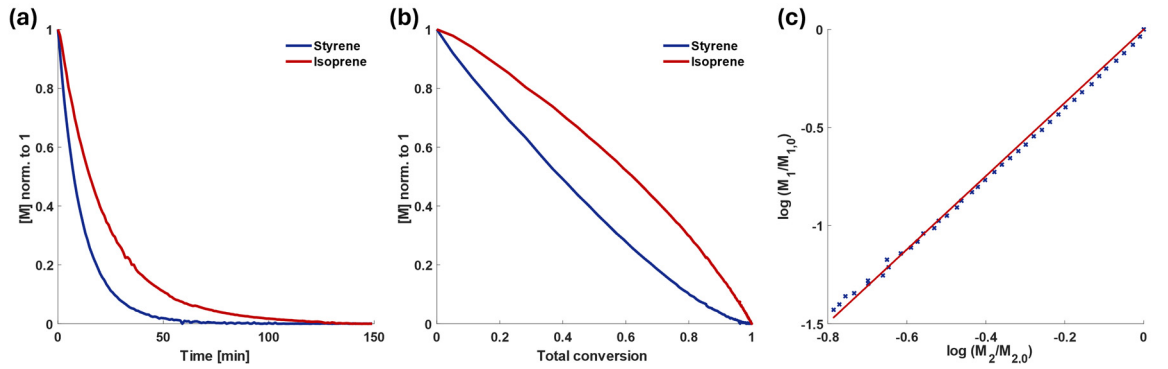

Figure S19. *In situ* ^{1}H NMR kinetics of the copolymerization of styrene and isoprene in MTBE at 23 °C, (a) time-conversion plot, (b) monomer consumption vs. total consumption, (c) Jaacks-fit of the copolymerization; r_I=0.53 and r_S=1.87.

6.2 *In Situ* NIR Kinetics

For the determination of the influence of an increasing amount of MTBE added to the copolymerization in cyclohexane, *in situ* NIR kinetics experiments were performed. The equivalents of [MTBE]/[Li] were steadily increased from 5 to 20, 40, 240, 1000, 2350 to 4700 equivalents, respectively. Pure MTBE was achieved by 4700 equivalents. In the following, the time-conversion and monomer-total conversion-plots and the respective fits for the determination of the reactivity ratios are given, see **Figure S20-S26**.

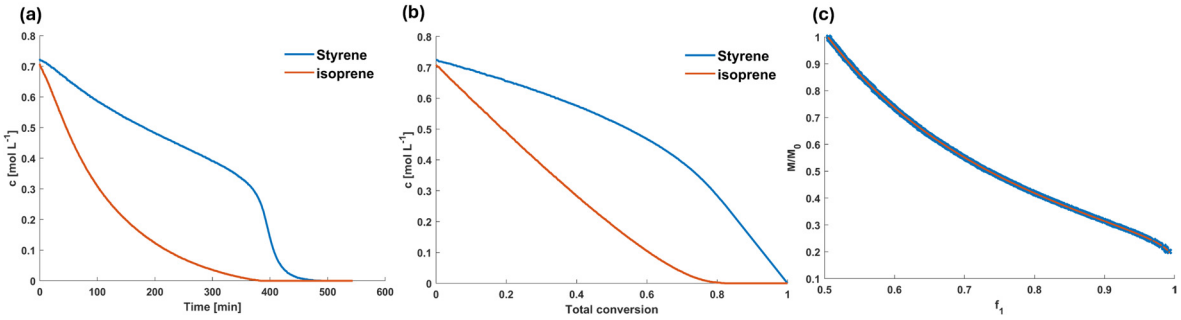

Figure S20. *In situ* NIR kinetics of the copolymerization of styrene and isoprene in CHx and 5 eq MTBE at 20 °C, (a) time-conversion plot, (b) monomer consumption vs. total consumption, (c) Meyer Lowry-fit of the copolymerization, r_I=3.13 and r_S=0.09.

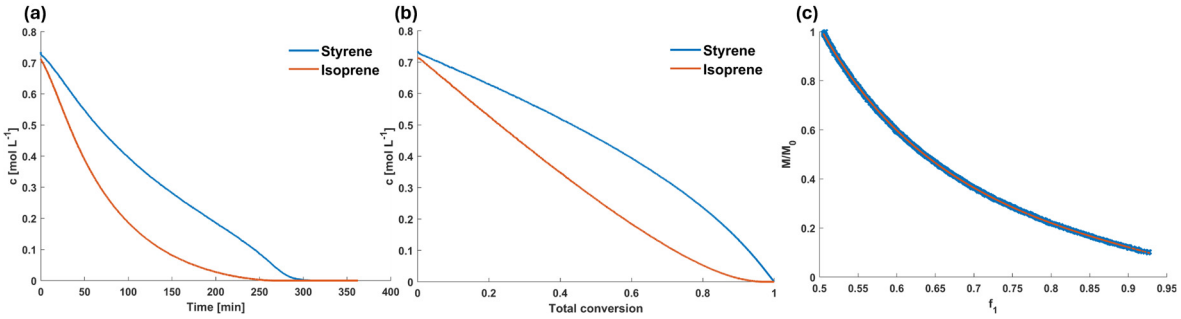

Figure S21. *In situ* NIR kinetics of the copolymerization of styrene and isoprene in CHx and 20 eq MTBE at 20 °C, (a) time-conversion plot, (b) monomer consumption vs. total consumption, (c) Meyer Lowry-fit of the copolymerization, r_I=1.74 and r_S=0.31.

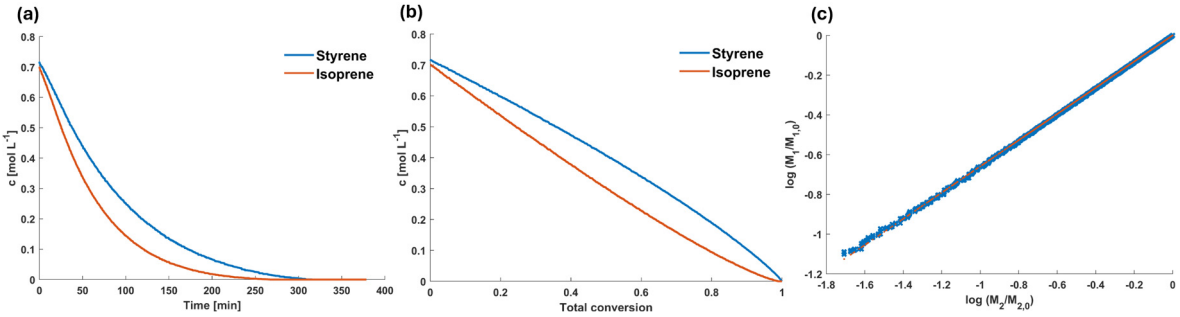

Figure S22. *In situ* NIR kinetics of the copolymerization of styrene and isoprene in CHx and 40 eq MTBE at 20 °C, (a) time-conversion plot, (b) monomer consumption vs. total consumption, (c) Jaacks-fit of the copolymerization, r_I=1.52 and r_S=0.66.

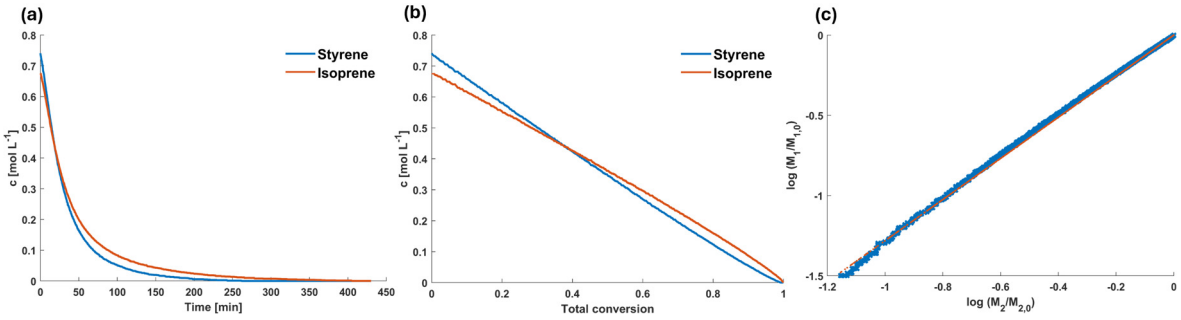

Figure S23. *In situ* NIR kinetics of the copolymerization of styrene and isoprene in CHx and 240 eq MTBE at 20 °C, (a) time-conversion plot, (b) monomer consumption vs. total consumption, (c) Jaacks-fit of the copolymerization, r_I=0.78 and r_S=1.28.

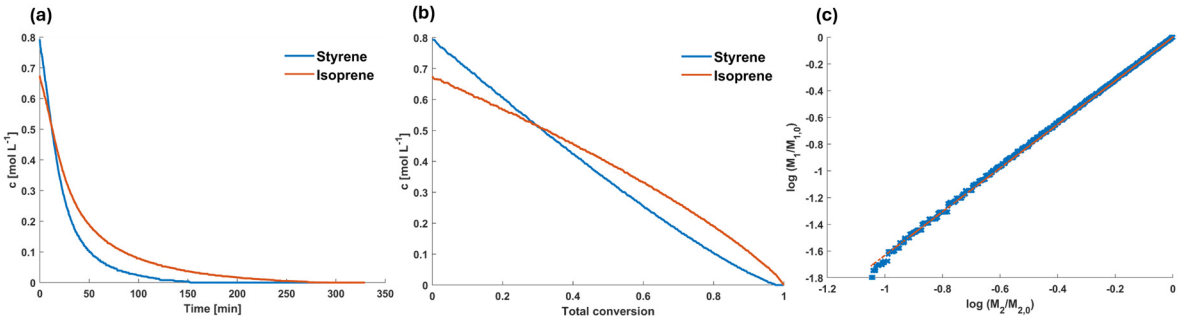

Figure S24. *In situ* NIR kinetics of the copolymerization of styrene and isoprene in CHx and 1000 eq MTBE at 20 °C, (a) time-conversion plot, (b) monomer consumption vs. total consumption, (c) Jaacks-fit of the copolymerization, r_I=0.61 and r_S=1.63.

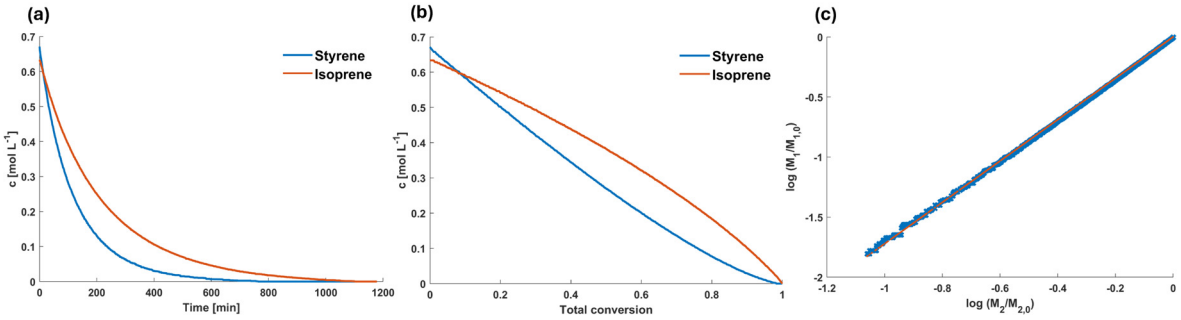

Figure S25. *In situ* NIR kinetics of the copolymerization of styrene and isoprene in CHx and 2350 eq MTBE at 20 °C, (a) time-conversion plot, (b) monomer consumption vs. total consumption, (c) Jaacks-fit of the copolymerization, r_I=0.58 and r_S=1.72.

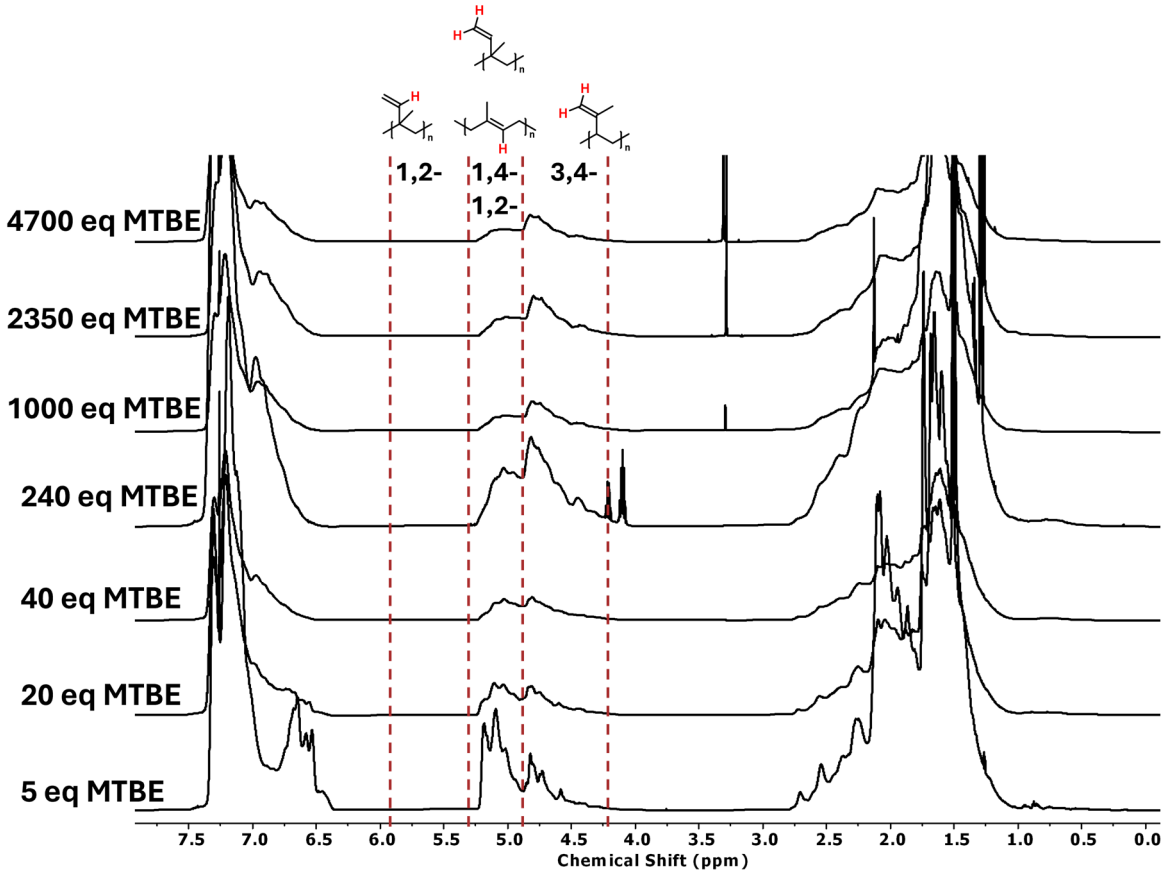

Figure S26. ^{1}H NMR results of all synthesized *in situ* NIR PS-*co*-PI copolymers indicating signals of the respective PI microstructure, measured in $CDCl_3$ and 600 MHz.

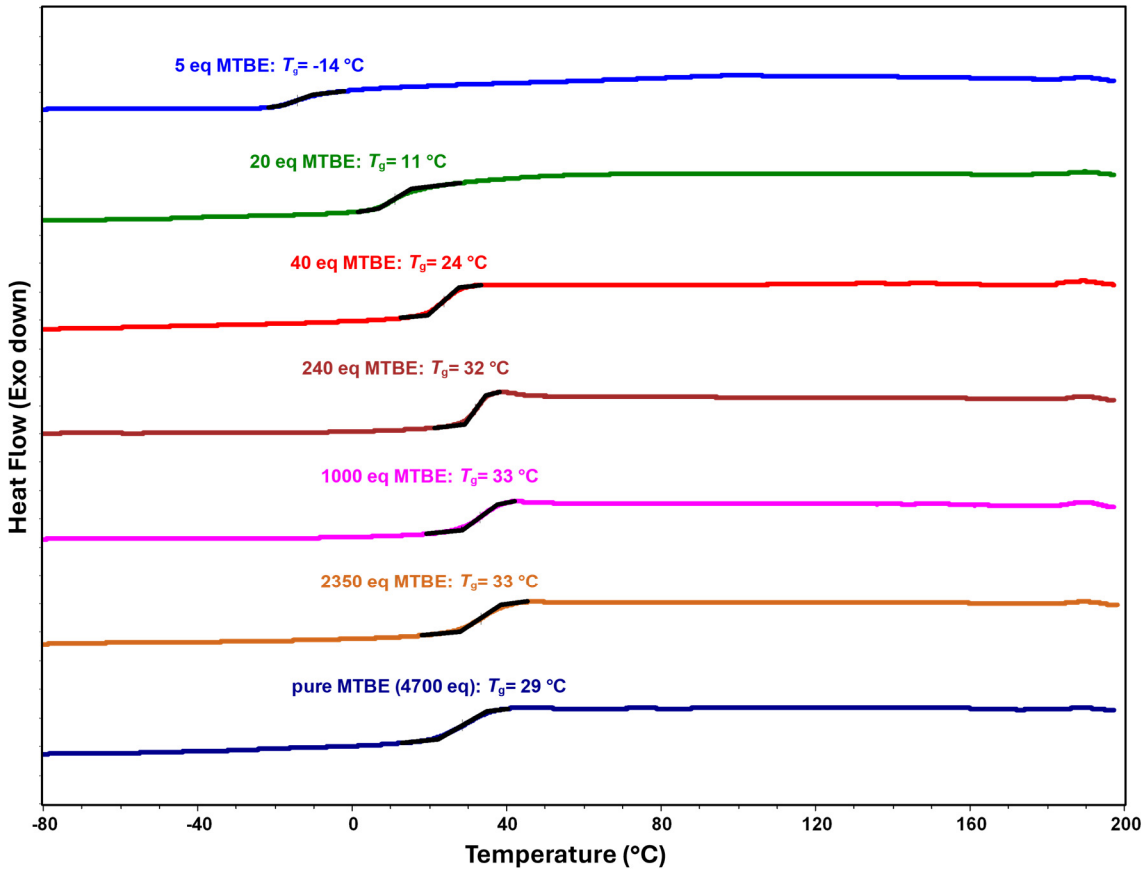

Figure S27. Second DSC heating curve of all synthesized PS-*co*-PI copolymers, measured with a heating rate of 10 K·min^{-1}.

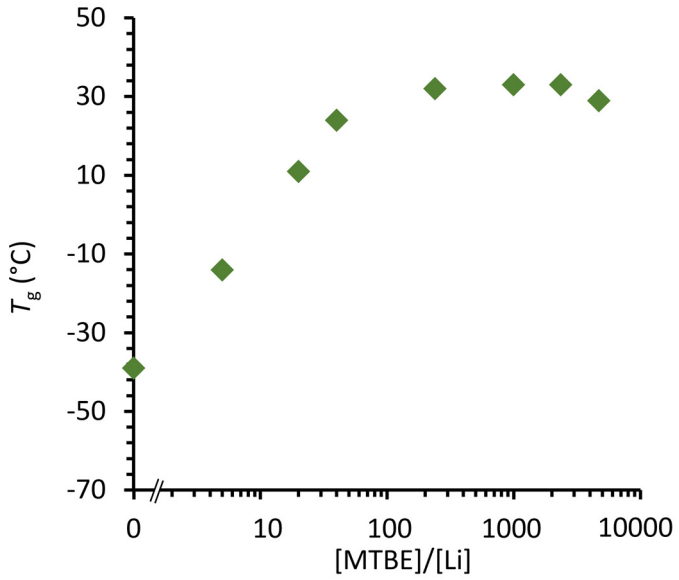

Figure S28. Glass temperature versus [MTBE]/[Li] ratio of all PS-*co*-PI copolymers.

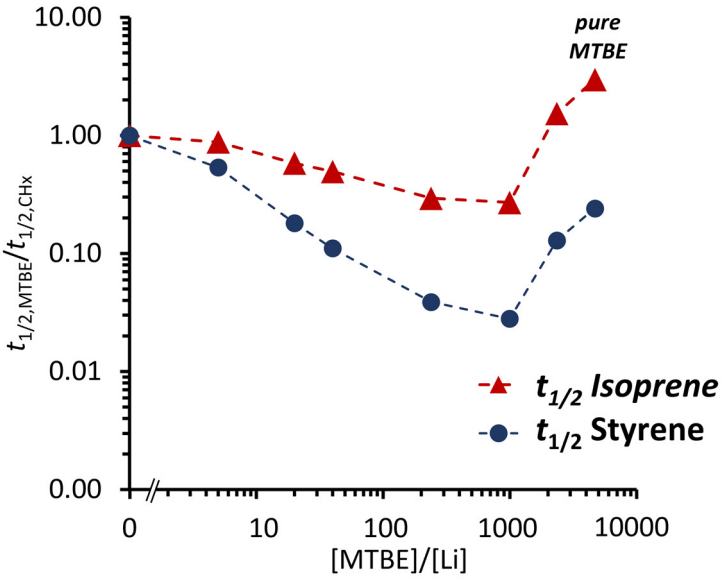

Figure S29. Half-lives of styrene and isoprene with increasing ratio [MTBE]/[Li] normalized to values in cyclohexane ($t_{1/2}^{S,CHx}$= 614 min, $t_{1/2}^{I,CHx}$= 96 min), lines connecting the symbols are a guide to the eye only.

6.3 Blockiness Study

The so-called blockiness of a PS-*co*-PI copolymer can be described by the ratio of SSS-triads in relation to all triads (ISS, ISI, SSS). The triads have slightly different shifts in the respective ^{1}H NMR spectra and can be used to quantify the SSS-triads. This can be used to get a rough estimate on the parameter "blockiness" that corresponds to the block-like PS-domains of at least 3 repeating units.[2],[6]–[8] The results for all PS-*co*-PI copolymer samples of this work is summarized in **Figure S30**.

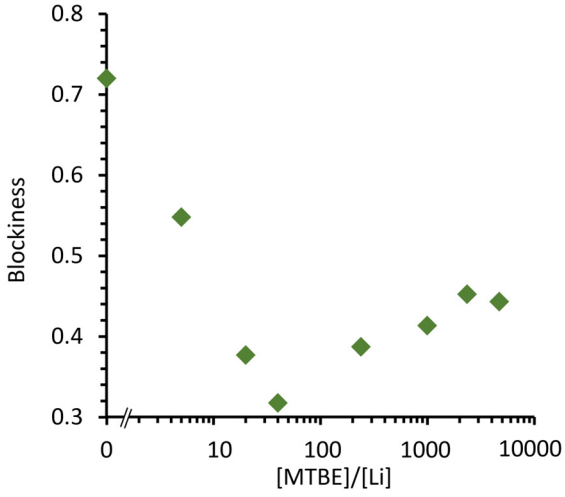

Figure S30. Blockiness of PS content of all PS-*co*-PI copolymers with increasing ratio [MTBE]/[Li], value in pure cyclohexane taken from ref[2].

References

[1] Steube, M.; Johann, T.; Plank, M.; Tjaberings, S.; Gröschel, A. H.; Gallei, M.; Frey, H.; Müller, A. H. E. Kinetics of Anionic Living Copolymerization of Isoprene and Styrene Using in Situ NIR Spectroscopy: Temperature Effects on Monomer Sequence and Morphology. *Macromolecules*, **2019**, *52* (23), 9299‑9310.

[2] Steube, M.; Johann, T.; Hübner, H.; Koch, M.; Dinh, T.; Gallei, M.; Floudas, G.; Frey, H.; Müller, A. H. E. Tetrahydrofuran: More than a "Randomizer" in the Living Anionic Copolymerization of Styrene and Isoprene: Kinetics, Microstructures, Morphologies, and Mechanical Properties. *Macromolecules*, **2020**, *53* (13), 5512‑5527.

[3] Meier-Merziger, M.; Fickenscher, M.; Hartmann, F.; Kuttich, B.; Kraus, T.; Gallei, M.; Frey, H. Synthesis of phase-separated super-H-shaped triblock architectures: poly(l-lactide) grafted from telechelic polyisoprene. *Polym. Chem.*, **2023**, *14* (23), 2820‑2828.

[4] Meier-Merziger, M.; Imschweiler, J.; Hartmann, F.; Niebuur, B.-J.; Kraus, T.; Gallei, M.; Frey, H. Bifunctional Carbanionic Synthesis of Fully Bio-Based Triblock Structures Derived from *β*-Farnesene and ll-Dilactide: Thermoplastic Elastomers. *Angew. Chem. Int. Ed.*, **2023**, *62* (42), e202310519.

[5] Jaacks, V. A Novel Method of Determination of Reactivity Ratios in Binary and Ternary Copolymerizations. *Makromol. Chem.*, **1972**, *161* (1), 161‑172.

[6] Bovey, F. A.; v. d. Tiers, G.; Filipovich, G. Polymer NSR spectroscopy. I. The motion and configuration of polymer chains in solution. *J. Polym. Sci.*, **1959**, *38* (133), 73‑90.

[7] V. D. Mochel. Nuclear Magnetic Resonance-Analog Computer Method for "Block Styrene". *Macromolecules*, **1969**, *2* (5), 537‑540.

[8] Handlin, D. L.; Williamson, D. T.; Willis, C. L. Block copolymer. US20020289833 20021107.

Chapter 4

Bifunctional Carbanionic Synthesis of Fully Bio-Based Triblock Structures Derived from β-Farnesene and LL-Dilactide: Thermoplastic Elastomers

Moritz Meier-Merziger,[a] *Jan Imschweiler,*[a] *Frank Hartmann,*[b] *Bart-Jan Niebuur,*[c] *Tobias Kraus,*[c,d] *Markus Gallei,*[b,e] *and Holger Frey* [a]*

* Corresponding authors

[a] Department of Chemistry, Johannes Gutenberg University Mainz, Duesbergweg 10-14, 55128 Mainz, Germany

[b] Chair in Polymer Chemistry, Saarland University, Campus Saarbrücken C4 2, 66123 Saarbrücken, Germany

[c] INM—Leibniz-Institute for New Materials, Campus D2 2, Saarland University, 66123 Saarbrücken, Germany

[d] Colloid and Interface Chemistry, Saarland University, Campus D2 2, 66123 Saarbrücken, Germany

[e] Saarene, Saarland Center for Energy Materials and Sustainability, Campus C4 2, 66123 Saarbrücken, Germany

Published in: *Angewandte Chemie International Edition*, **2023**, 62 (42), e202310519.
https://doi.org/10.1002/anie.202310519

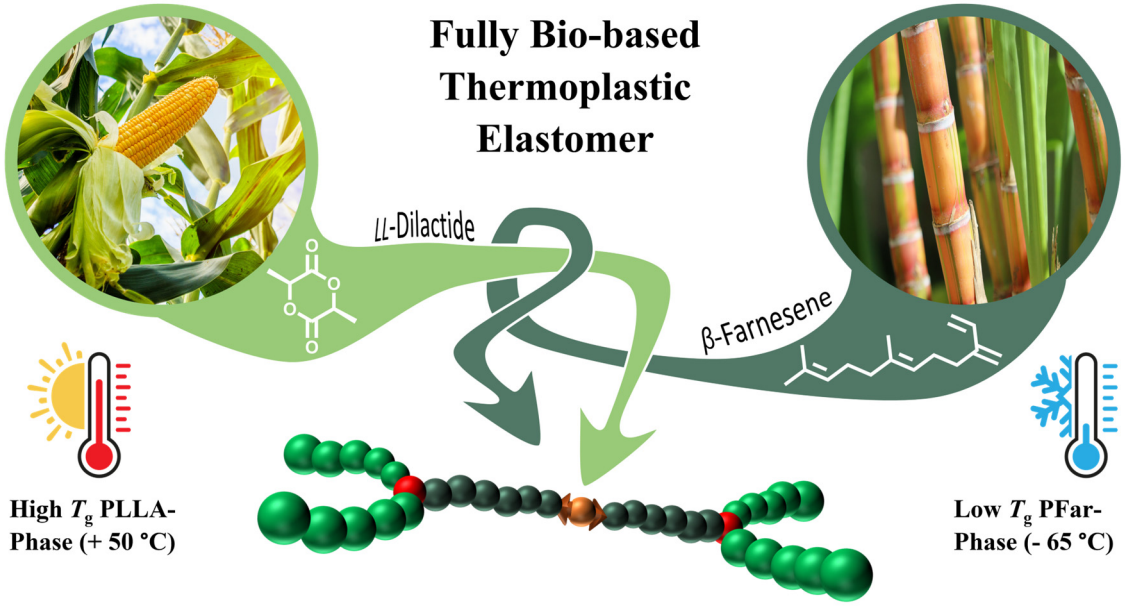

The following publication is adapted with permission from Meier-Merziger, M.; Imschweiler J.; Hartmann, F.; Niebuur, B.-J.; Kraus, T.; Gallei, M.; and Frey, H.; Bifunctional Carbanionic Synthesis of Fully Bio-Based Triblock Structures Derived from *β*-Farnesene and LL-Dilactide: Thermoplastic Elastomers, *Angewandte Chemie International Edition*, **2023**, 62 (42), e202310519.

Abstract

Current environmental challenges and the shrinking fossil fuel feedstock are important criteria for the next generation of polymer materials. In this context, we present a fully bio-based material, which shows promise as a thermoplastic elastomer (TPE). Due to the use of *β*-farnesene and LL-dilactide as monomers, bio-based feedstocks, namely sugar cane and corn, can be used. A bifunctional initiator for the carbanionic polymerization was employed, to permit an efficient synthesis of ABA-type block structures. In addition, the "green" solvent MTBE (methyl *tert*-butyl ether) was used for the anionic polymerization, enabling excellent solubility of the bifunctional anionic initiator. This afforded low dispersity (*Đ*= 1.07 to 1.10) and telechelic polyfarnesene macroinitiators. These were employed for lactide polymerization to obtain *H*-shaped triblock copolymers. TEM and SAXS revealed clearly phase-separated morphologies, and tensile tests demonstrated elastic mechanical properties. The materials featured two glass temperatures, at – 66 °C and 51 °C as well as gyroid or cylindrical morphologies, resulting in soft elastic materials at room temperature.

Introduction

Thermoplastic elastomers (TPEs) are extensively studied because of their advantages over classically vulcanized elastomers for specific applications. Especially in terms of their potential recyclability, TPEs are superior and therefore important to respond to current environmental challenges. They offer thermoplastic processability, retaining elastomeric properties at service temperatures.[1] The finite availability of fossil resources and their enormous impact on the environment lead to one of the key objectives of current research: the search for alternatives to fossil fuel-based materials. Established thermoplastic elastomers of the SBS or SIS type consist of two glassy polystyrene (PS) end-blocks, which are covalently connected to a rubber-like polybutadiene (PB) or polyisoprene (PI) mid-block. Hillmyer et al.[2],[3] showed that the PS-phase can be substituted with another high glass temperature (T_g) material, e.g., polylactide (PLA), to obtain partly bio-based TPE structures. They demonstrated the combination of different polymerization techniques to create new materials of clearly phase-separated block copolymers. Further, some examples of fully bio-based TPE structures have recently been presented in literature, showing materials that can be obtained from purely renewable raw material. They cover materials based on polyesters, polyurethanes and polyamides.[4],[5] Herein, terpenes offer great potential as alternative sources for sustainable materials.[4] For instance, β-myrcene (Myr) has been considered as a bio-based substitute for the soft phase in TPEs in various works. Anionic polymerization,[6] subsequent LA grafting[7] – [9] and also RAFT[10] were used to develop bio-based TPE structures derived from diene monomers.

A major challenge for actual application is to identify scalable processes with monomers that can be produced on large scale.[4] We recently presented a partly bio-based material with a low T_g PI midblock, flanked by outer high T_g lactide blocks.[11] Here we aim at fully bio-based TPEs, which are synthesized by combining carbanionic and ring-opening polymerization.

A rather less considered, bio-based monomer can be found in the group of terpenes: the diene β-farnesene (Far) is already produced on an industrial scale.[12] β-Farnesene is based on the renewable feedstock sugar cane, and the corresponding polyfarnesene (PFar) shows different thermal and rheological properties in bulk compared to its homologues, PI and PB. The unusual bottlebrush-like architecture leads to a significantly higher entanglement molar mass (M_e) of PFar of ≈ 49.7 kg·mol^{-1} and an even higher critical molar mass (M_c) of >105 g·mol^{-1}.[13] In comparison the M_c values of PB (5.6 kg·mol^{-1})[14] and PI (14 kg·mol^{-1})[15] are much lower. Further, both PI and PB show a strong T_g dependency on their microstructure ratio. The T_g of PI with 9% of vinyl content can be found at – 67 °C and increases to 0 °C at a vinylic fraction of 85%.[16] In comparison, PFar retains a low T_g below – 70 °C independent of the vinylic content up to 52%.[16] Therefore, Far is a highly suitable monomer for carbanionic polymerization in

polar aprotic media (i.e., ethers), in which polydienes with a high vinylic content >52% are obtained. This further facilitates the use of a bifunctional initiator for the carbanionic polymerization, which reduces the number of necessary monomer addition steps, but is known to be hardly soluble in pure hydrocarbons. As polar solvents lead to an increase in the vinylic fraction, this normally limits their relevance for widely used dienes, such as butadiene (B) and isoprene (I). Even though there are several reported bifunctional initiators available for non-polar solvents,[17] their preparation is rather complex and challenging to implement in scale-up procedures.[18] Here we demonstrate that it is possible to take full advantage of both the characteristics of Far as a building block and the use of a polar solvent for efficient dissolution of the bifunctional initiator.

We employed 1,3-diisopropenylbenzene (DIB), a commercially available initiator precursor, for our synthesis route, which is transformed to the dilithiated species by the addition of two equivalents of *tert*-BuLi.[19],[20] To further overcome undesired decomposition reactions, observed in widely used polar solvents like THF and diethyl ether in the presence of carbanionic species, methyl *tert*-butyl ether (MTBE) was investigated as an more inert alternative.[21] Besides its stability against side reactions with the nucleophilic chain end, it also established as a more sustainable solvent.[22] Even though large-scale production is currently based on the fossil resources isobutene and methanol, some partly bio-based variants, e.g. bio-MTBE, are already available on the market.[23] Other advantages, such as safer handling (no peroxide formation), have found attention in organic chemistry, but surprisingly have never gained importance in polymer chemistry.[24]

Polyfarnesyl lithium was transformed to hydroxyl functional telechelics by end-functionalization of the living chain ends with a glycidyl ether, namely ethoxy ethyl glycidyl ether (EEGE). After acidic deprotection, telechelic tetrahydroxyl macroinitiators with a high degree of end-functionalization are accessible in a highly controlled manner.[25] The targeted 100% bio-based A_2BA_2-type triblock-type structure was further generated by polymerization of LL-dilactide (LLA), one of the most abundant bio-based materials to date. The corresponding poly-(L)-lactide (PLLA) has a T_g of ≈ 60 °C and therefore acts as a suitable candidate for the "hard" block of TPEs.[26] By simply varying the respective glycidyl ether, different and more elaborate structures are accessible. The step-by-step synthesis route can be followed in **Scheme 1**. Pitet et al. recently demonstrated that lactide polymerization onto PFar macroinitiators is also suitable for flow synthesis, highlighting the potential for scale-up.[27]

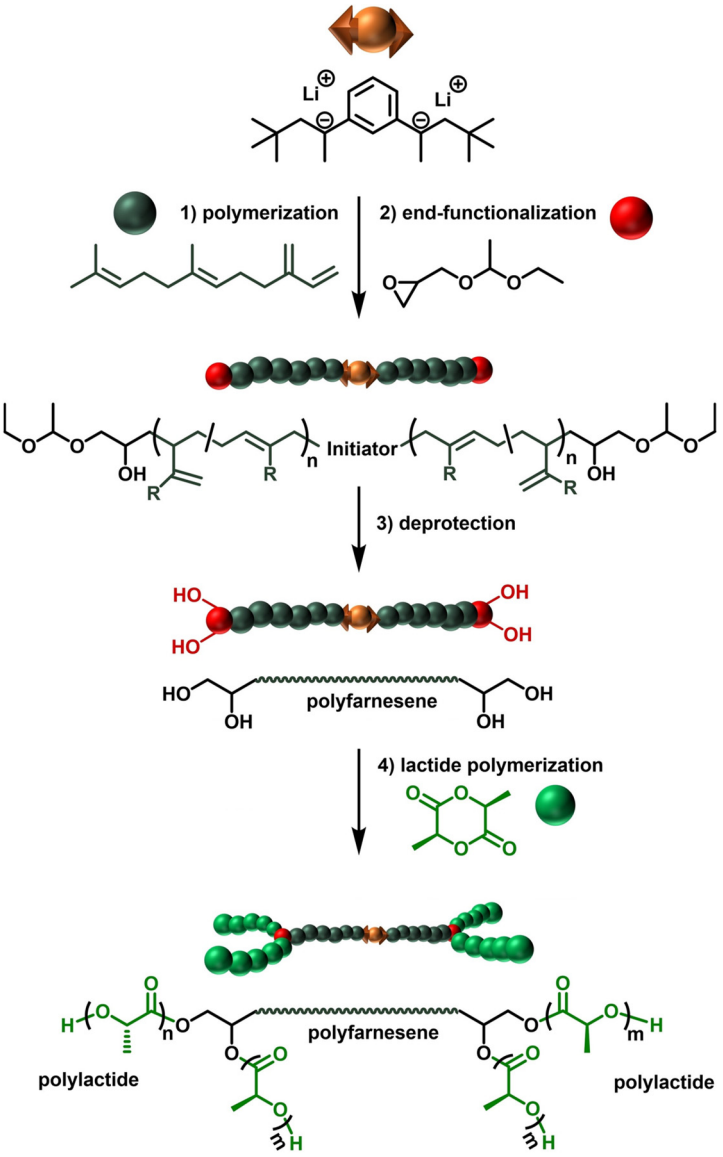

Scheme 1. Synthesis pathway: Far initiated by DIB/*tert*-BuLi and subsequent end-functionalization using EEGE, then deprotection followed by organocatalyzed ROP of LLA to form H-shaped A_2BA_2-type triblock copolymers.

Results and Discussion

The successful preparation of the active initiator species derived from the reaction of DIB/*tert*-BuLi was tracked by ^{1}H NMR spectroscopy. Full conversion of the respective benzylic double bonds was observed within the first monitored time frame (<1 min) (**Figure S1**). The deep red colored solution was diluted, and the color faded to a slightly yellowish color upon the addition of Far, showing the crossover from the benzylic carbanions of the initiator to the farnesyl lithium chain ends. After full monomer consumption, the addition of a tenfold excess of EEGE led to an instant decolorization due to the introduction of alkoxide groups at the chain ends and formation of a highly viscous organo-gel. Upon protonation of the chain ends by addition

of degassed methanol a polymer solution of low viscosity was obtained. Since end-group determination by NMR spectroscopy leads to reliable results only for low molar masses (M_n), a low M_n sample of 5000 g·mol^{-1} was prepared. An end-group functionality of 94% for EEGE-PFar(5k)-EEGE was determined by comparison of the signal of the methyl groups (≈ 0.88 ppm) of the initiating species with the proton signals of the end-group in the respective ^{1}H NMR (**Figure S2**). Likewise, the spectra can be used to determine the M_n by NMR. The obtained M_n^{NMR} of 6600 g·mol^{-1} differs slightly from the size-exclusion-chromatography (SEC) results M_n^{SEC} = 5700 g·mol^{-1}), which can be explained by the utilization of a PI-calibration for the SEC measurement. Both methods lead to a value close to the expected M_n. Combining all observations leads to the conclusion that a highly controlled bifunctional polymerization and subsequent termination occurs.

Consequently, three additional high molar mass macroinitiators (targeted M_n: 30k, 50k and 80k) were synthesized for the preparation of triblock copolymers. The SEC traces of the telechelic EEGE-PFar-EEGE samples are displayed in **Figure 1**, showing low dispersity ($Đ$) of 1.07 to 1.10, reflecting the controlled and living behavior of the synthesis. A slight shoulder is observed for the higher molar mass samples, which is caused by inevitable initiation of *tert*-BuLi utilized for the preparation of the bifunctional initiator. This, however, indicates the presence of a mainly bifunctional species during the polymerization. The remaining low dispersity of the samples emphasizes a negligible monofunctional content.

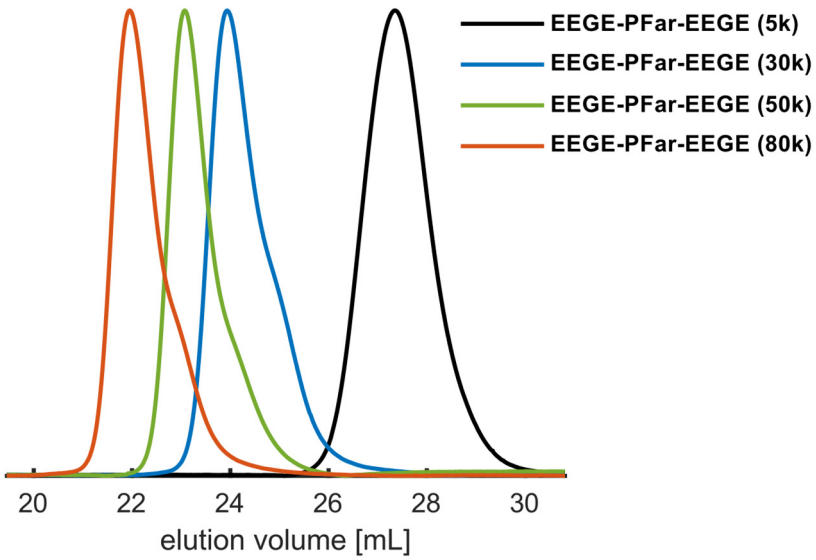

Figure 1. SEC traces of all end-capped EEGE-PFar-EEGE telechelics targeting 5k, 30k, 50k and 80k (eluent: THF, PI-calibration).

Characterization results are summarized in **Table 1**, including the ratio of the different microstructures of all samples determined by ^{1}H NMR spectroscopy, see Supporting Information. The 1,4-PFar content decreases to approximately 61%. In non-polar solvents, e.g., heptane, a 1,4-PFar content of 91% is obtained.[13] It is interesting to note that only 3,4-PFar is observed, and 1,2-PFar units were absent. In a next step, the partially acetal-protected hydroxyl groups at the chain ends were deprotected under acidic conditions *via* addition of ion-exchange resin (DOWEX) to the polymer solution. It is important to note that these reaction conditions are applicable for larger scales, due to the straight-forward separation of the resin *via* filtration.

Table 1. Data of the synthesized A_2BA_2-type triblock copolymers and their respective macroinitiators.

Sample	M_n^{target} [g·mol^{-1}] / $\Phi_{LA}^{targeted}$	M_n^{SEC} [a] [g·mol^{-1}]	$Đ$ [a]	1,4-Far[b] [%]	Φ_{LA} [c] [%]	T_g^1 [d] [°C]	T_g^2 [d] [°C]	T_m [e] [°C]	SAXS [f]	TEM [f]
EEGE-PFar-EEGE (5k)	**5 000**	**5 700**	**1.17**	**59.0**	**-**	**-**	**-**	**-**	**-**	**-**
EEGE-PFar-EEGE (30k)	**30 000**	**24 100**	**1.10**	**61.2**	**-**	**-**	**-**	**-**	**-**	**-**
(PLLA$_{2.6k}$)$_2$-*b*-PFar(30k)-*b*-(PLLA$_{2.6k}$)$_2$	+ 20% PLLA	30 200	1.17	61.2	18.3	-	-	-	mix	H
(PLLA$_{4.5k}$)$_2$-*b*-PFar(30k)-*b*-(PLLA$_{4.5k}$)$_2$	+ 30% PLLA	39 100	1.14	61.2	28.6	- 64	50	149	H	G
EEGE-PFar-EEGE (50k)	**50 000**	**36 300**	**1.07**	**61.8**	**-**	**-**	**-**	**-**	**-**	**-**
(PLLA$_{4.4k}$)$_2$-*b*-PFar(50k)-*b*-(PLLA$_{4.4k}$)$_2$	+ 20% PLLA	43 600	1.19	61.8	20.0	-	-	-	H	#NA
(PLLA$_{7.5k}$)$_2$-*b*-PFar(50k)-*b*-(PLLA$_{7.5k}$)$_2$	+ 30% PLLA	54 600	1.18	61.8	28.5	- 66	51	136	#NA	#NA
EEGE-PFar-EEGE (80k)	**80 000**	**57 400**	**1.09**	**63.5**	**-**	**-**	**-**	**-**	**-**	**-**
(PLLA$_{7.0k}$)$_2$-*b*-PFar(80k)-*b*-(PLLA$_{7.0k}$)$_2$	+ 20% PLLA	59 800	1.36	63.5	20.6	-	-	-	S	S
(PLLA$_{12k}$)$_2$-*b*-PFar(80k)-*b*-(PLLA$_{12k}$)$_2$	+ 30% PLLA	79 400	1.27	63.5	23.6	- 66	51	134	L	G

[a] Eluent: THF, calibration: PI. [b] Calculated from ^{1}H NMR, see SI. [c] Calculated from PFar:PLLA ratio from ^{1}H NMR assuming the homopolymer density ρ(PFar): 0.900 g·cm^{-3} [13] and ρ(PLLA): 1.264 g·cm^{-3}.[28] [d] From second heating curve measured by DSC, with a heating rate of 10 K·min^{-1}. [e] DSC value of the first heating curve. [f] Determined by TEM and SAXS, S: spherical, G: gyroidal, H: hexagonally packed cylinders, L: lamellar.

Complete disappearance of the methine proton signals of the protecting group at 4.55 ppm in the ^{1}H NMR spectrum (**Figure S3**) confirmed successful cleavage. In the following step, the desired fully bio-based block copolymer structure was obtained *via* organobase catalyzed ring-opening polymerization (ROP) of LLA with 1,8-diazabicyclo(5.4.0)undec-7-ene (DBU), using the telechelic multihydroxyl functional PFar. The polymerization technique is known to

provide narrow molar mass distributions and short reaction times despite the mild reaction conditions.[29],[30]

After work-up, a solid material was isolated. The expected shift towards higher molar masses was observed by SEC, see **Figure 2** (a–c). As the methine proton signals of PLLA and the 3,4-PFar signals overlap in the ^{1}H NMR spectrum, determination of the PLLA volume fraction is not straightforward. Since the 1,4-PFar to 3,4-PFar ratios of the macroinitiators are known, the 3,4-PFar proton content can be subtracted from the combined ^{1}H NMR signal. The remaining integral of the signal is due to the methine signal of PLLA. Thereby, the molar ratio can be calculated. The volume fraction of PLLA (Φ_{LA}) is approximated by the literature-known densities of the PFar and PLLA, ρ(PFar): 0.900 g·cm^{-3};[13] ρ(PLLA): 1.264 g·cm^{-3}.[28]

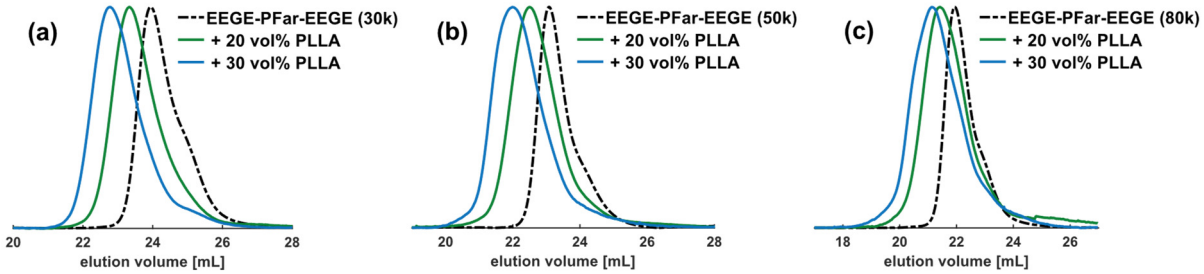

Figure 2. SEC traces of all telechelic macroinitiators and their corresponding triblock copolymers: (a) EEGE-PFar-EEGE (30k) with +20 vol% and +30 vol% PLLA; (b) EEGE-PFar-EEGE (50k) with +20 vol% and +30 vol% PLLA; (c) EEGE-PFar-EEGE (80k) with +20 vol% and +30 vol% PLLA; (c) EEGE-PFar-EEGE (80k) with +20 vol% and +30 vol% PLLA; (eluent: THF, PI-calibration).

Based on the ^{1}H NMR results shown in **Table 1**, PLLA volume fractions between 18 and 29 vol% were determined that are near the theoretical values. A slight broadening is observed in the SEC diagram (see **Figures 2** and **S9–11**), which is explained by the presence of different initiating species. However, as the SEC distribution remains unimodal, successful chain extension is confirmed. The absence of a PLLA homopolymer species in diffusion-ordered-spectroscopy measurements (**Figure S5**) indicates successful and controlled initiation by the PFar macroinitiator.

The successful triblock copolymer synthesis motivated further studies of the newly formed materials with respect to TPE properties. Evidence for phase-separation was found by differential scanning calorimetry (DSC) measurements (**Figure 3**), showing two distinct T_gs for each sample. The lower T_g between – 66 °C and – 64 °C is caused by the PFar phase and the higher one at around 50 °C can be attributed to PLLA. In addition to the observed T_gs, all samples showed a melting point (T_m) in the temperature range of 134 °C to 149 °C, see **Figures S6–8**. However, the melting endotherms were only visible in the first heating run of

the measurements. The time frame or cooling rate upon cooling was therefore not sufficient to allow for (re)crystallization of PLLA. A recrystallization peak was also absent in the cooling curve.

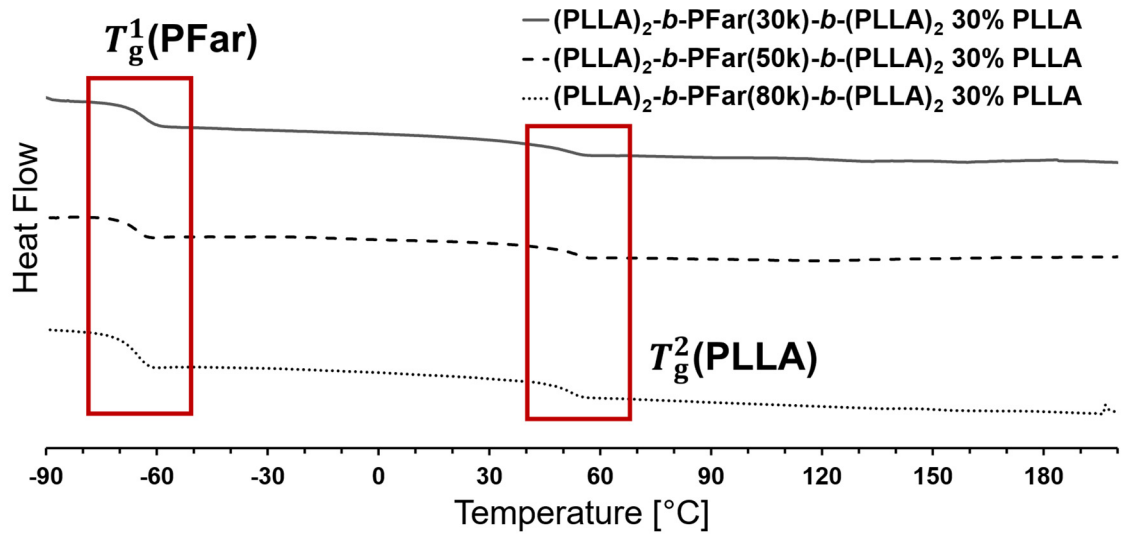

Figure 3. Second DSC heating curve of all (PLLA)$_2$-*b*-PFar-*b*-(PLLA)$_2$ with a targeted PLLA volume fraction of 30 vol%, (heating rate of 10 K·min^{-1}).

Phase-separation was confirmed by transmission electron microscopy (TEM) for most samples, see **Figure 4** and **S15**. Hexagonal (**Figure 4a**), gyroidal (**Figure 4b**) and spherical (**Figure 4c**) morphologies were observed, some of which comprise phase-separation of several domain sizes within one sample. Remarkably, the complex gyroid morphology was present in two of the samples, which is explained by the elaborate *H*-shaped architecture that leads to curvature at the interface.[31]

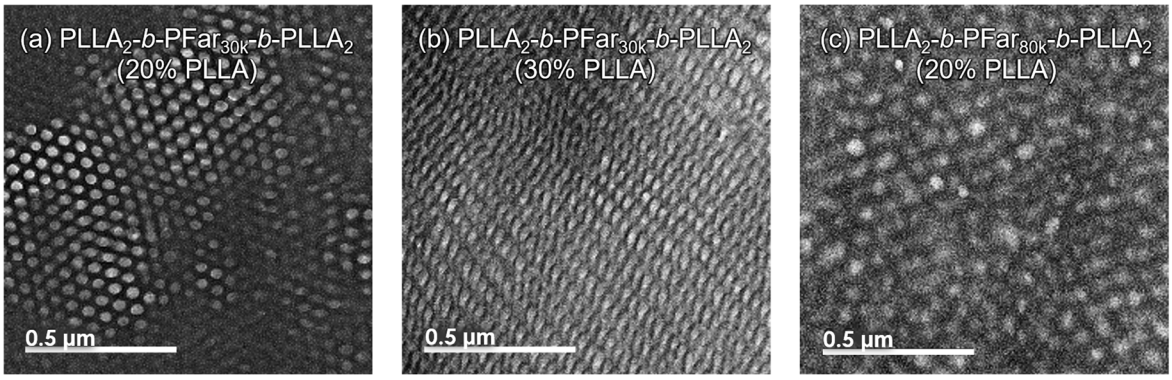

Figure 4. TEM Images of (PLLA)$_2$-*b*-PFar-*b*-(PLLA)$_2$ samples of different compositions, solvent cast, 16 h annealing at 80 °C and OsO_4 stained; (a) (PLLA)$_2$-*b*-PFar(30k)-*b*-(PLLA)$_2$ 20% PLLA; (b) (PLLA)$_2$-*b*-PFar(30k)-*b*-(PLLA)$_2$ 30% PLLA; (c) (PLLA)$_2$-*b*-PFar(80k)-*b*-(PLLA)$_2$ 20% PLLA.

The different architecture of the polymers leads to a deviation of the morphology from the phase diagram of classical linear block copolymers at given volume ratios. In some cases, the determination of the phase-separation resulted in some deviation between the applied analytical techniques. DSC results suggest phase-separation for all measured samples, but in case of the 50k PFar samples no phase-separation was observed in the TEM images. Despite well-defined phase-separation for most samples, the morphology could not be determined in every case. Therefore, additional validation studies were performed using small-angle X-ray scattering (SAXS), which probes the bulk structural properties and averages over larger sample volumes compared to TEM. As is described in the SI, the SAXS measurements revealed different morphologies compared to the ones assigned by TEM for most samples. PFar(30k) with 20 vol% PLLA (**Figure S16a**) even showed a combination of reflections that can be attributed to a mixed morphology. The obtained volume fraction of PLLA appears to be at the transition point of two morphologies in the phase diagram. To which extent the *H*-shaped architecture plays a peculiar role for the morphology will be a subject of future work. The determined morphologies for all samples are listed in **Table 1**.

ABA-type triblocks are widely used thermoplastic elastomers, based on domain bridging due crosslinking by the vitrified high T_g domains.[32] Tensile tests were performed for the samples with a targeted Φ_{LA} of 30%. Films were prepared *via* solvent casting process. The measurements revealed almost exclusively elastic deformation for the sample with the lowest M_n (**Figure 5**). The elongation at break (ε_{break}) was 66%, and at lower deformation the samples showed full elastic recovery. The higher M_n samples exhibited plastic deformation and strain hardening in addition to elastic deformation. This is in line with the behavior of non-bio-based SIS-rubbers.[33] The mentioned results and the Young's modulus (E) are shown in **Table S1**, and all remaining stress-strain curves are presented in **Figures S12–13**.

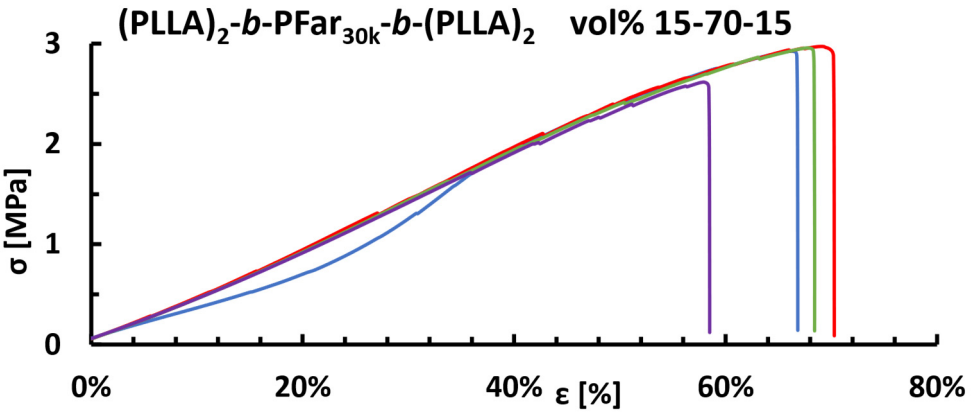

Figure 5. Stress-strain experiments of $(PLLA)_2$-*b*-PFar(30k)-*b*-$(PLLA)_2$ 30 vol% PLLA, four measurements for each sample.

The obtained values are low compared to the characteristics of triblocks consisting of styrene copolymerized with isoprene or myrcene.[33] This is most likely due to the aforementioned, considerably higher M_e of PFar, which requires even longer PFar midblocks to achieve higher strength and elongation.[34] Further, by distributing the lactide units over 4 arms of the *H*-shaped architecture, each arm of the respective chain has still a rather low molar mass of 2.6 kg·mol^{-1} up to 12 kg·mol^{-1}. This could explain the low degree of crystallization of PLLA observed in the DSC measurements. Thus, the obtained mechanical characteristics can clearly be attributed to the targeted structure and the moderate molar masses. Further tailoring and improvement of the material properties for specific applications and to obtain stronger TPEs is possible *via* the synthesis sequence introduced in this work.

Conclusions

In summary, we capitalize on the hardly used, slightly polar bio-based solvent MTBE for the bifunctional, anionic initiation and at the same time rely on the low T_g of PFar, despite its increased vinyl content in this solvent. Telechelic multi α,ω-hydroxyl PFar macroinitiators were generated *via* controlled end-functionalization of the living anionic chain ends. By using LLA for the subsequent polymerization, *H*-shaped A_2BA_2-type copolymers were accessible. These materials showed microphase-segregation, manifest in two distinct T_gs for all samples, covering a broad service temperature range from – 66 °C to 51 °C. Longer PLLA chains that crystallize may considerably increase the upper service temperature of the TPEs in the future. TEM and SAXS of the copolymers showed different morphologies e.g. gyroid and hexagonal cylinders, and surprisingly also mixtures of those. As the obtained morphologies deviate from expectation for classical linear polymers, these results pave the way for a variety of further materials by varying the content of both components and even the nature of the diene and the aliphatic polyester. Since the monomers *β*-farnesene and LL-dilactide are derived from renewable feedstocks, the materials are an example of fully bio-based thermoplastic elastomers.

References

[1] Holden, G. *Understanding thermoplastic elastomers*; Hanser understanding books; Hanser, 2000.

[2] Frick, E. M.; Hillmyer, M. A. Synthesis and characterization of polylactide-block-polyisoprene-block-polylactide triblock copolymers: new thermoplastic elastomers containing biodegradable segments **2000**, *18* (21), 1317‑1322.

[3] Frick, E. M.; Zalusky, A. S.; Hillmyer, M. A. Characterization of Polylactide-b-polyisoprene-b-polylactide Thermoplastic Elastomers. *Biomacromolecules* **2003**, *4* (2), 216‑223.

[4] Tang, S.; Li, J.; Wang, R.; Zhang, J.; Lu, Y.; Hu, G.-H.; Wang, Z.; Zhang, L. Current trends in bio-based elastomer materials. *SusMat* **2022**, *2* (1), 2‑33.

[5] Wahlen, C.; Frey, H. Anionic Polymerization of Terpene Monomers: New Options for Bio-Based Thermoplastic Elastomers. *Macromolecules* **2021**, *54* (16), 7323‑7336.

[6] Bolton, J. M.; Hillmyer, M. A.; Hoye, T. R. Sustainable Thermoplastic Elastomers from Terpene-Derived Monomers. *ACS Macro Lett.* **2014**, *3* (8), 717‑720.

[7] Wahlen, C.; Rauschenbach, M.; Blankenburg, J.; Kersten, E.; Ender, C. P.; Frey, H. Myrcenol-Based Monomer for Carbanionic Polymerization: Functional Copolymers with Myrcene and Bio-Based Graft Copolymers. *Macromolecules* **2020**, *53* (20), 9008‑9017.

[8] Zhou, C.; Wei, Z.; Jin, C.; Wang, Y.; Yu, Y.; Leng, X.; Li, Y. Fully biobased thermoplastic elastomers: Synthesis of highly branched linear comb poly(*β*-myrcene)-graft-poly(l-lactide) copolymers with tunable mechanical properties. *Polymer* **2018**, *138*, 57‑64.

[9] Zhou, C.; Wei, Z.; Lei, X.; Li, Y. Fully biobased thermoplastic elastomers: synthesis and characterization of poly(l -lactide)-b-polymyrcene-b-poly(l -lactide) triblock copolymers. *RSC Adv.* **2016**, *6* (68), 63508‑63514.

[10] Fang, C.; Wang, X.; Chen, X.; Wang, Z. Mild synthesis of environment-friendly thermoplastic triblock copolymer elastomers through combination of ring-opening and RAFT polymerization. *Polym. Chem.* **2019**, *10* (26), 3610‑3620.

[11] Meier-Merziger, M.; Fickenscher, M.; Hartmann, F.; Kuttich, B.; Kraus, T.; Gallei, M.; Frey, H. Synthesis of phase-separated super-H-shaped triblock architectures: poly(l-lactide) grafted from telechelic polyisoprene. *Polym. Chem.* **2023**, *14* (23), 2820‑2828.

[12] McCoy, M. Amyris Puts A Price On Farnesene. *Chemical & Engineering News* **2015**, *93* (41).

[13] Iacob, C.; Yoo, T.; Runt, J. Molecular Dynamics of Polyfarnesene. *Macromolecules* **2018**, *51* (13), 4917–4922.

[14] Gruver, J. T.; Kraus, G. Rheological properties of polybutadienes prepared by n-butyllithium initiation. *J. Polym. Sci. A Gen. Pap.* **1964**, *2* (2), 797–810.

[15] Lewis J. Fetters. Determination of the Inermolecular Entanglement Coupling Spacing in Polyisoprene by Viscosity Measurments. *J. Res. Natl. Bur. Stds.* **1965** (69A), 33–37.

[16] Yoo, T.; Henning, S. K. Synthesis and Characterization of Farnesene-Based Polymers. *Rubber Chemistry and Technology* **2017**, *90* (2), 308–324.

[17] Yu, Y. S.; Jerome, R.; Fayt, R.; Teyssie, P. Efficiency of the sec-Butyllithium/m-Diisopropenylbenzene Diadduct as an Anionic Polymerization Initiator in Apolar Solvents. *Macromolecules* **1994**, *27* (21), 5957–5963.

[18] Schultz, A. R.; Bobade, S.; Scott, P. J.; Long, T. E. Hydrocarbon-Soluble Piperazine-Containing Dilithium Anionic Initiator for High Cis -1,4 Isoprene Polymerization. *Macromol. Chem. Phys.* **2018**, *219* (1), 1700201.

[19] Beinert, G.; Lutz, P.; Franta, E.; Rempp, P. A bifunctional anionic initiator soluble in non-polar solvents. *Makromol. Chem.* **1978**, *179* (2), 551–555.

[20] Yu, J. M.; Dubois, P.; Jérôme, R. Synthesis and Properties of Poly[isobornyl methacrylate (IBMA)- b -butadiene (BD)- b -IBMA] Copolymers: New Thermoplastic Elastomers of a Large Service Temperature Range. *Macromolecules* **1996**, *29* (23), 7316–7322.

[21] Stanetty, P.; Mihovilovic, M. D. Half-Lives of Organolithium Reagents in Common Ethereal Solvents. *J. Org. Chem.* **1997**, *62* (5), 1514–1515.

[22] Jordan, A.; Hall, C. G. J.; Thorp, L. R.; Sneddon, H. F. Replacement of Less-Preferred Dipolar Aprotic and Ethereal Solvents in Synthetic Organic Chemistry with More Sustainable Alternatives. *Chemical reviews* **2022**, *122* (6), 6749–6794.

[23] Nawaz, Z. Methyl-Tert-Butyl-Ether Synthesis Reactor Modelling and Optimization Using an Aspen Custom Modeler. *Hungarian Journal of Industry and Chemistry* **2017**, *45* (2), 1-7.

[24] Hamid, S. H.; Ali, M. A. Effect of MTBE Blending on the Properties of Gasoline. *Fuel Science and Technology International* **1995**, *13* (5), 509–544.

[25] Dreier, P.; Ahn, J.; Chang, T.; Frey, H. End Group Functionality of 95-99%: Epoxide Functionalization of Polystyryl-Lithium Evaluated via Solvent Gradient Interaction Chromatography. *Macromol. Rapid Commun.* **2022**, e2200560.

[26] Taib, N.-A. A. B.; Rahman, M. R.; Huda, D.; Kuok, K. K.; Hamdan, S.; Bakri, M. K. B.; Julaihi, Muhammad Rafiq Mirza Bin; Khan, A. A review on poly lactic acid (PLA) as a biodegradable polymer. *Polym. Bull.* **2022**, 1‑35.

[27] Haese, M. den; Gemoets, H. P. L.; van Aken, K.; Pitet, L. M. Fully biobased triblock copolymers generated using an unconventional oscillatory plug flow reactor. *Polym. Chem.* **2022**, *13* (30), 4406‑4415.

[28] Witzke, D. R.; Narayan, R.; Kolstad, J. J. Reversible Kinetics and Thermodynamics of the Homopolymerization of l -Lactide with 2-Ethylhexanoic Acid Tin(II) Salt. *Macromolecules* **1997**, *30* (23), 7075‑7085.

[29] Lohmeijer, B. G. G.; Pratt, R. C.; Leibfarth, F.; Logan, J. W.; Long, D. A.; Dove, A. P.; Nederberg, F.; Choi, J.; Wade, C.; Waymouth, R. M.; Hedrick, J. L. Guanidine and Amidine Organocatalysts for Ring-Opening Polymerization of Cyclic Esters. *Macromolecules* **2006**, *39* (25), 8574‑8583.

[30] Sherck, N. J.; Kim, H. C.; Won, Y.-Y. Elucidating a Unified Mechanistic Scheme for the DBU-Catalyzed Ring-Opening Polymerization of Lactide to Poly(lactic acid). *Macromolecules* **2016**, *49* (13), 4699‑4713.

[31] Hadjichristidis, N.; Iatrou, H.; Behal, S. K.; Chludzinski, J. J.; Disko, M. M.; Garner, R. T.; Liang, K. S.; Lohse, D. J.; Milner, S. T. Morphology and miscibility of miktoarm styrene-diene copolymers and terpolymers. *Macromolecules* **1993**, *26* (21), 5812‑5815.

[32] Matsushita, Y.; Mogi, Y.; Mukai, H.; Watanabe, J.; Noda, I. Preparation and morphology of multiblock copolymers of the (AB)n type. *Polymer* **1994**, *35* (2), 246‑249.

[33] Wahlen, C.; Blankenburg, J.; Tiedemann, P. von; Ewald, J.; Sajkiewicz, P.; Müller, A. H. E.; Floudas, G.; Frey, H. Tapered Multiblock Copolymers Based on Farnesene and Styrene: Impact of Biobased Polydiene Architectures on Material Properties. *Macromolecules* **2020**, *53* (23), 10397‑10408.

[34] Tzourtzouklis, I.; Hahn, C.; Frey, H.; Floudas, G. Molecular Dynamics and Viscoelastic Properties of the Biobased 1,4-Polymyrcene. *Macromolecules* **2022**, *55* (19), 8766‑8775.

Supporting Information

1. Experimental Details

1.1 Ethoxy Ethyl Glycidyl Ether (EEGE)

Ethoxy ethyl glycidyl ether (EEGE) was synthesized according to the procedure of Fitton et al.[1] In a three-necked 500 mL round-bottom flask, ethyl vinyl ether (150 g, 200 mL, 2 mol) and freshly distilled glycidol (40 g, 36 mL, 0.55 mol) were cooled to 0 °C. Then, *para*-toluene sulfonic acid (1 g, 0.005 mol) was added portion wise, that the reaction temperature would not exceed 20 °C. The mixture was stirred for 3 hours and then mixed with 100 mL of a saturated aqueous solution of sodium hydrogen carbonate. The organic layer was separated and the excess ethyl vinyl ether was removed using the rotary evaporator. The product was purified by fractionated distillation (50 °C at 5 mbar) to yield 67 g (85%) of a colorless liquid. ^{1}H NMR: (DMSO-d_6, 400 MHz) δ [ppm] = 1.12 (m, g, 3H), 1.21 (m, e, 3H), 2.57 (m, a, 1H), 2.74 (m, a', 1H), 3.09 (m, b, 1H), 3.35 (m, f, c, 2H), 3.58 (m, f', 1H), 3.73 (m, c', 1H), 4.71 (q, d, 1H, J=6 Hz).

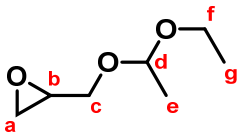

1.2 Anionic Polymerization

For the carbanionic polymerizations all used glassware was flame dried prior use. Methyl *tert*-butyl ether (MTBE) was dried over *sec*-BuLi and 1,1-diphenyl ethylene (DPE) and freshly distilled for every experiment. The monomer *β*-farnesene was first freed from its stabilizer by passing though alkaline aluminum oxide. Then it was dried over calcium hydride with three *freeze-pump-thaw* cycles. It was distilled under high vacuum ($1 \cdot 10^{-3}$ mbar) just prior use. EEGE was dried by reacting 1 eq with 0.2 eq *sec*-BuLi. The dried EEGE was distilled. By using high vacuum techniques great importance was set on a dry and oxygen free environment. All substances were put into an argon filled glove box.

As described in **Scheme S1**, a 0.1 molar stock solution of 1,3-diisopropenylbenzene (DIB) was activated by the addition of 2.05 eq *tert*-BuLi. More detailed information of the preparation of the active species of the bifunctional initiator is given in chapter "2. Activation of DIB/*tert*-BuLi". After activation the active and deep red colored initiator solution was diluted to obtain a 5 vol% monomer concentration. *β*-Farnesene was added and a color change to yellow was observed within the first two minutes. The polymerization was stirred overnight to allow full conversion of the monomer. Then 10 eq to each chain end of EEGE were added to the yellow

solution. An instant decolorization was observed. The solution got highly viscous. To allow a sufficient mixing through stirring and later through diffusion, degassed methanol was not added before 2 hours after the end capping reagent was added. By the addition of methanol, the solution got low viscous again. The polymer was isolated by precipitation in cold methanol. The yield for all samples was between 97% to 99%, indicating full conversion.

Scheme S1. Synthesis pathway for EEGE-PFar-EEGE polymer samples.

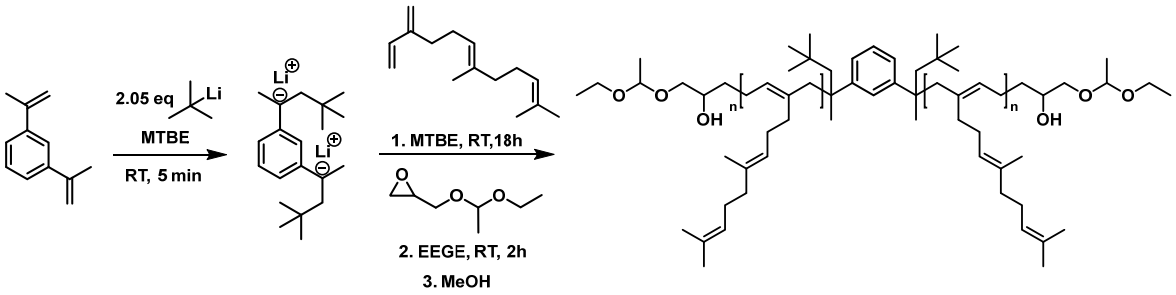

Detailed information about the allocation of protons in the respective ^{1}H NMR is given in the chapter "3. Additional NMR Results". All samples were investigated by NMR and SEC.

1.3 Deptrotection

As can be followed in **Scheme S2**, the end-functionalized PFar samples were dissolved in methylene chloride (DCM) and methanol was added to such an extent that no precipitation of the polymer occurred. DOWEX® hydrogen form, regenerated with concentrated. hydrochloric acid, was added and the suspension was stirred overnight. The deprotection was confirmed by ^{1}H NMR and the polymer was isolated by filtration of the DOWEX and then precipitation into cold methanol. For the upcoming LL-dilactide (LLA) grafting the polymers were prepared by freeze-drying from benzene.

Scheme S2. Cleavage of protecting group of EEGE-PFar-EEGE polymers.

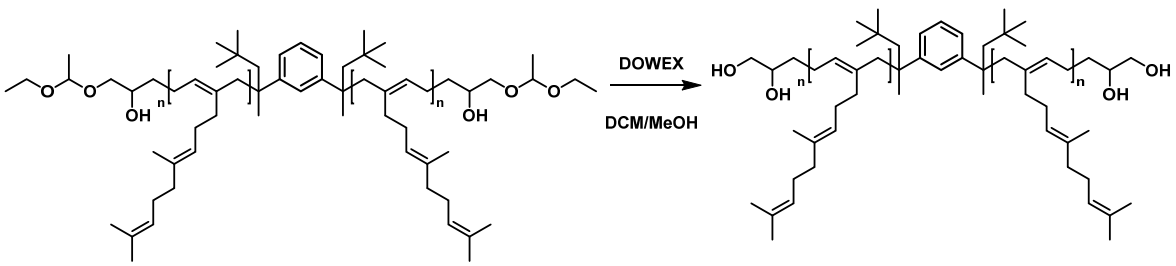

1.4 Organocatalyzed LLA Polymerization

To introduce PLLA to the macroinitiator LLA was recrystallized and then freeze-dried from benzene. It was inserted into an argon filled glovebox, alongside with the respective PFar macroinitiator and dry DCM. 1,8-Diaza-bicyclo-[5.4.0]-undec-7-ene (DBU), as the organobase catalyst, was dried over calcium hydride and three *freeze-pump-thaw* cycles. The polymerization was prepared by dissolving LLA and the PFar macroinitiator in DCM. The concentration was set to a 0.4 mol L^{-1} solution of LLA. DBU was added with respect to the exact ratio of [OH]/[DBU] = 5 to start the polymerization. The reaction solution turned slightly yellow upon the addition. After 1 hour the polymerization was quenched by the addition of ~ 2 eq of benzoic acid referred to the amount of DBU. The polymer was isolated by precipitation into cold methanol. The characterization was done through NMR and SEC. The exact determination of the PFar/PLLA ratio can be followed in chapter "7. Mathematic Calculations".

1.5 Analytic Measurements and Preparation

Nuclear Magnetic Resonance Spectroscopy (NMR). The measured 300 MHz NMR spectra were recorded on a *Bruker Avance III HD 300* and for the 400 MHz measurements, the *Bruker Avance II 400* and *Bruker Avance III HD 400* were used. The measurements, consisting of ^{1}H, ^{13}C, HSQC, COSY and DOSY NMR spectra, were recorded at the respective maximum frequency of the spectrometer (300 MHz and 400 MHz) for the ^{1}H measurement and at 75 MHz and 101 MHz for ^{13}C measurements. Subsequent analysis of the measured spectra was performed using the software "*MestReNova v14.2.0*" from Mestrelab Research S.L., Santiago de Compostela, Spain. The chemical shift (δ) of the signals is given in ppm in each case and were normalized to the proton signal of the deuterated solvent used.

Size Exclusion Chromatography (SEC). The measurement of the samples according to their hydrodynamic radius was performed in tetrahydrofuran (THF) as solvent and a PI-calibration. The setup consists of a set of columns (SDV 10e6/10e4/500) along with a *PSS SECcurity* pump. As detectors a RI detector (*SECcurity RID*) and a UV detector (*PSS SECcurity UV 254 nm*) at 254 nm were used.

Dynamic Scanning Calorimetry (DSC). Thermal properties of the samples were studies using a differential scanning calorimeter (DSC) instrument *DSC-823* of Mettler-Toledo, USA. The instrument was calibrated using indium, zinc and water. Two heating and one cooling cycle were performed in a temperature range between – 100 °C and 200 °C and a heat- and cool-rate of 10 K min^{-1}.

Tensile Testing. Stress-strain experiments were performed on a *EZ Test EZ-LX* instrument by Shimadzu, Japan. Polymer films were prepared by solvent casting from chloroform (1.5 g in 20 mL $CHCl_3$). Then "dog-bones" (DIN 53 504.S 3A) were cut out. For all measurements a pre-load force of 0.1 N was applied. A force transducer (50 N Capacity) *SM-50N-168* was used with a speed of 1 mm min^{-1}. All measurements were recorded using the software *TRAPEZIUMX* by Shimadzu, Japan.

Transmission Electron Microscopy (TEM). Ultrathin sections (40 nm) were prepared with an ultramicrotome (*Reichert Ultracut* by Leica Microsystems, Wetzlar, Germany) and placed on a copper grid. The samples were stained with Osmium oxide for 5 min of vapor exposition before imaging. Images were obtained using a *JEOL JEM-2100* (JEOL Ltd., Tokyo, Japan) electron microscope with 200 kV acceleration voltage; 0.14 nm resolution and a *Gatan Orius SC1000* camera (binning 2; 1024 x 1024 pixels) in the brightfield mode.

Small-angle X-ray Scattering (SAXS). Experiments were performed on a *Xeuss 2.0* system (Xenocs SAS, Grenoble, France). The incident beam from a Copper K_α source with a wavelength $\lambda = 0.154$ nm was collimated and focused on the sample with a spot size of 0.25 mm^2. 2D scattering intensity patterns were collected using a *Pilatus 300K* detector (pixel size 172 x 172 μm^2) located at a sample-detector distance of ~2500 mm, calibrated using a silver behenate standard. For each measurement, the acquisition time was 3600 s. As no signs of anisotropic scattering were observed, the scattering patterns were azimuthally averaged to obtain the scattered intensity I in dependence on momentum transfer $q = 4\pi \sin(\theta/2)\, \lambda^{-1}$, with θ being the scattering angle.

2. Activation of DIB/*tert*-BuLi

To evaluate the effective activation of the bifunctional initiator the reaction was tracked using offline ^{1}H NMR kinetics. The reaction was performed inside the glovebox to secure an oxygen and water free environment. The solution of the precursor 1,3-diisopropenylbenzene (DIB) (0.1 mol L^{-1}) was mixed with 2.05 equivalents of *tert*-BuLi. Samples were terminated after different time frames with degassed methanol. A complete activation results in a total disappearance of the proton signals at 5.2 ppm and 5.5 ppm, attributed to the benzylic double bonds, upon the addition of *tert*-BuLi. As it can be followed in **Figure S1**, the reaction occurs really fast and the first sample taken (1 min) already shows complete activation. Therefore, a rapid and complete activation is assured for the preparation of the polymers by choosing an activation time of greater than 5 min.

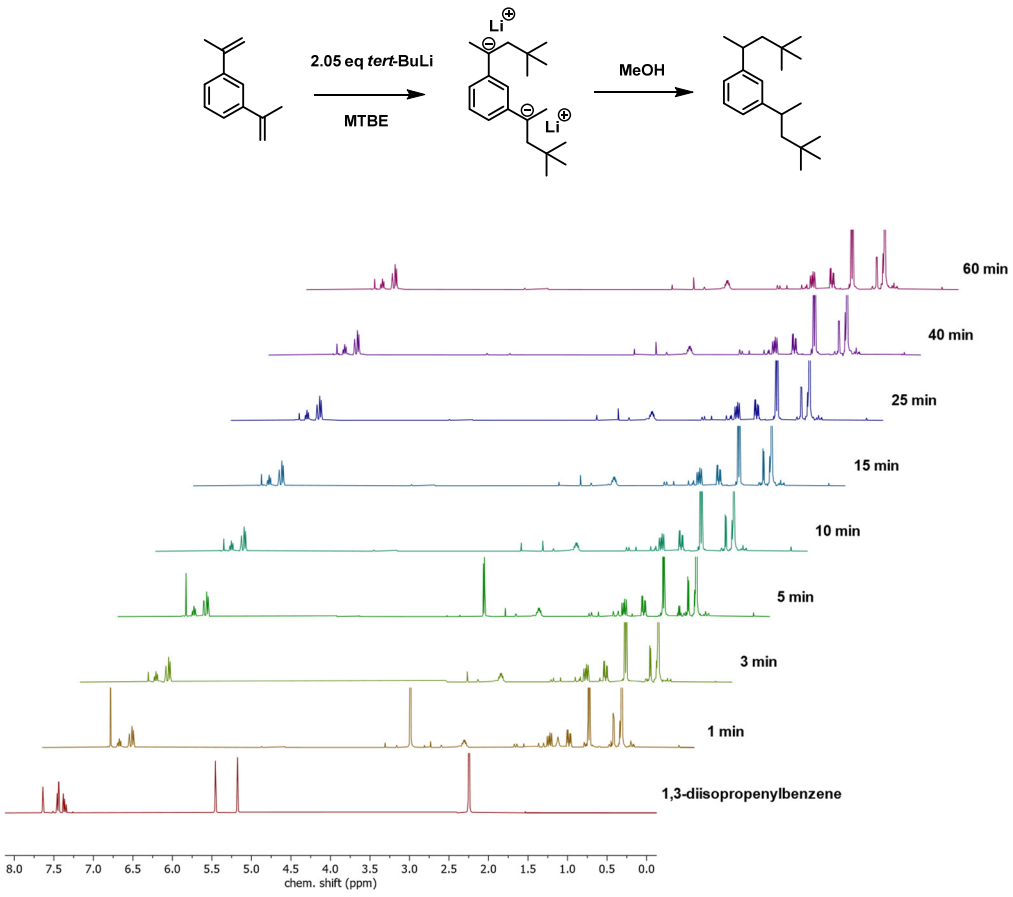

Figure S1. Offline ^{1}H NMR kinetics of the activation of DIB using 2.05 eq *tert*-BuLi.

3. Additional NMR Results

To identify key characteristics of the synthesized EEGE-PFar-EEGE macroinitiators they were analyzed by ^{1}H NMR. Only the low molar mass (M_n) sample allows a reliable determination of the degree of end functionalization and the molar mass by NMR, M_n^{NMR}. Therefore, the proton signal of the methyl groups of the initiator (~0.88 ppm) can be set to the respective 18 protons and the integral of the resulting proton signals of EEGE and Far can be used to calculate the mentioned values. The exact mathematic consideration can be followed in the chapter "7. Mathematic Calculations". The ^{1}H NMR of the targeted 5000 g·mol^{-1} sample is shown in **Figure S2** including all necessary allocations.

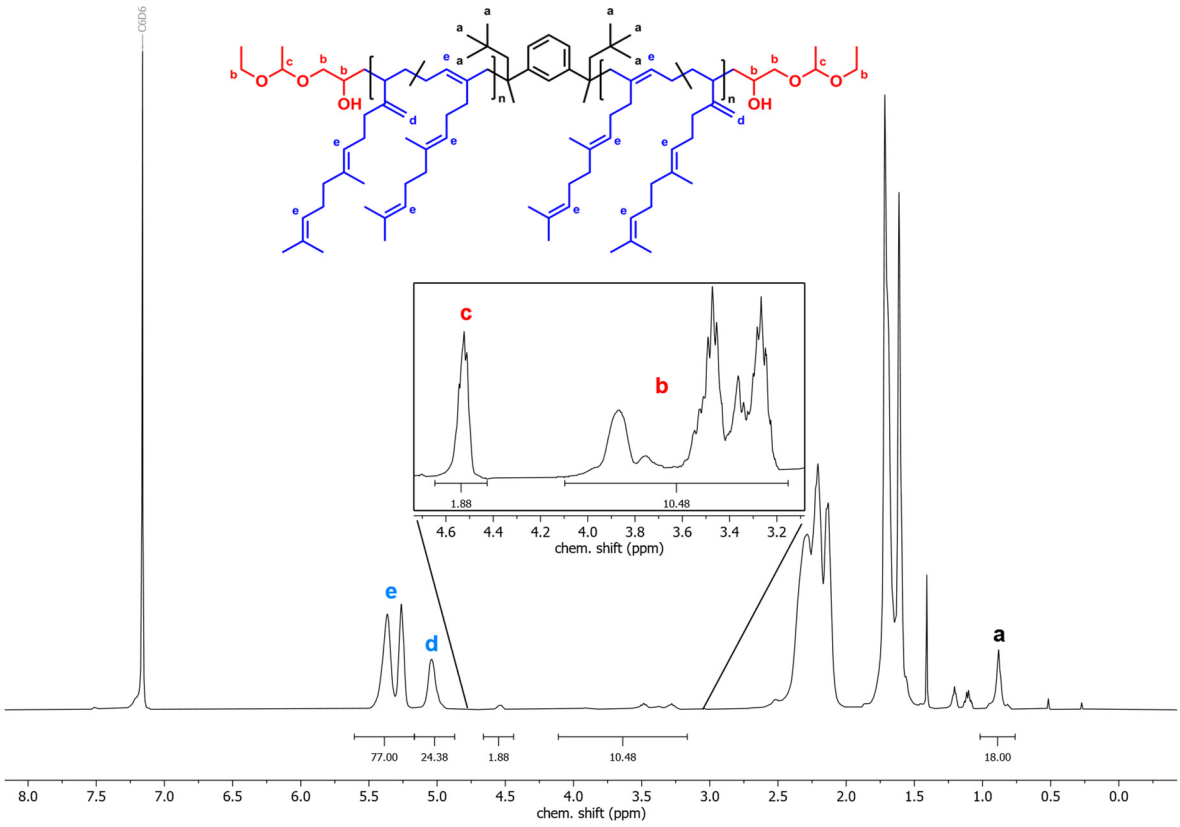

Figure S2. ^{1}H NMR: C_6D_6 400 MHz, EEGE-PFar(5k)-EEGE sample with allocation of the proton signals.

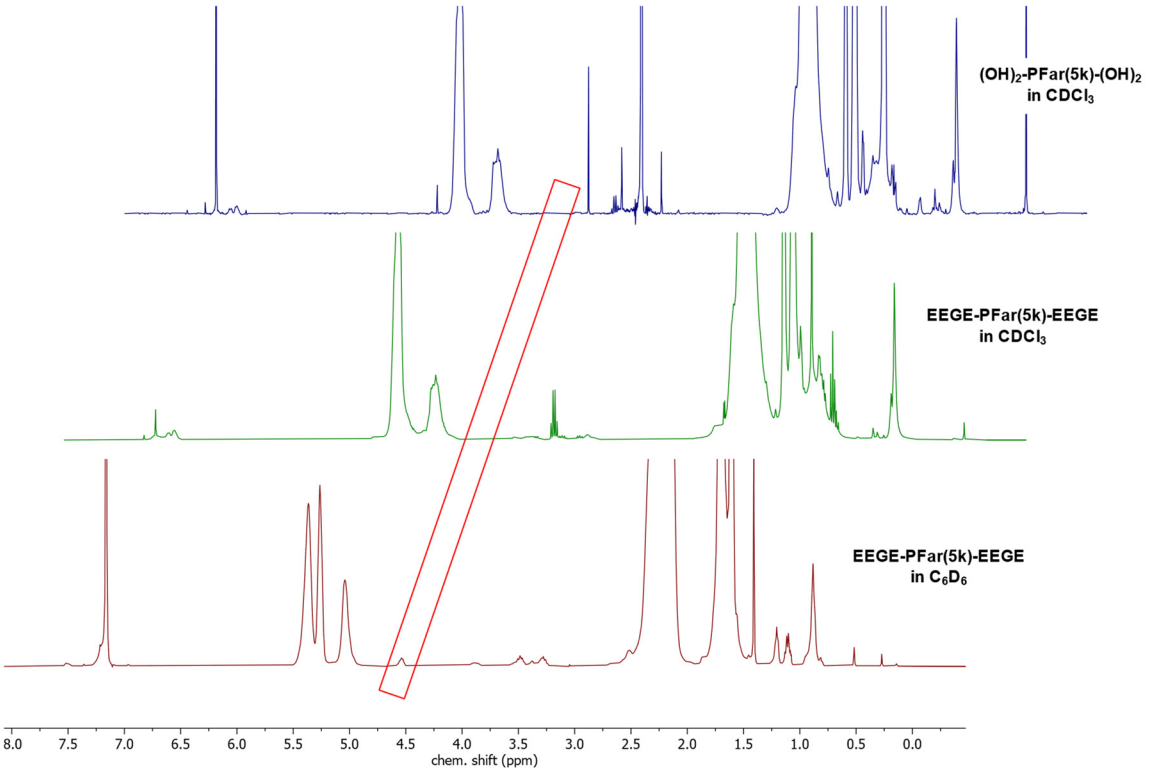

Figure S3. Stacked ^{1}H NMR of EEGE-PFar(5k)-EEGE sample measured in $CDCl_3$ and C_6D_6 against ^{1}H NMR of deprotected sample $(OH)_2$-PFar(5k)-$(OH)_2$.

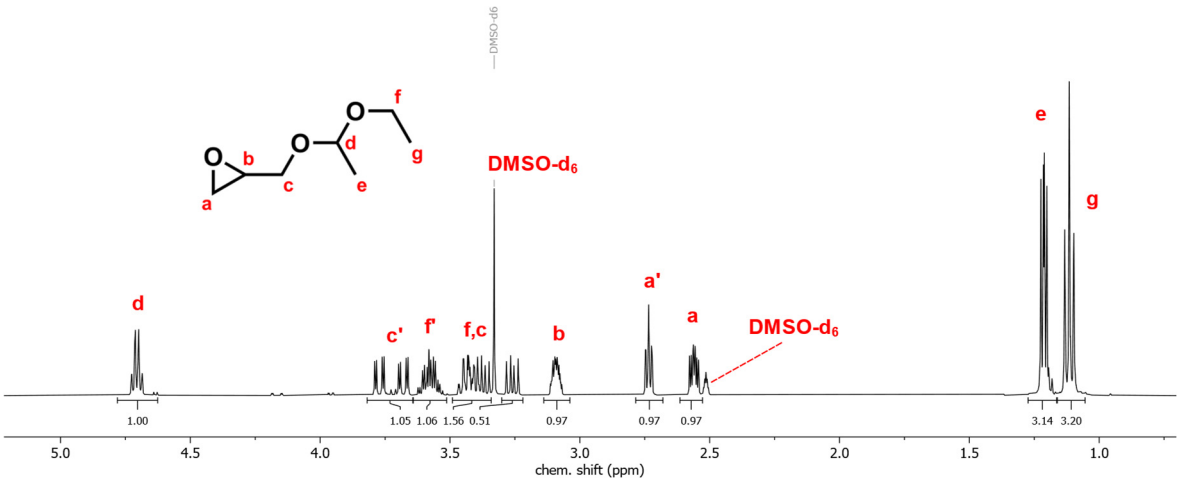

Figure S4. ^{1}H NMR of EEGE with allocation of all the proton signals, DMSO-d_6, 400 MHz.

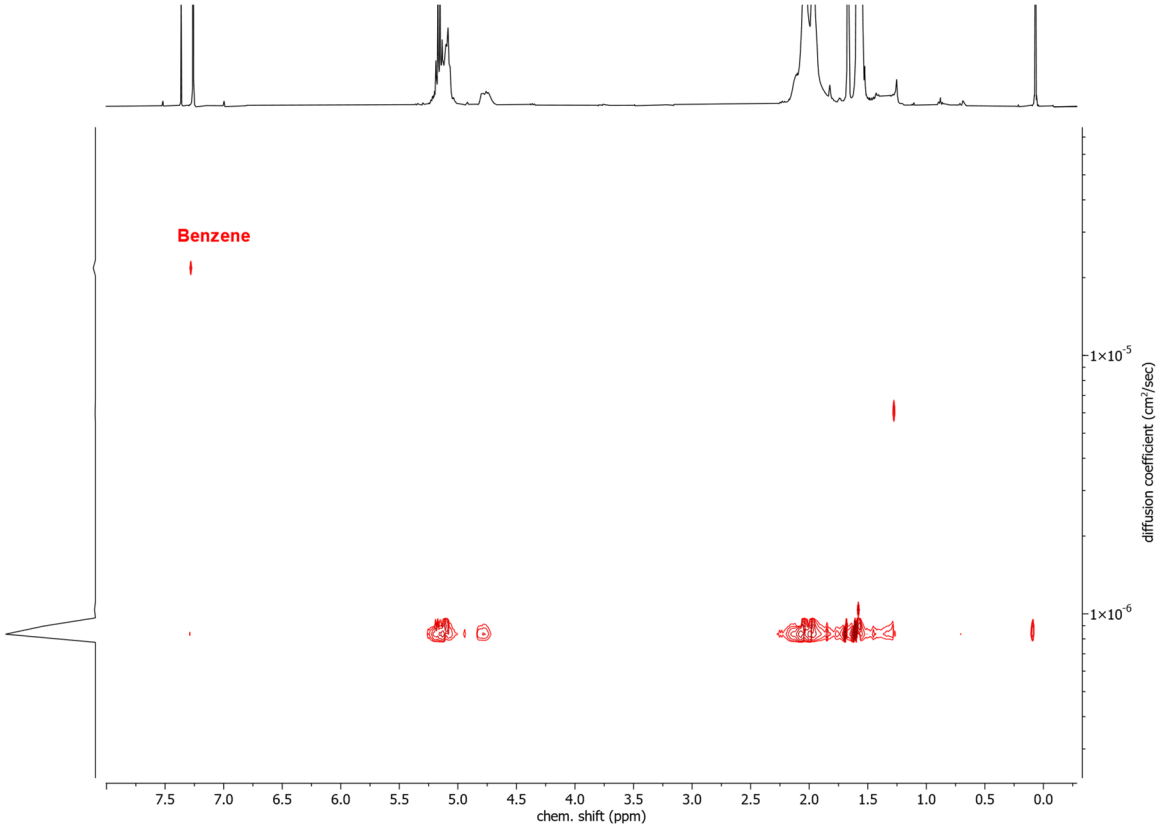

Figure S5. DOSY of $(PLLA)_2$-*b*-PFar(30k)-*b*-$(PLLA)_2$ 30 vol% PLLA, $CDCl_3$, 400 MHz.

4. DSC Measurements

DSC measurements were performed in the range of – 100 °C to 200 °C with a heat and cooling rate of 10 K·min^{-1}. As shown below, all samples show a melting point at temperatures between 134 °C to 149 °C of the PLLA-Phase. The cooling time and rate is not sufficient to allow recrystallisation. Thereby, the samples show no sign of recrystallization upon cooling and the melting point is absent in the second heat curve, which is used to determine the glass temperatures (T_g's).

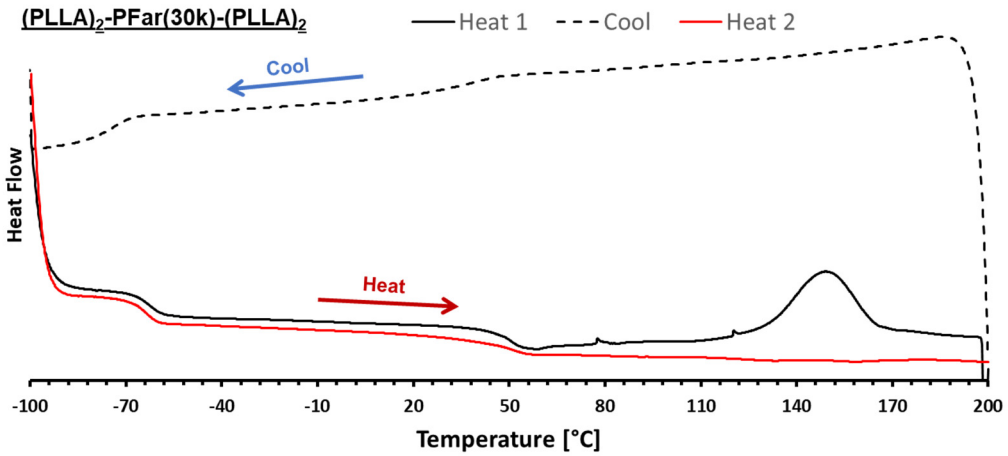

Figure S6. DSC results of sample $(PLLA)_2$-*b*-PFar(30k)-*b*-$(PLLA)_2$ 30 vol% PLLA, all heat and cool curves, measured with a heat and cool rate of 10 $K \cdot min^{-1}$.

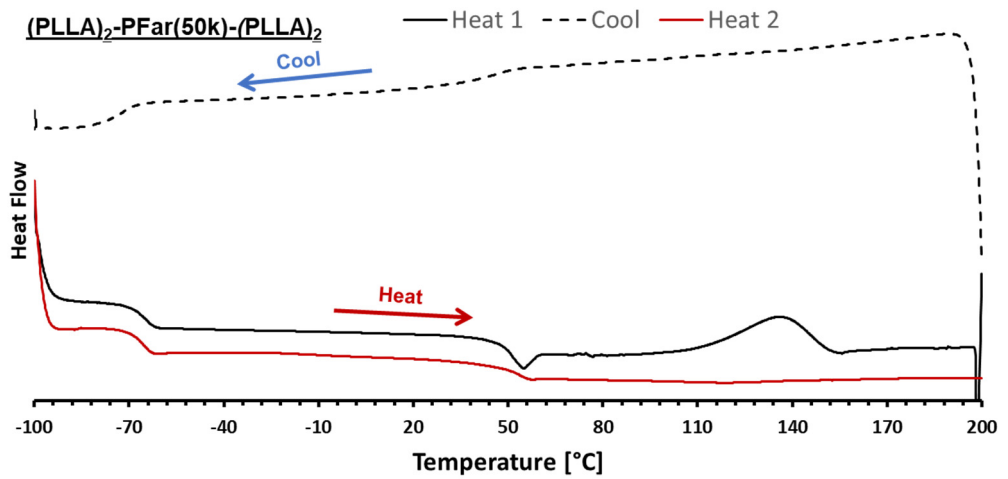

Figure S7. DSC results of sample $(PLLA)_2$-*b*-PFar(50k)-*b*-$(PLLA)_2$ 30 vol% PLLA, all heat and cool curves, measured with a heat and cool rate of 10 $K \cdot min^{-1}$.

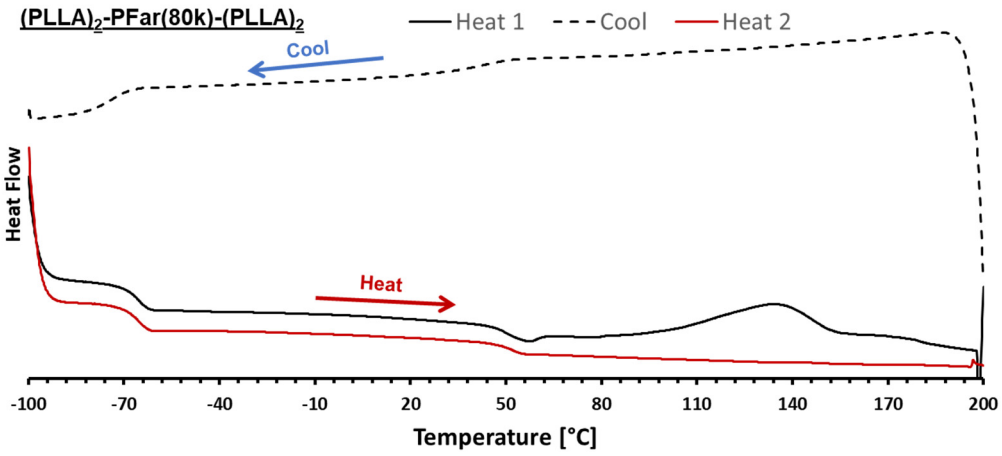

Figure S8. DSC results of sample $(PLLA)_2$-*b*-PFar(80k)-*b*-$(PLLA)_2$ 30 vol% PLLA, all heat and cool curves, measured with a heat and cool rate of 10 $K \cdot min^{-1}$.

5. Additional SEC Results

Below, the SEC traces of all samples are illustrated. The macroinitiator is always displayed as a dashed line. The clear shift towards higher molar masses can be followed for all samples, depending on the targeted vol% of PLLA. The observed broadening of the distribution while grafting can be explained by the inevitable monofunctional content and an uneven distribution of lactide units to the four possible initiating sites each chain.

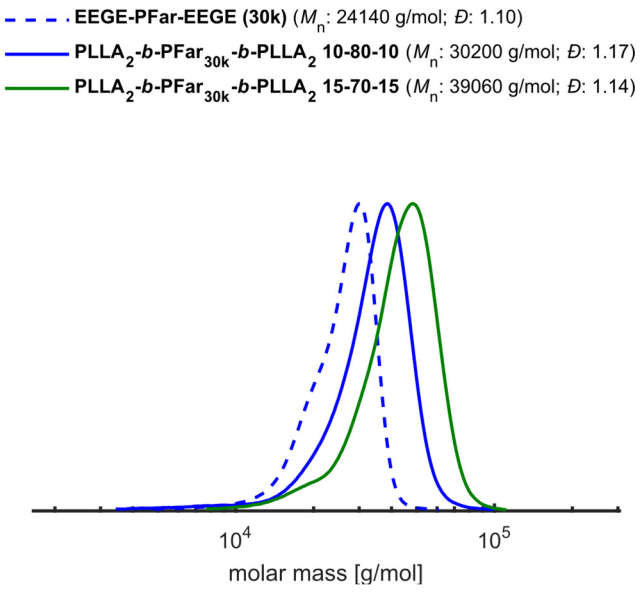

Figure S9. SEC results of 30k samples with 20% and 30% of PLLA, eluent: THF, PI-calibration.

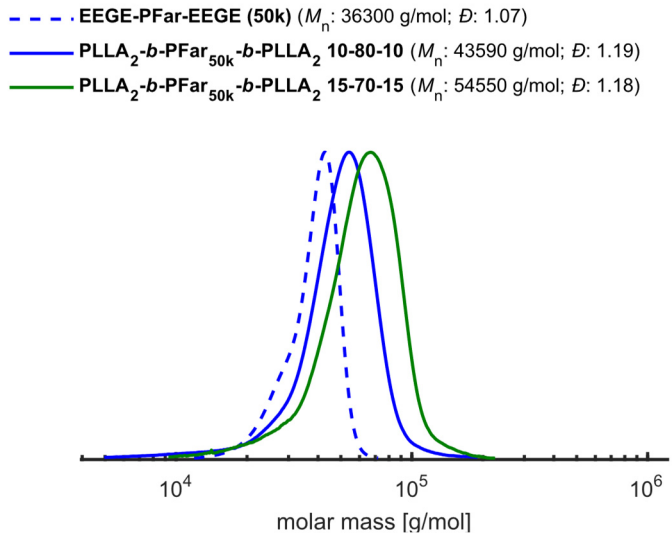

Figure S10. SEC results of 50k samples with 20% and 30% of PLLA, eluent: THF, PI-calibration.

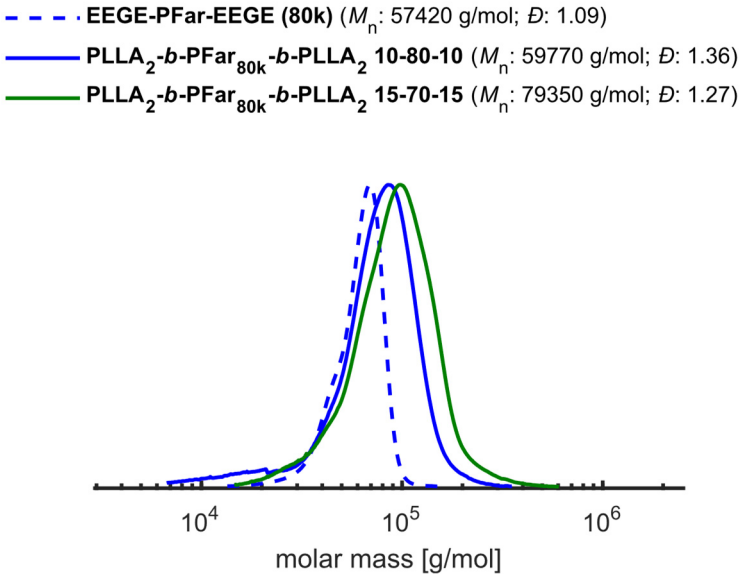

Figure S11. SEC results of 80k samples with 20% and 30% of PLLA, eluent: THF, PI-calibration.

6. Tensile Test

All stress-strain experiments were performed 4 times each sample. The average values presented in **Table S1** show the elongation at break (ε_{break}) and the Young's modulus (E). Below the stress-strain curves of the 50k and 80k samples are also given.

Table S1. Mechanical properties of the samples with a targeted Φ_{LA} of 30%.

Sample	M_n^{SEC}[a] [g·mol^{-1}]	Φ_{LA} [%]	ε_{break}[c] [%]	E [c] [MPa]
(PLLA)$_2$-*b*-PFar(30k)-*b*-(PLLA)$_2$	39 100	28.6	66 ± 5	4.51 ± 0.03
(PLLA)$_2$-*b*-PFar(50k)-*b*-(PLLA)$_2$	54 600	28.5	81 ± 6	33 ± 2
(PLLA)$_2$-*b*-PFar(80k)-*b*-(PLLA)$_2$	79 400	23.6	66 ± 12	11.7 ± 0.4

[a] Eluent: THF, calibration: Polyisoprene. [b] See **Table 1**. [c] Values calculated from stress-strain tests, values were determined for each sample three to four times and are displayed as average values with their respective standard deviations.

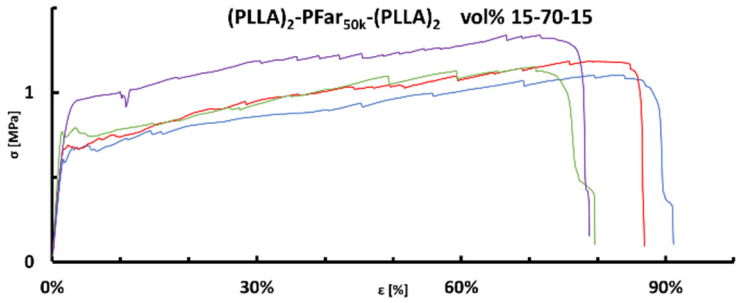

Figure S12. Tensile test of (PLLA)$_2$-*b*-Far(50k)-*b*-(PLLA)$_2$ 30% PLLA.

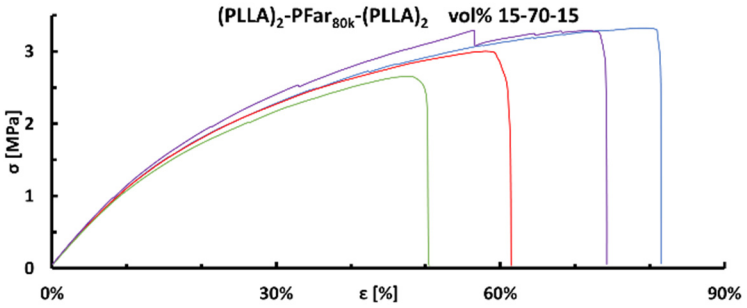

Figure S13. Tensile test of (PLLA)$_2$-*b*-PFar(80k)-*b*-(PLLA)$_2$ 30% PLLA.

7. Mathematic Calculations

7.1 Microstructure of Polyfarnesene [$PFar_{1,4}$-share]

Below the calculation of the microstructure of PFar is shown. To calculate the amount of 1,4 units, the degree of polymerization (P_n) of each individual microstructure is calculated. Therefore, the methylene signal (~5.02 ppm) I(d) and methine signal (5.39 ppm) I(e) are taken from the 5k EEGE-PFar(5k)-EEGE sample, see **Figure S2**.

$$P_n(\mathrm{Far}_{1,4}) = \frac{I(\mathrm{e})\text{-}I(\mathrm{d})}{3} = \frac{77.00\text{-}24.38}{3} = 17.54 \quad \textbf{(S1)}$$

$$P_n(\mathrm{Far}_{3,4}) = \frac{I(\mathrm{d})}{2} = \frac{24.38}{2} = 12.19 \quad \textbf{(S2)}$$

$$P_n(\mathrm{PFar}) = P_n(\mathrm{Far}_{3,4}) + P_n(\mathrm{Far}_{3,4}) = 17.54 + 12.19 = 29.73 \quad \textbf{(S3)}$$

$$\mathrm{PFar}_{1,4} = \frac{P_n(\mathrm{PFar}_{1,4})}{P_n(\mathrm{PFar})} = \frac{17.54}{29.73} = 59.0\% \quad \textbf{(S4)}$$

7.2 Molar mass by NMR [M_n^{NMR} (EEGE-PFar(5k)-EEGE)]

The molar mass by NMR (M_n^{NMR}) can be calculated as followed. Next to the molar mass of the Far units, the initiator and end-capping reagent (EEGE) need to be included.

$$M_n^{NMR}(\text{EEGE-PFar(5k)-EEGE}) = M(C_{20}H_{34}) + P_n(\mathrm{Far}) \cdot M(C_{15}H_{24}) + 2 \cdot M(C_7H_{14}O_3) \quad \textbf{(S5)}$$

$$= 274.49\ \mathrm{g \cdot mol^{-1}} + 29.73 \cdot 204.36\ \mathrm{g \cdot mol^{-1}} + 2 \cdot 146.19\ \mathrm{g \cdot mol^{-1}} \cong 6600\ \mathrm{g \cdot mol^{-1}}$$

7.3 End-group Functionalization

To determine the degree of end group functionalization, the proton signals of the end capping reagent (EEGE) can be compared to the methyl signals of the initiator. The methyl signal in the ^{1}H NMR at (0.88 ppm) is normalized to the respective 18 protons of the two tert-butyl groups. Thereby, the integral of the proton signals of EEGE (e.g. the methine signal (**c**, see **Figure S2**) at ~ 4,54 ppm) can be used to calculate the degree of end group functionalization. Both chain ends need be considered. So, by dividing the integral by the maximum possible value of two protons the percentual value is determined.

$$\text{end group functionalization} = \frac{I(\mathrm{c})}{2} \cdot 100\% = \frac{1.88}{2} \cdot 100\% = 94\% \quad \textbf{(S6)}$$

7.4 Volume Fraction of Polylactide [ϕ_{LA}]

The degree of polymerization of each comonomer is not easily accessible through NMR. End group determination does not lead to reliable results due to the high molar mass. Nevertheless, the ratio between PFar/PLLA units can be determined precisely. This leads to the determination of the volume share of PLLA (ϕ_{LA}).

In the respective ^{1}H NMR the methylene of the 3,4-PFar and the methine signal of the PLLA overlap. As the ratio of 1,4-PFar and 3,4-PFar of the macroinitiator is known, the proton share of 3,4-PFar can be subtracted. Thereby, the integrals of PLLA and PFar can be compared as followed. The relative integrals of PFar and PLLA are given by I_{rel}(PFar) and I_{rel}(PLLA).

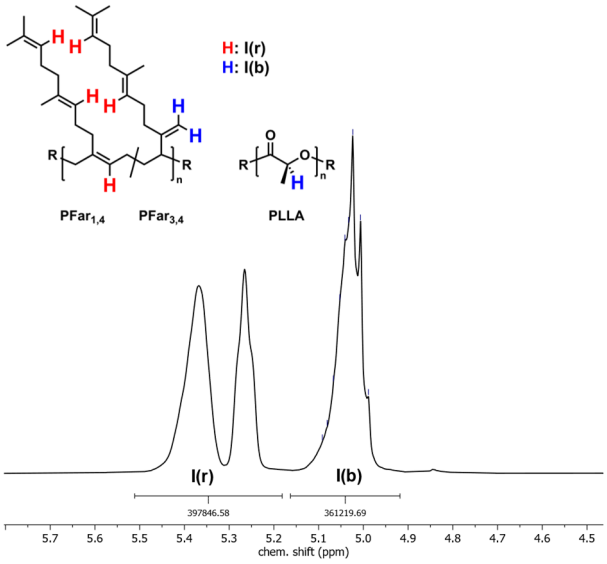

Figure S14. ^{1}H NMR of $(PLLA)_2$-*b*-PFar-*b*-$(PLLA)_2$ 30%PLLA, range of significant PFar and PLLA proton signals and their allocations, C_6D_6, 400 MHz.

$$I_{rel}(\text{PFar}) = \frac{I(\text{r})}{\text{PFar}_{1,4}\cdot 3 + \text{PFar}_{3,4}\cdot 2} = \frac{397846.58}{61.16\%\cdot 3 + 38.84\%\cdot 2} = 152337.84 \quad \textbf{(S7)}$$

$$I_{rel}(\text{PLLA}) = I(\text{b}) - \left(I_{rel}(\text{PFar})\cdot \text{PFar}_{3,4}\cdot 2\right) = 361219.69 - (152337.84\cdot 38.84\%\cdot 2) = 242885.79 \quad \textbf{(S8)}$$

From there the mass ratio (m(%)$_{Far}$ and m(%)$_{PLLA}$) can be determined by taking the molar mass of the monomer units:

M(Far)=204.36 g·mol^{-1}; M(LA)=72.07 g·mol^{-1}

$$\mathrm{m}(\%)_{\mathrm{Far}} = \frac{I_{\mathrm{rel}}(\mathrm{PFar}) \cdot M(\mathrm{Far})}{\left(I_{\mathrm{rel}}(\mathrm{PFar}) \cdot M(\mathrm{Far}) + I_{\mathrm{rel}}(\mathrm{PLLA}) \cdot M(\mathrm{PLLA})\right)}$$

$$= \frac{152337.84 \cdot 204.36\ \mathrm{g \cdot mol^{-1}}}{(152337.84 \cdot 204.36\ \mathrm{g \cdot mol^{-1}} + 242885.79 \cdot 72.07\ \mathrm{g \cdot mol^{-1}})} = 64.01\% \quad \textbf{(S9)}$$

$$\mathrm{m}(\%)_{\mathrm{PLLA}} = \frac{I_{\mathrm{rel}}(\mathrm{PLLA}) \cdot M(\mathrm{PLLA})}{\left(I_{\mathrm{rel}}(\mathrm{PFar}) \cdot M(\mathrm{Far}) + I_{\mathrm{rel}}(\mathrm{PLLA}) \cdot M(\mathrm{PLLA})\right)}$$

$$= \frac{242885.79 \cdot 72.07\ \mathrm{g \cdot mol^{-1}}}{(152337.84 \cdot 204.36\ \mathrm{g \cdot mol^{-1}} + 242885.79 \cdot 72.07\ \mathrm{g \cdot mol^{-1}})} = 35.99 \quad \textbf{(S10)}$$

This can be converted with the respective densities of the homopolymers ρ(PLLA)=1.264 g·cm^{-3} [2] and PFar ρ(PFar)=0.900 g·cm^{-3} [3] to the volume share:

$$\Phi_{\mathrm{LA}} = \frac{\frac{\mathrm{m}(\%)_{\mathrm{PLLA}}}{\rho(\mathrm{PLLA})}}{\frac{\mathrm{m}(\%)_{\mathrm{PLLA}}}{\rho(\mathrm{PLLA})} + \frac{\mathrm{m}(\%)_{\mathrm{PFar}}}{\rho(\mathrm{PFar})}} = \frac{\frac{35.99\%}{1.246\ \mathrm{g \cdot cm^{-3}}}}{\frac{35.99\%}{1.246\ \mathrm{g \cdot cm^{-3}}} + \frac{64.01\%}{0.900\ \mathrm{g \cdot cm^{-3}}}} = 28.6\% \quad \textbf{(S11)}$$

8. Additional TEM and SAXS Results

Sample	Φ_{LA} [%]	
$(PLLA)_2$-PFar(30k)-$(PLLA)_2$ 20% PLLA	18.3	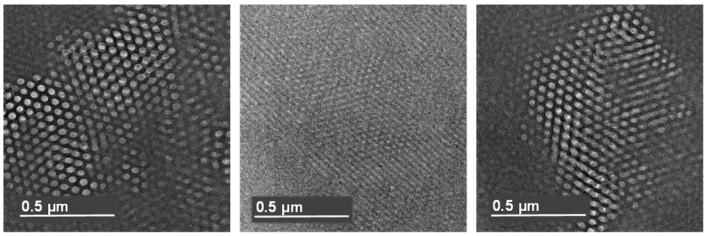
$(PLLA)_2$-PFar(30k)-$(PLLA)_2$ 30%PLLA	28.6	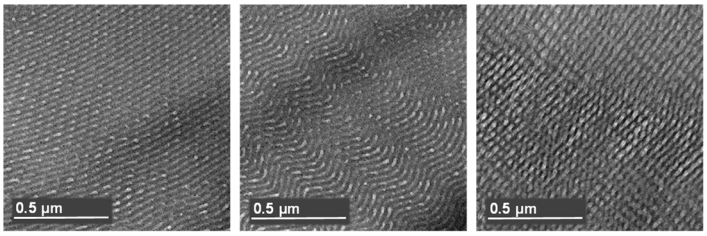
$(PLLA)_2$-PFar(50k)-$(PLLA)_2$ 20% PLLA	20. 0	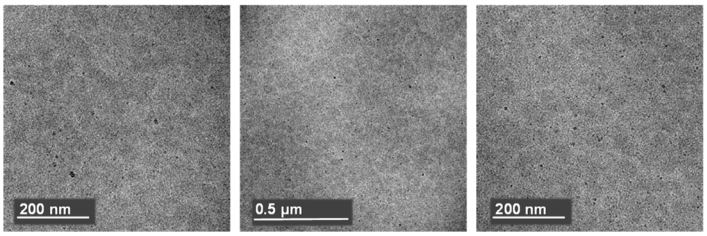
$(PLLA)_2$-PFar(50k)-$(PLLA)_2$ 30% PLLA	28.5	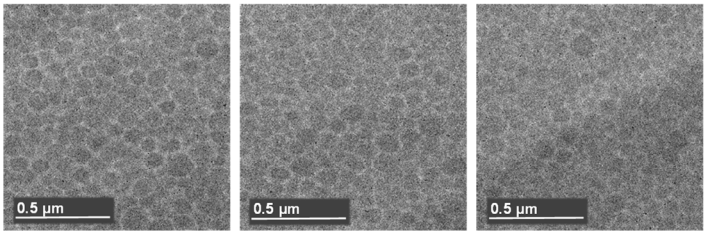
$(PLLA)_2$-PFar(80k)-$(PLLA)_2$ 20% PLLA	20.6	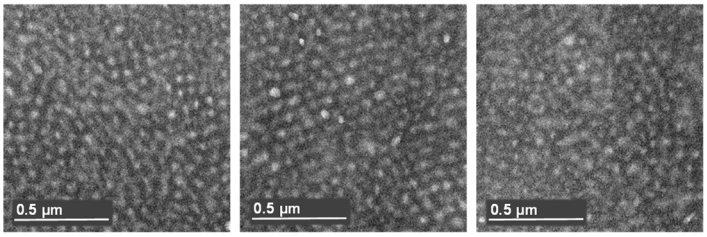
$(PLLA)_2$-PFar(80k)-$(PLLA)_2$ 30% PLLA	23.6	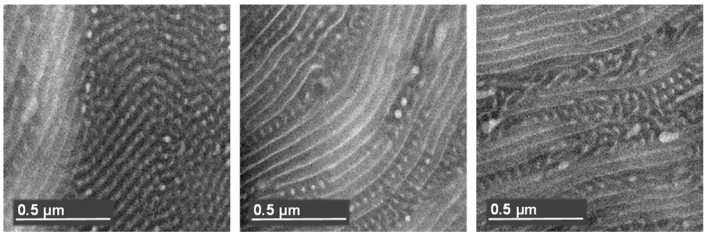

Figure S15. TEM images of all *H*-shape A_2BA_2-type triblock samples, stained with OsO_4.

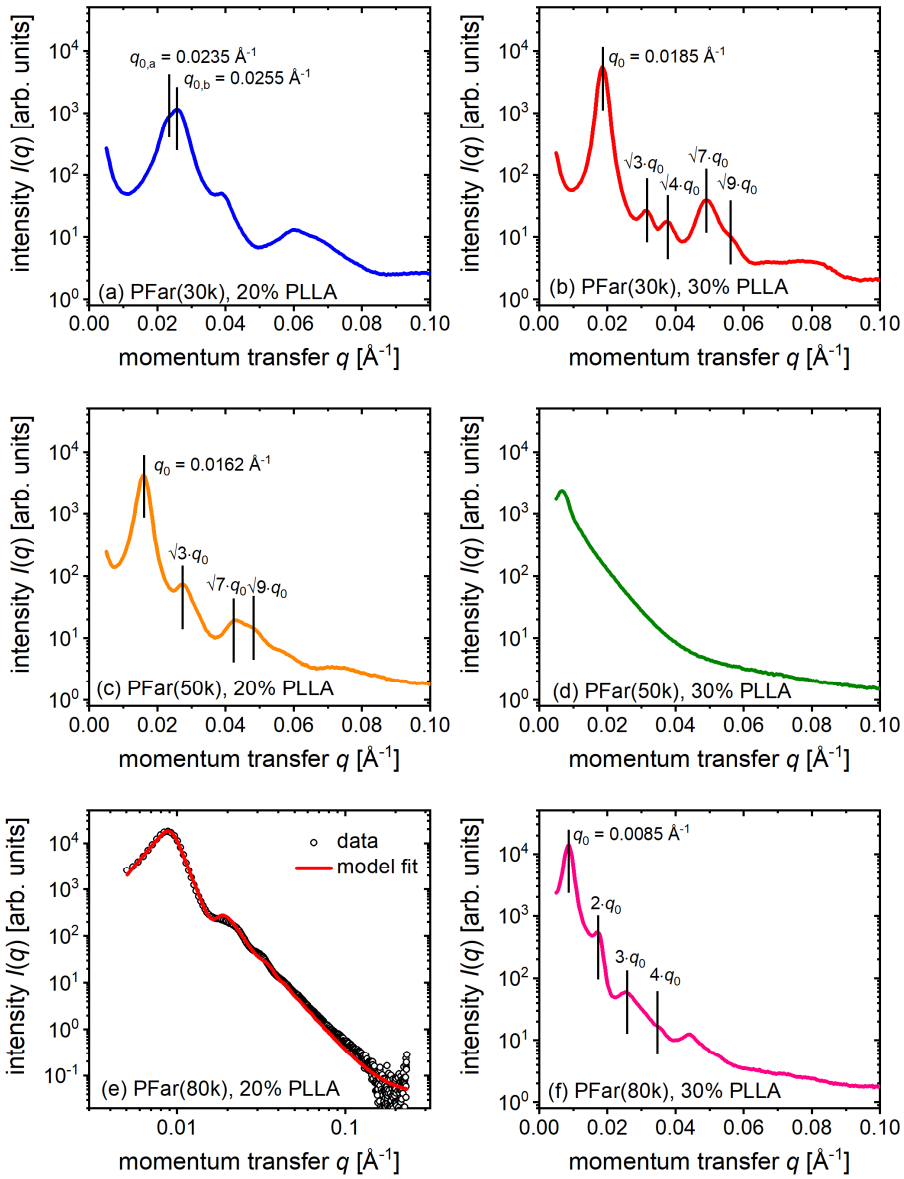

Figure S16. SAXS results of all $(PLLA)_2$-*b*-PFar-*b*-$(PLLA)_2$ samples.

Figure S16 presents the SAXS patterns of all $(PLLA)_2$-*b*-PFar-*b*-$(PLLA)_2$ samples. PFar(30k) with 20% PLLA (**Figure S16a**) shows a broad Bragg reflection at small *q*-values, which is composed of two primary peaks at $q_{0,a} = 0.0235$ Å^{-1} and $q_{0,b} = 0.0255$ Å^{-1}, and suggests the presence of two separate structure types with repeat distances of $2\pi/q_{0,a} = 26.7$ nm and $2\pi/q_{0,b} = 24.6$ nm, respectively. The secondary peak at ~0.04 Å^{-1} implies that at least one of them is crystalline, but we could not unambiguously assign it to a specific structure.

The scattering curve of PFar(30k) with 30% PLLA (**Figure S16b**) has a distinct primary Bragg reflection at q_0 = 0.0185 Å^{-1}. Secondary peaks are found at √3· q0, √4· q0, √7· q0 and √9· q_0, which implies that the polymers microphase separated in a hexagonal structure with a repeat distance of $2\pi/q_0$ = 34.0 nm.[4]

PFar(50k) with 20% PLLA (**Figure S16c**) shows a primary Bragg reflection at q_0 = 0.0162 Å^{-1}, which corresponds to a repeat distance of $2\pi/q_0$ = 38.8 nm. Secondary peaks at positions corresponding to a hexagonal structure are present, too.

The scattering curve obtained for PFar(50k) with 30% PLLA (**Figure S16d**) has strong intensities at small q values, but no Bragg peaks indicative of ordered structures. The sample appears entirely disordered.

We compared the scattering of PFar(80k) with 20% PLLA (**Figure S16e**) to that expected for spheres arranged in a random close packing as described by the function:

$$I(q) = S_{HS}(q) P_S(q) + I_{bkg} \qquad \textbf{(S12)}$$

with $P_S(q)$ a sphere formfactor with a Gaussian size distribution, which yields the size of the spheres, R_S, and the width of the distribution, σ.[5] $S_{HS}(q)$ is a hard-sphere structure factor, which accounts for the disordered arrangement of the spheres, and gives the hard sphere radius, R_{HS}, i.e., half the center-to-center distance between the spheres, and the hard-sphere volume fraction, η.[6] Using R_S = 26.5 nm and R_{HS} = 34.9 nm, a good agreement of the model with the data is obtained, which suggest a microstructure that is well-described by randomly packed spheres.

PFar(80k) with 30% PLLA (**Figure S16f**) displays a primary Bragg reflection at q_0 = 0.0162 Å^{-1}, and secondary peaks at 2· q_0, 3· q_0 and 4· q_0, indicative of a lamellar structure.[4]

References

[1] Fitton, A. O.; Hill, J.; Jane, D. E.; Millar, R. Synthesis of Simple Oxetanes Carrying Reactive 2-Substituents. *Synthesis* **1987**, *1987* (12), 1140‑1142.

[2] Witzke, D. R.; Narayan, R.; Kolstad, J. J. Reversible Kinetics and Thermodynamics of the Homopolymerization of l -Lactide with 2-Ethylhexanoic Acid Tin(II) Salt. *Macromolecules* **1997**, *30* (23), 7075‑7085.

[3] Iacob, C.; Yoo, T.; Runt, J. Molecular Dynamics of Polyfarnesene. *Macromolecules* **2018**, *51* (13), 4917‑4922.

[4] Hamley, I. W.; Castelletto, V. Small-angle scattering of block copolymers. *Progress in Polymer Science* **2004**, *29* (9), 909‑948.

[5] Lindner, P., Ed. *Neutrons, X-rays and light*:*Scattering methods applied to soft condensed matter*, Transferred to digital print; North-Holland delta series; Elsevier, 2006.

[6] Percus, J. K.; Yevick, G. J. Analysis of Classical Statistical Mechanics by Means of Collective Coordinates. *Phys. Rev.* **1958**, *110* (1), 1‑13.

Chapter 5

One-Step Synthesis of Fully Bio-based Two-Sided Tapered ABA-Type Thermoplastic Elastomers

Moritz Meier-Merziger,[a] *Nikolaos Fotaras,*[b] *Ioannis Tzourtzouklis,*[b] *Chaymaa Allouch,*[a] *Manfred Wagner,*[c] *Axel H. E. Müller,*[a]* *George Floudas,*[b,c]* *and Holger Frey* [a]*

* Corresponding authors

[a] Department of Chemistry, Johannes Gutenberg University Mainz, Duesbergweg 10-14, 55128 Mainz, Germany

[b] Department of Physics, University of Ioannina, P.O. Box 1186, 45110 Ioannina, Greece

[c] Max Planck Institute for Polymer Research, Ackermannweg 10, 55128 Mainz, Germany

Published in: *ACS Sustainable Chemistry and Engineering*, **2024**, 12 (26), 9922-9933.
https://doi.org/10.1021/acssuschemeng.4c02530

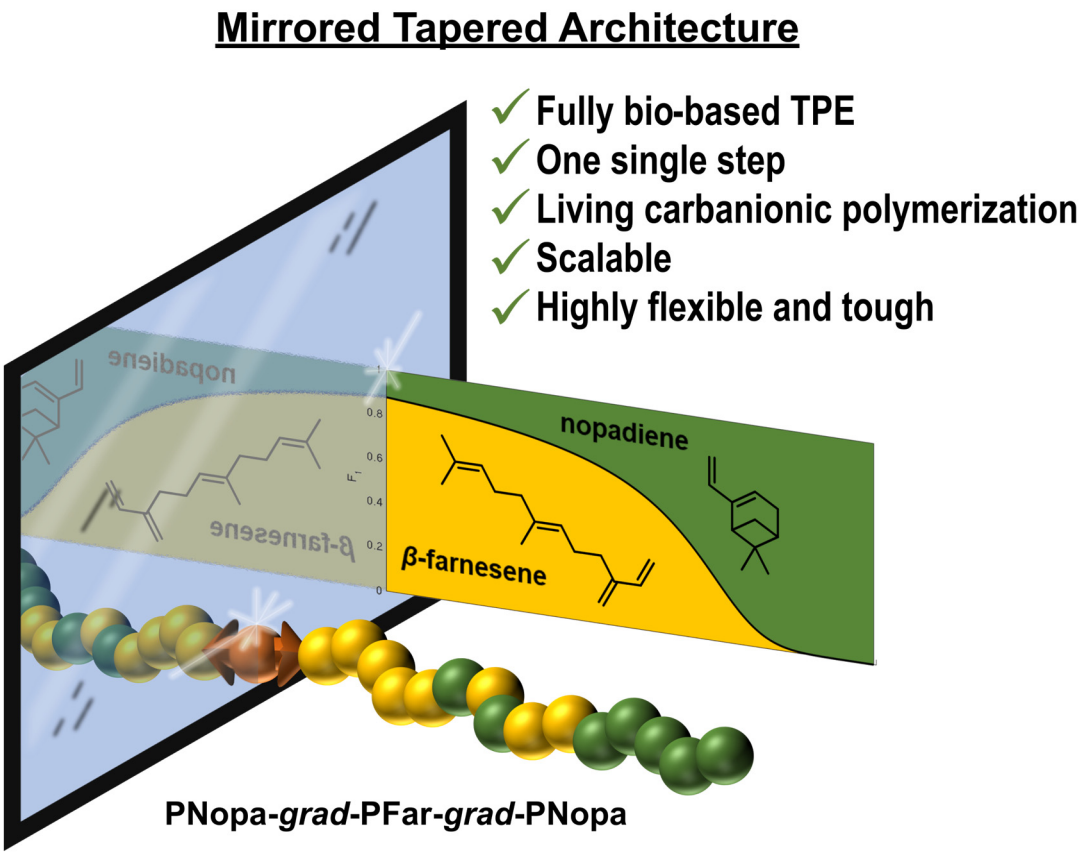

The following publication is adapted with permission from Meier-Merziger, M.; Fotaras N.; Tzourtzouklis, I.; Allouch, C.; Wagner, M.; Müller, A. H. E., Floudas, G., and Frey, H.; One-step Synthesis of Fully Bio-based Two-Sided Tapered ABA-type Thermoplastic Elastomers, *ACS Sustainable Chemistry and Engineering*, **2024**, 12 (26), 9922-9933.

Abstract

The synthesis of a fully bio-based thermoplastic elastomer (TPE) is presented as an alternative to classical styrene/isoprene derived TPEs. Limitations of classical systems, e.g., the microstructure of dienes or elaborate multistep addition pathways can be overcome by the combination of bifunctional initiation in the scarcely used, moderately polar solvent methyl *tert*-butyl ether (MTBE) and by using the monomers *β*-farnesene and nopadiene. The monomers can be derived from renewable sugar cane and pine tree feedstocks. Excellent control of carbanionic copolymerization is confirmed by *in situ* NMR kinetics. The study reveals that two-sided tapered ABA triblock copolymers are accessible in a one-step approach, capitalizing on a difunctional initiator in MTBE. The material properties can be tuned in a broad range — highly elastic materials with elongation exceeding 1300% as well as tough materials with Young's modulus exceeding 500 MPa were obtained. Small-angle X-ray scattering, temperature-modulated differential scanning calorimetry, rheology and dielectric spectroscopy were employed to relate the material properties to the phase state. They revealed local phase segregation accompanied by respective glass temperatures, albeit in the absence of long-range order.

Introduction

Thermoplastic elastomers (TPEs) can be considered a more sustainable material class than classical elastomers, as they are reprocessable. Covalent cross-linking, present in vulcanized rubber, is replaced by physical cross-linking of phase-separated ABA triblock copolymers in TPEs. They consist of a center block with a low glass temperature (T_g) that offers flexibility and two vitrified high-T_g outer blocks.[1],[2] Consequently, processing by extrusion is much simpler as compared to covalently crosslinked elastomers, which must be cured in their final shape. The triblock structure also enables functional processing techniques such as 3D printing, making TPEs much broader applicable.[3]

Commercially established examples are styrene (S)-, butadiene (B)-, and isoprene (I)-derived SBS and SIS block copolymers, used in a broad range of applications. Their properties can be tuned by various parameters, such as composition, molar mass, additives and fillers.[4] Finding an equivalent but more sustainable replacement is an important focus of current research, as fossil fuel feedstocks are limited and have a negative impact on the environment.[2] In this context, terpenes represent versatile feedstocks. They can be obtained from a large variety of natural resources, and due to their structural diversity, they offer great potential for use in a variety of polymerization methods and to achieve a wide range of properties. The basic structure of terpenes is based on the isoprene C_5H_8 unit.[5]–[7] The bio-based C_{10} and C_{15} homologues, *β*-myrcene (Myr) and *β*-farnesene (Far), comprise the same 2-substituted 1,3-diene functionality. The 1,3-diene structure can be incorporated along the polymer chains in different possible patterns, i.e., microstructures, specifically divided into regio- and stereostructure, see **Scheme 1**a. Changes in reaction conditions such as solvent polarity, counterion, modifier, and temperature are known to strongly affect the resulting microstructure and thereby the material properties. For classical dienes, e.g., polyisoprene (PI), a T_g of -67 °C for mainly 1,4-PI and only 9% vinyl content can be obtained. In polar solvents or in the presence of modifiers, the vinyl content can increase up to 85%, leading to a T_g up to 0 °C.[8] This renders the material unsuitable for many applications and thus limits the variation of reaction conditions in classical systems.[9]

As proposed by Henning and co-workers, the longer side chain in polyfarnesene (PFar) leads to a bottlebrush-like architecture of the polymers' backbone. This leads to the remarkable feature of a low T_g of < -70 °C of polyfarnesene (PFar), even with a vinyl content exceeding 50%.[8] The lower T_g was attributed to the high density of end-groups that effectively mobilize the polymer backbone.[10],[11] Thereby, many shortcomings of classical dienes are eliminated, allowing a much more versatile synthesis pathway for the synthesis of PFar. This "chain thickening" caused by the side chains greatly affects the viscoelastic properties: The

entanglement molar mass increases from 6.4 kg·mol^{-1} in PI to 22 kg·mol^{-1} in PMyr to 50 kg·mol^{-1} in PFar.[11],[12] Likewise, the packing length (p) increases (from 3.1 Å in PI to 4.7 Å in PMyr and to 6.3 Å in PFar) and the plateau modulus (G_N^0) decreases. The latter follows the proposed empirical relation (**Eq. 1**):

$$G_N^0 = 0.00226\ k_B T/p^3 \qquad \textbf{(1)}$$

consistent with the proportionality between the tube diameter and the packing length.[13] As a result, a higher molar mass is mandatory to achieve good mechanical properties. Farnesene is mostly derived from sugar cane, a renewable feedstock, albeit with the drawback of competing with the human food chain. It is an industrially relevant compound studied for its use as a sustainable alternative for rubber (commercialized by *Kuraray* and *Amyris*),[14] jet fuels, tires, and polyurethanes. This and ongoing investigations for alternative feedstocks for microbacterial production will likely result in farnesene becoming price-competitive in the future.[15]–[18]

Scheme 1. A) Possible microstructures of 1,3-diene monomers, B) Structural comparison of the monomer nopadiene, its natural feedstock β-pinene and the different microstructures of polynopadiene.[19].

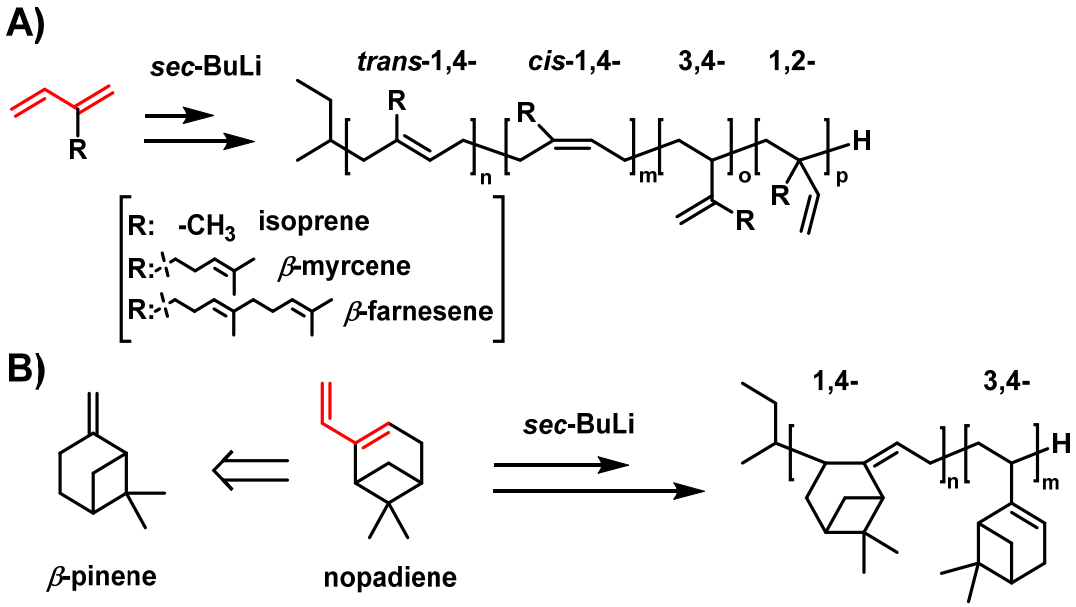

PFar is ideally suited to form the center block in TPEs due to its above-mentioned advantages, however, a sustainable substitute for the styrene-based hard block remains a challenge. We recently introduced nopadiene (Nopa), 1*R*,5*S*-2-ethenyl-6,6-dimethylbicyclo[3.1.1]hept-2-ene, a terpene-derived 1,2-substituted 1,3-diene.[19] Besides the anionic and catalytic polymerization reported by us it was recently also polymerized using rare-earth catalysts.[20] It can be synthesized from myrtenal[21],[22] or nopol,[23] both derived from β-pinene, which can both be converted to the respective diene structure. Due to the rigid structure of the sterically hindered Nopa units within the polymer backbone, see **Scheme 1**b, the T_g of PNopa is found at

160 °C.[19] This is in line with other dienes containing cyclic structures, as the works of Ishizone and co-workers and others have shown.[24]–[26] This makes it an ideal bio-based substitute for styrene, even extending the upper service temperature of polystyrene (PS) ($T_g \sim 100$ °C).

The first option to synthesize TPEs based on these bio-based monomers is simple sequential monomer addition, relying on a living polymerization technique. However, this strategy is also the most complex one, as it requires at least three sequential monomer additions. This can be optimized by relying on statistical living copolymerization, capitalizing on disparate reactivity ratios. In most cases, the relative rates of comonomer conversion differ, resulting in a comonomer gradient along the polymer chains. Classical systems, e.g., styrene/isoprene (S/I) polymerized in cyclohexane, form steep gradients, so-called tapered block copolymers, as isoprene ($r_I = 10.0$) polymerizes first, followed by styrene upon depletion of isoprene ($r_S = 0.015$).[27] Thereby, the required monomer addition steps for ABA triblock copolymers can be reduced to two. First, monomer A is polymerized, and then a mixture of both monomers A and B is added to the living chain end, yielding A-*b*-(B-*grad*-A).

In this work, living statistical copolymerization with a bifunctional initiator is presented for the synthesis of "two-sided tapered ABA triblock copolymers" from a mixture of both monomers in a single step, circumventing monomer addition steps. The more reactive diene monomer is incorporated first in both directions of the growing chains, followed by the second monomer, which forms the outer blocks. **Figure 1** indicates the advantage of this more efficient bifunctional route compared to the classical, complex three-step addition pathway. The use of bifunctional initiators for the synthesis of ABA triblock copolymers is described in various Kraton™ patents.[28]

The reactivity ratios can be determined by tracking the conversion of the comonomers in real time. Several analytic techniques have been used, e.g., *in situ* NMR,[29],[30] mid-IR,[31] or NIR spectroscopies,[27],[32] to gain a picture of the copolymerization kinetics, and various models are known to convert the comonomer consumptions into the respective reactivity ratios. A comprehensive compilation of the different models and their pros and cons can be found elsewhere.[33],[34]

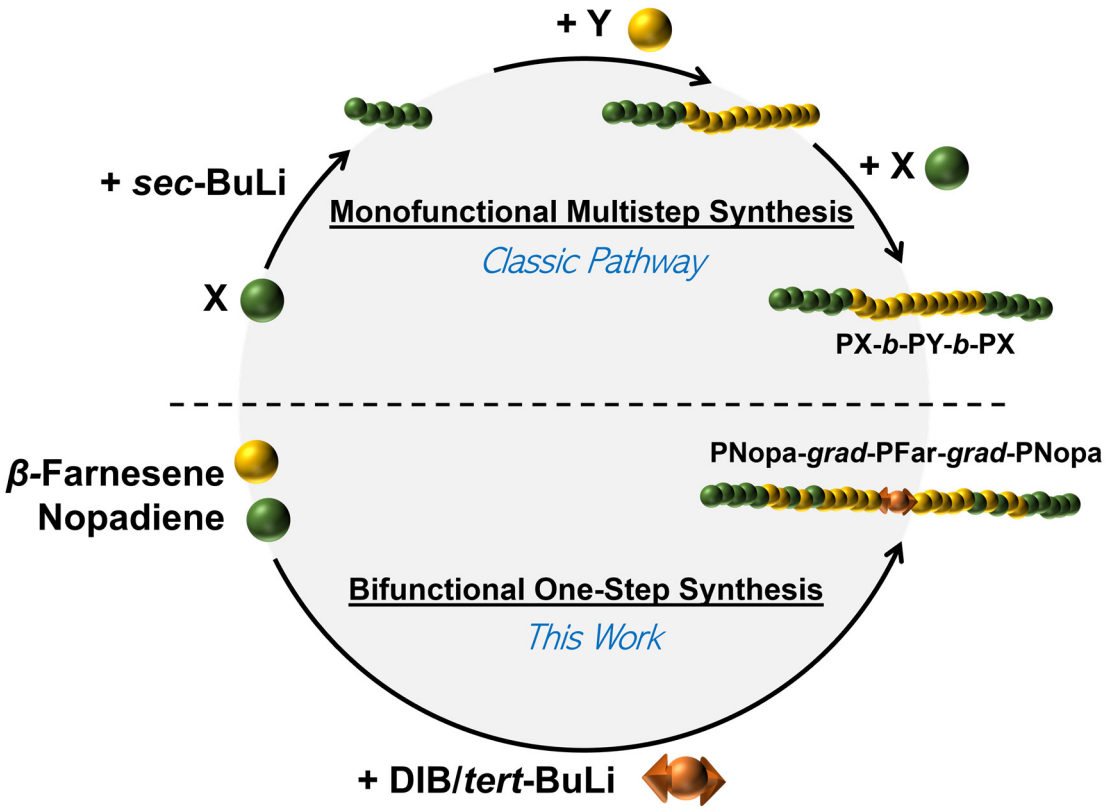

Figure 1. Benefits resulting from bifunctional initiation (lower part) over sequential multistep monomer addition syntheses of ABA triblock copolymers.

The poor solubility of bifunctional initiators in pure hydrocarbon solvents has resulted in only a few successful recent reports for classical systems of rather complex structures.[35]–[37] The addition of polar solvents or modifiers can prevent the aggregation of the bifunctional initiators, albeit with the drawback of an undesired high vinyl content of the resulting polydienes.[38],[39] As the T_g of PFar is not affected by the increased vinyl content, the use of a polar solvent is now feasible. The moderately polar solvent methyl *tert*-butyl ether (MTBE) was used due to its good solubilization of bifunctional initiators as well as its higher stability toward nucleophiles, which is a major limitation of other polar solvents, e.g., THF, and therefore restricts them to low temperatures.[40] Moreover, besides being an established compound in industry and organic synthesis, MTBE possesses the potential for sustainable production from bio-based methanol and bio-based isobutane.[41] As MTBE has been rarely used in carbanionic polymerization, its impact on copolymerization on Far and Nopa is investigated in the first section.[8],[38],[42]–[44]

Results and Discussion

Kinetics of Statistical Copolymerization

The statistical, living copolymerization of Far and Nopa (molar ratio 1:1) in cyclohexane was investigated using *in situ* ^{1}H NMR kinetics. The consumption of Far and Nopa can be followed individually, see **Figure 2**a. To gain reliable and quantitative results within the NMR experiment, the T_1-relaxation times of the protons under consideration were predetermined, see **Figure S1**. Both dienes contribute to the integral at ~ 6.55 ppm, attributed to the proton of the conjugated 1,3-diene. Nopa has another isolated proton in its diene structure. This methine proton is connected to both the diene and the six-membered ring structure and shifts upfield to ~ 5.72 ppm, see **Figure 2**. Simple subtraction of the Nopa integral of the combined proton signal gives the Far content. Thus, individual monomer consumption as a function of time and of total conversion can be followed (**Figures S2-S12)**. Within this work, the nonterminal model (Jaacks equation[45], **Equation S5**) was studied to describe the copolymerization using only one independent parameter, i.e., $r_1 \cdot r_2 = 1$.[34],[45] The nonterminal model assumes that an ideal copolymerization is independent of the chain end nature. The more complex terminal model relies on two parameters, making it prone to overfitting. All kinetic data and fits can be found in **Figures S4-S13** and T**able S1**.

In the hydrocarbon solvent cyclohexane, Far is consumed first, followed by Nopa. The determination of the respective reactivity ratios resulted in $r_{Far} = 6.50$ and $r_{Nopa} = 0.155$. Even though a gradient of comonomer incorporation is achieved, it is less pronounced than the one found for the classical S/I system in cyclohexane ($r_I = 10.0$, $r_S = 0.015$).[27] As the polymerization of Far is not limited to hydrocarbon solvents, polar solvents and modifiers were also investigated. This revealed different reactivity ratios, as summarized in **Table 1**. Using MTBE as a moderately polar solvent leads to a slightly stronger gradient. 1,3-Di(2-tetrahydrofuryl)propane (DTHFP) was used as a highly efficient modifier.[46] By using MTBE as a solvent in the presence of two equivalents (2 eq) of DTHFP with respect to lithium, more disparate reactivity ratios are obtained (r_{Far}=11.2 and r_{Nopa}=0.09) that resemble the values of the classical S/I system. Thus, the MTBE/DTHFP solvent/modifier system yields a rather strong gradient resulting in tapered block copolymers. All gradients are depicted in **Table S1**. One significant observation is the faster reaction in the solvent/modifier system since the consumption of Far ($t_{1/2}$) in cyclohexane of ~11 min is reduced to ~1 min in MTBE and DTHFP. This is explained by the breakup of chain end aggregates in the polar environment.[47]

Table 1. Reactivity ratios of Far and Nopa under different conditions determined by *in situ* ^{1}H NMR kinetics using the Jaacks[45] equation (**Eq. S1**).

Solvent	Initiator	r_{Far}	r_{Nopa}	R^2
Cyclohexane	*sec*-BuLi	6.50 ± 0.04	0.155 ± 0.001	0.99
MTBE	*sec*-BuLi	7.23 ± 0.30	0.138 ± 0.005	0.95
MTBE + 2 eq DTHFP	*sec*-BuLi	11.2 ± 1.0	0.090 ± 0.008	0.92
MTBE + 2 eq DTHFP	DIB-Li_2	10.8 ± 0.9	0.093 ± 0.008	0.96

The kinetic investigation suggests that initiating a mixture of Far and Nopa with a bifunctional initiator should enable the preparation of ABA-type, two-sided tapered triblock copolymers that require no additional monomer addition steps. Far will therefore be incorporated first in both directions, and Nopa forms the outer blocks of the tapered triblock. To prove this behavior, a kinetics study was performed using the bifunctional initiator DIB-Li_2, derived from 1,3-diisopropenyl benzene and *tert*-BuLi, see **Scheme 2**.

Scheme 2. Synthesis of DIB-Li_2 followed by initiation of Nopa and Far.

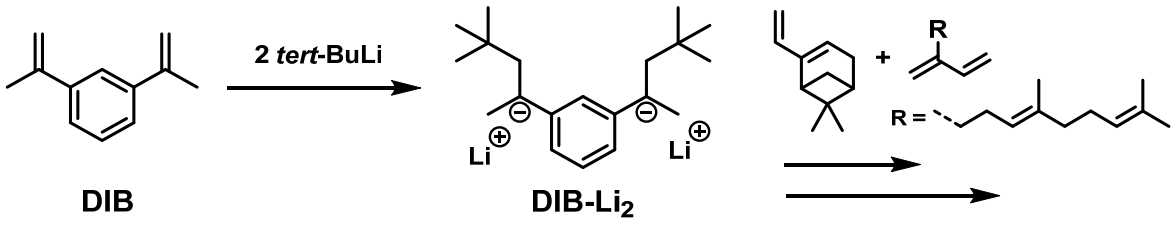

This initiator is established[48],[49] and shows reliable results in moderately polar solvents like MTBE.[8],[42] Both synthesis and in-depth investigation of this bifunctional initiator were introduced in our previous work.[42] As can be followed in **Figure 2** and **Table 1**, the bifunctional initiator instead of *sec*-BuLi does not influence the results obtained before.

The living behavior, i.e., fast initiation and absence of chain termination or transfer of the polymerization, is reflected by the linearity of the pseudo-first-order plot of $\ln([M]_0/[M])$ vs time, see **Figure 2**c. Further, the steep gradient shown in **Figure 2**d has to be imagined in a mirrored fashion since the chain growth occurs in both directions of the bifunctional initiator. The significantly larger volume fraction of PFar compared to PNopa can be explained by the higher molar mass of Far over Nopa, resulting in a larger weight fraction of Far, w_{Far}, of 58 wt%. This effect becomes even more pronounced in the volume fraction, Φ_{Far} = 60 vol%, due to the slightly lower density of the homopolymer PFar (0.900 g·cm^{-3}) compared to PNopa (0.987 g·cm^{-3}).

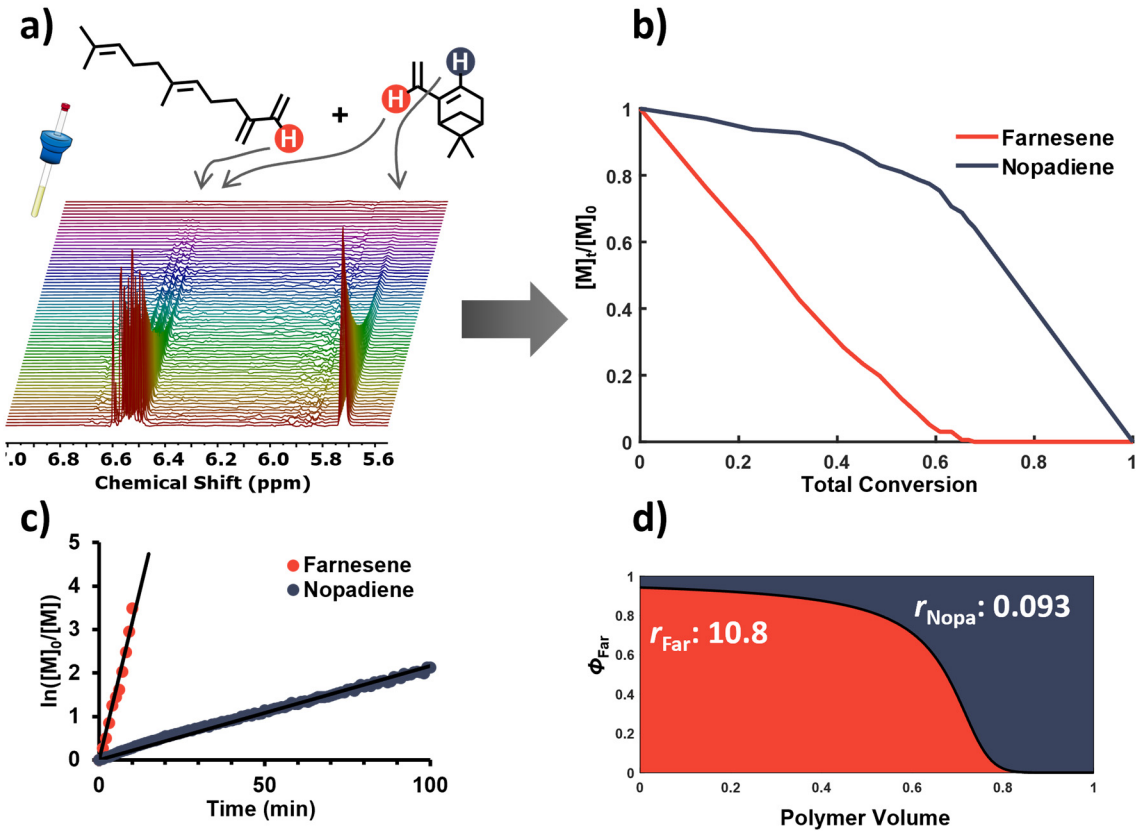

Figure 2. a) *In situ* ^{1}H NMR kinetics of Far and Nopa in MTBE with 2 eq DTHFP using the bifunctional initiator DIB-Li_2; b) comonomer consumption vs total conversion; c) pseudo-first order plot; d) volume gradient using the reactivity ratios determined by the Jaacks[45] fit.

Molecular and Thermal Properties of PFar and PNopa Synthesized in MTBE/DTHFP

The copolymerization kinetics point to a highly efficient synthesis route for two-side tapered ABA-triblock copolymers in a single polymerization step by bifunctional initiation in MTBE, using 2 eq of DTHFP as a modifier. Since changes of the reaction conditions (i.e., solvent and modifier) can have a drastic impact on the polymer properties of polydienes, homopolymers have also been prepared from each monomer using *sec*-BuLi as the initiator. Size-exclusion chromatography (SEC) revealed that the reaction conditions are suitable for the carbanionic polymerization of Far and Nopa, as both polymers show low dispersity. The results, summarized in **Table 2** and **Figure S22**, are in good agreement with molar masses obtained by additional studies *via* multi-angle light scattering (MALS) detection. In fact, the observations indicate an even lower dispersity for PNopa polymerized in MTBE than in pure hydrocarbon solvents. In cyclohexane, higher dispersity is observed due to stronger aggregated initiators, resulting in slow initiation.[19] Accordingly, we assume that the more polar character of

MTBE/DTHFP leads to suppression of aggregation, as is also indicated by the strongly increased reaction rates.

Both homopolymers were characterized in terms of their microstructural composition. The regiostructure of PFar can be determined by ^{1}H NMR spectroscopy.[42],[50] The integration is shown in **Figure 3**, and the results are given in **Table 2**. In MTBE/DTHFP 37.3% 1,4-, 60.2% of 3,4-, and 2.5% 1,2-units are observed. In contrast, polymerization in pure hydrocarbons results in 91-94%[8],[50] 1,4-units, whereas in pure MTBE the amount decreases to 61% 1,4-units.[42]

For PNopa the determination is not straightforward due to overlapping signals in the olefinic region in the respective ^{1}H NMR, see **Figures S17-S19**. A reasonable solution can be found using *inverse gated*-^{13}C NMR as described in greater detail earlier.[19] As shown in **Figure 3**, the microstructure of PNopa in MTBE/DTHFP is composed of 54.8% 1,4-PNopa and 45.2% 3,4-PNopa. PNopa synthesized in pure hydrocarbon media resulted in 51% 1,4-incorparation.[19]

Table 2. Characterization results for both homopolymers PFar and PNopa synthesized in MTBE and 2 eq DTHFP.

Sample	M_n^{SEC} [g·mol^{-1}]	$Đ$	M_w^{MALS} [g·mol^{-1}]	1,4- [%] d)	3,4- [%] d)	1,2- [%] d)	T_g [°C] e)	ρ [g·cm^{-3}] f)
PFar	15 700 a)	1.05	17 200	37.3	60.2	2.5	-67±1	0.900
PNopa	15 800 b)	1.06	14 900	54.8	45.2	0	151±2	0.987

[a] Measured by SEC with PI-calibration; eluent: THF. [b] Measured by SEC with PS-calibration; eluent: THF. [c] Measured by SEC using a MALS detector; eluent: THF. [d] PFar determined by ^{1}H NMR spectroscopy; PNopa determined by *inverse gated*-^{13}C NMR spectroscopy. [e] Determined by DSC experiments using a heating rate of 10 K·min^{-1}. [f] Density determined using helium pycnometer at 298 K.

Thermal analysis *via* differential scanning calorimetry (DSC) was performed for both homopolymers, and the heat flow curves are presented in **Figure S23**. For PFar, known for its T_g being rather unaffected by its microstructure, a T_g of -67 °C was found, whereas PNopa showed a high T_g of 151 °C, both measured with a heating rate of 10 K·min^{-1}. This difference is even higher than the one found for classical SIS or SBS rubber systems (PI: -67 °C, polybutadiene (PB): -96 °C, PS: 100 °C).[51] Both homopolymers show properties that are ideally suited for TPEs. To calculate the volume fraction of both polymers in the tapered graft copolymers, the densities of the bulk materials were determined by a helium pycnometer (**Table 2**). The density of PFar corresponds to the value reported in the literature.[11]

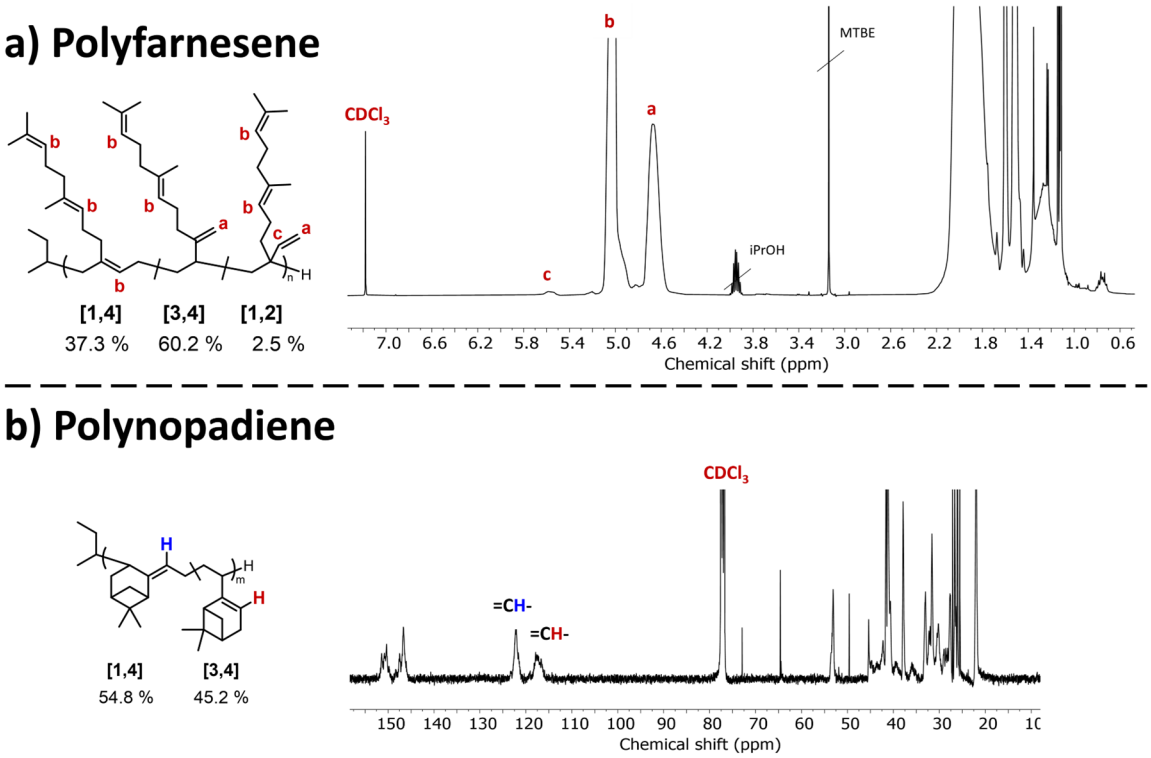

Figure 3. a) ^{1}H NMR spectra of PFar with all olefinic protons assigned, 400 MHz, $CDCl_3$, 30 s delay; b) *inverse gated*-^{13}C NMR spectum of PNopa with carbons of each microstructure assigned, 100 MHz, $CDCl_3$, 12 s delay.

Synthesis and Molecular Properties of Tapered ABA Triblock Copolymers

Based on these results, a series of tapered triblock copolymers, PNopa-*grad*-PFar-*grad*-PNopa, were synthesized using the bifunctional initiator DIB-Li_2, see **Scheme 2**. By choosing the ratio $[M]_0/[Ini]_0$ a series of molar masses was obtained. The mole fraction, x_{Far}, defines the length, i.e., number of monomer units, of the respective blocks. As most of Nopa is incorporated after polymerization of Far, it is found at both chain ends of the tapered ABA structure, leading to a mirrored molar mass composition of 25k-50k-25k at a molar composition of x_{Far}=0.42 and a target molar mass of 100 kg·mol^{-1}. Thereby equivalent molar masses for each comonomer are achieved due to the higher molar mass of the Far monomer (204 g·mol^{-1}) compared to Nopa (148 g·mol^{-1}). **Figure 4** and **Table 3** compile the SEC results of two different series of triblock copolymers prepared in this work.

First, a series of different molar mass copolymers targeting 50k, 100k and 200k with 50% comonomer weight fraction (42 mol% Far) was synthesized, followed by a series of 100k samples of various compositions. The midblock of PFar was varied from 20k up to 80k using 10k intervals, resulting in a total of seven samples. The targeted molar compositions are displayed using the format "P(N_x-F_y-N_x)-M_n^{target}" with "*x*" and "*y*" referring to each copolymer's

molar mass proportion. The volume fraction of PFar, Φ_{Far}^{target}, within the copolymers can be calculated using the homopolymer densities determined in the previous section.

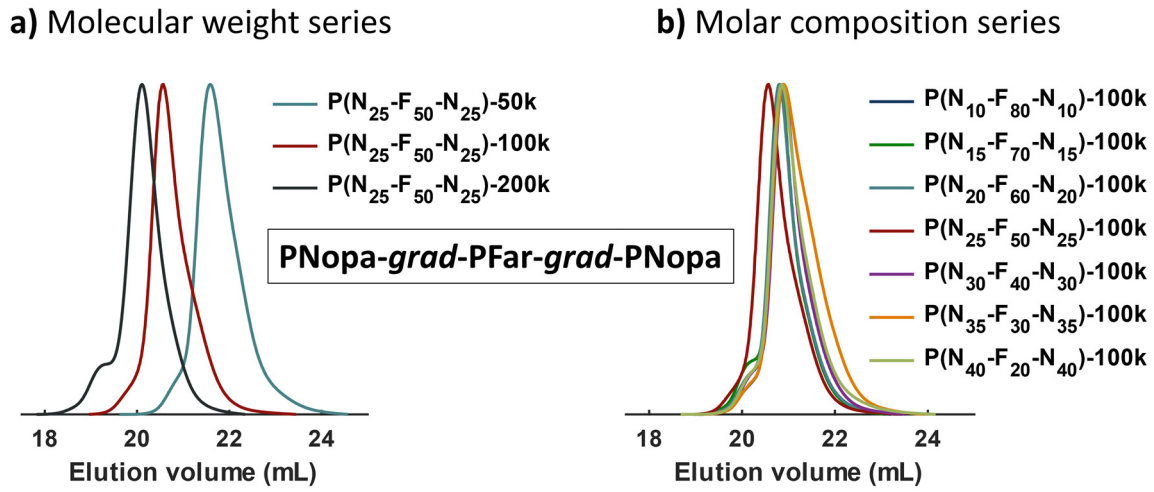

Figure 4. Compilation of SEC traces of synthesized tapered triblock series of PNopa-*grad*-PFar-*grad*-PNopa; a) samples of increasing molar mass; b) samples of different compositions.

Table 3. Summary of characterization data of all tapered triblock copolymers.

Sample	x_{Far}	Φ_{Far}^{target} a)	M_n^{target} [kg·mol^{-1}]	M_n^{SEC} b) [kg·mol^{-1}]	$Đ$ b)	$T_{g,\,Far}$ [°C]	$T_{g,\,Nopa}$ d) [°C]
$P(N_{25}\text{-}F_{50}\text{-}N_{25})$-50k	0.42	0.52	50	45.2	1.18	-45±4 d)	70±10
$P(N_{25}\text{-}F_{50}\text{-}N_{25})$-100k	0.42	0.52	100	86.4	1.18	-44±5 d)	60±10
$P(N_{25}\text{-}F_{50}\text{-}N_{25})$-200k	0.42	0.52	200	171.1	1.22	-46±3 d)	108±6
$P(N_{10}\text{-}F_{80}\text{-}N_{10})$-100k	0.74	0.81	100	88.2	1.14	-57±1 c)	-
$P(N_{15}\text{-}F_{70}\text{-}N_{15})$-100k	0.63	0.72	100	91.3	1.16	-53±2 c)	-
$P(N_{20}\text{-}F_{60}\text{-}N_{20})$-100k	0.52	0.62	100	89.1	1.16	-44±4 d)	58±8
$P(N_{30}\text{-}F_{40}\text{-}N_{30})$-100k	0.33	0.42	100	82.3	1.17	-53±4 d)	67±12
$P(N_{35}\text{-}F_{30}\text{-}N_{35})$-100k	0.24	0.32	100	71.7	1.21	NA	NA
$P(N_{40}\text{-}F_{20}\text{-}N_{40})$-100k	0.15	0.22	100	78.1	1.21	NA	NA

[a] determined using the homopolymer densities: ρ(PFar)= 0.900 g·cm^{-3}; ρ(PNopa)= 0.987 g·cm^{-3}. [b] measured by SEC with PS-calibration; eluent: THF. [c] determined by DSC using a heating rate of 10 K·min^{-1}. [d] determined by temperature modulated DSC, period of modulation, T=20 s.

All results are summarized in **Table 3**, showing that both the molar mass and composition of the copolymers can be tailored. The slight deviation in M_n (SEC) of the samples of different compositions, but the same M_n^{target} of 100 kg·mol^{-1} can be attributed to the different

hydrodynamic radii of both copolymer blocks. The dispersity of the tapered triblocks, despite being somewhat higher than that for the homopolymers, can be considered to be rather low taking into account bifunctional initiation. As both monomers are 1,3-dienes, individual characterization within the copolymer is not accessible *via* NMR spectroscopy, as all signals obtained stem from protons of both monomers (see **Figure S21**). The nearly quantitative precipitated polymer yield (>90%) indicates good prediction of its composition.

Thermal and Morphological Properties of Tapered Triblock Copolymers

DSC measurements were conducted for all tapered triblock copolymer samples. As can be seen in **Table 3** and **Figure S24**, the T_g of the PFar phase decreases with increasing PFar molar mass. This is in contrast to the Flory-Fox equation for homopolymers.[52] However, this can be tentatively attributed to the tapered nature of the architecture, which leads to some extent of phase mixing and less pronounced phase separation for lower chain lengths. **Table 3** and **Figure S25** show an increasing T_g of PFar with a decreasing Far content. This was most noticeable in the appearance of the two samples of high PFar content that were obtained as viscous materials, leading to the assumption of the absence of phase separation. The T_g values of the PFar-triblock domains approach that of the PFar homopolymer with increasing PFar content and molar mass. Surprisingly, the T_g of PNopa was not detectable in standard DSC experiments. We will return to this point below with respect to the results from temperature-modulated DSC.

More insights regarding the phase state of the copolymers were gained by variable temperature small-angle X-ray scattering (SAXS). As an example, in **Figure 5**, we compare the SAXS patterns of three copolymers with the same composition (25/50/25 by weight) as a function of molar mass (45.2, 86.4, and 171.1 kg·mol^{-1}). In most cases, a single broad peak is evident, revealing correlation hole scattering from the disordered (DIS) phase. The domain spacing extracted from the peak position, as $d = 2\pi/q^*$, scales as $d \sim N^{0.5}$, suggesting Gaussian chains in the DIS phase. The only exception is the scattering curve from P(N_{25}-F_{50}-N_{25})-200k with the higher molar mass, where a shoulder is evident at approximately twice q^*, suggesting a lamellar structure with a short-range order.

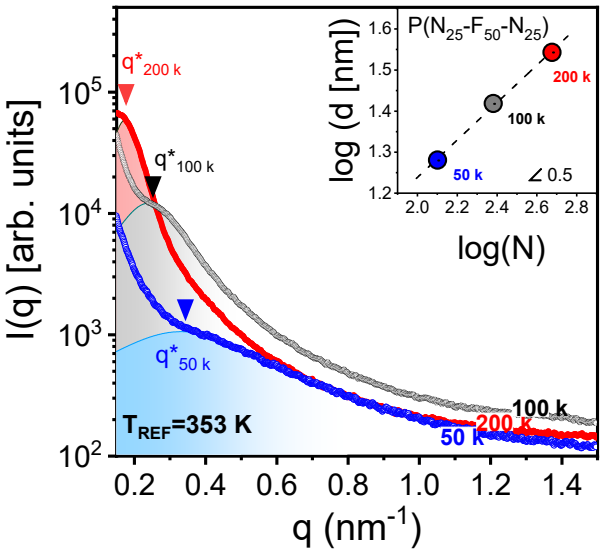

Figure 5. SAXS patterns at a common temperature of 353 K (80 °C), for the three copolymers P(N_{25}-F_{50}-N_{25})-50k, P(N_{25}-F_{50}-N_{25})-100k and P(N_{25}-F_{50}-N_{25})-200k, with the same composition (25/50/25) and with molar masses of 45.2, 86.4, and 171.1 kg·mol^{-1}, respectively. All samples exhibit a very broad peak corresponding to the DIS state. In the inset, the domain spacing is plotted as a function of the total degree of polymerization in a double logarithmic representation. A line with a slope of ~1/2 is shown.

Some temperature dependent SAXS curves are shown in **Figure 6** for tapered P(N_{30}-F_{40}-N_{30})-100k. The patterns indicate a single broad peak related to correlation hole scattering (with a period of ~25 nm), corresponding to the disordered state (DIS). The temperature dependence of the broad peak as q^* is very informative of the state of the copolymer. **Figure 6**b indicates a distinctly different $q^*(T)$ dependence below and above ~365 K. This behavior reflects changes in electron density originating from changes in the specific volume when crossing a glass temperature. Hence, we identify a SAXS glass temperature of PNopa at ~ 365 K (92 °C).

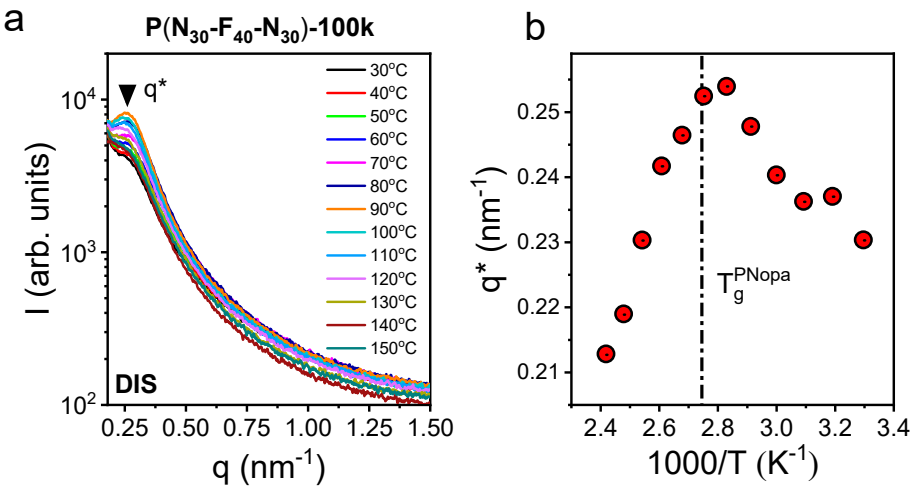

Figure 6. (a) Temperature-dependent SAXS patterns of the tapered P(N_{30}-F_{40}-N_{30})-100k, obtained on heating from 30 to 150 °C in 10 °C steps. (b) Temperature dependence of the primary peak (q*). The glass temperature of PNopa is indicated by the change in the temperature dependence of q*.

More detailed information about the thermodynamic state and the molecular dynamics of the copolymers can be extracted by temperature-modulated DSC (TM-DSC) and dielectric spectroscopy (DS), respectively. The temperature dependence of the reversing heat capacity of P(N_{25}-F_{50}-N_{25})-200k, obtained from TM-DSC at two different periods of modulation (T = 40 s, 20 s), is depicted in **Figure 7**. The reversing heat capacity (Rev c_p) and, in particular, its first derivative with respect to temperature are very informative regarding the thermodynamic arrest at some temperatures as indicated by arrows. The peak at lower temperatures (-46 °C) clearly corresponds to the T_g of the soft phase, PFar. The peak at the highest temperature (112 °C) corresponds to the T_g of the hard phase, PNopa. Interestingly, there exists a weak feature at intermediate temperatures (~ 6 °C). Based on earlier studies of gradient copolymers this feature is assigned to the glass temperature of the "interphase".[53],[54] Additional TM-DSC curves for the other copolymers are shown in **Figure S26**.

Isochronal rheology measurements (at ω = 10 rad·s^{-1}) of the shear moduli provide additional evidence for the lower and higher T_g in the copolymer, **Figure 7**c. Master curves of the loss and storage shear moduli are discussed with respect to **Figure S27**. In general, the rheology experiments revealed cross-linking of the copolymers at temperatures exceeding 150 °C.

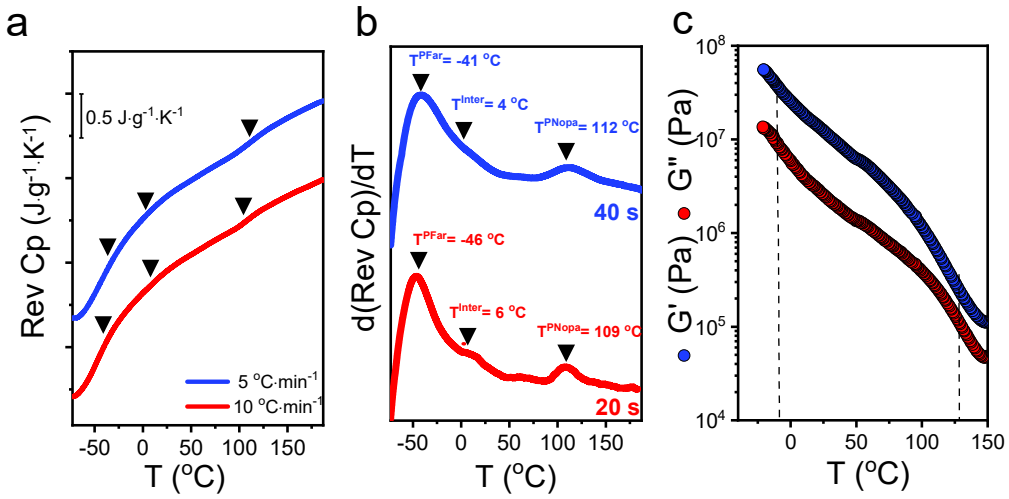

Figure 7. (a) Temperature dependence of the reversing heat capacity (Rev c_p) for the sample P(N_{25}-F_{50}-N_{25})-200k, obtained from TM-DSC, at two different periods of modulation (T = 40 s, 20 s). Arrows indicate characteristic "transition" temperatures (see text). Data are shifted vertically for clarity. (b) Temperature dependence of the first derivative of the reversing heat capacity, for the two aforementioned oscillation periods. In both cases, three peaks are evident, related to the T_g of PFar, an "interphase" T_g corresponding to the gradient interface, and to PNopa. (c) Storage (blue) and loss (red) shear moduli obtained on heating with a rate of 5 K·min^{-1} at a frequency of 10 rad·s^{-1}. Dashed lines indicate approximate values for the PFar and PNopa T_g's at the particular (higher) frequency.

The molecular dynamics were subsequently investigated by dielectric spectroscopy.[55],[56] **Figure 8** provides a representative loss curve for P(N_{25}-F_{50}-N_{25})-200k at 323 K, revealing two relaxation mechanisms. The faster one corresponds to the segmental dynamics of PFar. It has the usual Vogel-Fulcher-Tammann (VFT) dependence, **Eq. 2**,

$$f_{max} = f_{\infty} \cdot \exp\left(-\frac{B}{T \cdot T_0}\right) \quad \textbf{(2)}$$

where f_∞, is a pre-exponential factor, B is the activation parameter, and T_0 is the Vogel temperature (also called "ideal" glass temperature). The VFT parameters of the PFar segmental mode are: -log(f_{max}/Hz) = 12 (held fixed), B = 2600 ± 30 K, and T_0 = 140 ± 1 K. The slower process, although it has a temperature dependence similar to the longest normal mode of the homopolymer PFar 100k (also shown in the figure with a solid line; corresponding VFT parameters -log(f_{max}/Hz) = 5, B = 1230 ± 20 K, and T_0 = 183 ± 3 K), it is not assigned to this mode for two reasons. First, the chain modes are suppressed in the copolymers as PFar is attached from both sides to the relatively immobile PNopa.[57] Second, this mode freezes at the DSC temperature corresponding to the interphase T_g. Therefore, it has been assigned to a segmental-type process of PFar and PNopa units located at the interphase. A third process corresponding to the PNopa segmental relaxation (as seen in DSC) could not be identified in DS.

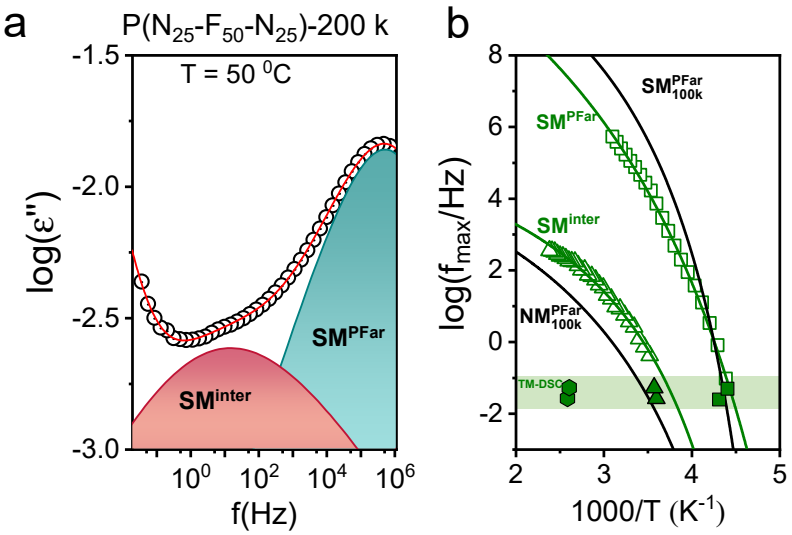

Figure 8. (a) Dielectric loss curve as a function of frequency for the sample P(N_{25}-F_{50}-N_{25})-200k, at 50 °C. Two relaxation processes are evident: a fast one corresponding to the segmental relaxation of PFar, and a slower one corresponding to the segmental relaxation of the gradient interphase. (b) Characteristic frequencies at maximum loss plotted as a function of inverse temperature. Open green squares refer to the segmental mode (SM) of PFar and open green triangles correspond to the SM of the interphase. For comparison, the relaxation times of the SM and NM of the homopolymer PFar 100k are also depicted with black lines. The latter data are shifted so as to coincide with the SM mode of the P(N_{25}-F_{50}-N_{25})-200k copolymer. Green-filled symbols are obtained from TM-DSC (squares: PFar, triangles: interface, and polygons: PNopa).

The slower segmental process corresponding to PNopa could be identified in the copolymer P(N_{30}-F_{40}-N_{30})-100k with higher PNopa content. The results are listed in **Figure 9**. The figure depicts three segmental processes corresponding to PFar, the interphase, and PNopa at higher temperatures [VFT parameters: -log(f_{max}/Hz) = 12 (held fixed), B = 2730 ± 40 K, T_0 = 161 ± 2 K; -log(f_{max}/Hz) = 10 (held fixed), B = 4160 ± 50 K, T_0 = 152± 3 K for the segmental and interphase processes, respectively]. The three segmental processes freeze at temperatures corresponding to the ones in TM-DSC (**Figure S26**).

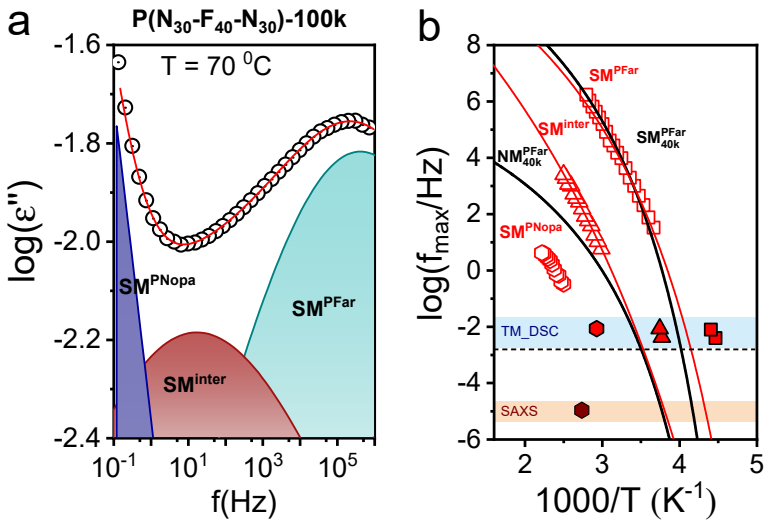

Figure 9. (a) Dielectric loss curve as a function of frequency for the sample P(N_{30}-F_{40}-N_{30})-100k, at the reference temperature of 70 °C. Two relaxation processes are evident: a fast one corresponding to the segmental relaxation of the PFar and a slower one corresponding to the segmental relaxation of the interphase. (b) Relaxation map of the same sample. Open red squares refer to the segmental mode (SM) of PFar, open red triangles correspond to the SM of the interphase, and open red circles correspond to the SM of PNopa. For comparison, the relaxation times of the SM and NM of the bulk PFar 40k (black lines) are depicted and shifted so as to coincide with the SM mode of P(N_{30}-F_{40}-N_{30})-100k. Red filled symbols are obtained from TM-DSC (squares: PFar, triangles: interface, and polygons: PNopa), while the filled symbol is obtained from SAXS measurements (the characteristic frequency corresponding to the slow effective rate in this experiment).

Overall, results from variable temperature SAXS, temperature-modulated DSC, and DS as a function of temperature identified three local segmental processes in the tapered P(Nopa-*grad*-Far-*grad*-Nopa) copolymers and the corresponding glass temperatures. The lowest and highest correspond to the freezing of the segmental dynamics of the soft (PFar) and hard (PNopa) segments, whereas the intermediate corresponds to the collective freezing of the Far and Nopa segments located at the "interphase".

The absence of long-range order *via* the SAXS measurements can be attributed to the unusual two-sided tapered structure that leads to diffuse boundaries of the domains. We assume that it prevents the formation of a periodic structure. Despite the absence of long-range order, the combination of the thermal, SAXS, dielectric spectroscopy, and rheology results revealed local segregation similar to classical TPEs.

Mechanical Properties of Tapered Block Copolymers

Films were prepared by solvent casting ($CHCl_3$), and dog-bone-shaped test specimens were punched out. They were analyzed using a preload of 0.1 N and pulled at a speed of 20 mm·min^{-1}.

Figure 10 shows a selection of individual stress-strain curves of the second series of triblock copolymers of different comonomer compositions. A complete compilation of all stress-strain experiments can be found in **Figures S28** and **S29**. The data are collected in **Table 4**. Limitations for such measurements were the viscous nature of samples with 80 and 70 wt% PFar as well as the brittle nature of the samples with 20 wt% PFar. As can be seen in **Figure 10** and **Figure 11**a, an increasing content of PNopa within the triblock copolymer leads to a decrease in elongation at break, ε_{max}. The triblock P(N_{20}-F_{60}-N_{20})-100k has an ε_{max} of 1300% decreasing to 210% for the P(N_{35}-F_{30}-N_{35})-100k sample. The Young's modulus, E, on the other hand, shows just the opposite trend. The material properties change from low modulus (2.5 MPa) and high flexibility to tough materials that reach a high modulus of up to 550 MPa. Both samples with the highest amount of PNopa, i.e., 60 and 70 wt%, show distinctive yielding behavior, in line with previously reported results.[19] The higher content of vitrified PNopa domains leads to greater plastic deformation and lower elasticity due to less elongation within the shorter PFar-chains. Hence, similar magnitudes as known for classical and petrol-based materials, e.g., SBS-rubbers (Styroflex and Styrolux), can be achieved. Differences can be attributed to the much higher M_e of PFar (50 kg·mol^{-1}) compared to polybutadiene (M_e ~ 1.9 kg·mol^{-1}).[11],[12] A summary of the measurement results is given in **Table 4**.

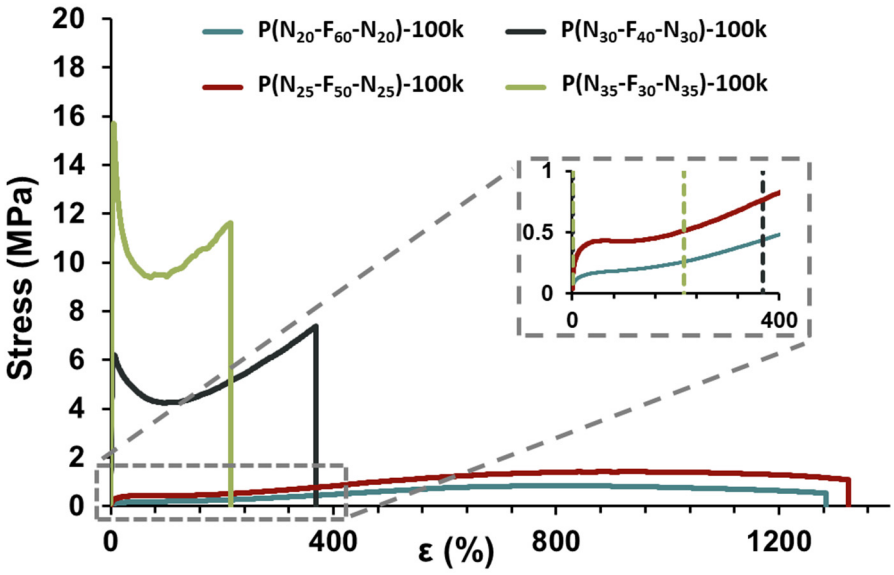

Figure 10. Stress-strain curves of the triblock series of different compositions; each sample was measured three times; as an example, one curve of each was selected.

Table 4. Summary of tensile-test results of all tapered triblock copolymers.

Sample	M_n^{SEC} a) [kg·mol^{-1}]	$Đ$ a)	E b) [MPa]	ε_{max} c) [%]
P(N_{25}-F_{50}-N_{25})-50k	45.2	1.18	20 ± 2 (16)[d]	1 030 ± 40
P(N_{25}-F_{50}-N_{25})-100k	86.4	1.18	9.4 ± 0.6 (5.9)[d]	1 280 ± 80
P(N_{25}-F_{50}-N_{25})-200k	171.1	1.22	7.0 ± 0.2 (33)[d]	660 ± 170
P(N_{10}-F_{80}-N_{10})-100k	88.2	1.14	*viscous* (0.04)[d]	*viscous*
P(N_{15}-F_{70}-N_{15})-100k	91.3	1.16	*viscous* (0.24)[d]	*viscous*
P(N_{20}-F_{60}-N_{20})-100k	89.1	1.16	2.5 ± 0.4	1 300 ± 100
P(N_{30}-F_{40}-N_{30})-100k	82.3	1.17	246 ± 1	370 ± 20
P(N_{35}-F_{30}-N_{35})-100k	71.7	1.21	550 ± 20	210 ± 30
P(N_{40}-F_{20}-N_{40})-100k	78.1	1.21	*brittle*	*brittle*

[a] Measured by SEC in THF with PS-calibration. [b] Determined by the initial slope of each stress-strain curve (1% stretching); values are presented as the average of three measurements done for each sample, accompanied by their standard deviation. [c] Values given the as average of three measurements performed per sample, accompanied by their standard deviation. [d] Values obtained from rheology.

A much less pronounced effect was found when changing molar mass, **Figure 11**b. The Young's modulus decreases from 19.7 MPa to 7.0 MPa when increasing M_n from 50 kg·mol^{-1} up to 200 kg·mol^{-1} and the highest value of ε_{max} was found for the 100 kg·mol^{-1} sample with an ε_{max} of 1280%. The thermal stability of the polymer samples presented in **Figure 11** were examined *via* thermal gravimetric analysis (TGA), yielding $T_{5\%}$-values (temperature of 5% weight loss) in the range of 339 °C to 349 °C. These values are well above the glass temperature of the vitrified PNopa domains and thus ensures thermal processing. All measurements are presented in **Figure S35**.

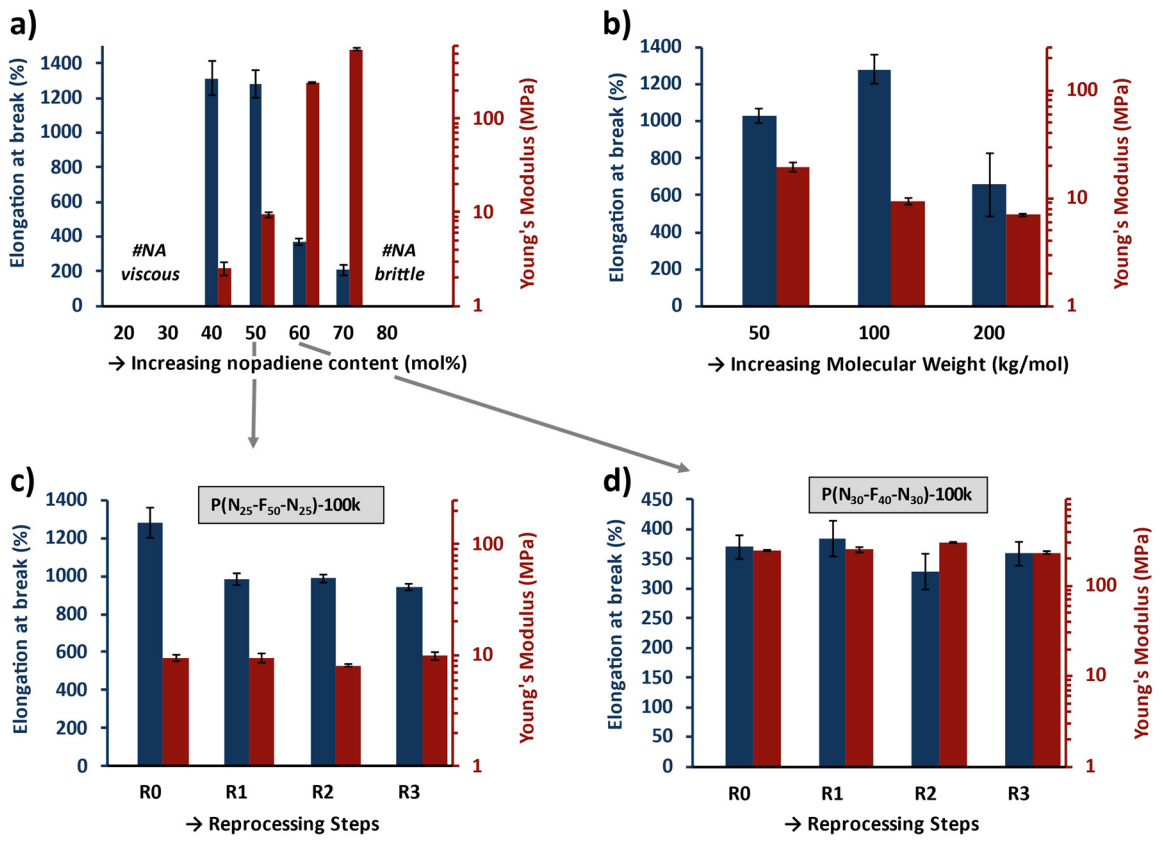

Figure 11. Tensile test results of both triblock series; a) variation of composition of PFar/PNopa with M_n^{target} = 100k; b) variation of molar mass at an individual M_n ratio of PFar and PNopa of 50:50; c) reprocessing of $P(N_{25}\text{-}F_{50}\text{-}N_{25})$-100k; d) reprocessing of $P(N_{30}\text{-}F_{40}\text{-}N_{30})$-100k.

Further, the elastic recovery of the lowest modulus sample $P(N_{20}\text{-}F_{60}\text{-}N_{20})$-100k was determined to be 96%, showing only minor plastic deformation for the low-strain region, see **Figure S30**. One major advantage of TPEs over classical elastomers is the possibility of facile (re)processing.

As covalent cross-linking of vulcanized elastomers is replaced by noncovalent physical cross-linking of the glassy PNopa domains, the material can be (re)dissolved after use. Thereby, multiple reshaping is feasible. One highly flexible, $P(N_{25}\text{-}F_{50}\text{-}N_{25})$-100k, and one rather high modulus sample, $P(N_{30}\text{-}F_{40}\text{-}N_{30})$-100k, were reprocessed four times each by dissolving and film casting. Tensile tests provide rather constant moduli, as presented in **Figure 11**c and d. After each measurement, the torn pieces and remains of the samples were redissolved, and new films were prepared; see **Figure 11** and **Figures S31-S34**. As only nanophase segregated materials are expected to exhibit this level of mechanical properties, the previously observed local phase segregation is further underlined.

We emphasize that all obtained values represent a close match to their industrially produced crude-oil-derived competitors and benchmarks, *Styroflex* and *Styrolux*. They can likewise be

tuned into the same range of magnitude, both in elongation and modulus.[4] Hence, we introduce a fully bio-based thermoplastic elastomer alternative that can be produced in a highly efficient, single-step, one-pot reaction. The efficiency can be attributed to the kinetically driven tapered incorporation of the monomers within a bifunctional initiator system.

Conclusions

Identifying a more sustainable but adequate substitute for established fossil fuel-based SBS and SIS rubber materials was the key objective of this work. A synthesis pathway toward fully bio-based thermoplastic elastomers, derived from *β*-farnesene and nopadiene, is presented. *In situ* NMR kinetics of the statistical copolymerization revealed a strong compositional gradient after optimizing the polymerization conditions. Polymerization with a bifunctional initiator in the moderately polar solvent MTBE results in two-sided tapered ABA triblock copolymers. It is a key feature of the approach presented that these ABA-tapered triblock copolymers are obtained directly in a single-step synthesis. Although SAXS measurements revealed the absence of long-range periodic order in the copolymer, local phase segregation was clearly shown by temperature-modulated DSC and dielectric spectroscopy measurements. They revealed not only the T_g of the PFar and PNopa domains but also the appearance of a mixed interphase T_g. Mechanical testing showed that material properties can be tailored by the variation of the comonomer ratio. The mechanical properties vary from highly elastic, > 1300% in elongation and 2.5 MPa modulus, toward reasonably tough materials, 550 MPa and 210% in elongation. We believe that the one-step strategy reported here is of general relevance for the field of thermoplastic elastomers.

Experimental Section

All data concerning the materials, instruments, and monomer synthesis is included in the Supporting Information.

Polymerization Kinetics

In situ NMR kinetic experiments were performed on the *Bruker Acance III* 500 MHz and *Bruker Avance III HD* 400 MHz instruments. All kinetic experiments were performed using an initiator concentration of $[Ini]_0$= 0.03 mol·L^{-1} and a monomer concentration of *β*-farnesene and nopadiene of $[Far]_0$= $[Nopa]_0$= 0.3 mol·L^{-1}. Prior to the measurement, the T_1-relaxation of the respective protons of *β*-farnesene and nopadiene were determined *via* inversion recovery experiments, see **Figure S1**. Therefore, the delay using a pulse angle of 30° or 90° need to be set to approximately 2.5 or 5 times the T_1-relaxation time of the protons of interest to ensure a reliable and quantitative evaluation.[58],[59] As the solvent MTBE cannot be purchased in its deuterated form, experiments in MTBE were performed using a capillary with dimethyl sulfoxide-d_6 or even without any deuterated solvent. The signal-to-noise ratio suffers by the decreased amount of sample within the measuring volume and by the decrease in receiver gain caused by the high abundance of protons of the nondeuterated solvent. Nevertheless, the individual consumption of the monomers can be tracked and the slightly increased fluctuation does not have a large impact on the determination of the reactivity ratios from the respective fit model. Data was evaluated using the software NIREVAL.[60] Systematic errors due to fluctuations in the data points were corrected by preventing negative concentrations and allowing only monomer concentration changes in one orientation.

Homopolymerization

All used glassware was flame-dried prior to use. Both monomers, *β*-farnesene and nopadiene, were dried in a two-step procedure: first over calcium hydride, followed by three *freeze-pump-thaw* cycles, and second using trioctylaluminum. MTBE and DTHFP were dried using *sec*-BuLi and diphenyl ethylene. Cyclohexane-d_{12} was dried over calcium hydride only. All reagents were inserted into an argon-filled glovebox. DTHFP was used as a stock solution in MTBE at a concentration of 0.05 mol·L^{-1}. Monomer, solvent and modifier were mixed, and *sec*-BuLi was added to initiate the polymerization. The amount of initiator is directed by the relation P_n = $[M]_0/[Ini]_0$, where $[M]_0$ is the initial monomer concentration, $[Ini]_0$ is the initiator concentration, and P_n is the degree of polymerization at full monomer conversion.

Polymerizations were performed using monomer concentrations of 10 - 15 vol% and an initiator concentration of [Ini] = 0.005 mol·L^{-1}. Active polymerization solutions were terminated after one night of polymerization at room temperature by adding degassed methanol. Polymers were isolated by precipitation into methanol following centrifugation, decantation, and removal of the solvent under reduced pressure. Irganox 1520 (1000 ppm) was added to all polymers to enhance stability.

Triblock Copolymerization

In addition to the homopolymerization, 1,3-diisopropenyl benzene (DIB) was dried over calcium hydride and used as a 0.85 mol·L^{-1} stock solution in MTBE. Activation of DIB was performed by mixing 1 mL of DIB stock solution, 2 mL of dry MTBE, and 1 mL of *tert*-BuLi. The mixture was stirred for 5 min. In our previous work, the activation procedure was introduced and investigated by NMR kinetics in greater detail.[42] The mixture of both monomers, solvent, and modifier was initiated with the amount of initiator solution again directed by the relation $P_n = [M]_0/[Ini]_0$. Polymerizations were performed at a monomer concentration of 10 - 15 vol% and an initiator concentration of [Ini] = 0.0015 mol·L^{-1}. To ensure full conversion for all high-molar mass samples, bifunctional polymerizations were performed over a time span of 5 days, followed by termination by degassed methanol. The workup of the polymers was done as described for the homopolymers and was likewise stabilized by the addition of Irganox 1520 (1000 ppm).

References

[1] Bonart, R. Thermoplastic elastomers. *Polymer*, **1979**, *20* (11), 1389–1403.

[2] Jeon, J. H.; Jung, J. H.; Choi, C. Toward a greener future: Exploring sustainable thermoplastic elastomers. *J. Polym. Sci.*, **2024**, *62*, 662–678.

[3] Asadi, V.; Dolleman, R.; van der Gucht, J.; Kodger, T. E. 3D Printable Soft and Solvent-free Thermoplastic Elastomer Containing Dangling Bottlebrush Chains. *Mater. Adv.*, **2023**, *4*, 5535.

[4] Knoll, K.; Nießner, N. Styrolux + and styroflex + - from transparent high impact polystyrene to new thermoplastic elastomers: Syntheses, applications and blends with other styrene based polymers. *Macromol. Symp.*, **1998**, *132* (1), 231–243.

[5] Sahu, P.; Bhowmick, A. K.; Kali, G. Terpene Based Elastomers: Synthesis, Properties, and Applications. *Processes*, **2020**, *8* (5), 553.

[6] Wahlen, C.; Frey, H. Anionic Polymerization of Terpene Monomers: New Options for Bio-Based Thermoplastic Elastomers. *Macromolecules*, **2021**, *54* (16), 7323–7336.

[7] Bolton, J. M.; Hillmyer, M. A.; Hoye, T. R. Sustainable Thermoplastic Elastomers from Terpene-Derived Monomers. *ACS Macro Lett.*, **2014**, *3* (8), 717–720.

[8] Yoo, T.; Henning, S. K. Synthesis and Characterization of Farnesene-Based Polymers. *Rubber Chem. Technol.*, **2017**, *90* (2), 308–324.

[9] Baskaran, D.; Müller, A. H. E. Anionic Vinyl Polymerization. In *Controlled and living polymerizations*:*Methods and materials*; Müller, A. H. E., Matyjaszewski, K., Eds.; Wiley-VCH-Verl., **2009**; pp 1–56.

[10] Tzourtzouklis, I.; Hahn, C.; Frey, H.; Floudas, G. Molecular Dynamics and Viscoelastic Properties of the Biobased 1,4-Polymyrcene. *Macromolecules*, **2022**, *55* (19), 8766–8775.

[11] Iacob, C.; Yoo, T.; Runt, J. Molecular Dynamics of Polyfarnesene. *Macromolecules*, **2018**, *51* (13), 4917–4922.

[12] Fetters, L. J.; Lohse, D. J.; Colby, R. H. Chain Dimensions and Entanglement Spacings. In *Physical properties of polymers handbook,* 2nd ed.; Mark, J. E., Ed.; Springer, **2007**; pp 447–454.

[13] Everaers, R.; Sukumaran, S. K.; Grest, G. S.; Svaneborg, C.; Sivasubramanian, A.; Kremer, K. Rheology and microscopic topology of entangled polymeric liquids. *Science (New York, N.Y.)*, **2004**, *303* (5659), 823–826.

[14] Sá, M. C. C. de; Córdova, T.; Melo, P. A.; León, R. D. de; Pinto, J. C. Modelling and parameter estimation of trans-β-farnesene coordination polymerization. *Can J Chem Eng*, **2023**, *101* (9), 5256–5269.

[15] Milker, S.; Holtmann, D. First time β-farnesene production by the versatile bacterium Cupriavidus necator. *Microbial cell factories*, **2021**, *20* (1), 89.

[16] McCoy, M. Amyris Puts A Price On Farnesene. *Chemical & Engineering News*, **2015**, *93* (41).

[17] Sahu, P.; Young Ko, J.; Uk Ha, J.; Oh, J. S. Toward Biosourced Elastomer from β-Farnesene and Styrene: Synthesis, Properties, and Mechanical Performance. *Ind. Eng. Chem. Res.*, **2023**, *62* (22), 8726–8735.

[18] Zhang, J.; Chen, J.; Yao, M.; Jiang, Z.; Ma, Y. Hydrolysis-resistant polyurethane elastomers synthesized from hydrophobic bio-based polyfarnesene diol. *J. Appl. Polym. Sci.*, **2019**, *136* (25).

[19] Hahn, C.; Göttker-Schnetmann, I.; Tzourtzouklis, I.; Wagner, M.; Müller, A. H. E.; Floudas, G.; Mecking, S.; Frey, H. Nopadiene: A Pinene-Derived Cyclic Diene as a Styrene Substitute for Fully Biobased Thermoplastic Elastomers. *J. Am. Chem. Soc.*, **2023**, *145* (49), 26688-26698.

[20] Liu, H.; You, F.; Shi, W.; Hu, X.; So, Y.-M.; Shi, X. Rare-earth-metal catalyzed highly regio- and stereoselective polymerization of terpene-derived conjugated dienes. *Polym. Chem.*, **2023**, *14* (38), 4474–4480.

[21] Wu, J. Y.; Moreau, B.; Ritter, T. Iron-catalyzed 1,4-hydroboration of 1,3-dienes. *J. Am. Chem. Soc.*, **2009**, *131* (36), 12915–12917.

[22] Salzer, A.; Schmalle, H.; Stauber, R.; Streiff, S. Optically active transition-metal complexes. *Journal of Organometallic Chemistry*, **1991**, *408* (3), 403–424.

[23] Kitchen, L. J. Nopadiene. *J. Am. Chem. Soc.*, **1951**, *73* (5), 2368–2369.

[24] Uchida, S.; Togii, K.; Miyai, S.; Goseki, R.; Ishizone, T. Allylidene Monomers: Anionically Polymerizable 1,1-Disubstituted 1,3-Diene Derivatives. *Macromolecules*, **2020**, *53* (22), 10107–10116.

[25] Barent, R. D.; Wagner, M.; Frey, H. Geometric requirements for living anionic polymerization: polymerization of rotationally constrained 1,3-dienes. *Polym. Chem.*, **2022**, *13* (38), 5478–5485.

[26] Hahn, C.; Rauschenbach, M.; Frey, H. Merging Styrene and Diene Structures to a Cyclic Diene: Anionic Polymerization of 1-Vinylcyclohexene (VCH). *Angew. Chem. Int. Ed.*, **2023**, *62* (28), e202302907.

[27] Steube, M.; Johann, T.; Hübner, H.; Koch, M.; Dinh, T.; Gallei, M.; Floudas, G.; Frey, H.; Müller, A. H. E. Tetrahydrofuran: More than a "Randomizer" in the Living Anionic Copolymerization of Styrene and Isoprene: Kinetics, Microstructures, Morphologies, and Mechanical Properties. *Macromolecules*, **2020**, *53* (13), 5512–5527.

[28] Willis, C. L.; Goodwin, D. E.; Haddix, G. W.; Tutunjian, P. N.; Cocchiara, J. P.; Atwood, H. E.; Stevens, C. A. Anionic Polymerization Diinitiator and Process for Preparing Same. US20070876596 20071022.

[29] Obermeier, B.; Wurm, F.; Frey, H. Amino Functional Poly(ethylene glycol) Copolymers via Protected Amino Glycidol. *Macromolecules*, **2010**, *43* (5), 2244–2251.

[30] Natalello, A.; Werre, M.; Alkan, A.; Frey, H. Monomer Sequence Distribution Monitoring in Living Carbanionic Copolymerization by Real-Time 1 H NMR Spectroscopy. *Macromolecules*, **2013**, *46* (21), 8467–8471.

[31] Quinebèche, S.; Navarro, C.; Gnanou, Y.; Fontanille, M. In situ mid-IR and UV–visible spectroscopies applied to the determination of kinetic parameters in the anionic copolymerization of styrene and isoprene. *Polymer*, **2009**, *50* (6), 1351–1357.

[32] Miller, C. E.; Eichinger, B. E.; Gurley, T. W.; Hermiller, J. G. Determination of microstructure and composition in butadiene and styrene-butadiene polymers by near-infrared spectroscopy. *Anal. Chem.*, **1990**, *62* (17), 1778–1785.

[33] Blankenburg, J.; Kersten, E.; Maciol, K.; Wagner, M.; Zarbakhsh, S.; Frey, H. The poly(propylene oxide- co -ethylene oxide) gradient is controlled by the polymerization method: determination of reactivity ratios by direct comparison of different copolymerization models. *Polym. Chem.*, **2019**, *10* (22), 2863–2871.

[34] Steube, M.; Johann, T.; Barent, R. D.; Müller, A. H.; Frey, H. Rational design of tapered multiblock copolymers for thermoplastic elastomers. *Progress in Polymer Science*, **2022**, *124*, 101488.

[35] Ying, W. B.; Ko, N. Y.; Yao, C. K.; Kwak, N. H.; Zhang, R.; Lee, K. J.; Lee, B. A Convenient Dual-Side Anionic Initiator Based on 2,6-Luditine/s-Butyl Lithium. *Macromol. Res.*, **2019**, *27* (6), 601–605.

[36] Schultz, A. R.; Bobade, S.; Scott, P. J.; Long, T. E. Hydrocarbon-Soluble Piperazine-Containing Dilithium Anionic Initiator for High Cis -1,4 Isoprene Polymerization. *Macromol. Chem. Phys.*, **2018**, *219* (1), 1700201.

[37] Meier-Merziger, M.; Fickenscher, M.; Hartmann, F.; Kuttich, B.; Kraus, T.; Gallei, M.; Frey, H. Synthesis of phase-separated super-H-shaped triblock architectures: poly(l-lactide) grafted from telechelic polyisoprene. *Polym. Chem.*, **2023**, *14* (23), 2820–2828.

[38] Yu, Y.; Dubois, P.; Teyssié, P.; Jérôme, R. Difunctional Initiator Based on 1,3-Diisopropenylbenzene. 6. Synthesis of Methyl Methacrylate−Butadiene−Methyl Methacrylate Triblock Copolymers. *Macromolecules*, **1997**, *30* (15), 4254–4261.

[39] Quirk, R. P.; Ma, J.-J. Dilithium initiators based on 1,3-bis(1- phenylethenyl)benzene. Tetrahydrofuran and lithium sec-butoxide effects. *Polym. Int.*, **1991**, *24* (4), 197–206.

[40] Stanetty, P.; Mihovilovic, M. D. Half-Lives of Organolithium Reagents in Common Ethereal Solvents. *J. Org. Chem.*, **1997**, *62* (5), 1514–1515.

[41] van Leeuwen, B. N. M.; van der Wulp, A. M.; Duijnstee, I.; van Maris, A. J. A.; Straathof, A. J. J. Fermentative production of isobutene. *Applied microbiology and biotechnology*, **2012**, *93* (4), 1377–1387.

[42] Meier-Merziger, M.; Imschweiler, J.; Hartmann, F.; Niebuur, B.-J.; Kraus, T.; Gallei, M.; Frey, H. Bifunctional Carbanionic Synthesis of Fully Bio-Based Triblock Structures Derived from β-Farnesene and ll-Dilactide: Thermoplastic Elastomers. *Angew. Chem. Int. Ed.*, **2023**, *62* (42), e202310519.

[43] Novoa-Carballal, R.; Nosov, S.; Pfaff, S.; Schmalz, H.; Müller, A. H. E. Hyperbranched and Hyperstar Polybutadienes via Anionic Self-Condensing Vinyl Copolymerization. *Macromolecules*, **2021**, *54* (12), 5774–5783.

[44] Iovu, M. C.; Buzdugan, E.; Teodorescu, M.; Britchi, A. G.; Hubca, G.; Iovu, H. Copolymerization of styrene with butadiene using methyl tert -butyl ether as active center modifier. *Angew. Makromol. Chemie*, **1999**, *271* (1), 18–23.

[45] Jaacks, V. A Novel Method of Determination of Reactivity Ratios in Binary and Ternary Copolymerizations. *Makromol. Chem.*, **1972**, *161* (1), 161–172.

[46] Fuchs, D. A. H.; Hübner, H.; Kraus, T.; Niebuur, B.-J.; Gallei, M.; Frey, H.; Müller, A. H. E. The effect of THF and the chelating modifier DTHFP on the copolymerisation of β-myrcene and styrene: kinetics, microstructures, morphologies, and mechanical properties. *Polym. Chem.*, **2021**, *12* (32), 4632–4642.

[47] Morton, M.; Fetters, L. J. Homogeneous anionic polymerization. V. Association phenomena in organolithium polymerization. *J. Polym. Sci. A Gen. Pap.*, **1964**, *2* (7), 3311–3326.

[48] Foss, R. P.; Jacobson, H. W.; Sharkey, W. H. A New Difunctional Anionic Initiator. *Macromolecules*, **1977**, *10* (2), 287–291.

[49] Yu, Y. S.; Dubois, P.; Jérôme, R.; Teyssié, P. Difunctional Initiators Based on 1,3-Diisopropenylbenzene. 3. Synthesis of a Pure Dilithium Adduct and Its Use as Difunctional Anionic Polymerization Initiator. *Macromolecules*, **1996**, *29* (8), 2738–2745.

[50] Wahlen, C.; Blankenburg, J.; Tiedemann, P. von; Ewald, J.; Sajkiewicz, P.; Müller, A. H. E.; Floudas, G.; Frey, H. Tapered Multiblock Copolymers Based on Farnesene and Styrene: Impact of Biobased Polydiene Architectures on Material Properties. *Macromolecules*, **2020**, *53* (23), 10397–10408.

[51] Meerwall, E. D. von; Amelar, S.; Smeltzly, M. A.; Lodge, T. P. Solvent and probe diffusion in Aroclor solutions of polystyrene, polybutadiene, and polyisoprene. *Macromolecules*, **1989**, *22* (1), 295–304.

[52] Fox, T. G.; Flory, P. J. Second-Order Transition Temperatures and Related Properties of Polystyrene. I. Influence of Molecular Weight. *Journal of Applied Physics*, **1950**, *21* (6), 581–591.

[53] Steube, M.; Johann, T.; Galanos, E.; Appold, M.; Rüttiger, C.; Mezger, M.; Gallei, M.; Müller, A. H. E.; Floudas, G.; Frey, H. Isoprene/Styrene Tapered Multiblock Copolymers with up to Ten Blocks: Synthesis, Phase Behavior, Order, and Mechanical Properties. *Macromolecules*, **2018**, *51* (24), 10246–10258.

[54] Galanos, E.; Grune, E.; Wahlen, C.; Müller, A. H. E.; Appold, M.; Gallei, M.; Frey, H.; Floudas, G. Tapered Multiblock Copolymers Based on Isoprene and 4-Methylstyrene: Influence of the Tapered Interface on the Self-Assembly and Thermomechanical Properties. *Macromolecules*, **2019**, *52* (4), 1577–1588.

[55] Kremer, F.; Schönhals, A. *Broadband dielectric spectroscopy*; Springer, **2003**.

[56] Floudas, G. Dielectric Spectroscopy. In *Polymer science*:*A comprehensive reference,* [New ed.]; Matyjaszewski, K., Möller, M., Eds.; Elsevier Science, **2012**; pp 825–845.

[57] Livitsanou, C.; Steube, M.; Johann, T.; Frey, H.; Floudas, G. Local and Subchain Relaxation of Polyisoprene in Multiblock Copolymers with a Tapered Interface. *Macromolecules*, **2020**, *53* (8), 3042–3051.

[58] Traficante, D. D. Optimum tip angle and relaxation delay for quantitative analysis. *Concepts Magn. Reson.*, **1992**, *4* (2), 153–160.

[59] Malz, F.; Jancke, H. Validation of quantitative NMR. *Journal of pharmaceutical and biomedical analysis*, **2005**, *38* (5), 813–823.

[60] Steube, M.; Johann, T.; Plank, M.; Tjaberings, S.; Gröschel, A. H.; Gallei, M.; Frey, H.; Müller, A. H. E. Kinetics of Anionic Living Copolymerization of Isoprene and Styrene Using in Situ NIR Spectroscopy: Temperature Effects on Monomer Sequence and Morphology. *Macromolecules*, **2019**, *52* (23), 9299–9310.

Supporting Information

1. Experimental Section

1.1 Materials

Materials were used as received if not specified otherwise. Chemicals were purchased from the following suppliers: *Amyris*: *β*-farnesene (95%); *TCI*: methyltriphenylphosphonium bromide (98%), potassium *tert*-butoxide (97%), 1,3-diisopropenyl benzene (97%); *Lanxess*: trioctylaluminium; *VWR*: trichloromethane (99,4%), *n*-pentane (99%), methanol (>99.9%); *Sigma-Aldrich*: (-)myrtenal (97%), *sec*-butlylithium (1.3 mol·L^{-1}), *tert*-butyl lithium (1.7 mol·L^{-1}); *Fisher Scientific*: tetrahydrofuran (99.5%), calciumhydride (93%), cyclohexane (99.8%); *Thermo Scientific*: methyl *tert*-butylether (99.9%), aluminium oxide (alkaline, 40-300 µm, 60A); *Arlanxeo:* 2,2'-di(tetrahydrofuryl)propane; Irganox 1520; *Deutero*: trichloromethane-d_1 (99.8%), cyclohexane-d_{12} (99.8%), benzene-d_6 (99.5%), dimethyl-sulfoxide-d_6 (99.8%).

1.2 Instruments

Nuclear Magnetic Resonance Spectroscopy (NMR). All ^{1}H NMR measurements (^{1}H, ^{13}C, COSY, HSQC, DOSY, T_1-determination) were conducted on either *Bruker Avance II HD* 400 MHz *(*5 mm *BBFO-head* with z-gradient, ATM and *SampleXPress 60* autosampler), *Bruker Avance III HD* 400 MHz (5 mm N_2-cooled *BBO-cryo-head (BB/H+F)* with z-gradient, ATM and *SampleXPress 60* autosampler) or *Bruker Avance III* 500 MHz (5 mm *BBFO-Probe* with z-gradient and ATM, temperature control was done with a *VTU* (variable temperature unit) with an accuracy of ± 0.1 K) instruments. All spectra are referenced to the internal residual proton signal of the deuterated solvent used. Evaluation was performed using *MestReNova* by *Mestrelab Research S.L.*, Spain.

Size-Exclusion Chromatography (SEC). SEC of all samples was performed on an Agilent *1260 Infinity II* setup using a *MZ-Gel SDPlus e5/e3/100* column set provided by *MZ-Analysentechnik,* Mainz, Germany. Samples were prepared as 1 mg·mL^{-1} THF solutions and normalized to an internal toluene standard. The molar masses are referenced to either 1,4-polyisoprene or polystyrene standards provided by *Polymer Standard Service*, Mainz, Germany.

Differential Scanning Calorimetry (DSC). Thermal analysis using differential scanning calorimetry (DSC) was performed on a *TA Instruments DSC 250* instrument connected to a *TA Instruments RCS 90* cooling system, both obtained from *Waters Corporation*, United States.

Samples were measured with a heating rate of 10 K·min^{-1} and the second heating curve was used for the determination using the software *TRIOS*. Further, additional measurements were investigated through a QA 2000 (TA Instruments) system. The instrument was calibrated for the baseline using a sapphire standard, for the enthalpy and temperature using indium as a standard, and for the heat capacity using sapphire as a standard. In each case, the under-investigation sample was heated-up to 473 K, in order to delete its history and after that cooling/heating cycles were performed at the rates of 10 K·min^{-1} and 20 K·min^{-1} in a temperature range between 173 K and 473 K.

Temperature-Modulated Differential Scanning Calorimetry (TM DSC). Temperature-modulated differential scanning calorimetry (TM-DSC) measurements were made for the two-sided tapered copolymers PNopa-*grad*-PFar-*grad*-PNopa with the same *Q2000* (*TA Instruments*) using cooling/heating rates in the range of 10 to 1 K·min^{-1} and oscillation periods from 20 to 60 s. A specific rate/period pair was employed for each measurement according to **Eq. S1**:

$$\beta = \frac{\Delta T_g}{c \cdot P} \cdot 60 \text{ s} \cdot \text{min}^{-1} \quad \textbf{(S1)}$$

Here, β is the cooling/heating rate, ΔT_g is the range of T_g, c is the number of cycles across the T_g width, and P is the oscillation period. The rate/period pairs used were as follows: 20 s, 10 K·min^{-1}; 40 s, 5 K·min^{-1}; 60 s, 2 K·min^{-1}. TM-DSC measurements were made within the temperature range from 173 K to 473 K.

Dielectric Spectroscopy (DS). Dielectric spectroscopy measurements as a function of temperature (*i.e.* under "isobaric" conditions) were performed with the *Novocontrol Alpha* high-resolution frequency analyzer, within the frequency range from 10^{-2} Hz to 10^{7} Hz, and for temperatures in the range from 173.15 K to 423.15 K. Samples were prepared as melts under vacuum by pressing the electrodes to the spacer thickness. The DS measuring cell consisted of two platinum electrodes (of 20 mm diameter) forming a capacitor. A Teflon spacer was inserted in the sample to keep the distance of the electrodes fixed (about 50 μm). By applying an alternating electric field to the capacitor, the complex dielectric function (ε^*) is obtained as a function frequency (ω) and temperature (T). The latter is defined as $\varepsilon^* = \varepsilon' - i\varepsilon''$, where the real part (the dielectric permittivity) refers to the energy which is reversibly stored in the dielectric, and the imaginary part to the dielectric losses. The analysis of the DS resulted curves was based on the empirical equation of Havriliak and Negami (**Eq. S2**)

$$\varepsilon^*_{HN}(\omega, T, P) = \varepsilon_\infty(T, P) - \frac{\Delta\varepsilon(T,P)}{[1+(i\omega\tau_{HN}(T,P))^m]^n} + \frac{\sigma_0(T,P)}{i\varepsilon_0\omega} \quad \textbf{(S2)}$$

where $\varepsilon_\infty(T,P)$ is the high frequency permittivity, $\varepsilon_0(T,P)$ is the permittivity of free space, $\tau_{HN}(T,P)$ refers to the characteristic relaxation time of this model, $\Delta\varepsilon(T,P) = \varepsilon_0(T,P) - \varepsilon_\infty(T,P)$ is the relaxation strength of the process under investigation, $\sigma_0(T,P)$ is the DC conductivity, *m* and *n* describe, respectively, the symmetrical and asymmetrical broadening of the relaxation times distribution, and finally ω (= $2\pi f = 1/\tau$) is the angular frequency of the external electric field. From the τ_{HN} the relaxation times at maximum loss, $\tau_{\max}$, were obtained analytically from the HN equation, **Eq. S3**, as follows:

$$\tau_{\max} = \tau_{HN} \sin^{-1/m}\left(\frac{\pi m}{2(1+n)}\right) \sin^{-1/m}\left(\frac{\pi n m}{2(1+n)}\right) \quad \textbf{(S3)}$$

In the temperature range where two, or more, relaxation processes contribute to ε^*, a summation of HN functions was used, assuming statistical independence in the frequency domain.

Density Pycnometer. Density measurements were performed on a *Micro Ultrapyc 1200e* helium pycnometer of *Quantachrome*, Austria.

Small-Angle X-ray Scattering. Small-angle (SAXS) measurements were made with the *N8 Horizon* vertical setup (*Bruker*), using a 50W CuKα radiation (IμS micro-focus source with integrated MONTEL optics). The diffraction patterns were recorded on the *VÅNTEC-500 2D* detector (*Bruker*) at a sample-detector distance of 660 mm. Intensity distributions as a function of the modulus of the total scattering vector, $q = (4\pi/\lambda)\sin(2\theta/2)$, where 2θ is the scattering angle and λ=0.154 nm is the wavelength, were obtained by radial averaging of the 2D datasets. The samples P(N_{20}-F_{60}-N_{20})-100k, P(N_{25}-F_{50}-N_{25})-50k, P(N_{25}-F_{50}-N_{25})-200k and P(N_{25}-F_{50}-N_{25})-100k were prepared in the form of fiber, while the samples P(N_{30}-F_{40}-N_{30})-100k, P(N_{35}-F_{30}-N_{35})-100k, and P(N_{40}-F_{20}-N_{40})-100k were prepared in the form of thick films (~1 mm). Temperature-dependent measurements of 1 hour long were made by slowly heating the films from 303 K to 423 K in 10 K steps – with 1 hour equilibration time at each temperature - and subsequent cooling.

Rheology. A *TA Instruments AR-G2* with a magnetic bearing that allows for nanotorque control was used for recording the viscoelastic properties of the copolymers. Measurements were made with the environmental test chamber (ETC) as a function of temperature. The samples were prepared on the lower rheometer plate (8 mm), the upper plate was brought into contact, and the sample thickness was adjusted accordingly. The linear and non-linear of viscoelastic regions were determined *via* strain amplitude dependence of the complex shear modulus $|G^*|$ at ω = 10 rad·s^{-1} at each temperature. Subsequently, isothermal frequency sweeps within the angular frequency range of $0.1 < \omega < 100$ rad·s^{-1} were made for different temperatures. Before each isothermal measurement, a thermal stabilization of 30 min was employed to ensure

thermal equilibrium. Master curves were constructed by using the time-temperature superposition principle (tTs). The extracted shift factors, α_T, were fitted according to WLF equation, **Eq. S4**, as

$$log\alpha_T = -\frac{C_1(T-T_r)}{C_2+(T-T_r)} \quad \textbf{(S4)}$$

where C_1, C_2 are empirical parameters at the reference temperature (T_r). The WLF coefficients at T_g were calculated as $c_1^g = c_1^r c_2^r/(c_2^r+T_g-T_r)$ and $c_2^g = c_2^r + T_g-T_r$.

Mechanical Analysis. Tensile tests were performed on an *EZ Test EZ-LX* instrument by *Shimadzu*, Japan. Polymer films were prepared by solvent casting from chloroform and the respective (60x10 mm STEG 4.5) "dog-bones" were cut out. For all measurements a pre-load force of 0.1 N was applied. Then the samples were measured using speed of 20 mm·min^{-1} using a 50 N capacity *SM-50N-168* force transducer. Results were recorded using *TRAPEZIUMX* by *Shimadzu*, Japan.

Thermal Gravimetric Analysis. To investigate the thermal stability of the samples, thermal gravimetric analysis (TGA) was performed on a *Mettler Toledo TGA 2 Star* instrument in alumina (aluminum oxide) 300 µL crucible and N_2 atmosphere. The samples were annealed at 30 °C for 10 minutes followed by heating to 800 °C using a heat rate of 10 K min^{-1}. The temperature at a weight loss of 5%, $T_{5\%}$, is determined for each sample.

1.3 Monomer Synthesis

Nopadiene was synthesized from (-)myrtenal as described elsewhere in more detail.[1] After work-up by distillation at 100 °C at 85 mbar the product was further purified by passing through alkaline alumina to yield 82% of colorless liquid. Nopadiene was characterized using ^{1}H and ^{13}C NMR as well as 2D NMR experiments, see **Figures S14-S16**. ^{1}H NMR (400 MHz, $CDCl_3$, δ[ppm]): 6.41 – 6.34 (m, 1H, b), 5.58 – 5.55 (m, 1H, d), 5.09 – 4.88 (m, 2H, a), 2.60 – 2.57 (m, 1H, h), 2.47 – 2.42 (m, 1H, j), 2.39 – 2.29 (m, 2H, e), 1.35 (s, 3H, i), 1.17 – 1.15 (d, 1H, j), 0.81 (s, 3H, i); ^{13}C NMR (100 MHz, $CDCl_3$, δ[ppm]): 146.91 (C), 137.95 (B), 124.57 (D), 109.70 (A), 41.17 (F), 40.44 (H), 37.83 (G), 32.01 (E), 31.38 (J), 26.50 (I), 20.88 (I).

2. *In Situ* NMR kinetics results

All NMR results were monitored using the parameters noted in greater detail in the experimental section of the manuscript. To yield a reliable and quantitative ^{1}H NMR signal the longitudinal relaxation times, T_1, of the respective protons of interest need to be determined. The results are given in **Figure S1**. With longer T_1-relaxation time less data points can be recorded for the respective fit, as the delay between each data point is restricted by the T_1-relaxation time of the protons tracked. The T_1-time of the monitored protons range from 10.0 s to 11.8 s at 298 K. Consequently, the reactivity ratios exhibit a greater error, reflected by the decrease of the R-squared (R^2) value, see **Table 1**. The choice of settings is of great importance to get quantitative NMR kinetic results and a detailed compilation can be found in the experimental section.

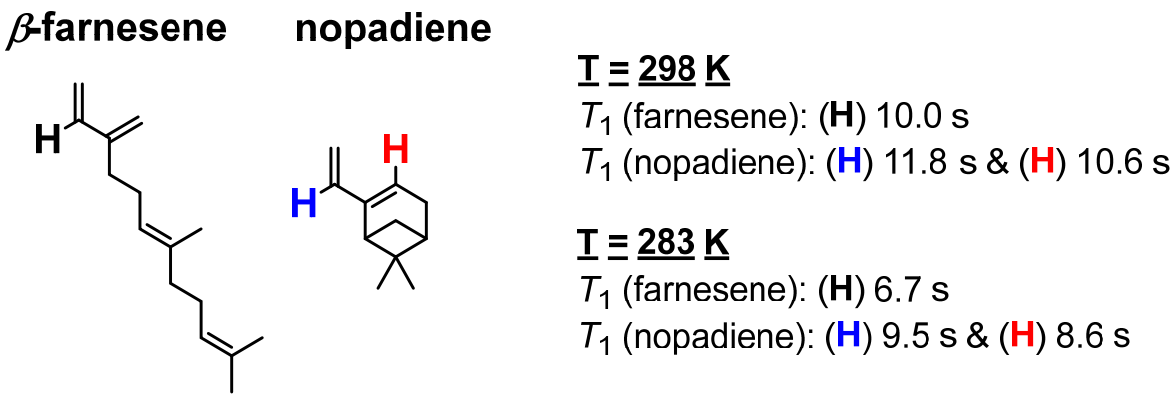

Figure S1. Results of T_1-time determination of the protons of interest of the copolymerization of Far and Nopa in MTBE and 2 eq DTHFP at 298 K and 283 K.

The individual monomer consumption can be then tracked by ^{1}H NMR as presented below.

Determination reactivity ratios

The Jaacks[2] equation, **Eq. S5**, was used to determine the reactivity ratios of Far (r_{Far}) and Nopa (r_{Nopa}) from the individual monomer consumptions as a function of time (**Eq. S5**):

$$\ln\frac{[M_1]_0}{[M_1]_t} = r_1 \ln\frac{[M_2]_0}{[M_2]_t}; \qquad r_2 = 1/r_1 \tag{S5}$$

An overview of reactivity ratios determined for each solvent is given in **Table S1**. The respective kinetic and *Jaacks* plots are presented thereafter. **Table S1** also contains the respective volume gradients derived from the respective reactivity ratios and the volume share. A monomer molar feed of 50:50 of Far and Nopa gives a volume fraction of PFar Φ_{PFar} = 60% taking the densities of PFar and PNopa (**Table 2**) into account.

Table S1. Summary of all reactivity ratios of the copolymerization of Far and Nopa under different conditions and their respective volume gradient.

Solvent	r_{Far}	r_{Nopa}	Volume-based Gradient*
Cyclohexane (*sec*-BuLi)	6.50 ± 0.04	0.155 ± 0.001	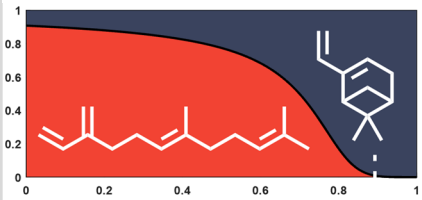
MTBE (*sec*-BuLi)	7.23 ± 0.30	0.138 ± 0.005	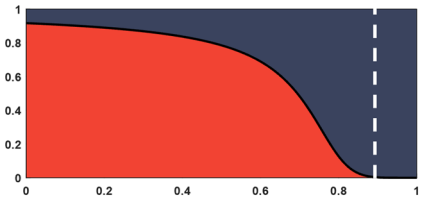
MTBE + 2 eq DTHFP (*sec*-BuLi)	11.2 ± 1.0	0.090 ± 0.008	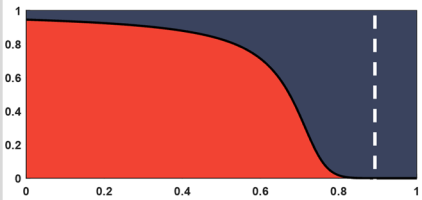
MTBE + 2 eq DTHFP (DIB-Li_2)	10.8 ± 0.9	0.093 ± 0.008	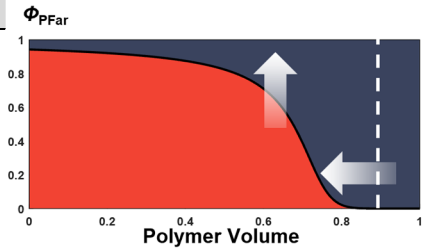

* Volume gradient derived from reactivity ratios determined by the Jaacks equation and assuming a molar ratio of 50:50 of Far and Nopa.

2.1 Copolymerization in Cyclohexane

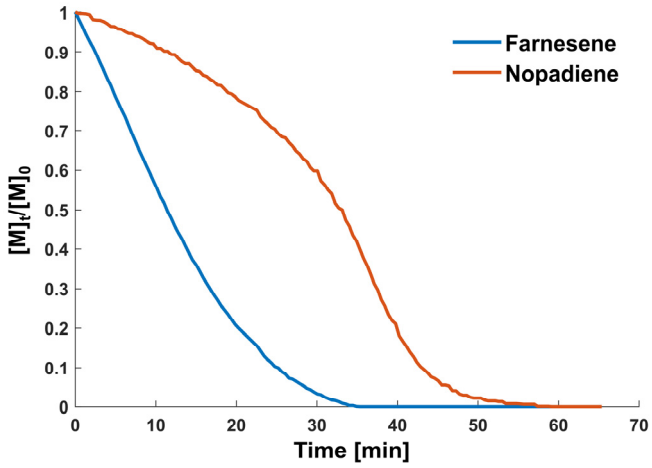

Figure S2. Time-monomer-consumption-plot of copolymerization of Far and Nopa in pure cyclohexane.

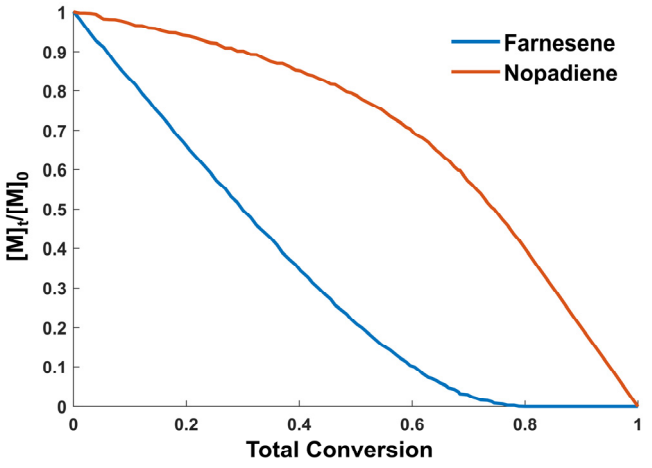

Figure S3. Total conversion-monomer consumption-plot of copolymerization of Far and Nopa in pure cyclohexane.

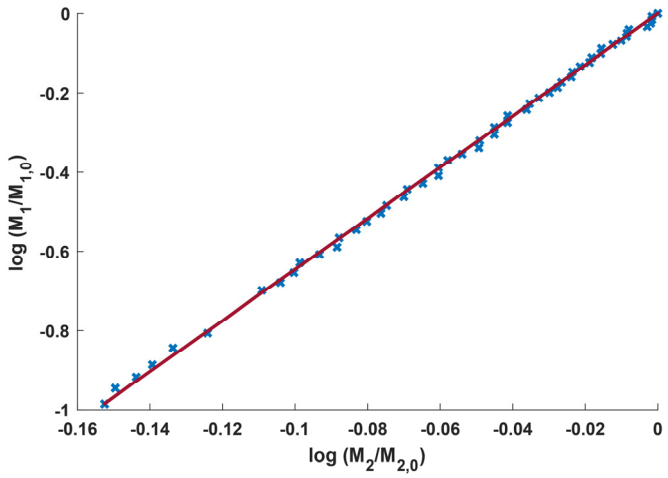

Figure S4. Jaacks plot of copolymerization of Far and Nopa in pure cyclohexane.

2.2 Copolymerization in pure MTBE

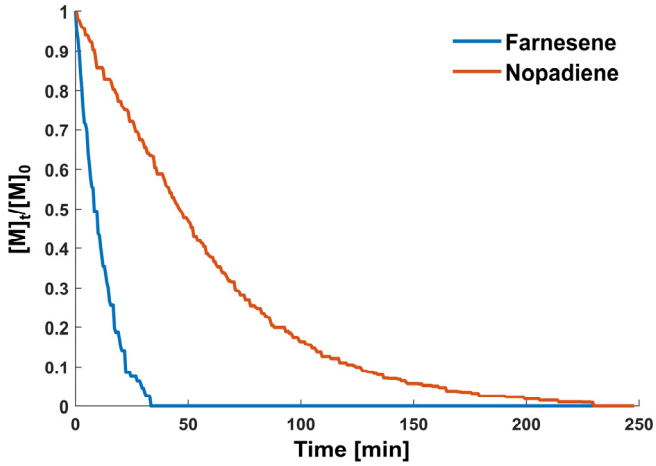

Figure S5. Time-conversion plot of copolymerization of Far and Nopa in pure MTBE.

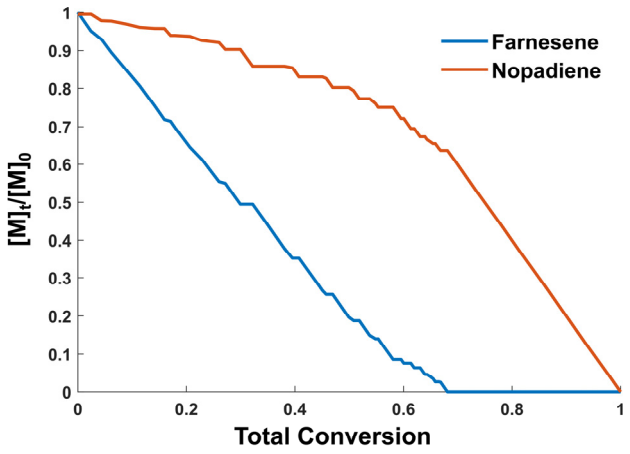

Figure S6. Plot of comonomer conversions vs total conversion in the copolymerization of Far and Nopa in pure MTBE.

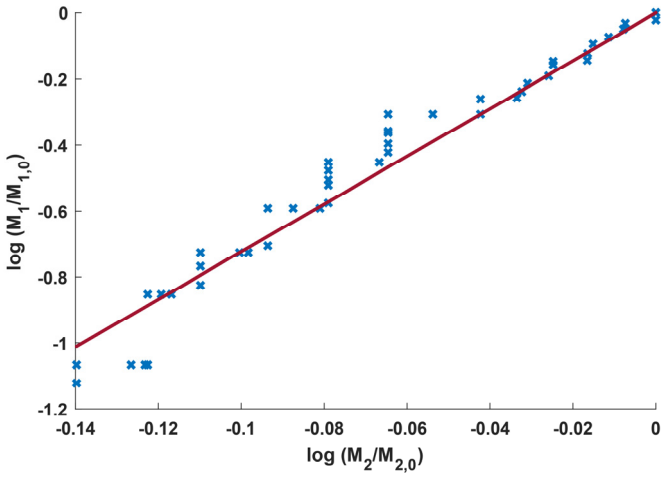

Figure S7. Jaacks plot of copolymerization of Far and Nopa in pure MTBE.

2.3 Copolymerization in MTBE and 2 eq. DTHFP

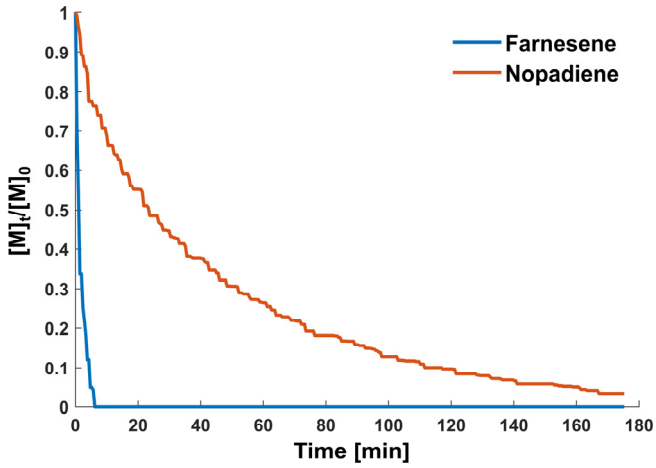

Figure S8. Time-conversion plot of copolymerization of Far and Nopa in MTBE and 2 eq. DTHFP.

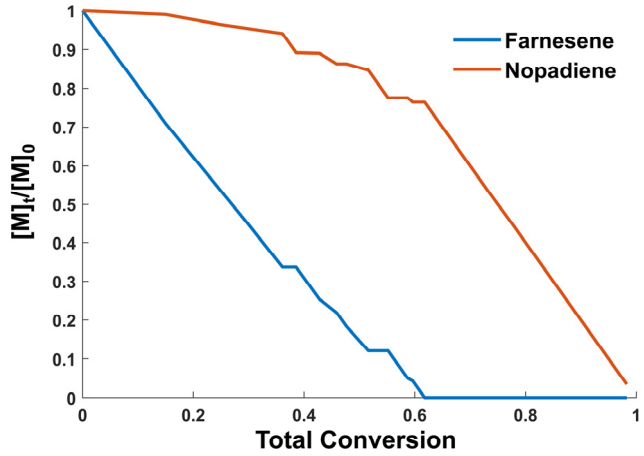

Figure S9. Plot of comonomer conversion vs. total conversion in the copolymerization of Far and Nopa in MTBE and 2 eq. DTHFP.

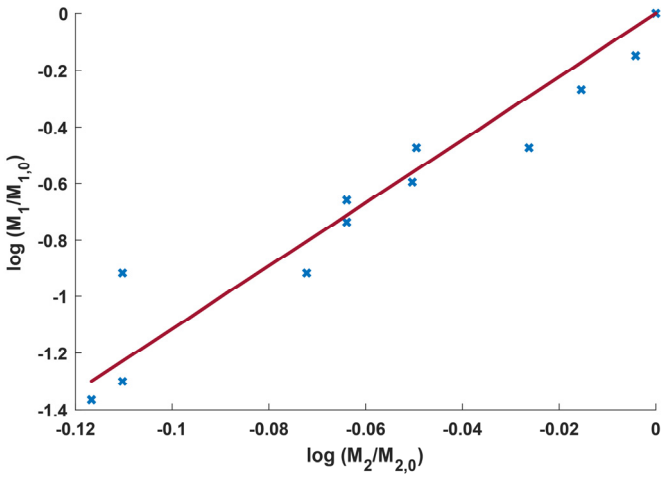

Figure S10. Jaacks plot of copolymerization of Far and Nopa in MTBE and 2 eq. DTHFP.

2.4 Copolymerization using the Bifunctional Initiator DIB-Li2

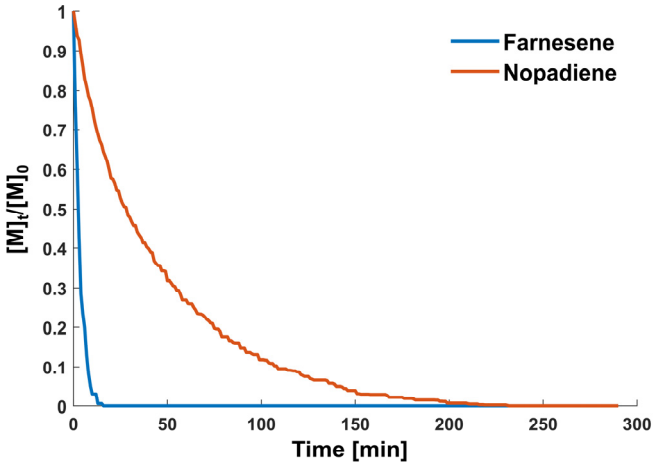

Figure S11. Time-conversion plot of copolymerization of Far and Nopa in MTBE and 2 eq. DTHFP using the bifunctional initiator DIB-Li_2.

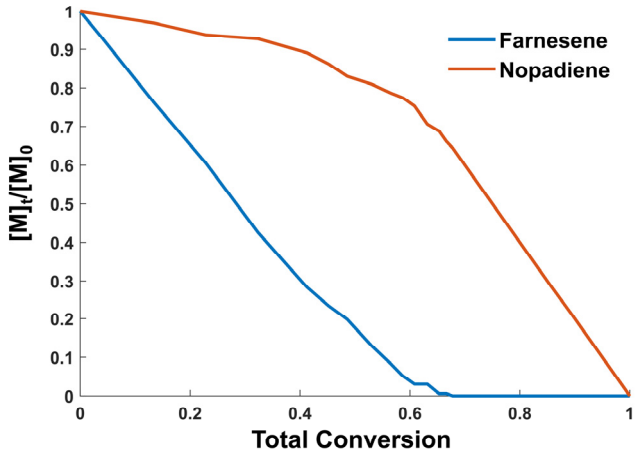

Figure S12. Plot of comonomer conversion vs. total conversion in the copolymerization of Far and Nopa in MTBE and 2 eq. DTHFP using the bifunctional initiator DIB-Li_2.

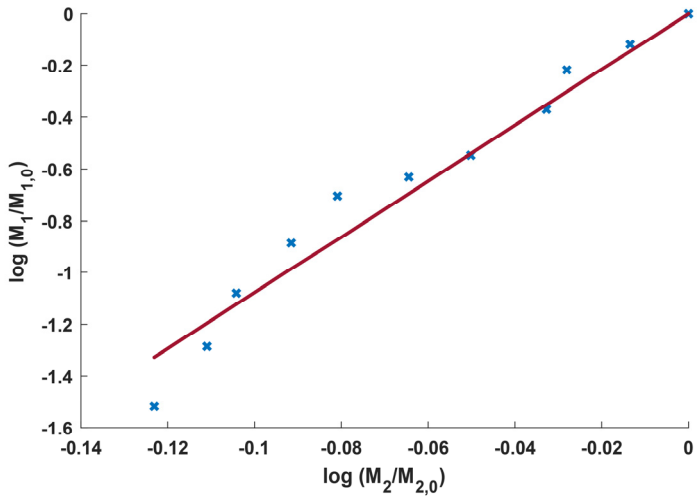

Figure S13. Jaacks plot of copolymerization of Far and Nopa in MTBE and 2 eq. DTHFP using the bifunctional initiator DIB-Li_2.

3. Additional NMR Results

All presented NMRs were baseline corrected and normalized to the respective signal of the deuterated solvent. For each copolymer, one NMR was chosen as representee of the whole series.

3.1 Nopadiene

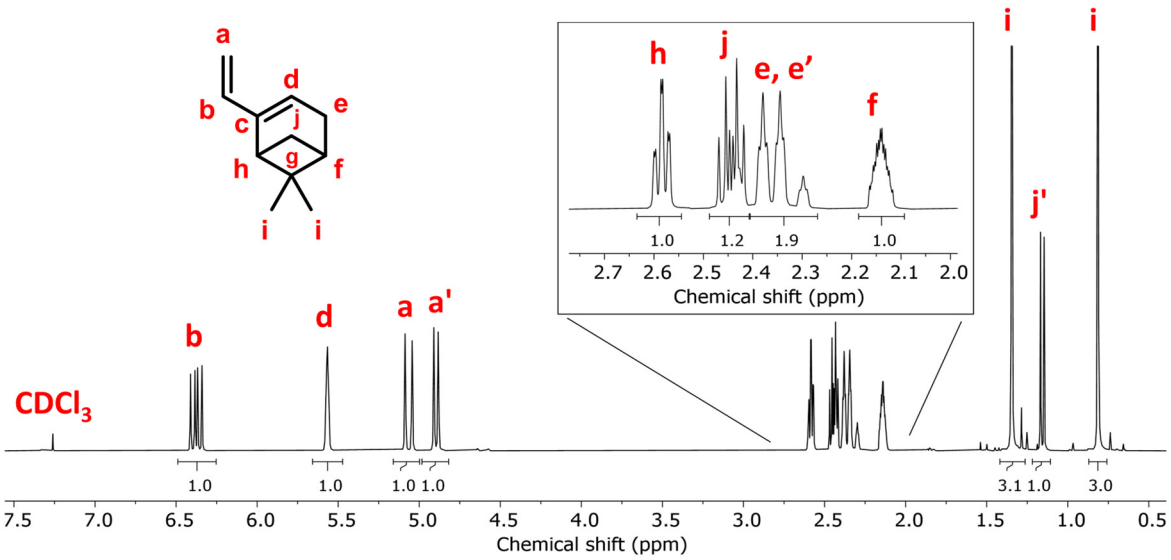

Figure S14. ^{1}H NMR of Nopa with all proton signals assigned, measured in $CDCl_3$, 400 MHz.

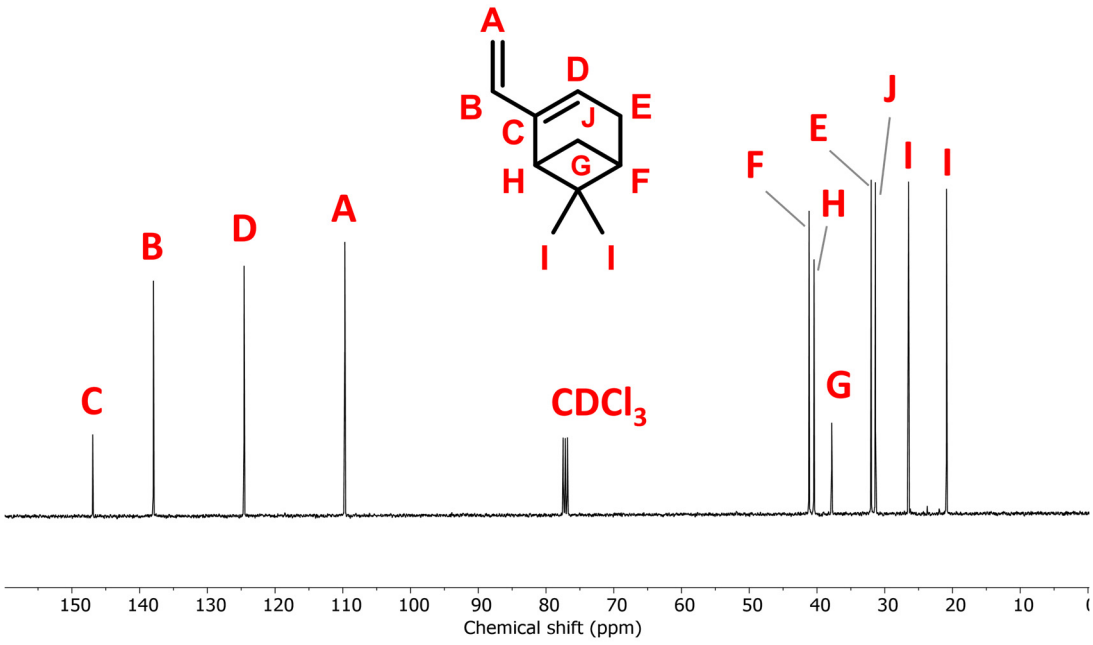

Figure S15. ^{13}C NMR of Nopa with all carbon signals assigned, measured in $CDCl_3$, 100 MHz.

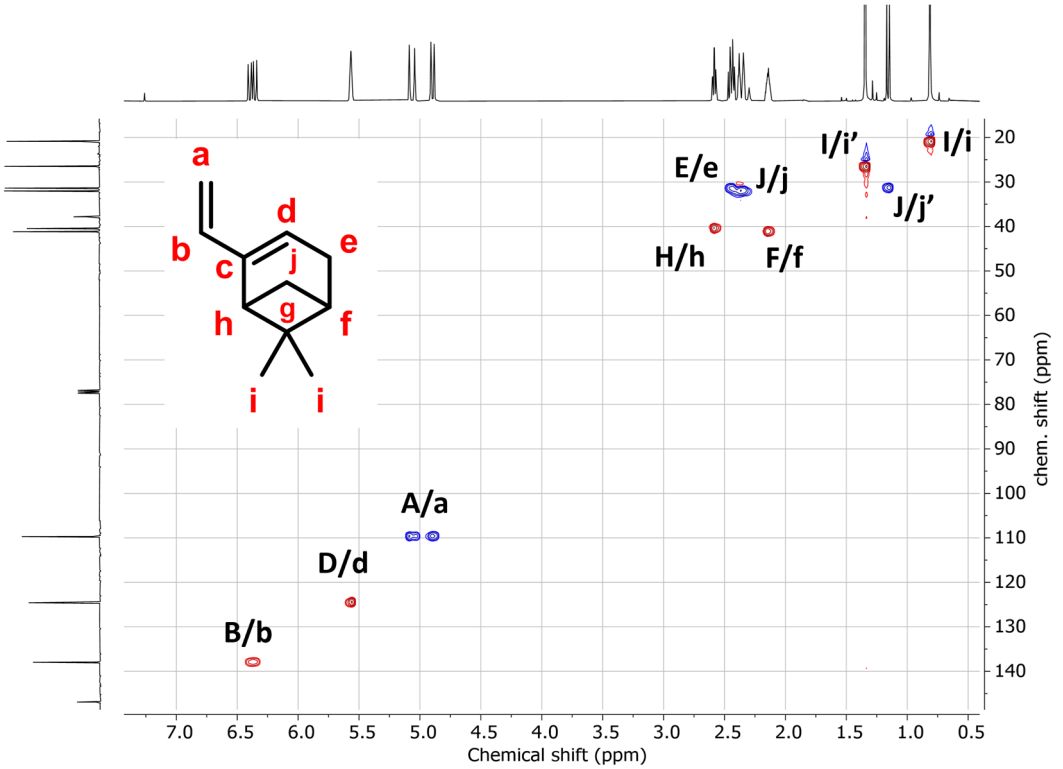

Figure S16. $^{1}H/^{13}C$-HSQC NMR of Nopa with all proton and carbon couplings assigned, measured in $CDCl_3$, 400 MHz (^{1}H) and 100 MHz (^{13}C).

3.2 Polynopadiene

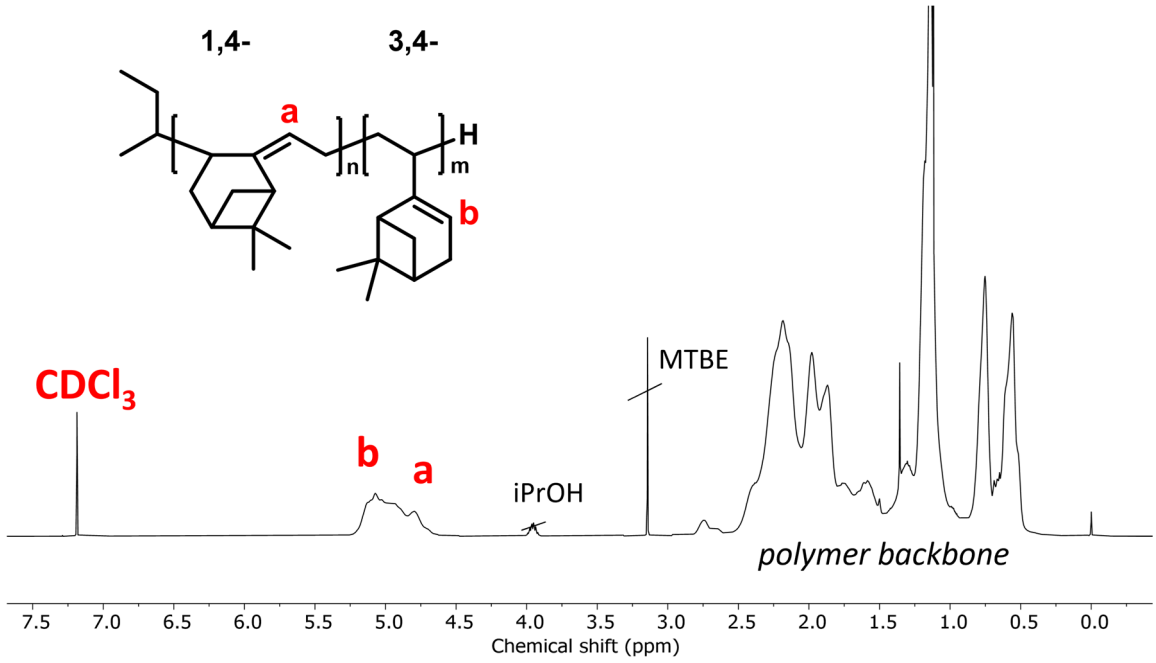

Figure S17. ^{1}H NMR of PNopa with overlapping olefinic proton signals, measured in $CDCl_3$, 400 MHz.

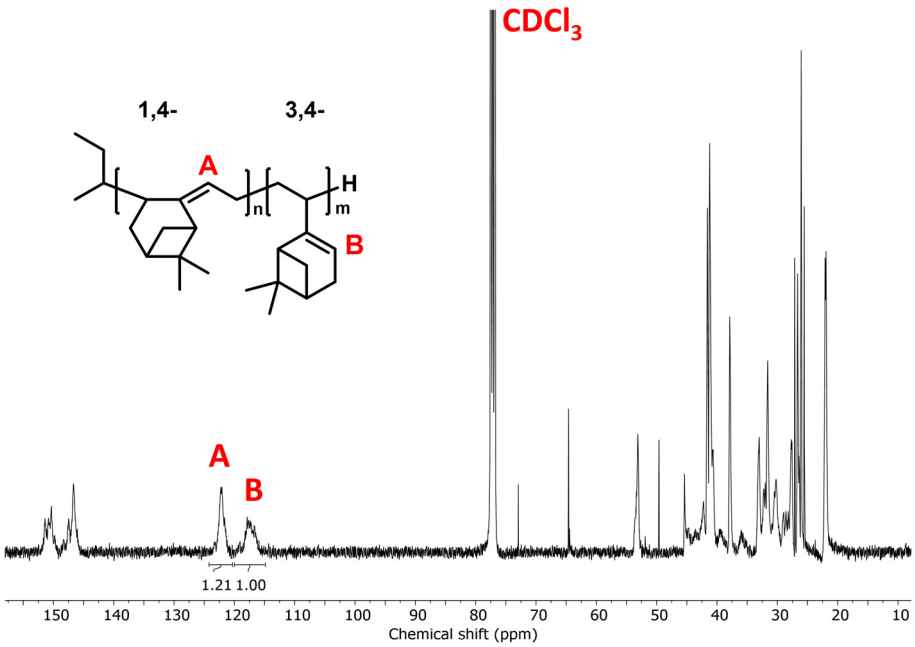

Figure S18. ^{13}C NMR of PNopa with olefinic carbon signals assigned, measured in $CDCl_3$, 100 MHz.

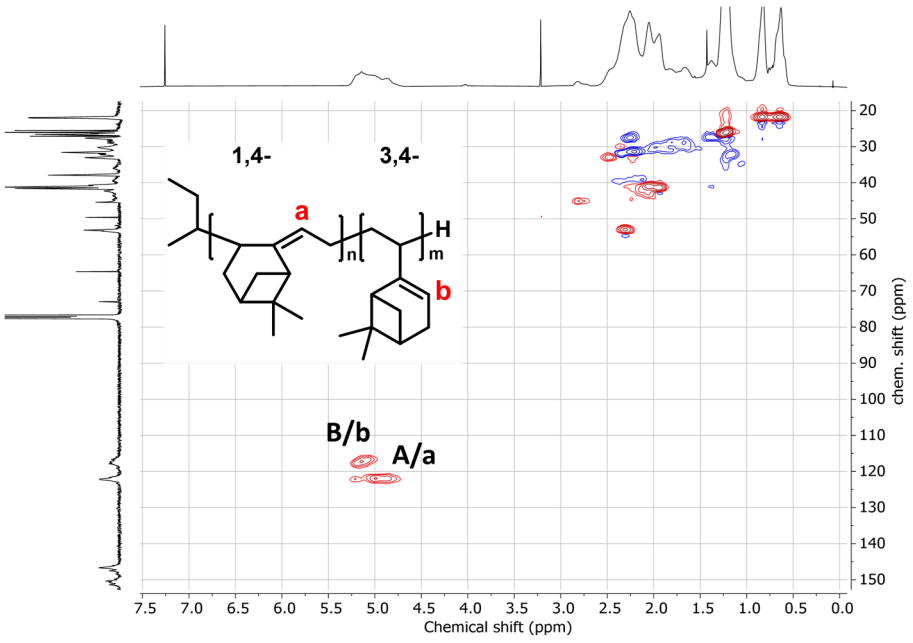

Figure S19. $^{1}H/^{13}C$-HSQC NMR of PNopa with olefinic proton and carbon couplings assigned, measured in $CDCl_3$, 400 MHz (^{1}H) and 100 MHz (^{13}C).

3.3 Polyfarnesene

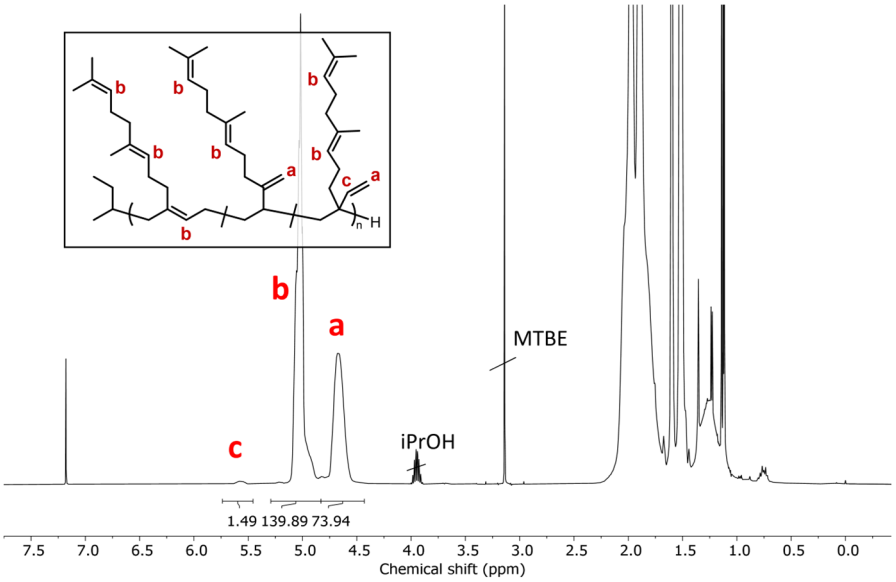

Figure S20. ^{1}H NMR of PFar with all olefinic proton signals assigned, measured in $CDCl_3$, 400 MHz.

3.4 PNopa-*grad*-PFar-*grad*-PNopa

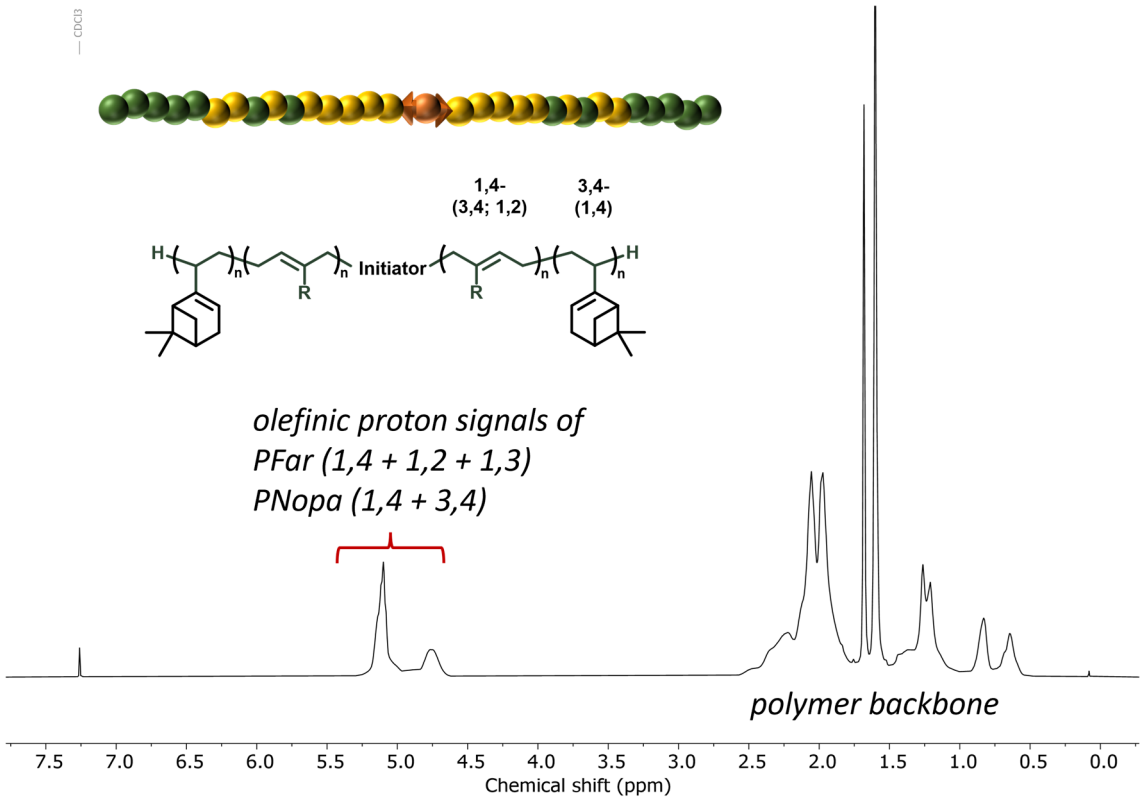

Figure S21. ^{1}H NMR of PNopa-*grad*-PFar-*grad*-PNopa triblock: $P(N_{20}\text{-}F_{60}\text{-}N_{20})$-100k, measured in $CDCl_3$, 400 MHz.

4. SEC Results

Each homopolymer is measured against its closest available calibration. Therefore, PI calibration is used for PFar and PNopa is compared to a PS calibration.

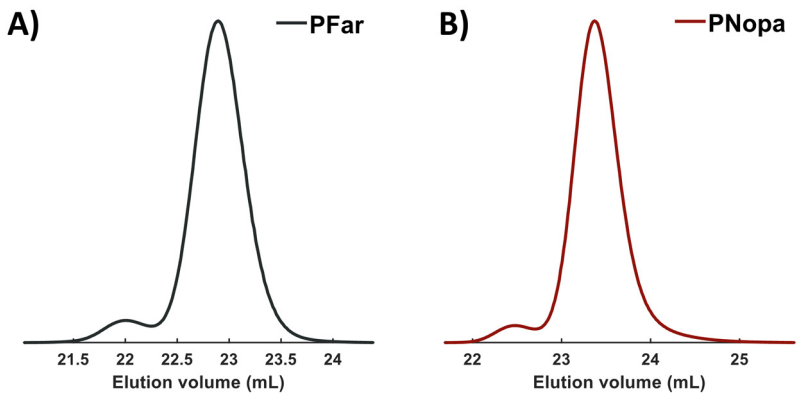

Figure S22. SEC traces of homopolymers measured in THF; A) PFar and B) PNopa. The peaks at lower elution volume are due coupling by traces of oxygen in the quenching agent.

5. DSC Results

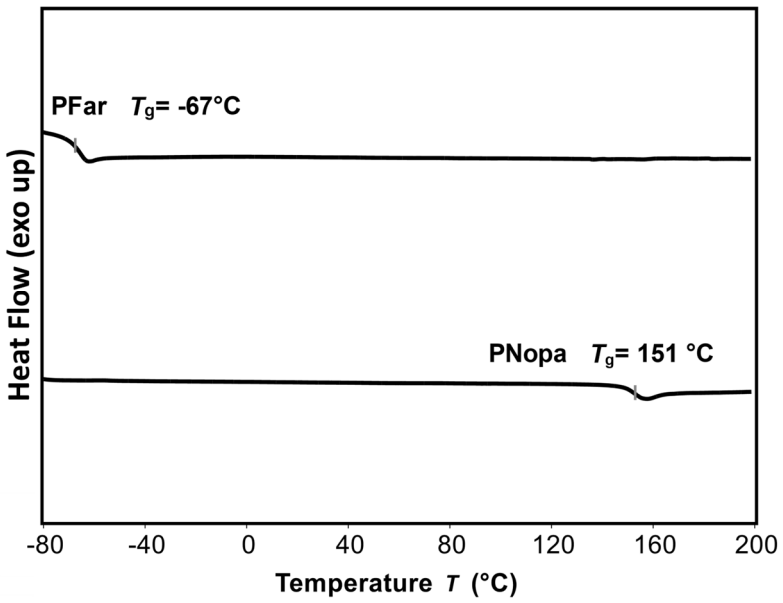

Figure S23. DSC results of homopolymer PFar and PNopa, second heat curve, measured with a heat rate of 10 K·min^{-1}.

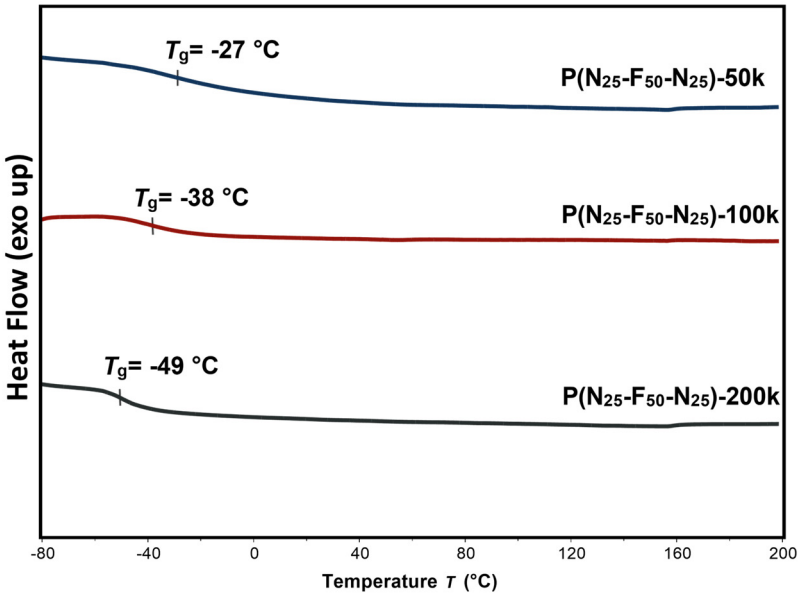

Figure S24. Compilation of DSC results of triblock series with increasing molar mass, second heat curve, measured with a heat rate of 10 K·min^{-1}.

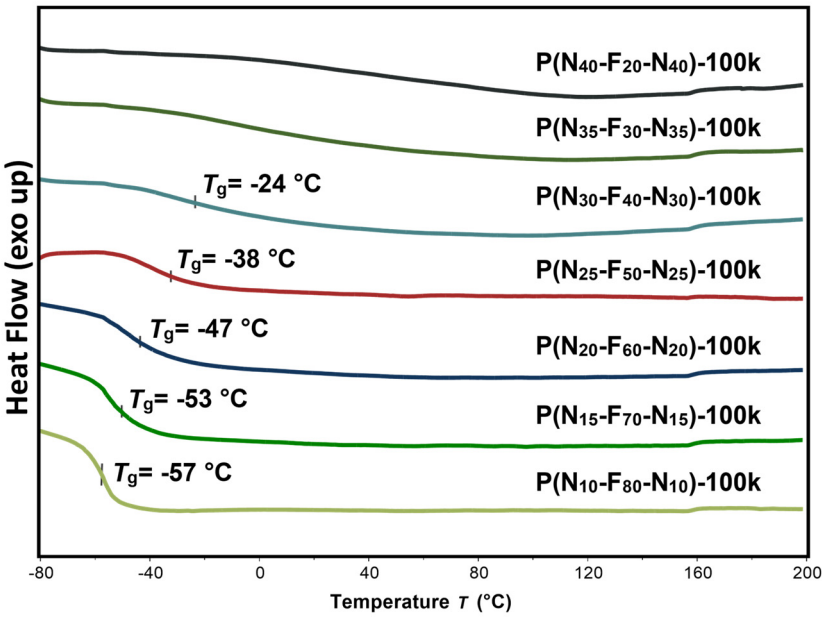

Figure S25. Compilation of DSC results of triblock series with increasing molar mass, second heat curve, measured with a heat rate of 10 K·min^{-1}.

6. Temperature-Modulated DSC

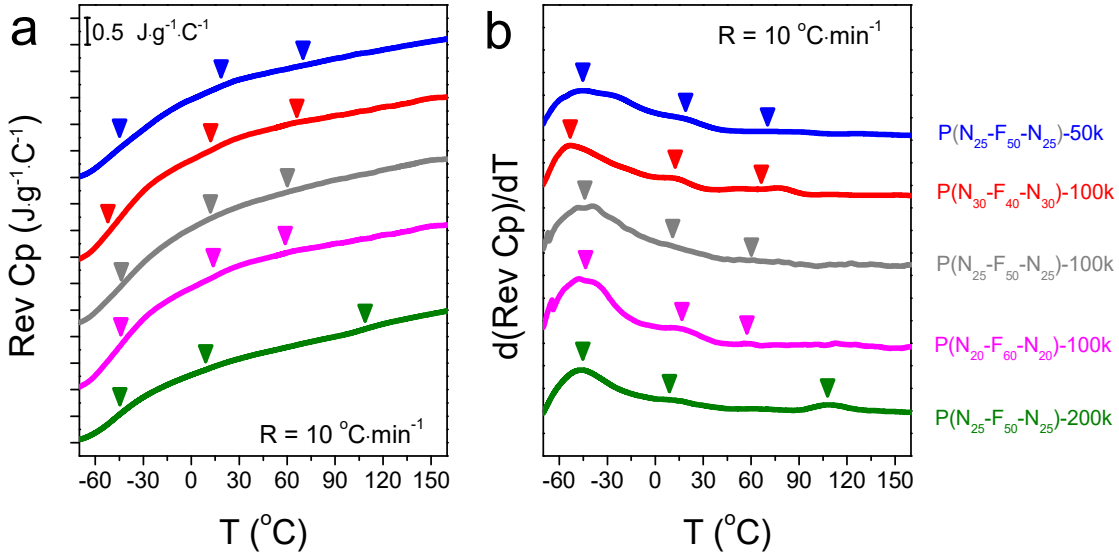

Figure S26. (a) Temperature dependence of the reversing heat capacity (Rev C_p) for the different samples: P(N_{25}-F_{50}-N_{25})-50k (blue), P(N_{30}-F_{40}-N_{30})-100k (red), P(N_{25}-F_{50}-N_{25})-100k (grey), P(N_{20}-F_{60}-N_{20})-100k (magenta) and P(N_{25}-F_{50}-N_{25})-200k (olive), obtained from TM-DSC, at a period of modulation of T=20 s. Arrows indicate characteristic "transition" temperatures. Data are shifted vertically for clarity. (b) Temperature dependence of the first derivative of the reversing heat capacity, for the same oscillation period. In all cases, at least two peaks are evident, related to the T_g of PFar and an "interphase" T_g corresponding to the gradient interface. In P(N_{25}-F_{50}-N_{25})-50k, P(N_{30}-F_{40}-N_{30})-100k and P(N_{25}-F_{50}-N_{25})-200k, a third peak is also evident, corresponding to the T_g of PNopa.

7. Rheology

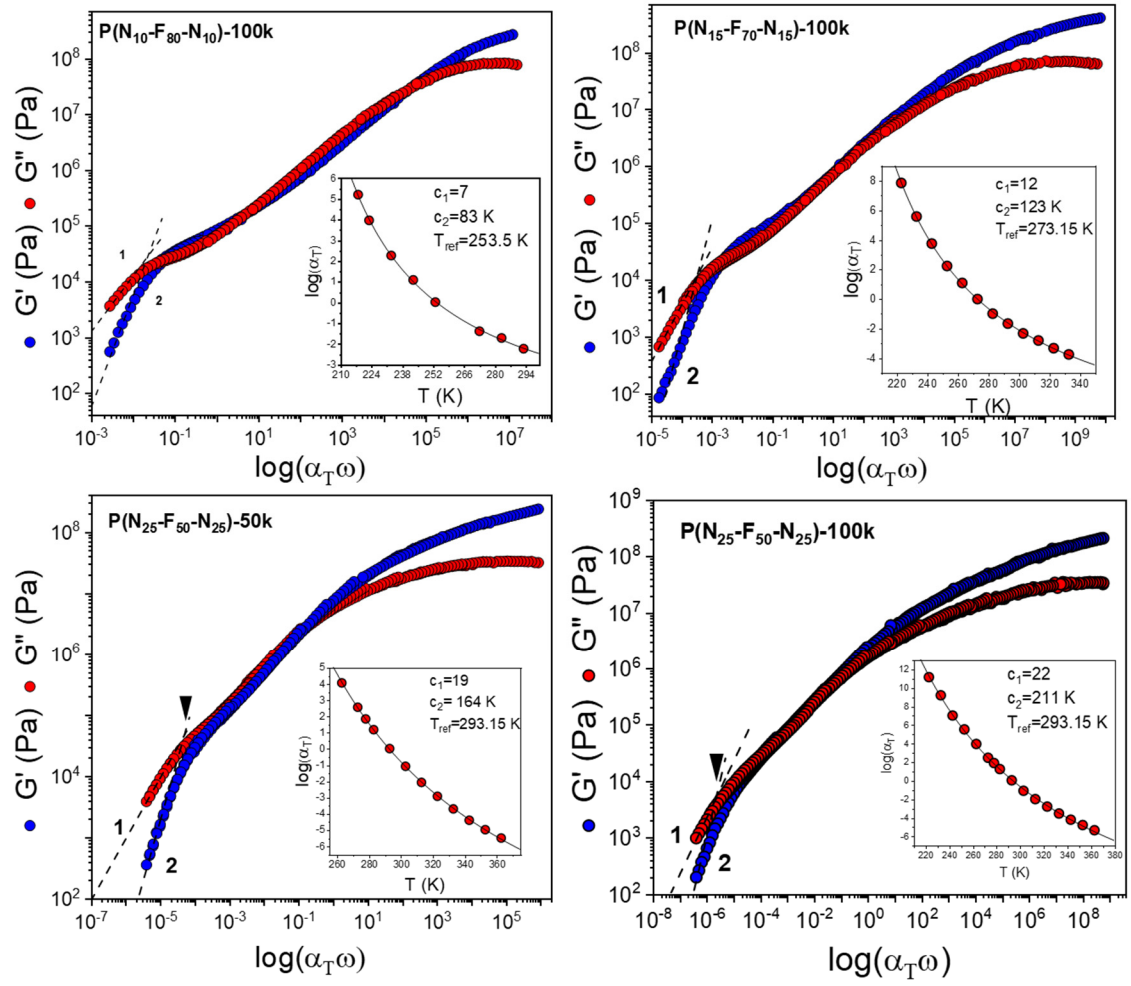

Figure S27. Master curves of the storage and loss moduli for four copolymers with increasing PNopa content and respective WLF coefficients (inert). The extreme broadening at the liquid-to-glass temperature range suggests multiple dynamic processes operating in the tapered triblock copolymers.

8. Tensile-Test Results

Each sample was measured three times and the material properties, i.e. elongation at break (ε_{max}) and Young's modulus (E), are given in **Table 4** as average values along with their standard deviation.

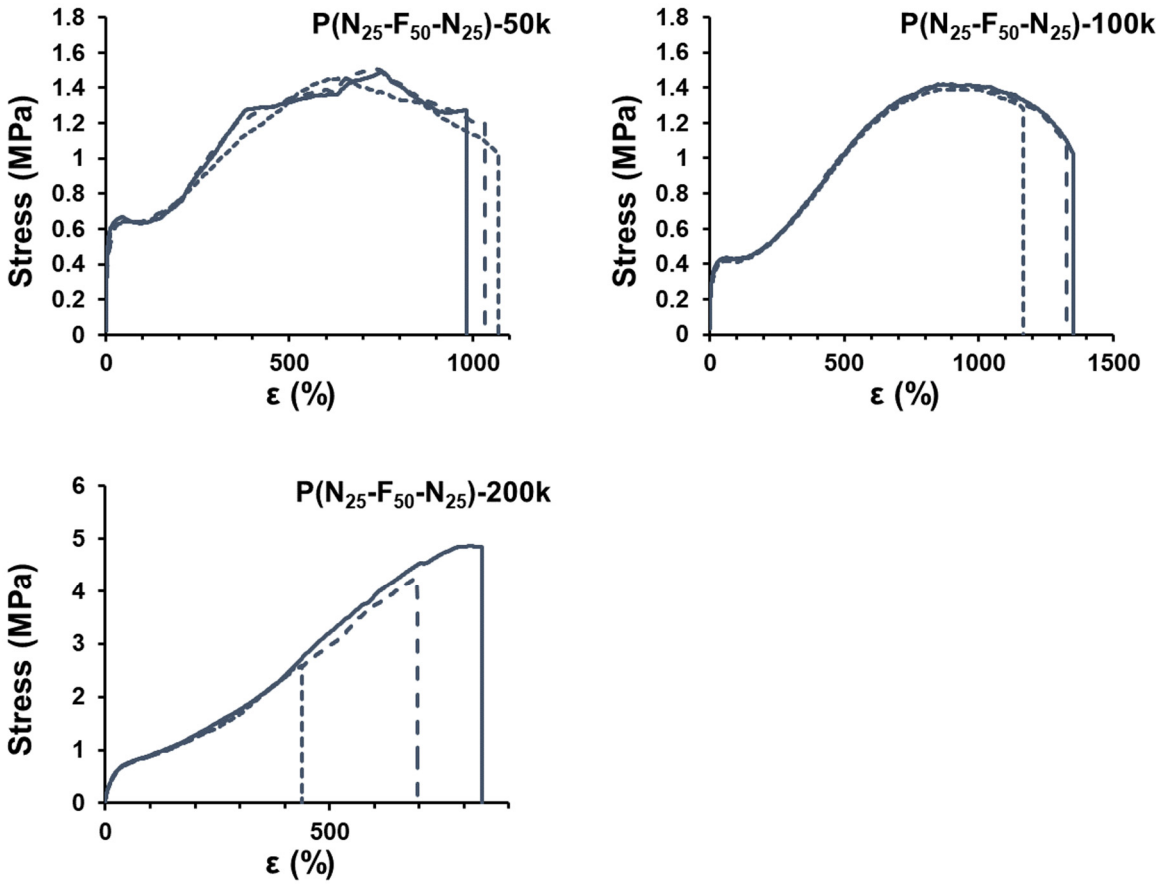

Figure S28. Stress-Strain curves of triblock series of different molar mass and constant molar composition of 25-50-25; each sample measured three times.

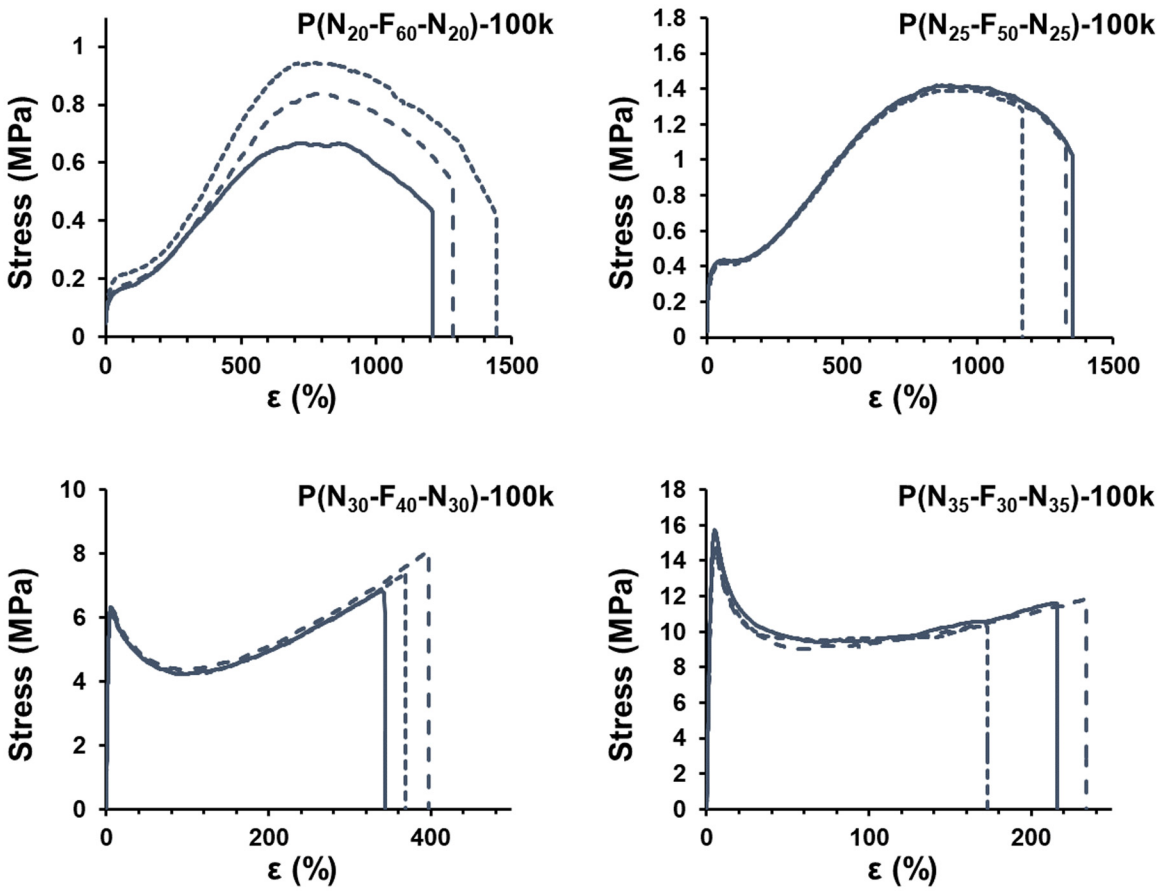

Figure S29. Stress-Strain curves of 100 k triblocks series of different molar compositions; each sample measured three times.

9. Elastic Recovery

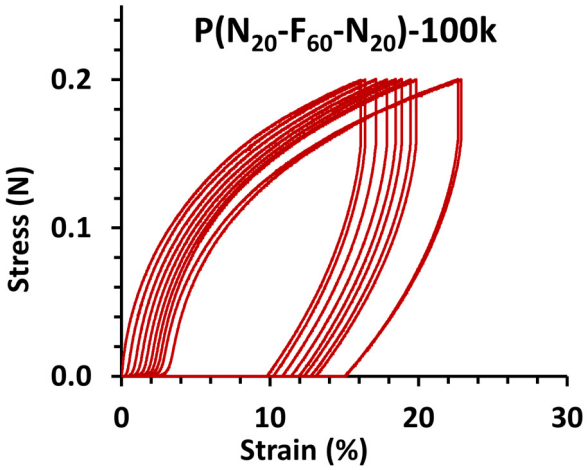

Figure S30. Elastic recovery experiment of sample P(N_{20}-F_{60}-N_{20})-100k using a stress of 0.2 N over ten cycles of hysteresis and a delay of ten minutes.

The elastic recovery (R_n) was determined using **Equation S6**. The value strain_{max}^{n} corresponds to the maximum strain that was observed for each cycle *n* and $\text{strain}_{max}^{n+1}$ the maximum strain for the next cycle n*+1*.

$$R_n = \left(\frac{\text{strain}_{max}^{n}}{\text{strain}_{max}^{n+1}}\right) \cdot 100\% \quad (6)$$

10. Reprocessing as main advantage of TPEs

The slight decrease in ε_{max} by reprocessing, visible in the complete constellation of all stress-strain curves presented in the **Figure S31-S32** and **Figure 11**c and d, is caused by the loss of material and consequently film thickness. As the determination of *E* takes the thickness by the cross-section of the test specimen into account, these values are much better suited for the comparison. In addition, SEC measurements were done after each tensile measurement to track any structural changes. As can be followed in the respective SEC-traces, see **Figure S29,** both samples keep their unimodal distribution even though both show slight broadening. This can be accounted to the large number of olefinic bonds along the whole polymer structure that can lead to some extent of crosslinking. This behavior is known for other double-bond rich polymers and can be prevented by the addition of more stabilizer. This change in distribution had only a minor influence on the properties and still enabled full dilution of the polymer material.

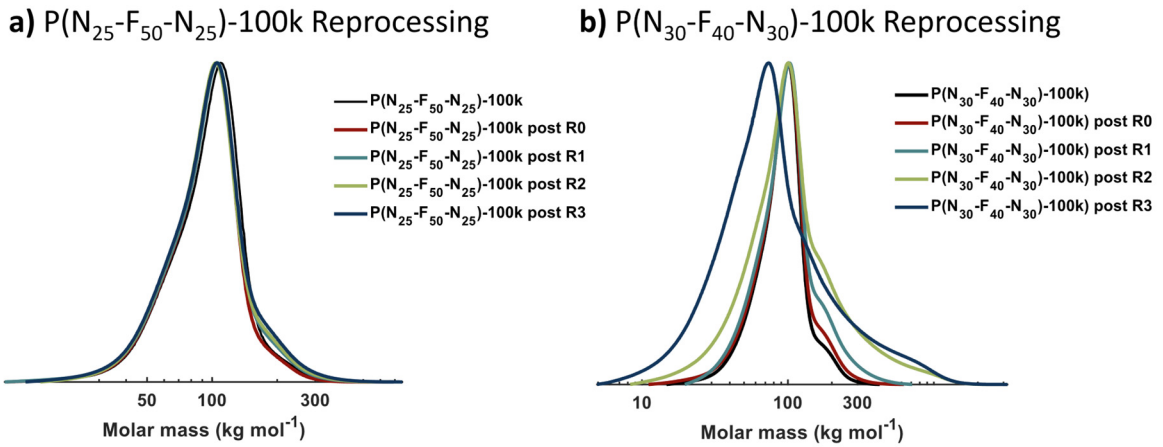

Figure S31. SEC traces of P(N_{25}-F_{50}-N_{25})-100k and P(N_{30}-F_{40}-N_{30})-100k after each tensile experiment, measured in THF against PS-calibration.

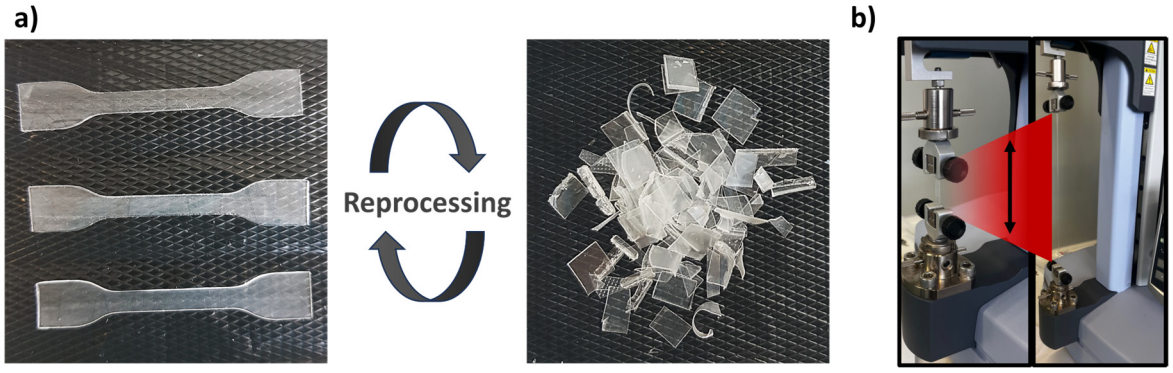

Figure S32. a) Dogbone test specimens before measurement and torn pieces for reprocessing; b) dogbone test specimen during tensile measurement indicating high elasticity.

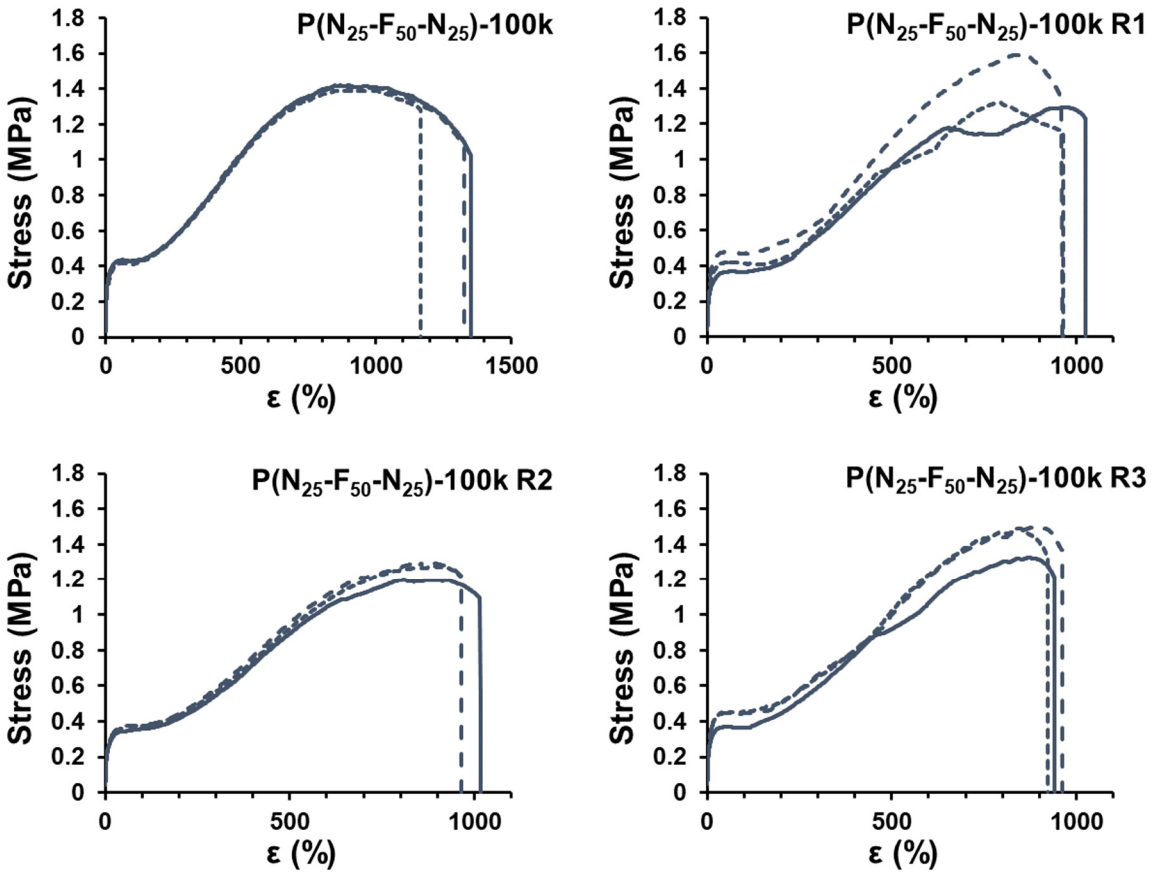

Figure S33. Stress-Strain curves of sample P(N_{25}-F_{50}-N_{25})-100k and its respective recycling steps; each sample measured three times.

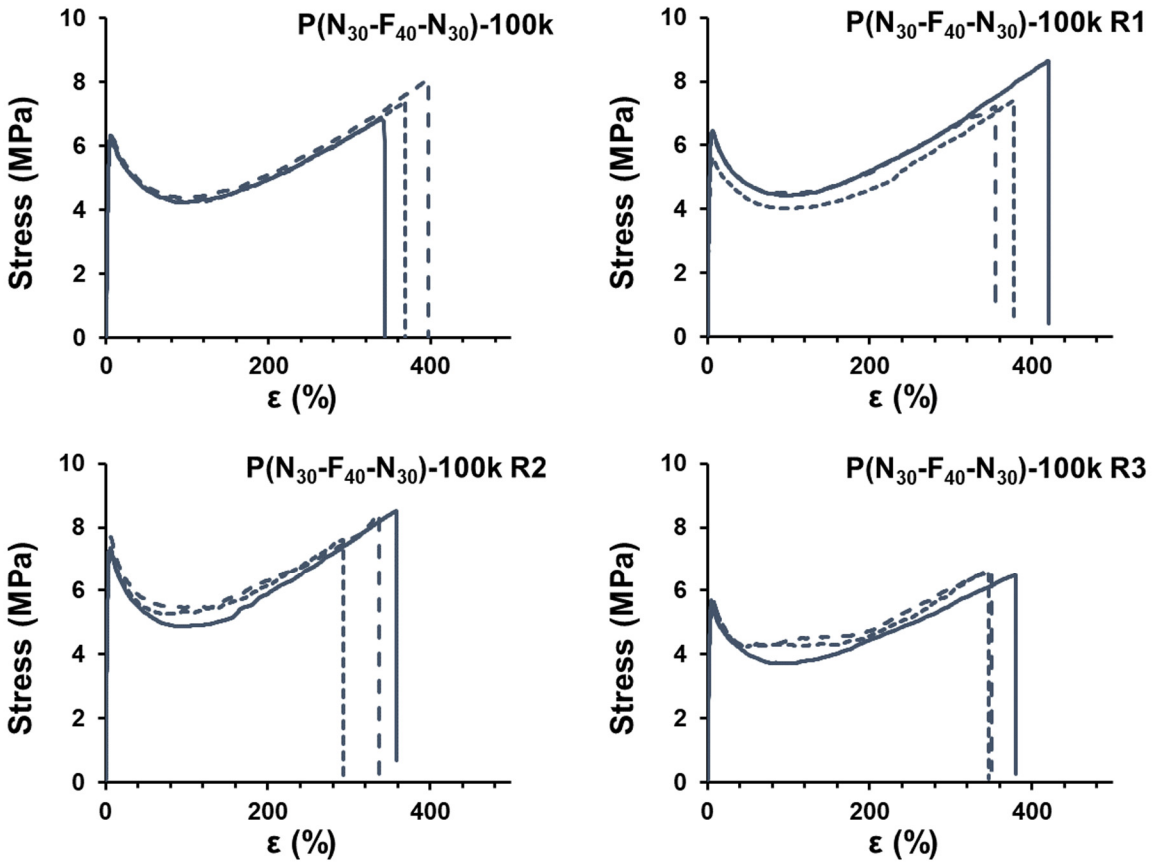

Figure S34. Stress-Strain curves of sample P(N_{30}-F_{40}-N_{30})-100k and its respective recycling steps, each sample measured three times.

11. TGA Results

All polymer samples that were tested *via* tensile test were examined for their thermal stability using thermal gravimetric analysis (TGA). **Figure S35** indicates a similar stability of all triblocks independent of their molar mass and composition.

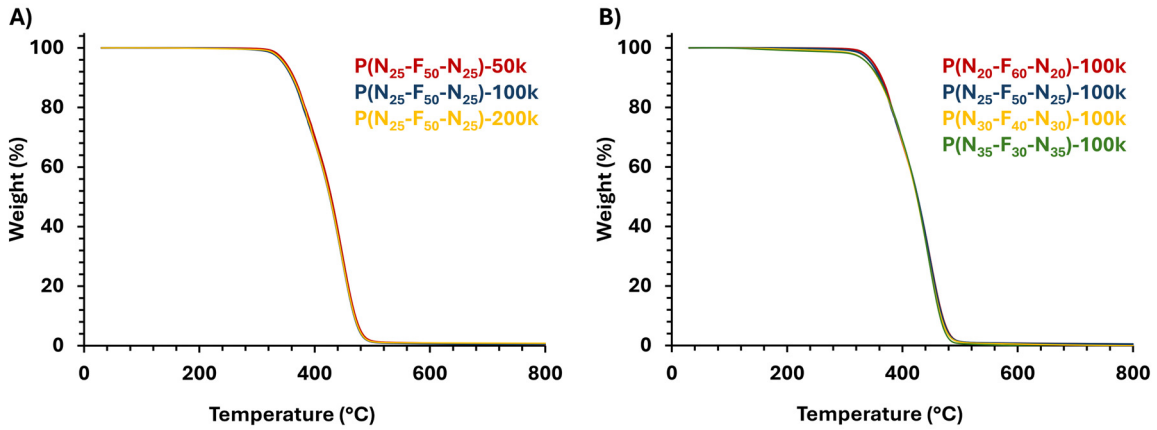

Figure S35. TGA measurements of triblock samples measured from 30 °C to 800 °C with a heat rate of 10 K min^{-1}.

References

[1] Hahn, C.; Göttker-Schnetmann, I.; Tzourtzouklis, I.; Wagner, M.; Müller, A. H. E.; Floudas, G.; Mecking, S.; Frey, H. Nopadiene: A Pinene-Derived Cyclic Diene as a Styrene Substitute for Fully Biobased Thermoplastic Elastomers. *J. Am. Chem. Soc.*, **2023**, *145* (49), 26688-26698.

[2] Jaacks, V. A Novel Method of Determination of Reactivity Ratios in Binary and Ternary Copolymerizations. *Makromol. Chem.*, **1972**, *161* (1), 161‑172.

Chapter 6

Heterotelechelic Initiation to access A_2B-type Block Copolymers via LL-Dilactide Grafting from α-Functionalized Polyisoprene

Moritz Meier-Merziger [a] *and Holger Frey* [a]*

* Corresponding author

[a] Department of Chemistry, Johannes Gutenberg University Mainz, Duesbergweg 10-14, 55128 Mainz, Germany

To be submitted

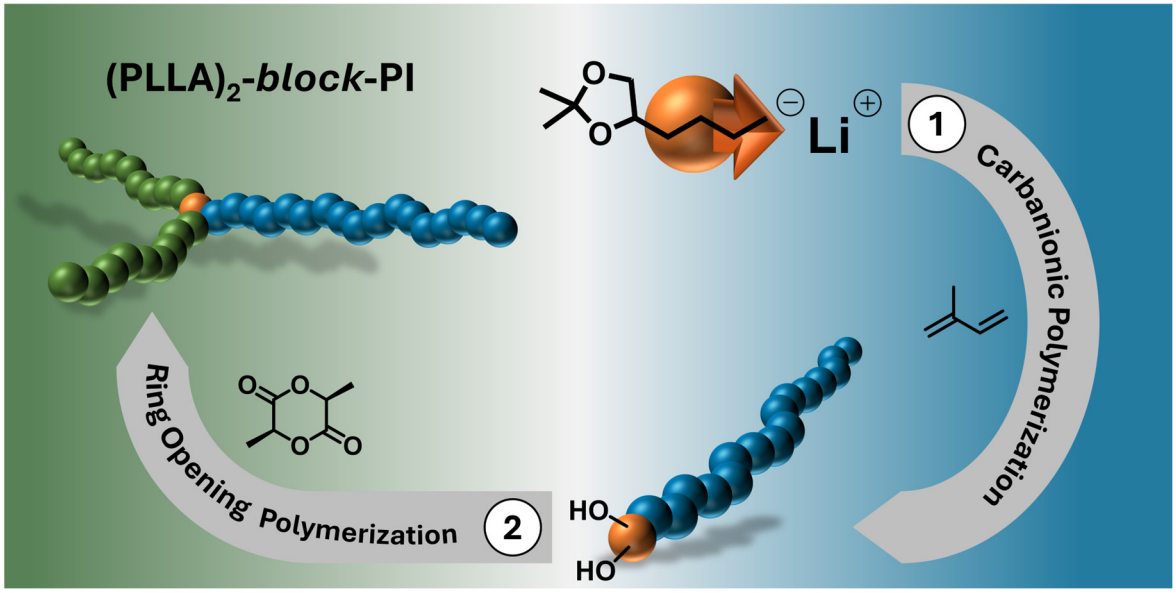

The following chapter's results are based on a collaboration of Arlanxeo with the Johannes Gutenberg-University, Mainz.

Abstract

The synthesis of a heterotelchelic initiator for the formation of α-functionalized polyisoprene that is further extended by lactide grafting to yield A_2B-type copolymers is presented. The initiator was accessed *via* titration using an iodine alkyl precursor and *tert*-butyl lithium. The functional alkyl lithium initiator, bearing two ketal-protected hydroxyl functionalities, is used for the carbanionic polymerization of isoprene. MALDI-ToF MS measurements verified an effective and quantitative end-group functionalization of polyisoprene in α-position. To yield low dispersity ($Đ < 1.1$) polymers and ensuring a high 1,4-polyisoprene content (60%), the required amount of polar modifier was optimized. Following deprotection, the polyisoprene macroinitiators are used to polymerize LL-dilactide in a subsequent organocatalyzed ring-opening polymerization. SEC, NMR, and DOSY measurements are used to demonstrate the successful chain-extension *via* lactide grafting and DSC experiments indicate phase-separation within the block copolymers.

Introduction

Anionic polymerization is a sensitive method that requires careful attention to the reaction set-up and materials used. The absence of any protic impurities is required to ensure a "living" polymerization in absence of termination and transfer reactions.[1],[2] Thereby, a high precision polymerization proceeds which enables the synthesis of low dispersity ($Đ$ << 1.1) polymers, often referred to as benchmark in controlled polymerization.[3] Other polymer properties, i.e., molar mass, microstructure, architecture, copolymer composition, and comonomer incorporation can be precisely tailored. This makes it a versatile method, to access high precision and high performance materials, to match nature derived materials properties such as wool, silk, cotton, natural rubber, etc.[4] A readily available large-scale material obtained *via* anionic polymerization of 1,3-dienes is synthetic rubber. Important material properties, e.g. glass temperature (T_g) of butadiene(B)/isoprene(I)-styrene(S) copolymers can be customized by influencing the incorporation within the copolymerization or by affecting the resulting microstructure of the poly(1,3-diene). For many applications, i.e., tires and seals, a low T_g is desirable to ensure a good performance even at low temperature without turning brittle.[5],[6]

One challenge in the carbanionic polymerization, is the incorporation of functional groups to the polymer structure. A common pathway to address the chain end of the polymer, i.e., ω-position, is to terminate the polymerization with a suitable electrophile.[7] Epoxides are known to add exactly one monomer unit to the chain end if lithium is used as a counter ion due to the strong O-Li bond formation.[8] – [11] Other termination reactions are known to insert functional groups including hydroxyl,[10],[12] amino,[13],[14] halide,[15] and carboxylate[16] beside others.[7] To yield high degrees of functionalization, again precise consideration of the preparation of the substrates and in some cases the suppression of side reactions is required. For instance, the insertion of a carboxyl group using CO_2 usually results in numerous side reactions.[17] – [19]

A much more demanding approach is to insert functional groups in α-position as they need to withstand the strongly basic conditions of the carbanionic polymerization. The use of functional initiators is usually regarded as a quantitative pathway to functionalized polymers.[20] Several suitable protecting groups were reported, including siloxy,[21],[22] acetal,[23],[24] and silyl amines.[25] A broad application of functional initiators is often restricted due to poor solubility in hydrocarbon solvents.[10] Moreover, the addition of polar solvents, e.g. ethers, is often required in the synthesis step, usually comprising the reaction of the respective halide and lithium metal.[23] As it is known that an increase in solvent polarity enhances the amount of vinyl incorporation of 1,3-dienes – associated with an increase in T_g – it limits their relevance for a majority of applications.[26]

A pathway to access lithium alkyl compounds without the use of lithium metal, intentionally designed for organic synthesis, was introduced by Bailey et al.[27], see **Scheme 1**. It was reported that undesired side reactions, i.e., coupling and elimination, of the reaction of a primary alkyl iodide with *tert*-butyl lithium (*tert*-BuLi), can be suppressed by adding small quantities of ether as co-solvent and low temperatures. Thereby, the lithium-iodine exchange reaction occurs quantitatively and hence, offers access to a variety of initiators for the carbanionic polymerization.

Scheme 1. Synthesis of alkyl lithium structures based on a lithium-iodine exchange reaction; A) different reaction condition show different reaction pathways; B) subsequent reaction of the formed *tert*-butyl iodide and *tert*-butyl lithium; scheme based on results reported of Bailey et al.[27]

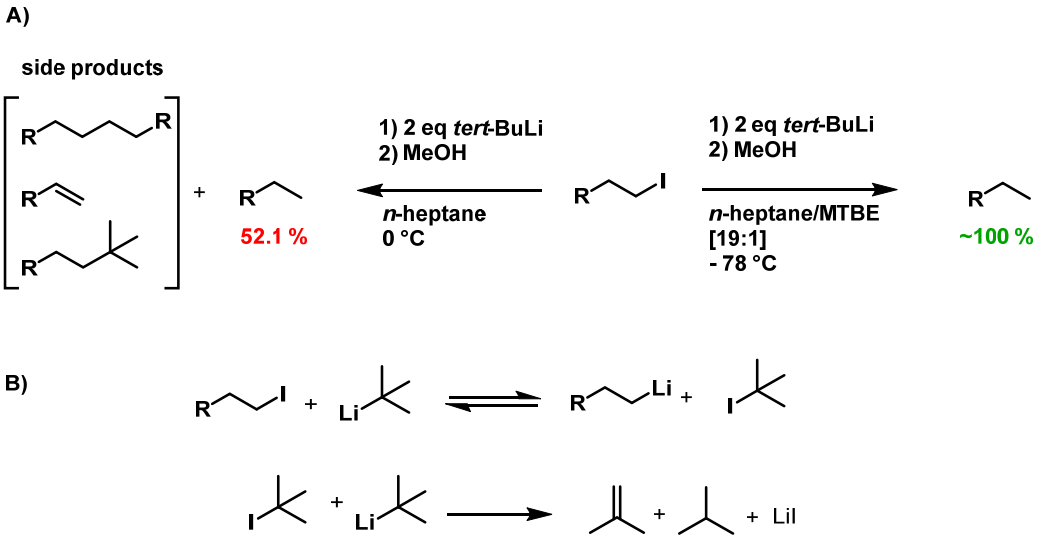

Methyl *tert*-butyl ether (MTBE) as co-solvent was reported to yield the best results. The aim of this work was to transfer this approach to the field of functional initiators for carbanionic polymerizations and introduce a new reaction pathway for the synthesis of heterotelechelic polydienes. Key objective was to introduce hydroxyl groups in α-position of polydienes and to further address them *via* chain-extension by LL-dilactide (LLA) grafting to yield block copolymers.

Moreover, the incorporation of hydrophilic groups to the chain end of synthetic rubber is a major challenge for the synthetic rubber industry, to improve the performance of tires and make them more environmentally friendly. This is mainly achieved by introducing silica particles as filler to the tire composite to improve wet grip and to reduce fuel-consumption by lowering the rolling resistance.[28] The higher hydrophilicity of silica, compared to carbon black, results in a poor rubber-filler interaction and requires the use of coupling agents to ensure a good silica reinforcement. Still, their performance is limited as the silane coupling agents do not achieve the particle scale desired, i.e., 15 - 30 nm.[29] Furthermore, it is known,

that the hysteresis loss of rubber can be attributed to the free terminals – dangling ends – of the polymer chains in a vulcanized network. Their possible random motion generates more heat due to friction and consequently increases the rolling resistance.[29],[30] Addressing the chain ends by functional groups, which interact with the filler material, can potentially tackle both challenges: enhance the rubber-filler interaction and hinder the motion of free terminals. Both are important aspects to produce more environmentally friendly tires.

Results and Discussion

The precursors for the functional initiators were synthesized according to reported procedures.[31] – [33] For the propyl-derivate, 4-(iodomethyl)-2,2-dimethyl-1,3-dioxolan (**DiOx-I**), the hydroxyl group of solketal was substituted with iodine using the Appel-reaction, see **Scheme 2**a. The hexyl derivate, 4-(4-iodobutyl)-2,2-dimethyl-1,3-dioxolan (**DiOxHex-I**) was synthesized using a more elaborate three-step synthesis, starting from the readily available 1,2,6-hexanetriol, **Scheme 2**b.

Scheme 2. Synthesis pathway of: A) one-step synthesis of **DiOx-I**, starting from solketal; B) three-step synthesis of **DiOxHex-I**, starting from 1,2,6-hexanetriol; C) lithium-iodine exchange reaction.

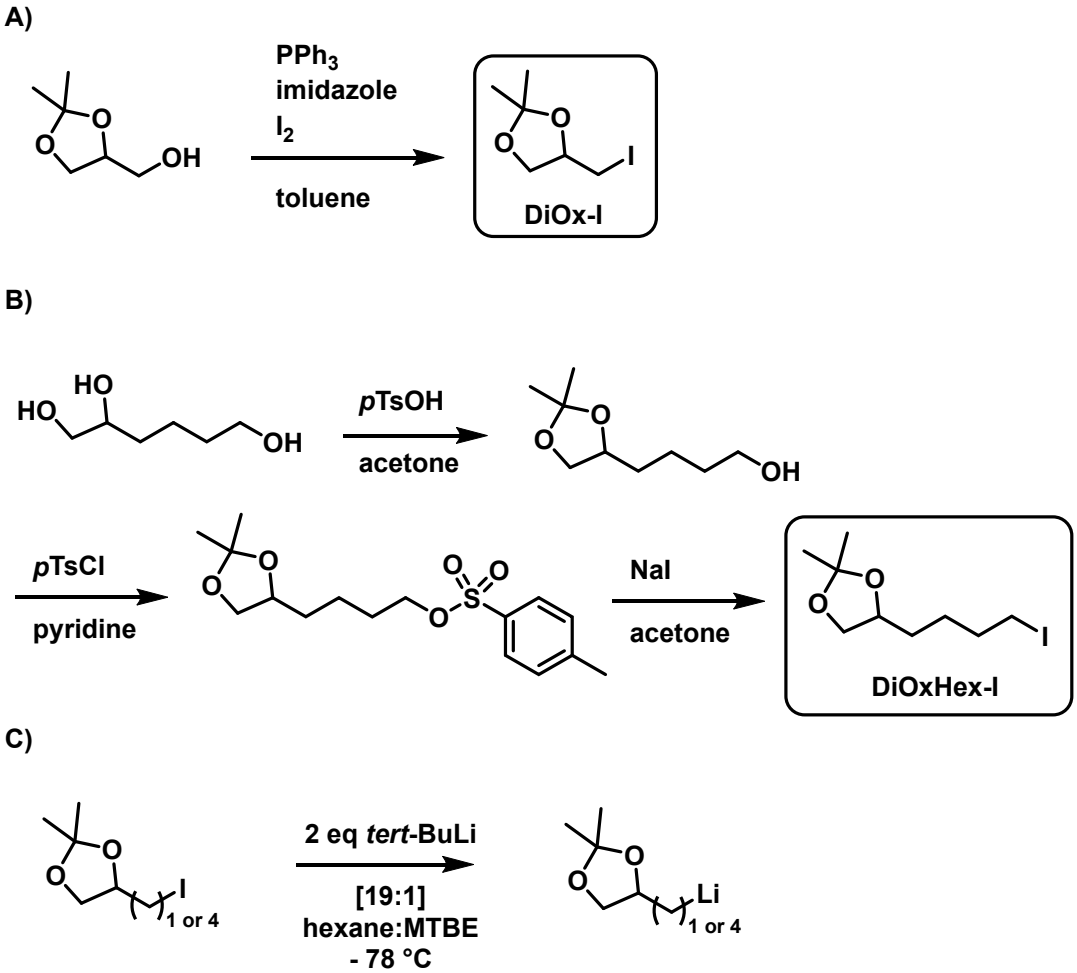

Further, **Scheme 2**c indicates the lithium-iodine exchange reaction yielding the respective alkyl lithium structure. Detailed characterization of each intermediate was done by ^{1}H, ^{13}C, and 2D NMR spectroscopy and the respective spectra are summarized in the **Supporting Information**, see **Figure S1-S10**.

The lithium-iodine exchange reaction was performed as described in greater detail in the experimental section. First, the activation step without the addition of monomer was investigated. Upon the addition of *tert*-BuLi to the DiOx-I solution, a colorless precipitate (lithium iodide) was observed. After one hour of stirring at – 78 °C, the reaction was quenched by the addition of degassed methanol. Consequently, the formed alkyl lithium compound should add a proton at the former position of the halide atom. Surprisingly, new signals emerge in the olefinic region (> 5 ppm) of the respective ^{1}H NMR spectrum of the propyl derivate, **Figure S11**. Further, using the "active" initiator solution to initiate isoprene polymerization did not yield any polymeric material, indicating the absence of any active alkyl lithium species. Based on the olefinic signals observed after quenching with methanol, we assume that the lithium-iodide exchange reaction is directly followed by decomposition of the alkyl lithium compound. The signals observed indicate the formation of allyl alkoxide. The formation can be attributed to the ring-opening of the 1,3-dioxolane structure. Hence, DiOx-Li is not stable under the reaction conditions and rearranges into the open allyl alkoxide, which is not capable of initiating isoprene, see **Scheme 3**.

Scheme 3. Activation of DiOx-I and DiOxHex-I, indicating the side reaction and proposed formation of allyl alkoxide for the DiOx-I structure. DiOxHex-I indicates the successful synthesis of α-functionalized polyisoprene.

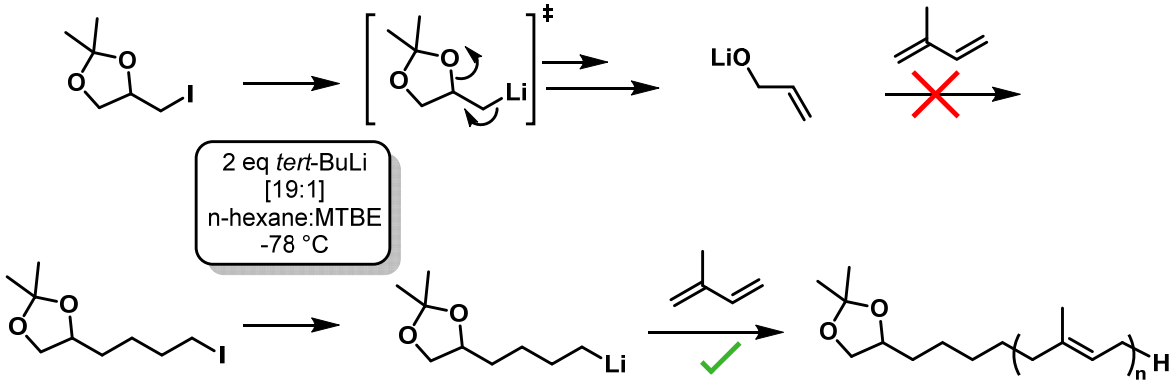

Introducing an alkyl spacer between the 1,3-dioxolane and the alkyl lithium functionality should prevent this side reaction. Therefore, the same reaction was performed with the DiOxHex-I derivate. ^{1}H NMR spectroscopy indicates a successful lithium-iodine exchange reaction with absence of the above-mentioned side reaction, see **Figure S12**. Again, a colorless precipitate was obtained. The characteristic methylene signal at ~ 3.2 ppm disappears after

the reaction with *tert*-BuLi and subsequential quenching with degassed isopropyl alcohol. Therefore, after activation with *tert*-BuLi at – 78 C, the reaction solution was allowed to reach room temperature and used to initiate isoprene in cyclohexane (chx). Size-exclusion chromatography (SEC) indicated the formation of a polymer but with a strong tailing of the molar mass distribution towards low molar masses. The obtained dispersity, $Đ$ = 1.34, is close to the theoretical value of a slow initiation process ($Đ \sim 1.3$).[34] As alkyl lithium structures are known to form aggregates in pure hydrocarbon solvents, we assume that the increased polarity of the dioxolan group further enhances strong aggregation and precipitation of the active DiOx-Li structure.[35] As the addition of isoprene units eventually increases the fraction of non-polar structures, i.e., increasing the solubility in hydrocarbons, we postulate a faster propagation compared to initiation.

It is known that polar additives can be used to prevent the formation of aggregates.[36] Therefore, different polar modifiers were tested. First, 50 vol% of MTBE as moderately polar co-solvent was used, as MTBE is already present in the system due to the activation process.[37] Secondly, 2,2-di-tetrahydrofuryl propane (DTHFP), a much more potent modifier,[38] was used to an extent of 5 vol%. As evident from SEC, both additives show a positive effect by lowering the dispersity of the respective SEC-traces, see **Figure 1**. The shoulder at lower elution volumes of the distributions can be attributed to oxygen coupling during the termination step.

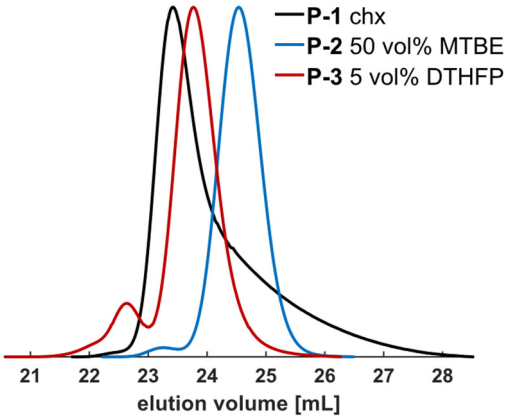

Figure 1. SEC traces of DiOxHex-Li initiated PI in pure cyclohexane (black), using 50 vol% MTBE (blue), and 5 vol% DTHFP (red) as polar modifier, eluent: THF, 1,4-PI-calibration.

As the change in polarity of the solvent and the strong chelating effect of DTHFP are known to affect the propagation mechanism and the resulting microstructure of polyisoprene (PI), ^{1}H NMR spectroscopy was used to determine the ratio of 1,4- : 3,4- : 1,2-additions, **Figures S13** and **S14**. A more detailed description of the determination *via* ^{1}H NMR spectroscopy is described in an earlier publication.[39] The 1,4-PI content decreases from 68% in cyclohexane

including 4 eq of MTBE (present due to the lithium-iodine exchange reaction), to 47% by the presence of 50 vol% of MTBE. In contrast, DTHFP shows a much stronger effect, as 5 vol% decreases the 1,4-PI content further down to 13%. This is in line with reported values.[38],[40] The amount of added modifier is given as equivalents (eq) compared to the active chain ends, i.e., [Modifier]:[Li]. This, along with all corresponding polymer characteristics is summarized in **Table 1**.

Table 1. Summary of PI samples initiated with DiOxHex-Li using different additives, 4 eq of MTBE is always present, due to the active DiOxHex-Li solution.

Sample	Solvent + Modifier*	M_n^{target} [g·mol^{-1}]	M_n^{SEC} [a] [g·mol^{-1}]	$Đ$ [a]	1,4-PI[b]	3,4-PI[b]	1,2-PI[b]	T_g [c] [°C]
P-1 261	chx	5 000	5 200	1.34	67.7	31.8	0.5	- 43
P-2 262	chx + 50 vol% MTBE	5 000	4 700	1.05	47.4	49.3	3.3	- 31
P-3 263	chx + 9 eq DTHF	5 000	7 200	1.12	13.2	76.3	10.5	5

[a] Determined by SEC: eluent: THF, calibration: 1,4-PI. [b] Calculated from ^{1}H NMR. [c] Determined *via* DSC measurements using a heating rate of 10 K·min^{-1}. *4 eq of MTBE always present.

To proof the successful α-functionalization, the low dispersed polymer sample, **P-2**, was investigated *via* matrix assisted laser desorption ionization time-of-flight mass spectrometry (MALDI-ToF MS), see **Figure 2**a. A single polymer species can be clearly assigned to DiOxHex-PI. The main distribution consists of the polymer, the end-group and Ag^+ as counter ion. The second distribution can be attributed to Li^+ as counter ion. The spacing matches the molar mass of the isoprene repeating unit of ~ 68 g·mol^{-1}. This indicates a quantitative end-group functionalization. It should be noted that the second distribution also matches pure polyisoprene bearing a *tert*-butyl end-group and Ag^+ as counter ion. This species can be excluded by the chain-extension reactions performed in the last section of this work. By ^{1}H NMR spectroscopy, the appearance of proton signals of the end-group can also be observed, see **Figure S13**.

The cleavage of the dioxolane group was performed on **P-2**, using a standard protocol with DOWEX® ion-exchange resin.[39] The simple handling and separation by filtration makes it an ideal procedure for lab-scale applications. Again, MALDI-ToF MS measurements were performed to confirm the successful cleavage (**P-2***). As can be followed in **Figure 2**b, the molar mass is reduced by the loss of the ketal-protecting group. Thereby, polyisoprene with two hydroxyl functionalities in α-position was obtained. The SEC traces remain monomodal and are presented in the last sections of this work, **Figure 5**. Moreover, ^{1}H NMR spectroscopy indicates cleavage of the protecting group by the shift of the characteristic proton signals of the ketal group, see **Figure S16**.

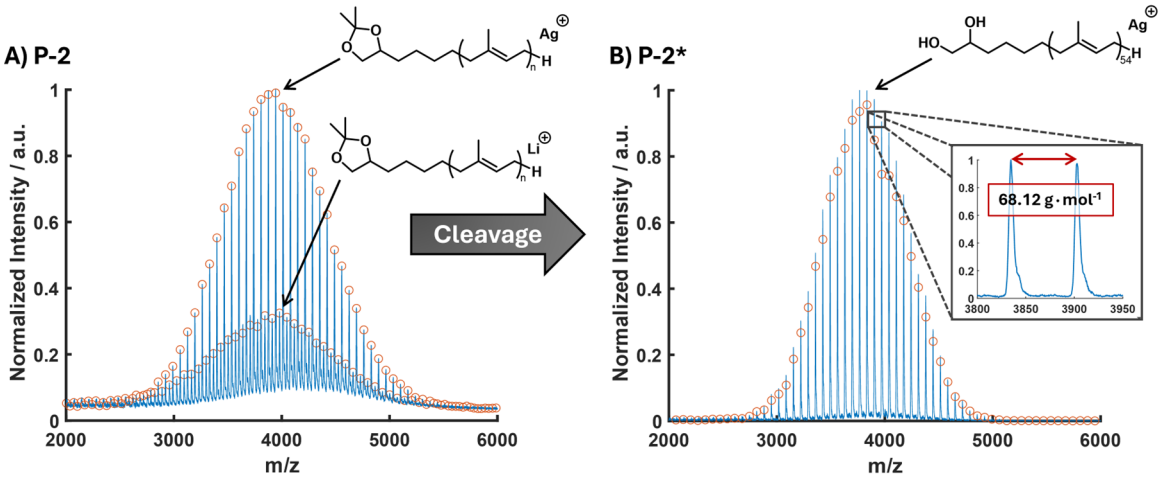

Figure 2. A) MALDI-ToF MS measurement of polymer **P-2**, polymer is detected with Ag+ and Li+ as counter ion, Matrix: DCTB + AgTFA; B) MALDI-ToF MS measurement after cleavage, **P-2***, only one species with Ag+-counter ion detected, Matrix: DCTB + AgTFA.

Prior to addressing the hydroxyl groups in a subsequent reaction step, the amount of required polar additives was optimized. The amount of DTHFP was successively reduced from 1 eq down to 0.25 eq. This has a strong effect on the polymer characteristics. As evident from SEC, **Figure 3**b, 0.75 eq DTHFP is sufficient to maintain a low dispersity ($Đ$ < 1.1), whereas lower amounts lead to broadening – again attributed to the formation of aggregates. It was also shown that the molar mass can be tailored by synthesizing a 10 and 20 kg·mol^{-1} sample, see **Figure 3**a. All polymer characteristics are summarized in **Table 2**.

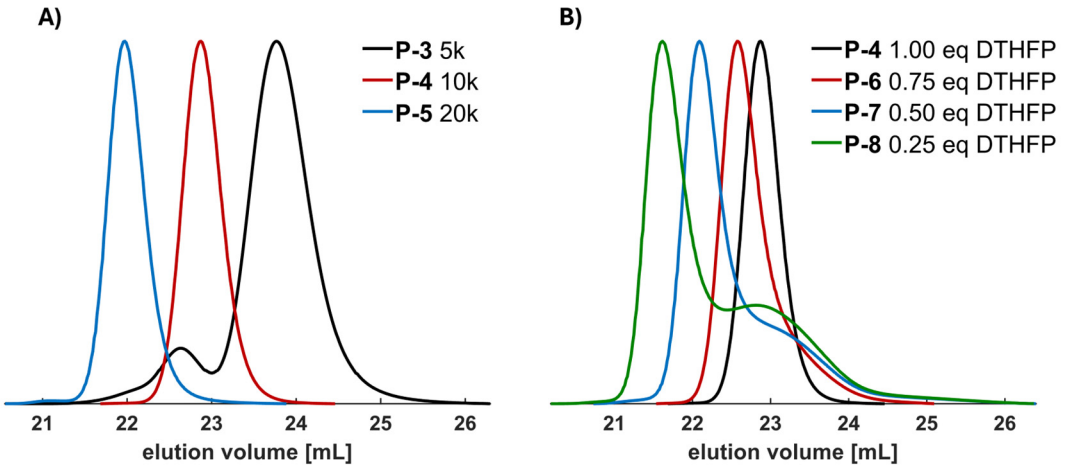

Figure 3. SEC traces of DiOxHex-Li initiated polyisoprene; A) variating the targeted molar mass; B) decreasing the amounts of DTHFP equivalents.

Table 2. Polymer characteristics of all DiOxHex-PI polymer samples synthesized using different equivalents of DTHFP incl. 4 eq of MTBE and varying the targeted molar mass from 5 to 10 to 20 kg·mol^{-1}.

Sample	[DTHFP]:[Li]*	M_n^{target} [g·mol^{-1}]	M_n^{SEC} [a] [g·mol^{-1}]	$Đ$ [a]	1,4-PI[b] [%]	3,4-PI[b] [%]	1,2-PI[b] [%]	T_g [c] [°C]
P-3 263	9	5 000	7 200	1.12	13.2	76.3	10.5	- 39
P-4 284	1	10 000	14 400	1.03	38.9	57.5	3.7	- 39
P-5 289	1	20 000	27 000	1.04	51.0	47.3	1.8	- 39
P-6 286	0.75	10 000	15 500	1.08	56.4	42.3	1.3	- 48
P-7 287	0.50	10 000	17 100	1.25	60.5	38.6	0.9	- 53
P-8 288	0.25	10 000	19 300	1.42	64.6	34.7	0.7	- 54

[a] Determined by SEC: eluent: THF, calibration: 1,4-PI. [b] Calculated from ^{1}H NMR. [c] Determined *via* DSC measurements using a heating rate of 10 K·min^{-1}; *4 eq of MTBE always present.

The determination of the respective microstructure reveals the expected trend of higher vinyl content by an increasing amount of DTHFP, see **Figure S14**. As this is known to directly affect the resulting T_g of the material, differential scanning calorimetry (DSC) measurements were performed, **Figure S19** and **S20**. Decreasing the DTHFP content results in a lower T_g. The trends on the microstructure and T_g are illustrated in the following **Figure 4**:

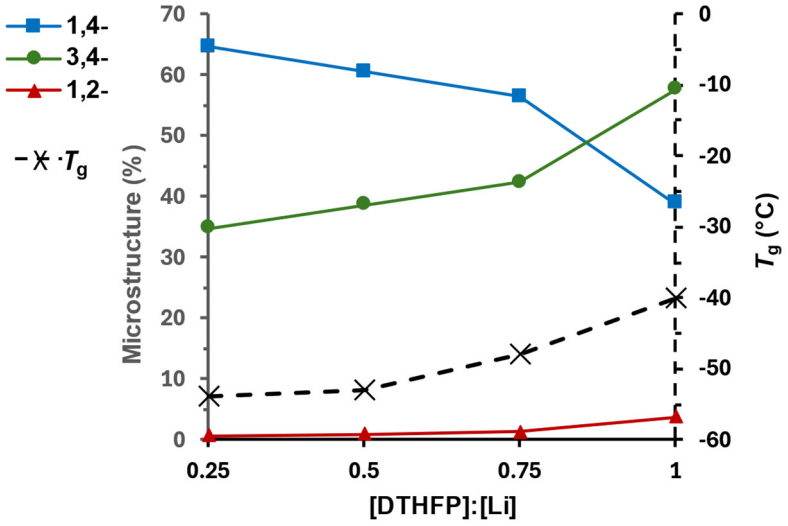

Figure 4. Effect of an increasing DTHFP content on the microstructure and T_g of the respective DiOxHex-PI samples.

Organocatalyzed ring-opening polymerization (ROP) of LLA was investigated to address the chain ends hydroxyl groups. It was reported, that 1,8-diazabicyclo[5.4.0]undec-7-ene (DBU) can be used as catalyst for the ROP of LLA, yielding narrowly distributed polymers with high

molar mass under considerably mild reaction conditions.[41] Since the above mentioned cleavage of the ketal protecting group generates two hydroxyl groups, both can add LLA monomers. Consequently, A_2B-type block copolymers architectures are obtained. The 5 kg·mol^{-1} (**P-2***) and the 10 kg·mol^{-1} (**P-4***) $(OH)_2$-PI macroinitiators were examined for the chain-extension reaction. The smaller macroinitiator was used to add the same molar mass of poly(L)lactide (PLLA) targeting an overall molar mass of 10 kg·mol^{-1}, where the PLLA chains are distributed across two arms, yielding $(PLLA_{2.5k})_2$-*b*-PI_{5k}. The larger macroinitiator was used to add 10 and 20 kg·mol^{-1} of PLLA, respectively. As presented in **Figure 5**, SEC reveals a clear shift towards a higher molar mass, indicating a successful chain-extension. For the copolymers **CP-2** and **CP-3** it is evident that a higher proportion of LLA leads to further chain-growth. The dispersity of the copolymers remains rather low, $Đ < 1.15$, attributed to the great control found by the DBU catalyzed ROP. **Table 3** summarizes all characteristics of the copolymers and macroinitiators. Characterization *via* ^{1}H NMR spectroscopy can be followed in **Figure S15**.

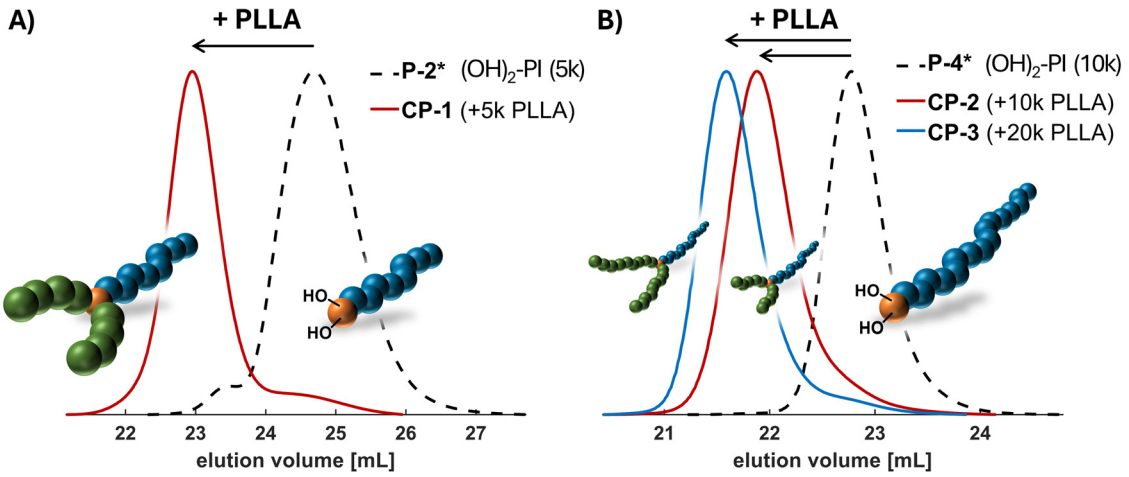

Figure 5. SEC traces of all copolymers and their respective macroinitiators (dashed line); a) **P-2*** used to yield **CP-1**; b) **P-4*** used to yield **CP-2** and **CP-3**.

By this means, the presence of hydroxyl groups at the α-position can be confirmed. Therefore, the initiator DiOxHex-Li is suitable to synthesize heterotelchelic copolymers. Block copolymers are known for their exceptional properties, mainly derived from the phase separation in the bulk material, attributed to the immiscibility of different polymer types. Block copolymers derived from polyisoprene and poly(L)lactide are readily reported in the respective literature in terms of thermoplastic elastomers or compatibilizers for polymer blends.[39],[42]–[44] PI-PLLA block copolymers can be used to enhance the brittle properties of neat PLLA and toughen the material.[45],[46] Thereby, the scope of application of PLLA, as one of the most important and large-scale produced biomaterials can be extended.

Table 3. Characteristics of $(OH)_2$-PI macroinitiators and A_2B-type PI/PLLA copolymers (CP).

Macroinitiators	M_n^{target} [g·mol^{-1}]	M_n^{SEC} [a] [g·mol^{-1}]	$Đ$ [a]	T_g [d] [°C]
P-2*	5 000	4 500	1.12	-29
P-4*	10 000	15 000	1.04	-24

Copolymers	M_n^{target} [g·mol^{-1}]	M_n^{SEC} [a] [g·mol^{-1}]	$Đ$ [a]	wt%^{PLLA} target	wt%^{PLLA} [%] [b]	1,4-PI [c] [%]	T_g1 [d] [°C]	T_g2 [d] [°C]
CP-1	10 000	12 300	1.15	50	60.8	47.4	-26	43
CP-2	20 000	26 800	1.07	50	51.0	38.9	-17	50
CP-3	30 000	32 700	1.07	66	61.3	38.9	-16	53

[a] Determined by SEC: eluent: THF, calibration: 1,4-PI. [b] Determined from ^{1}H NMR. [c] Based on PI-macroinitiators. [d] Determined from second heating cycle of DSC measurements using a heating rate of 10 K·min^{-1}.

To further confirm the chain-extension, diffusion-ordered spectroscopy (DOSY) NMR experiments were performed. As evident from **Figure 6**, characteristic signals of PLLA and PI share the same diffusion coefficient, proofing the successful synthesis of the $PLLA_2$-*b*-PI block copolymers. DOSY measurements of **CP-1** and **CP-3** can be followed in **Figures S16** and **S17**.

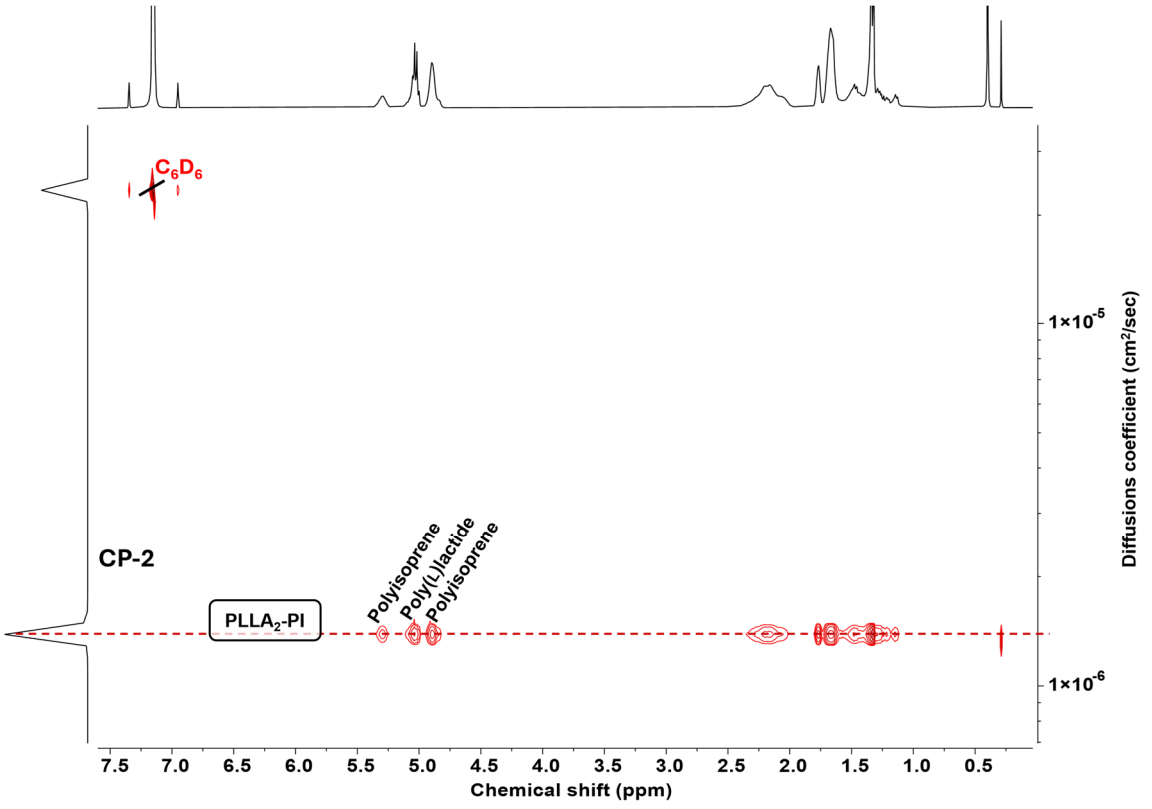

Figure 6. ^{1}H DOSY NMR of copolymer CP-2 with signals assigned to characteristic protons of PLLA and PI, measured in C_6D_6, 400 MHz.

Thermal analysis of the samples can be utilized to investigate the phase state of the copolymers. Therefore, all samples were measured *via* differential scanning calorimetry (DSC). As evident from **Figure 7** the second heat curve reveals two distinct T_gs which can be assigned to PI and PLLA. This indicates the presence of phase separation of PI- and PLLA-domains within the bulk material. Noteworthy, all samples showed no melting point, T_m, in the second heating cycle of the DSC experiment, which suggests that the chain-length of PLLA is too short to allow crystallization.

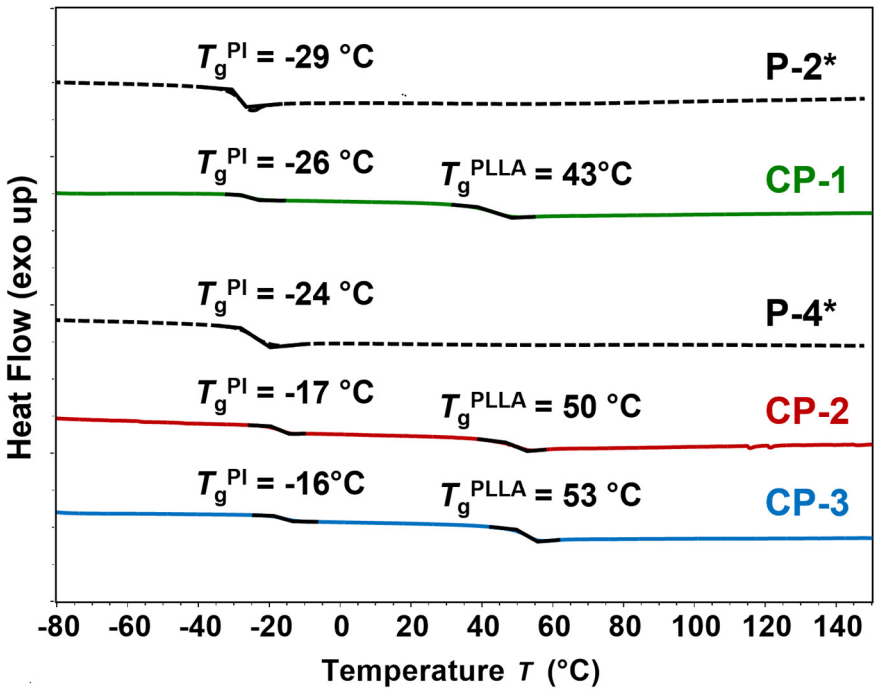

Figure 7. DSC measurements of all PI-macroinitiators and A_2B-type copolymers, measured with a heating rate of 10 K·min^{-1}, second heating curve used for determination.

Future investigations will combine this functional initiator, DiOxHex-Li, with controlled end-functionalization using different epoxides. Ethylene oxide, ethoxy ethyl glycidyl ether, and 1,2-isopropylidene glyceryl glycidyl are known to introduce 1, 2, and 3 hydroxyl groups, respectively.[10],[47] Thereby, α,ω-functionalized polydienes are accessible as well as a variety of asymmetric polymer architectures.

Conclusions

Key finding of this work is the introduction of a general pathway to access functional initiators for carbanionic polymerization. The pathway relies on the lithium-iodine exchange reaction, which yields alkyl lithium compounds, capable of initiating 1,3-diene monomers, i.e., isoprene. This route offers the possibility to introduce protected hydroxyl functionalities in α-position of a polydiene. The 1,3-dioxolane group is utilized to simultaneously introduce two hydroxyl groups at the α chain end. MALDI-ToF MS measurements prove the successful quantitative end-functionalization. Organocatalyzed ring-opening polymerization of LL-dilactide was used to demonstrate the use of these α-functionalized polyisoprenes as macroinitiators. The presented structure, DiOxHex-Li, is therefore capable of heterotelechelic synthesis of polyisoprene/poly(L)lactide copolymers. We emphasize the general nature of this synthesis, since the access to active organolithium compounds can be beneficial to introduce numerous functionalities within the field of anionic polymerization. The successfully synthesized A_2B-type block copolymers represent an impression of polymer architecture accessible *via* this route.

References

[1] Szwarc, M. 'Living' Polymers. *Nature*, **1956**, *178* (4543), 1168-1169.

[2] Frey, H.; Ishizone, T. Living Anionic Polymerization Celebrates 60 Years: Unique Features and Polymer Architectures. *Macromol. Chem. Phys.*, **2017**, *218* (12).

[3] Ntetsikas, K.; Ladelta, V.; Bhaumik, S.; Hadjichristidis, N. Quo Vadis Carbanionic Polymerization? *ACS polymers Au*, **2023**, *3* (2), 158-181.

[4] Webster, O. W. Living polymerization methods. *Science (New York, N.Y.)*, **1991**, *251* (4996), 887-893.

[5] Steube, M.; Johann, T.; Hübner, H.; Koch, M.; Dinh, T.; Gallei, M.; Floudas, G.; Frey, H.; Müller, A. H. E. Tetrahydrofuran: More than a "Randomizer" in the Living Anionic Copolymerization of Styrene and Isoprene: Kinetics, Microstructures, Morphologies, and Mechanical Properties. *Macromolecules*, **2020**, *53* (13), 5512-5527.

[6] Forens, A.; Roos, K.; Dire, C.; Gadenne, B.; Carlotti, S. Accessible microstructures of polybutadiene by anionic polymerization. *Polymer*, **2018**, *153*, 103-122.

[7] Tasdelen, M. A.; Kahveci, M. U.; Yagci, Y. Telechelic polymers by living and controlled/living polymerization methods. *Progress in Polymer Science*, **2011**, *36* (4), 455-567.

[8] Richards, D. H.; Szwarc, M. Block polymers of ethylene oxide and its analogues with styrene. *Trans. Faraday Soc.*, **1959**, *55*, 1644.

[9] Quirk, R. P.; Ma, J.-J. Characterization of the functionalization reaction product of poly(styryl)lithium with ethylene oxide. *J. Polym. Sci. A Polym. Chem.*, **1988**, *26* (8), 2031-2037.

[10] Tonhauser, C.; Frey, H. A road less traveled to functional polymers: epoxide termination in living carbanionic polymer synthesis. *Macromolecular rapid communications*, **2010**, *31* (22), 1938-1947.

[11] Zhang, J.; Pointer, W.; Patias, G.; Al-Shok, L.; Hand, R. A.; Smith, T.; Haddleton, D. M. End functionalization of polyisoprene and polymyrcene obtained by anionic polymerization via one-pot ring-opening mono-addition of epoxides. *European Polymer Journal*, **2023**, *183*, 111755.

[12] Hirao, A.; Hayashi, M. Synthesis of Well-Defined Functionalized Polystyrenes with a Definite Number of Chloromethylphenyl Groups at Chain Ends or in Chains by Means of

Anionic Living Polymerization in Conjunction with Functional Group Transformation. *Macromolecules*, **1999**, *32* (20), 6450-6460.

[13] Hirao, A.; Hattori, I.; Sasagawa, T.; Yamaguchi, K.; Nakahama, S.; Yamazaki, N. Synthesis of polymers with primary amino end groups, 1. Reactions of anionic living polymers with protected aminating reagents. *Makromol. Chem., Rapid Commun.*, **1982**, *3* (1), 59-63.

[14] Ueda, K.; Hirao, A.; Nakahama, S. Synthesis of polymers with amino end groups. 3. Reactions of anionic living polymers with α-halo-ω-aminoalkanes with a protected amino functionality. *Macromolecules*, **1990**, *23* (4), 939-945.

[15] Hirao, A.; Tohoyama, M.; Nakahama, S. Synthesis of End-Functionalized Polymers by Means of Living Anionic Polymerization. 8. Reactions of Living Anionic Polymers with α, ω-Dihaloalkanes. *Macromolecules*, **1997**, *30* (12), 3484-3489.

[16] Hirao, A.; Nagahama, H.; Ishizone, T.; Nakahama, S. Synthesis of polymers with carboxy end groups by reaction of polystyryl anions with 4-bromo-1,1,1-trimethoxybutane. *Macromolecules*, **1993**, *26* (9), 2145-2150.

[17] Wyman, D. P.; Allen, V. R.; Altares, T. Reaction of polystyryllithium with carbon dioxide. *J. Polym. Sci. A Gen. Pap.*, **1964**, *2* (10), 4545-4550.

[18] Månsson, P. Reactions of polystyryl anions with carbon dioxide and oxygen. Analysis of products by silica gel chromatography. *J. Polym. Sci. Polym. Chem. Ed.*, **1980**, *18* (6), 1945-1956.

[19] Quirk, R. P.; Yin, J.; Fetters, L. J. Carbonation and related reactions of poly(styryl)lithium. *Macromolecules*, **1989**, *22* (1), 85-90.

[20] Hirao, A.; Hayashi, M. Recent advance in syntheses and applications of well-defined end-functionalized polymers by means of anionic living polymerization. *Acta Polym.*, **1999**, *50* (7), 219-231.

[21] Handlin, D. L., JR; Bening, R. C.; Willis, C. L. Low viscosity terminally functionalized isoprene polymers. US19930160341 19931201.

[22] Shepherd, N.; Stewart, M. J. Polymerisation of olefinic-containing monomers employing anionic initiators. US19930142966 19931029.

[23] Schulz, D. N.; Halasa, A. F.; Oberster, A. E. Anionic polymerization initiators containing protected functional groups and functionally terminated diene polymers. *J. Polym. Sci. Polym. Chem. Ed.*, **1974**, *12* (1), 153-166.

[24] Weißmüller, M.; Burchard, W. Preparation and end-linking of hydroxyl-terminated polystyrene star macromolecules. *Macromol. Chem. Phys.*, **1999**, *200* (3), 541‐551.

[25] Schulz, D. N.; Halasa, A. F. Anionic polymerization initiators containing protected functional groups. II. *J. Polym. Sci. Polym. Chem. Ed.*, **1977**, *15* (10), 2401‐2410.

[26] Yoo, T.; Henning, S. K. Synthesis and Characterization of Farnesene-Based Polymers. *Rubber Chem. Technol.*, **2017**, *90* (2), 308‐324.

[27] Bailey, W. F.; Brubaker, J. D.; Jordan, K. P. Effect of solvent and temperature on the lithium‐iodine exchange of primary alkyl iodides: reaction of t-butyllithium with 1-iodooctane in heptane‐ether mixtures. *Journal of Organometallic Chemistry*, **2003**, *681* (1-2), 210‐214.

[28] Dierkes, W.; Blume, A. Silica Reinforcement. In *Encyclopedia of Polymeric Nanomaterials*; Kobayashi, S., Müllen, K., Eds.; Springer Berlin Heidelberg, **2020**; pp 1‐7.

[29] Liu, X.; Zhao, S.; Zhang, X.; Li, X.; Bai, Y. Preparation, structure, and properties of solution-polymerized styrene-butadiene rubber with functionalized end-groups and its silica-filled composites. *Polymer*, **2014**, *55* (8), 1964‐1976.

[30] Medalia, A. I. Heat Generation in Elastomer Compounds: Causes and Effects. *Rubber Chemistry and Technology*, **1991**, *64* (3), 481‐492.

[31] Tanis, S. P.; Raggon, J. W. Pyrroles as terminators in cationic cyclizations. The preparation of 5,6,7,8-tetrahydroindolizidines and 6,7,8,9-tetrahydro-5H-pyrrolo[1,2-a]azepines. *J. Org. Chem.*, **1987**, *52* (5), 819‐827.

[32] Procter, G.; Russell, A. T.; Murphy, P. J.; Tan, T. S.; Mather, A. N. Epoxy-silanes in organic synthesis. *Tetrahedron*, **1988**, *44* (13), 3953‐3973.

[33] Lioux, T.; Drocourt, D.; Vernejoul, F.; Tiraby, G.; Perouzel, E. Conjugated TLR7 and/or TLR8 and TLR2 polycationic agonists. EP20130305207 20130222.

[34] Gold, L. Statistics of Polymer Molecular Size Distribution for an Invariant Number of Propagating Chains. *The Journal of Chemical Physics*, **1958**, *28* (1), 91‐99.

[35] Worsfold, D. J.; Bywater, S. Degree of Association of Polystyryl-, Polyisoprenyl-, and Polybutadienyllithium in Hydrocarbon Solvents. *Macromolecules*, **1972**, *5* (4), 393‐397.

[36] Morton, M.; Fetters, L. J. Homogeneous anionic polymerization. V. Association phenomena in organolithium polymerization. *J. Polym. Sci. A Gen. Pap.*, **1964**, *2* (7), 3311‐3326.

[37] Iovu, M. C.; Buzdugan, E.; Teodorescu, M.; Britchi, A. G.; Hubca, G.; Iovu, H. Copolymerization of styrene with butadiene using methyl tert -butyl ether as active center modifier. *Angew. Makromol. Chemie*, **1999**, *271* (1), 18‑23.

[38] Fuchs, D. A. H.; Hübner, H.; Kraus, T.; Niebuur, B.-J.; Gallei, M.; Frey, H.; Müller, A. H. E. The effect of THF and the chelating modifier DTHFP on the copolymerisation of *β*-myrcene and styrene: kinetics, microstructures, morphologies, and mechanical properties. *Polym. Chem.*, **2021**, *12* (32), 4632‑4642.

[39] Meier-Merziger, M.; Fickenscher, M.; Hartmann, F.; Kuttich, B.; Kraus, T.; Gallei, M.; Frey, H. Synthesis of phase-separated super-H-shaped triblock architectures: poly(l-lactide) grafted from telechelic polyisoprene. *Polym. Chem.*, **2023**, *14* (23), 2820‑2828.

[40] Meier-Merziger, M.; Fuchs, D. A. H.; Frey, H.; Müller, A. H. E. Spotlight on Methyl tert-Butyl Ether - Underrated or Overlooked? Unveiling Its Role for Living Anionic Polymerization. *In Revision*, **2024**.

[41] Lohmeijer, B. G. G.; Pratt, R. C.; Leibfarth, F.; Logan, J. W.; Long, D. A.; Dove, A. P.; Nederberg, F.; Choi, J.; Wade, C.; Waymouth, R. M.; Hedrick, J. L. Guanidine and Amidine Organocatalysts for Ring-Opening Polymerization of Cyclic Esters. *Macromolecules*, **2006**, *39* (25), 8574‑8583.

[42] Frick, E. M.; Hillmyer, M. A. Synthesis and characterization of polylactide-block-polyisoprene-block-polylactide triblock copolymers: new thermoplastic elastomers containing biodegradable segments. *Macromol. Rapid Commun.*, **2000**, *21* (18), 1317‑1322.

[43] Frick, E. M.; Zalusky, A. S.; Hillmyer, M. A. Characterization of Polylactide-b-polyisoprene-b-polylactide Thermoplastic Elastomers. *Biomacromolecules*, **2003**, *4* (2), 216‑223.

[44] Fang, C.; Wang, X.; Chen, X.; Wang, Z. Mild synthesis of environment-friendly thermoplastic triblock copolymer elastomers through combination of ring-opening and RAFT polymerization. *Polym. Chem.*, **2019**, *10* (26), 3610‑3620.

[45] Gramlich, W. M. Toughening Polylactide with Phase-Separating Complex Copolymer Architectures. *Macromol. Chem. Phys.*, **2015**, *216* (2), 145‑155.

[46] Krishnan, S.; Pandey, P.; Mohanty, S.; Nayak, S. K. Toughening of Polylactic Acid: An Overview of Research Progress. *Polymer-Plastics Technology and Engineering*, **2016**, *55* (15), 1623‑1652.

[47] Dreier, P.; Ahn, J.; Chang, T.; Frey, H. End Group Functionality of 95-99%: Epoxide Functionalization of Polystyryl-Lithium Evaluated via Solvent Gradient Interaction Chromatography. *Macromol. Rapid Commun.*, **2022**, e2200560.

Supporting Information

1. Experimental Section

1.1 Materials

All materials were purchased from common suppliers (*Sigma Aldrich, Alfa Aesar, Acros, TCI, VWR, Thermo Fisher, Fisher Scientific*, and *Deutero*) and used without further treatment, unless otherwise stated.

1.2. Instruments

Nuclear magnetic resonance spectroscopy (NMR). Experiments (^{1}H, ^{13}C and 2D) were performed on a *Bruker Avance II* 400 MHz instrument, equipped with: *SampleXPress 60* autosampler, a 5 mm *BBFO-head* with z-gradient and ATM or on a *Bruker Avance III HD* 300 MHz instrument, equipped with: *BACS 60* autosampler, 5 mm *BBFO-head* with z-gradient and ATM by *Bruker*, United States. All samples were measured in deuterated solvents: $CDCl_3$, DMSO-d_6, and benzene-d_6 from *Deutero GmbH*. Evaluation of the data was done using the software *MestReNova* by Mestrelab Research S.L., Spain.

Size-exclusion chromatography (SEC). Molar mass and molar mass distribution was measured on an *Agilent 1260 Infinity II* setup by *Agilent Technologies*, United States, using a *MZ-Gel SDPlus e5/e3/100* column-set provided by *MZ-Analysentechnik,* Mainz, Germany. The system was operated with tetrahydrofuran (THF) and all samples were normalized to an internal toluene standard. Calibration was done using a 1,4-polyisoprene calibration set, purchased from *Polymer Standard Service*, Mainz, Germany.

Differential-scanning calorimetry (DSC). Measurements were performed on a *TA Instruments DSC 250* instrument connected to a *TA Instruments RCS 90* cooling system from *Waters Corporation*, United States. A heating rate of 10 $K \cdot min^{-1}$ was applied, and the second heating curve of each measurement was used for the determination. Evaluation of the data was done using the software *TRIOS* by *Waters Corporation*, United States.

1.3 Initiator Synthesis

4-(Iodomethyl)-2,2-dimethyl-1,3-dioxolane (DiOx-I). The synthesis is based on a reported patent procedure.[1] A round-bottomed flask was loaded with 295 mL dry toluene, 14.7 g (0.11 mol, 1 eq) isopropylidene glycerol, 22.8 g (0.33 mol, 3 eq) imidazole, 35.1 g (0.13 mol,

1.2 eq) triphenylphosphine, and 36.8 g (0.15 mol, 1.3 eq) iodine in an argon-atmosphere. The mixture was stirred for 3 hours at 90 °C. The mixture was allowed to reach room temperature and toluene was removed in vacuo. The residue was mixed with 250 mL dichloromethane (DCM) and washed with 100 mL saturated $Na_2S_2O_3$ solution, water, and brine. The organic layer was dried over magnesium sulfate and concentrated in vacuo. The product was purified *via* fractional distillation ($T_{b,product}$= 120 °C at 19-30 mbar). 15 g (55.7%) DiOx-I was obtained as a colorless liquid and characterized *via* ^{1}H and COSY NMR spectroscopy, see **Figure S1** and **S2**. ^{1}H NMR (300 MHz, $CDCl_3$, δ[ppm]): 4.34 – 4.20 (m, 1H, c), 4.14 (dd, $^2J_{d,d'}$=8.6 Hz, $^3J_{d,c}$=6.0 Hz, 1H, d), 3.78 (dd, $^2J_{d',d}$=8.7 Hz, $^3J_{d',c}$=5.5 Hz, 1H, d'), 3.25 (dd, $^2J_{b,b'}$=9.8 Hz, $^3J_{b,c}$=4.6 Hz, 1H, b), 3.13 (dd, $^2J_{b',b}$=9.9 Hz, $^3J_{b',c}$=8.5 Hz, 1H, b'), 1.45 (s, 3H, a), 1.34 (s, 3H, a').

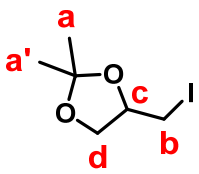

4-(4-Hydroxybutyl)-2,2-dimethyl-1,3-dioxolane (DiOxHex-OH). The synthesis is based on a procedure reported by Procter et al.[2] A round-bottomed flask was loaded with 8 g (0.06 mol, 1 eq) 1,2,3-hexanetriol, 100 mL dry acetone, and 0.98 g (0.005 mol, 0.01 eq) p-toluene sulfonic acid in an argon-atmosphere. The reaction was stirred at room temperature for 21 hours. Then, solid sodium hydrogen carbonate was added, and the mixture was stirred for two hours. This was followed by filtration and the removal of acetone in vacuo. The product was distilled at 96 °C and $5 \cdot 10^{-2}$ mbar and yielded 9.2 g (86%) of the pure DiOxHex-OH as a colorless liquid. Characterization was done *via* ^{1}H, ^{13}C, and 2D NMR spectroscopy, see **Figure S3-S6**. ^{1}H NMR (400 MHz, DMSO-d_6, δ[ppm]): 4.31 (t, $^3J_{OH,b}$=5.2 Hz, 1H, OH), 3.99 – 3.86 (m, 2H, f, g), 3.40 – 3.27 (m, 3H, g', b), 1.53 – 1.26 (m, 6H, c, d, e), 1.24 (s, 3H, a), 1.19 (s, 3H, a'); ^{13}C NMR (100 MHz, DMSO-d_6, δ[ppm]): 107.8 (H), 75.5 (F), 68.8 (G), 60.6 (B), 33.1 (c), 32.5 (E), 26.9 (A), 25.7 (A'), 22.0 (D).

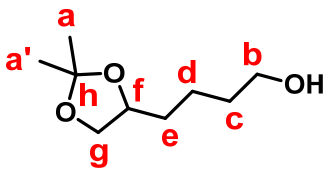

4-(4-Iodobutyl)-2,2-dimethyl-1,3-dioxolane (DiOxHex-I). First, the hydroxyl group of DiOxHex-OH was transferred to the respective tosylate, **DiOxHex-Tos**, according to a reported procedure.[3] Therefore, 16 g (0.09 mol, 1 eq) DiOxHex-OH was mixed with 50 mL dry pyridine and immersed in an ice-water bath under an argon-atmosphere. Then, 21.9 g (0.1 mol, 1.25 eq) *para*-toluene sulfonyl chloride was added. The reaction was stirred for 2 hours at 0 °C and eventually allowed to reach room temperature. The reaction solution was casted into an ice/saturated hydrochloric acid solution (300 g/300 mL) mixture and extracted with 600 mL diethyl ether. The organic layer was swiftly washed with 1 molar hydrochloric acid solution, water, saturated sodium bicarbonate, and brine. The organic layer was dried using sodium sulfate and concentrated in vacuo to give 29 g (97%) of DiOxHex-Tos as colorless liquid that was used without further purification.

DiOxHex-Tos was transferred to the respective iodo-derivate following a procedure reported by Tanis et al.[3] A 250 mL Schlenk-flask was loaded with 183 mL dry acetone and 15 g (0.05 mol, 1 eq) DiOxHex-Tos in an argon-atmosphere. 7.5 g sodium iodide was added, and the solution was heated under reflux for 5 hours. After cooling to room temperature, the solution was filtered, and the filtrate mixed with 250 mL diethyl ether. The organic layer was washed with, each 200 mL of 10% sodium thiosulfate solution, water, saturated sodium bicarbonate solution, and brine. The organic layer was dried over sodium sulfate and concentrated in vacuo. The residue was bulb-to-bulb distilled at $5 \cdot 10^{-2}$ mbar and 200 °C. The product was distilled a second time at $1 \cdot 10^{-3}$ mbar and 80-100 °C. The resulting pale-yellow liquid was passed through alkaline aluminum oxide using ethyl acetate and concentrated to yield 5.64 g (43%) pure DiOxHex-I as a colorless liquid. It was characterized using ^{1}H, ^{13}C, and 2D NMR spectroscopy, **Figure S7-S10**. ^{1}H NMR (400 MHz, $CDCl_3$, δ[ppm]): 4.16 – 4.02 (m, 2H, g, f), 3.52 (t, $^{3}J_{g',f}$=7.1 Hz, 1H, g'), 3.20 (t, $^{3}J_{b,c}$=7.0 Hz, 2H, b), 1.94 – 1.82 (m, 2H, c), 1.71 – 1.43 (m, 4H, d, e), 1.42 (s, 3H, a), 1.36 (s, 3H, a'); ^{13}C NMR (100 MHz, $CDCl_3$, δ[ppm]): 108.8 (H), 75.8 (F), 69.5 (G), 33.4 (C), 32.6 (E), 27.0 (A), 26.8 (D), 25.8 (A'), 6.6 (B).

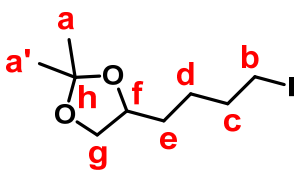

1.4 Initiator activation

The "active", lithiated species was obtained using the respective precursors, DiOx-I and DiOxHex-I. The synthesis follows the procedure reported by Bailey et al.[4] First, the respective iodine dioxolane structure was dried over calcium hydride for 24 hours. After removal of hydrogen by three *freeze-pump-thaw* cycles, the dried structures were distilled and transferred into an argon-filled glove box. Likewise, *n*-heptane and methyl *tert*-butyl ether (MTBE) were dried using *sec*-butyl lithium (BuLi) and diphenyl ethylene (DPE), freshly distilled and transferred into the glove box. A 0.1 mol·L^{-1} solution of DiOx-I and DiOxHex-I were prepared with a volume ratio of *n*-heptane:MTBE of [19:1]. Thereafter, the solutions were removed from the glovebox in a sealed anionic reaction-flask, equipped with a septum, and placed into a -78 °C acetone/N_2-cooling bath. Then, 2.2 eq of *tert*-BuLi solution (1.7 mol·L^{-1}) was slowly added using a syringe and the solution was stirred for 1 hour. A direct formation of colorless precipitate was observed. Then the solution was either quenched with methanol or isopropyl alcohol, for further investigation, or transferred back into the glove box and used as initiator stock solution for the polymerization of isoprene.

1.5 Anionic Polymerization

All glassware was flame-dried before usage. Isoprene was dried over calcium hydride for 24 hours and hydrogen was removed *via* three *freeze-pump-thaw* cycles. Then, isoprene was transferred into a new empty flask *via* cryotransfer and transferred into an argon-filled glove box. Cyclohexane, MTBE, and 2,2-ditetrahydrofurfuryl propane (DTHFP) were separately dried using *sec*-BuLi and DPE and freshly distilled directly before usage. All anionic polymerizations were performed inside an argon-filled glove box. Polymers were prepared on a 1-3 g scale and a monomer concentration of 10-20 vol%. The amount of initiator, i.e. concentration, $[Ini]_0$ is given by targeted molar mass (M_n), the initial monomer concentration $[M]_0$ and the monomers molar mass, $M_{mon.}$ following, $M_n = [M]/[Ini]\cdot M_{mon.}$. Mixtures of monomer, solvent, and polar additives were prepared and freshly activated DiOxHex-Li initiator solution was used to initiate the polymerization. The polymerizations were performed overnight and terminated by the addition of degassed methanol or isopropyl alcohol. The polymers were precipitated in isopropyl alcohol, and isolated *via* centrifugation and decantation. After drying in vacuo, the polymers were characterized *via* SEC, NMR spectroscopy, MALDI-ToF MS, and DSC.

1.6 Cleavage of Ketal Protecting Group

Cleavage of the ketal protecting groups was conducted according to reported procedures using the ion-exchange resin DOWEX®.[5] First, the resin was activated and washed using concentrated hydrochloric acid. The polymer was dissolved in dichloromethane (10 mL for 1.5 g polymer) and 1 g DOWEX® was added. Thereafter, methanol was added until the polymer was just barely maintained in solution. The solution was stirred for 15 hours, filtered, and the polymer was precipitated in isopropyl alcohol. The samples were characterized *via* SEC and NMR spectroscopy and the deprotected low M_n-sample (**P-2***) was additionally investigated *via* MALDI-ToF MS.

1.7 Organocatalyzed ROP of LL-dilactide

1,8-Diazabicyclo[5.4.0]undec-7-en (DBU) was dried over calcium hydride for 24 hours and hydrogen was removed *via* three *freeze-pump-thaw* cycles. DBU was distilled and transferred to an argon-filled glovebox. LL-Dilactide (LLA) was recrystallized from toluene, dissolved in benzene and freeze-dried overnight. Separately, two $(OH)_2$-PI macroinitiators (**P-2*** and **P-4***) were freeze-dried from benzene and transferred into the glove box. PI macroinitiator and LLA were mixed and dissolved in dry dichloromethane (5 mL for 300 mg LLA). Then, DBU was added to initiate the organocatalyzed ring-opening polymerizations ([ROH]/[DBU]=5). The reactions were stirred for 1 hour at room temperature and quenched by the addition of 2 eq (compared to DBU) benzoic acid. The polymer solutions were removed from the glove box and the polymers were precipitated into isopropyl alcohol, dried from benzene and stabilized using Irganox 1520 (1000 ppm). Characterization of the copolymers was done *via* SEC, NMR and DSC.

2. Additional NMR Results

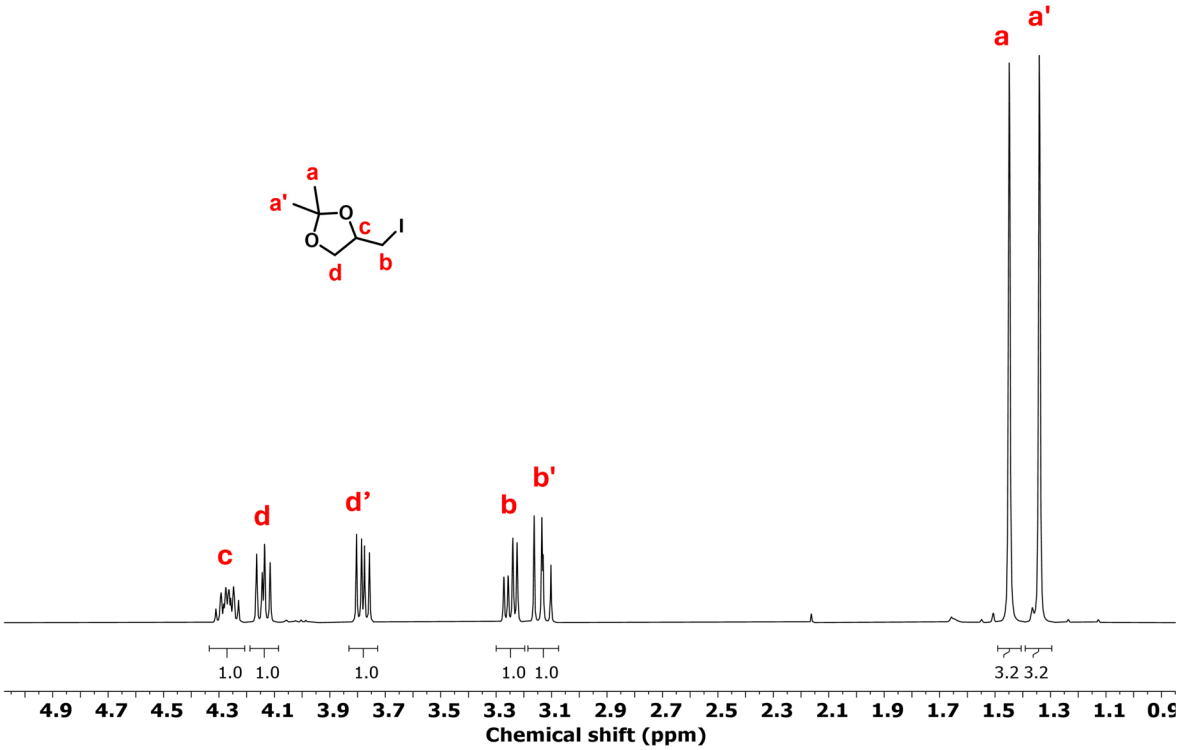

Figure S1. ^{1}H NMR spectrum of DiOx-I with all proton signals assigned, measured in $CDCl_3$, 300 MHz.

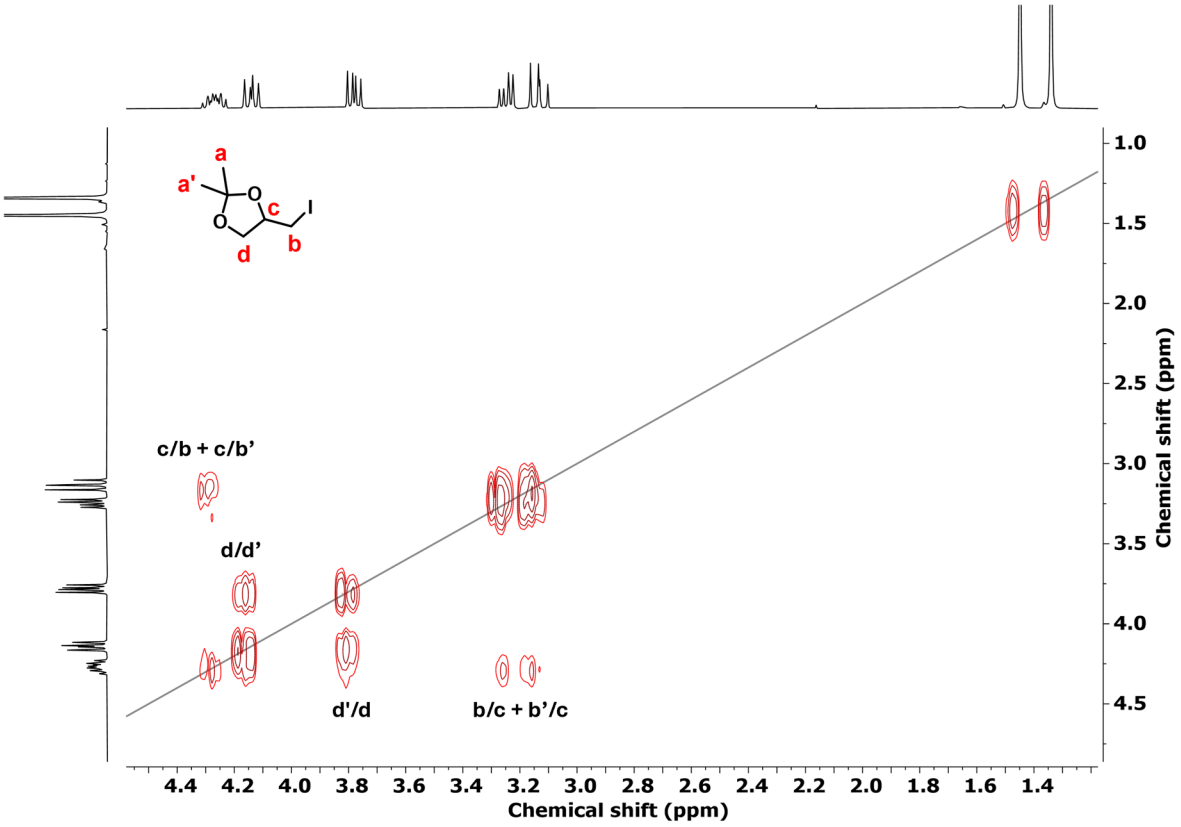

Figure S2. ^{1}H-^{1}H COSY NMR spectrum of DiOx-I with all proton couplings assigned, measured in $CDCl_3$, 300 MHz.

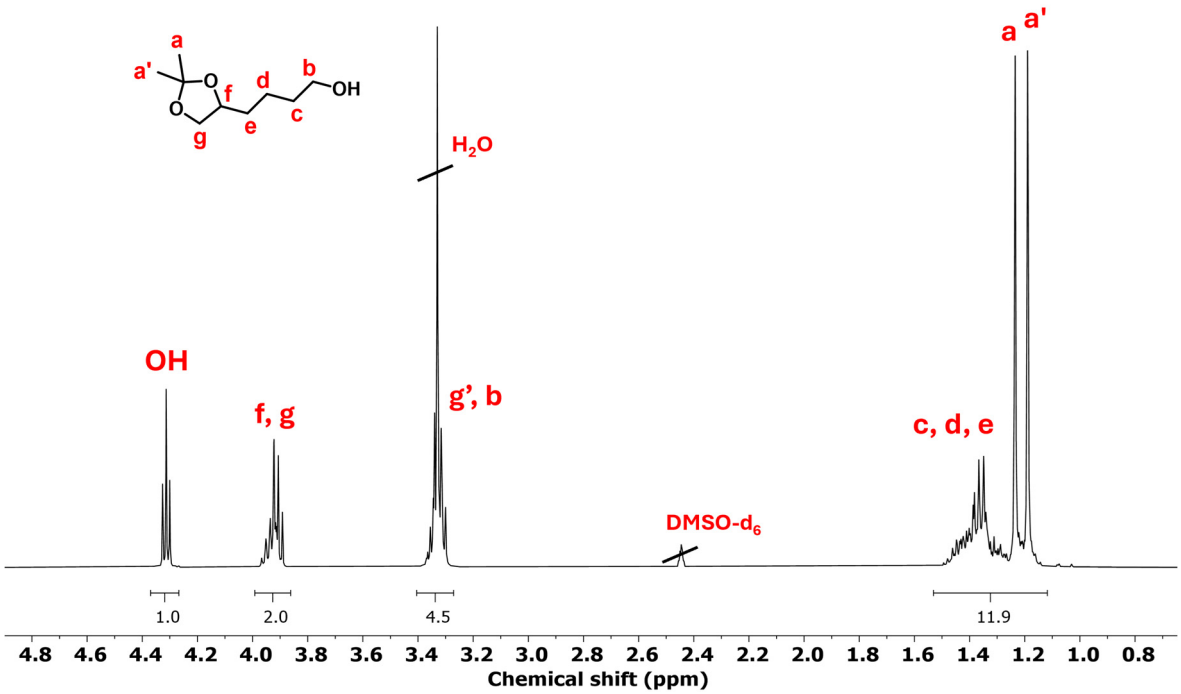

Figure S3. ^{1}H NMR spectrum of DiOxHex-OH with all proton signals assigned, measured in DMSO-d_6, 400 MHz.

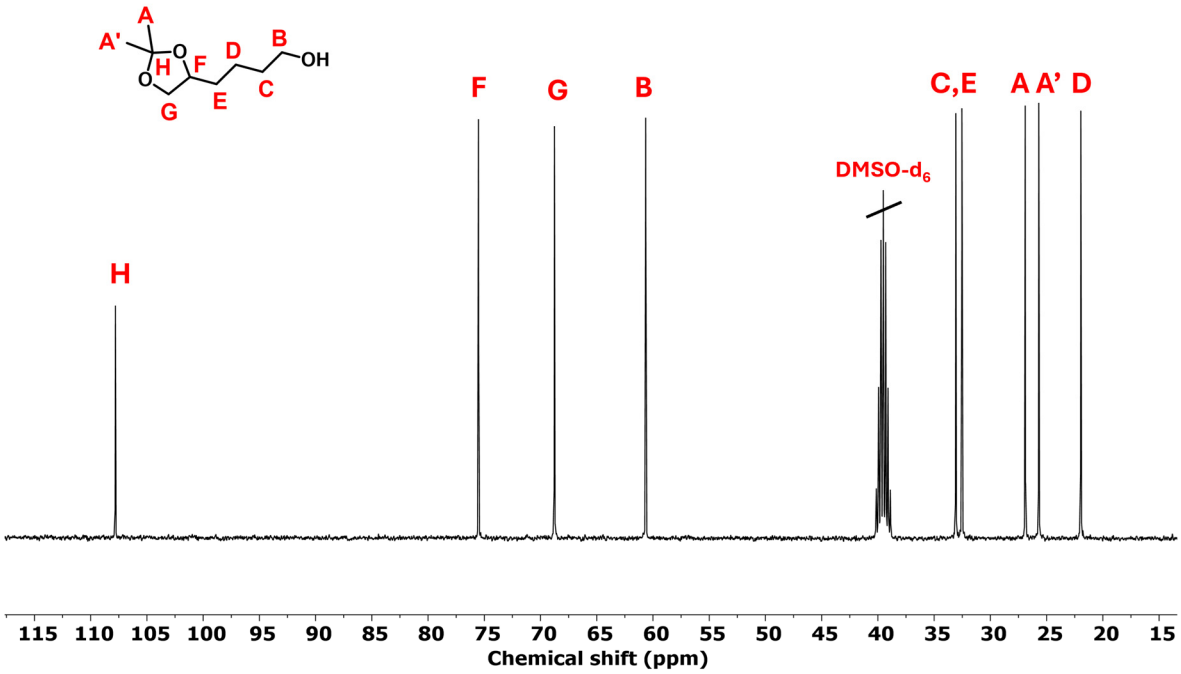

Figure S4. ^{13}C NMR spectrum of DiOxHex-OH with all carbon atom signals assigned, measured in DMSO-d_6, 100 MHz.

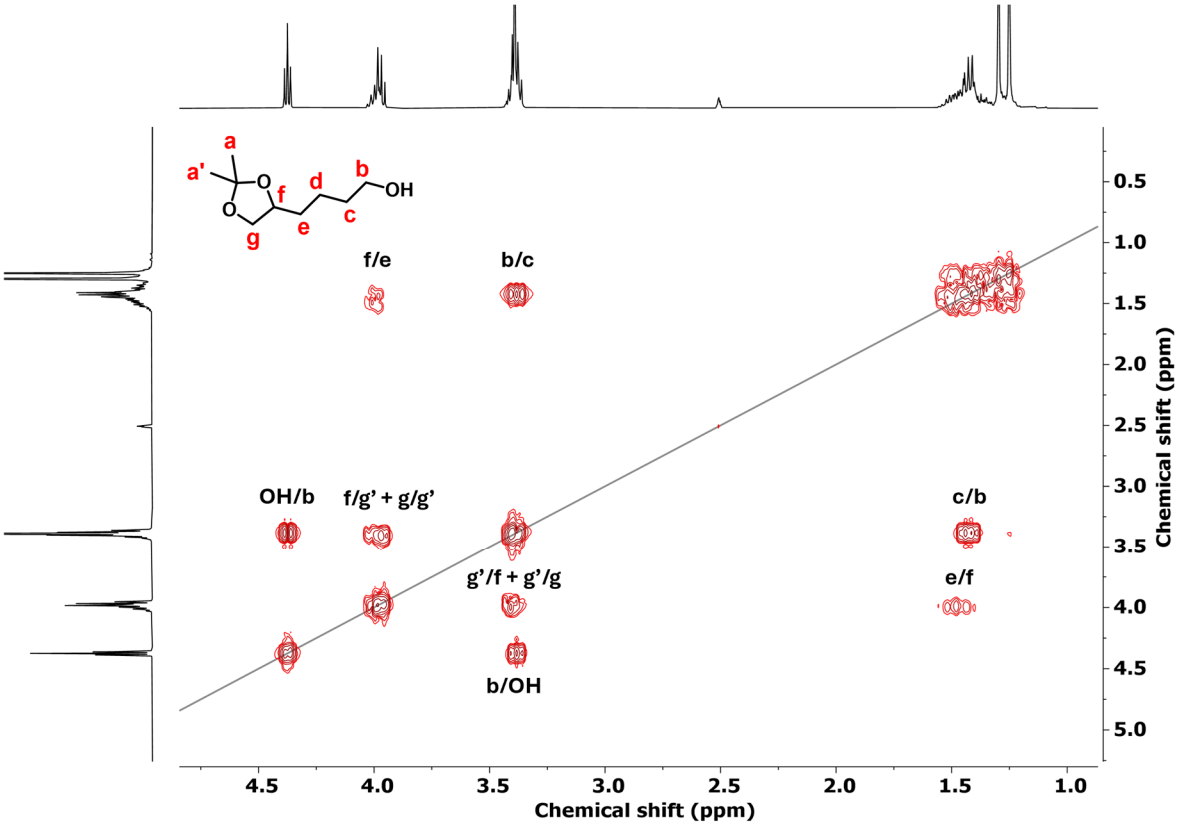

Figure S5. ^{1}H-^{1}H COSY NMR spectrum of DiOxHex-OH with all proton couplings assigned, measured in DMSO-d_6, 400 MHz.

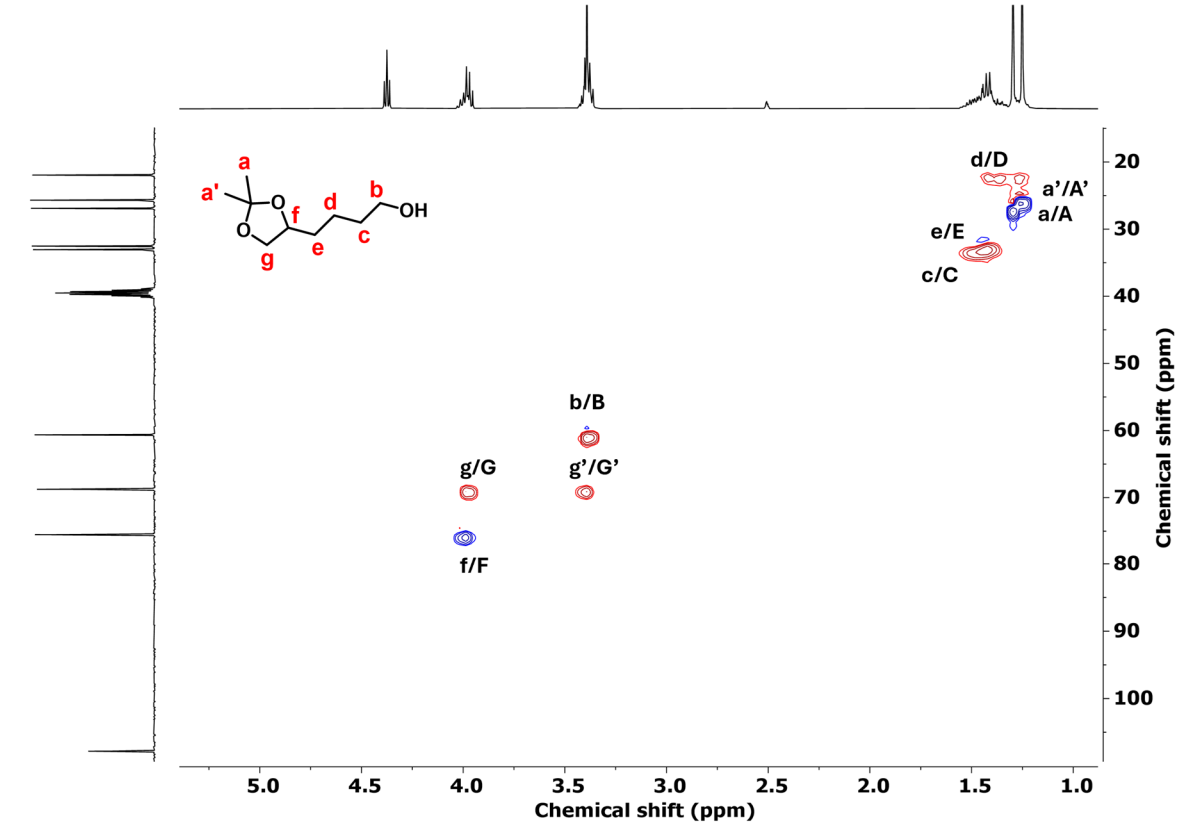

Figure S6. ^{1}H-^{13}C HSQC NMR spectrum of DiOxHex-OH with all proton/carbon couplings assigned, measured in DMSO-d_6, 400 MHz.

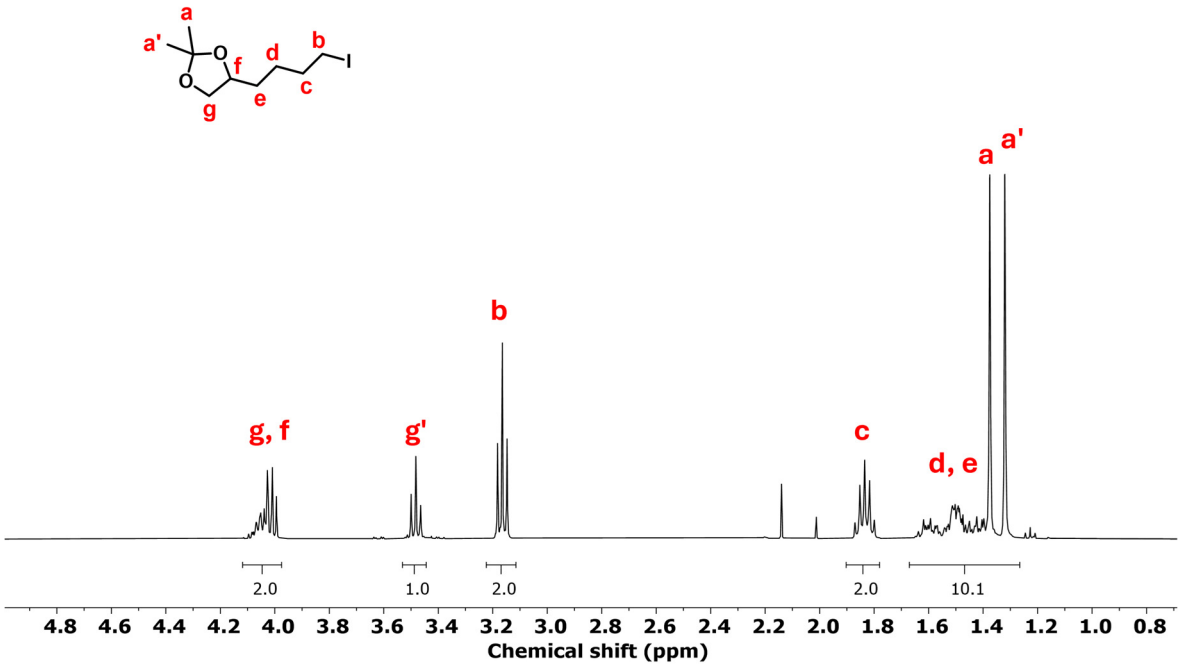

Figure S7. ^{1}H NMR spectrum of DiOxHex-I with all proton signals assigned, measured in $CDCl_3$, 400 MHz.

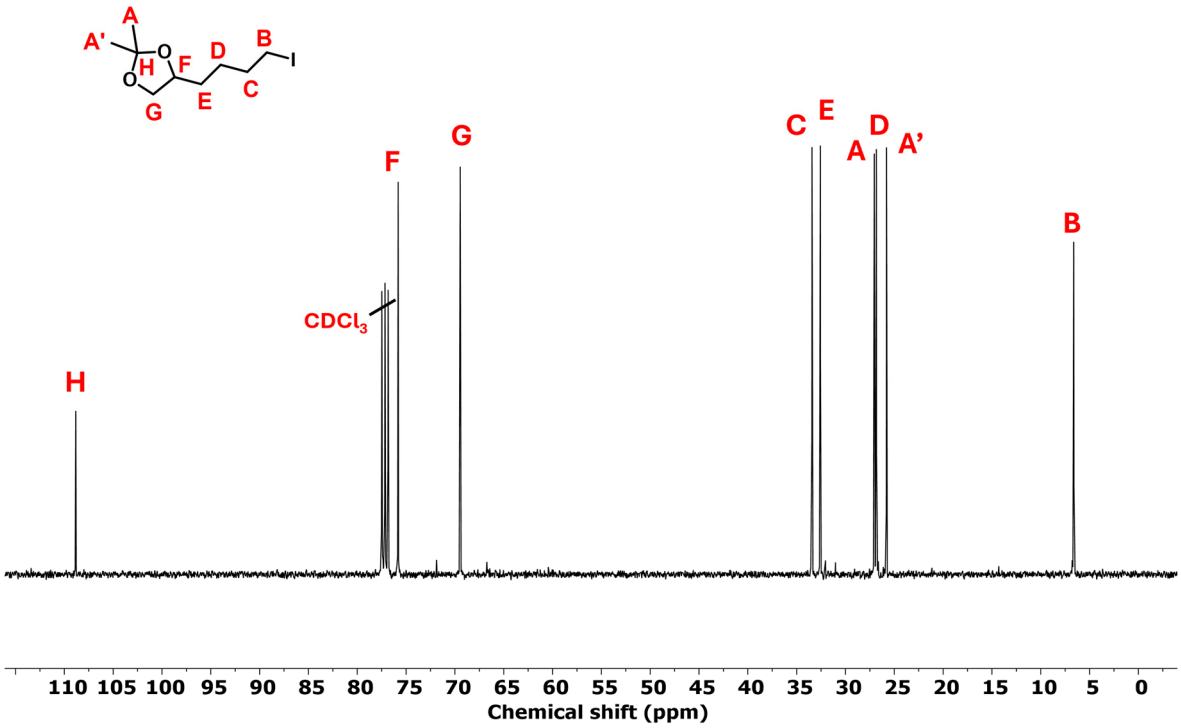

Figure S8. ^{13}C NMR spectrum of DiOxHex-I with all carbon atom signals assigned, measured in $CDCl_3$, 100 MHz.

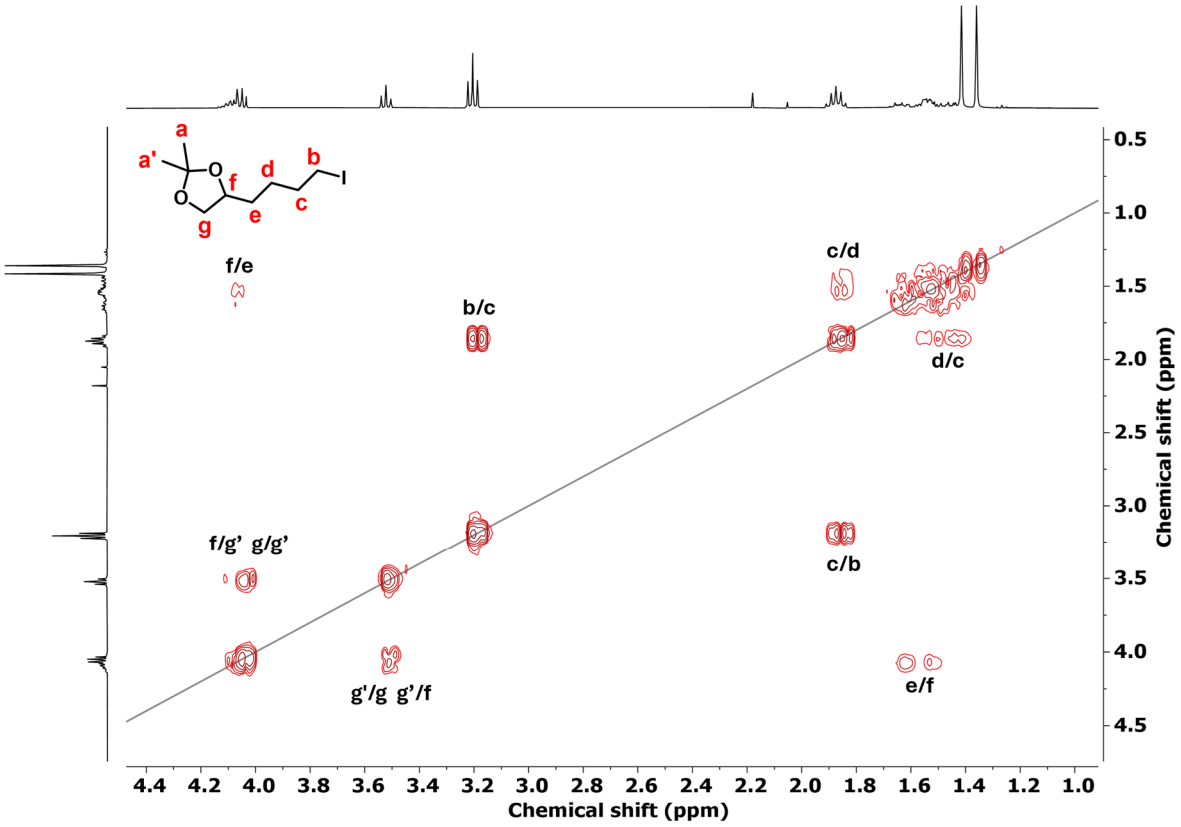

Figure S9. ^{1}H-^{1}H COSY NMR spectrum of DiOxHex-I with all proton couplings assigned, measured in $CDCl_3$, 400 MHz.

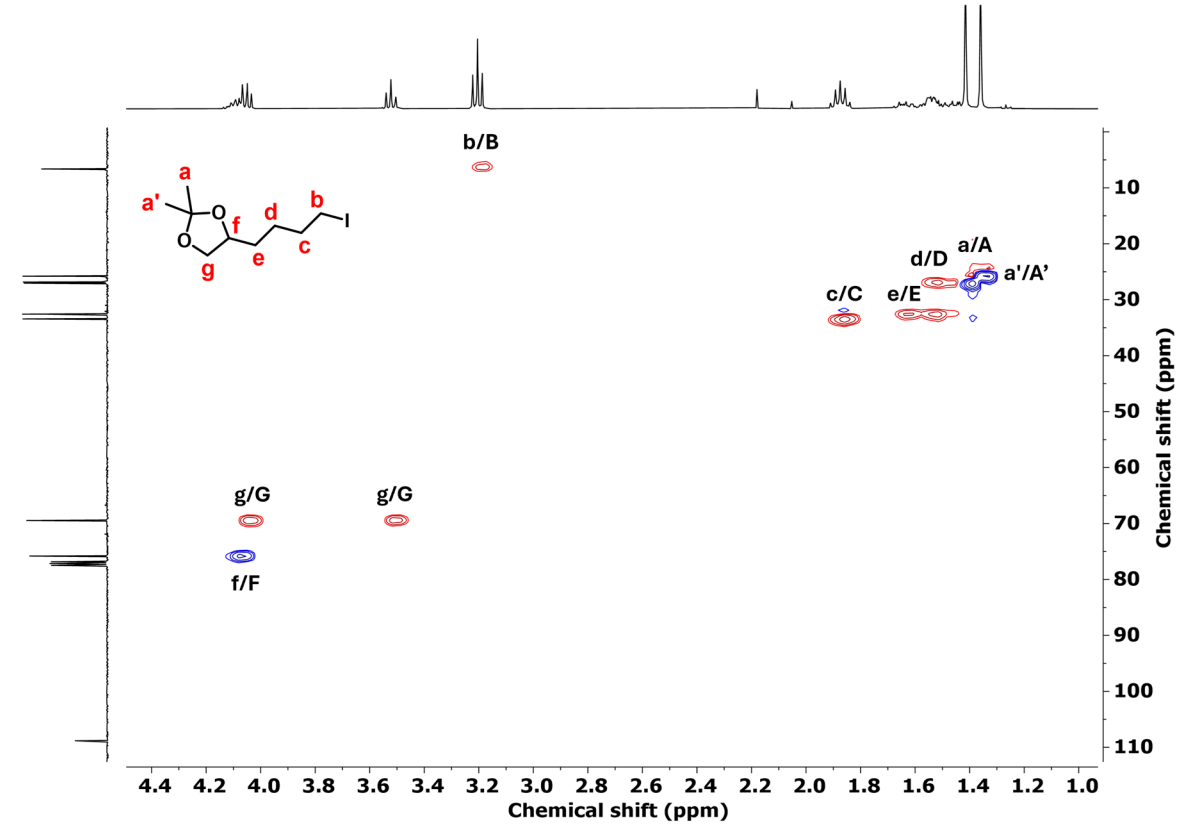

Figure S10. ^{1}H-^{13}C HSQC NMR spectrum of DiOxHex-I with all proton/carbon couplings assigned, measured in $CDCl_3$, 400 MHz.

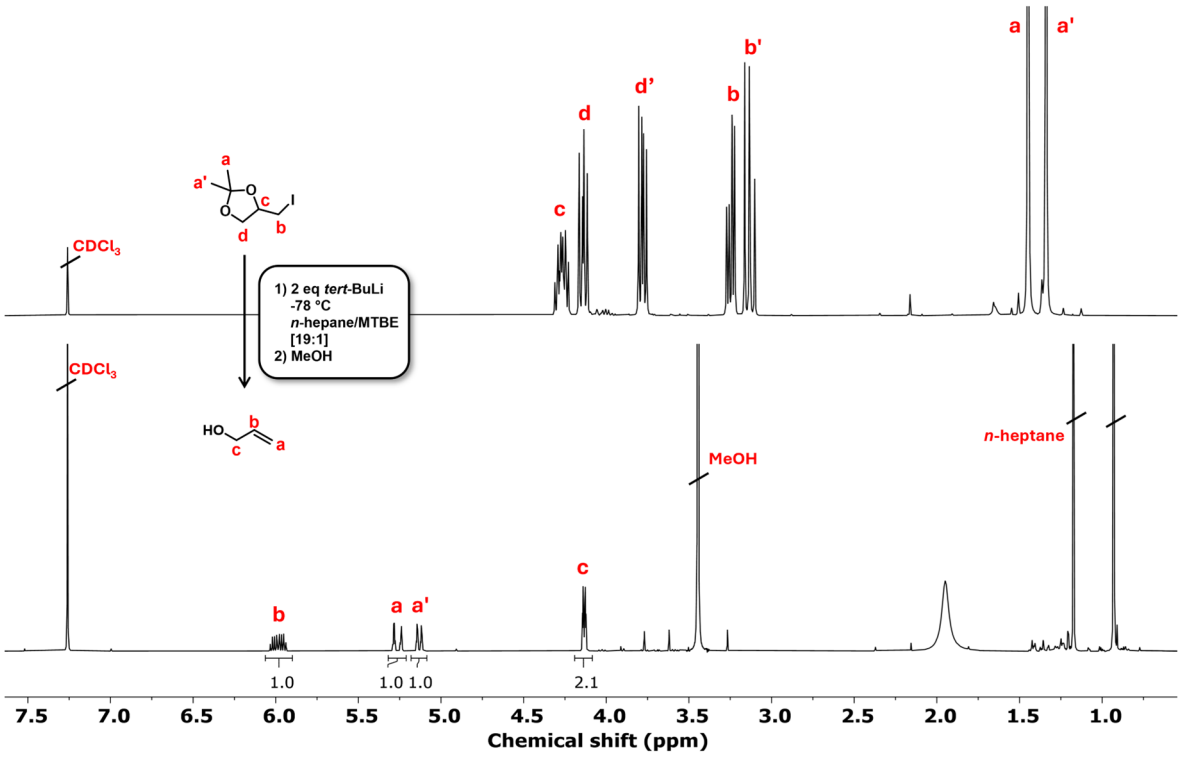

Figure S11. ^{1}H NMR investigation of the activation reaction of DiOx-I with *tert*-BuLi indicating the side reaction towards allyl-alcohol, measured in $CDCl_3$, top spectrum at 300 MHz and bottom spectrum at 400 MHz.

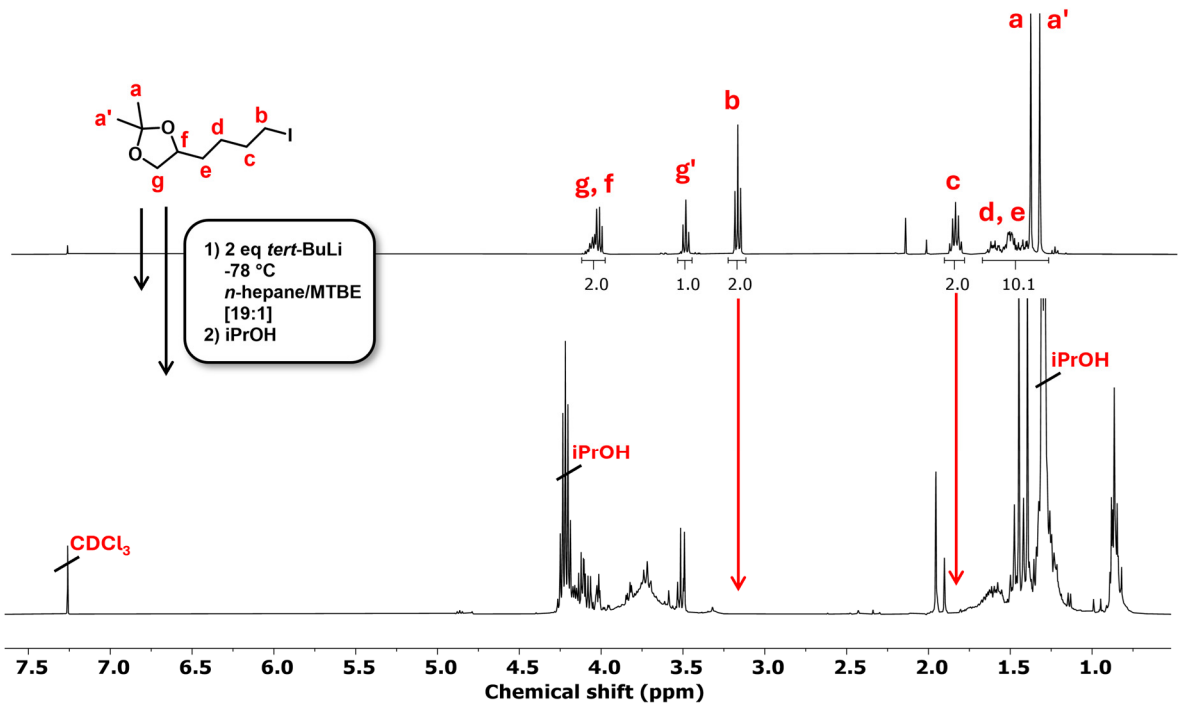

Figure S12. ^{1}H NMR investigation of activation reaction of DiOxHex-I with *tert*-BuLi, measured in $CDCl_3$, 400 MHz.

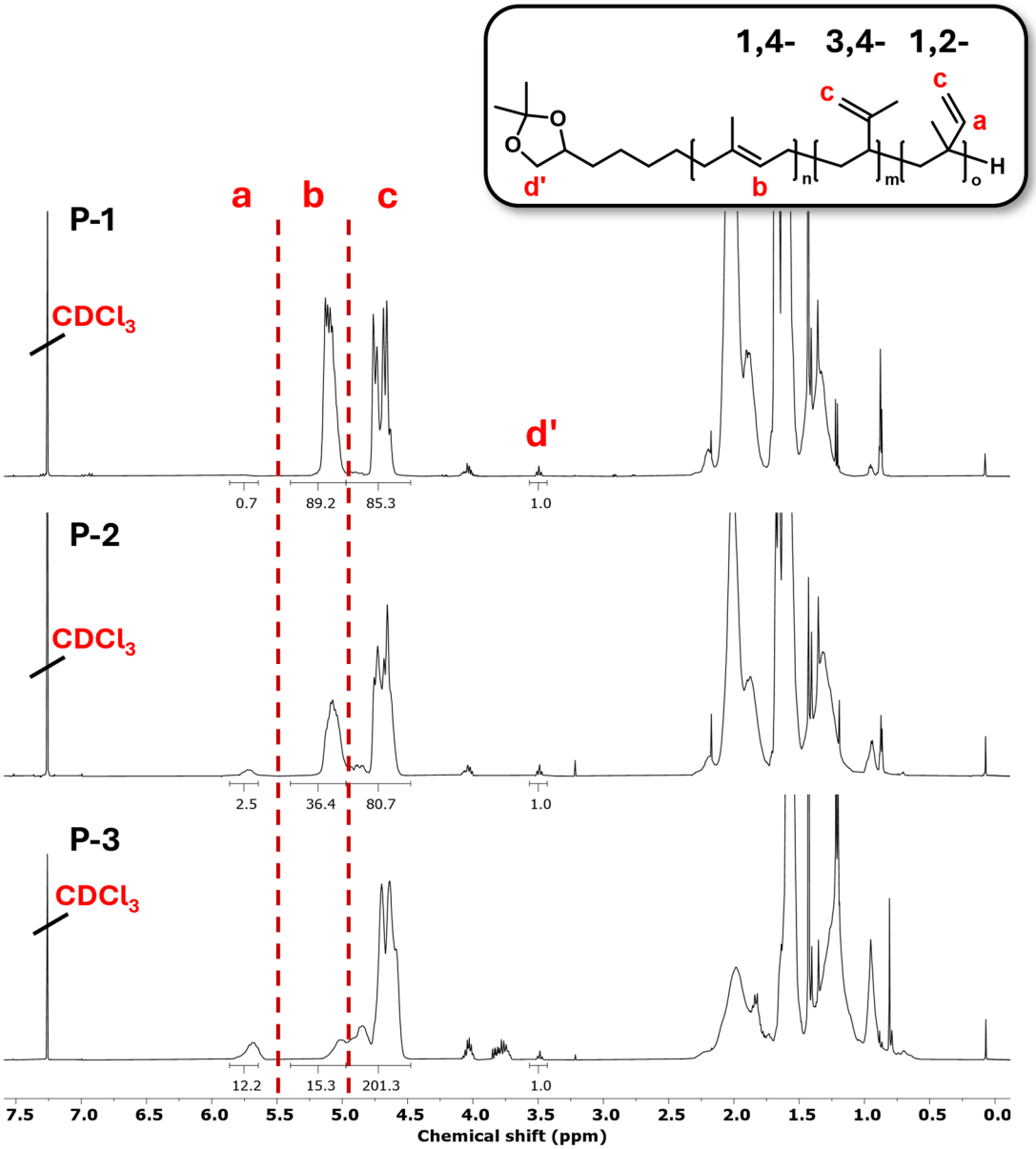

Figure S13. ^{1}H NMR spectra of polymers **P-1**, **P-2**, and **P-3** with signals assigned to characteristic protons of the different possible microstructures, measured in $CDCl_3$, 400 MHz.

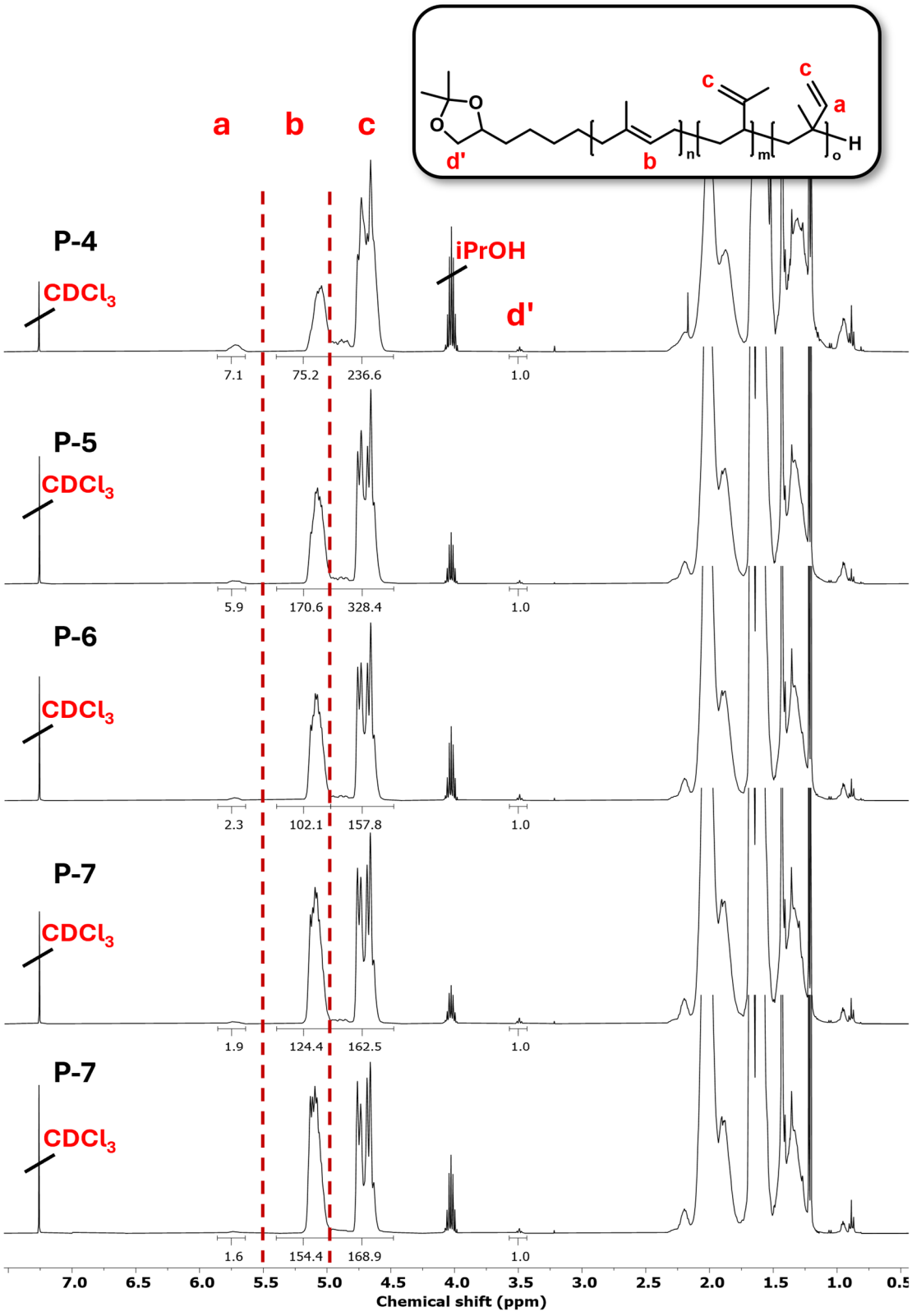

Figure S14. ^{1}H NMR spectra of polymers **P-4**, **P-5**, **P-6**, **P-7**, and **P-8** with signals assigned to characteristic protons of the different possible microstructures, measured in $CDCl_3$, 400 MHz.

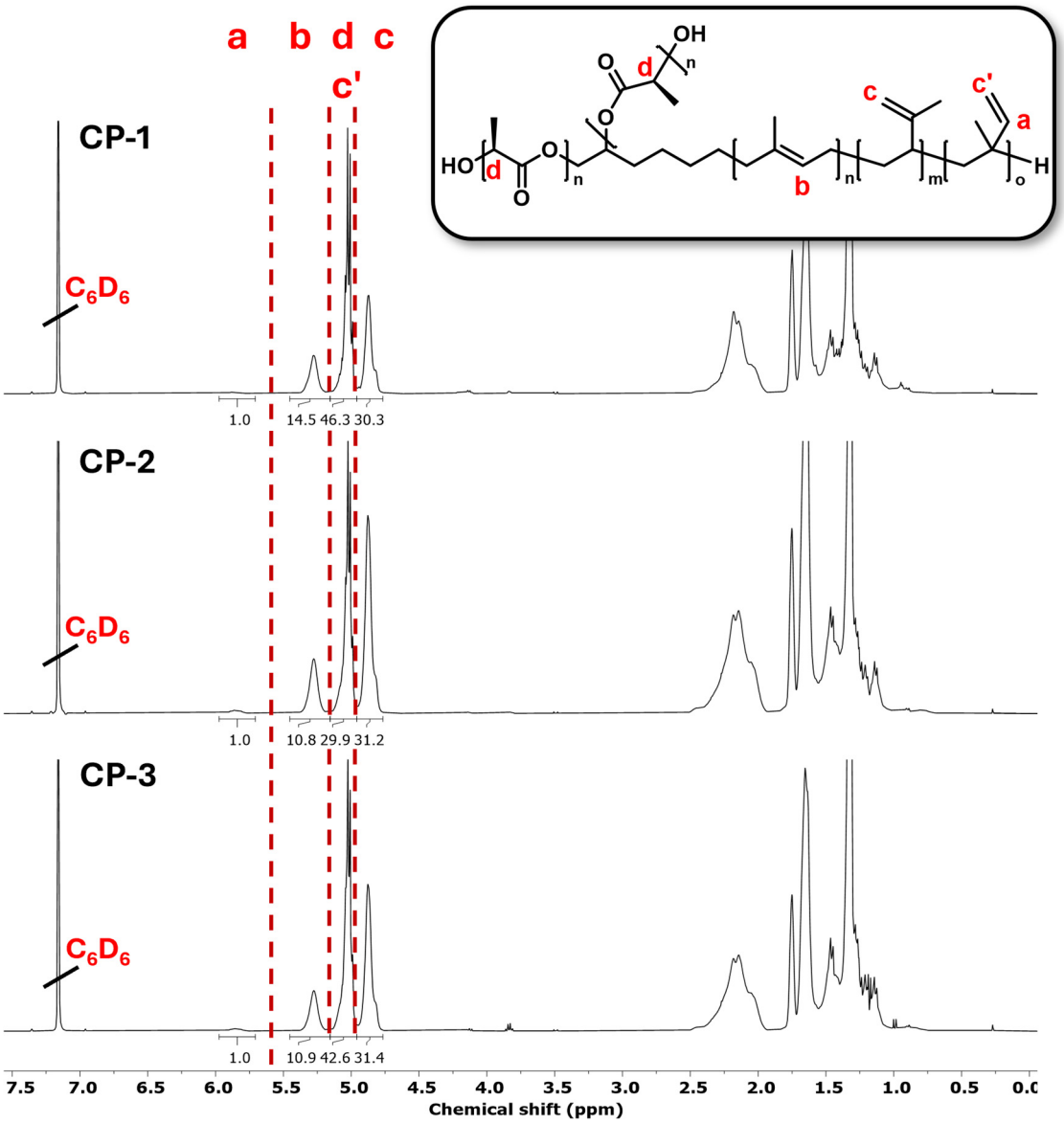

Figure S15. ^{1}H NMR spectra of copolymers **CP-1**, **CP-2**, and **CP-3** with signals assigned to characteristic protons of PLLA and PI, measured in C_6D_6, 400 MHz.

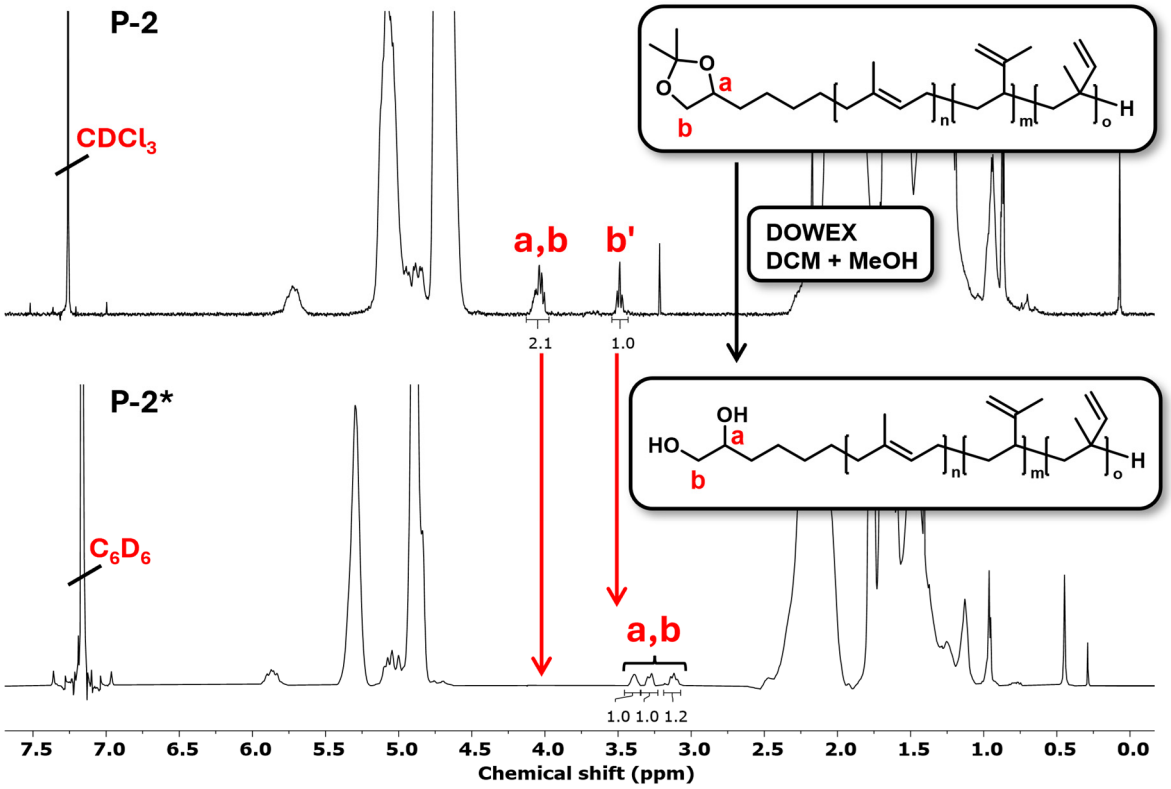

Figure S16. ^{1}H NMR investigation of cleavage reaction of **P-2** to **P-2*** using DOWEX, measured in $CDCl_3$ (top, **P-2**) and C_6D_6 (bottom, **P-2***), each at 400 MHz.

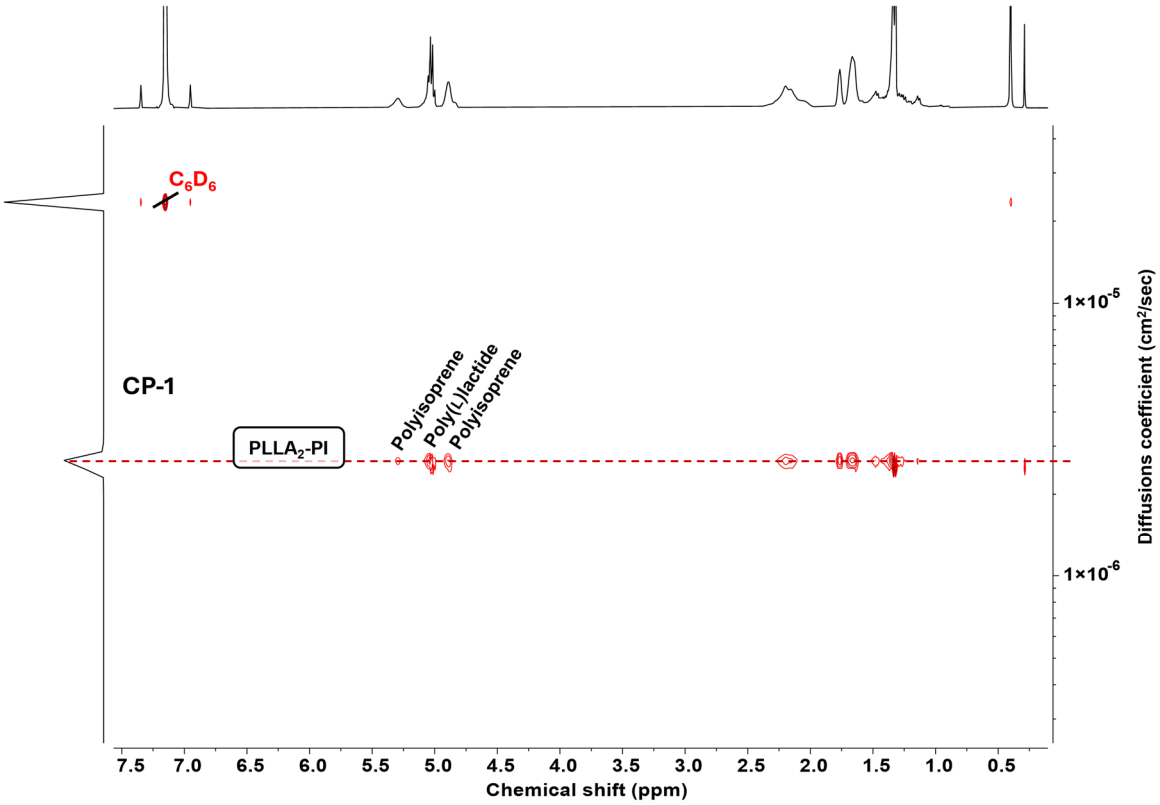

Figure S17. ^{1}H DOSY NMR spectrum of copolymer **CP-1** with signals assigned to characteristic protons of PLLA and PI, measured in C_6D_6, 400 MHz.

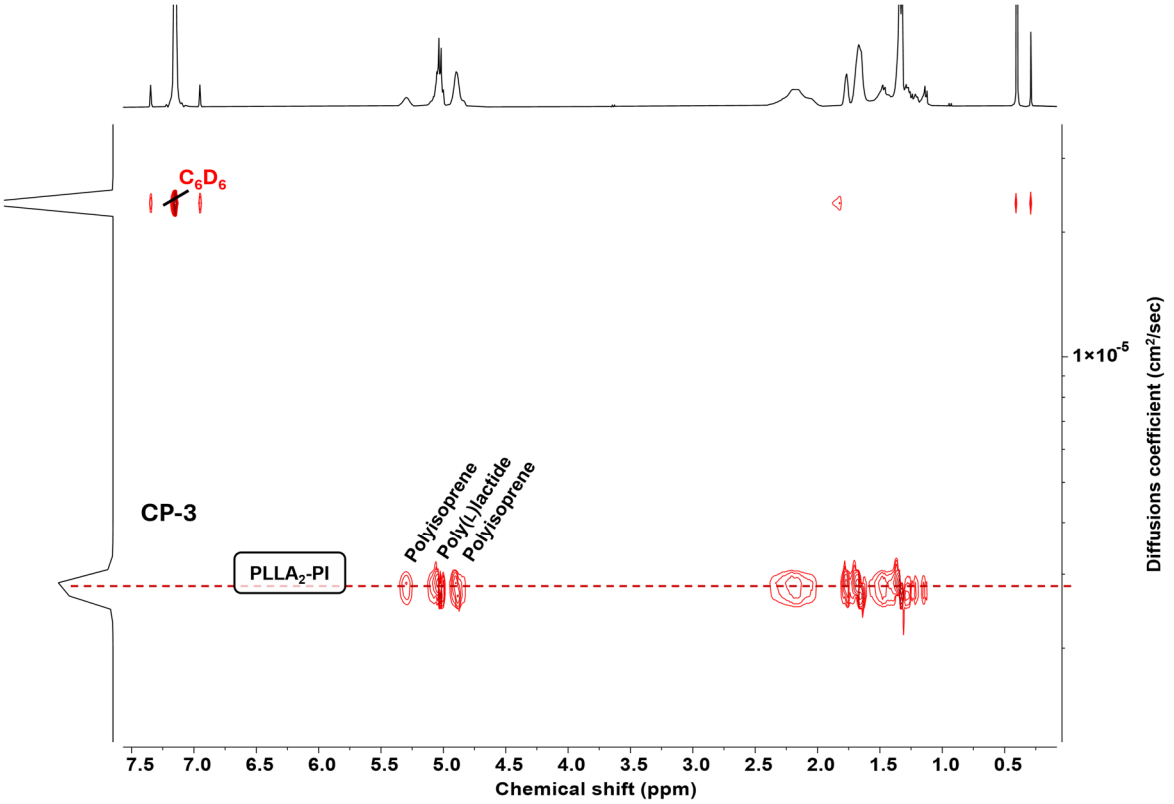

Figure S18. ^{1}H DOSY NMR spectrum of copolymer **CP-3** with signals assigned to characteristic protons of PLLA and PI, measured in C_6D_6, 400 MHz.

3. Additional DSC Results

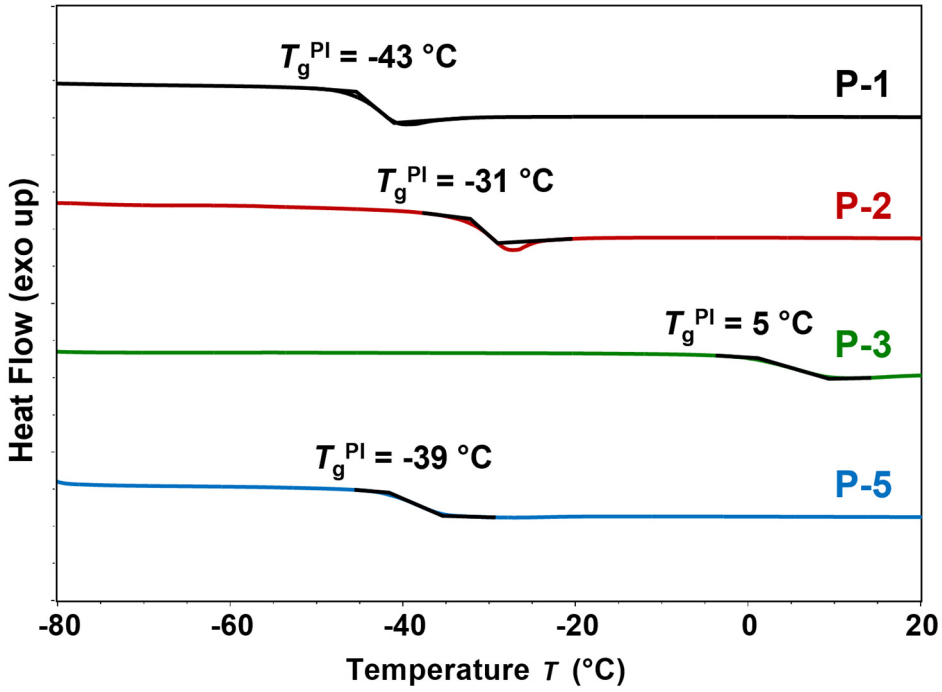

Figure S19. DSC measurements of polymers **P-1**, **P-2**, **P-3**, and **P-5**, showing the second heating curve and measured with a heating rate of 10 K·min^{-1}.

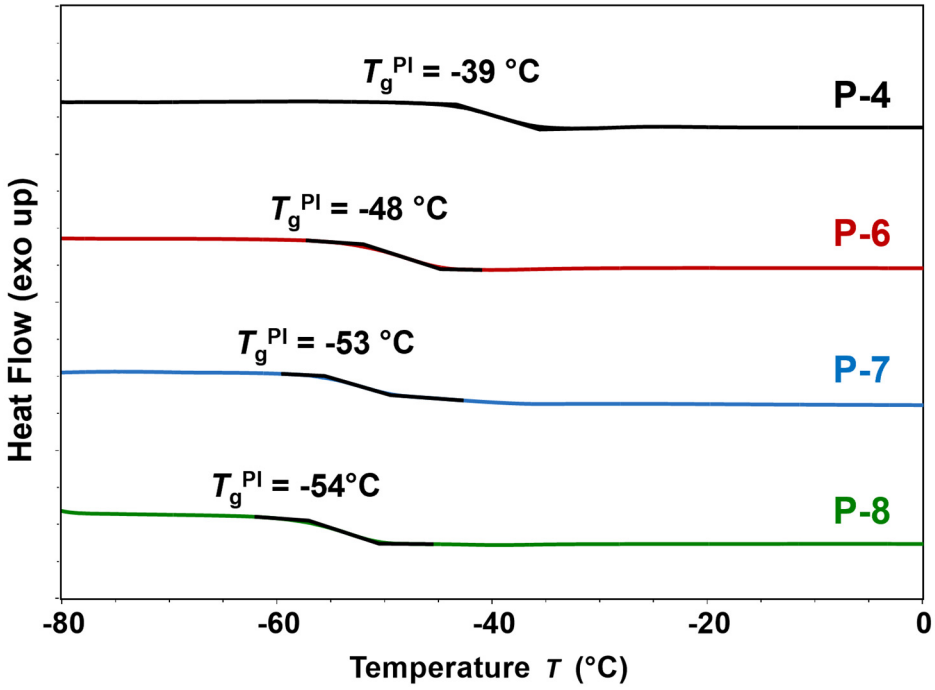

Figure S20. DSC measurements of polymers **P-4**, **P-6**, **P-7**, and **P-8**, showing the second heating curve and measured with a heating rate of 10 K·min^{-1}.

References

[1] Lioux, T.; Drocourt, D.; Vernejoul, F.; Tiraby, G.; Perouzel, E. Conjugated TLR7 and/or TLR8 and TLR2 polycationic agonists. EP20130305207 20130222.

[2] Procter, G.; Russell, A. T.; Murphy, P. J.; Tan, T. S.; Mather, A. N. Epoxy-silanes in organic synthesis. *Tetrahedron*, **1988**, *44* (13), 3953‑3973.

[3] Tanis, S. P.; Raggon, J. W. Pyrroles as terminators in cationic cyclizations. The preparation of 5,6,7,8-tetrahydroindolizidines and 6,7,8,9-tetrahydro-5H-pyrrolo[1,2-a]azepines. *J. Org. Chem.*, **1987**, *52* (5), 819‑827.

[4] Bailey, W. F.; Brubaker, J. D.; Jordan, K. P. Effect of solvent and temperature on the lithium‑iodine exchange of primary alkyl iodides: reaction of t-butyllithium with 1-iodooctane in heptane‑ether mixtures. *Journal of Organometallic Chemistry*, **2003**, *681* (1-2), 210‑214.

[5] Meier-Merziger, M.; Fickenscher, M.; Hartmann, F.; Kuttich, B.; Kraus, T.; Gallei, M.; Frey, H. Synthesis of phase-separated super-H-shaped triblock architectures: poly(l-lactide) grafted from telechelic polyisoprene. *Polym. Chem.*, **2023**, *14* (23), 2820‑2828.

Chapter A1

Synthesis of Phase-Separated *super-H*-shaped Triblock Architectures: Poly(L-Lactide) grafted from Telechelic Polyisoprene

Moritz Meier-Merziger,[a] *Marcel Fickenscher,*[a] *Frank Hartmann,*[b] *Björn Kuttich,*[c] *Tobias Kraus,*[c,d] *Markus Gallei,*[b,e] *and Holger Frey* [a]*

* Corresponding author

[a] Department of Chemistry, Johannes Gutenberg University Mainz, Duesbergweg 10-14, 55128 Mainz, Germany.

[b] Chair in Polymer Chemistry, Saarland University, Campus Saarbrücken C4 2, 66123 Saarbrücken, Germany

[c] INM−Leibniz-Institute for New Materials, Campus D2 2, Saarland University, 66123 Saarbrücken, Germany

[d] Colloid and Interface Chemistry, Saarland University, Campus D2 2, 66123 Saarbrücken, Germany

[e] Saarene, Saarland Center for Energy Materials and Sustainability, Campus C4 2, 66123 Saarbrücken, Germany

Published in: *Polymer Chemistry*, **2023**, 14 (23), 2820–2828.
Supplementary material associated with this article can be found in the online version:
https://doi.org/10.1039/d3py00230f

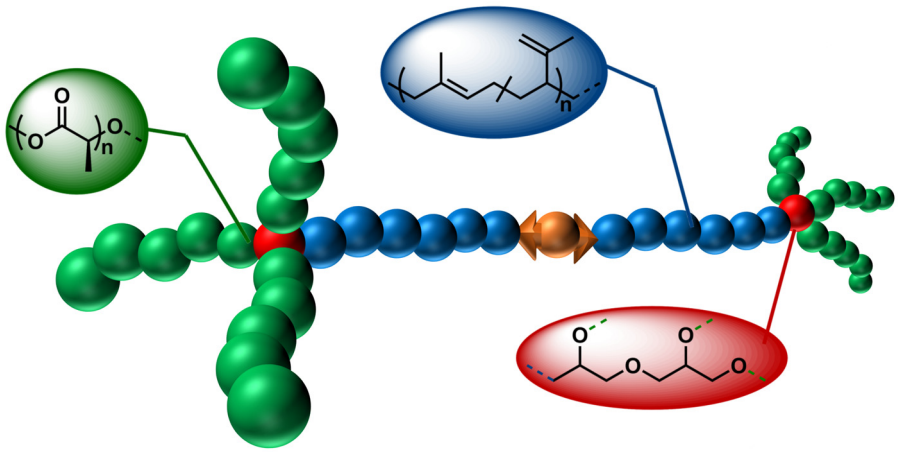

The following publication is adapted with permission from Meier-Merziger, M.; Fickenscher, M.; Hartmann, F.; Kuttich, B.; Kraus, T.; Gallei, M.; and Frey, H.; Synthesis of phase-separated *super-H*-shaped triblock architectures: poly(L-lactide) grafted from telechelic polyisoprene, *Polymer Chemistry*, **2023**, 14 (23), 2820 – 2828.

Polymer Chemistry

ROYAL SOCIETY OF CHEMISTRY

PAPER

Cite this: *Polym. Chem.*, 2023, **14**, 2820

Synthesis of phase-separated super-H-shaped triblock architectures: poly(L-lactide) grafted from telechelic polyisoprene†

Moritz Meier-Merziger, [a] Marcel Fickenscher,[a] Frank Hartmann, [b] Björn Kuttich,[c] Tobias Kraus,[c,d] Markus Gallei [b,e] and Holger Frey [a]*

In the field of carbanionic polymerization bifunctional initiators permit the synthesis of complex triblock copolymer structures. Using 1,3-bis(1-phenylethenyl)benzene (PEB), isoprene was polymerized in cyclohexane, yielding a high content of 1,4-PI units of 93%. Subsequently, 3 hydroxyl groups were introduced simultaneously both in α- and ω-position by means of end-functionalization of the living anionic dilithiated polyisoprene (PI) chains with 1,2-isopropylidene glyceryl glycidyl ether (IGG) and subsequent acidic deprotection. The resulting hexa-hydroxy functional PI-macroinitiators were then used to initiate L-lactide (LLA) in a DBU-catalysed polymerisation, ultimately yielding super-H-shaped $(PLLA)_3$-*b*-PI-*b*-$(PLLA)_3$ triblock structures with molecular weights of 23–49 kg mol^{-1}. Narrow molecular weight distributions with dispersity in the range of 1.19–1.35 were obtained, and thermal characterisation revealed two distinct glass transition temperatures (T_g), indicating phase separation. The PI-domains feature a low T_g between −55 °C and −59 °C, whereas the PLLA-domains exhibit a higher T_g of 41 °C to 49 °C. Further, the block copolymers were analyzed by TEM and SAXS, confirming clearly phase-separated cylindrical and lamellar morphologies. The reported bifunctional approach combining carbanionic polymerization with the ROP of lactones represents an efficient and general synthesis pathway for a large variety of complex polymer architectures.

Received 2nd March 2023,
Accepted 16th May 2023

DOI: 10.1039/d3py00230f

rsc.li/polymers

1. Introduction

A key feature of block copolymers is self-assembly leading to different morphologies in bulk. This microphase separation can be utilized *e.g.* to increase toughness, when combining a brittle polymer with a highly flexible segment.[1] Supramolecular elastomers based on ABA triblock structures consisting of a hard, semi-crystalline outer A block and a soft, elastic B midblock, so-called thermoplastic elastomers (TPE), offer a wide range of applications.[2] In addition to simple ABA triblock structures, more complex *e.g.* multiblock[3] or bottlebrush[4] structures have been subject of many investigations. An increasing demand for such materials is explained by several advantages: thermoplastic processability and the possibility of remolding at temperatures above the order-disorder transition or melting temperature of the hard block are attractive features, while retaining excellent toughness due to non-covalent cross-linking at room temperature.[5] In principle, this opens the possibility to remold and reuse TPEs and represents a recycling option.

The advantages of TPEs over classical elastomers can be further enhanced when changing from fossil fuel-based materials to more renewable and sustainable alternatives. Consequently, polylactide (PLA) as one of a few renewable, large-scale produced materials is a key component for consideration.[6] Different approaches have been reported to combine brittle PLA with low glass transition temperature (T_g) material. As a further advantage, plasticizers can be avoided, as a permanently toughened PLA can also be obtained in this manner.[7] Copolymerization with unsaturated polyesters such as crystalline poly(*cis*-butene succinate)succinate (PcBS) or amorphous poly(*cis*-butene glutarate) (PcBG) leads to fully biodegradable materials due to the polyester structure. However, the T_g of the soft phase at −27 °C and −47 °C, respectively, is

[a]*Department of Chemistry, Johannes Gutenberg University Mainz, Duesbergweg 10-14, 55128 Mainz, Germany. E-mail: hfrey@uni-mainz.de*
[b]*Chair in Polymer Chemistry, Saarland University, Campus Saarbrücken C4 2, 66123 Saarbrücken, Germany*
[c]*INM—Leibniz-Institute for New Materials, Campus D2 2, Saarland University, 66123 Saarbrücken, Germany*
[d]*Colloid and Interface Chemistry, Saarland University, Campus D2 2, 66123 Saarbrücken, Germany*
[e]*Saarene, Saarland Center for Energy Materials and Sustainability, Campus C4 2, 66123 Saarbrücken, Germany*

†Electronic supplementary information (ESI) available. See DOI: https://doi.org/10.1039/d3py00230f

higher than the values known for established styrene–butadiene–styrene TPEs (SBS).[8] This also applies to copolymers based on polymenthide with a T_g of −22 °C.[9] As the temperature range for application is restricted by both T_gs of the copolymer, rather high values of the low T_g-phase are a major limitation. If the temperature falls below the T_g of the soft phase, the material becomes brittle. To ensure a wide temperature range for application a partly bio-based material was investigated in this work. Polyisoprene is employed as the soft phase due to its known low T_g (<−60 °C).[10]

Hillmyer *et al.*[11,12] showed that with a silyl ether protected initiator, followed by termination with ethylene oxide (EO), α,ω-hydroxy functionalized polyisoprenes (PI) are accessible in cyclohexane. The resulting well-defined low T_g PI was employed as a macroinitiator for the subsequent L-lactide (LLA) polymerization, generating linear triblock structures. Despite the seminal character of this work, a drawback of this route is the rather high effort to synthesize the initiator. In general, the use of a monofunctional initiator limits possible changes to the ω-chain end, since the α-position is fixed. A similar, albeit biobased pathway was presented by Zhou *et al.*[13] by investigating myrcene for the soft phase. The same ABA-type structure can be obtained by reversible addition–fragmentation chain transfer polymerization (RAFT) of myrcene as reported by Fang *et al.*[14,15]

Here we present a synthesis route for $(PLLA)_3$-*b*-PI-*b*-$(PLLA)_3$ that requires only few reaction steps and offers a broad range of possibilities for end-functionalization. Tonhauser *et al.*[16] demonstrated that glycidyl ethers are ideally suited to introduce multiple hydroxy groups at a living anionic chain end, leading to multifunctional macroinitiators.[17] This technique was recently used by Haddleton *et al.*[18] to introduce a variety of different end groups at PI and polymyrcene, capitalizing on different substituted epoxides.

Facile and scalable pathways to complex architectures such as super-H-shaped[19] (pom–pom[20] or dumbbell[21]) block copolymers can hardly be found in literature. In the few reported cases they showed improvements with an increasing number of branch points with respect to strain at break and increased tensile strength. In general, branched structures are known for their lower viscosity in the melt, which translates to facilitated processing.[20,22]

The reaction steps shown in Scheme 1 illustrate the synthesis route developed in this work. 1,3-Bis(1-phenylethenyl) benzene (PEB) is one of only few reported bifunctional initiators for carbanionic polymerization in non-polar media.[23] The often observed aggregation of di-lithium compounds in non-polar solvents is prevented by the high steric demand of the phenyl rings.[24] For polar solvents or the use of so-called "modifiers" (*e.g.*, ethers), several studies can be found. It has been demonstrated that although an increased vinyl content in the diene polymerization occurs, end-functionalization can simultaneously address both end groups.[25] The use of 1,2-isopropylidene glyceryl glycidyl ether (IGG) as an end-functionalization reagent enables the introduction of a total of six hydroxyl groups at both ends of the

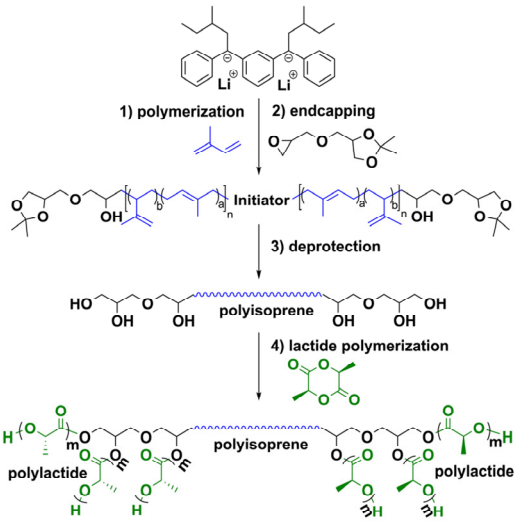

Scheme 1 Synthetic route starting from a bifunctional initiator to yield super-H-shaped $(PLLA)_3$-*b*-PI-*b*-$(PLLA)_3$ block copolymer structures.

chain after cleavage of the acetal protective groups.[16,26] After deprotection these macroinitiators were used for the organocatalyzed polymerization of L-lactide with 1,8-diazabicyclo[5.4.0] undec-7-ene (DBU). As reported by Lohmeijer *et al.*,[27] this synthesis strategy leads to high molecular weights with narrow distribution under rather mild conditions and short reaction times.

2. Results and discussion

2.1 Model reaction

Prior to the use of a bifunctional initiator system, the feasibility of introducing 3 terminal hydroxyl groups by IGG end-functionalization to polyisoprene was studied by means of a linear, monofunctional model polymerization. The results are briefly summarized in Fig. 1, showing narrow and monomodal molar mass distributions. Table 1 gives an overview of the polymer characterization by means of SEC and NMR, as well as the calculated polyisoprene microstructure and the level of end-functionalization. The fraction of 1,4-PI-units can be calculated by means of NMR spectroscopy, following eqn (1) (see ESI† for further information). In addition, the characteristic signals of the IGG group, introduced to the polymeric chain end, can be observed in the NMR spectra in range of a chemical shift between 3.2 ppm to 4.3 ppm.

$$1,4-\mathrm{PI} = \frac{I(\mathrm{methine})}{I(\mathrm{methine}) + I(\mathrm{methylidene}) \times 0.5} \times 100\% \quad (1)$$

The subsequent cleavage of the ketal protecting group with the acidic DOWEX® resin was tracked by NMR spectroscopy, as demonstrated in Fig. 1(d). Particularly noteworthy is the

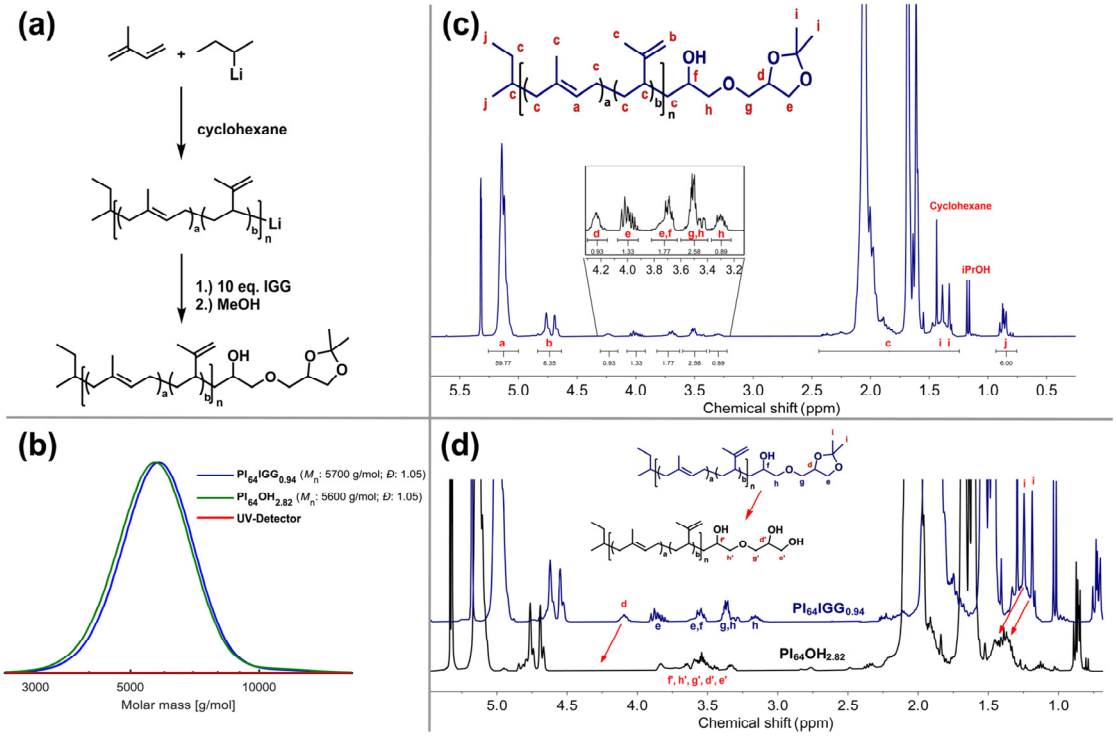

Fig. 1 Summarized results for *sec*-BuLi initiated PI, end-functionalized with IGG. (a) Reaction scheme; (b) SEC-traces, measured in THF, PI-calibration and RI-detector; (c) ^{1}H NMR spectrum of IGG end-functionalized PI and assignment of ^{1}H signals; (d) ^{1}H NMR spectrum, evidence for ketal cleavage.

Table 1 Results of low molecular weight IGG end-functional PI-samples

	M_n^{theor} [g mol^{-1}]	$M_n^{NMR\ a}$ [g mol^{-1}]	$M_n^{SEC\ b}$ [g mol^{-1}]	$Đ^b$	End-function-alization^c	1,4-PI^d
$PI_{64}IGG_{0.94}$	4800	4600	5700	1.05	94%	93%
$IGG_{0.91}PI_{91}IGG_{0.91}$	5000	6900	4300	1.08	91%	93%

^{a} Calculated from ^{1}H NMR by ratio of methyl signal of *sec*-BuLi *vs.* PI signals. ^{b} Determinated by SEC in THF and PI-calibration from RI-signal. ^{c} Calculated from ^{1}H NMR spectra from ratio of methyl signal of *sec*-BuLi *vs.* IGG signals. ^{d} Calculated from ^{1}H NMR spectra from the ratio of 1,4-PI *vs.* 3,4-PI signals.

complete disappearance of the methyl groups of the 2,2-dimethyl-1,3-dioxolane protecting group and the upfield shift of the methine proton. This corresponds to known literature results.[26,28] Thus, three terminal hydroxy groups are released and accessible for the ensuing lactide polymerization.

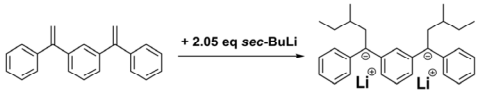

Scheme 2 Conversion of PEB to the active dilithium initiating species.

2.2 Activation of PEB and difunctional PI synthesis

As shown in Scheme 2, a 0.1 M solution of PEB was activated with *sec*-BuLi, followed by the addition of isoprene. After complete polymerization of isoprene an excess of 10 eq. IGG was added to introduce the end-functionalization. The activation time of the bifunctional initiator is a key parameter for the outcome of the reaction. While a longer activation time led to a lower extent of chain coupling, thus reducing the high molecular weight shoulder of the distributions, an increase of low molecular weight tailing was observed. This was assumed to be caused by delayed dissolution of aggregates formed by the active initiator species.

These trends were monitored and the optimization towards unimodal SEC traces can be followed in Fig. S22.†

The best compromise between (tolerated) tailing and high molecular weight shoulder was found for an activation time of 145 min for PEB at 20 °C. Based on the optimized activation conditions, a sample of 5000 g mol^{-1} of bifunctional PI end-functionalized with IGG was synthesized for more detailed characterization. The results, listed in Table 1, agree with expectation. By means of NMR spectroscopy (see Fig. S6†), the targeted high extent of 1,4-PI units of 93% and a high level of end-functionalization of 91% can be confirmed. This coincides with a low dispersity of 1.08, obtained by SEC measurements (PI-standard). Compared to the monofunctional samples, Fig. 1(b), the UV detector can now also be used, due to the presence of the PEB units in the PI chains formed (Fig. S23†). DOSY NMR spectroscopy confirms the successful introduction (Fig. 2), since the PEB-, isoprene- and IGG-signals show the same diffusion coefficient. The level of end-functionalization of the bifunctional initiated PI samples were again determined by ^{1}H NMR spectroscopy. The results represent the high level of control that is achieved, when using carbanionic polymerization techniques in non-polar solvents with the lithiated PEB initiator.

2.3 Preparation of the macroinitiators

These results were used to synthesize a series of different macroinitiators ranging from 20 to 40 kg mol^{-1} in targeted molecular weight range. The results of the synthesized polymers before and after deprotection are summarized in Table 2. Fig. 3 gives an overview of the respective SEC traces. Again, a close correlation of experimental and the targeted molecular weight by means of SEC, using THF as an eluent and PI-calibration is observed. The content of 1,4-PI microstructure was calculated using NMR spectroscopy and is in line with expectation of PI polymerized in non-polar media. The respective low T_g of −59 °C to −56 °C also complies with literature values and therefore fulfills the basic requirements for elastomers.

All macroinitiators showed a monomodal distribution (Fig. 3), yet slight shoulders hint at chain coupling of a minor fraction of unreacted PEB in the system. This imperfection is difficult to avoid due to the titration used for initiator activation, but should have negligible effect on the final polymer properties, given their relatively small proportion.

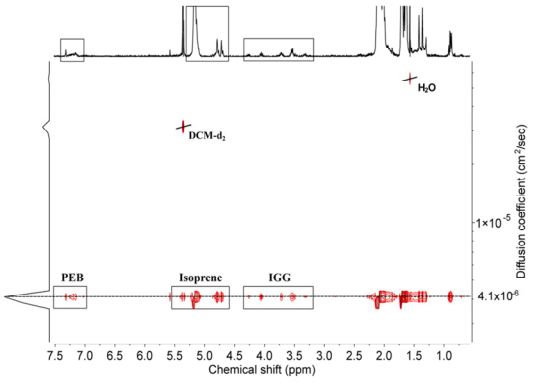

Fig. 2 DOSY NMR spectrum showing signals of the PEB initiator, isoprene and IGG at the same diffusion coefficient, confirming successful telechelic end-functionalization.

Table 2 Synthesized PI-macroinitiators before and after deprotection; results of SEC characterization and thermal properties

	M_n^{theor} [g mol^{-1}]	$M_n^{SEC\ a}$ [g mol^{-1}]	D^a	1,4-PI^b	$T_g{}^c$ [°C]
$IGG_1PI_{254}IGG_1$	20 000	17 300	1.22	94%	−59
$IGG_1PI_{459}IGG_1$	30 000	31 300	1.44	94%	−56
$IGG_1PI_{617}IGG_1$	40 000	42 000	1.32	94%	−57
$OH_3PI_{254}OH_3$	20 000	20 000	1.28	94%	−56
$OH_3PI_{459}OH_3$	30 000	33 400	1.37	94%	−57
$OH_3PI_{617}OH_3$	40 000	42 200	1.30	94%	−59

^{a} Determined by SEC in THF and PI-calibration from RI-signal. ^{b} Calculated from ^{1}H NMR by ratio of 1,4-PI *vs.* 3,4-PI signals. ^{c} Determined by means of DSC with a heat rate of 20 K min^{-1}.

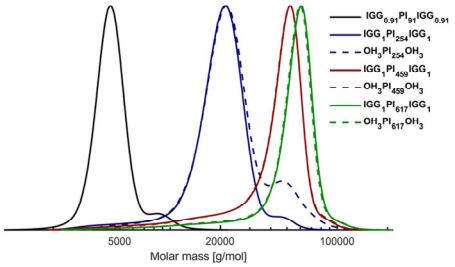

Fig. 3 SEC-traces of 5k, 20k, 30k and 40k macroinitiators before and after deprotection, measured in THF using a PI-calibration and RI-detector.

The shift of the SEC traces towards higher molecular weight after the deprotection is caused by a change of the hydrodynamic radius in the respective solvent (*vs.* PI-standard). The now exposed hydroxyl groups lead to a change of the hydrophilicity of the polymer chains. Despite a comparatively small effect, the successful deprotection can be confirmed. As the end group determination *via* NMR spectroscopy can only be carried out for low molecular weights, all higher molecular weight samples were investigated by SEC. For this reason, the level of end-functionalization achieved for the 5k sample is also assumed for all macroinitiators and used for the ensuing lactide polymerizations. Note, that a level of end-functionalization of 91% for a bifunctional system, *i.e.*, 9% non-functionalized chain ends statistically leads to an amount of only $(0.09)^2$ = 0.81% PI-chains with no functionalization at all. Thus, most of the polymer chains carry the end-functionalization at both chain ends (82.81%), and a smaller fraction at least on one side (16.38%). All functionalized chains can participate in the subsequent lactide polymerization.

2.4 Lactide polymerization

Various polymerization techniques are suitable for the synthesis of polylactide. The route chosen here was the organoca-

talytic DBU ring-opening polymerization (ROP) of L-lactide. Key advantages, such as the polymerization at room temperature and tolerance against functional groups, accompanied by excellent control of the molecular weight were suitable for the reported PI-macroinitiator, which bears multiple potentially reactive double bonds in its backbone. Short reaction times were also preferable to reduce the risk of undesired cross-linking and side reactions. As demonstrated by Sherck *et al.*[29] a [ROH]/[DBU] ratio of 2.1 is favored to suppress side reactions and to obtain narrow distributions. The present results showed quantitative conversion for the 20k and 30k samples on a timescale of one hour. First experiments using the highest molecular weight (40k) macroinitiator showed an additional low molecular weight mode by SEC (Fig. S19†) and a PLLA homopolymer impurity by DOSY NMR spectroscopy (Fig. S15†). To suppress homopolymerization, the ratio had to be adjusted to [ROH]/[DBU] = 5. Following this adjustment, a monomodal SEC trace was achieved (Fig. S19 and S21†). A possible explanation is the "nucleophilic-attack-pathway" mechanism proposed by Sherck *et al.*,[29] which describes the autocatalyzed polymerization of lactide without an alcohol as initiator. Based on the assumption that – due to the higher molecular weight – the hydroxyl groups are not as exposed as within the lower M_n samples, the amount of DBU was decreased. Thereby, monomodal SEC traces were obtained and by DOSY NMR spectroscopy (Fig. S16†) no polylactide homopolymer was observed. The shift to higher M_n, dependent of the targeted amount of PLLA, can be followed by SEC (Fig. 4).

This meets the essential demand for successful preparation of a graft copolymer: shift and growth of the monomodal SEC traces towards higher molecular weights and a common, single diffusion coefficient measured by DOSY NMR spectroscopy.

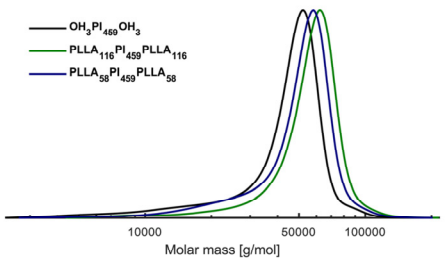

Fig. 4 SEC traces of 30k PI macroinitiator, converted to two different triblock copolymers with targeted 20 and 30 vol% of PLLA.

2.5 Copolymer characterization

To investigate the general features and characteristics of these triblock compositions, two different ratios of PI : PLLA were employed for each macroinitiator. The targeted ratios of 10–80–10 and 15–70–15 are confirmed by ^{1}H NMR spectroscopy measurements and the determination is described in more detail in the ESI.† Here the intensity of the methine signal of PLLA (~5.1 ppm) was compared to the signals of 1,4-PI (~5.3 ppm) and 3,4-PI (~4.8 ppm). In this manner the degree of polymerization (P_n) of PLLA can be calculated in relation to the P_n of PI, which is known from the respective macroinitiator employed. A uniform distribution of the lactide units at both chain ends is assumed for statistical reasons. Thus, a P_n(LA) of 76 and P_n(PI) of 254 results in the following sample-ID: PLLA$_{38}$-*b*-PI$_{254}$-*b*-PLLA$_{38}$. It is worth noticing that due to the unique architecture of three hydroxy groups at each chain end, the P_n of PLLA is actually distributed over six arms per polymer chain. The P_n of both materials can be used to calculate the volume fraction of polylactide (Φ_{LA}) (see ESI†).

Based on the successful polymer syntheses, the thermal properties as well as the microphase separation capability of the materials were studied. A comprehensive overview of the results is given in Table 3.

2.6 Thermal analysis

As displayed in Fig. 5, all samples showed two distinct T_gs by differential scanning calorimetry (DSC). The lower value (−55 °C to −59 °C) corresponds to the PI midblock, and the higher value (41 °C to 49 °C) to PLLA, both in excellent agreement with the respective values in literature.[15] Since the average chain length of the individual PLLA segments is rather low due to the unusual architecture, no crystallization was observed for most samples. A melting point (T_m) of 102 °C for PLLA can only be detected for the sample with the highest amount of PLLA (total P_n = 232). This is significantly lower than values of PLLA (T_m^{lit} = 148–154 °C)[31] and is attributed to the rather short average length of the polylactide chains. Compared to literature values of the melt enthalpy (ΔH), $\Delta H_{PLLA}^{lit.}$ = 5.22 J

Table 3 Results of synthesized PLLA$_x$-*b*-PI$_y$-*b*-PLLA$_x$ triblock copolymers with determent analytic data

Sample ID[d]	Ratio (target)	M_n^{SEC} [a] [g mol^{-1}]	$Đ$[a]	1,4-PI[e]	Φ_{LA} [b]	TEM	SAXS	T_g^1 [c] [°C]	T_g^2 [c] [°C]	T_m [c] [°C]
PLLA$_{38}$PI$_{254}$PLLA$_{38}$	10–80–10	22 500	1.31	94%	0.19	H	H	−56	44	—
PLLA$_{64}$PI$_{254}$PLLA$_{64}$	15–70–15	23 600	1.35	94%	0.28	H	—	−59	45	—
PLLA$_{58}$PI$_{459}$PLLA$_{58}$	10–80–10	41 600	1.25	94%	0.16	H	—	−55	46	—
PLLA$_{116}$PI$_{459}$PLLA$_{116}$	15–70–15	48 200	1.19	94%	0.28	L	L	−57	49	102
PLLA$_{81}$PI$_{617}$PLLA$_{81}$	10–80–10	49 400	1.24	94%	0.17	H	—	−56	41	—
PLLA$_{70}$PI$_{617}$PLLA$_{70}$	15–70–15	49 100	1.25	94%	0.15	H	—	−55	48	—

[a] M_n measured by SEC, using a PI calibration and THF as an eluent. [b] Calculated assuming the homopolymer densities ρ(PLA) = 1.154 g cm^{-3} (ref. 30) and ρ(PI) = 0.830 g cm^{-3} (ref. 15) at 140 °C. [c] Determined by means of DSC with a heat rate of 20 K min^{-1}. [d] Derived from M_n of the corresponding PI-macroinitiator and ^{1}H NMR of the PLLA-*b*-PI-*b*-PLLA. [e] Calculated from ^{1}H NMR signals of the corresponding.

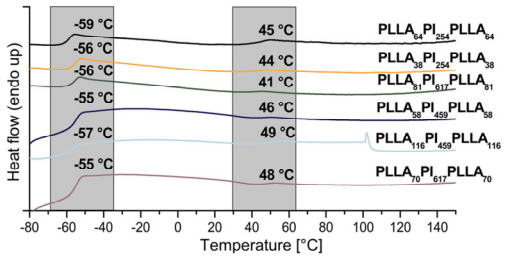

Fig. 5 DSC results of all triblock copolymers, showing the second heating curve with a heat rate of 20 K min^{-1}.

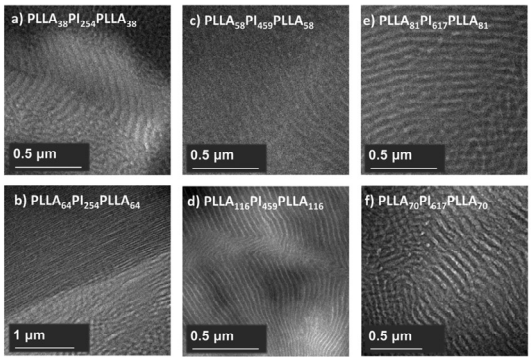

Fig. 7 TEM images of $PLLA_x$-*b*-PI_y-*b*-$PLLA_x$ samples: annealed (16 h, 80 °C), stained with OsO_4 and measured on a JEOL JEM-2100 instrument, 200 kV acceleration voltage; 0.14 nm resolution and a Gatan Orius SC1000 camera (binning 2; 1024 × 1024 pixels) in the brightfield mode was used.

g $^{-1}$,[31] this further explains the low values obtained of the sample ($PLLA_{116}$-*b*-PI_{459}-*b*-$PLLA_{116}$) $\Delta H = 0.6$ J g^{-1}.

In order to elucidate the results of the thermal characterization with respect to the underlying morphology, transmission electron microscopy (TEM) of the samples was performed (Fig. 7). Prior to the measurement, the samples were prepared as thin films by solvent casting of benzene and DCM (0.33 g mL^{-1}) solutions and thermally annealed at 80 °C for 16 hours. Thin slices were prepared by ultramicrotome and subsequent staining for 2–5 min with osmium tetroxide (OsO_4) increased the contrast between both copolymer components. Hence, the PI domains appear dark and the PLLA domains bright in the resulting TEM images.

Branched polymer structure are known to show characteristic differences within the phase diagram compared to linear architectures. It was previously described that for miktoarm stars of AB_n structure, an increased number of B-chains leads to curvature at the interface due to a higher demand for space (Fig. 6).[32,33]

Given that the phase diagram of ABA triblock copolymers is almost identical to the one of AB diblock copolymers, the B_3AB_3 structure prepared in this work is compared with the phase diagram of AB_n miktoarm stars.[34] As a result of the increased space requirement of the B phase, a shift occurs in the phase diagram. A lamellar morphology is achieved with a Φ_B as low as 22.5% (B-block) for AB_2-structures, which is in contrast to the classical morphology diagram for linear diblock structures.[34]

From the measured TEM images, a cylindrical morphology was concluded for all samples with one exception ($PLLA_{116}$-*b*-PI_{459}-*b*-$PLLA_{116}$). This can be observed mainly by the non-continuous bright PLLA domains inside the continuous dark PI-phase (*cf.* Fig. 7b). Cylinders, which are oriented vertically, were found to have the characteristic hexagonal structure. These two features can be observed most clearly for sample (b) in Fig. 7 ($PLLA_{64}$-*b*-PI_{254}-*b*-$PLLA_{64}$).

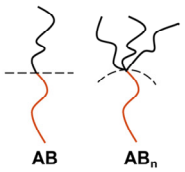

Fig. 6 Illustration of the different curvature at the interface comparing AB and AB_n structures, inspired by literature.[33]

The exception matches the sample that was already conspicuous in the DSC measurements, being the only one to show a T_m. It has the highest P_n of PLLA and shows the only lamellar morphology with a Φ_{LA} of 28%, Fig. 7(d). For regular linear block copolymers, this would still result in an expected hexagonal structure, as demonstrated by Hillmyer *et al.*[11] for linear PLLA-*b*-PI-*b*-PLLA structures, comprising a similar fraction of PLLA. Due to the high-volume difference, different lamellar thickness can also be observed in the TEM image for both components (*cf.* Fig. 7d). This observation is in line with expectation based on the calculated volume fractions of the different blocks. The bright PLLA areas are clearly thinner than the darker PI areas.

In addition to the TEM results, small-angle X-ray scattering (SAXS) measurements were performed for each of the two different morphologies obtained for verification. The two samples (a and d) shown in Fig. 7 were examined in more detail, and the results can be followed in Fig. 8. A clear dependence on the thermal history of the sample is observed. Without thermal annealing the peak positions cannot be precisely assigned to any morphology. In contrast, after annealing for 16 h at 80 °C the relative peak positions agree very well with values of peak sequences known in literature for the hexagonal cylindrical morphology ($1 : \sqrt{3} : \sqrt{4} : \sqrt{7} : \sqrt{9} : \sqrt{12}$).[35]

This effect is attributed to the fact that the sample has a kinetically inhibited, non-continuous morphology as a result of different affinities of the two copolymer components to the solvent during film production.[36] By means of annealing the material above the T_g of PLLA, the copolymer chains subsequently arrange in their thermodynamically preferred mor-

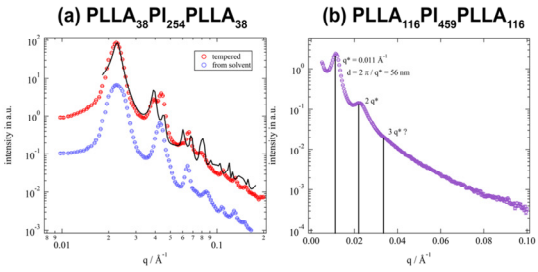

Fig. 8 SAXS results measured on a laboratory-scale Xeuss 2.0 instrument (Xenocs, Grenoble, France); a: $PLLA_{38}PI_{254}PLLA_{38}$ red: tempered, blue: from solvent cast, black: hexagonally arranged cylinder-model; b: $PLLA_{116}PI_{459}PLLA_{116}$ tempered.

phology. Therefore, all samples were always annealed prior to TEM measurements.

In summary, the morphologies obtained by SAXS match with the TEM results. Again, a lamellar morphology for the sample with a Φ_{LA} of 28% and highest P_n(LA) was observed.

3. Experimental

3.1 Materials

Chemicals were purchased from the following suppliers: cyclohexane (Fischer Scientific, 99.8%), benzene (Roth, 99.5%), dichloromethane (DCM) (Fischer Scientific, 99.8%), L-lactide (BASF SE, 99%), *sec*-BuLi (Acros Organics, 1.3 M), 1,1-diphenylethylene (abcr, 98%), isoprene (Acros Organics, stabilized, 98%), calcium hydride (Sigma Aldrich, 97%), methanol (Fischer Scientific, 99.9%), DOWEX 50WX8 hydrogen form (Acros Organics, 200–400 mesh), isopropylidene glycerol (Acros Organics, 97%), tetrabutylammonium hydrogen sulfate (Acros Organics, 98%), epichlorohydrin (Acros Organics, 99%), DBU (TCI, 98%), benzoic acid (Sigma Aldrich, 99.5%), dry DCM (Acros Organics, 99.8%, molecular sieve). If not stated otherwise they were used without further purification.

3.2 Characterization

^{1}H NMR measurements were carried out at room temperature on a Bruker Avance III HD 300 MHz, Bruker Avance II 400 MHz or Bruker Avance III HD 400 MHz. Size-exclusion chromatography (SEC) was performed with the autosampler Waters 717 plus with a MZ-Gel SD plus e5/e3/100 column from MZ-Analysetecchnik, Mainz and a SpectraSeries-P100 pump. An Agilent G1362A RI-detector and MZ-Messanalytik TSP UV (254 nm) UV-detector were used. Samples were measured against a PI calibration in concentrations of 3–5 mg in 6 mL tetrahydrofuran (THF) and toluene as an internal standard. FT-IR measurements were performed using a Nicoleti iS10FT-IR spectrometer of Thermo Fisher Scientific in a wavenumber range of 650 cm^{-1} to 4000 cm^{-1}, and all samples were pasted as solid. High-resolution mass spectroscopy (HRMS) was performed on an Agilent 6545 QTOF-HRAM-MS instrument.

3.3 Thermal analysis

Differential scanning calorimetry (DSC) to determine the glass transition and crystallization temperatures was performed on a Perkin Elmer 8500 device and a Perkin Elmer Thermal Analysis Controller TAC7/DX. Samples were measured after sufficient drying under reduced pressure with a heat rate of 20 K min^{-1} and analyzed by their second heating run. The chosen temperature range for pure PI-samples was −95 °C to 0 °C and for the block copolymers −95 °C to 200 °C.

3.4 *Morphology analysis*

The phase separation behavior was characterized using transmission electron microscopy. A JEOL JEM-2100 device with LaB_6-cathode, HR pole piece, 200 kV accelerating voltage and a line resolution of 0.14 nm was used. The camera used was a Gatan Orius CCSD. Films were prepared by evaporation from solutions of benzene and DCM and tempered at 80 °C for 16 h. Cuts were prepared by microtome and stained for 2–5 min with osmium tetroxide (OsO_4) prior measurement. Small-angle X-ray scattering (SAXS) measurements were performed using a Xeuss 2.0 setup, Xenocs, Grenoble, France. The setup involved a copper Kα X-ray source (λ = 1.54 Å). The data were recorded with a 2D Pilatus 3R 1M detector, Dectris, Baden, Switzerland. Since scattering of the samples was completely isotropic, the 2D detector images were azimuthally averaged to obtain 1D scattering curves.

3.5 Synthesis of 1,2-isopropylidene glyceryl glycidyl ether (IGG)

Following the procedure of Wurm *et al.*[26] IGG was synthesized by the addition of 30.97 mL (36.41 g, 0.40 mol, 2 eq.) epichlorohydrin to a mixture of 40 mL 50% w/w NaOH, 40 mL benzene, 24.50 mL (26.00 g, 0.20 mol, 1 eq.) isopropylidene glycerol and 2.67 g (7.90 mmol, 0.04 eq.) tetrabutylammonium hydrogen sulfate at 0 °C. Then the reaction mixture was allowed to heat up to room temperature and stirred for 98 hours. The product was diluted with 500 mL diethyl ether and 100 mL water. The organic phase was separated, washed three times with water and brine and subsequently dried with magnesium sulfate prior to the evaporation of the solvent and subsequent distillation under reduced pressure. 17.02 g (0.08 mol, 46%) of IGG were obtained as a colorless liquid. The product was characterized by HRMS (Fig. S26†), IR (Fig. S25†), ^{1}H and ^{13}C NMR spectroscopy (Fig. S2 and S3†).

3.6 Synthesis of the PEB initiator

1,3-Bis(1-phenylethenyl)benzene was synthesized from 1,3-dibenzoylbenzene and methyl Grignard, followed by dehydration.[37] Purification was carried out *via* column chromatography and confirmed by ^{1}H NMR, (Fig. S4†).

3.7 Synthesis of α,ω-multi hydroxy PI-macroinitiators

An anionic reaction flask, loaded with 5 mL of 0.1 molar PEB stock solution in benzene was activated for 145 min at 20 °C by addition of 2.05 eq. of 1.3 molar *sec*-BuLi solution in an Ar-atmosphere. After activation, 9.61 g (0.14 mol) freshly distilled dry isoprene (three freeze–pump–thaw cycles over CaH_2) and 95 mL of dry cyclohexane were added simultaneously *via* an ampule. After stirring for 30 min at 20 °C, the flask was placed in a 40 °C oil bath, and the polymerization proceeded for 150 min. IGG was dried by the addition of a small amount of *sec*-BuLi and distilled for further use. The living polyisoprene reaction mixture was end-functionalized by the addition of 1.9 g (10 eq.) of IGG and stirred for another 2 hours before termination with degassed methanol. The polymer was precipitated in methanol and dried under reduced pressure.

The ketal protecting group was cleaved in DCM, using DOWEX (50WX8 hydrogen form) over night. After quantitative cleavage of the protecting group the polymer was precipitated in methanol and dried under reduced pressure.

3.8 Preparation of super-H-shaped triblock structures

The polyisoprene macroinitiator was dissolved in benzene and freeze-dried under reduced pressure. Under an inert argon-atmosphere 0.5 g (0.015 mmol) PI and 0.1738 g (1.21 mmol) dry LLA and 4 mL dry DCM were added. After complete dissolution, the polymerization was initiated by the addition of 2.7 μL (0.018 mmol) water free DBU ([OH]/[DBU] = 5). The polymerization was quenched after one hour by adding 5 mg (0.041 mmol) benzoic acid, followed by precipitation in methanol to yield the colorless copolymers in quantitative yield. Additional experimental and characterization data can be found in the ESI.†

4 Conclusions

We have developed a general synthesis pathway for $(PLLA)_3$-*b*-PI-*b*-$(PLLA)_3$ super-H-shaped copolymers, taking advantage of the living carbanionic polymerization for the difunctional macroinitiator synthesis, combined with epoxide termination. Using the bifunctional initiator PEB for isoprene polymerization in a non-polar medium, good control over molecular weights and microstructure (high degree of 94% 1,4-PI) was achieved for the PI midblock. The subsequent addition of IGG permitted end-functionalization of the living chain end due to inhibited propagation of the stable lithium alkoxide chain ends. Thereby, precisely three terminal hydroxyl groups were introduced at both chain termini. Ultimately, a super-H-shaped architecture was obtained by using these telechelic, hexahydroxy-functional polymers as macroinitiators for a DBU-catalyzed L-lactide ring-opening polymerization. Consequently, a low T_g of −55 °C to −59 °C attributed to PI and a second distinct T_g in the range of 41 °C to 49 °C, ascribed to PLLA, were observed for the resulting super-H-shaped copolymers. Further characterization techniques (TEM and SAXS) proved well-ordered, microphase separated morphologies for all synthesized samples, unexpectedly showing a lamellar morphology at a PLLA volume fraction Φ_{LA} of only 28%.

As the super-H-shaped architecture shows a peculiar effect on the resulting morphologies in comparison to common linear architectures, future studies will focus on tailoring polymer morphologies and resulting material properties. Mechanical properties as well as a fully bio-based approach by substituting isoprene by naturally occurring terpene-based dienes are currently under investigation.

The synthesis strategy developed here is of a general nature and permits to prepare a large range of polydiene- and polyester-based super-H shaped copolymers, combining carbanionic polymerization with the ROP of lactones. According to a recent study, hydroxyl-diene structures can be used to initiator lactide also in a flow process, offering promise for upscaling.[38] By varying the end-functionalization reagent, a wide range of other architectures besides super-H structures is accessible.

Author contributions

M. Meier-Merziger, M. Fickenscher, and H. Frey primarily created the concept and design of the article. All synthetic work was performed by M. Meier-Merziger and detailed characterization by TEM and SAXS was contributed by F. Hartmann, B. Kuttich, T. Kraus and M. Gallei.

Conflicts of interest

There are no conflicts to declare.

Acknowledgements

We are grateful to Sandra Schüttner for help with the lactide polymerizations and to Monika Schmelzer for her valuable assistance with the SEC measurements. M. Meier-Merziger thanks the BASF SE for their personal financial support through the "Deutschlandstipendium". The authors thank Marcus Koch for support in TEM measurements.

References

1 F. S. Bates and G. H. Fredrickson, *Phys. Today*, 1999, **52**, 32–38.
2 A. L. Holmberg, K. H. Reno, R. P. Wool and T. H. Epps, *Soft Matter*, 2014, **10**, 7405–7424.
3 (*a*) M. Steube, T. Johann, E. Galanos, M. Appold, C. Rüttiger, M. Mezger, M. Gallei, A. H. E. Müller, G. Floudas and H. Frey, *Macromolecules*, 2018, **51**, 10246–10258; (*b*) M. Steube, T. Johann, R. D. Barent, A. H. Müller and H. Frey, *Prog. Polym. Sci.*, 2022, **124**, 101488; (*c*) C. Wahlen, J. Blankenburg, P. von Tiedemann, J. Ewald, P. Sajkiewicz, A. H. E. Müller, G. Floudas and H. Frey, *Macromolecules*, 2020, **53**, 10397–10408.

4 C. Wahlen, M. Rauschenbach, J. Blankenburg, E. Kersten, C. P. Ender and H. Frey, *Macromolecules*, 2020, **53**, 9008–9017.

5 (*a*) J. Markarian, *Plast. Addit. Compd.*, 2004, **6**, 22–25; (*b*) S. Amin and M. Amin, *Rev. Adv. Mater. Sci.*, 2011, **29**, 15–30.

6 (*a*) J. Pretula, S. Slomkowski and S. Penczek, *Adv. Drug Delivery Rev.*, 2016, **107**, 3–16; (*b*) R. E. Drumright, P. R. Gruber and D. E. Henton, *Adv. Mater.*, 2000, **12**, 1841–1846.

7 (*a*) S. C. Schmidt and M. A. Hillmyer, *Macromolecules*, 1999, **32**, 4794–4801; (*b*) K. Bechtold, M. A. Hillmyer and W. B. Tolman, *Macromolecules*, 2001, **34**, 8641–8648.

8 (*a*) J.-F. Masson, S. Bundalo-Perc and A. Delgado, *J. Polym. Sci., Part B: Polym. Phys.*, 2005, **43**, 276–279; (*b*) Y. Wang, X. Leng, Z. Wei, Y. Zhao, L. Zheng and Y. Li, *J. Mater. Sci.*, 2020, **55**, 9129–9143.

9 C. L. Wanamaker, M. J. Bluemle, L. M. Pitet, L. E. O'Leary, W. B. Tolman and M. A. Hillmyer, *Biomacromolecules*, 2009, **10**, 2904–2911.

10 J. M. Widmaier and G. C. Meyer, *Macromolecules*, 1981, **14**, 450–452.

11 E. M. Frick and M. A. Hillmyer, *Macromol. Rapid Commun.*, 2000, **18**, 1317–1322.

12 E. M. Frick, A. S. Zalusky and M. A. Hillmyer, *Biomacromolecules*, 2003, **4**, 216–223.

13 (*a*) C. Zhou, Z. Wei, C. Jin, Y. Wang, Y. Yu, X. Leng and Y. Li, *Polymer*, 2018, **138**, 57–64; (*b*) C. Zhou, Z. Wei, X. Lei and Y. Li, *RSC Adv.*, 2016, **6**, 63508–63514.

14 (*a*) S. Ding, C. Fang, J. Zhang, X. Wang and Z. Wang, *Polymer*, 2020, **202**, 122724; (*b*) S. Ding, C. Fang, X. Wang and Z. Wang, *Polymer*, 2020, **186**, 121993.

15 C. Fang, X. Wang, X. Chen and Z. Wang, *Polym. Chem.*, 2019, **10**, 3610–3620.

16 C. Tonhauser and H. Frey, *Macromol. Rapid Commun.*, 2010, **31**, 1938–1947.

17 (*a*) J. Morsbach, A. Natalello, J. Elbert, S. Winzen, A. Kroeger, H. Frey and M. Gallei, *Organometallics*, 2013, **32**, 6033–6039; (*b*) C. Tonhauser, M. Mazurowski, M. Rehahn, M. Gallei and H. Frey, *Macromolecules*, 2012, **45**, 3409–3418.

18 J. Zhang, W. Pointer, G. Patias, L. Al-Shok, R. A. Hand, T. Smith and D. M. Haddleton, *Eur. Polym. J.*, 2023, **183**, 111755.

19 H. Iatrou, A. Avgeropoulos and N. Hadjichristidis, *Macromolecules*, 1994, **27**, 6232–6233.

20 T. C. B. McLeish and R. G. Larson, *J. Rheol.*, 1998, **42**, 81–110.

21 U. Bayer and R. Stadler, *Macromol. Chem. Phys.*, 1994, **195**, 2709–2722.

22 (*a*) R. Weidisch, S. P. Gido, D. Uhrig, H. Iatrou, J. Mays and N. Hadjichristidis, *Macromolecules*, 2001, **34**, 6333–6337; (*b*) L. D. Moore, *J. Polym. Sci.*, 1959, **36**, 155–172.

23 R. P. Quirk and F. Ignatz-Hoover, in *Recent Advances in Anionic Polymerization*, ed. T. E. Hogen-Esch and J. Smid, Springer Netherlands, Dordrecht, 1987, pp. 393–401.

24 (*a*) T. Bastelberger and H. Höcker, *Angew. Makromol. Chem.*, 1984, **125**, 53–67; (*b*) L. H. Tung, G. Y.-S. Lo and D. E. Beyer, *Macromolecules*, 1978, **11**, 616–617.

25 (*a*) B. Gao, L. Sun, X. Chen, X. Zhai, J. Zheng, X. Ye, J. Lu, A. Feng and L. Zhang, *J. Appl. Polym. Sci.*, 2022, **139**(43), e53061; (*b*) P.-C. Lee, C.-C. Wang and C.-Y. Chen, *Polymer*, 2020, **210**, 123028.

26 F. Wurm, J. Nieberle and H. Frey, *Macromolecules*, 2008, **41**, 1909–1911.

27 B. G. G. Lohmeijer, R. C. Pratt, F. Leibfarth, J. W. Logan, D. A. Long, A. P. Dove, F. Nederberg, J. Choi, C. Wade, R. M. Waymouth and J. L. Hedrick, *Macromolecules*, 2006, **39**, 8574–8583.

28 P. Ziemczonek, M. Gosecka, M. Gosecki, M. Marcinkowska, A. Janaszewska and B. Klajnert-Maculewicz, *Int. J. Mol. Sci.*, 2021, **22**, 8386.

29 N. J. Sherck, H. C. Kim and Y.-Y. Won, *Macromolecules*, 2016, **49**, 4699–4713.

30 D. R. Witzke, R. Narayan and J. J. Kolstad, *Macromolecules*, 1997, **30**, 7075–7085.

31 S. Fehri, P. Cinelli, M.-B. Coltelli, I. Anguillesi and A. Lazzeri, *Int. J. Chem. Eng. Appl.*, 2016, **7**, 85–88.

32 S. T. Milner, *Macromolecules*, 1994, **27**, 2333–2335.

33 N. Hadjichristidis, H. Iatrou, S. K. Behal, J. J. Chludzinski, M. M. Disko, R. T. Garner, K. S. Liang, D. J. Lohse and S. T. Milner, *Macromolecules*, 1993, **26**, 5812–5815.

34 M. W. Matsen, *Macromolecules*, 2012, **45**, 2161–2165.

35 *Anionic Polymerization*, ed. N. Hadjichristidis and A. Hirao, Springer, Japan, Tokyo, 2015.

36 (*a*) L. Ansaloni, Z. Dai, J. J. Ryan, K. P. Mineart, Q. Yu, K. T. Saud, M.-B. Hägg, R. J. Spontak and L. Deng, *Adv. Mater. Interfaces*, 2017, **4**, 1700854; (*b*) K. P. Mineart, X. Jiang, H. Jinnai, A. Takahara and R. J. Spontak, *Macromol. Rapid Commun.*, 2015, **36**, 432–438.

37 G. Y.-S. Lo, E. W. Otterbacher, R. G. Pews and L. H. Tung, *Macromolecules*, 1994, **27**, 2241–2248.

38 M. den Haese, H. P. L. Gemoets, K. van Aken and L. M. Pitet, *Polym. Chem.*, 2022, **13**, 4406–4415.

Chapter A2

Supersoft Polymer Melts in Binary Blends of bottlebrush *cis*-1,4-polyfarnesene and *cis*-1,4-polyisoprene

Ioannis Tzourtzouklis,[a] *Moritz Meier-Merziger,*[b] *Holger Frey,*[b]* *and George Floudas* [a,c,d]*

* Corresponding authors

[a] Department of Physics, University of Ioannina, P.O. Box 1186, 45110 Ioannina, Greece

[b] Department of Chemistry, Johannes Gutenberg University Mainz, Duesbergweg 10-14, 55128 Mainz, Germany

[c] Max Planck Institute for Polymer Research, Ackermannweg 10, 55128 Mainz, Germany

[d] University Research Center of Ioannina (URCI)-Institute of Materials Science and Computing, 45110 Ioannina, Greece

Published in: *Macromolecular Rapid Communications*, **2024**, 2400551.
https://doi.org/10.1002/marc.202400551

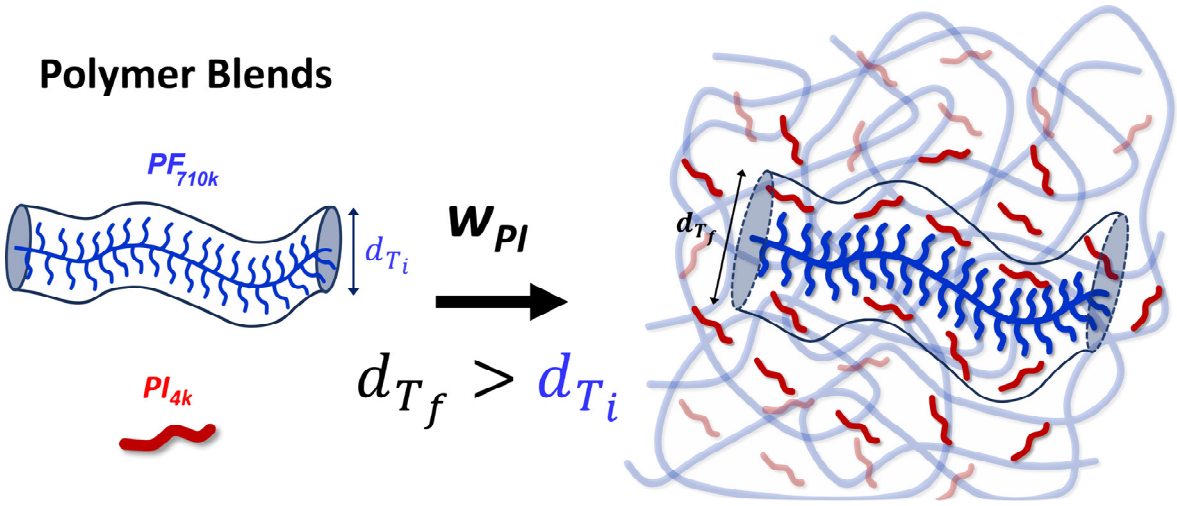

The following publication is adapted with permission from Tzourtzouklis, I.; Meier-Merziger, M.; Frey, H.; and Floudas, G.; Supersoft Polymer Melts in Binary Blends of bottlebrush cis-1,4-polyfarnesene and cis-1,4-polyisoprene, *Macromolecular Rapid Communications*, **2024,** 2400551.

Abstract

We employ binary blends of polyterpenes comprising *cis*-1,4-polyfarnesene (PF) with a bottlebrush architecture, and linear *cis*-1,4-polyisoprene (PI) as model systems towards supersoft polymer melts. The bottlebrush PF results in a low plateau modulus ($G_N^0 \sim 4.3 \times 10^4$ Pa) that can further be reduced with the addition of PI. Depending on the fraction of short PI chains in the *athermal* and nearly *isofrictional* blends, plateau moduli in the range from 1 to 10 kPa can be achieved. Tube dilation is very efficient in the present binary blends as compared to more common blends comprising long/short or linear/star chains of identical polymer structure.

1. Introduction

Biological materials have elastic moduli that range from ~ 10 Pa (supersoft tissues) to ~ 10^7 Pa (skin and tendons).[1],[2] Mimicking soft biological tissues with polymeric materials requires specific architectural design based on brush-like motifs.[3]–[6] The underlying idea is that the bottlebrush architecture will increase the diameter of polymer chains, and as a result, dilute the entanglements (i.e., increase the entanglement molar mass, M_e). Linear polymer melts fail this exercise, with M_e in the range from 10^3 to 10^4 g·mol^{-1} the rubbery plateau modulus, G_N^0, ($G_N^0 = \frac{4}{5}\frac{\rho RT}{M_e}$, where ρ is the mass density, T is the temperature and R is the Avogadro number) is in the range from 10^5 Pa to 10^6 Pa, i.e., much higher than the one encountered in soft biological tissues. Contrasting this with bottlebrush polymers, scaling arguments predict[7] that the plateau modulus scales with the tube diameter, d_T, and the number of units of the side chains (n_{sc}) as $G_N^0 \sim M_e^{-1} \sim d_T^{-3} \sim n_{sc}^{-3/2}$. In addition to n_{sc}, the mechanical response is controlled by the grafting density (n_g^{-1}); i.e., the number of side chains per backbone repeat unit. In networks made of bottlebrush polymers, another important parameter is the degree of polymerization of the strand backbone (n_x). In this case, the triplet (n_{sc}, n_g, n_x) controls the mechanical response of the network.

Earlier studies[4]–[6],[8] demonstrated that solvent-free polymer melts with the bottlebrush architecture comprising side chains attached to each repeat unit along the backbone, exhibit viscoelastic properties reminiscent of the bare backbone polymer in the presence of a diluent. Subsequent cross-linking of the undiluted bottlebrush polymer resulted in a plateau modulus of ~ 1 kPa, a value typically found in networks swollen by a diluent.[8]

Here we employ a different approach towards supersoft polymer melts. It is based on a recent investigation of the viscoelastic and dielectric properties of polymyrcene (PMyr)[9], a bio-based polymer belonging to the class of polyterpenes (other known members are the *cis*-1,4-polyisoprene (PI), and the *cis*-1,4-polyfarnesene (PF)[10]). Polyterpenes[11]–[14] constitute a class of type-A polymers, where by architectural design one can control the "thickness" of chains and henceforth the chain dynamics. As expected, chain thickening greatly affects the viscoelastic properties: In going from PI to PMyr and to PF, the entanglement molar mass increases (from 5 kg·mol^{-1} in PI, to 22 kg·mol^{-1} in PMyr, to 50 kg·mol^{-1} in PF). Similarly, the packing length increases (from 3.1 Å in PI to 4.7 Å in PMyr and to 6.3 Å in PF). Lastly, the plateau modulus decreases (from 0.35 MPa in PI, to 0.1 MPa in PMyr, and to 0.0426 MPa in PF). Furthermore, the plateau modulus followed the empirical relation: $G_N^0 = 0.00226\ k_B T/p^3$ consistent with the proportionality between the tube diameter and the packing length, p.[9],[15]

Motivated by the above findings, we employ binary blends of polyterpenes aiming to exert additional control over the plateau modulus and packing and henceforth to trigger the flow behavior. Inherent to the blend studies of long/short chains is the concept of constraint release (CR) of the long chain motions by the shorter chains, the latter acting effectively as a solvent.[16]–[20] In bidisperse blends with identical chemistry[21]–[24] comprising entangled long chains (molar mass, M_L, volume fraction, φ_L) and entangled short chains (molar mass, M_S) the terminal dynamics are determined by the relative relaxation of the reptating long chains, $\tau_{L,rept.} = 3\tau_e \left(\frac{M_L}{M_e}\right)^3$, vs the CR Rouse relaxation, $\tau_{CR} = 3\tau_e \left(\frac{M_S}{M_e}\right)^3 \left(\frac{M_L}{M_e}\right)^2$, and the final entanglement density, $Z = \left(\frac{M_L}{M_e}\right)\varphi_L^{\alpha}$, where α is the dilution exponent. In the present case the short/long chains form an athermal blend, but the components are not chemically identical, possessing very different M_e values. We show that athermal binary PF/PI blends where one component (PF) has a bottlebrush architecture and the other comprises linear chains (PI), constitute a new class of supersoft polymer melts. Depending on the fraction of short PI chains in the blend, plateau moduli as low as 1 kPa could be obtained.

2. Experimental Section

2.1 Synthesis

All polymerizations were made under an inert argon atmosphere as described elsewhere in detail.[9],[11]–[13] β-Farnesene was freed from its stabilizer by passing it through alkaline aluminum oxide. Subsequently it was dried over calcium hydride for 24 hours and degassed using at least three *freeze-pump-thaw* cycles. Then a 25 vol% solution of trioctyl aluminum in cyclohexane was added, and the solvent was removed in vacuo. The solvent *n*-heptane was dried using *sec*-butyl lithium (*s*-BuLi) and 1,1-diphenyl ethylene. Both monomer and solvent were freshly distilled prior to use and transferred into an argon filled glove box. Polymerizations were carried out at a volume concentration of β-farnesene to *n*-heptane of 1:9 and initiated using the respective amount of *s*-BuLi (1.3 molar solution) for the targeted molar mass (M_n=M_0·[M]$_0$/[I]); where M_0 = molar mass of β-farnesene, [M]$_0$ = monomer concentration and [I] = initiator concentration). The polymerizations were run over night at either ambient temperature or at 70 °C and terminated with degassed methanol. Thereafter, the reaction mixture was concentrated in vacuo and finally precipitated in isopropyl alcohol/methanol. By centrifugation and decantation, the polymeric material was separated from the solvent mixture. The polymer was redissolved in chloroform and precipitated a second time. The isolated polymer was dissolved in benzene and freeze-dried for at least 72 hours at 40 °C in vacuo ($1 \cdot 10^{-3}$ mbar) to remove any traces of solvents. Approximately quantitative yields of

>95% were obtained. The deviation can be attributed to a loss during purification. All samples were characterized *via* size-exclusion chromatography (SEC) and nuclear magnetic resonance spectroscopy (NMR).

The polyisoprene samples were purchased from *PSS Polymer Standards*, Mainz, Germany. As calibration standards for SEC instruments, they offer analytic purity and certificates, i.e., number average molar mass (M_n), mass average molar mass (M_w) and low dispersity ($Đ$). All values were measured by RI-detection in THF relying on a polyisoprene calibration. In addition, mass average molar mass (M_w^{MALS}) values obtained by multi-angle light scattering (MALS) are given. The molecular characteristics of the PF and PI samples are provided, respectively, in **Tables S1** & **S2**, Supporting Information.

2.2 Analytic Measurements

Size exclusion chromatography (SEC). All samples were measured using tetrahydrofuran (THF) as eluent and a polyisoprene calibration. A set-up consisting of: Waters 717 plus autosampler, a SpectraSeries-P100 pump, a column set (MZ-Gel SD plus e5/e3/100) of *MZ-Analysentechnik*, Mainz, an *Agilent G1362A* RI-Detector, and a *MZ-Messanalytik TSP* (254 nm) UV-detector were used. SEC traces for the PF homopolymers are shown in **Figure S1**, Supporting Information. As for the determination of the absolute molar mass, all samples were additionally measured using a multi-angle light scattering (MALS) detector. For these samples a column set PSS SDV 5 µm pc/ PSS SDV 5 µm 1 000 Å/ PSS SDV 5 µm 100 000 Å/ PSS SDV 5 µm 1 000 000 Å was used. It was measured on an *Agilent 1200* setup. The comparison of the molar mass of all PF and PI samples, determined by SEC with MALS detector is shown in **Figure S2** (Supporting Information).

Nuclear magnetic resonance spectroscopy (NMR). All samples were measured on a 400 MHz Bruker Avance II HD 400 instrument. Spectra (^{1}H, ^{13}C, COSY and HSQC) were recorded at the maximum frequency for each nucleus (400 MHz for ^{1}H and 101 MHz for ^{13}C). All measured spectra were processed using the software "*MestReNova v14.2.0*" from Mestrelab Research S.L., Santiago de Compostela, Spain. The spectra were normalized to the respective proton signal of the deuterated solvent of choice and phase and baseline corrected. ^{1}H NMR spectra of PF_{17} and PI_{64} are provided in **Figure S3** and **Figure S4**, respectively.

2.3 Rheology

The viscoelastic properties of all blends have been studied with the TA Instruments Rheometer AR-G2 equipped with a magnetic bearing that allows for nanotorque control. Measurements were performed in an environmental test chamber (ETC). Samples were prepared on the lower rheometer plate (8 mm), and the upper plate was adjusted aptly to ensure a uniform gap thickness. Temperature control was achieved through a nitrogen convection oven. The linear and non-linear viscoelastic regimes were determined by the strain amplitude dependence of the complex shear modulus $|G^*|$, at $\omega = 10$ rad·s^{-1}. Data of the complex shear modulus as a function of frequency were obtained by frequency sweeps in the range of 0.1–100 rad·s^{-1} for several temperatures near and above the glass temperature. According to the principle of time–temperature superposition (*tT*s), the frequency dependence of the complex shear modulus G^* at any temperature can be obtained from a master curve at a reference temperature (here $T_{\mathrm{ref}} = 253$ K for all the cases) according to the equation: $G^*(\omega,T) = b_{\mathrm{T}}G^*(a_{\mathrm{T}}\omega,T_{\mathrm{ref}})$.

2.4 Dielectric Spectroscopy

Dielectric spectroscopy measurements as a function of temperature (*i.e.* under "isobaric" conditions) were performed with the *Novocontrol Alpha* high-resolution frequency analyzer, within the frequency range from 10^{-2} Hz to 10^{7} Hz, and for temperatures in the range from 173.15 K to 333.15 K. All samples, before measurement, were placed into an oven under vacuum conditions in order to remove traces of water/solvent. The DS measuring cell consisted of two platinum electrodes (of 20 mm diameter) forming a capacitor. A Teflon spacer was inserted in the sample to keep the distance of the electrodes fixed (about 50 μm). By applying an alternating electric field to the capacitor, the complex dielectric function (ε^*) is obtained as a function frequency (ω) and temperature (T). The latter is defined as $\varepsilon^* = \varepsilon' - i\varepsilon''$, where the real part (the dielectric permittivity) refers to the energy which is reversibly stored in the dielectric, and the imaginary part to the dielectric losses. The analysis of the DS resulted curves was based on the empirical equation of Havriliak and Negami (Eq. 1)[25]

$$\varepsilon^*_{HN}(\omega,T) = \varepsilon_\infty(T) + \sum_j \frac{\Delta\varepsilon_j(T)}{\left[1+(i\omega\tau_{HN\,j}(T))^{m_j}\right]^{n_j}} + \frac{\sigma_0(T)}{i\varepsilon_f\omega} \qquad \textbf{(1)}$$

where $\varepsilon_\infty(T)$ is the high frequency permittivity, ε_f is the permittivity of free space, $\tau_{HN}(T)$ refers to the characteristic relaxation time of this model, $\Delta\varepsilon(T) = \varepsilon_0(T) - \varepsilon_\infty(T)$ is the relaxation strength of the process under investigation, m and n are the two shape parameters of the HN equation (with $0 \le m_{\mathrm{j}}$, $m_{\mathrm{j}}n_{\mathrm{j}} \le 1$), ω ($= 2\pi f = 1/\tau$) is the angular frequency of the

external electric field, and $\sigma_0(T)$ introduces the conductivity contribution. From the τ_{HN} the relaxation times at maximum loss, τ_{max}, were obtained analytically from the HN equation as follows:

$$\tau_{max} = \tau_{HN}\left[sin\left(\frac{\pi m}{2(1+n)}\right)\right]^{-1/m}\left[sin\left(\frac{\pi mn}{2(1+n)}\right)\right]^{1/m} \quad \textbf{(2)}$$

In the temperature range where two or more relaxation processes contribute to ε^*, a summation of HN functions was used, assuming statistical independence in the frequency domain.

Table 1. Molar mass (M_n), number of entanglements (Z) and composition (w) of the binary bottlebrush/linear PF/PI blends.

BLENDS	**Name**	$\boldsymbol{M_n^{PI}}$ [g · mol^{-1}]	$\boldsymbol{M_n^{PF}}$ [g · mol^{-1}]	$\boldsymbol{Z_{PI}}$	$\boldsymbol{Z_{PF}}$	$\boldsymbol{w_{PI}}$	$\boldsymbol{w_{PF}}$
CASE I PF($3M_e$)/PI	BLD-PI(M_e)	4 500	129 000	0.9	2.6	0.5	0.5
	BLD-PI(2 M_e)	9 900	129 000	2.0	2.6	0.5	0.5
	BLD-PI(4 M_e)	19 000	129 000	3.8	2.6	0.5	0.5
	BLD-PI(8 M_e)	38 800	129 000	7.8	2.6	0.5	0.5
	BLD-PI(20 M_e)	103 000	129 000	20.6	2.6	0.5	0.5
	BLD-PI(30 M_e)	150 000	129 000	30	2.6	0.5	0.5
CASE II PI(M_e)/PF	BLD-PF(3 M_e)	4 500	129 000	0.9	2.6	0.5	0.5
	BLD-PF(8 M_e)	4 500	414 000	0.9	8.3	0.5	0.5
	BLD-PF(14 M_e)	4 500	710 000	0.9	14.2	0.5	0.5
CASE III PI(M_e)/PF($14M_e$)	BLD-PF(0.1)	4 500	710 000	0.9	14.2	0.9	0.1
	BLD-PF(0.2)	4 500	710 000	0.9	14.2	0.8	0.2
	BLD-PF(0.4)	4 500	710 000	0.9	14.2	0.6	0.4
	BLD-PF(0.5)	4 500	710 000	0.9	14.2	0.5	0.5
	BLD-PF(0.6)	4 500	710 000	0.9	14.2	0.4	0.6
	BLD-PF(0.9)	4 500	710 000	0.9	14.2	0.1	0.9

3. Results and Discussion

With the binary polyterpene blends of the "bottlebrush PF" and the linear PI we explore three cases. In the first section (**Case I**) we study the effect of PI molar mass on tube dilation by employing several symmetric PF/PI blends having an entangled PF (with Z_{PF}=2.6), and different PIs (molar masses from Z_{PI}=0.9 to 30). More efficient tube dilation effects can be obtained by exploring the effect of PF molar mass (Z_{PF}=2.6 to 14.2) in blends with a fixed PI (Z_{PI}=0.9) (**Case II**). In the last section (**Case III**) we employ the most efficient supersoft polymer melt (with Z_{PF}=14.2, and Z_{PI}=0.9) and explore the effect of blend composition.

3.1. CASE I: Effect of PI Molar Mass

In the first case we explore the effect of PI molar mass by preparing several symmetric PF/PI blends having a fixed PF molar mass (Z_{PF}=2.6) and different PI molar masses from unentangled (Z_{PI}=0.9) to well-entangled (Z_{PI}=30) (**Table 1**). The master curves of the blends are shown in **Figure 1**. They were constructed at the same reference temperature (T=253 K) and further normalized to the segmental relaxation time. A clear plateau is observed only in cases where the PI molar mass is above $\sim 8M_e$. The terminal relaxation in the blends shows a distinct dependence on PI molar mass (**Figure 1b**). When the PI molar mass is below $\sim 8M_e$ the terminal relaxation follows the corresponding PF relaxation (where Z_{PF}=2.6). On the other hand, for PI molar masses above $8M_e$ (Z_{PI}=7.8) the terminal relaxation is dictated by the longer PI chains. In this respect, the blend BLD-PI($8M_e$) lies at the borderline between PF- and PI-dominated terminal regimes. **Figure 1b** contains, in addition to the terminal relaxation from rheology, the longest normal mode as obtained from DS, for comparison. The results are in good agreement, as expected from the low polarity of PI and PF.

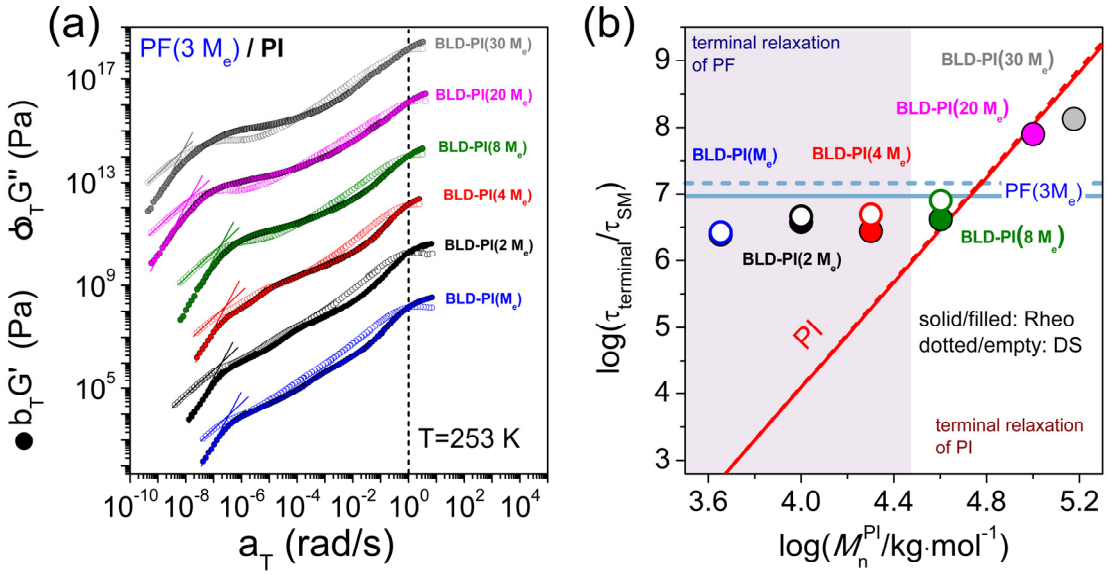

Figure 1. (a) Master curves for the storage (filled circles) and loss (open circles) moduli of the symmetric binary blends of PF/PI having a fixed PF molar mass (M_n^{PF} = 129000 g·mol^{-1}) and different PI molar masses: M_e (blue), $2M_e$ (black), $4M_e$ (red), $8M_e$ (green), $20M_e$ (magenta), and $30M_e$ (gray), all at T=253 K. Master curves are normalized to the segmental relaxation time, τ_{SM}, and are further shifted vertically for clarity. Linear fits with respective slopes 2 and 1 for the storage and loss moduli are shown, characteristic of the terminal relaxation. (b) Terminal relaxation times, normalized by the respective segmental times in the binary blends plotted as a function of PI molar mass. Solid lines give the τ_{term}/τ_{SM} for PI (shown in red) and PF (shown in blue) from rheology and corresponding dashed lines from DS. Symbols indicate the normalized τ_{term} from rheology (filled circles) and DS (open circles), respectively. Grey and white areas indicate regimes dominated by PF and PI terminal dynamics.

More informative with respect to the viscoelastic properties of the blends, and in particular regarding the applicability of time-temperature superposition, is the van Gurp-Palmen plot (vGP)[26],[27] of the phase angle δ vs. logG^* ($|G^*|=(G'(\omega)^2+G''(\omega)^2)^{1/2}$), see **Figure 2**. In a material following tTs, prior to any shift, all isothermal data in the vGP plot overlap in a single master curve. Starting from the terminal regime (where δ=90^0) and moving across the modulus scale, the modulus first decreases to a minimum value that is characteristic of the plateau modulus, G_N^0. The more entangled the polymer the deeper is the minimum. Subsequently, δ increases, goes through a maximum and decreases again to another minimum, in the vicinity of the glass "transition" ($|G^*|$=10^9 Pa). In the blends, one can observe several distinct features. First, tTs is only partially obeyed, especially on approaching the liquid-to-glass temperature. The reason is that PF has a lower T_g than PI (T_g(PF) ~ 200 K and T_g(PI) ~ 207 K).[9],[10] In the blends, there exists a single, albeit broad T_g giving rise to the lack of a perfect superposition. Nevertheless, to a good approximation the blends can be regarded as isofrictional. Second, in blends where the PI molar mass is higher than ~ $8M_e$, a clear minimum in δ is observed (with values in the

range $20^0 < \delta < 30^0$) at $|G^*|=10^5$ Pa giving the plateau modulus. In blends where $M(\mathrm{PI}) < 8M_e$, two shallow minima are observed suggestive of two quasi-elastic regimes. The first minimum in δ, $G^*_{\delta^1_{min}}$, between the terminal relaxation and the plateau modulus associates with the relaxation of the PF ($3M_e$) chains in the blend. As for the second minimum in δ, $G^*_{\delta^2_{min}}$, it was shown that it associates with the steady-state recoverable compliance, as it shifts with decreasing PI molar mass.[26]

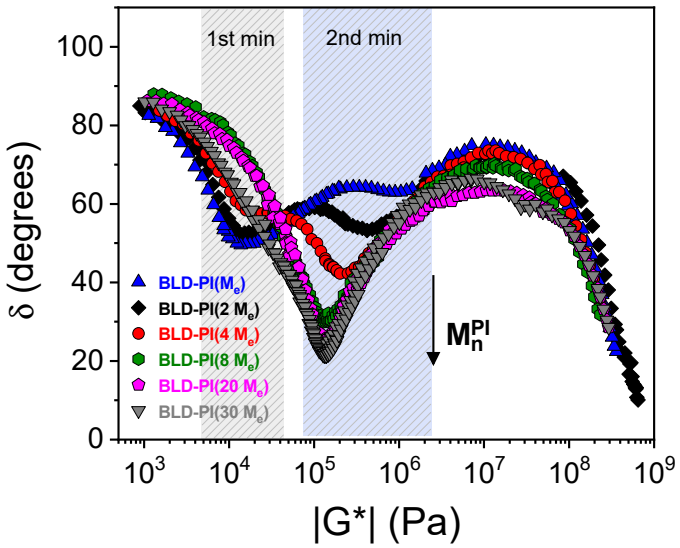

Figure 2. The van Gurp-Palmen plot for the symmetric binary blends of PF/PI shown for different PI molar masses: BLD-PI(M_e) (blue triangles), BLD-PI($2M_e$) (black rhombi), BLD-PI($4M_e$) (red spheres), BLD-PI($8M_e$) (green hexagons), BLD-PI($20M_e$) (magenta pentagons) and BLD-PI($30M_e$) (gray down-triangles). In the first three cases two weak minima are evident, while in the three latter cases one strong minimum below 40^o indicates the blend plateau modulus.

We can further explore the plateau modulus and obtain respective values for the entanglement molar mass, M_e, packing length, p, and tube diameter, d_T, using $M_e = \frac{4}{5}\frac{\rho RT}{G_N^0}$, where ρ is the mass density (ρ_{PI}=0.91 g·cm^{-3};[28] ρ_{PF}=0.90 g·cm^{-3} [10]), $M_e = 218\rho p^3$, and $d_T = 19p$.[28] The result is shown in **Figure 3**. We emphasize here, that the interpretation of the value of $|G^*|$ at the first and second (main) δ_{min} as corresponding to the plateau modulus is accurate only for the three blends with the strong single δ_{min}. For it is only in the latter case that the $G^*_{\delta^2_{min}}$ value corresponds exactly to the plateau modulus. Nevertheless, we calculate these quantities even for blends with $M(\mathrm{PI}) < 8M_e$ to explore some trends.

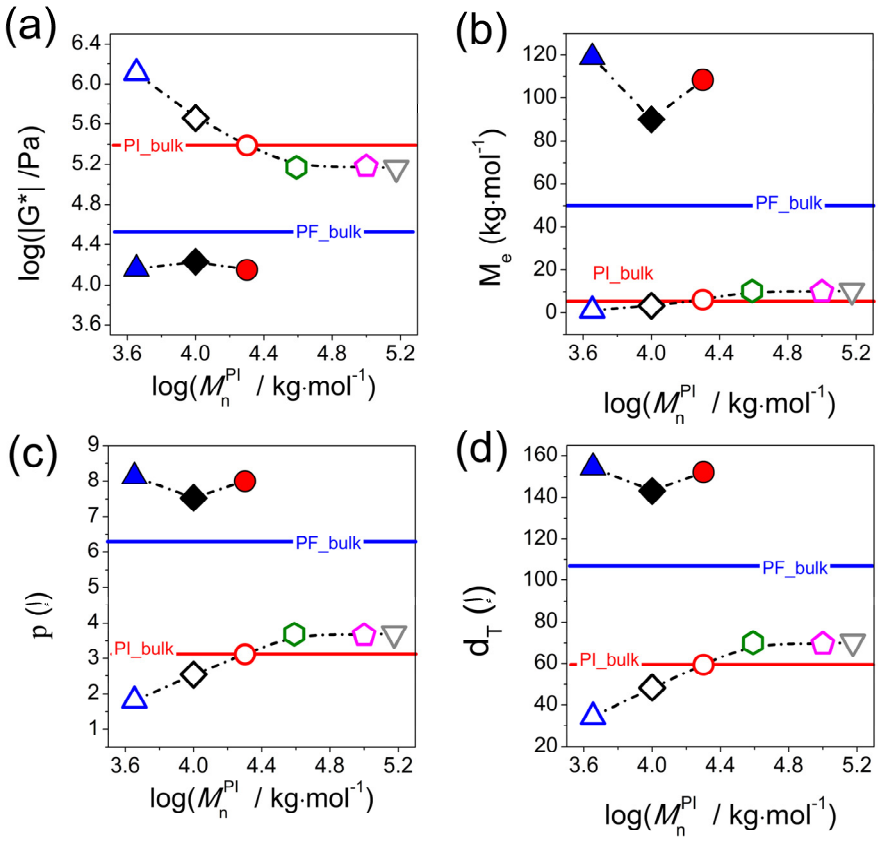

Figure 3. Viscoelastic properties of the symmetric binary blends PF/PI having a fixed PF molar mass (M_n^{PF} = 129000 g·mol^{-1}) and different PI molar masses. (a) Absolute value of the complex shear modulus as a function of PI molar mass. Filled symbols correspond to the first minimum in the van Gurp-Palmen plot, while open symbols correspond to the second minimum. (b) Entanglement molar mass plotted as a function of the PI molar mass. (c) Packing length over the molar mass of the PI component. (d) Tube diameter as a function of PI molar mass in the blend. Red and blue solid lines correspond to well-entangled homopolymers of PI and PF, respectively.

The value of the $G^*_{\delta^1_{min}}$ corresponding to the terminal relaxation of PF in the blends with M(PI)< 8M_e results to a higher M_e, p, and d_T values with respect to the PF homopolymer. This is one aspect of dynamic tube dilation in blends of long/short chains with identical chemistry that has been explored earlier.[16]–[19],[21]–[24] Effectively, the lower molar mass PI acts as a solvent to the PF component, alleviating the constraints and increasing the tube diameter of PF. More efficient tube dilation effects can be obtained by exploring the effect of PF molar mass in blends with a fixed PI molar mass (**Case II**, below).

3.2. CASE II: Effect of PF Molar Mass

Here we explore the viscoelastic properties in three blends having a fixed PI molar mass (M_e; Z_{PI}=0.9), and PF with increasing molar mass (from Z_{PF}=2.6 to 14.2). The master curves for the blends are compared with the pure components in **Figure 4**. For the BLD-PI(M_e)-PF($3M_e$), the rubbery plateau is not pronounced and the terminal relaxation speeds-up as compared to the PF homopolymer (**Figure 4a**). In the other extreme, the BLD-PI(M_e)-PF($14M_e$) blend, the rubbery plateau is clearly evident, but the plateau modulus is decreased nearly by an order of magnitude (**Figure 4c**). Evidently, blending high molar mass PF with short PI chains results in an efficient dynamic tube dilation (**Figure 4d**), giving rise to super-soft polymer melts.

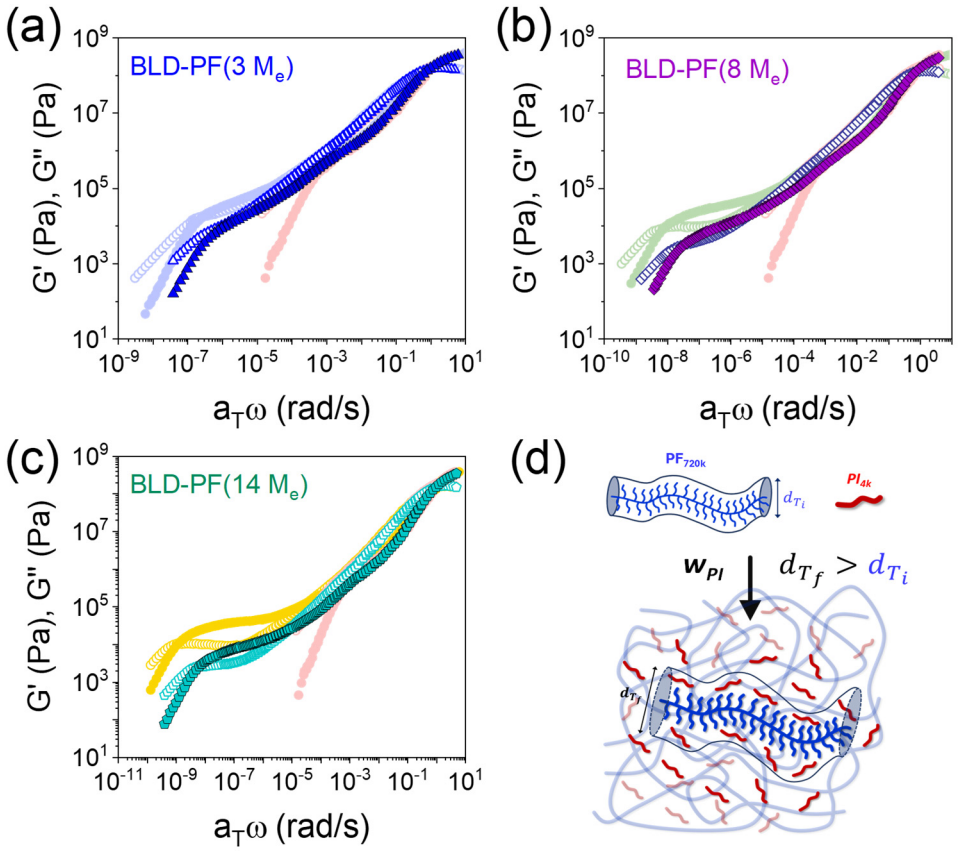

Figure 4. Master curves of the storage (filled symbols) and loss (open symbols) moduli for the bulk components (pale colors) and the PI(M_e) – PF blends for the three different cases of (a) BLD-PF($3M_e$), (b) BLD-PF($8M_e$) and (c) BLD-PF($14M_e$). In all cases, data are normalized to their segmental relaxation time. (d) Graphical representation of the tube dilation effect, where the low molar mass PI acts as a solvent for the well-entangled PF component.

How effective is the obtained supersoft polymer melt? To address this question, we explore the details of the vGP plot (**Figure 5**). The plot reveals one sharp minimum that is very distinct in the BLD-PF($14M_e$) (δ_{min}~20^0), and in BLD-PF($8M_e$) (δ_{min}~36^0), but much less distinct in BLD-PF($3M_e$) (δ_{min}~50^0). The value of modulus at the minimum shifts from $|G^*|$=4.3 ×10^4 Pa in

PF(14M_e) homopolymer, to |G^*|=7.3×10^3 Pa in the BLD-PF(14M_e), i.e., a 6-fold decrease in the plateau modulus. This again suggest that efficient supersoft polymers can be designed by mixing a well entangled bottlebrush polymer (PF component) with a low molar mass linear (PI component) polymer.

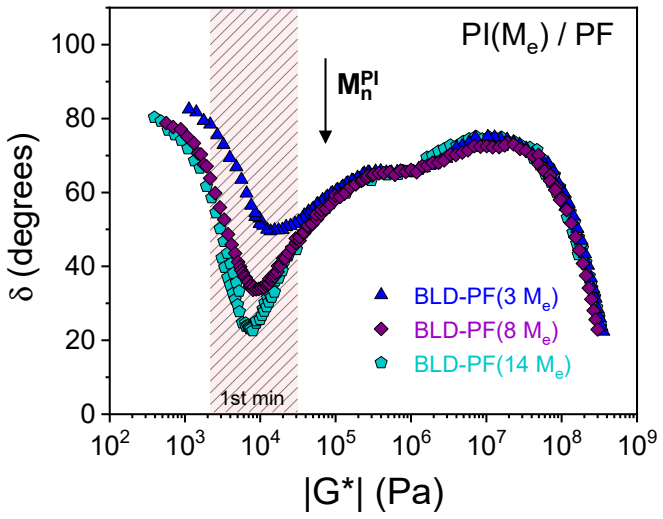

Figure 5. Van Gurp-Palmen plot for the three symmetric binary blends PF/PI having a fixed PI molar mass (M_n^{PI} = 4500 g·mol^{-1}) and different PF molar masses: BLD-PF(3M_e) (blue), BLD-PF(8M_e) (purple) and BLD-PF(14M_e) (light green). One strong minimum is evident in the latter two cases, together with a barely distinguishable second minimum, corresponding to the chain relaxation of the low molar mass constituent, PI(M_e). By increasing the molar mass of PF, |G^*| moves to lower values, adapting properties similar to those of supersoft polymers.

The effect of increasing PF molar mass on M_e, the packing length, p, and the tube diameter, d_T, are shown in **Figure 6**. The figure shows an increasing entanglement molar mass (**Figure 6b**), packing length (**Figure 6c**), and tube diameter (**Figure 6d**) with increasing PF molar mass in the blends. Interestingly, the PF tube diameter is nearly doubled by blending PF(14M_e) with a low molar mass PI(M_e) that acts as a diluent. In the next section we employ the most efficient supersoft polymer blend and explore the effect of blend composition on further controlling the plateau modulus.

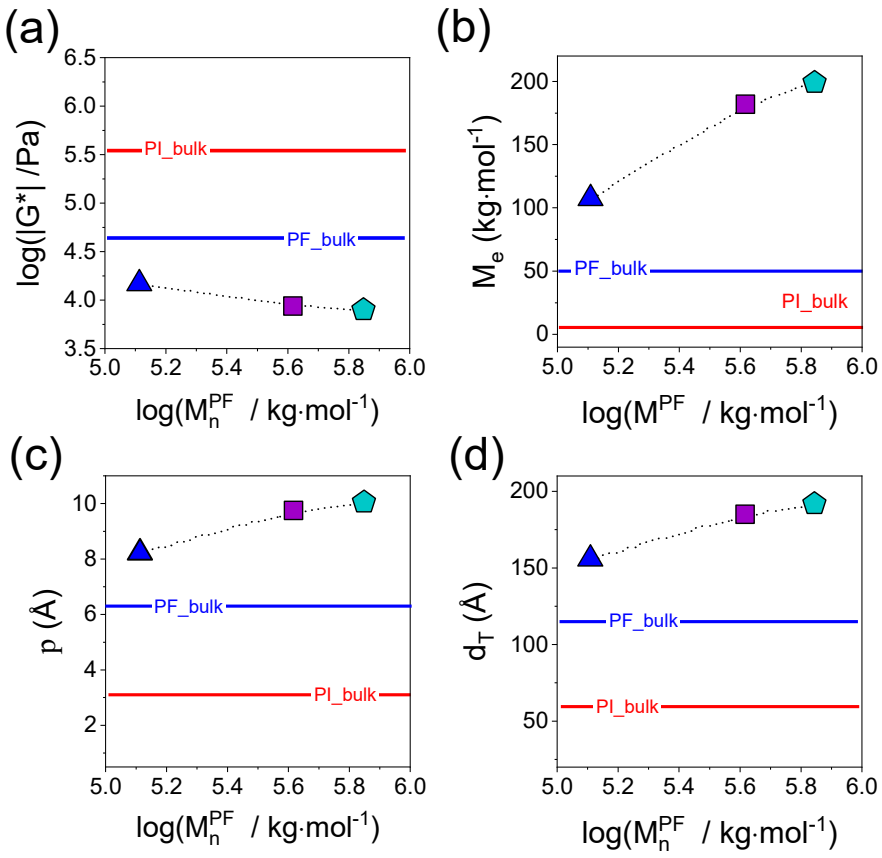

Figure 6. (a) Absolute value of the complex shear modulus as a function of PF molar mass for the three symmetric binary blends PF/PI having a fixed PI molar mass (M_n^{PI} = 4500 g·mol^{-1}) and different PF molar masses: BLD-PF($3M_e$) (blue triangle), BLD-PF($8M_e$) (purple square) and BLD-PF($14M_e$) (light green pentagon). For the extreme case of PF($14M_e$)-PI(M_e) the plateau value is lower than 10^4 Pa, exhibiting properties similar to supersoft polymer melts (see text). (b) Entanglement molar mass, (c) packing length, and (d) tube diameter plotted as a function of the PF molar mass in the blends. Red and blue solid lines give respective values for well entangled PI and PF homopolymers.

3.3. CASE III: Effect of Blend Composition on Tube Dilation.

Can we make better supersoft melts by controlling the bottlebrush/linear polymer blend composition? To this end we employ the well-entangled PF($14M_e$) and prepare blends with a low molar mass PI(M_e) at different ratios. **Figure 7** compiles the respective mastercurves for the storage modulus in the homopolymers and their blends. The results show a decreasing rubbery plateau with increasing PI content. In the inset, the normalized terminal relaxation times, are plotted as a function of the PF weight fraction in a double logarithmic representation. The results reveal a dependence as $\tau_{term} \sim w_{PF}^{1.5}$.

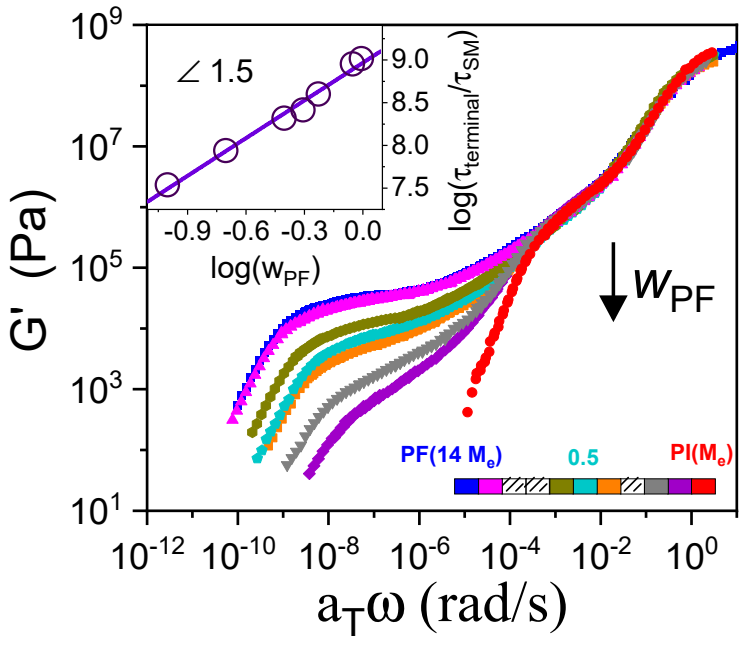

Figure 7. Mastercurves of the storage moduli (G') normalized at the segmental relaxation times, for blends with various blend compositions. A significant reduction in the plateau modulus is evident. In the inset, the terminal relaxation times, normalized to the segmental relaxation times, are plotted as a function of the PF weight fraction in a double logarithmic plot. A line with a slope of 1.5 is shown.

To explore further the details of the viscoelastic properties in the blends we discuss the vGP plot with the help of **Figure 8a**. Two minima are evident in some cases; the first minimum corresponds to the transition from the terminal relaxation of the blend to the rubbery plateau, whereas the second (shallow) minimum corresponds to the chain relaxation of the low molar mass component (PI). The first minimum in δ, $G^*_{\delta^1_{min}}$, is deep in the cases of $w_{PF} \geq 0.4$ and becomes shallow for $w_{PF} \leq 0.2$. As shown in **Figure 8b**, $1/G^*_{\delta^1_{min}} \sim w_{PF}^{-1.75}$, a somewhat weaker dependence than the one reported for blends of linear polymers (e.g. polystyrene).[26]

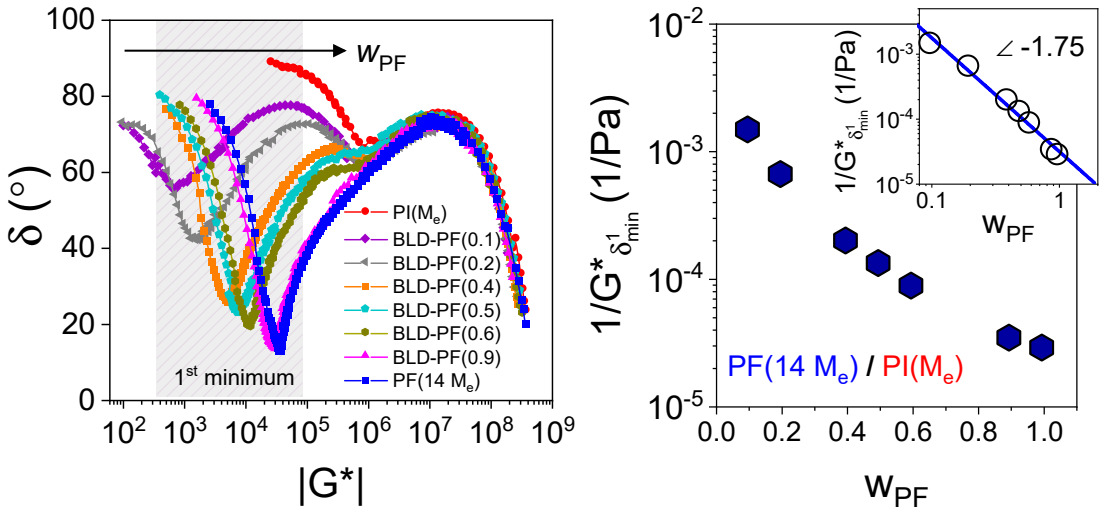

Figure 8. (Left) van Gurp-Palmen plot for the blends with different PF weight fraction: BLD-PF(0.1) (purple), BLD-PF(0.2) (gray), BLD-PF(0.4) (orange), BLD-PF(0.5) (light green), BLD-PF(0.6) (olive), BLD-PF(0.9) (magenta), PI(M_e) (red), PF(14M_e) (blue). (Right) The inverse of $|G^*|$ at the first δ minimum is plotted over the weight fraction of the high molar mass component, w_{PF}. In the inset, the same data are shown in a double logarithmic representation. The blue solid line indicates that $1/G^*_{\delta^1_{min}}$ varies with w_{PF} in the power of -1.75.

The extracted parameters from the absolute value of the complex shear modulus at $G^*_{\delta^1_{min}}$, i.e., the entanglement molar mass, the packing length, and the tube diameter, are plotted in **Figure 9** as a function of the weight fraction of PF in the blends. It is evident that the value of $|G^*|$ decreases with decreasing PF fraction in a nonlinear way. Data obtained for the M_e, p, and d_T in the case of the two blends with $w_{PF} \leq 0.2$ are shown in faint color, since a clear rubbery plateau is not observed in this case. For the remaining blends, results show significant tube dilation with increasing PI content. In the case of $w_{PF} = 0.4$ the entanglement molar mass increases to ~ 300 kg·mol^{-1} (from 50 kg·mol^{-1} in PF), the packing length to ~ 11.5 Å (from 6.3 Å in PF), and the tube diameter to 220 Å (from 116 Å in PF).[9],[10]

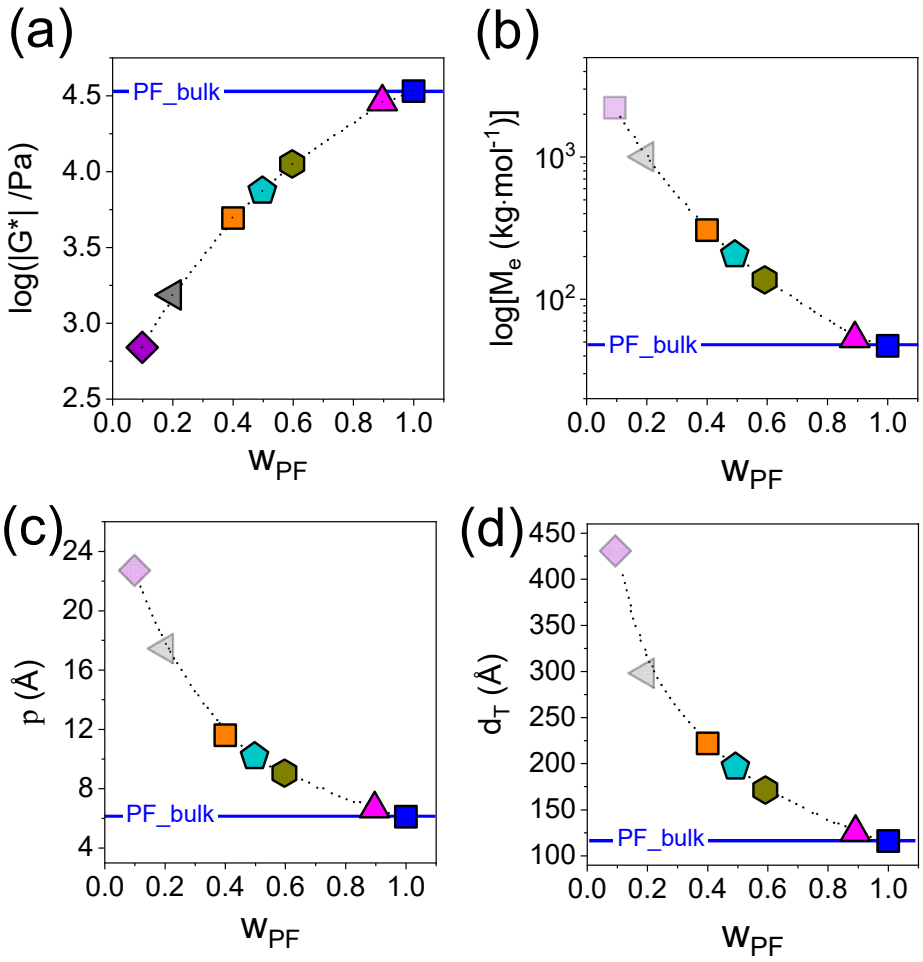

Figure 9. (a) Absolute value of the complex shear modulus at $G^*_{\delta^1_{min}}$ as a function of the weight fraction of the PF in the blends. Dependence of (b) the entanglement molar mass, (c) the packing length, and (d) the tube diameter, as a function of PF weight fraction. The dotted line is a guide for the eye. Blue solid line indicates the corresponding values for the PF($14M_e$) homopolymer.

The efficiency in tube dilation by chain architecture can be compared for different PI topologies (linear/linear, linear/star, and linear/bottlebrush) by plotting the dilated tube diameter in the blends reduced by the respective value in undiluted long homopolymer, as a function of the volume fraction of long chains, φ_L, in **Figure 10**. The figure depicts tube dilation in linear/linear PI blends scaling as $\varphi_L^{-0.5}$, and in linear/star PI blends scaling as $\varphi_L^{-0.375}$.[21] This should be contrasted with the present PF/PI (bottlebrush/linear) blends where tube dilation scales as $\varphi_L^{-0.56}$. Employing only blends where the rubbery plateau is more evident (e.g. ignoring the data points with $w_{PF} \leq 0.2$), it provides an even steeper dependence, e.g. scaling as $\varphi_L^{-0.73}$. Overall, the results show that among the different topologies examined, blends comprising of bottlebrush/linear chains are more effective in the process of tube dilation resulting in supersoft polymer melts. The explanation for this key observation is the low

rubbery plateau value of the bottlebrush polymer. Further crosslinking of the longer chains will result in supersoft elastomers.

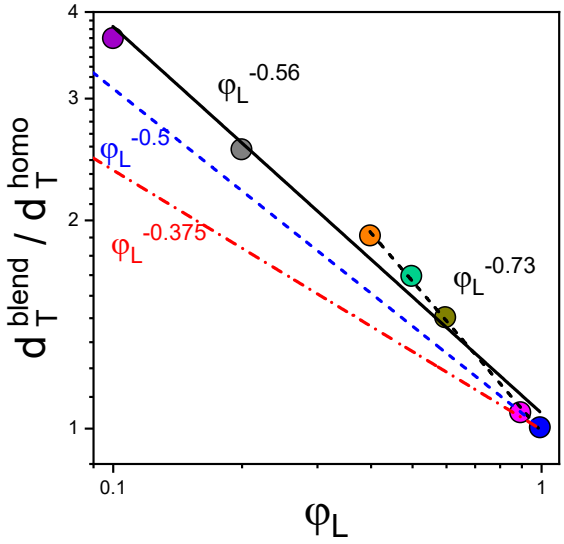

Figure 10. Architecture-induced tube dilation. Tube diameter in blends relative to the respective homopolymers for (a) linear PI blends (PI($16M_e$)/PI($2.4M_e$) shown with the red dash-dotted line, (b) blends of the same linear PI($16M_e$) with PI stars,[21] shown with the dashed blue line), and (c) the present bottlebrush/linear PF/PI blends shown with the black line.

3. Conclusions

Bottlebrush polymers are solvent-free melts with a plateau modulus as low as 1 kPa, a value typically found in swollen networks and required to match soft biological tissues. We employed binary blends of polyterpenes comprising linear (*cis*-1,4-PI) and bottlebrush (*cis*-1,4-PF) topologies to explore the possibility to further reduce the - already low - plateau modulus of PF (G_N^0~4.3×10^4 Pa) by tube dilation. The new *athermal* and largely *isofrictional* PF/PI blends constitute a new class of supersoft polymer melts with plateau moduli in the range from 10 to 1 kPa. The efficiency in tube dilation relates to polymer architecture; we deduce that blends of polyterpenes are more effective than long/short PI blends, as well as from linear/star PI blends, *i.e.*, blends with identical chemistry. This opens a new area, where bottlebrush/linear athermal polymer blends can be employed as a means to adjust the elasticity and flow behavior in polymer melts and thereby lead to supersoft elastomer materials after crosslinking.

References

[1] Meyers, M. A.; Chen, P.-Y.; Lin, A. Y.-M.; Seki, Y. Biological materials: Structure and mechanical properties. *Progress in Materials Science*, **2008**, *53* (1), 1‑206.

[2] Fung, Y. C. *Biomechanics: Mechanical Properties of Living Tissues*; Springer Nature; Springer, **2013**.

[3] Li, Z.; Tang, M.; Liang, S.; Zhang, M.; Biesold, G. M.; He, Y.; Hao, S.-M.; Choi, W.; Liu, Y.; Peng, J.; Lin, Z. Bottlebrush polymers: From controlled synthesis, self-assembly, properties to applications. *Progress in Polymer Science*, **2021**, *116*, 101387.

[4] Sheiko, S. S.; Dobrynin, A. V. Architectural Code for Rubber Elasticity: From Supersoft to Superfirm Materials. *Macromolecules*, **2019**, *52* (20), 7531‑7546.

[5] Liang, H.; Morgan, B. J.; Xie, G.; Martinez, M. R.; Zhulina, E. B.; Matyjaszewski, K.; Sheiko, S. S.; Dobrynin, A. V. Universality of the Entanglement Plateau Modulus of Comb and Bottlebrush Polymer Melts. *Macromolecules*, **2018**, *51* (23), 10028‑10039.

[6] Daniel, W. F. M.; Burdyńska, J.; Vatankhah-Varnoosfaderani, M.; Matyjaszewski, K.; Paturej, J.; Rubinstein, M.; Dobrynin, A. V.; Sheiko, S. S. Solvent-free, supersoft and superelastic bottlebrush melts and networks. *Nature materials*, **2016**, *15* (2), 183‑189.

[7] Kavassalis, T. A.; Noolandi, J. Entanglement scaling in polymer melts and solutions. *Macromolecules*, **1989**, *22* (6), 2709‑2720.

[8] Pakula, T.; Zhang, Y.; Matyjaszewski, K.; Lee, H.; Boerner, H.; Qin, S.; Berry, G. C. Molecular brushes as super-soft elastomers. *Polymer*, **2006**, *47* (20), 7198‑7206.

[9] Tzourtzouklis, I.; Hahn, C.; Frey, H.; Floudas, G. Molecular Dynamics and Viscoelastic Properties of the Biobased 1,4-Polymyrcene. *Macromolecules*, **2022**, *55* (19), 8766‑8775.

[10] Iacob, C.; Yoo, T.; Runt, J. Molecular Dynamics of Polyfarnesene. *Macromolecules*, **2018**, *51* (13), 4917‑4922.

[11] Grune, E.; Bareuther, J.; Blankenburg, J.; Appold, M.; Shaw, L.; Müller, A. H. E.; Floudas, G.; Hutchings, L. R.; Gallei, M.; Frey, H. Towards bio-based tapered block copolymers: the behaviour of myrcene in the statistical anionic copolymerisation. *Polym. Chem.*, **2019**, *10* (10), 1213‑1220.

[12] Wahlen, C.; Blankenburg, J.; Tiedemann, P. von; Ewald, J.; Sajkiewicz, P.; Müller, A. H. E.; Floudas, G.; Frey, H. Tapered Multiblock Copolymers Based on Farnesene and Styrene: Impact of Biobased Polydiene Architectures on Material Properties. *Macromolecules*, **2020**, *53* (23), 10397‑10408.

[13] Wahlen, C.; Frey, H. Anionic Polymerization of Terpene Monomers: New Options for Bio-Based Thermoplastic Elastomers. *Macromolecules*, **2021**, *54* (16), 7323‑7336.

[14] Tang, C.; Ryu, C. Y., Eds. *Sustainable polymers from biomass*, [1. Auflage]; Wiley-VCH Verlag GmbH & Co. KGaA, **2017**.

[15] Everaers, R.; Sukumaran, S. K.; Grest, G. S.; Svaneborg, C.; Sivasubramanian, A.; Kremer, K. Rheology and microscopic topology of entangled polymeric liquids. *Science (New York, N.Y.)*, **2004**, *303* (5659), 823‑826.

[16] Viovy, J. L.; Rubinstein, M.; Colby, R. H. Constraint release in polymer melts: tube reorganization versus tube dilation. *Macromolecules*, **1991**, *24* (12), 3587‑3596.

[17] Doi, M.; Graessley, W. W.; Helfand, E.; Pearson, D. S. Dynamics of polymers in polydisperse melts. *Macromolecules*, **1987**, *20* (8), 1900‑1906.

[18] Struglinski, M. J.; Graessley, W. W.; Fetters, L. J. Effects of polydispersity on the linear viscoelastic properties of entangled polymers. 3. Experimental observations on binary mixtures of linear and star polybutadienes. *Macromolecules*, **1988**, *21* (3), 783‑789.

[19] Marrucci, G. Relaxation by reptation and tube enlargement: A model for polydisperse polymers. *J. Polym. Sci. Polym. Phys. Ed.*, **1985**, *23* (1), 159‑177.

[20] Doi, M.; Edwards, S. F. *The theory of polymer dynamics*; The International series of monographs on physics (Oxford, England), Vol. 73; Clarendon Press; Oxford University Press, **2003, 1988**.

[21] Malo de Molina, P.; Alegría, A.; Allgaier, J.; Kruteva, M.; Hoffmann, I.; Prévost, S.; Monkenbusch, M.; Richter, D.; Arbe, A.; Colmenero, J. Tube Dilation in Isofrictional Polymer Blends Based on Polyisoprene with Different Topologies: Combination of Dielectric and Rheological Spectroscopy, Pulsed-Field-Gradient NMR, and Neutron Spin Echo (NSE) Techniques. *Macromolecules*, **2020**, *53* (14), 5919‑5936.

[22] van Ruymbeke, E.; Shchetnikava, V.; Matsumiya, Y.; Watanabe, H. Dynamic Dilution Effect in Binary Blends of Linear Polymers with Well-Separated Molecular Weights. *Macromolecules*, **2014**, *47* (21), 7653‑7665.

[23] van Ruymbeke, E.; Masubuchi, Y.; Watanabe, H. Effective Value of the Dynamic Dilution Exponent in Bidisperse Linear Polymers: From 1 to 4/3. *Macromolecules*, **2012**, *45* (4), 2085‑2098.

[24] Lee, J. H.; Fetters, L. J.; Archer, L. A.; Halasa, A. F. Tube Dynamics in Binary Polymer Blends. *Macromolecules*, **2005**, *38* (9), 3917‑3932.

[25] Kremer, F.; Schönhals, A. *Broadband dielectric spectroscopy*; Springer, **2003**.

[26] Qian, Z.; McKenna, G. B. Expanding the application of the van Gurp-Palmen plot: New insights into polymer melt rheology. *Polymer*, **2018**, *155*, 208-217.

[27] van Gurp, M.; Palmen, J. Time-Temperature Superposition For Polymeroc Blends. *Rheology Bulletin*, **1998**, *67*, 5-8.

[28] Fetters, L. J.; Lohse, D. J.; Graessley, W. W. Chain dimensions and entanglement spacings in dense macromolecular systems. *J. Polym. Sci. B Polym. Phys.*, **1999**, *37* (10), 1023-1033.

Supporting Information

1. Molecular Characterization

The carbanionic polymerization is considered a living polymerization technique. The absence of any termination and transfer reaction offers precise adjustment of the molar mass (M_n) by the simple relationship of the molar mass of the monomer unit (M_0) and the ratio of the monomer and initiator concentration ($[M]_0/[I]$): $M_n = M_0 \cdot [M]_0/[I]$

Great attention must be devoted to the purity of all compounds and the absence of any protic impurities. Polyfarnesene samples were synthesized using high vacuum technique and an argon filled glove box to assure these conditions. A series of samples of increasing molar mass of 3.5 kg·mol^{-1} to 720 kg·mol^{-1} were synthesized, all featuring a narrow molar mass distributions ($Đ$) of < 1.2 with the majority having a $Đ$ < 1.1. All SEC measurements performed on a regular SEC set-up used a RI-detector, THF as eluent and a polyisoprene calibration, see **Figure S1**.

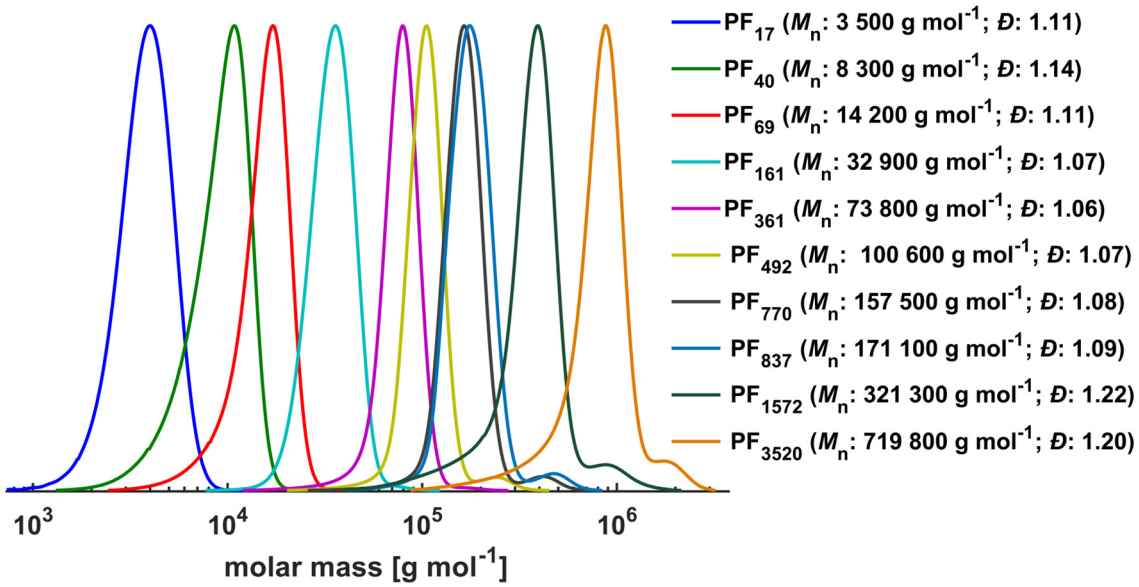

Figure S1. SEC traces of all synthesized PF samples measured in THF and against a PI calibration.

The architecture of the bio-based PF is different from its petrol-based and established alternatives, polyisoprene and polybutadiene. Besides the 1,3-diene structure, PF bears a long C_{11} alkyl chain in 2-position of the diene. Depending on the microstructure (1,4- or 3,4-), either 2 or 4 carbon atoms are incorporated along the polymer backbone. This leaves 11 or 13 carbons at the side chain, resulting in a bottlebrush structure. Due to this characteristic, we expected a significant deviation of the hydrodynamic radius of PF compared to polyisoprene

and polystyrene. The determination against these standards by SEC is therefore only an indication of the true molar mass. Consequently, all synthesized samples were measured using a multi-angle light scattering (MALS) detector. The data is summarized in **Table S1**.

As *n*-heptane as an apolar solvent and lithium as counter ion was used for the synthesis, primarily 1,4-incooperation of the *β*-farnesene monomer units was observed. The ratio of the microstructures can be determined from the respective ^{1}H NMR spectra. As illustrated in **Figure S3**, all samples comprise a 1,4-content of >93%, being in accordance with reported values. All measured values are summarized in **Table S1**. For this work, polyisoprene samples of similar molar mass compared to the PF samples were purchased. For the best comparison, the molar masses determined by MALS were used. As it can be followed in **Figure S2**, each PF sample was successfully matched with a PI sample with a similar molar mass. The microstructure of the PI-samples was determined, again using ^{1}H NMR spectroscopy, see **Figure S4**. All samples comprise a 1,4-content of >93%.

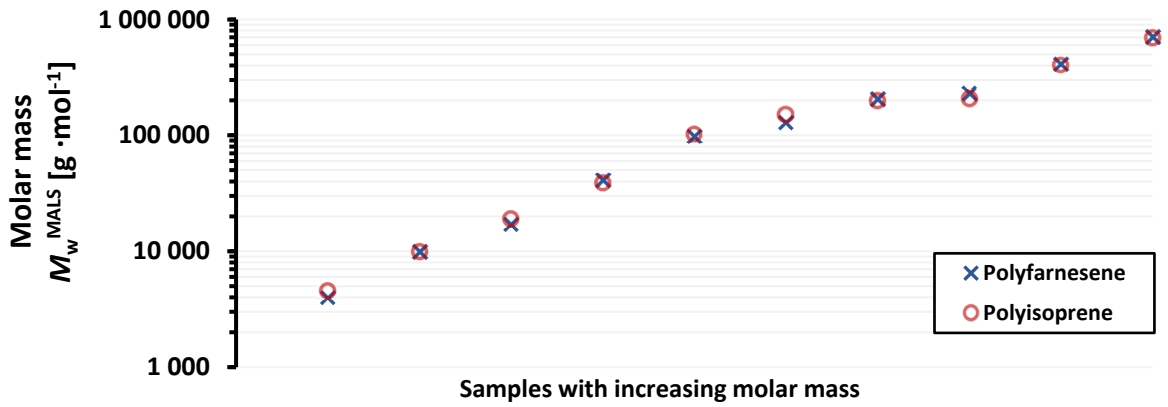

Figure S2. Comparison of the molar mass of all PF and PI samples, determined by SEC using a MALS detector, eluent: THF.

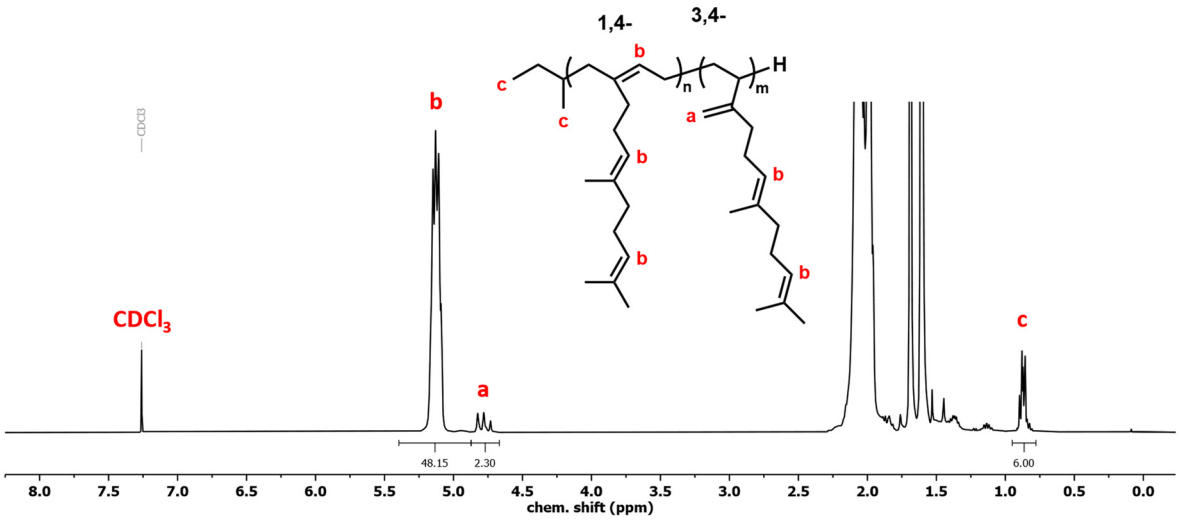

Figure S3. ^{1}H NMR spectrum of the PF_{17} sample with assignment of the signals to the respective protons of the 1.4- and 3.4- microstructure, measured in $CDCl_3$ at 400 MHz.

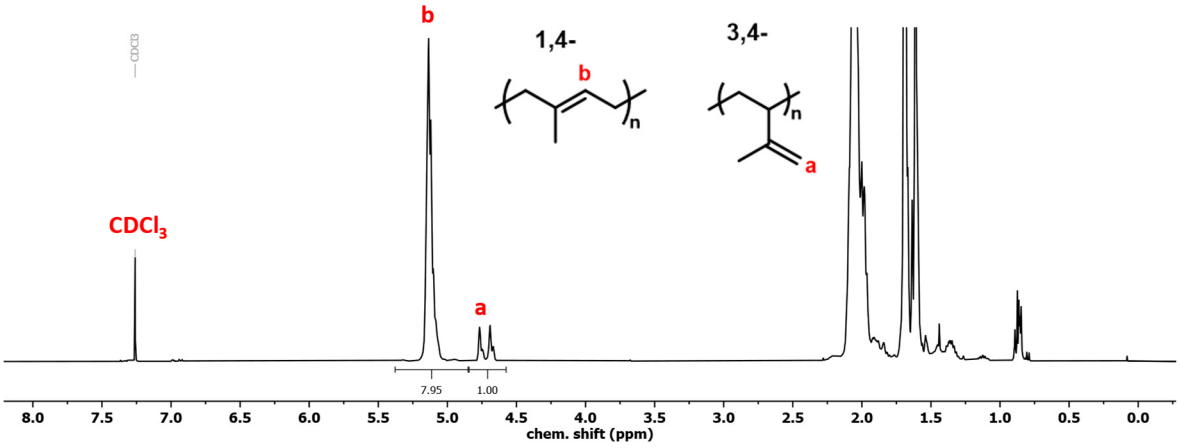

Figure S4. ^{1}H NMR spectrum of the PI_{64} sample with assignment of the signals to the respective protons of the 1.4- and 3.4- microstructure, measured in $CDCl_3$ at 400 MHz.

Table S1. Summary of polymer characteristics of all synthesized PF samples.

Sample	M_n^{SEC} [a] [g·mol^{-1}]	M_w^{SEC} [a] [g·mol^{-1}]	$Đ$ [a]	M_w^{MALS} [b] [g·mol^{-1}]	1,4-PF [c] [%]	3,4-PF [c] [%]
PF_{17}	3 500	3 900	1.11	4 000	93.0	7.0
PF_{40}	8 300	9 500	1.14	10 000	93.1	6.9
PF_{69}	14 200	15 800	1.11	17 100	93.5	6.5
PF_{161}	32 900	35 200	1.07	41 100	93.5	6.5
PF_{361}	73 800	78 500	1.06	98 600	93.4	6.6
PF_{492}	100 600	107 700	1.07	129 000	94.0	6.0
PF_{770}	157 500	170 600	1.08	205 000	93.7	6.3
PF_{837}	171 100	186 800	1.09	231 000	93.6	6.4
PF_{1572}	321 300	393 000	1.21	414 000	93.0	7.0
PF_{3520}	719 800	860 800	1.20	710 000	94.4	5.6

[a] M_n^{SEC} and M_w^{SEC} were determined by SEC using a PI calibration and THF as eluent. [b] M_w^{MALS} values were determined by SEC using a MALS detector and THF as eluent. [c] Determined by ^{1}H NMR spectroscopy.

Table S2. Summary of polymer characteristics of all PI samples.

Sample	M_n^{SEC} [a] [g·mol^{-1}]	M_w^{SEC} [a] [g·mol^{-1}]	$Đ$ [a]	M_w^{MALS} [a] [g·mol^{-1}]	1,4-PI [b] [%]	3,4-PI [b] [%]
PI_{64}	4 450	4 610	1.04	4 570	94.1	5.9
PI_{146}	10 000	10 500	1.04	9 960	94.7	5.3
PI_{287}	19 600	20 400	1.04	19 000	94.1	5.9
PI_{616}	42 000	42 500	1.01	38 800	94.7	5.3
PI_{1626}	110 800	111 000	1.01	103 000	93.9	6.1
PI_{2275}	155 000	157 000	1.01	150 000	93.4	6.6
PI_{2612}	178 000	182 000	1.02	198 000	94.4	5.6
PI_{3332}	227 000	231 000	1.02	208 000	95.1	4.9
PI_{6297}	429 000	443 000	1.03	405 000	94.8	5.2
PI_{10407}	709 000	735 000	1.04	694 000	94.7	5.3

[a] Values: M_n^{SEC}, M_w^{SEC}, and M_w^{MALS} are taken from analysis certificates of the SEC reference materials. M_n^{SEC}, M_w^{SEC} were determined by SEC using a PI calibration and THF as eluent; M_w^{MALS} using a MALS Detector. [b] Determined by ^{1}H NMR spectroscopy.

Chapter A3

German Translation: Bifunktionelle Carbanionische Synthese Vollständig Biobasierter Triblock-Copolymere aus *β*-Farnesene und LL-Dilactid: Thermoplastische Elastomere

Moritz Meier-Merziger,[a] *Jan Imschweiler,*[a] *Frank Hartmann,*[b] *Bart-Jan Niebuur,*[c] *Prof. Tobias Kraus,*[c,d] *Prof. Markus Gallei,*[b,e] *and Prof. Holger Frey* [a]*

* Corresponding author

[a] Department of Chemistry, Johannes Gutenberg University Mainz, Duesbergweg 10-14, 55128 Mainz, Germany.

[b] Chair in Polymer Chemistry, Saarland University, Campus Saarbrücken C4 2, 66123 Saarbrücken, Germany

[c] INM—Leibniz-Institute for New Materials, Campus D2 2, Saarland University, 66123 Saarbrücken, Germany

[d] Colloid and Interface Chemistry, Saarland University, Campus D2 2, 66123 Saarbrücken, Germany

[e] Saarene, Saarland Center for Energy Materials and Sustainability, Campus C4 2, 66123 Saarbrücken, Germany

Published in: *Angewandte Chemie*, **2023**, 135 (42), e202310519.
Supplementary material associated with this article can be found in the online version:
https://doi.org/10.1002/ange.202310519

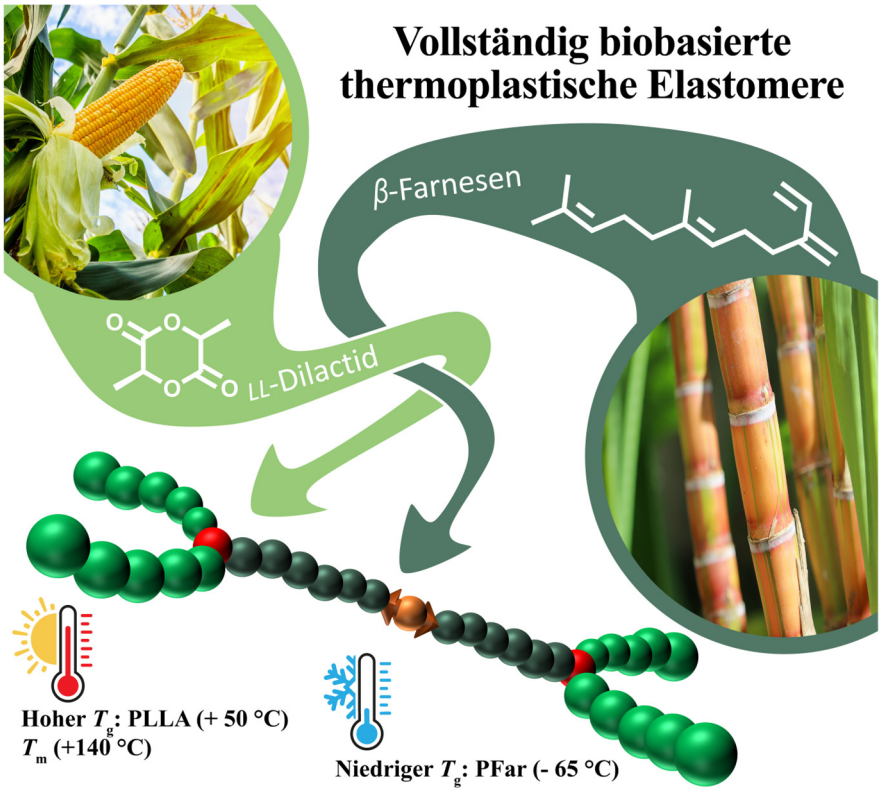

The following publication is adapted with permission from Meier-Merziger, M.; Imschweiler J.; Hartmann, F.; Niebuur, B.-J..; Kraus, T.; Gallei, M.; and Frey, H.; Bifunktionelle Carbanionische Synthese Vollständig Biobasierter Triblock-Copolymere aus *β*-Farnesene und LL-Dilactid: Thermoplastische Elastomere, *Angewandte Chemie*, **2023**, 135 (42), e202310519.

GDCh Zuschriften Angewandte Chemie www.angewandte.org

Zitierweise: Angew. Chem. Int. Ed. 2023, e202310519
doi.org/10.1002/anie.202310519

Polymerisation

Bifunktionelle carbanionische Synthese vollständig biobasierter Triblock-Copolymere aus β-Farnesen und LL-Dilactid: Thermoplastische Elastomere

*Moritz Meier-Merziger, Jan Imschweiler, Frank Hartmann, Bart-Jan Niebuur, Tobias Kraus, Markus Gallei, und Holger Frey**

Abstract: Aktuelle ökologische Herausforderungen und die Endlichkeit fossiler Rohstoffe sind wichtige Kriterien, welche für die nächste Generation von Polymermaterialien eine zentrale Rolle spielen. In diesem Zusammenhang wird ein vollständig biobasiertes Material mit potenzieller Anwendung als thermoplastisches Elastomer (TPE) vorgestellt. Durch die Verwendung der Monomere *β*-Farnesen und L-Lactid können biobasierte Rohstoffe wie Zuckerrohr und Mais verwendet werden. Für die carbanionische Polymerisation wurde ein bifunktioneller Initiator eingesetzt, um eine effiziente Synthese von ABA-artigen Blockstrukturen zu ermöglichen. Zusätzlich kam das potenziell nachhaltige Lösungsmittel MTBE (Methyl-*tert*-butylether) zum Einsatz, da es eine hervorragende Löslichkeit des bifunktionellen Initiators gewährleistet. Dies ermöglichte die Herstellung von telechelen Polyfarnesen-Makroinitiatoren mit niedrigen Dispersitäten ($Đ = 1.07$ bis 1.10). Diese wurden anschließend für die Lactidpolymerisation verwendet, um *H*-förmige Triblockcopolymere zu erhalten. TEM und SAXS-Messungen zeigten deutlich phasengetrennte Morphologien, und mittels Zugversuche konnten elastische Eigenschaften nachgewiesen werden. Die Triblockstrukturen weisen jeweils zwei Glasübergangstemperaturen bei −66 °C und 51 °C sowie gyroide oder zylindrische Morphologien auf, was bei Raumtemperatur zu weichelastischen Materialien führt.

Thermoplastische Elastomere (TPE) werden aufgrund ihrer Vorteile gegenüber klassisch vulkanisierten Elastomeren für spezifische Anwendungen umfassend untersucht. Insbesondere hinsichtlich ihrer potenziellen Recyclingfähigkeit sind TPEs überlegen und daher wichtig, um aktuellen ökologischen Herausforderungen gerecht zu werden. Sie sind thermoplastisch verarbeitbar und besitzen bei Gebrauchstemperaturen elastische Eigenschaften.[1] Zudem führen die Endlichkeit fossiler Ressourcen und ihre enormen Auswirkungen auf die Umwelt zu einem der zentralen Ziele der aktuellen Forschung: die Suche nach alternativen Materialien, welche nicht auf fossilen Grundstoffen basieren. Etablierte TPEs vom Typ SBS oder SIS bestehen aus zwei Endblöcken aus glasartigem Polystyrol (PS), die kovalent mit einem "weichen", langen Mittelblock aus Polybutadien (PB) oder Polyisopren (PI) verbunden sind. Hillmyer et al.[2] zeigten, dass die PS-Phase durch ein anderes Material mit hoher Glasübergangstemperatur (T_g), z.B. Polylactid (PLA), ersetzt werden kann, um teilweise biobasierte TPE-Strukturen zu erhalten. Die Autoren konnten zeigen, dass die Kombination verschiedener Polymerisationstechniken geeignet ist, um neue Materialien aus klar phasengetrennten Blockcopolymeren herzustellen. Darüber hinaus wurden kürzlich einige Beispiele vollständig biobasierter TPE-Strukturen in der Fachliteratur vorgestellt, die Materialien beschreiben, welche aus rein nachwachsenden Rohstoffen gewonnen werden können. Sie umfassen Materialien auf Basis von Polyestern, Polyurethanen und Polyamiden.[3,4] Terpene bieten hier ein großes Potenzial als alternative Quellen für nachhaltige Materialien.[4] So wurde z.B. *β*-Myrcen (Myr) in verschiedenen Arbeiten als biobasierter Ersatz für die Weichphase in TPEs untersucht. Anionische Polymerisation,[5] darauffolgendes Lactid-Grafting[6] und

[*] M. Meier-Merziger, J. Imschweiler, Prof. H. Frey
Johannes Gutenberg-Universität, Mainz, Department Chemie
Dusbergweg 10–14, 55128 Mainz (Deutschland)
E-mail: hfrey@uni-mainz.de

F. Hartmann, Prof. M. Gallei
Universität des Saarlandes, Lehrstuhl für Polymerchemie
Campus C4 2, 66123 Saarbrücken (Deutschland)

B.-J. Niebuur, Prof. T. Kraus
INM - Leibniz-Institut für neue Materialien
Campus D2 2, 66123 Saarbrücken (Deutschland)

Prof. T. Kraus
Universität des Saarlandes, Kolloid-und Grenzflächenchemie
Campus D2 2, 66123 Saarbrücken (Deutschland)

Prof. M. Gallei
Saarene, Saarland Zentrum für Energiematerialien und Nachhaltigkeit
Campus C4 2, 66123 Saarbrücken (Deutschland)

RAFT[7] wurden bereits vorgestellt, um biobasierte TPE-Strukturen aus Dien-Monomeren herzustellen.

Eine der größten Herausforderungen für eine großtechnische Anwendung ist es, einen skalierbaren Prozess zu finden, mit technisch herstellbaren Monomeren.[3] Erst kürzlich haben wir ein teilweise biobasiertes Material mit einem niedrigen T_g durch einen PI-Mittelblock, flankiert von äußeren, starren Lactidblöcken, vorgestellt.[8] Bei der vorliegenden Arbeit werden dagegen vollständig biobasierte TPEs angestrebt, welche durch die Kombination von carbanionischer und ringöffnender Polymerisation synthetisiert werden.

Ein selten beachtetes, biobasiertes Monomer findet sich in der Gruppe der Terpene: Das 1,3-Dien β-Farnesen (Far) wird bereits im industriellen Maßstab hergestellt.[9] β-Farnesen basiert auf dem nachwachsenden Rohstoff Zuckerrohr, und das daraus herstellbare Polyfarnesen (PFar) weist deutliche abweichende thermische und rheologische Eigenschaften zu seinen Homologen PI und PB auf. Die ungewöhnliche Bürstenarchitektur führt zu einem deutlich erhöhten Verschlaufungsmolekulargewicht (M_e) von PFar von $\approx$49.7 kg·mol^{-1} und einem noch höheren kritischen Molekulargewicht (M_c) von $>$105 g·mol^{-1}.[10] Die M_c-Werte von PB (5.6 kg·mol^{-1})[11] und PI (14 kg·mol^{-1})[12] sind im Vergleich dazu deutlich niedriger. Des Weiteren zeigen sowohl PI als auch PB eine starke T_g-Abhängigkeit zum vorliegenden Mikrostrukturverhältnis. Der T_g von PI mit 9 % Vinylanteil liegt bei -67 °C und steigt bei einem Vinylanteil von 85 % auf 0 °C an.[13] Polyfarnesen (PFar) dagegen behält einen niedrigen Glasübergang von unter -70 °C, unabhängig vom Vinylanteil bis 52 %.[13] Das Monomer β-Farnesen ist daher gut geeignet für die carbanionische Polymerisation in polaren aprotischen Medien (z.B. Ether), in denen Polydiene mit einem hohen Vinylgehalt $>$52 % erhalten werden.

Zudem ermöglichen Ether als Lösungsmittel die Verwendung eines bifunktionellen Initiators für die carbanionische Polymerisation, sodass die benötigte Anzahl der Monomeradditions-Schritte verringert werden kann. Dies ist in reinen Kohlenwasserstoffen aufgrund von Löslichkeitsproblemen bifunktioneller Initiatoren nur schwer realisierbar. Da polare Lösungsmittel zu einem erhöhten Vinylanteil führen, ist ihre Relevanz für klassische Diene wie Butadien (B) und Isopren (I) in der Regel begrenzt. Obwohl mehrere bifunktionelle Initiatoren für die Verwendung in apolaren Lösungsmitteln bekannt sind,[14] ist ihre Herstellung komplex und somit schwierig großtechnisch zu implementieren.[15] Mit der vorliegenden Arbeit wird gezeigt, dass es möglich ist, sowohl die Vorteile von Far als Baustein als auch die effiziente Verwendung eines bifunktionellen Initiators aufgrund guter Löslichkeit in einem polaren Lösemittel voll auszuschöpfen und zu vereinen.

Kommerziell erhältliches 1,3-Diisopropenylbenzol (DIB) wurde als Vorstufe eines bifunktionellen Initiators in der vorgestellten Syntheseroute verwendet. Es wurde durch die Zugabe von zwei Äquivalenten *tert*-BuLi in die dilithierte Spezies überführt.[16] Außerdem wurde aufgrund der unerwünschten Protonenabstraktion bei geläufigen polaren Lösungsmitteln, wie THF und Diethylether in Gegenwart von carbanionischen Verbindungen, Methyl-*tert*-butylether (MTBE) als inerte Alternative untersucht.[17] Neben seiner Stabilität gegenüber Nebenreaktionen mit dem nukleophilen Kettenende hat MTBE sich auch als nachhaltiges Lösungsmittel etabliert.[18] Obwohl die großtechnische Herstellung derzeit noch auf den fossilen Rohstoffen Isobuten und Methanol basiert, sind teilweise biobasierte Varianten, z.B. *Bio-MTBE*, bereits auf dem Markt erhältlich.[19] Andere Vorteile, wie eine sicherere Handhabung (keine Peroxidbildung), haben zwar in der organischen Chemie Beachtung gefunden, aber überraschenderweise in der Polymerchemie bislang nie an Bedeutung gewonnen.[20]

Polyfarnesyllithium wurde durch Endfunktionalisierung der lebenden Kettenenden mit dem Glycidylether Ethoxyethyl-glycidylether (EEGE) zu hydroxy-funktionellen Telechelen umgesetzt. Nach saurer Abspaltung der Schutzgruppe sind telechele Tetrahydroxy-Makroinitiatoren mit einem hohen Endfunktionalisierungsgrad über eine sehr kontrollierte Synthese zugänglich.[21] Die angestrebte vollständig biobasierte A_2BA_2-Triblockstruktur wurde anschließend durch Polymerisation von LL-Dilactid (LLA) zu Poly-(L)-Lactid (PLLA), einem der gängigsten biobasierten Materialien, erhalten. Der hohe T_g von PLLA von $\approx$60 °C prädestiniert es für den Einsatz als glasartige äußere Blöcke von TPEs.[22] Durch die Variation des verwendeten Glycidylethers sind unterschiedliche und komplexe Strukturen zugänglich. Der beschriebene Syntheseweg ist in Schema 1 dargestellt. Pitet et al. haben kürzlich gezeigt, dass die Lactid Polymerisation mittels PFar-Makroinitiatoren auch zur Anwendung in der kontinuierlichen Durchflusssynthese geeignet ist, was das Scale-Up Potenzial unterstreicht.[23]

Die Herstellung der aktiven Initiator-Spezies aus der Reaktion von DIB/*tert*-BuLi wurde mittels ^{1}H NMR-Spektroskopie verfolgt. Vollständige Reaktion der Benzyl Doppelbindungen wurde bereits nach dem ersten Messwert ($<$ 1 min) beobachtet (Abbildung S1). Die tiefrote Lösung wurde verdünnt, und nach Zugabe von Far kam es zu einem Farbumschlag zu schwach gelb. Dies kann auf den Übergang des Benzylcarbanions des Initiators zum Farnesyllithium-Kettenende zurückgeführt werden. Nach vollständigem Monomerumsatz ergab die Zugabe eines zehnfachen Überschusses an EEGE eine sofortige Entfärbung der Lösung aufgrund der Bildung von Alkoxidgruppen an den Kettenenden, wodurch es zudem zur Ausbildung eines hochviskosen Organogels kam. Bei Protonierung der Kettenenden durch Zugabe von entgastem Methanol wurde eine Polymerlösung niedriger Viskosität zurückgewonnen. Da die Endgruppenbestimmung mittels NMR-Spektroskopie nur für kleine Molekulargewichte (M_n) zuverlässige Ergebnisse liefert, wurde eine Probe mit geringerem M_n von 5000 g·mol^{-1} hergestellt. Ein Endfunktionalisierungsgrad von 94 % für EEGE-PFar(5k)-EEGE wurde über den Vergleich des Signals der Methylgruppen ($\approx$0.88 ppm) der initiierenden Spezies mit den Protonensignalen der Endgruppe im entsprechenden ^{1}H NMR ermittelt (Abbildung S2). Das Spektrum kann außerdem zur Bestimmung des M_n mittels NMR verwendet werden. Das erhaltene M_n^{NMR} von 6600 g·mol^{-1} weicht geringfügig von den Ergebnissen der Gel-Permeations-Chromatographie (GPC) ab (M_n^{GPC} = 5700 g·mol^{-1}), was sich durch die Verwendung einer PI-Kalibrierung in der

GDCh Zuschriften Angewandte Chemie

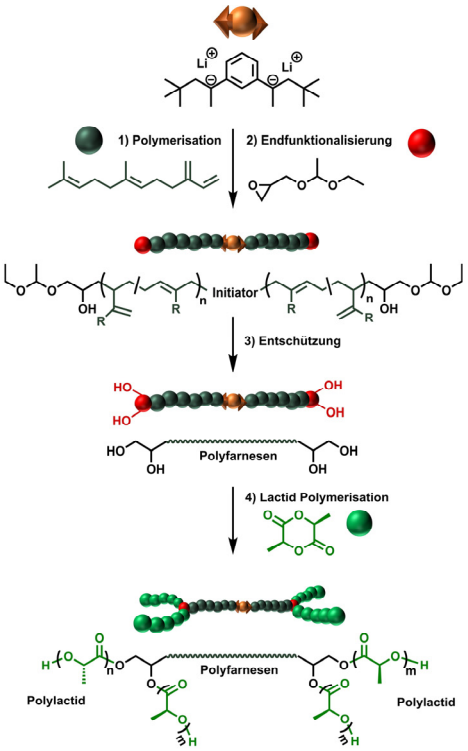

Schema 1. Syntheseübersicht: Far Initiierung durch DIB/*tert*-BuLi und anschließende Endfunktionalisierung mittels EEGE; danach saure Entschützung, gefolgt von basenkatalysierter ROP von LLA zur Herstellung *H*-förmiger A_2BA_2-Triblockcopolymere.

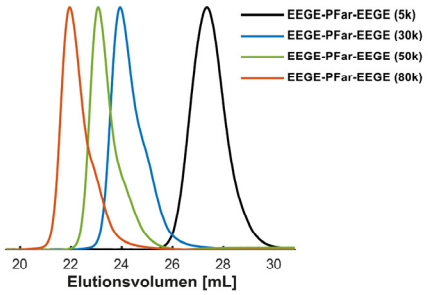

Abbildung 1. GPC-Kurven aller endfunktionalisierten EEGE-PFar-EEGE Telechele mit angestrebten Molekulargewichten von 5k, 30k, 50k und 80k (Laufmittel: THF, PI-Eichung).

GPC-Messung erklären lässt. Beide Verfahren ergeben einen Wert der dicht am angestrebten M_n liegt. Dies lässt auf eine kontrollierte bifunktionelle Polymerisation mit anschließender Endfunktionalisierung schließen.

Es wurden drei zusätzliche hochmolekulare Makroinitiatoren (angestrebtes M_n: 30k, 50k and 80k) für die Herstellung der Triblockcopolymere synthetisiert. Die GPC-Kurven aller telechelen EEGE-PFar-EEGE Proben sind in Abbildung 1 dargestellt und zeigen geringe Dispersitäten ($Đ$) von 1.07 bis 1.10, was die hohe Kontrolle und den lebenden Charakter der Synthese widerspiegelt. Eine leichte Schulter kann bei den hochmolekularen PFar-Proben beobachtet werden, was durch den unvermeidbaren Anteil an *tert*-BuLi entsteht, welcher für die Herstellung des bifunktionellen Initiators nötig ist. Dies weist somit auf eine größtenteils bifunktionelle Polymerisation hin. Die erhaltene geringe Dispersität der Proben deutet zudem auf einen vernachlässigbar kleinen monofunktionellen Anteil hin.

Die Charakterisierungsdaten aller Polymere sowie das Verhältnis der erhaltenen Mikrostrukturen (siehe Hintergrundinformationen), sind in Tabelle 1 zusammengefasst.

Der 1,4-PFar Anteil verringert sich auf ca. 61 %, wohingegen in apolaren Lösemitteln, z.B. *n*-Heptan, ein 1,4-PFar Anteil von 91 % erhalten wird.[10] Daneben wurde ausschließlich 3,4-PFar und kein 1,2-PFar nachgewiesen. Im nächsten Schritt wurden die partiell geschützten Hydroxylgruppen der Kettenenden unter Verwendung eines Ionenaustauscher-Harzes (DOWEX) unter sauren Bedingungen

Tabelle 1: Charakterisierungsdaten aller hergestellten A_2BA_2-Triblockcopolymerer sowie deren jeweiliger Makroinitiatoren.

Proben	M_n^{target} [g mol^{-1}]/$\Phi_{LA}^{targeted}$	M_n^{SEC}[a] [g mol^{-1}]	$Đ$ [a]	1,4-Far[b] [%]	Φ_{LA}[c] [%]	T_g^1[d] [°C]	T_g^2[d] [°C]	T_m[e] [°C]	SAXS [f]	TEM [f]
EEGE-PFar-EEGE (5k)	**5000**	**5700**	**1.17**	**59.0**	–	–	–	–	–	–
EEGE-PFar-EEGE (30k)	**30000**	**24100**	**1.10**	**61.2**	–	–	–	–	–	–
$(PLLA_{2.6k})_2$-*b*-PFar(30k)-*b*-$(PLLA_{2.6k})_2$	+20% PLLA	30200	1.17	61.2	18.3	-	-	-	*mix*	*H*
$(PLLA_{4.5k})_2$-*b*-PFar(30k)-*b*-$(PLLA_{4.5k})_2$	+30% PLLA	39100	1.14	61.2	28.6	−64	50	149	H	G
EEGE-PFar-EEGE (50k)	**50000**	**36300**	**1.07**	**61.8**	–	–	–	–	–	–
$(PLLA_{4.4k})_2$-*b*-PFar(50k)-b-$(PLLA_{4.4k})_2$	+20% PLLA	43600	1.19	61.8	20.0	-	-	-	*H*	*#NA*
$(PLLA_{7.5k})_2$-*b*-PFar(50k)-*b*-$(PLLA_{7.5k})_2$	+30% PLLA	54600	1.18	61.8	28.5	−66	51	136	#NA	#NA
EEGE-PFar-EEGE (80k)	**80000**	**57400**	**1.09**	**63.5**	–	–	–	–	–	–
$(PLLA_{7.0k})_2$-*b*-PFar(80k)-*b*-$(PLLA_{7.0k})_2$	+20% PLLA	59800	1.36	63.5	20.6	-	-	-	*S*	*S*
$(PLLA_{12k})_2$-*b*-PFar(80k)-*b*-$(PLLA_{12k})_2$	+30% PLLA	79400	1.27	63.5	23.6	−66	51	134	L	G

[a] Laufmittel: THF, Eichung: PI. [b] bestimmt über ^{1}H NMR, siehe Hintergrundinformationen. [c] berechnet vom PFar/PLLA Verhältnis aus dem ^{1}H NMR unter der Annahme der Dichten der Homopolymere ϱ(PFar): 0.900 g·cm^{-3} [10] und ϱ(PLLA): 1.264 g·cm^{-3} [25]. [d] zweite Heizkurve der DSC-Messung, gemessen mit einer Heizrate von 10 K/min. [e] DSC-Wert der ersten Heizkurve. [f] bestimmt über TEM und SAXS, S: Kugel (engl. *spherical*), G: Gyroid, H: hexagonal gepackte Zylinder, L: Lamellen.

GDCh Zuschriften Angewandte Chemie

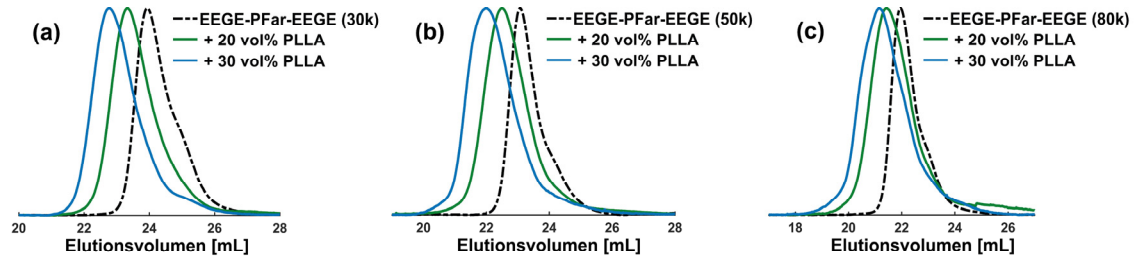

Abbildung 2. GPC-Kurven aller telechelen Makroinitiatoren und der jeweiligen Triblockcopolymere: (a) EEGE-PFar-EEGE (30k) mit + 20 vol % und + 30 vol % PLLA; (b) EEGE-PFar-EEGE (50k) mit + 20 vol % und + 30 vol % PLLA; (c) EEGE-PFar-EEGE (80k) mit + 20 vol % und + 30 vol % PLLA; (Laufmittel: THF, PI-Eichung).

entschützt. Diese Reaktionsbedingungen lassen sich leicht auf technische Anwendungen übertragen, da die Trennung des Polymers vom Harz durch einfaches Filtrieren möglich ist. Das vollständige Verschwinden der Methin-Protonensignale der Schutzgruppe bei 4.55 ppm im ^{1}H NMR-Spektrum (Abbildung S3) bestätigt die komplette Entschützung. Im nächsten Schritt wird die angestrebte, vollständig biobasierte Blockcopolymerstruktur über eine basenkatalysierte ringöffnende Polymerisation (ROP) von LLA mit 1,8-Diazabicyclo[5.4.0]undec-7-en (DBU) unter Verwendung der funktionellen telechelen multihydroxy PFar Proben erreicht. Die Polymerisationstechnik ist bekannt dafür, trotz milder Reaktionsbedingungen enge Molekulargewichtsverteilungen bei kurzen Reaktionszeiten zu ermöglichen.[24]

Nach Aufarbeitung wurde ein festes Material erhalten. Die zu erwartende Verschiebung zu höheren Molekulargewichten kann in den zugehörigen GPC-Kurven verfolgt werden, siehe Abbildung 2 (a–c). Der Volumenanteil von PLLA ist nicht direkt zugänglich, da die Signale der Methinprotonen von PLLA mit denen von 3,4-PFar im ^{1}H NMR-Spektrum überlappen. Da das Verhältnis von 1,4-PFar zu 3,4-PFar der Makroinitiatoren bekannt ist, kann der 3,4-PFar Anteil vom gemeinsamen Protonenintegral abgezogen werden. Das verbleibende Integral entspricht somit ausschließlich dem Signal der Methinprotonen von PLLA. Daraus ergibt sich das Molverhältnis, welches über die literaturbekannten Dichten von PFar und PLLA, ρ(PFar): 0.900 g·cm^{-3};[10] ρ(PLLA): 1.264 g·cm^{-3},[25] den Volumenanteil von PLLA (Φ_{LA}) ergibt.

Basierend auf diesen ^{1}H NMR-Bestimmungen ergeben sich die in Tabelle 1 dargestellten Volumenanteile von PLLA von 18 vol % bis 29 vol %, welche nahe an den angestrebten Werten liegen. Eine leichte Verbreiterung der Größenverteilungen kann in den GPC-Kurven beobachtet werden (siehe Abbildung 2 und Abbildung S9–11), was durch eine gewisse Mischung an Initiatoren erklärt werden kann.

Das Bewahren der unimodalen GPC-Verteilung zeigt eine erfolgreiche Kettenverlängerung durch PLLA. Diffusions-NMR Experimente (Abbildung S5) zeigen keine Spuren des PLLA-Homopolymers, und somit kann von einer erfolgreichen und kontrollierten Initiierung der PFar-Makroinitiatoren ausgegangen werden.

Die erfolgreiche Synthese der Triblockcopolymere motivierte weiterführende Untersuchungen des Materials im Hinblick auf dessen TPE-Eigenschaften. Erste Indizien für eine Phasenseparation konnte mittels Differenzkalorimetrie (DSC) Messungen (Abbildung 3) gefunden werden, welche zwei getrennte T_gs bei jeder Probe aufzeigten: einen niedrigen T_g zwischen −66 °C und −64 °C, welcher der PFar-Phase zugeschrieben werden kann, sowie einen hohen T_g bei ca. 50 °C der PLLA-Phase. Zudem konnte bei allen Proben ein Schmelzpunkt (T_m) im Temperaturbereich 134 °C bis 149 °C nachgewiesen werden (siehe Abbildung S6–8). Dieser war jedoch ausschließlich in der ersten Heizkurve zu beobachten. Die Kühlrate bzw. die Dauer der Abkühlung ist daher nicht ausreichend, um eine (Re)Kristallisation von PLLA zu ermöglichen. Ein Rekristallisationspeak war zudem in keiner Kühlkurve zu beobachten.

Phasenseparation konnte durch Transmissionselektronen-mikroskopie (TEM) für die meisten Proben bestätigt werden, siehe Abbildung 4 und Abbildung S15. Es konnten hexagonale Morphologien (Abbildung 4-a), Gyroidstrukturen (Abbildung 4-b) und Kugelmorphologien (Abbildung 4-c), bei denen einige unterschiedliche Domänengrößen in einer einzigen Probe zeigten, nachgewiesen werden. Erstaunlicherweise konnte die komplexe Gyroidstruktur bei zwei Proben nachgewiesen werden. Dies wird der ungewöhnlichen *H*-Architektur zugeschrieben, welche zu einer Krümmung an der Grenzfläche führt.[26]

Aufgrund der ungewöhnlichen Architektur der hergestellten Polymere kommt es zu einer Abweichung der

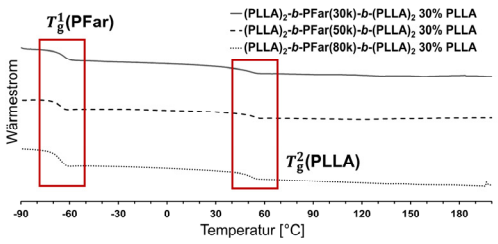

Abbildung 3. Zweite DSC-Heizkurve aller (PLLA)$_2$-*b*-PFar-*b*-(PLLA)$_2$ Proben mit einem angestrebten PLLA-Volumenanteil von 30 vol %, (Heizrate: 10 K/min).

GDCh Zuschriften Angewandte Chemie

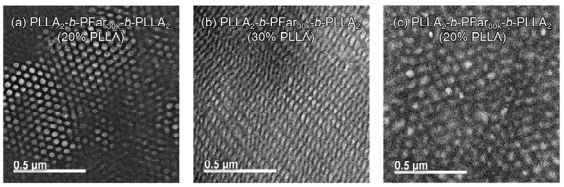

Abbildung 4. Transmissionselektronenmikroskopie der $(PLLA)_2$-*b*-PFar-*b*-$(PLLA)_2$ Proben unterschiedlicher Zusammensetzung; Film aus Lösung, 16 h bei 80 °C temperiert und mit OsO_4 behandelt; (a) $(PLLA)_2$-*b*-PFar(30k)-*b*-$(PLLA)_2$ 20 % PLLA; (b) $(PLLA)_2$-*b*-PFar(30k)-*b*-$(PLLA)_2$ 30 % PLLA; (c) $(PLLA)_2$-*b*-PFar(80k)-*b*-$(PLLA)_2$ 20 % PLLA.

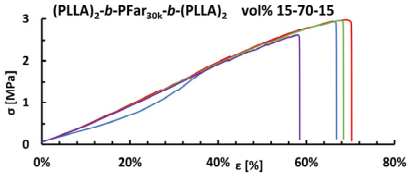

Abbildung 5. Zug-Dehnungs-Experiment der Serie $(PLLA)_2$-*b*-PFar(30k)-*b*-$(PLLA)_2$ mit 30 vol % PLLA, jeweils vier Messungen pro Probe.

resultierenden Morphologie im Vergleich zum Phasendiagramm klassischer linearer Blockcopolymere bei den gegebenen Volumenverhältnissen. Bei einigen Proben kam es bei der Bestimmung der Phasenseparation zu einer Abweichung zwischen den unterschiedlichen Analysemethoden. DSC-Messungen ließen auf eine Phasenseparation für alle Proben schließen, wohingegen bei den 50k PFar Blockcopolymeren keine klare Phasenseparation in den TEM-Bildern zu erkennen ist. Obwohl für die meisten Proben eine klare Phasenseparation zu beobachten war, konnte nicht immer eine klare Zuordnung zu einer Morphologie erfolgen. Daher wurde eine zusätzliche Untersuchung mittels Kleinwinkelstreuung (SAXS) durchgeführt, welche die Ordnung durch Phasenseparation im Gegensatz zu den TEM-Messungen über ein größeres Probenvolumen betrachtet. Wie in den Hintergrundinformationen genauer beschrieben, zeigen bei einigen Proben die SAXS-Messungen eine abweichende Morphologie zu der über TEM bestimmten auf. PFar(30k) mit 20 vol % PLLA (Abbildung S16a) zeigt sogar eine Kombination von Reflexen, welche eine Koexistenz unterschiedlicher Morphologien zugeschrieben werden kann. Der erhaltene Volumenanteil von PLLA scheint demnach genau am Übergangspunkt zweier Morphologien im Phasendiagramm zu sein. Welchen Beitrag die *H*-förmige Architektur in diesem Zusammenhang hat, wird in zukünftigen Arbeiten genauer untersucht werden. Die erhaltene Morphologie aller Proben ist in Tabelle 1 zusammengestellt.

ABA-Triblockcopolymere sind weit verbreitet in der Anwendung als thermoplastische Elastomere, deren physikalische Vernetzung auf der Domänenverbrückung der erstarrten Domänen mit hohem Glasübergang beruhen.[27] Zugversuche wurden für alle Proben mit einem angestrebten Φ_{LA} von 30 % durchgeführt. Die Folien für die mechanischen Messungen wurden durch Abdampfen aus Lösung hergestellt. Die Messungen ergaben eine ausschließlich elastische Verformung der Probe mit dem niedrigsten M_n (Abbildung 5). Die erhaltene Bruchdehnung (ε_{break}) lag bei 66 %, und bei geringer Verformung zeigte die Probe vollständige Reversibilität. Die hochmolekularen Proben zeigten neben der elastischen Verformung plastische Verformung sowie Kaltumformung. Dies steht im Einklang mit dem Verhalten nicht biobasierter SIS-Kautschuke.[28] Alle erhaltenen Ergebnisse sowie die E-Module (E) sind in Tabelle S1 zusammengefasst, und zusätzliche Zug-Dehnungs-Kurven sind in den Abbildungen S12–13 dargestellt.

Die mechanischen Charakteristika sind noch vergleichsweise niedrig zu denen von Triblöcken aus Styrol und Isopren bzw. Myrcen.[28] Dies ist wahrscheinlich auf das eingangs erwähnte deutlich höhere M_e von PFar zurückzuführen, sodass deutlich längere PFar Mittelblöcke nötig sind, um eine hohe Zugfestigkeit und Bruchdehnung zu erhalten.[28,29] Daneben hat jedes PLLA-Kettensegment aufgrund der Aufteilung der Einheiten auf die vier Arme der Architektur ein relativ geringes Molekulagewicht von 2.6 kg·mol^{-1} bis 12 kg·mol^{-1}. Dies erklärt zusätzlich den geringen Kristallisationsgrad, welcher in den DSC-Messungen erhalten wurde. Demnach können die erhaltenen mechanischen Eigenschaften klar der angestrebten Architektur und den noch moderaten Molekulargewichten zugeschrieben werden. Weitere Anpassung und Verbesserung der Materialeigenschaften für spezifische Anwendungen, wie formstabilere TPEs, ist mit der hier vorgestellten Syntheseroute leicht möglich.

Zusammenfassend konnte gezeigt werden, dass das selten genutzte, leicht polare und zudem biobasierte Lösungsmittel MTBE für bifunktionelle, anionische Initiatoren geeignet ist, da PFar einen niedrigen T_g behält, obwohl es zu einem erhöhten Vinylgehalt bei PFar in diesem Lösungsmittel kommt. Telechele α,ω-multihydroxy PFar-Makroinitiatoren wurden durch kontrollierte Endfunktionalisierung der lebenden Kettenenden hergestellt. Durch den Einsatz von LLA für die darauffolgende Ringöffnungspolymerisation sind *H*-förmige A_2BA_2-Triblockcopolymere zugänglich. Die erhaltenen Materialen zeigten klare Mikrophasenseparation und zudem jeweils zwei Glasübergänge, welche einen breiten Anwendungstemperaturbereich von −66 °C bis 51 °C ermöglichen. Durch Kristallisation längerer PLLA Ketten könnte die obere Anwendungstemperatur der TPEs in Zukunft weiter erhöht werden. TEM und SAXS-Messungen ergaben unterschiedliche Morphologien, wie Gyroid und hexagonale Zylinder und überraschenderweise auch Mischungen davon. Da die erhaltenen Morphologien von den Erwartungen für analoge lineare Blockcopolymere abweichen, zeigen diese Ergebnisse exemplarisch den Weg zu einer Vielfalt von denkbaren Materialien auf, welche über die Variation des Copolymerverhältnisses oder des Diens bzw. der Polyesterstruktur realisierbar sind. Da die hier verwendeten Monomere β-Farnesen und L-Dilactid aus erneuerbaren Rohstoffen gewonnen werden, stellt das hergestellte Material ein Beispiel für ein vollständig biobasiertes thermoplastisches Elastomer dar.

Danksagung

Wir danken der Firma Amyris für das zur Verfügung gestellte β-Farnesen. Weiter möchten wir Sandra Seywald und Petra Räder vom MPI-P für die DSC und GPC-Messungen danken. Spezieller Dank gilt Dr. Philip Dreier für das sorgfältige Korrekturlesen des Manuskripts. Open Access Veröffentlichung ermöglicht und organisiert durch Projekt DEAL.

Interessenkonflikt

Die Autoren erklären, dass keine Interessenkonflikte vorliegen.

Erklärung zur Datenverfügbarkeit

Die Daten, die die Ergebnisse dieser Studie unterstützen, sind auf begründete Anfrage beim Autor erhältlich.

Stichwörter: Anionische Polymerisation · Bifunktionell · Phasenseparation · Polyfarnesen · Thermoplastische Elastomere

[1] G. Holden in *Rubber Technology* (Ed.: M. Morton), Springer, New York, **1987**, pp. 465–481.
[2] a) E. M. Frick, A. S. Zalusky, M. A. Hillmyer, *Biomacromolecules* **2003**, *4*, 216; b) E. M. Frick, M. A. Hillmyer, *Macromol. Rapid Commun.* **2000**, *21*, 1317.
[3] S. Tang, J. Li, R. Wang, J. Zhang, Y. Lu, G.-H. Hu, Z. Wang, L. Zhang, *SusMat* **2022**, *2*, 2.
[4] C. Wahlen, H. Frey, *Macromolecules* **2021**, *54*, 7323.
[5] J. M. Bolton, M. A. Hillmyer, T. R. Hoye, *ACS Macro Lett.* **2014**, *3*, 717.
[6] a) C. Wahlen, M. Rauschenbach, J. Blankenburg, E. Kersten, C. P. Ender, H. Frey, *Macromolecules* **2020**, *53*, 9008; b) C. Zhou, Z. Wei, C. Jin, Y. Wang, Y. Yu, X. Leng, Y. Li, *Polymer* **2018**, *138*, 57; c) C. Zhou, Z. Wei, X. Lei, Y. Li, *RSC Adv.* **2016**, *6*, 63508.
[7] C. Fang, X. Wang, X. Chen, Z. Wang, *Polym. Chem.* **2019**, *10*, 3610.
[8] M. Meier-Merziger, M. Fickenscher, F. Hartmann, B. Kuttich, T. Kraus, M. Gallei, H. Frey, *Polym. Chem.* **2023**, *14*, 2820.
[9] M. McCoy, *Chem. Eng. News* **2015**, 93.
[10] C. Iacob, T. Yoo, J. Runt, *Macromolecules* **2018**, *51*, 4917.
[11] J. T. Gruver, G. Kraus, *J. Polym. Sci. Part A* **1964**, *2*, 797.
[12] L. J. Fetters, *J. Res. Natl. Bur. Stand.* **1965**, *69A*, 33.
[13] T. Yoo, S. K. Henning, *Rubber Chem. Technol.* **2017**, *90*, 308.
[14] Y. S. Yu, R. Jerome, R. Fayt, P. Teyssie, *Macromolecules* **1994**, *27*, 5957.
[15] A. R. Schultz, S. Bobade, P. J. Scott, T. E. Long, *Macromol. Chem. Phys.* **2018**, *219*, 1700201.
[16] a) G. Beinert, P. Lutz, E. Franta, P. Rempp, *Makromol. Chem.* **1978**, *179*, 551; b) J. M. Yu, P. Dubois, R. Jérôme, *Macromolecules* **1996**, *29*, 7316.
[17] P. Stanetty, M. D. Mihovilovic, *J. Org. Chem.* **1997**, *62*, 1514.
[18] A. Jordan, C. G. J. Hall, L. R. Thorp, H. F. Sneddon, *Chem. Rev.* **2022**, *122*, 6749.
[19] Z. Nawaz, *Hung. J. Ind. Chem.* **2017**, *45*, 1.
[20] S. H. Hamid, M. A. Ali, *Fuel Sci. Technol. Int.* **1995**, *13*, 509.
[21] P. Dreier, J. Ahn, T. Chang, H. Frey, *Macromol. Rapid Commun.* **2022**, *43*, 2200560.
[22] N.-A. A. B. Taib, M. R. Rahman, D. Huda, K. K. Kuok, S. Hamdan, M. K. B. Bakri, Julaihi, M. R. M. Bin, A. Khan, *Polym. Bull.* **2022**, *1*.
[23] M. den Haese, H. P. L. Gemoets, K. van Aken, L. M. Pitet, *Polym. Chem.* **2022**, *13*, 4406.
[24] a) B. G. G. Lohmeijer, R. C. Pratt, F. Leibfarth, J. W. Logan, D. A. Long, A. P. Dove, F. Nederberg, J. Choi, C. Wade, R. M. Waymouth et al., *Macromolecules* **2006**, *39*, 8574; b) N. J. Sherck, H. C. Kim, Y.-Y. Won, *Macromolecules* **2016**, *49*, 4699.
[25] D. R. Witzke, R. Narayan, J. J. Kolstad, *Macromolecules* **1997**, *30*, 7075.
[26] N. Hadjichristidis, H. Iatrou, S. K. Behal, J. J. Chludzinski, M. M. Disko, R. T. Garner, K. S. Liang, D. J. Lohse, S. T. Milner, *Macromolecules* **1993**, *26*, 5812.
[27] Y. Matsushita, Y. Mogi, H. Mukai, J. Watanabe, I. Noda, *Polymer* **1994**, *35*, 246.
[28] C. Wahlen, J. Blankenburg, P. von Tiedemann, J. Ewald, P. Sajkiewicz, A. H. E. Müller, G. Floudas, H. Frey, *Macromolecules* **2020**, *53*, 10397.
[29] I. Tzourtzouklis, C. Hahn, H. Frey, G. Floudas, *Macromolecules* **2022**, *55*, 8766.

Manuskript erhalten: 23. Juli 2023
Akzeptierte Fassung online: 28. Juli 2023
Endgültige Fassung online: 28. Juli 2023

Curriculum Vitae

Curriculum Vitae

Publications